THE CHALLENGE OF NEW THERAPEUTIC APPROACHES FOR UNMET THERAPEUTIC NEEDS

EDITED BY: Arianna Carolina Rosa, Mitsunobu Mio, Ioanna Andreadou and Vadim V. Sumbayev

PUBLISHED IN: Frontiers in Pharmacology

frontiers Research Topics

ISSN 1664-8714
ISBN 978-2-88966-178-7
DOI 10.3389/978-2-88966-178-7

About Frontiers

Frontiers is more than just an open-access publisher of scholarly articles: it is a pioneering approach to the world of academia, radically improving the way scholarly research is managed. The grand vision of Frontiers is a world where all people have an equal opportunity to seek, share and generate knowledge. Frontiers provides immediate and permanent online open access to all its publications, but this alone is not enough to realize our grand goals.

Frontiers Journal Series

The Frontiers Journal Series is a multi-tier and interdisciplinary set of open-access, online journals, promising a paradigm shift from the current review, selection and dissemination processes in academic publishing. All Frontiers journals are driven by researchers for researchers; therefore, they constitute a service to the scholarly community. At the same time, the Frontiers Journal Series operates on a revolutionary invention, the tiered publishing system, initially addressing specific communities of scholars, and gradually climbing up to broader public understanding, thus serving the interests of the lay society, too.

Dedication to Quality

Each Frontiers article is a landmark of the highest quality, thanks to genuinely collaborative interactions between authors and review editors, who include some of the world's best academicians. Research must be certified by peers before entering a stream of knowledge that may eventually reach the public - and shape society; therefore, Frontiers only applies the most rigorous and unbiased reviews.
Frontiers revolutionizes research publishing by freely delivering the most outstanding research, evaluated with no bias from both the academic and social point of view. By applying the most advanced information technologies, Frontiers is catapulting scholarly publishing into a new generation.

What are Frontiers Research Topics?

Frontiers Research Topics are very popular trademarks of the Frontiers Journals Series: they are collections of at least ten articles, all centered on a particular subject. With their unique mix of varied contributions from Original Research to Review Articles, Frontiers Research Topics unify the most influential researchers, the latest key findings and historical advances in a hot research area! Find out more on how to host your own Frontiers Research Topic or contribute to one as an author by contacting the Frontiers Editorial Office: researchtopics@frontiersin.org

THE CHALLENGE OF NEW THERAPEUTIC APPROACHES FOR UNMET THERAPEUTIC NEEDS

Topic Editors:
Arianna Carolina Rosa, University of Turin, Italy
Mitsunobu Mio, Shujitsu University, Japan
Ioanna Andreadou, National and Kapodistrian University of Athens, Greece
Vadim V. Sumbayev, University of Kent, United Kingdom

Citation: Rosa, A. C., Mio, M., Andreadou, I., Sumbayev, V. V., eds. (2020). The Challenge of New Therapeutic Approaches for Unmet Therapeutic Needs. Lausanne: Frontiers Media SA. doi: 10.3389/978-2-88966-178-7

Table of Contents

frontiers in Pharmacology

EDITORIAL
published: 30 September 2020
doi: 10.3389/fphar.2020.01341

Editorial: The Challenge of New Therapeutic Approaches for Unmet Therapeutic Needs

Arianna Carolina Rosa[1]*, *Mitsunobu Mio*[2], *Ioanna Andreadou*[3] and *Vadim V. Sumbayev*[4]

[1] Department of Scienza e Tecnologia del Farmaco, University of Turin, Turin, Italy, [2] Department of Pharmacology, School of Pharmacy, Shujitsu University, Okayama, Japan, [3] Laboratory of Pharmacology, Faculty of Pharmacy, National and Kapodistrian University of Athens, Athens, Greece, [4] Medway School of Pharmacy, Universities of Kent and Greenwich, Chatham, United Kingdom

Keywords: pharmacology innovation, drug-design, innovative therapies, pharmaceutical innovations, efficacy/risk ratio

Editorial on the Research Topic

The Challenge of New Therapeutic Approaches for Unmet Therapeutic Needs

In light of the recent worldwide emergency caused by the coronavirus disease (COVID-19), it has become even more urgent that we solve unmet medical needs (UMNs). The COVID-19 pandemic has placed national health systems, as well as scientific research communities under enormous pressures in terms of drug repositioning, which is considered to be the quickest possible transition from bench to bedside for UMNs (Singh et al., 2020). Conceived before the pandemic occurred, this Research Topic is topical and relevant to this context but does not fully address the pitfalls of COVID-19 management. As many working in this area are aware, the larger the disease burden, the greater the degree to which important needs are not met. Consistently, clinical testing and the approval of new medicines involves an accelerated authorization procedure. According to the article 4 paragraph 2 of the Commission Regulation EC (No. 507/2006 of 29 March 2006), the conditional authorization of medicinal products for human use (falling within the scope of Regulation, EC No. 726/2004 of the European Parliament and the Council UMN) takes place when there is "a condition for which there exists no satisfactory method of diagnosis, prevention or treatment in the Union or, even if such a method exists, in relation to which the medicinal product concerned will be of major therapeutic advantage to those affected".

This topic is focused around a review by Scavone et al. entitled "The New Paradigms in Clinical Research: From Early Access Programs to the Novel Therapeutic Approaches for Unmet Medical Needs", an extended review which describes the regulatory framework and the more importantly, criticism of new drugs covering UMNs. The other 16 papers in this Research Topic include reviews and research papers which cover an apparent and high heterogeneity of subjects. This collection aims to reflect on a number of important UMNs in different medical areas, to address the lack of a real consensus on the definition and interpretation of UMN (Vreman et al., 2019). Consistently, a search on PubMed.gov using the keyword "unmet therapeutic needs" retrieves 5,100 results, with a variety of specific therapeutic areas that reflect the complexity of the topic. The above definition of UMN includes the concept of "satisfactory method" or, in other words, "adequate treatment" and "major therapeutic advantage", also meaning "significant benefit". This implies: (i) a degree of disease severity or burden; (ii) a lack of effective drugs; (iii) the existence of non-responders among the treated patients; (iv) poor adherence to the prescribed regimen affecting the extent of

OPEN ACCESS

Edited and reviewed by:
Martin C. Michel,
Johannes Gutenberg University
Mainz, Germany

***Correspondence:**
Arianna Carolina Rosa
ariannacarolina.rosa@unito.it

Specialty section:
This article was submitted to Experimental Pharmacology and Drug Discovery, a section of the journal Frontiers in Pharmacology

Received: *19 July 2020*
Accepted: *11 August 2020*
Published: *30 September 2020*

Citation:
Rosa AC, Mio M, Andreadou I and Sumbayev VV (2020) Editorial: The Challenge of New Therapeutic Approaches for Unmet Therapeutic Needs. Front. Pharmacol. 11:01341. doi: 10.3389/fphar.2020.01341

concordance or compliance in medicine taking, and therefore conditioning the pharmacotherapy response; (v) the need for safer drugs; and (vi), that the route of drug administration is eventually related to the delivery formulation, to improve both the pharmacokinetic and the compliance in medicine taking. These are the main areas covered by the papers collected in the present Research Topic.

One of the areas where the UMNs are evident is oncology. The burden of cancer and mortality is associated with a need to face up to these different challenges (Smith et al., 2015). This Research Topic includes several exemplary studies. For instance, the paper "Transcriptome-Wide Effects of Sphingosine Kinases Knockdown in Metastatic Prostate and Breast Cancer Cells: Implications for Therapeutic Targeting" by Alshaker et al., which studied oncogenic signaling to explore the potential advantages of certain molecular therapy combinations in targeting prostate and breast cancers, which reveals the importance of the RNA transcriptome microarray analysis.

A research snapshot article by Sakhnevych et al. on "Mitochondrial Defunctionalization Suppresses Tim-3-Galectin-9 Secretory Pathway in Human Colorectal Cancer Cells and Thus Can Possibly Affect Tumor Immune Escape", further indicates the importance of understanding oncogenic signaling and how it controls immune escape. This enables medical practitioners to select the correct therapeutic targets and develop new approaches for immunotherapy of cancer.

Personalized medicine emphasizes the importance of predicting which patients can experience the best benefits, as well as in anticipating adverse effects. A paper from Giri and Aittokallio on how "DNMT Inhibitors Increase Methylation in the Cancer Genome" approaches this topic, identifying 638 novel hypermethylated molecular targets that influence responses to DNA methyltransferase inhibitors. The synergic effect of different compounds to improve the long-term survival of oncologic patients subjected to conventional chemotherapy is another topic of interest. Accordingly, a prototype for a novel antileukemic therapy is described by Trachtenberg et al., exploring the "Synergistic Cytotoxicity of Methyl 4-Hydroxycinnamate and Carnosic Acid to Acute Myeloid Leukemia Cells via Calcium-Dependent Apoptosis Induction".

The topic of dose reduction, as a way of limiting multiple the side effects of chemotherapeutic regimens, is critical to solving at least part of the UMNs in oncology. Paclitaxel together with other microtubule inhibitors, such as nocodazole and vinorelbine dose-response curves, were investigated by Potashnikova et al. in the study "Non-linear Dose Response of Lymphocyte Cell Lines to Microtubule Inhibitors", who demonstrate, at the cellular level, how the dose can influence the clinical response in terms of cell cycle arrest and cell death. The development of new formulations, and how these are applied to oncology is also reported. The paper on "Paclitaxel-Loaded Nanosponges Inhibit Growth and Angiogenesis in Melanoma Cell Models" by Clemente et al. assess the problem of how an already existing agent, like paclitaxel, could increase the positive efficacy/risk ratio through an innovative technological approach, based on nanoformulation.

A wide spectrum of nanoformulations is constantly under investigation, to address the need for improving the pharmacological and therapeutic properties of drugs (Bamrungsap et al., 2012). Apart from the study of paclitaxel-loaded nanosponges cited above, an example of functionalized gold nanoparticles is also described by Yasinska et al. The paper "Targeting of Basophil and Mast Cell Pro-Allergic Reactivity Using Functionalised Gold Nanoparticles", discuss how gold nanoparticles can be used as a platform for the non-toxic delivery of signaling inhibitors, circumventing the side effects of toxic agents such as calcineurin inhibitors, and thus furnishing potential new antiallergic drugs based on a disease-modifying approach (targeting allergic effector cells).

The review articles by Ingusci et al. on "Gene Therapy Tools for Brain Diseases" and by Chazot et al. on "Histamine and Delirium: Current Opinion" focus the attention on another therapeutic area known to present a number of UMNs, the area of cognitive disorders and other central nervous system disorders, including neurodegenerative diseases. The specific topic of brain disease is very complex and wide. The UMNs in this context are related to unique biological/pathological mechanism(s) that reflect the many as yet unaddressed facets of diseases (Smith et al., 2019). Therefore, as described by Ingusci S. and colleagues, gene therapy represents an attractive option that could address this gap. This Research Topic reports a paper on the search for new antiepileptic drugs is reported, however, an exhaustive exploration of the UMNs for brain disease would require a dedicated issue in itself. Another paper on how "Embelin Prevents Seizure and Associated Cognitive Impairments in a Pentylenetetrazole-Induced Kindling Zebrafish Model" by Kundap et al. discusses the development of a new drug, embelin (produced by *Embelia ribes*), a potential candidate against chronic epilepsy-related cognitive dysfunction with an improved efficacy/risk ratio (retarding seizure and improving cognitive impairment).

This Research Topic also includes another approach to different therapeutic areas such as pathological bone resorptive diseases, osteoporosis, periodontitis, and rheumatoid arthritis. Outlining the novel imidazole derivative KP-A038, Ihn et al. describe the "Inhibitory Effect of KP-A038 on Osteoclastogenesis and Inflammatory Bone Loss Is Associated With Downregulation of Blimp1". Durante et al. also write about the "Effects of PARP-1 Deficiency and Histamine H4 Receptor Inhibition in an Inflammatory Model of Lung Fibrosis in Mice". Their focus on lung fibrosis, is based on the new target identification approach, expanding this concept to the possibility of a combination strategy to improve the benefit/risk ratio adding the selective inhibition of the histamine H4 receptor to non-toxic doses of selective PARP-1 inhibitors.

This idea of the identification of a new potential target to solve pitfalls in the effectiveness of existing therapies reflects the review "Glucocorticoid-Induced Leucine Zipper: A Novel Anti-inflammatory Molecule" by Bereshchenko et al., which provides a clear and complete description, focusing on how a consolidated therapeutic area like inflammation, should involve the design of new therapeutic approaches to improve the glucocorticoids benefit/risk ratio.

According to the WHO, cardiovascular diseases (CVDs) are the leading cause of death worldwide. Therefore, CVDs represent another important area in which UMNs persist. Two papers approach this specific topic: the one by Huang et al. entitled "Rolipram, a PDE4 Inhibitor, Enhances the Inotropic Effect of Rat Heart by Activating SERCA2a" and another by Loi et al. on how "Metformin Protects the Heart Against Hypertrophic and Apoptotic Remodeling After Myocardial Infarction". The first used the prototype of phosphodiesterase-4 inhibitors to validate this target in developing agents for the treatment of heart failure. The second one examined the opportunity of a drug repositioning approach in the treatment of hypertrophic remodeling after myocardial infarction. As an approach, the latter could have important clinical benefits in reducing the experimental time and is based on a well-known commercially available drug-like metformin in the specific.

Some research on UMNs examines polychemical medical approaches, such as those used in Traditional Chinese Medicine, as a possible way to fill that gap (Cheng, 2015). In the paper "Epigoitrin, an Alkaloid From Isatis indigotica, Reduces H1N1 Infection in Stress-Induced Susceptible Model in vivo and in vitro" by Luo et al., this approach is validated by the consistency of preparation, evidence-based clinical efficacy, safety, and knowledge of the mechanism of action.

In conclusion, this Research Topic (containing 3 review articles, 1 mini-review, 3 brief research reports, 1 research snapshot, and 9 original research papers) explores and exemplifies the main challenges in approaching the UMNs. These include: (i) the identification of disease etiopathology and the underlying determinant molecules; (ii) the development of new drugs against novel targets or agents with higher selectivity for existing targets to improve the positive efficacy/risk ratio of the available therapeutic options; and (iii), new strategies for drug administration that could offer better clinical outcomes.

AUTHOR CONTRIBUTIONS

ACR conceived and wrote the text. MM, IA, and VVS co-edited the Research Topic and approved the Editorial final version. All authors contributed to the article and approved the submitted version.

FUNDING

This work was supported by Fondo Finanziamento delle Attivita Base di Ricerca - ROSA_FFABR_17_01.

REFERENCES

Bamrungsap, S., Zhao, Z., Chen, T., Wang, L., Li, C., Fu, T., et al. (2012). Nanotechnology in therapeutics: a focus on nanoparticles as a drug delivery system. *Nanomed. (Lond.)* 7 (8), 1253–1271. doi: 10.2217/nnm.12.87

Cheng, Y. C. (2015). Opportunities for traditional Chinese medicine to address unmet challenges in modern healthcare. *J. Tradit. Complement. Med.* 5 (1), 2–4. doi: 10.1016/j.jtcme.2014.12.001

Singh, H., Kakkar, A. K., and Chauhan, P. (2020). Repurposing minocycline for COVID-19 management: mechanisms, opportunities, and challenges. *Expert Rev. Anti Infect. Ther.* 18, 1–7. doi: 10.1080/14787210.2020.1782190

Smith, A., Hyde, Y. M., and Stanford, D. (2015). Supportive care needs of cancer patients: A literature review. *Palliat Support Care* 13 (4), 1013–1017. doi: 10.1017/S1478951514000959

Smith, E. S., Porterfield, J. E., and Kannan, R. M. (2019). Leveraging the interplay of nanotechnology and neuroscience: Designing new avenues for treating central nervous system disorders. *Adv. Drug Deliv. Rev.* 148, 181–203. doi: 10.1016/j.addr.2019.02.009

Vreman, R. A., Heikkinen, I., Schuurman, A., Sapede, C., Garcia, J. L., Hedberg, N., et al. (2019). Unmet Medical Need: An Introduction to Definitions and Stakeholder Perceptions. *Value Health* 22 (11), 1275–1282. doi: 10.1016/j.jval.2019.07.007

Conflict of Interest: The authors declare that the research was conducted in the absence of any commercial or financial relationships that could be construed as a potential conflict of interest.

frontiers in Pharmacology

ORIGINAL RESEARCH
published: 07 February 2019
doi: 10.3389/fphar.2019.00078

Epigoitrin, an Alkaloid From *Isatis indigotica*, Reduces H1N1 Infection in Stress-Induced Susceptible Model *in vivo* and *in vitro*

Zhuo Luo[1,2], Li-Fang Liu[1,2], Xiao-Hua Wang[1,2], Wen Li[1,2], Chong Jie[1,2], Huan Chen[1,2], Fan-Qin Wei[3], Dan-Hua Lu[1,2], Chang-Yu Yan[1,2], Bo Liu[4], Hiroshi Kurihara[1,2], Yi-Fang Li[1,2] and Rong-Rong He[1,2]**

[1] Guangdong Engineering Research Center of Chinese Medicine & Disease Susceptibility, Jinan University, Guangzhou, China, [2] Guangdong Province Key Laboratory of Pharmacodynamic Constituents of TCM and New Drugs Research, College of Pharmacy, Jinan University, Guangzhou, China, [3] Department of Otorhinolaryngology, Head and Neck Surgery, The First Affiliated Hospital, Sun Yat-sen University, Guangzhou, China, [4] State Key Laboratory of Biotherapy, West China Hospital, Sichuan University, Chengdu, China

OPEN ACCESS

Edited by:
Ioanna Andreadou,
National and Kapodistrian University of Athens, Greece

Reviewed by:
Alan G. Goodman,
Washington State University, United States
Ivan Tattoli,
Columbia University, United States

***Correspondence:**
Yi-Fang Li
liyifang706@jnu.edu.cn
Rong-Rong He
rongronghe@jnu.edu.cn

Specialty section:
This article was submitted to Experimental Pharmacology and Drug Discovery, a section of the journal Frontiers in Pharmacology

Received: 01 October 2018
Accepted: 21 January 2019
Published: 07 February 2019

Citation:
Luo Z, Liu L-F, Wang X-H, Li W, Jie C, Chen H, Wei F-Q, Lu D-H, Yan C-Y, Liu B, Kurihara H, Li Y-F and He R-R (2019) Epigoitrin, an Alkaloid From Isatis indigotica, Reduces H1N1 Infection in Stress-Induced Susceptible Model in vivo and in vitro. Front. Pharmacol. 10:78. doi: 10.3389/fphar.2019.00078

Stress has been proven to modulate an individual's immune system through the release of pituitary and adrenal hormones such as the catecholamines, growth hormone, and glucocorticoids. These signal molecules can significantly alter the host immune system and make it susceptible to viral infection. In this study, we investigate whether epigoitrin, a natural alkaloid from *Isatis indigotica*, provides protection against influenza infection by reducing the host's susceptibility to influenza virus under stress and its underlying mechanism. To support it, the mouse restraint stress model and the corticosterone-induced stress model were employed. Our results demonstrated that epigoitrin significantly decreased the susceptibility of restraint mice to influenza virus, evidenced by lowered mortality, attenuated inflammation, and decreased viral replications in lungs. Further results revealed that epigoitrin reduced the protein expression of mitofusin-2 (MFN2), which elevated mitochondria antiviral signaling (MAVS) protein expression and subsequently increased the production of IFN-β and interferon inducible transmembrane 3 (IFITM3), thereby helping to fight viral infections. In conclusion, our study indicated that epigoitrin could reduce the susceptibility to influenza virus via mitochondrial antiviral signaling.

Keywords: epigoitrin, influenza virus, stress-induced susceptibility, MFN2, MAVS

INTRODUCTION

Influenza A viruses (IAVs), highly contagious pathogens, are responsible for severe respiratory infection in humans and animals worldwide with pandemic potential (Chen et al., 2018). At present, antiviral drugs and vaccines are the main treatment for IAVs infection. Due to the high mutation rate and antiviral-drug-resistant strains of IAVs (Kumar et al., 2018), developing vaccines and antiviral drugs for IAVs infection are still full of challenges. Hence, there is an urgent need to identify novel antiviral therapies or complementary strategies.

Many herbal extracts or natural products have been demonstrated to possess potent anti-influenza, preventive and immunomodulatory effects. The dry root of *Isatis indigotica* (Ban Lan Gen, BLG), a traditional Chinese medicine, has been used for anti-influenza in clinics over thousands of years in China (Zhou and Zhang, 2013). Chemical studies showed that BLG contains various compounds such as alkaloids, nucleosides, amino acids, organic acids (Xiao et al., 2014). Epigoitrin as an alkaloid was used as a marker compound of BLG in the 2015 edition of the Chinese Pharmacopoeia (National Pharmacopoeia Commission, 2015). It has previously been reported that epigoitrin exerts antiviral activity against influenza A1 virus FM1 via inhibiting virus attachment and multiplication *in vitro* (Xiao et al., 2016). However, no *in vivo* pharmacological studies confirmed the anti-influenza activities. Our previous studies indicated that restraint stress could increase the susceptibility to the influenza virus in mice and provide a useful model basis for evaluating the effectiveness of the herbal medicinal product and natural products (He et al., 2011; Tang et al., 2014; Chen et al., 2017). It is well known that stressful events take a toll in the development of disease, especially in infectious disease. Stressors can increase susceptibility to infectious agents, dysregulate the humoral and cellular immune responses to pathogens and increase the risk of catching infectious diseases. Restraint is a commonly used stressor for mice. Mice are placed in tubes with holes such that they can breathe and move forward or backward but cannot turn around, which is often applied overnight during the most active time for mice (Glaser and Kiecolt-Glaser, 2005). Moreover, influenza and pneumonia are the fifth leading cause of death among individuals over 50 years old, which was related to greater immunological impairments associated with distress or depression in the old than that in the young (Glaser and Kiecolt-Glaser, 2005). Accordingly, stress-related immune disorders may be a core mechanism behind multiple infectious diseases, and if antiviral drugs or compounds have the ability to regulate stress-mediated immune disorders, they might play a more important role in the treatment of influenza. In this study, we employed the restraint-stress induced susceptible model to investigate the preventive effects of epigoitrin on influenza infection and its related mechanisms.

MATERIALS AND METHODS

Compounds

Epigoitrin with 98% purity was purchased from Aladdin Biochemical Technology Co., Ltd. (Shanghai, China). Oseltamivir was obtained from Yichang Changjiang Pharmaceutical Co., Ltd. (Wuhan, China). Corticosterone was purchased from Sigma (MO, United States).

Virus

The human HlN1 prototype strain, mouse-adapted A/FM/1/47 virus (Smeenk and Brown, 1994), was provided by College of Veterinary Medicine of South China Agricultural University (Guangzhou, China). Viruses were propagated in the allantoic cavities of specific-pathogen-free fertilized eggs. The allantoic fluid containing virus was harvested and stored in aliquots at −80°C until used. Median tissue culture infective dose ($TCID_{50}$) was measured in MDCK cells and calculated according to the Reed-Muench formula after serial dilution of the stock. Amounts of 10 $TCID_{50}$ value were used for viral infection in all the cell experiments.

Mice and Experimental Design

Specific-pathogen-free male Kunming mice with 4 weeks of age and weighing 12–15 g were purchased from Guangdong Medical Laboratory Animal Center (Guangzhou, China). The animals performed in this study were housed in plastic cages and lived under standard laboratory conditions. Animal experiments were approved by the Animal Care and Use Committee of Jinan University (Approval ID: SYXK 20150310001) and performed in compliance with the National Institute of Health's Guide for the Care and Use of Laboratory Animals (7th edition, United States).

To evaluate the anti-influenza virus effects of epigoitrin on mice loaded with restraint stress, mice were randomly distributed to six groups: Control, Virus, "Restraint + Virus," Oseltamivir (30 mg/kg/d oseltamivir + restraint + virus), Epigoitrin-L (88 mg/kg/d epigoitrin + restraint + virus), and Epigoitrin-H (176 mg/kg/d epigoitrin + restraint + virus). Oseltamivir and epigoitrin were administered orally to mice for 7 consecutive days, while other groups were received oral administration of water only. After the first day of administration, mice except those in Control and Virus groups were physically restricted in the plastic centrifuge tube of 50 mL with holes for 22 h. On the second day after restraint, mice were anesthetized by inhalation of diethyl ether vapor and then were inoculated intranasally with 500 PFU Influenza virus in PBS. Subsequently, the daily changes of mice in survival and their typical influenza symptoms, including hunched back, ruffled fur, altered respiration and unresponsiveness, were observed and recorded for 21 days or until death. The morbidity of the mouse was estimated when its weight was decreased over 1 $g{\cdot}d^{-1}$. The survival rate was also calculated.

Mice were weighed and euthanized after 5 days post infection (dpi), and the lungs were removed and weighed. The lung index was calculated according to the formula: Lung index (mg/g) = lung weight/body weight. Samples of lung tissue were reserved for histopathological examination, virus titers, and western blotting analysis.

The second animal experiment was conducted to investigate the effect and mechanism of epigoitrin on type I IFN secretion in stressed mice. Mice were distributed at random to five groups: Control, Virus, "Restraint+Virus," Epigoitrin-L, and Epigoitrin-H. The following treatment was the same as described above. The lung tissues were collected to determine the protein expressions related with IFN-β and MAVS signaling. To explore the effects of epigoitrin on corticosterone level, Mice were randomly divided into four groups: Virus, "Restraint+H1N1," Epigoitrin-L and Epigoitrin-H. On the second day after restraint, mice were challenged with virus. Blood samples were collected from the heart to determine the plasma corticosterone levels. For investigating the anti-viral activity against H1N1

in unstressed mice, Mice were orally administered with epigoitrin-L (88 mg/kg/d epigoitrin + virus) and epigoitrin-H (176 mg/kg/d epigoitrin + virus) for 7 days prior to H1N1 infection. After 5 dpi, Lung samples were collected for $TCID_{50}$ assay.

Histological Analysis of Lung Injury

The lungs of the mice were fixed in 10% neutral buffered formalin and processed routinely. Paraffin sections, 5–10 μm thick, were stained with hematoxylin and eosin and then examined under microscopy in a blinded fashion. Pathological changes were scored based on the criteria (Fang et al., 2011): 0, no pneumonia; 1, mild interstitial pneumonia (<25% of the lung); 2, moderate interstitial pneumonia (25–50% of the lung); 3, severe interstitial pneumonia (>50% of the lung). The sums of scores of different animals were averaged.

Quantification of Cells and Measurement of Cytokines From Bronchoalveolar Lavage Fluid (BALF)

Mice were anesthetized after 5 dpi and lungs were lavaged by instillation and withdrawal of 1 ml PBS through a tracheal cannula and BAL fluid (BALF) was collected. Total BAL cell numbers were determined using a hemocytometer. After centrifuged at 1500 rpm at 4°C for 5 min, Supernatants were collected to determine the levels of TNF-α and IL-1β using enzyme-linked immunosorbent assay (ELISA) kits (Thermo Fisher Scientific, Waltham, MA, United States) according

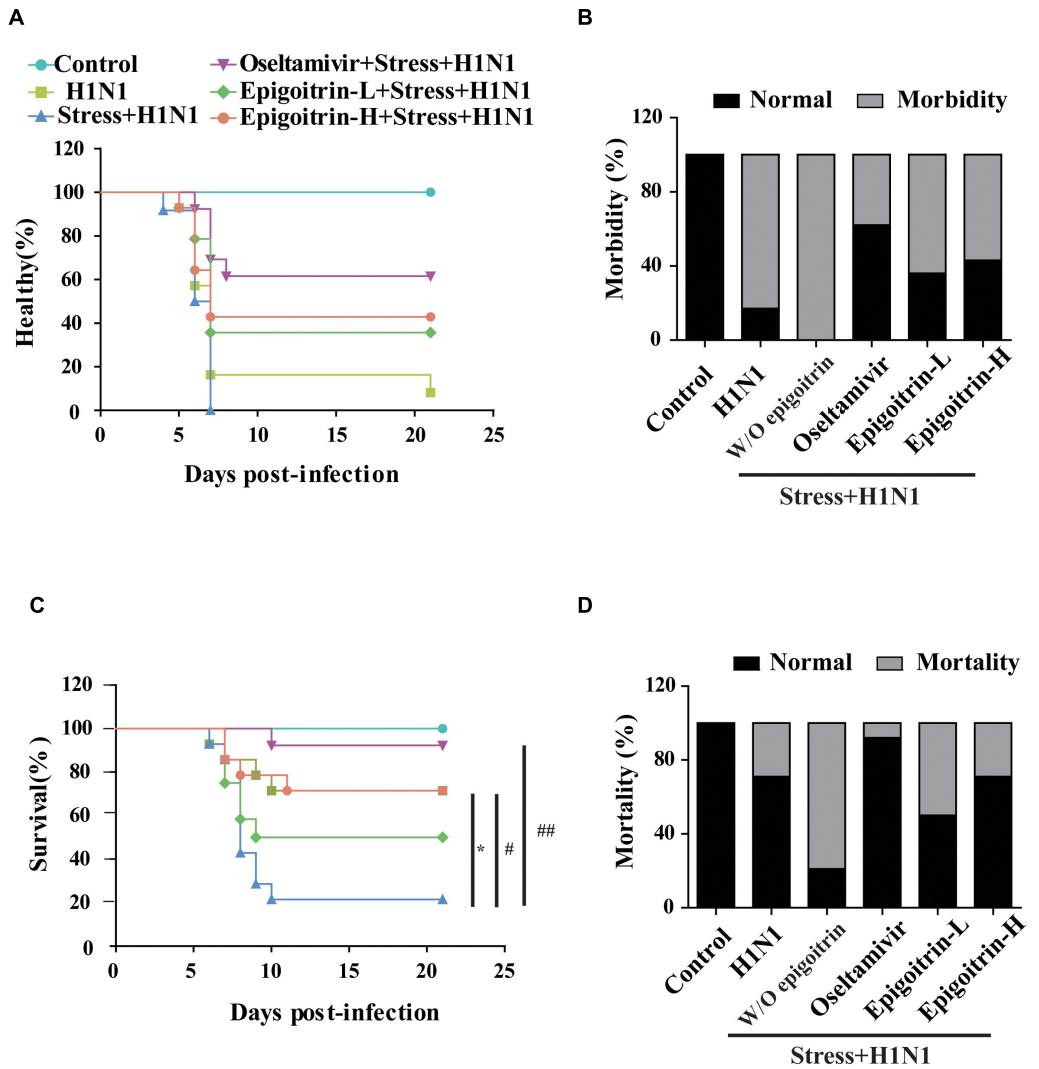

FIGURE 1 | Epigoitrin attenuated the morbidity and mortality caused by influenza infection in stressed mice. **(A,B)** Healthy curve and morbidity caused by influenza infection in restraint mice. **(C,D)** Survival curve and mortality caused by influenza infection in restraint mice. "W/O epigoitrin" indicates without epigoitrin treatment. Epigoitrin-H and Epigoitrin-L, respectively, represent the higher dose of epigoitrin (176 mg/kg/d) and the lower dose of epigoitrin (88 mg/kg/d). The difference was considered statistically significant at $^{*}P < 0.05$ vs. H1N1 group; $^{\#}P < 0.05$ and $^{\#\#}P < 0.01$ vs. "Stress+H1N1" group. Data were obtained from 10–14 animals in each group.

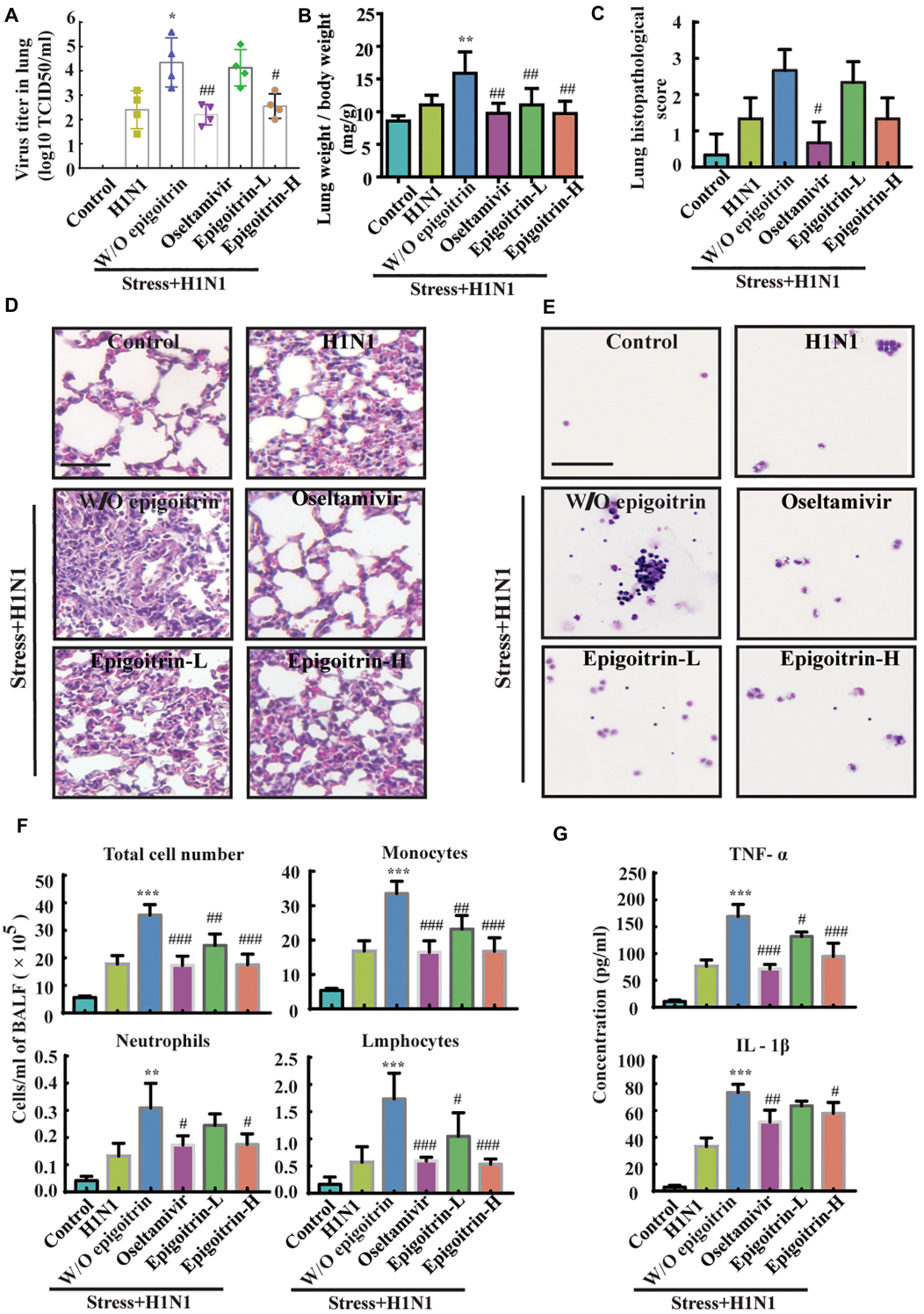

FIGURE 2 | Epigoitrin protected against pneumonia caused by influenza infection in stressed mice. **(A,B)** The effects of epigoitrin on the viral titres in the lungs (n = 4) and the lung index (n = 6). **(C,D)** Lung pathological scores (n = 3) and histopathologic changes on the 5th day after influenza virus challenge, stained by H&E (scale bar = 50 μm). **(E,F)** Effects of epigoitrin on the changes of types of infiltrated inflammatory cells and cell numbers in BALF (scale bar = 100 μm). **(G)** Effects of epigoitrin on the levels of TNF-α, IL-1β in BALF (n = 4). The difference was considered statistically significant at $^{*}P < 0.05$, $^{**}P < 0.01$, $^{***}P < 0.001$ vs. H1N1 group; $^{\#}P < 0.05$, $^{\#\#}P < 0.01$, $^{\#\#\#}P < 0.001$ vs. "Stress+H1N1" group.

to the manufacturer's protocol, and compared with known standards. Cell pellets were resuspended in 200 μl PBS and cellular infiltration was assessed on Wright-Giemsa-stained slides (Nanjing Jiancheng Bioengineering Institute, Nanjing, China).

Determination of Corticosterone Level in Plasma

Corticosterone was extracted from the plasma and quantified by HPLC as we previously reported (Chen et al., 2017). Briefly, the plasma was collected from blood samples pretreated with 10 μl of heparin after centrifugation at 2500 × *g* for 10 min. Cortisol solution (100 μl, 500 ng/ml) as an internal standard was mixed into plasma (1 ml), and then were extracted by mixing with 2 ml of ethyl acetate thoroughly for three times. The organic phase was collected, washed, and evaporated under nitrogen. The residue was dissolved and analyzed by HPLC with a UV detection at 254 nm (Agilent 1200).

Cell Culture and Treatment

Human alveolar epithelial cell line (A549) and Madin-Darby canine kidney (MDCK) cells were grown at 37°C in 5% CO_2 atmosphere in Dulbecco's modified Eagle's medium (DMEM; high glucose, with L-glutamine) supplemented with 10% fetal bovine serum (FBS), 100 IU/ml penicillin, and 100 μg/ml streptomycin. For simulating the stress-induced susceptibility to influenza virus infection *in vitro*, corticosterone, an indicator of the stress response, was employed to establish a "Corticosterone + Virus" A549 cell model. Cells were treated with corticosterone (100 μM) for 48 h and then infected with 10 $TCID_{50}$ for 12 h. Based on the "Corticosterone + Virus" model, we then evaluate the antiviral activity of epigoitrin against IAVs. Cells pretreated for 2 h with different concentrations of epigoitrin were challenged with corticosterone for 48 h in the presence of epigoitrin prior to infection, then was infected with H1N1 influenza virus of 10 $TCID_{50}$ for 1.5 h. Twelve hours post infection (hpi), the cells were harvested for RT-qPCR and $TCID_{50}$ assay.

Viral RNA Quantification by RT-qPCR

Total RNA was extracted using TRIzol reagent (Invitrogen) at indicated time according to manufacturer's instructions. RNA concentrations were determined by optical density measurement at 260 nm on a spectrophotometer (Thermo Fisher Scientific) and cDNA was synthesized from the purified RNA by both random and oligo (dT) priming using an iScript cDNA synthesis kit (Bio-Rad). Intracellular NP and IFN-β RNA levels were measured using the SYBR green method (Applied Biosystems) on a reverse transcription (RT) machine (CFX Connect™; Applied Biosystems) and the relative values of Actin. The fold induction of viral RNA or innate immune genes over the levels of induction for either mock-infected cells or DMSO-treated control cells was calculated. Primer sequences were as follows: NP forward, 5′-CAGGTACTGGGCCATAAGGAC-3′, and reverse, 5′-GCATTGTCTCCGAAGAAATAAG-3′; IFN-β forward, 5′-CTTACAGGTTACCTCCGAAACTGAA-3′, and reverse, 5′-TTGAAGAATGCTTGAAGCAATTGT-3′; Actin forward, 5′-TGACGTGGACATCCGCAAAG-3′, and reverse, 5′-CTGGAAGGTGGACAGCGAGG-3′.

$TCID_{50}$ Assay

Briefly, a confluent monolayer of MDCK cells grown in 96-well plates were washed two times with PBS and then inoculated with

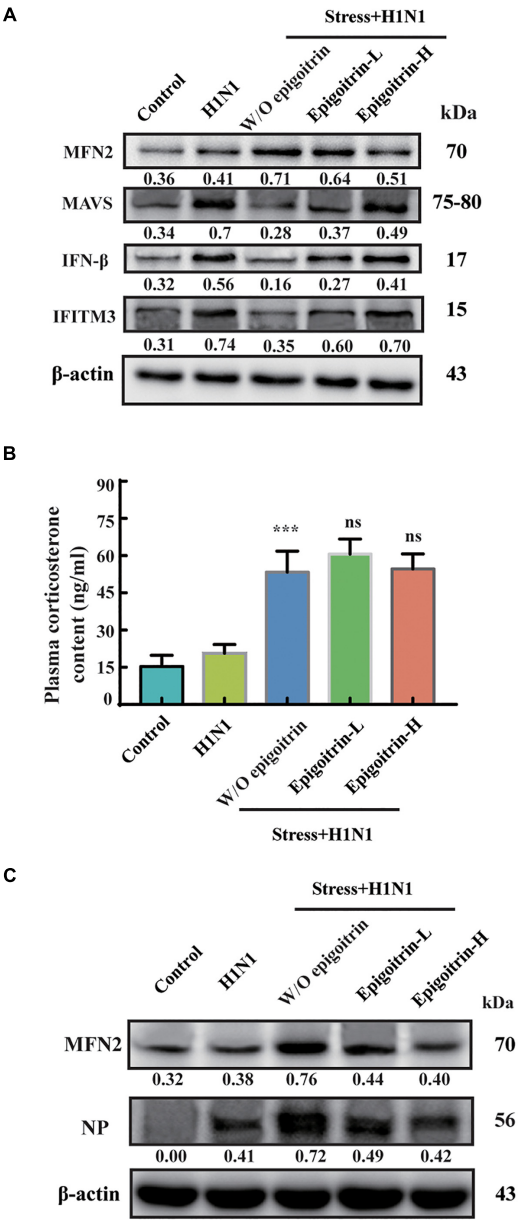

FIGURE 3 | Epigoitrin improved MAVS antiviral signaling after influenza infection in stressed mice. **(A)** Effects of epigoitrin on MFN2, MAVS, IFN-β, and IFITM3 protein expressions in the lung tissues. **(B)** Effects of epigoitrin on corticosterone level in the plasma. **(C)** Effects of epigoitrin on MFN2, NP protein expressions in the lung tissues. Actin was used as an internal control and the relative densities of the measured protein were quantified by image J software. ***$P < 0.001$ vs. H1N1 group; ns, no significance ($P \geq 0.05$) vs. Stress+H1N1 group.

threefold serial dilution of the virus-containing supernatants in DMEM for 2 h. The inoculum was removed, and cells washed and incubated with 200 μL DMEM containing 1 μg/mL TPCK-trypsin. After 48 h of incubation, the cytopathic effect was scored microscopically, and the $TCID_{50}$ dose was calculated according to the Reed–Muench methods.

Immunofluorescence Assay (IFA)

Cells from each group were fixed with 4% paraformaldehyde for 30 min, and then were permeabilized with 0.1% Triton-X100 for 5 min. After blocking with 2% bovine serum albumin for 20 min, they stained with a rabbit polyclonal antibody against NP (GTX125989) or a mouse Monoclonal antibody against MFN2 (ab56889, Abcam, United States) in 1:100 dilution at 4°C for 12 h. The secondary antibodies conjugated with Alexa Fluor 488 anti-mouse IgG in 1:200 dilution or 555 conjugated goat-rabbit IgG (Life Technology, NY, United States) in 1:200 dilution were applied for 45 min at room temperature. Nuclei were counterstained with DAPI (Beyotime, Shanghai, China), and the cells were visualized and analyzed using a confocal laser scanning microscope.

Lung Histopathology and Virus Titers

Lungs from each group of mice after 5 dpi were removed and immediately fixed in 4% buffered formalin. Subsequently, the lung tissue was embedded in paraffin wax and 4 μm thick sections were sliced and stained with hematoxylin and eosin (H&E). For determination of virus titer in lung, lung tissues from euthanized mice were aseptically removed and homogenized in DMEM plus antibiotics to achieve 10% (w/v) suspensions, followed by centrifuged at 1400 *g* for 20 min at 4°C. $TCID_{50}$ assay was performed to determine the infectivity of virus in the supernatant as described above.

EGFP-MFN2 Plasmid Transfection

A549 cells were cultured on 6-well plate (NEST Biotech) in 50000 cells/ml and subsequently prepared for EGFP-MFN2 (TransGen Biotech) transfection to reach 50–60% confluence. A non-targeting vector (TransGen Biotech) was used as negative control. The transfection, using Lipofectamine® LTX & PLUS™ Reagent (Invitrogen), was carried out as described in the instructions of the manufacturer. Forty eight hours after transfection, cells were infected with 10 $TCID_{50}$ H1N1 for 2 h. Subsequently, cells were performed to western blotting analysis at 12 hpi.

Western Blotting Analysis

For immunoblotting analysis, lung samples and cell lysates lysed by RIPA buffer (Beyotime, China) were resolved by SDS–PAGE and transferred to the polyvinylidene fluoride membrane (Millipore, United States). Immunoblots were visualized by the ECL system (Fdbio Science, China). The following antibodies were used in immunoblotting analysis: antibodies for anti-IFITM3 (1:2,000), anti-MFN2 (1:2,000), anti-IFN-β (1:500) antibody and anti-IL-1β (1:1,000) were from Abcam. β-actin antibody (1:2,000) was purchased from Fude Biotechnology. Anti-phospho-IRF3 (1:1,000), and anti-TNF-α (1:2,000) antibodies were purchased from Cell Signaling Technology. Anti-MAVS (1:500) antibodies were obtained from Proteintech Group. β-actin was used as an internal control and the relative densities of the measured protein were quantified by image J software.

Statistical Analysis

All data are expressed as mean ± standard deviation (SD) from at least three independent experiments. Differences during experiments were analyzed by unpaired one-way ANOVA (Tukey test) of the GraphPad Prism 5 system. Kinetics of mortality and morbidity are analyzed by Kaplan–Meier curves and log-rank test with Bonferroni adjustment. A value of $P < 0.05$ was defined as statistically significant.

RESULTS

Protective Effects of Epigoitrin on Influenza Infection in Restraint-Stress Mice

To establish a susceptible animal model, mice were loaded with restraint stress for 22 h before H1N1 virus challenge were employed. The experimental mice were monitored daily for 21 days. Compared with "H1N1" group, the emergence of clinical symptoms, including lack of appetite, inactivity, ruffled fur, a hunched posture and respiratory distress had an earlier tendency in "Restraint stress + H1N1" group (**Figure 1A**). Moreover, the morbidity of "Restraint stress + H1N1" group increased to 100% (**Figure 1B**). These results suggested that restraint stress could exacerbate clinical development of influenza disease and make the host susceptible to the influenza virus. Based on this model, the protective effects of epigoitrin against H1N1 virus in mice were investigated. As shown in **Figures 1C,D**, mice in the "Restraint stress + H1N1" group had a higher morbidity rate (100% vs. 83%) and lower mean time to sickness (6.33 ± 0.89 vs. 8.43 ± 5.36 days) compared to the "H1N1" alone group. Likewise, the survival rate of "Restraint stress + H1N1" group decreased from 71 to 50.0% compared with the "H1N1" alone group ($P < 0.01$), and the mean day to death (MDD) decreased from 17.29 ± 6.16 to 10.86 ± 5.7 days ($P < 0.05$). However, the administration of epigoitrin at 176, 88 mg/kg/d saved 50 and 29% of "Restraint stress + H1N1" group, respectively, and prolonged MDD with a lower morbidity sign. As a positive control, oseltamivir remarkable decreased the morbidity rate to 38% and markedly raised the survival rate to 92%. These results demonstrated that epigoitrin treatment effectively increased survival rate and protected mice from lethal infection with influenza.

Effects of Epigoitrin on Influenza Infection in the Lung of Restraint-Stress Mice

To further evaluate the therapeutic efficacy of epigoitrin against influenza infection in stressed mice, virus titers in the lung were measured after 5 dpi. No virus was detected in lung tissues of the Control group. The virus titer in "Restraint stress + H1N1"

group was significantly higher than that in "H1N1" alone group (4.35 ± 0.50 vs. 2.40 ± 0.39 Log10 $TCID_{50}$/ml), whereas virus titer were 2.55 ± 0.25 Log10 $TCID_{50}$/ml and 4.13 ± 0.37 Log10 $TCID_{50}$/ml in the high- and low-dose epigoitrin-treated groups (**Figure 2A**), respectively. H1N1 virus titers in stressed mice after epigoitrin treatment markedly decreased. Histopathological examination by H&E staining was performed to investigate pathological changes after virus infection. As shown in **Figure 2C**, mild inflammatory cell infiltration was observed in the lungs of mice infected H1N1 virus. More severe inflammatory cell infiltration in the interstitium and alveoli (**Figure 2D**) were found in the "Restraint stress +H1N1" group. Meanwhile, a higher lung index and histopathological score presented in the "Restraint stress + H1N1" group (**Figures 2B,C**), compared to the "Virus" alone group. In contrast, treatment with oseltamivir, or epigoitrin-H significantly reduced the numbers of total cell and infiltration of neutrophils, monocytes and lymphocytes in BALF (**Figures 2E,F**) with a lower index and histopathological score. Moreover, epigoitrin treatment effectively lowered TNF-α and IL-1β levels in BALF from "Restraint stress + H1N1" group (**Figure 2G**).

Epigoitrin Improved the MAVS Antiviral Signaling Pathway in Restraint Stressed Mice

Previous studies had suggested that restraint stress-induced influenza viral susceptibility was closely related to innate immunity (Glaser and Kiecolt-Glaser, 2005). After infection, H1N1 virus mRNA was recognized by RIG-I/MAVS/IRF3 pathway and induced type I IFNs secretion, which could suppress viral replication, boost adaptive immunity, and limit acute lung injury (Arimori et al., 2013; McNab et al., 2015). To confirm that the differences in virus pathogenicity between the "Restraint stress + Virus" and epigoitrin groups were due to an improvement in type I IFNs pathway, the expression

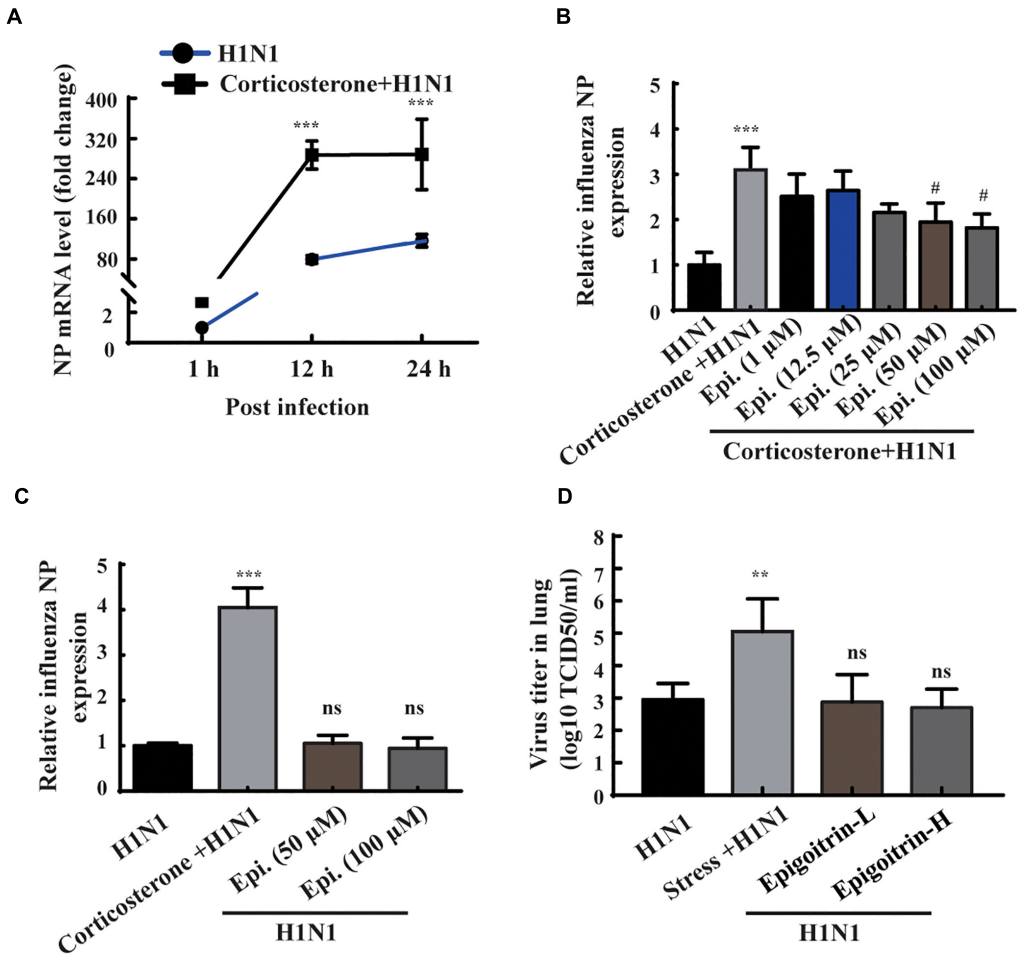

FIGURE 4 | Epigoitrin reduced H1N1 viral expression in corticosterone-loaded A549 cell. **(A)** A549 cells were treated with or without corticosterone (100 μM) for 48 h before viral infection and the NP gene expression were measured by RT-qPCR at the indicated time. **(B,C)** Effects of epigoitrin on the NP gene expression in H1N1-infected A549 cell pretreated with or without corticosterone. **(D)** Effects of epigoitrin on the viral titers of lungs in stressed or unstressed mice (n = 4). The difference was considered statistically significant at $^{**}P < 0.01$, $^{***}P < 0.001$ vs. H1N1 group; $^{\#}P < 0.05$ vs. corticosterone +H1N1 group; ns, no significance ($P \geq 0.05$) vs. H1N1 group.

levels of protein related to this pathway were evaluated. The protein expressions of MAVS, IFN-β and IFITM3 were assayed in the lung tissue. Large increases in the protein expressions of MAVS, IFN-β, and IFITM3 were observed upon viral infection. Compared to the "H1N1" group, restraint stress obviously reduced these protein expressions with a higher MFN2 level. However, this process was improved by epigoitrin treatment (**Figure 3A**). Stressors could activate the hypothalamic-pituitary-adrenal axis and thereby trigger increases in stress hormone levels, which lead to dysregulation of immune function. Our previous study revealed that restraint stress-induced influenza viral susceptibility was specifically associated

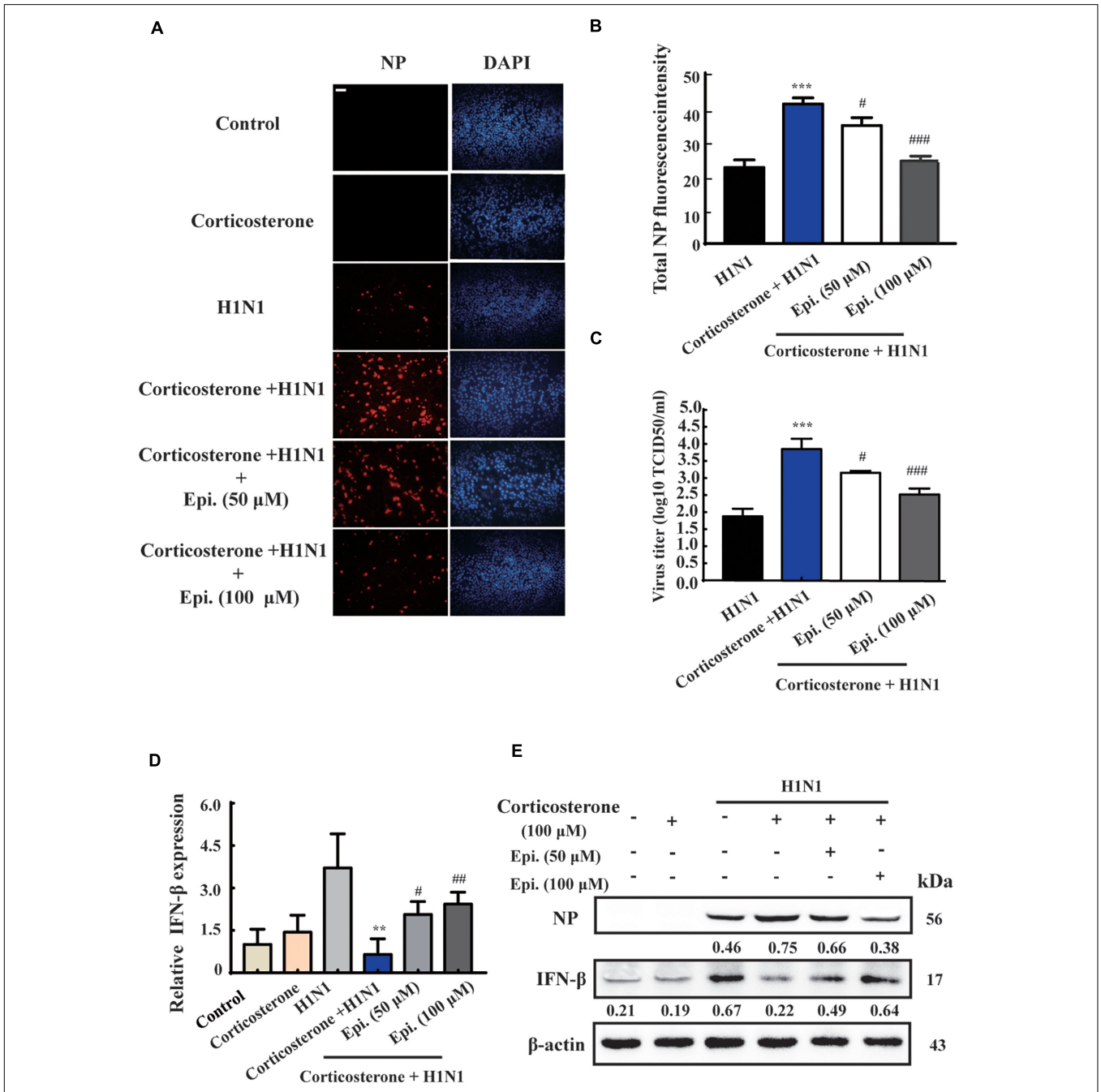

FIGURE 5 | Epigoitrin inhibited H1N1 replication and promoted IFN-β generation after influenza infection in stress cell model. **(A)** Cells stained for influenza A virus NP at 12 hpi (red) and the cell nuclei were stained by DAPI (blue). Bar = 50 μm. **(B)** The total fluorescent intensity was determined to reflect the levels of NP. **(C)** Related infectious viral titer was detected by $TCID_{50}$ assay. **(D,E)** Effects of epigoitrin on IFN-β gene and protein expression were analyzed by qRT-PCR and Western blotting. The difference was considered statistically significant at $^{**}P < 0.01$, $^{***}P < 0.001$ vs. H1N1 group; $^{\#}P < 0.05$, $^{\#\#}P < 0.01$, $^{\#\#\#}P < 0.001$ vs. corticosterone +H1N1 group.

with corticosterone secretion (Chen et al., 2017). Hence, effects of epigoitrin on corticosterone level in the plasma of stressed mice were investigated. As show in **Figures 3B,C**, restraint stress significantly elevated the plasma corticosterone levels and the expression of MFN2 and virus nucleoprotein (NP) in lungs of mice. Interestingly, Epigoitrin-H and Epigoitrin-L had no significant effects on the plasma corticosterone level, but decreased the protein level of MFN2 and NP in stressed mice. It could be inferred that restraint stress-induced influenza viral susceptibility might be associated with

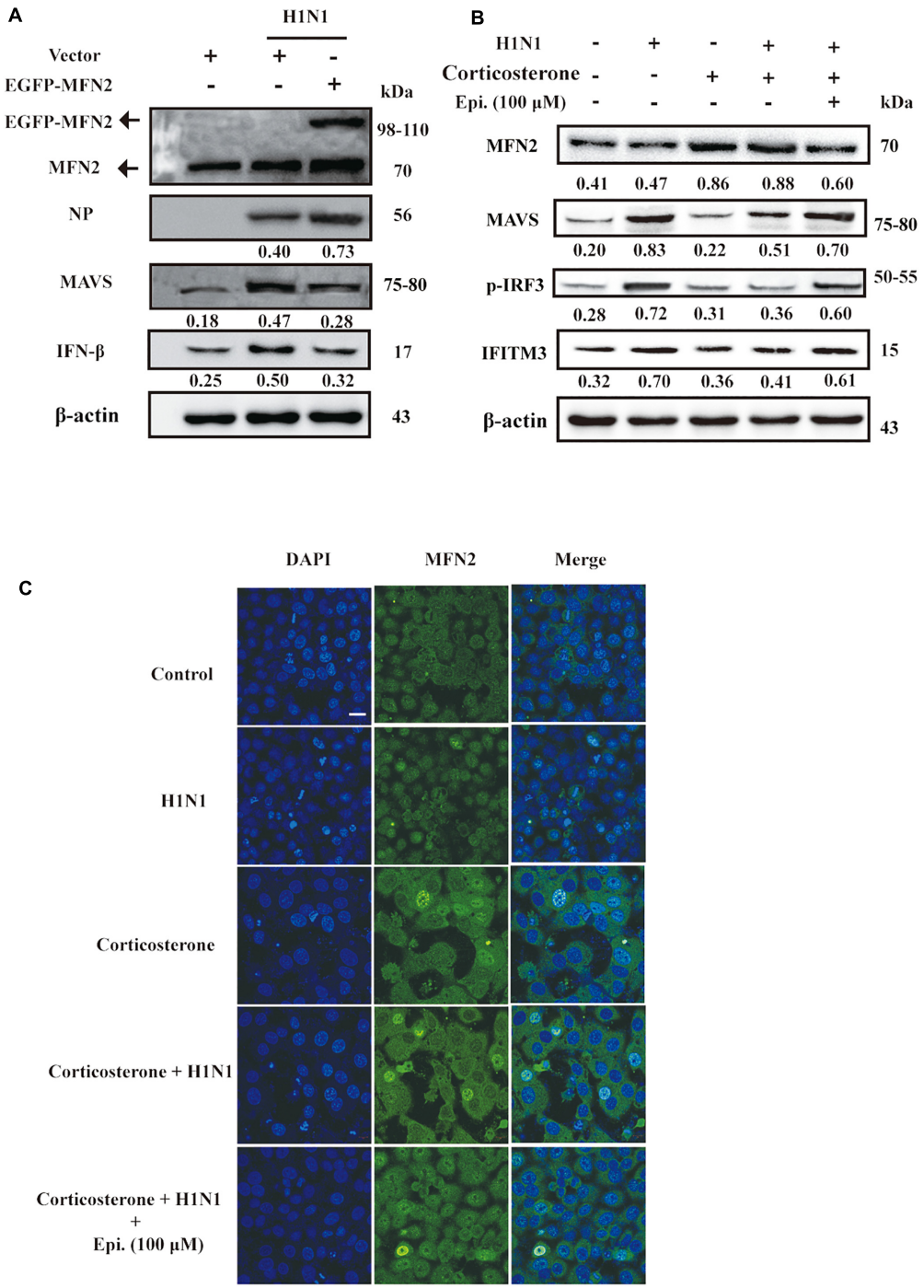

FIGURE 6 | MFN2 was involved in the regulation of IFN-β production by epigoitrin in stress cell model. **(A)** Effects of EGFP-MFN2 overexpression on H1N1 infection. **(B)** The levels of protein expression by the MFN2, MAVS, p-IRF3, and IFITM3 gene relative to the level of β-actin expression were determined using the respective antibodies. **(C)** Representative fluorescence images showing the levels of MFN2 protein expression. Bar = 20 μm.

corticosterone secretion. Epigoitrin treatment would boost resistance to influenza through the mitochondrial antiviral signaling pathway independent of inhibiting corticosterone secretion.

Epigoitrin Reduced H1N1 Viral Expression in Corticosterone-Loaded A549 Cell

According to the results of animal experiments (**Figure 3B**), restraint stress-induced influenza viral susceptibility was associated with corticosterone secretion. Thus, corticosterone was utilized to establish a stress-induced susceptibility model *in vitro*. The gene expression of NP was assessed to reflect the viral replication level. As shown in **Figure 4A**, the intracellular viral abundance in the cells treated with corticosterone and H1N1 was significantly higher than that in cells only treated with virus at 12 and 24 hpi. The susceptibility to H1N1 infection caused by corticosterone is independent of viral entry, because there was no statistically significant difference in NP gene expression between the two groups level at 1 hpi. Based on this model, we examined the antiviral effects of epigoitrin. A dose-dependent inhibition in the mRNA expression of NP was observed in cells pretreated by epigoitrin compared with levels in untreated cells after corticosterone load (**Figure 4B**). However, this preventive effect of epigoitrin on NP gene expression in H1N1 susceptibility model may be not due to its direct antiviral ability, because epigoitrin pretreatment had no significantly inhibitory effect on the expression of viral gene NP in A549 cell (**Figure 4C**) and virus titer in the lungs of unstressed mice after H1N1 infection (**Figure 4D**). These result were consistent with the fact that pre-treatment with epigoitrin didn't exert a prophylaxis effect on H1N1 infection (Xiao et al., 2016).

Epigoitrin Inhibited H1N1 Replication Through Promoting IFN-β Generation in Corticosterone-Induced Viral Susceptibility Model

To further investigate the protective effect of epigoitrin on reducing influenza susceptibility *in vitro*, NP protein levels and virus titers were measured. As shown in **Figure 5A**, no immunofluorescence of viral NP was found in the "Control" and "Corticosterone" group. A significant increase of red fluorescence intensity (**Figure 5B**) and virus titer (**Figure 5C**) were observed in H1N1-infected cells with corticosterone pretreatment, which could be attenuated by epigoitrin treatment. Moreover, in cells pretreated with corticosterone, the expression levels of H1N1-triggered IFN-β gene (**Figure 5D**) and protein

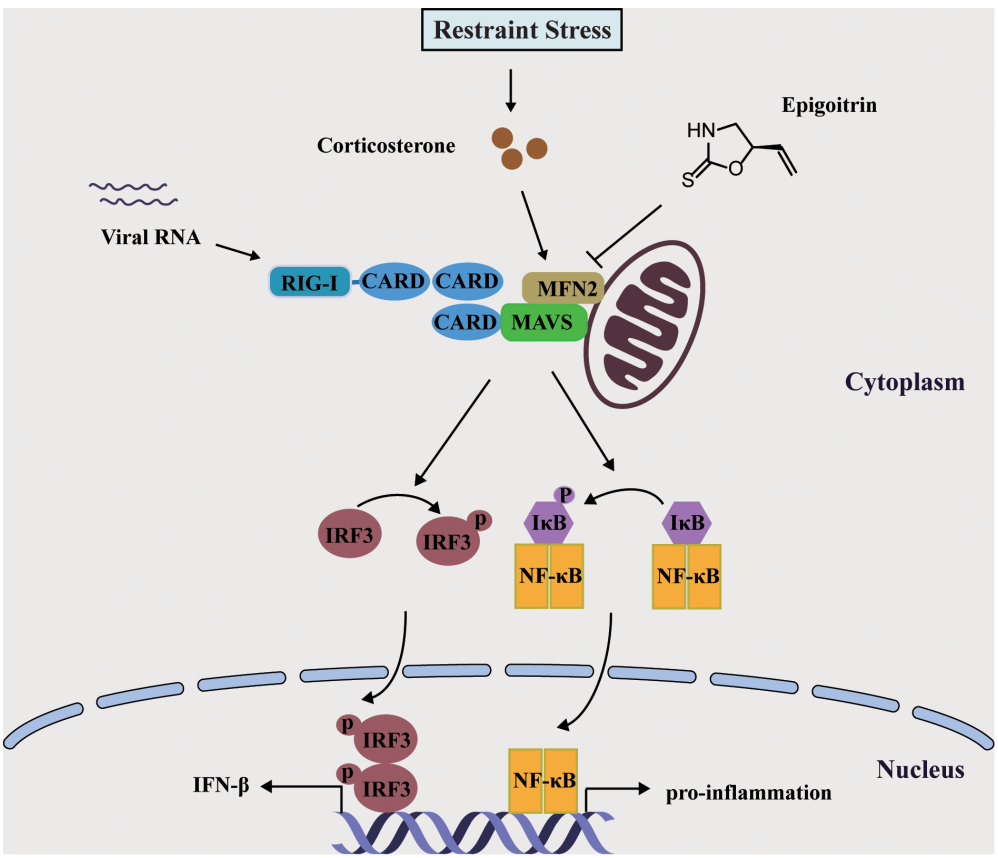

FIGURE 7 | Schematic diagram of the mechanism of Epigoitrin-induced attenuation of H1N1 pathogenesis in the susceptible model.

(**Figure 5E**) were significantly reduced, while epigoitrin treatment improved their production and reduced viral NP protein.

MFN2 Was Engaged in the Regulation of IFN-β Production by Epigoitrin in Corticosterone-Induced Viral Susceptibility Model

The antiviral RIG-I-like Receptor (RLR) signaling played a key role for IFN-β production in the mammalian immune response during H1N1 infection. Accumulated findings had unveiled that mitochondrial dynamics participated in RLR signaling transduction, functioning as signaling platforms and contributing to effector responses (West et al., 2011). MFN2, a mitofusin protein, had been shown to interact with MAVS and suppressed MAVS activating the IFN-β generation (Yasukawa et al., 2009). To examine the effects of MFN2 overexpression on H1N1 infection, we transfected cells with EGFP-MFN2 for western blot analysis. H1N1-infected cells showed higher IFN-β, an indicator of RLR signaling activation, and lower NP production when compared to cells transfected with MFN2. Moreover, higher MAVS expression was also noted in H1N1-infected cells without MFN2 transfection while lower antiviral activity appeared in the MFN2-overexpressing cells (**Figure 6A**). Hence, to explore whether epigoitrin could down-regulate the level of MFN2 protein and improved the MAVS antiviral signaling in H1N1 susceptibility model. Increased MFN2 protein was detected in both "Corticosterone" and "Corticosterone +Virus" groups, which resulted in a decreased level of the MAVS antiviral signaling-related proteins, MAVS, p-IRF3, and IFITM3. However, epigoitrin treatment could reduce the MFN2 protein expression and improve MAVS antiviral signaling-related proteins production (**Figure 6B**). We also determined the effect of epigoitrin on MFN2 expression by immunofluorescence and the results were coincided with that from western blotting (**Figure 6C**).

DISCUSSION

Previously, we had utilized restraint stress, a commonly used stressor to establish mouse H1N1 susceptibility model and evaluate the anti-viral effect of medicines and compounds. Based on this model the protective effect of epigoitrin on influenza susceptibility *in vivo* was evaluated. Our results showed that substantially increased morbidity and mortality in restraint stress animals challenged with H1N1 virus. Moreover, restraint stress also significantly increased the virus titer and induced excessive production of pro-inflammatory cytokines such as IL-1β, TNF-α, which aggravated pathological changes of the lung tissues in H1N1-infected mice. In comparison, treatment with epigoitrin prior to infection led to improvement of these pathological indicators and reduced the risk of influenza virus infection in restraint-stressed mice.

The principal peripheral effectors of the stress system are glucocorticoids, which are regulated by the hypothalamic–pituitary–adrenal axis (Chrousos, 2009). Studies indicated that restraint stress-induced influenza viral susceptibility was associated with corticosterone secretion (Konstantinos and Sheridan, 2001; Chen et al., 2017). Thus, we utilized corticosterone to establish an A549 cell stress model, and evaluated the preventive effects of epigoitrin on H1N1 infection. In the present study, we found that corticosterone *in vitro* could disrupt the interferon innate immune pathways and increased influenza viral susceptibility, which eventually facilitated its own replication in host cells. This effect of corticosterone-induced immunosuppression on virus infection is improved by epigoitrin. Epigoitrin treatment could improve the MAVS antiviral signaling and promoted the generation of IFN-β in corticosterone-loaded A549 cells and stressed mice following H1N1 infection.

Mitochondria were essential for triggering the cellular innate immune responses via MAVS against invading viruses, especially RNA viruses. This subsequently activated a signaling cascade that resulted in the phosphorylation and nuclear translocation of IRF3, leading to the expression of type I IFN (Iwasaki and Pillai, 2014). MFN2 acted as an inhibitor in regulating MAVS signaling independent of its function in mitochondrial fusion (Yasukawa et al., 2009). In accordance with this report, we also observed that overexpressed MFN2 dampened the generation of IFN-β following viral infection and increased H1N1 replication. The expression of MFN2 was considerably increased under restraint stress and corticosterone load, which was reduced by epigoitrin to improve the activation of MAVS antiviral signaling. These data indicated that epigoitrin could improve the suppression of innate immunity by restraint stress via downregulating MFN2 expression (**Figure 7**). Nevertheless, we do not know the underlying mechanism, further studies are required to investigate it.

In summary, our results demonstrated that epigoitrin reduced the susceptibility to H1N1 virus and the production of pro-inflammatory cytokines to alleviate pneumonia in restraint-stressed mice. Based on both the restraint-stressed mice model and corticosterone-loaded A549 cell model, epigoitrin was found to maintain MAVS antiviral signaling following H1N1 infection to ensure IFN-β production.

AUTHOR CONTRIBUTIONS

R-RH and Y-FL developed the study design and revised the manuscript. ZL participated in the study design, performed the experiments, analyzed the data, and wrote the manuscript. L-FL, X-HW, CJ, HC, D-HL, C-YY performed the experiments and analyzed the data. BL, F-QW, and HK participated in the study design and analyzed the data. All authors have read and approved the final version of the manuscript.

FUNDING

This work was supported, in part, by the National Natural Science Foundation of China (Grant Numbers 81622050,

81673709, 81560661, 81573675 and 81873209), the Young Top-notch Talent Support Program of Guangdong Province (Grant Numbers 2014TQ01R229 and 2016TQ03R586), the Science and Technology Program of Guangzhou (Grant Numbers 201604046016 and 201610010182), Guangdong Science and Technology Foundation for Distinguished Young Scholars (2017A030306004), and the National Key Research and Development Program of China (2017YFC1700404).

REFERENCES

Arimori, Y., Nakamura, R., Yamada, H., Shibata, K., Maeda, N., Kase, T., et al. (2013). Type I interferon limits influenza virus-induced acute lung injury by regulation of excessive inflammation in mice. *Antiviral Res.* 99, 230–237. doi: 10.1016/j.antiviral.2013.05.007

Chen, H., Jie, C., Tang, L. P., Meng, H., Li, X. B., Li, Y. B., et al. (2017). New insights into the effects and mechanism of a classic traditional chinese medicinal formula on influenza prevention. *Phytomedicine* 27, 52–62. doi: 10.1016/j.phymed.2017.02.004

Chen, X., Liu, S., Goraya, M. U., Maarouf, M., Huang, S., and Chen, J. L. (2018). Host immune response to influenza a virus infection. *Front. Immunol.* 9:320. doi: 10.3389/fimmu.2018.00320

Chrousos, G. P. (2009). Stress and disorders of the stress system. *Nat. Rev. Endocrinol.* 5, 374–381. doi: 10.1038/nrendo.2009.106

Fang, M., Wan, M., Guo, S., Sun, R., Yang, M., Zhao, T., et al. (2011). An oligodeoxynucleotide capable of lessening acute lung inflammatory injury in mice infected by influenza virus. *Biochem. Biophys. Res. Commun.* 415, 342–347. doi: 10.1016/j.bbrc.2011.10.062

Glaser, R., and Kiecolt-Glaser, J. K. (2005). Stress-induced immune dysfunction: implications for health. *Nat. Rev. Immunol.* 5, 243–251. doi: 10.1038/nri1571

He, R. R., Wang, M., Wang, C. Z., Chen, B. T., Lu, C. N., Yao, X. S., et al. (2011). Protective effect of apple polyphenols against stress-provoked influenza viral infection in restraint mice. *J. Agric. Food Chem.* 59, 3730–3737. doi: 10.1021/jf104982y

Iwasaki, A., and Pillai, P. S. (2014). Innate immunity to influenza virus infection. *Nat. Rev. Immunol.* 14, 315–328. doi: 10.1038/nri3665

Konstantinos, A. P., and Sheridan, J. F. (2001). Stress and influenza viral infection: modulation of proinflammatory cytokine responses in the lung. *Respir. Physiol.* 128, 71–77. doi: 10.1016/S0034-5687(01)00266-3

Kumar, B., Asha, K., Khanna, M., Ronsard, L., Meseko, C. A., and Sanicas, M. (2018). The emerging influenza virus threat: status and new prospects for its therapy and control. *Arch. Virol.* 163, 831–844. doi: 10.1007/s00705-018-3708-y

McNab, F., Mayer-Barber, K., Sher, A., Wack, A., and O'Garra, A. (2015). Type I interferons in infectious disease. *Nat. Rev. Immunol.* 15, 87–103. doi: 10.1038/nri3787

National Pharmacopoeia Commission. (2015). *Chinese Pharmacopoeia*. Beijing: China Medical Science and Technology Press.

Smeenk, C. A., and Brown, E. G. (1994). The influenza virus variant A/FM/1/47-MA possesses single amino acid replacements in the hemagglutinin, controlling virulence, and in the matrix protein, controlling virulence as well as growth. *J. Virol.* 68, 530–534.

Tang, L. P., Mao, Z. F., Li, X. X., Chen, M., Li, S. B., Tsoi, B., et al. (2014). ReDuNing, a patented Chinese medicine, reduces the susceptibility to H1N1 influenza of mice loaded with restraint stress. *Eur. J. Integr. Med.* 6, 637–645. doi: 10.1016/j.eujim.2014.07.018

West, A. P., Shadel, G. S., and Ghosh, S. (2011). Mitochondria in innate immune responses. *Nat. Rev. Immunol.* 11, 389–402. doi: 10.1038/nri2975

Xiao, P., Huang, H. Z., Chen, J., and Li, X. (2014). Radix Isatidis extract and bioaccessibility of six bioactive compounds after simulated gastro-intestinal digestion. *J. Ethnopharmacol.* 157, 55-61. doi: 10.1016/j.jep.2014.09.005

Xiao, P., Ye, W., Chen, J., and Li, X. (2016). Antiviral activities against influenza virus (FM1) of bioactive fractions and representative compounds extracted from banlangen (*Radix isatidis*). *J. Tradit. Chin. Med.* 36, 369–376. doi: 10.1016/S0254-6272(16)30051-6

Yasukawa, K., Oshiumi, H., Takeda, M., Ishihara, N., Yanagi, Y., Seya, T., et al. (2009). Mitofusin 2 inhibits mitochondrial antiviral signaling. *Sci. Signal.* 2:ra47. doi: 10.1126/scisignal.2000287

Zhou, W., and Zhang, X. (2013). Research progress of chinese herbal medicine *Radix isatidis* (banlangen). *Am. J. Chin. Med.* 41, 743–764. doi: 10.1142/S0192415X1350050X

Conflict of Interest Statement: The authors declare that the research was conducted in the absence of any commercial or financial relationships that could be construed as a potential conflict of interest.

frontiers in Pharmacology

REVIEW
published: 13 February 2019
doi: 10.3389/fphar.2019.00111

The New Paradigms in Clinical Research: From Early Access Programs to the Novel Therapeutic Approaches for Unmet Medical Needs

Cristina Scavone†, Gabriella di Mauro†, Annamaria Mascolo, Liberato Berrino, Francesco Rossi‡ and Annalisa Capuano‡*

Campania Regional Centre for Pharmacovigilance and Pharmacoepidemiology, Department of Experimental Medicine, Section of Pharmacology "L. Donatelli", University of Campania "Luigi Vanvitelli", Naples, Italy

OPEN ACCESS

Edited by:
Ioanna Andreadou, National and Kapodistrian University of Athens, Greece

Reviewed by:
Emilio Russo, Università degli Studi Magna Græcia di Catanzaro, Italy
Tero Aittokallio, Institute for Molecular Medicine Finland, Finland

***Correspondence:**
Annalisa Capuano
annalisa.capuano@unicampania.it

† These authors have contributed equally to this work
‡ These authors are both lead authors

Specialty section:
This article was submitted to Experimental Pharmacology and Drug Discovery, a section of the journal Frontiers in Pharmacology

Received: *07 December 2018*
Accepted: *28 January 2019*
Published: *13 February 2019*

Citation:
Scavone C, di Mauro G, Mascolo A, Berrino L, Rossi F and Capuano A (2019) The New Paradigms in Clinical Research: From Early Access Programs to the Novel Therapeutic Approaches for Unmet Medical Needs. Front. Pharmacol. 10:111. doi: 10.3389/fphar.2019.00111

Despite several innovative medicines gaining worldwide approval in recent years, there are still therapeutic areas for which unsatisfied therapeutic needs persist. For example, high unmet clinical need was observed in patients diagnosed with type 2 diabetes mellitus and hemophilia, as well as in specific age groups, such as the pediatric population. Given the urgent need to improve the therapy of clinical conditions for which unmet clinical need is established, clinical testing, and approval of new medicines are increasingly being carried out through accelerated authorization procedures. Starting from 1992, the Food and Drug Administration and the European Medicines Agency have supported the so-called Early Access Programs (EAPs). Such procedures, which can be based on incomplete clinical data, allow an accelerated marketing authorization for innovative medicines. The growth in pharmaceutical research has also resulted in the development of novel therapeutic approaches, such as biotech drugs and advanced therapy medicinal products, including new monoclonal antibodies for the treatment of asthma, antisense oligonucleotides for the treatment of Duchenne muscular dystrophy and spinal muscular atrophy, and new anticancer drugs that act on genetic biomarkers rather than any specific type of cancer. Even though EAPs and novel therapeutic approaches have brought huge benefits for public health, their implementation is limited by several challenges, including the high risk of safety-related label changes for medicines authorized through the accelerated procedure, the high costs, and the reimbursement and access concerns. In this context, regulatory agencies should provide the best conditions for the implementation of the described new tools.

Keywords: clinical research, early access programs, novel therapeutic approaches, unmet medical needs, challenges

INTRODUCTION

The development of a new medicine is a long, expensive and risky process. The entire time that passes from the R&D phase until the drug's marketing approval can last up to 15 years, and it is characterized by extremely high costs, usually exceeding $1.2 billion (Saadi and White, 2014). At the initial phase, before clinical trials can be carried out in humans, preclinical studies on animals, which are mainly aimed to characterize the mechanisms of action, the toxicity, the dosage or route of administration of the new medicine, are provided (Andrade et al., 2016). Based on the positive results of preclinical research, the new drug can be evaluated in humans during the four main phases of the clinical development. In particular, phase I–III studies are those that evaluate the efficacy and safety profile of the new drug in humans until the marketing authorization. Differently from phase I studies, which involve healthy patients and whose study design is relatively simple, phase II and III studies enroll patients affected by the disease for which the new drug is indicated, and are characterized by a more structured study design, which is usually randomized and controlled (randomized controlled trials, or RCTs). Once the new medicine is authorized, based on data demonstrating the positive benefit/risk profile, the real-world effectiveness and safety of the drug is assessed during phase IV studies (Auricchio et al., 2017; Mascolo et al., 2017). In this last phase, pharmacovigilance is included. Therefore, the "clinical value" of a new drug is observed during a rigorous clinical program, in which it is compared with the best available treatments, if they exist (Morgan et al., 2008). Apart from the traditional design of RCT, in recent years further study designs, including umbrella, basket and platform trials, were developed and applied to new therapies, especially in the area of oncology research (Simon, 2017). The reason for the introduction of these new study designs lies in the discovery of cancer genomic features and consequently in the development of target therapies able to recognize specific oncogenes.

Despite RCTs representing the highest level of the evidence-based medicine pyramid, they suffer from several limitations in predicting effectiveness, which mainly include the limited duration, the highly controlled setting, and the exclusion of frail populations, including children, the elderly, pregnant women, as well as patients affected by multiple diseases and those receiving concomitant medications (Wang et al., 2018). Furthermore, during the premarketing phase, the efficacy and safety data are frequently evaluated using a non-inferiority or equivalence study design and surrogate outcomes. Considering these limitations, the real value of a new drug can be confirmed only when it will be used in real life conditions (Oyinlola et al., 2016).

UNMET CLINICAL NEEDS AND EARLY ACCESS PROGRAMS

Generally, the main objective of the development of a new medicine is to respond to an unmet medical need (Kaplan et al., 2013; U.S. Department of Health and Human Services, 2014). Indeed, when a new medicine obtains the marketing authorization, the respective regulatory agency performs a global evaluation of the clinical benefit associated to the new drug as well as an evaluation of the therapeutic need. This latter action is carried out through the analysis of the global burden of the disease for which the new drug is indicated and the prediction of the trend of the disease's burden. Both evaluations are based on epidemiological and demographic data. Those assessments include the evaluation of the Disability-Adjusted Life Year (DALYs), which is a measure of mortality and disability associated with a clinical condition, and the efficacy and safety profiles of medicines already available for treating that disease. In addition, unmet clinical need is further demonstrated when the new drug has significant effects on serious outcomes, if it demonstrates efficacy in patients who do not tolerate or do not respond to the available drug therapies, and better safety/compliance/drug-drug interactions profiles (Ujeyl et al., 2012). Although several innovative therapies were recently approved worldwide, there are still therapeutic areas for which unsatisfied therapeutic needs persist (**Figure 1**). Indeed, the so-called "white spots" – clinical conditions for which no efficacious treatments are approved – still exist among pharmaceutical pipelines (Papaluca et al., 2015). For example, a high unmet clinical need was observed in patients diagnosed with type 2 diabetes mellitus (T2DM), which represents an increasing health concern worldwide and is a leading risk factor for cardiovascular diseases. Bennett et al. (2014) evaluated outcomes in T2DM patients in United Kingdom general practice and described the unmet clinical need in T2DM as the failure to meet targets for blood pressure, total cholesterol, or glycated hemoglobin levels. The authors suggested that conventional therapies for T2DM are not able to manage all the clinical aspects of this condition; thus, there is a need for new therapeutic agents in order to alleviate the health and economic burden associated with T2DM (Bennett et al., 2014). Unmet needs were identified also in the management of hemophilia. Indeed, even though several improvements were made in this field, the development of inhibitors, namely the immune response that occurs in patients treated with clotting factor concentrates, negatively affects treatment (Dargaud et al., 2016). A high rate of unmet clinical needs is also found in specific age groups, such as the pediatric population. For these patients, the lack of data from the premarketing development, including the lack of age-specific dose and long-term efficacy and safety data, has significant impact on pharmacological treatments. This is particularly true in the case of psychiatric disorders, which still represent a challenge in children and adolescents (Pozzi et al., 2018; Rafaniello et al., 2018). Indeed, drugs indicated for these conditions are frequently used as off-label in children, based on data from RCTs that have involved only adult patients (Capuano et al., 2014; Persico et al., 2015; Rafaniello et al., 2016). Similarly, the therapeutic area of respiratory diseases, such as asthma, still represents a concern for children. Once again, this is mainly related to the lack of clinical efficacy and safety evidence, but also to the limited availability of non-steroid-based alternative therapies for children < 6 years of age (Lindly et al., 2016).

Given the urgent need to improve the therapeutic armamentarium of particular clinical conditions for which

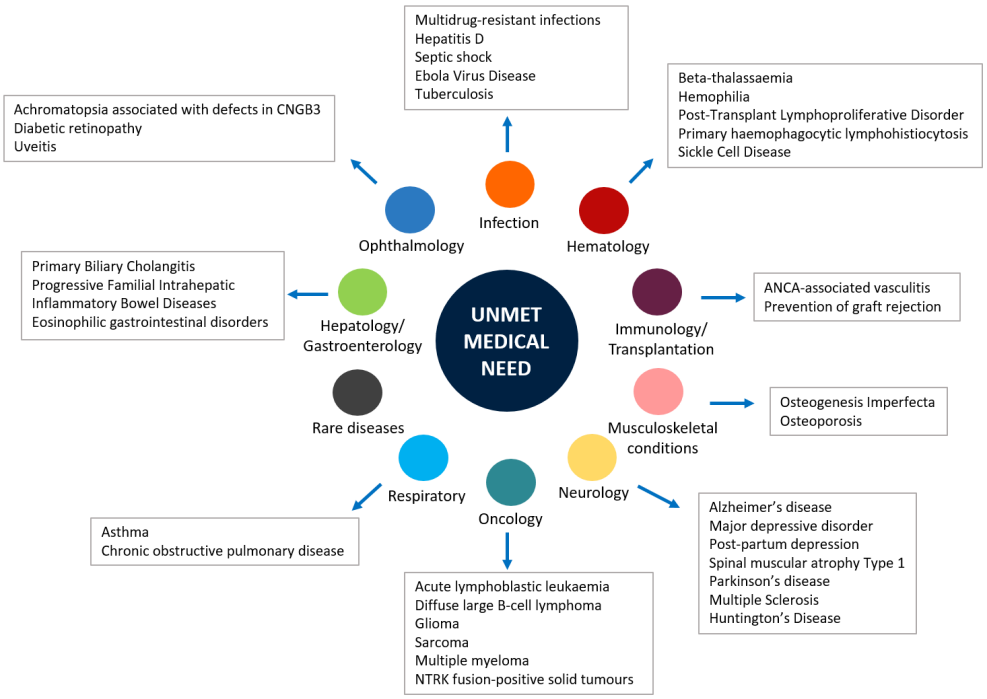

FIGURE 1 | Main unmet medical needs in therapeutic areas.

unmet clinical need is confirmed, clinical testing and approval of new medicines are increasingly carried out through accelerated authorization procedures. As a matter of fact, both the Food and Drug Administration (FDA) and the European Medicines Agency (EMA) have supported the so-called "Early Access Programs" (EAPs). Since 1992, the FDA has introduced the "Priority Review" or "Fast Track," designed to make available new drugs for the treatment of serious or life-threatening diseases (conditions associated with morbidity that have significant impact on specific factors, such as survival or day-to-day functioning) without therapeutic alternatives. For these drugs the "breakthrough designation" can be expected. The FDA's "Fast track" imposes on the pharmaceutical company lower standards than the regular procedure (U.S. Department of Health and Human Services, 2014). Similarly, in the European context, specific regulatory procedures, including approval under exceptional circumstances as well as conditional and accelerated approval, have been introduced in order to accelerate the marketing authorization of a new drug. With such procedures, the marketing authorization application should be based on incomplete clinical data (even data from phase II studies), and its evaluation can be reduced from 210 to 150 days if the applicant provides sufficient justification for an accelerated assessment (**Figure 2**; European Medicines Agency, 2018). Furthermore, the EMA has recently introduced new tools to support the EAPs, Adaptive Licensing and PRIority Medicines (PRIME). The first one is a prospective authorization process that allows an initial approval based on limited scientific evidence only for a small group of patients. When further evidence is collected, the drug's access can be expanded to larger patients' populations (Vella Bonanno et al., 2017). In 2016, EMA implemented the PRIME scheme, which offers early and enhanced dialog between the EMA and the pharmaceutical industry in order to enhance development plans and speed up the evaluation process (European Medicines Agency, 2017). In **Table 1**, a few examples of medicines evaluated within the PRIME scheme are reported.

NOVEL THERAPEUTIC APPROACHES

Whilst regulatory agencies have promoted EAPs, which have increased over time during the past 25 years (Beaver et al., 2018), the growth in pharmaceutical research has resulted in the discovery and development of novel therapeutic approaches, mainly represented by biotech drugs and gene-, cell- and tissue-therapies. Starting from the marketing approval of the first monoclonal antibody in 1986, the entire class of biotech drugs has grown significantly. In 2013, the global sales revenue for all mAbs was almost $75 billion, representing half of the total sales of all biopharmaceutical products (Ecker et al., 2015). Most of these novel therapeutic approaches are indicated for the management of different diseases with recognized unmet medical needs. For example, until recently the pharmaceutical armamentarium of asthma included muscarinic antagonists, beta2-agonists and corticosteroids, but approximately half of patients do not adequately respond to the available therapies. For this condition, four monoclonal antibodies (mAbs) recently

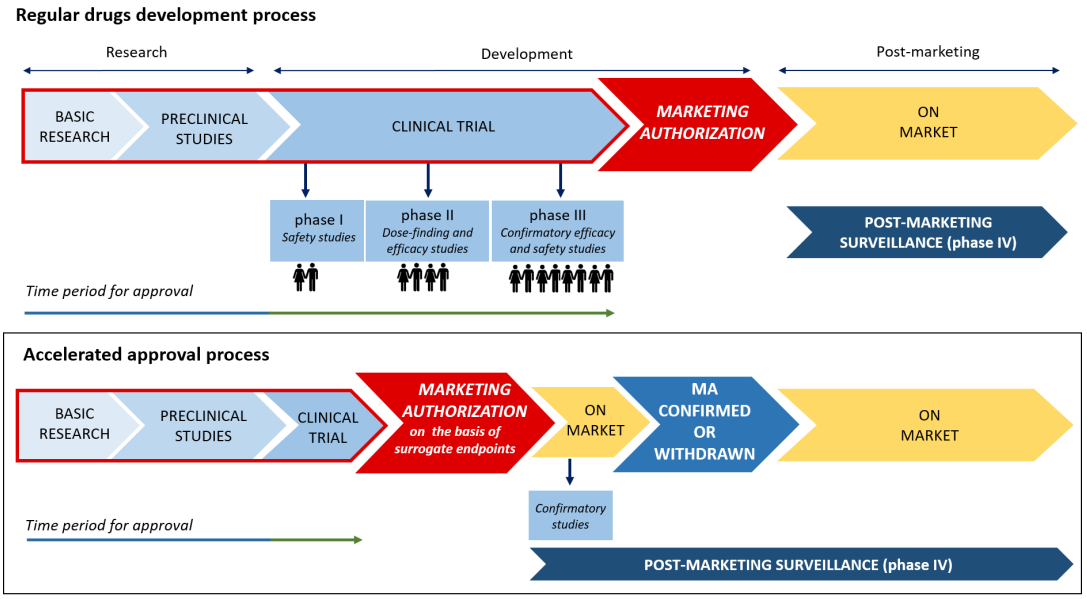

FIGURE 2 | Traditional vs. accelerated development and approval process.

obtained the marketing authorization (Bateman et al., 2008; Swedin et al., 2017). Omalizumab is a recombinant humanized mAb that binds to the F_C portion of the IgE antibody, preventing the binding of IgE to high-affinity IgE receptors on mast cells and basophils and the release of inflammatory mediators induced by allergen exposure (Thomson and Chaudhuri, 2012; Sattler et al., 2017). Mepolizumab, benralizumab, and reslizumab are anti-IL-5 mAbs that bind IL-5Rα, causing apoptosis of eosinophils and basophils through the antibody-dependent cellular cytotoxicity (Farne et al., 2017; Chung, 2018). Currently, these mAbs are indicated as add-on treatment in adults, adolescents and children aged ≥6 years with severe persistent allergic (omalizumab) and refractory eosinophilic (mepolizumab, benralizumab, and reslizumab) asthma inadequately controlled with other available treatments.

Among novel therapeutic approaches, Advanced Therapy Medicinal Products (ATMPs), including cell-, gene-, and tissue-engineered therapies, are particularly noteworthy, especially in the field of neurodegenerative and neuromuscular diseases, for which effective treatments have been limited. The antisense oligonucleotides (ASOs) are synthetic single-stranded strings of nucleic acids, which selectively bind to specific pre-messenger ribonucleic acid (pre-mRNA)/mRNA sequences leading to an alteration of the synthesis of proteins. The FDA approved in 2016 two ASOs for the treatment of Duchenne muscular dystrophy and spinal muscular atrophy. Their role was envisaged also in further clinical conditions, such as Huntington's disease, amyotrophic lateral sclerosis and Alzheimer's disease (Wurster and Ludolph, 2018). It should be highlighted that in most cases ATMPs are indicated for the treatment of very rare conditions but, unlike traditional drugs that are administered with a certain frequency, they require administration only once, which is then able to provide for years or for the entire life the biological activity and clinical benefit. This is the case, for example, with axicabtagene ciloleucel, also known as CAR-T therapy, which is indicated for the treatment of diffuse large B-cell lymphoma.

Lastly, a new generation of anticancer drugs is going to be developed. Recently, Drilon et al. (2018) have performed a phase I/II trial, using a basket design, in order to evaluate the safety and efficacy of larotrectinib, a selective inhibitor of TRK proteins, in 55 patients with NTRK genetic alterations regardless of tumor types (Ghosh and Tabrizi, 2017). According to its peculiar pharmacodynamic features, larotrectinib acts on genetic biomarkers rather than any specific type of cancer. On the basis of the efficacy and safety data of this cutting-edge cancer therapy, in November 2018 the FDA granted Priority Review for larotrectinib for the treatment of adult and pediatric patients with locally advanced or metastatic solid tumors harboring an NTRK gene fusion (Drilon et al., 2018). Furthermore, in cancer settings as well as in other therapeutics areas, new drug-drug and drug-antibody combinations are increasingly emerging as therapeutic approaches to fulfill several unmet needs. For example, in the treatment of hemophilia the conjugation of immunogenic peptides to a non-immunogenic protein carrier, such as in the case of the recombinant FVIII–Fc fusion protein, decreases the immunogenicity of FVIII, leading to better clinical outcomes. Similarly, in the treatment of leukemia, the conjugation of PEG to the native asparaginase enzyme leads to fewer allergic reactions than asparaginase enzyme alone (U.S. Food and Drug Administration, 2018). New antibody-drug conjugates (ADCs), mainly indicated for the treatment of hematological and solid malignancies, are currently in the late stage of clinical development but are already showing promising results (Lieuw, 2017). Furthermore, the combination therapy of multiple drugs turned out to be useful also in the treatment of T2DM or hypertension, leading to better glycemic, and blood pressure

TABLE 1 | Medicines evaluated in PRIME scheme.

Medicine	Therapeutic indications	Reason for disease's unmet medical need
Avacopan	AAV	Rare disease
Axicabtagene ciloleucel (CAR-T)	DLBCL	Rare disease
Emapalumab	HLH	Rare disease
Onasemnogene abeparvovec	SMA Type 1 in pediatric patients	Rare disease
Tisagenlecleucel	R/R ALL	Less than 10% of patients achieve 5-year overall survival. Moreover, the R/R ALL is associated with high relapse rates (Papadantonakis and Advani, 2016)
Aducanumab	Alzheimer's disease	Current drugs improve symptoms, but do not have profound disease-modifying effects (Citron, 2010)
Asunercept	Glioblastoma	Rare disease
Brexanolone (Allopregnanolone, SAGE-547)	PPD	There is a need for new treatment options for mothers suffering from the disorder (Kanes et al., 2017)
Chimeric 2'-O-(2-methoxyethyl) modified oligonucleotide targeted to huntingtin RNA (RO7234292)	Huntington's Disease	Rare disease
Deoxycytidine / deoxythymidine	TK2	Rare disease
Givosiran	Prevention of acute attacks of hepatic porphyria	Rare disease
Lumasiran	PH1	Rare disease
MV-CHIK vaccine	Prevention of Chikungunya fever	Rare disease
Mycobacterium tuberculosis (MTBVAC)	TB Vaccine	Immune responses of human newborns and infants are distinct and cannot be predicted from those of human adults or animal models (Sanchez-Schmitz and Levy, 2011)
Olipudase alfa	Non-neurological manifestations of acid sphingomyelinase deficiency	Rare disease
Polatuzumab vedotin	R/R DLBCL	Rare disease
Rapastinel	Adjunctive treatment of MDD	Many patients with MDD fail to achieve a complete response with antidepressant medications and experience periods with residual symptom burdens (Rush et al., 2006)
Recombinant Vesicular Stomatitis Virus with Envelope Glycoprotein replaced by Zaire ebolavirus (Kikwit Strain) Glycoprotein	Vaccination against Ebola	Many survivors and their relatives continue to experience stigma and social isolation. Moreover, patients have health, psychological, and social needs (Calnan et al., 2017)
Seladelpar (MBX-8025)	Primary Biliary Cholangitis	Rare disease
Setmelanotide	Obesity and control of the hunger associated with deficiency disorders of the MC4R receptor pathway	Rare Genetic Disorders
Setrusumab	OI types I, III, and IV	Rare disease
Tasadenoturev	Recurrent glioblastoma	Rare disease
Vocimagene amiretrorepvec	Treatment of high-grade glioma	Rare disease
Voxelotor	SCD	Many patients experience poor clinical outcomes in short and longer term (Sarri et al., 2018)

AAV, active ANCA-associated vasculitis (including granulomatosis with polyangiitis and microscopic polyangiitis); DLBCL, large B-cell lymphoma; HLH, primary hemophagocytic lymphohistiocytosis, SMA: spinal muscular atrophy; R/R ALL, relapsed or refractory B cell acute lymphoblastic leukemia; PPD, Postpartum depression; TK2, Thymidine Kinase 2 Deficiency; PH1, Primary Hyperoxaluria Type 1; TB Vaccine, Active immunization against tuberculosis disease; R/R DLBCL, relapsed and refractory patients with diffuse large B cell lymphoma; MDD, major depressive disorder; OI, Osteogenesis Imperfecta; SCD, Sickle Cell Disease.

control. Despite these advantages, it should be stressed that the combination therapy of multiple drugs might increase treatment complexity and adverse events that affect long-term adherence (Mittermayer et al., 2015; Parslow et al., 2016). For these new drug-drug and drug-antibody combinations, a regular approval procedure is required, unless conditions for accelerated approval (confirmation of unmet need) exist. This is currently true also for new combination therapies, such as the polypill indicated for the treatment of hypertension or ADCs used in cancer settings; therefore, even though the individual drugs are already authorized, new approval is required. The novel therapeutic approaches do not necessarily refer solely to new medicines but also to already-existing ones that are used for different indications. This is the case, for example, with exenatide, a glucagon-like peptide-1 receptor agonist used for the treatment of T2DM, whose role is currently being evaluated for the treatment of Parkinson's disease (PD). Although available medications for PD have strong therapeutic effects, they are not able to stop the progression of the disease. Exenatide has demonstrated a neuroprotective effect in preclinical models of PD. In a clinical study that enrolled 62 patients with moderate PD, conflicting results were obtained (Cimmaruta et al., 2018). New drugs, including

those based on pluripotent stem cell therapy, are currently evaluated in clinical programs for the management of PD. Recent literature indicates that stem cells might represent a potential approach for developing novel treatment strategies for PD in humans (Athauda et al., 2017; Yasuhara et al., 2017).

THE CHALLENGES OF NEW PARADIGMS IN CLINICAL RESEARCH

Even though the new tools of clinical research and the discovery of novel therapeutic approaches have brought huge novelties and benefits, their implementation is limited by several challenges. First, EAPs should be applied only in fully justified circumstances in order to ensure the patient's safety. Furthermore, since the majority of EAPs are based on surrogate endpoints, the use of the new medicine in real life conditions must prove that it is able to improve the patient's health status and quality of life (patient-relevant endpoint), demonstrating significant benefit and a good safety profile. However, the interpretation of efficacy and safety data from clinical studies, especially when they are not complete, is extremely critical. Indeed, several medicines that underwent fast-track procedures by the FDA were withdrawn for safety reasons; this was the case with valdecoxib and rofecoxib, which were withdrawn due to an increased risk of cardiovascular events, and cerivastatin, which was associated with an increased risk of hepatic adverse events (Zhang et al., 2018). Similarly, the results of a recent study by Mostaghim et al. (2017) revealed that accelerated pathway drugs are associated to higher risks of safety-related label changes, including changes to boxed warnings and contraindications, compared with non-accelerated pathway drugs (Chary, 2016).

Another peculiar aspect of recently authorized therapies is their extremely high costs. As previously reported, except for rare cases, the novel therapeutic approaches are mainly represented by biological products and advanced therapies (Mostaghim et al., 2017). Those substances are characterized by highly complex development procedures as well as by large-scale molecules with huge heterogeneity (Abou-El-Enein et al., 2016; Scavone et al., 2017a,b). Given these intrinsic characteristics and considering the difficulties in their development, those medicines are defined by higher costs compared to traditional ones. For example, the new monoclonal antibodies targeting the PCSK9 had an average cost that exceed 8,000€/patient/year, while statins cost almost 50€/patient/year (Agenzia Italiana Del Farmaco, 2017; Scavone et al., 2017c). Understandably, the investment made in R&D should be at least partially reclaimed. In order to overcome issues related to the high costs of innovative medicines, each EU member state has implemented regulatory tools for reimbursement of medicinal products, the so-called Managed Entry Agreements (MEAs). These contracts, which are stipulated between the pharmaceutical industry and the payers/regulatory agencies, allow conditional access to the market for new drugs with unclear efficacy and safety profiles. Therefore, their objective is to improve access to new medicines in the context of uncertainty and high price. The use of MEAs has been implemented in several countries, including the United Kingdom (where MEAs are defined as "patient access schemes"), Italy, Belgium, and Australia. For example, in Italy the modulation of price and reimbursement schemes are planned by using two categories of MEAs, which include the health outcomes-based agreements (payment by result, risk sharing, and success fee) and the finance-based agreements (cost-sharing agreements and capping) (Mallya et al., 2017; Scavone et al., 2018).

Lastly, apart from the cost and safety concerns of new medicines approved through EAPs, a further challenge is represented by the lack of knowledge and infrastructure necessary for the storage, distribution and administration of the new therapeutics; this is true especially for the advanced therapy medicinal products (cell-, gene-, and tissue-engineered therapies) (Ferrario et al., 2017).

CONCLUSION

Despite the progress made in the field of clinical research, unmet therapeutic needs are still identified in several clinical areas (Miller, 2009; Taiwo et al., 2010; Aceves, 2014; Markowitz, 2015; Morrow et al., 2017). It is notable, for instance, that multidrug-resistant infections are rapidly increasing worldwide, but very few antibiotics able to treat these infections are currently under development. Therefore, this research area should be prioritized in the pharmaceutical industries' pipeline.

Recent developments in clinical research have also placed a series of challenges for regulatory agencies, which are required to create the best conditions for the implementation of the described new tools. Although the application of EAPs improves the patient's access to new medicines, obtaining new data on their real effectiveness and safety might be a concern. In this context, at least for EU countries, it is expected that the forthcoming application of Regulation No. 536/2014 on clinical trials will facilitate the conduct of clinical trials also in real-life conditions. Indeed, the active participation of patient organizations in clinical research will lead to better study designs, but also to improved reliability of study results and better applicability to patients in the real world. This will lead to increased knowledge of the effectiveness and safety profile of drugs also approved through EAPs. Furthermore, since Regulation No. 536/2014 introduces an authorization procedure based on a single submission via a single EU portal, clinical trial data on effectiveness and safety will be easily accessible. A further step for the better collection of clinical data would be the implementation of a health database and registries, whose potential are undisputed.

Finally, regarding the high costs characterizing new therapeutic approaches, it is advisable that price and reimbursement tools (i.e., MEAs), such as those used in several EU and non-EU countries, may also be applied in other countries. This will lead to an increased access to innovative therapies. Lastly, in order to further implement clinical research, especially in the field of ATMPs, a strengthening in research infrastructures and research training is what is required.

AUTHOR CONTRIBUTIONS

CS, GdM, AM, LB, FR, and AC drafted the work and revised it for important intellectual content, made substantial contributions to the acquisition, analysis, or interpretation of data for the work, wrote the manuscript, approved the final version of the manuscript to be published, and agreed to be accountable for all aspects of the work in ensuring that questions related to the accuracy or integrity of any part of the work are appropriately investigated and resolved. FR and AC developed the concept.

REFERENCES

Abou-El-Enein, M., Elsanhoury, A., and Reinke, P. (2016). Overcoming challenges facing advanced therapies in the EU market. *Cell Stem Cell* 19, 293–307. doi: 10.1016/j.stem.2016.08.012

Aceves, S. S. (2014). Unmet therapeutic needs in eosinophilic esophagitis. *Dig. Dis.* 32, 143–148. doi: 10.1159/000357131

Agenzia Italiana Del Farmaco. (2017). *Determina 16 Febbraio*. Available at: http://www.gazzettaufficiale.it/eli/id/2017/03/06/17A01583/sg%3Bjsessionid%3Dokjg9kmvS670yhHglsK8Lw__.ntc-as3-guri2a

Andrade, E. L., Bento, A. F., Cavalli, J., Oliveira, S. K., Freitas, C. S., Marcon, R., et al. (2016). Non-clinical studies required for new drug development - Part I: early in silico and in vitro studies, new target discovery and validation, proof of principles and robustness of animal studies. *Braz. J. Med. Biol. Res.* 49:e5644. doi: 10.1590/1414-431X20165644

Athauda, D., Maclagan, K., Skene, S. S., Bajwa-Joseph, M., Letchford, D., Chowdhury, K., et al. (2017). Exenatide once weekly versus placebo in parkinson's disease: a randomised, double-blind, placebo-controlled trial. *Lancet* 390, 1664–1675. doi: 10.1016/S0140-6736(17)31585-4

Auricchio, F., Scavone, C., Cimmaruta, D., Di Mauro, G., Capuano, A., Sportiello, L., et al. (2017). Drugs approved for the treatment of multiple sclerosis: review of their safety profile. *Expert Opin. Drug Saf.* 16, 1359–1371. doi: 10.1080/14740338.2017.1388371

Bateman, E. D., Hurd, S. S., Barnes, P. J., Bousquet, J., Drazen, J. M., FitzGerald, J. M., et al. (2008). Global strategy for asthma management and prevention: GINA executive summary. *Eur. Respir. J.* 31, 143–178. doi: 10.1183/13993003.51387-2007

Beaver, J. A., Howie, L. J., Pelosof, L., Kim, T., Liu, J., Goldberg, K. B., et al. (2018). A 25-year experience of us food and drug administration accelerated approval of malignant hematology and oncology drugs and biologics: a review. *JAMA Oncol.* 4, 849–856. doi: 10.1001/jamaoncol.2017.5618

Bennett, H., McEwan, P., Bergenheim, K., and Gordon, J. (2014). Assessment of unmet clinical need in type 2 diabetic patients on conventional therapy in the UK. *Diabetes Ther.* 5, 567–578. doi: 10.1007/s13300-014-0079-6

Calnan, M., Gadsby, E. W., Kondé, M. K., Diallo, A., and Rossman, J. S. (2017). The response to and impact of the ebola epidemic: towards an agenda for interdisciplinary research. *Int. J. Health Policy Manag.* 7, 402–411. doi: 10.15171/ijhpm.2017.104

Capuano, A., Scavone, C., Rafaniello, C., Arcieri, R., Rossi, F., and Panei, P. (2014). Atomoxetine in the treatment of attention deficit hyperactivity disorder and suicidal ideation. *Expert Opin. Drug Saf.* 13(Suppl. 1), S69–S78. doi: 10.1517/14740338.2014.941804

Chary, K. V. (2016). Expedited drug review process: fast, but flawed. *J. Pharmacol. Pharmacother.* 7, 57–61. doi: 10.4103/0976-500X.184768

Chung, K. F. (2018). Tralokinumab unsuccessful for management of severe, uncontrolled asthma. *Lancet Respir. Med.* 6, 480–481. doi: 10.1016/S2213-2600(18)30194-2

Cimmaruta, D., Lombardi, N., Borghi, C., Rosano, G., Rossi, F., and Mugelli, A. (2018). Polypill hypertension and medication adherence: the solution strategy? *Int. J. Cardiol.* 252, 181–186. doi: 10.1016/j.ijcard.2017.11.075

Citron, M. (2010). Alzheimer's disease: strategies for disease modification. *Nat. Rev. Drug Discov.* 9, 387–398. doi: 10.1038/nrd2896

Dargaud, Y., Pavlova, A., Lacroix-Desmazes, S., Fischer, K., Soucie, M., Claeyssens, S., et al. (2016). Achievements, challenges and unmet needs for haemophilia patients with inhibitors: report from a symposium in paris, france on 20 november 2014. *Haemophilia* 1(Suppl. 1), 1–24. doi: 10.1111/hae.12860

Drilon, A., Laetsch, T. W., Kummar, S., DuBois, S. G., Lassen, U. N., Demetri, G. D., et al. (2018). Efficacy of larotrectinib in TRK fusion-positive cancers in adults and children. *N. Engl. J. Med.* 378, 731–739. doi: 10.1056/NEJMoa1714448

Ecker, D. M., Jones, S. D., and Levine, H. L. (2015). The therapeutic monoclonal antibody market. *MAbs* 7, 9–14. doi: 10.4161/19420862.2015.989042

European Medicines Agency. (2017). *Prime Priority Medicines*. Available at: http://www.ema.europa.eu/ema/index.jsp?curl=pages/regulation/general/general_content_000660.jsp

European Medicines Agency. (2018). *Accelerated Assessment*. Available at: https://www.ema.europa.eu/en/human-regulatory/marketing-authorisation/accelerated-assessment

Farne, H. A., Wilson, A., Powell, C., Bax, L., and Milan, S. J. (2017). Anti-IL5 therapies for asthma. *Cochrane Database Syst. Rev.* 21:CD010834. doi: 10.1002/14651858.CD010834.pub3

Ferrario, A., Arâja, D., Bochenek, T., Èatiæ, T., Dankó, D., Dimitrova, M., et al. (2017). The implementation of managed entry agreements in central and eastern europe: findings and implications. *Pharmacoeconomics.* 35, 1271–1285. doi: 10.1007/s40273-017-0559-4

Ghosh, R., and Tabrizi, S. J. (2017). Gene suppression approaches to neurodegeneration. *Alzheimers Res. Ther.* 9:82. doi: 10.1186/s13195-017-0307-1

Kanes, S., Colquhoun, H., Gunduz-Bruce, H., Raines, S., Arnold, R., Schacterle, A., et al. (2017). Brexanolone (SAGE-547 injection) in post-partum depression: a randomised controlled trial. *Lancet* 390, 480–489. doi: 10.1016/S0140-6736(17)31264-3

Kaplan, W., Wirtz, V. J., Mantel-Teeuwisse, A., Stolk, P., Duthey, B., and Laing, R. (2013). *Priority Medicines for Europe and the World 2013 Update*. Geneva: World Health Organization.

Lieuw, K. (2017). Many factor VIII products available in the treatment of hemophilia a: an embarrassment of riches? *J. Blood Med.* 8, 67–73. doi: 10.2147/JBM.S103796

Lindly, O. J., Chavez, A. E., and Zuckerman, K. E. (2016). Unmet health services needs among us children with developmental disabilities: associations with family impact and child functioning. *J. Dev. Behav. Pediatr.* 37, 712–723. doi: 10.1097/DBP.0000000000000363

Mallya, U. G., Boklage, S. H., Koren, A., Delea, T. E., and Mullins, C. D. (2017). Budget impact analysis of PCSK9 inhibitors for the management of adult patients with heterozygous familial hypercholesterolemia or clinical atherosclerotic cardiovascular disease. *Pharmacoeconomics* 36, 115–126. doi: 10.1007/s40273-017-0590-5

Markowitz, C. E. (2015). Identifying and addressing unmet therapeutic needs in MS. *J. Clin. Psychiatr.* 76:e8. doi: 10.4088/JCP.13037nr4c

Mascolo, A., Scavone, C., Sessa, M., di Mauro, G., Cimmaruta, D., Orlando, V., et al. (2017). Can causality assessment fulfill the new european definition of adverse drug reaction? a review of methods used in spontaneous reporting. *Pharmacol. Res.* 123, 122–129. doi: 10.1016/j.phrs.2017.07.005

Miller, C. E. (2009). Unmet therapeutic needs for uterine myomas. *J. Minim. Invasive Gynecol.* 16, 11–21. doi: 10.1016/j.jmig.2008.08.015

Mittermayer, F., Caveney, E., De Oliveira, C., Gourgiotis, L., Puri, M., Tai, L. J., et al. (2015). Addressing unmet medical needs in type 2 diabetes: a narrative review of drugs under development. *Curr. Diabetes Rev.* 11, 17–31. doi: 10.2174/1573399810666141224121927

Morgan, S., Lopert, R., and Greyson, D. (2008). Toward a definition of pharmaceutical innovation. *Open Med.* 2, e4–e7.

Morrow, D., Ussi, A., and Migliaccio, G. (2017). Addressing pressing needs in the development of advanced therapies. *Front. Bioeng. Biotechnol.* 5:55. doi: 10.3389/fbioe.2017.00055

Mostaghim, S. R., Gagne, J. J., and Kesselheim, A. S. (2017). Safety related label changes for new drugs after approval in the US through expedited regulatory pathways: retrospective cohort study. *BMJ* 358:j3837. doi: 10.1136/bmj.j3837

Oyinlola, J. O., Campbell, J., and Kousoulis, A. A. (2016). Is real world evidence influencing practice? a systematic review of CPRD research in NICE guidances. *BMC Health Serv. Res.* 16:299. doi: 10.1186/s12913-016-1562-8

Papadantonakis, N., and Advani, A. S. (2016). Recent advances and novel treatment paradigms in acute lymphocytic leukemia. *Ther. Adv. Hematol.* 7, 252–269. doi: 10.1177/2040620716652289

Papaluca, M., Greco, M., Tognana, E., Ehmann, F., and Saint-Raymond, A. (2015). White spots in pharmaceutical pipelines-EMA identifies potential areas of unmet medical needs. *Expert Rev. Clin. Pharmacol.* 8, 353–360. doi: 10.1586/17512433.2015.1028918

Parslow, A. C., Parakh, S., Lee, F. T., Gan, H. K., and Scott, A. M. (2016). Antibody-drug conjugates for cancer therapy. *Biomedicines* 4:E14. doi: 10.3390/biomedicines4030014

Persico, A. M., Arango, C., Buitelaar, J. K., Correll, C. U., Glennon, J. C., Hoekstra, P. J., et al. (2015). European child and adolescent clinical psychopharmacology network. unmet needs in paediatric psychopharmacology: present scenario and future perspectives. *Eur. Neuropsychopharmacol.* 25, 1513–1531. doi: 10.1016/j.euroneuro.2015.06.009

Pozzi, M., Pisano, S., Marano, G., Carnovale, C., Bravaccio, C., Rafaniello, C., et al. (2018). Weight-change trajectories of pediatric outpatients treated with risperidone or aripiprazole in a naturalistic setting. *J. Child Adolesc. Psychopharmacol.* [Epub ahead of print]. doi: 10.1089/cap.2018.0092

Rafaniello, C., Pozzi, M., Pisano, S., Ferrajolo, C., Bertella, S., Sportiello, L., et al. (2016). Second generation antipsychotics in 'real-life' paediatric patients. adverse drug reactions and clinical outcomes of drug switch. *Expert Opin. Drug Saf.* 15(Suppl. 2), 1–8.

Rafaniello, C., Sessa, M., Bernardi, F. F., Pozzi, M., Cheli, S., Cattaneo, D., et al. (2018). The predictive value of ABCB1, ABCG2, CYP3A4/5 and CYP2D6 polymorphisms for risperidone and aripiprazole plasma concentrations and the occurrence of adverse drug reactions. *Pharmacogenomics J.* 18, 422–430. doi: 10.1038/tpj.2017.38

Rush, A. J., Kraemer, H. C., Sackeim, H. A., Fava, M., Trivedi, M. H., Frank, E., et al. (2006). CNP task force. report by the ACNP task force on response, and remission in major depressive disorder. *Neuropsychopharmacology* 31, 1841–1853. doi: 10.1038/sj.npp.1301131

Saadi, E., and White, G. (2014). Rewarding innovation in drug development. *Am. Health Drug Benefits.* 7, 373–374.

Sanchez-Schmitz, G., and Levy, O. (2011). Development of newborn and infant vaccines. *Sci. Transl. Med.* 3:90s27. doi: 10.1126/scitranslmed.3001880

Sarri, G., Bhor, M., Abogunrin, S., Farmer, C., Nandal, S., Halloway, R., et al. (2018). Systematic literature review and assessment of patient-reported outcome instruments in sickle cell disease. *Health Qual. Life Outcomes.* 16:99. doi: 10.1186/s12955-018-0930-y

Sattler, C., Garcia, G., and Humbert, M. (2017). Novel targets of omalizumab in asthma. *Curr. Opin. Pulm. Med.* 23, 56–61. doi: 10.1097/MCP.0000000000000340

Scavone, C., Carnovale, C., Ruggiero, R., Radice, S., Scatigna, M., Racagni, G., et al. (2018). On the policy of the italian government in the discovery, development, and access to medicines. *Clin. Ther.* 40, 1931–1940. doi: 10.1016/j.clinthera.2018.09.015

Scavone, C., Rafaniello, C., Berrino, L., Rossi, F., and Capuano, A. (2017a). Strengths, weaknesses and future challenges of biosimilars' development. an opinion on how to improve the knowledge and use of biosimilars in clinical practice. *Pharmacol. Res.* 126, 138–142. doi: 10.1016/j.phrs.2017.11.002

Scavone, C., Sportiello, L., Berrino, L., Rossi, F., and Capuano, A. (2017b). Biosimilars in the european union from comparability exercise to real world experience: what we achieved and what we still need to achieve. *Pharmacol. Res.* 119, 265–271. doi: 10.1016/j.phrs.2017.02.006

Scavone, C., Sportiello, L., Sullo, M. G., Ferrajolo, C., Ruggiero, R., Sessa, M., et al. (2017c). BIO-cam group. safety profile of anticancer and immune-modulating biotech drugs used in a real world setting in campania region (italy): bio-cam observational study. *Front. Pharmacol.* 8:607. doi: 10.3389/fphar.2017.00607

Simon, R. (2017). Critical review of umbrella, basket, and platform designs for oncology clinical trials. *Clin. Pharmacol. Ther.* 102, 934–941. doi: 10.1002/cpt.814

Swedin, L., Saarne, T., Rehnberg, M., Glader, P., Niedzielska, M., and Johansson, G. (2017). Patient stratification and the unmet need in asthma. *Pharmacol Ther* 169, 13–34. doi: 10.1016/j.pharmthera.2016.06.016

Taiwo, B., Hicks, C., and Eron, J. (2010). Unmet therapeutic needs in the new era of combination antiretroviral therapy for HIV-1. *J. Antimicrob. Chemother.* 65, 1100–1107. doi: 10.1093/jac/dkq096

Thomson, N. C., and Chaudhuri, R. (2012). Omalizumab: clinical use for the management of asthma. *Clin. Med. Insights Circ. Respir. Pulm. Med.* 6, 27–40. doi: 10.4137/CCRPM.S7793

U.S. Department of Health and Human Services. (2014). *Guidance for Industry Expedited Programs for Serious Conditions – Drugs and Biologics*. Available at https://www.fda.gov/downloads/Drugs/Guidances/UCM358301.pdf

U.S. Food and Drug Administration. (2018). *FDA Approves Larotrectinib for Solid Tumors with Ntrk Gene Fusions*. Available at: https://www.fda.gov/Drugs/InformationOnDrugs/ApprovedDrugs/ucm626720.htm

Ujeyl, M., Schlegel, C., Walter, S., and Gundert-Remy, U. (2012). New drugs: evidence relating to their therapeutic value after introduction to the market. *Dtsch. Arztebl. Int.* 109, 117–123. doi: 10.3238/arztebl.2012.0117

Vella Bonanno, P., Ermisch, M., Godman, B., Martin, A. P., Van Den Bergh, J., Bezmelnitsyna, L., et al. (2017). Adaptive pathways: possible next steps for payers in preparation for their potential implementation. *Front. Pharmacol.* 8:497. doi: 10.3389/fphar.2017.00497

Wang, S. V., Schneeweiss, S., Gagne, J. J., Evers, T., Gerlinger, C., Desai, R., et al. (2018). Using real world data to extrapolate evidence from randomized controlled trials. *Clin. Pharmacol. Ther.* [Epub ahead of print]. doi: 10.1002/cpt.1210

Wurster, C. D., and Ludolph, A. C. (2018). Antisense oligonucleotides in neurological disorders. *Ther. Adv. Neurol. Disord.* 11:1756286418776932. doi: 10.1177/1756286418776932

Yasuhara, T., Kameda, M., Sasaki, T., Tajiri, N., and Date, I. (2017). Cell therapy for parkinson's disease. *Cell Transplant* 26, 1551–1559. doi: 10.1177/0963689717735411

Zhang, Y., Ge, M., Hao, Q., and Dong, B. (2018). Induced pluripotent stem cells in rat models of parkinson's disease: a systematic review and meta-analysis. *Biomed. Rep.* 8, 289–296. doi: 10.3892/br.2018.1049

Conflict of Interest Statement: The authors declare that the research was conducted in the absence of any commercial or financial relationships that could be construed as a potential conflict of interest.

frontiers in Pharmacology

ORIGINAL RESEARCH
published: 27 February 2019
doi: 10.3389/fphar.2019.00154

Metformin Protects the Heart Against Hypertrophic and Apoptotic Remodeling After Myocardial Infarction

*Halyna Loi[1], Frederic Boal[2,3], Helene Tronchere[2,3], Mathieu Cinato[2,3], Solomiia Kramar[1], Oleksandra Oleshchuk[1], Mykhaylo Korda[1] and Oksana Kunduzova[2,3]**

[1] Department of Pharmacology, I. Horbachevsky Ternopil State Medical University, Ternopil, Ukraine, [2] National Institute of Health and Medical Research (INSERM) U1048, Institute of Cardiovascular and Metabolic Diseases, Toulouse, France, [3] UMR1048, Paul Sabatier University, Toulouse, France

Cardiovascular complications are the most prevalent cause of morbidity and mortality in diabetic patients. Metformin is currently the first-line blood glucose-lowering agent with potential relevance to cardiovascular diseases. However, the underpinning mechanisms of action remain elusive. Here, we report that metformin represses cardiac apoptosis at least in part through inhibition of Forkhead box O1 (FoxO1) pathway. In a mouse model of ischemia-reperfusion (I/R), treatment with metformin attenuated cardiac and hypertrophic remodeling after 14 days of post-reperfusion. Additionally, cardiac expression of brain-like natriuretic peptide (BNP) was significantly reduced in metformin-treated mice after 14 days of cardiac I/R. In cultured H9C2 cells, metformin counteracted hypertrophic and apoptotic responses to metabolic or hypoxic stress. FoxO1 silencing by siRNA abolished anti-apoptotic effect of metformin under hypoxic stress in H9C2 cells. Taken together, these results suggest that metformin protects the heart against hypertrophic and apoptotic remodeling after myocardial infarction.

Keywords: metformin, myocardial infarction, hypertrophy, apoptosis, cardiac remodeling

OPEN ACCESS

Edited by:
Vadim V. Sumbayev, University of Kent, United Kingdom

Reviewed by:
Elizaveta Fasler-kan, Universitätsspital Bern, Switzerland
Eric E. Kelley, West Virginia University, United States

***Correspondence:**
Oksana Kunduzova
oxana.koundouzova@inserm.fr

Specialty section:
This article was submitted to Experimental Pharmacology and Drug Discovery, a section of the journal Frontiers in Pharmacology

Received: *07 December 2018*
Accepted: *08 February 2019*
Published: *27 February 2019*

Citation:
Loi H, Boal F, Tronchere H, Cinato M, Kramar S, Oleshchuk O, Korda M and Kunduzova O (2019) Metformin Protects the Heart Against Hypertrophic and Apoptotic Remodeling After Myocardial Infarction. Front. Pharmacol. 10:154. doi: 10.3389/fphar.2019.00154

INTRODUCTION

The most prevalent form of diabetes mellitus in patients is type 2 diabetes (T2D) (Kannel and McGee, 1979). This form of metabolic disorders, which accounts for 90–95% of those with diabetes, circles subjects with insulin resistance and relative insulin deficiency (Kharroubi and Darwish, 2015). T2D mediates various cardiovascular manifestations, which have become the major cause of morbidity and mortality in the diabetic population (Townsend et al., 2016). A causative relationship between heart failure (HF) and diabetes has been well demonstrated (Aneja et al., 2008). HF is a frequent complication in diabetes mellitus with poor outcomes and five-year survival rates of <25% (Zinman et al., 2015). Diabetic cardiomyopathy (DCM) is the clinical condition associated with cardiac abnormalities mediated by diabetes. It has been estimated that DCM affects approximately 12% of the diabetic patients and may lead to HF and death (Aneja et al., 2008). The pathogenesis of DCM remains obscure, but is clearly of significant clinical priority, given the strong association of diabetes with HF and cardiovascular mortality (Zinman et al., 2015).

Cardiac hypertrophy, oxidative stress, inflammation, apoptosis, and uncontrolled interstitial fibrosis are the major features of DCM (Aneja et al., 2008). Decline in cardiac function linked to

DCM is attributable to initial rise in heart mass and unbalanced interventricular septal thickening. Cardiac hypertrophic reprogramming includes accelerated protein synthesis, up-regulation of atrial and brain natriuretic peptides and abnormal sarcomeric organization (Liu et al., 2016). Myocardial hypertrophic remodeling, triggered by signaling cascades in response to stress, is initially adaptive process. However, extended cardiac hypertrophy as a consequence of pathological stress leads to excessive production of reactive oxygen species, activation of apoptotic and inflammatory cascades which play a key role in DCM (Borner and Monney, 1999; Hunter and Chien, 1999; Clerk et al., 2003). These processes ultimately results in initiation of pro-fibrotic reprogramming and impaired cardiac function (Wynn and Ramalingam, 2012).

Metformin is currently the first-line blood glucose-lowering agent with potential relevance to cardiovascular diseases for the treatment of T2D. Two large-scale clinical trials suggested that apart from its antihyperglycemic effect, metformin has other potential effects. Metformin preserves cardiac function and prevents the incidence of myocardial infarction in patients with diabetes (UK Prospective Diabetes Study [Ukpds] Group, 1998; Holman et al., 2008). Compared with other glucose-lowering agents, use of metformin was associated with reduced risk of cardiovascular mortality and morbidity in patients with T2D (King et al., 1999). The potential mechanism of action of metformin involves activation of adenosine monophosphate-activated protein kinase (AMPK) and glucose metabolism (Gundewar et al., 2009; Sasaki et al., 2009; Paiva et al., 2010). Several studies reported that metformin may also acts via AMPK-independent pathways (Xu et al., 2014). However, the exact molecular mechanisms by which metformin regulates cardiac cell functions remain elusive.

In the present study, we show that metformin counteracts myocardial hypertrophy and apoptosis in a mouse model of cardiac I/R. Furthermore, we show that metformin could protect against stress-induced cardiac apoptosis through FoxO1 pathway.

MATERIALS AND METHODS

Cell Culture

The rat embryonic cardiomyoblast cell line H9C2 was cultured in DMEM medium (Life Technologies) supplemented with 10% fetal bovine serum (FBS) and 1% penicillin–streptomycin in a humidified atmosphere of 95% air-5% CO2 at 37°C. Cells were treated with 5 mM metformin 30 min before cell stress. In order to induce metabolic stress, H9C2 cells were exposed to 2-deoxy-D-glucose (2 mM) in 0% medium for 24 h. For hypoxic treatment cells were maintained at 37°C under hypoxic atmosphere (5% CO_2, 1% O_2, balance N_2) for 24 h.

Cell Transfection

H9C2 cells were seeded into 24-well plates and cultured with DMEM medium (Life Technologies) supplemented with 10% FBS and 1% penicillin–streptomycin in a humidified atmosphere of 95% air-5% CO2 at 37°C. Cells were transfected with FoxO1 siRNA and siRNA control at a final concentration of 200 nmol/L using Lipofectamine 2000 transfection reagent (Life Technologies) according to the manufacturer's instructions.

Histology

Oregon Green 488 coupled-wheat germ agglutinin (WGA) labeling was used in immunohistochemical preparations of 10-μm heart cryosections. The evaluation of cardiac structural alterations was performed using ImageJ software.

Evaluation of Apoptosis

Cardiac apoptosis was measured using the Terminal deoxynucleotidyl transferase dUTP nick end labeling (TUNEL) assay according to manufacturer's instructions (Promega). Briefly, cells fixed in 4% PFA were first incubated in 0.2% TritonX-100 for 5 min, then in Equilibration Buffer for 10 min. A solution which contained 5 μl of nucleotide mix and 1 μl of rTDT enzyme in 45 μl equilibration buffer was added for each well for 1 h at 37°C in the dark. Then, after adding saline sodium citrate and washing with phospho buffered saline (PBS) the slides were incubated with Dapi for 15 min. To detect and count the number of apoptotic cells, three fields of view were randomly selected per conditions in cardiac tissue.

Animal Studies

Animal investigations conform to the Guide for the Care and Use of Laboratory Animals published by the US National Institutes of Health (NIH Publication No. 85-23, revised 1985) and were performed in accordance with the recommendations of the French Accreditation of the Laboratory Animal Care (approved by the local Centre National de la Recherche Scientific ethics committee).

Three-month-old wild-type male C57BI/6J mice purchased from Janvier Labs were maintained in a temperature-controlled room (25°C) with a natural day/night cycle and fed a standard chow diet and given *ad libitum* access to water. A mouse model of I/R was used as previously described (Boal et al., 2016). The mice were intubated and placed under mechanical ventilation after undergoing general anesthesia with an intraperitoneal injection of ketamine (125 mg/kg) and xylazine (10 mg/kg). A left parasternotomy was performed to expose hearts, and a 0.4 mm polyethylene suture was placed around the left anterior descending coronary artery. A snare was placed on the suture, and regional myocardial ischemia was produced by tightening the snare. After 30 min of ischemia, the occlusive snare was released to initiate reperfusion. Sham-operated control mice underwent the same surgical procedures except that the snare was not tightened. Intraperitoneal (i.p.) treatment with metformin (5 mg/kg/day) in a final volume of 100 μl was started 15 min after the onset of reperfusion and maintained for 14 days. Animals were randomly divided into four groups as follows:

(1) Control+PBS (C) group ($n = 5$);
(2) Control+Metformin (C+M) group ($n = 5$);
(3) I/R+PBS (I/R) group ($n = 5$);
(4) I/R+Metformin (I/R+M) group ($n = 5$).

Quantitative RT-PCR Analysis

Total RNAs were isolated from mouse heart and cultured H9C2 cells using the GenElute^{TM} Mammalian Total RNA Miniprep Kit (Sigma-Aldrich). Total RNAs (500 ng) were reverse transcribed using High Capacity cDNA Reverse Transcription Kit (Applied Biosystems^{TM}) in the presence of random hexamers. Real−time quantitative PCR was performed as previously described (Boal et al., 2016). The expression of target mRNA was normalized to GAPDH mRNA expression. Sequence of the forward and reverse primer for BNP: Forward: 5′-GCACAAGATAGACCGGATCG-3′ Reverse: 5′-CCCAGGCAGAGTCAGAAAC-3′.

Statistical Analysis

Statistical comparison between two groups was performed by Student's *t*-test, while comparison of multiple groups was performed by One-way ANOVA followed by a Bonferroni's *post hoc* test using GraphPad Prism version 5.00 (GraphPad Software, Inc.). Data are expressed as mean ± SEM.

RESULTS

Metformin Inhibits Cell Hypertrophy in Response to Metabolic and Hypoxic Stress

In the first set of experiments, we investigated whether metformin affects metabolic- or oxidative stress-induced hypertrophic responses *in vitro*. As shown in **Figure 1**, cell treatment with 2 mM 2-deoxyglucose (2DG) for 24 h demonstrated significant increase in cell size. Metformin prevented cell hypertrophy in the presence of 2DG as compared to control untreated H9C2 cells (**Figure 1**). When H9C2 cells were exposed to hypoxic stress (1% O_2), significant increase in hypertrophy was

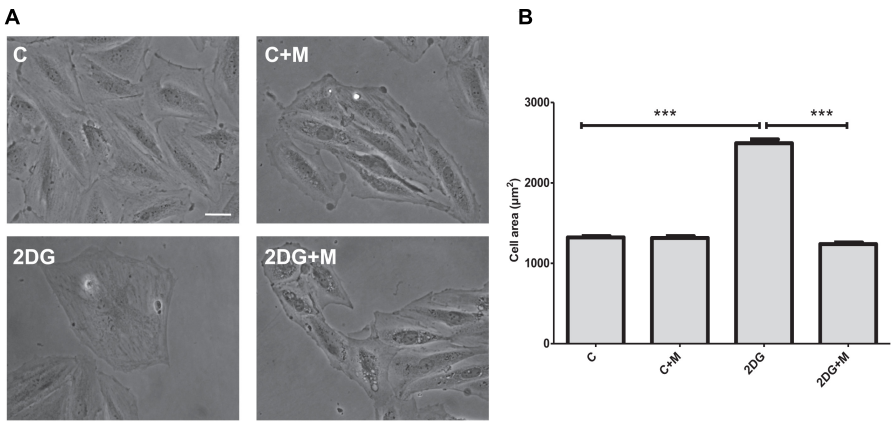

FIGURE 1 | Metformin attenuates cell hypertrophy in response to metabolic stress. **(A)** Representative images of H9C2 cells exposed to vehicle (C) or 2 mM 2-deoxyglucose (2DG) for 24 h in the presence or absence of 5 mM metformin (M). **(B)** Quantification of cell area from **(A)**. Data represents the mean ± SEM from at least three independent experiments. Scale bar is 100 µm. Statistical analysis was carried out by one-way ANOVA: ***$P < 0.001$ between indicated conditions.

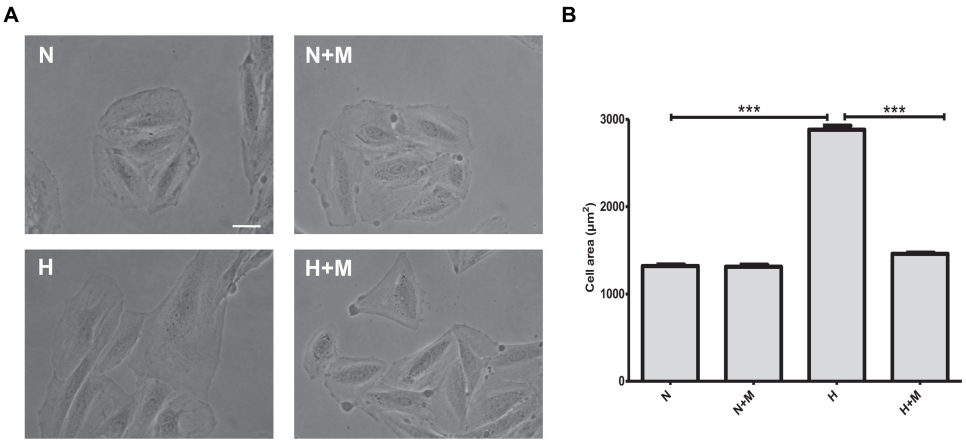

FIGURE 2 | Metformin prevents hypoxia-induced cell hypertrophy. **(A)** Representative images of H9C2 cells subjected to normoxia (N) or hypoxia (H) for 24 h in the presence or absence of 5 mM metformin (M). **(B)** Quantification of cell area from **(A).** Scale bar is 100 µm. Data represents the mean ± SEM from at least three independent experiments. Statistical analysis was carried out by one-way ANOVA: ***$P < 0.001$ between indicated conditions.

observed after 24 h (**Figure 2**). As shown in **Figure 2**, in the presence of metformin (5 mM), hypoxia-induced hypertrophy was markedly abolished in H9C2 cells. Thus, these data demonstrated that metformin prevents metabolic- or hypoxia-induced hypertrophy in H9C2 cells.

Metformin Inhibits Cell Apoptosis in Response to Metabolic Stress and Hypoxia

Excessive apoptotic cell death in human and animal hearts has been linked to ischemic and dilated cardiomyopathies (Narula et al., 1996; Olivetti et al., 1997; Saraste et al., 1997). In order to determine whether metformin affects apoptotic responses to metabolic or oxidative stress, we examined the effects of metformin on 2DG- or hypoxia-induced cell apoptosis by TUNEL staining. As shown in **Figure 3**, exposure of H9C2 cells to 2 mM 2DG for 24 h induced an increase in TUNEL positive cells. Treatment of H9C2 cells with metformin was able to attenuate 2DG-induced apoptotic cell death (**Figure 3**). Importantly, hypoxia-induced cell apoptosis was declined in metformin-treated cells as compared to control untreated cells (**Figure 4**).

Metformin Prevents H9C2 Cells From Hypoxia-Induced Apoptosis Through FoxO1 Pathway

The FoxO1 transcriptional factor plays an essential role in the regulation of apoptosis, energy metabolism and oxidative stress (O'Connor and Barr, 2009). We next examined whether knockdown of FoxO1 could affect anti-apoptotic effects of metformin. At 24 h after FoxO1 siRNA addition, qRT-PCR analysis showed that FoxO1 expression level was significantly decreased as compared to control cells receiving scrambled siRNA (**Figure 5**). Analysis of TUNEL-stained cells exposed to hypoxia for 24 h, demonstrated that metformin significantly

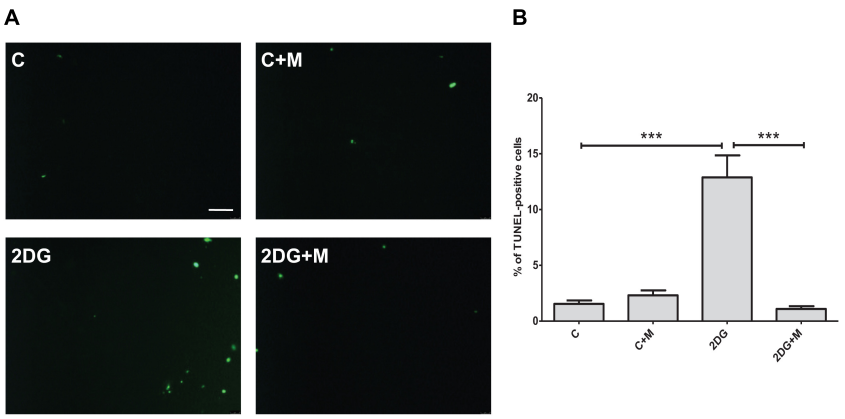

FIGURE 3 | Metformin abolishes cell apoptosis in response to metabolic stress. **(A)** Representative images of TUNEL staining of cultured H9C2 cells exposed to 2 mM 2-deoxyglucose (2DG) in the presence or absence of 5 mM metformin (M). **(B)** Quantification of apoptosis from **(A)**. Scale bar is 100 μm. Data represents the mean ± SEM from at least three independent experiments. Statistical analysis was carried out by one-way ANOVA: $^{***}P < 0.001$ between indicated conditions.

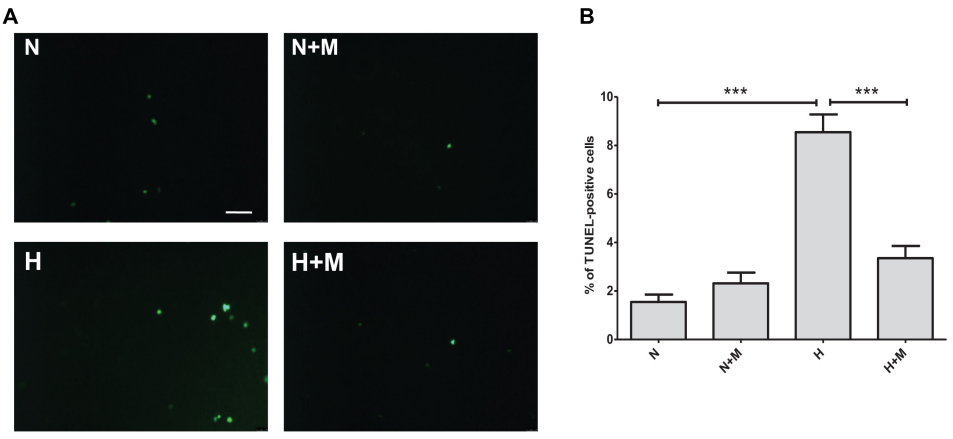

FIGURE 4 | Metformin protects against hypoxia-induced apoptosis in H9C2 cells. **(A)** TUNEL staining of apoptotic cells subjected to normoxia (N) or hypoxia (H) in the presence or absence of 5 mM metformin (M). **(B)** Quantification of TUNEL-positive cells from **(A)**. Scale bar is 100 μm. Data represents the mean ± SEM from at least three independent experiments. Statistical analysis was carried out by one-way ANOVA: $^{***}P < 0.001$ between indicated conditions.

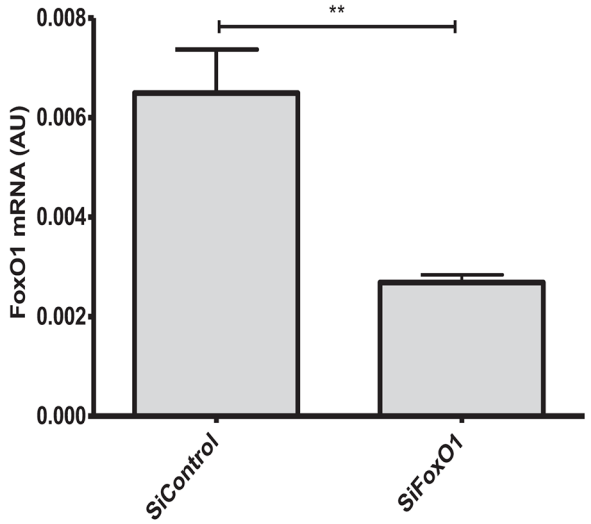

FIGURE 5 | Silencing of FoxO1 gene expression in H9C2 cells. HC92 cells were transfected with a control siRNA (siControl) or with a siRNA against Foxo1 (siFoxo1) and FoxO1 expression level was measured by qRT–PCR. Data are presented as mean ± SEM. Student's *t*–test: $^{**}P < 0.01$ between two conditions.

reduced cell apoptosis in control siRNA transfected cells. However, FoxO1 silencing by siRNA abrogated the effects of metformin on cell apoptosis, suggesting that anti-apoptotic activity of metformin is FoxO1-dependent (**Figure 6**).

Metformin Treatment Reduces Cardiac Hypertrophy in a Mouse Model of Cardiac I/R Injury

Considering *in vitro* effects of metformin on cellular stress responses, we next investigated *in vivo* activity of metformin on cardiac hypertrophic reprogramming in a mouse model of myocardial I/R injury. To examine the translational potential of metformin, *in vivo* study was designed to determine whether treatment with metformin (5 mg/kg/day, i.p.) initiated 15 min after the onset of reperfusion and maintained for 14 days induced cardioprotection in mice subjected to cardiac I/R. Histological analyses of cardiac sections stained with WGA (**Figures 7A,B**) demonstrated a significant decrease in myocyte hypertrophy in metformin-treated mice as compared with vehicle-treated mice. To further confirm the anti-hypertrophic effects of metformin, we examined expression of BNP, a marker of ventricular hypertrophy, in cardiac sections from vehicle- or metformin-treated mice after 14 days of I/R. As shown in **Figure 7C**, treatment of mice with metformin prevented I/R-induced up-regulation of BNP as compared to control mice.

Metformin Treatment Blunts Apoptotic Response to Cardiac I/R Injury

We next examined the effects of metformin on cardiac apoptosis in I/R-challenged hearts (**Figure 8**). In the group of vehicle-treated mice after myocardial infarction the number of apoptotic cells was significantly increased compared with control group (15.2% vs. 1.9%, $P < 0.001$). As shown by TUNEL staining in **Figure 8**, metformin treatment (5 mg/kg/day, i.p.) for 14 days markedly reduced cardiac apoptosis after I/R injury as compared to vehicle-treated mice (1.1% vs. 15.2%, $P < 0.001$, respectively).

DISCUSSION

The primary prominent features of the diabetic myocardium are cardiac hypertrophic reprogramming and activation of cell death programs (Bugger and Abel, 2014). We found that metformin, a drug commonly used in the treatment of T2D, attenuates cardiac hypertrophy and apoptosis *in vitro* and *in vivo*. In addition, we described FoxO1-dependent mechanism of anti-apoptotic effects of metformin in cardiomyoblasts exposed to stress. These studies implicate activation of myocardial apoptotic and hypertrophic reprogramming in the pathogenesis of adverse ventricular remodeling and suggest that metformin provides cardioprotective effects against I/R injury.

Metformin, according to the American Diabetes Association's current clinical practice recommendations, remains a first line pharmacological agent for T2D (American Diabetes Association, 2018) that can reduce risk of cardiovascular events and death (Holman et al., 2008). The beneficial effects of metformin on cardiac function have been attributed to direct actions on cell metabolism, endothelial function, platelet reactivity and calcium homeostasis (Kirpichnikov et al., 2002). Our studies demonstrated that metformin treatment blunts *in vitro* and *in vivo* hypertrophic and apoptotic responses to cardiac I/R injury. In H9C2 cells exposed to metabolic or oxidative stress, metformin inhibited apoptotic cell death. The rat cardiomyoblast cell line H9C2 has emerged as a valuable tool for studying pathophysiology of cardiac remodeling processes and mechanisms of disease progression in hypertrophic cardiomyopathy (Hescheler et al., 1991). The reason for the wide popularity of H9C2 cell model is that they have well-characterized properties in terms of morphology and cardiac molecular physiology (Watkins et al., 2011). We also demonstrated that a significantly decreased hypertrophic response to I/R was observed in hearts of C57BL/6 mice that exhibit functional and structural abnormalities recapitulating human cardiac remodeling processes (Eguchi et al., 2012).

Several lines of evidence suggest that maladaptive cardiac hypertrophy is one of the most common features of DCM (Aneja et al., 2008). At the level of cardiomyocytes, hypertrophic response is characterized by an increase in cell size, accelerated protein synthesis, profound organization of the sarcomere and fetal gene reprogramming (Dorn et al., 2003; Frey et al., 2004). Stress-induced reactivation of fetal genes in the failing heart plays a pivotal role in the progression of ventricular remodeling and HF in humans and in mouse models (Frey et al., 2004). Importantly, we found that treatment with metformin decreases BNP expression in I/R-challenged hearts suggesting that metformin can

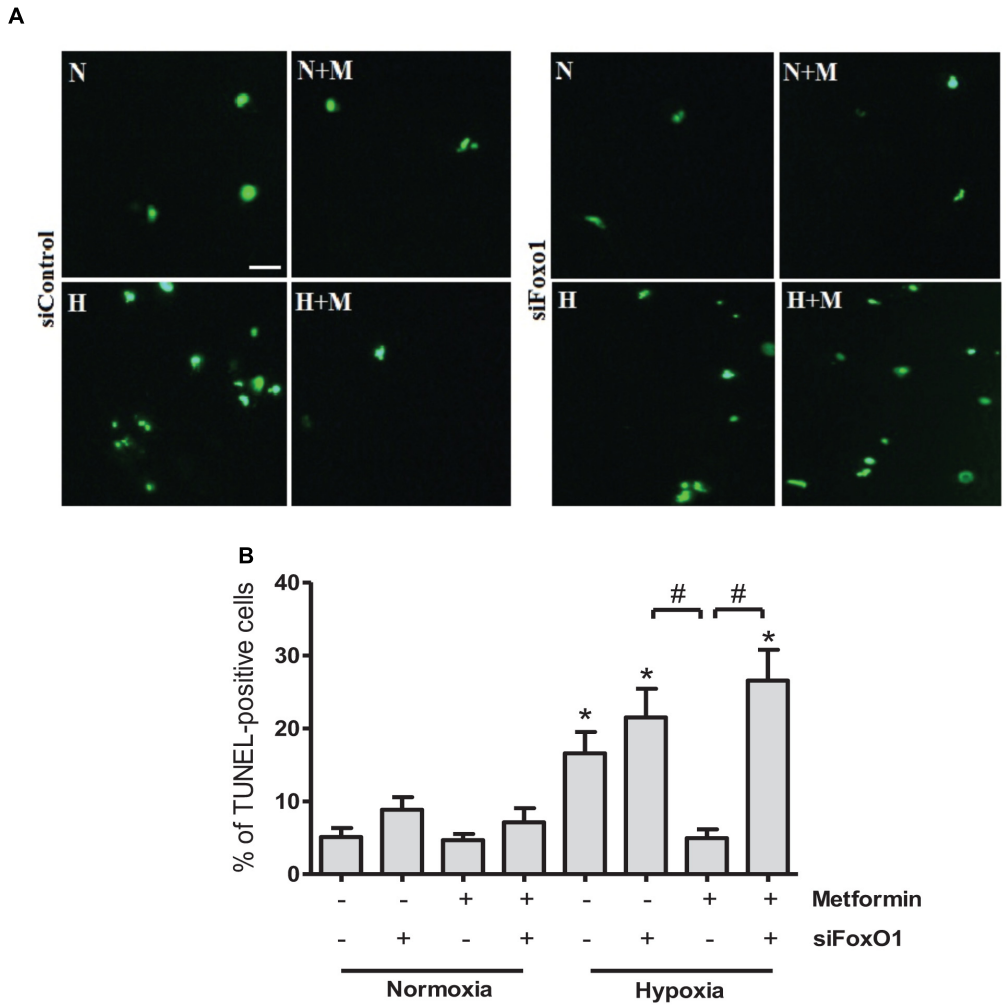

FIGURE 6 | Metformin prevents H9C2 cells from hypoxia-induced apoptosis through FoxO1 pathway. **(A)** Representative images of TUNEL staining of H9C2 cells transfected with control siRNA (siControl) or siRNA targeting FoxO1 (siFoxO1). Scale bar is 25 μM. **(B)** Quantification of apoptotic cells from **(A)**. Data are presented as mean ± SEM. Statistical analysis was carried out by one-way ANOVA: $^{*}P < 0.05$ vs. control, $^{\#}P < 0.05$ between indicated conditions.

counteract activation of pro-hypertrophic gene program in the failing myocardium.

Results from this study demonstrated that metformin inhibits stress-activated apoptotic cell death via FoxO1 pathway. FoxO-family proteins including FoxO1, FoxO3, FoxO4, and FoxO6 orchestrate various physiological and pathological functions by controlling the expression of genes associated with cell cycle arrest, apoptosis, DNA damage repair, oxidative stress resistance and cell metabolism (Accili and Arden, 2004; Huang and Tindall, 2007; Eijkelenboom and Burgering, 2013). A recent study reports that metformin regulates FoxO1 activities in endothelial cells (Li et al., 2015). Another study (Arunachalam et al., 2014) supports the notion that metformin can negatively regulate FoxO1-dependent apoptotic gene transcription and cell cycle. Our *in vitro* results suggest that metformin represses cell apoptosis through FoxO1 pathway in H9C2 cells. In line with these data, a recent study found that cardiomyocyte expression of FoxO1 inhibits cell hypertrophic growth and calcineurin phosphatase activity (Ni et al., 2006).

The adult heart is comprised of terminally differentiated myocytes that are responsible for contractile performance. In this context, the failing heart displays more pronounced adverse effects as a consequence of excessive cell death. The limited capacity of the myocardium to efficiently regenerate highlights the importance of preservation of resting cardiomyocytes to support contractile function. Maintenance of cardiovascular homeostasis depends on cardiac cell death and renewal, and excessive apoptotic loss of cardiomyocytes has been implicated in many cardiovascular diseases (Narula et al., 1996). The results of our study have demonstrated that metformin inhibits cardiac apoptosis in I/R-challenged mice, suggesting that metformin can prevent cell loss in the failing heart. Recent studies found that metformin may inhibit cell apoptosis in kidney and cisplatin-induced acute kidney injury (Li et al., 2016) indicating the anti-apoptotic potential of metformin in peripheral

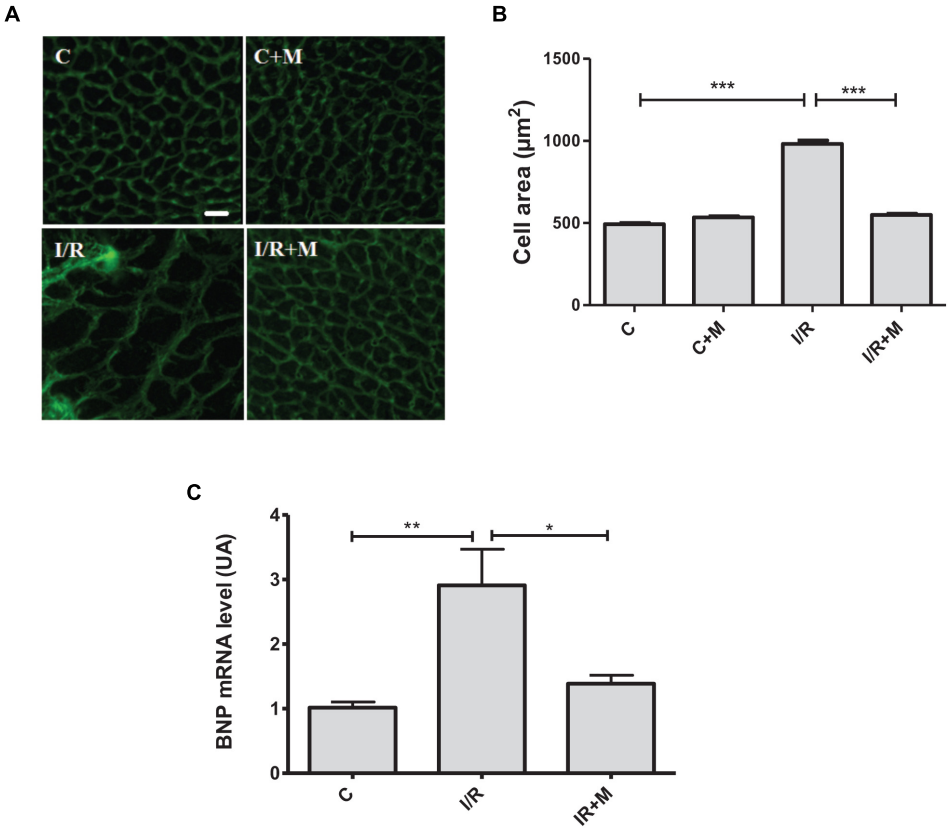

FIGURE 7 | Metformin treatment reduces cardiac hypertrophy in I/R-challenged hearts. **(A)** Representative images of wheat germ agglutinin (WGA) staining of heart frozen tissue sections. Mice were subjected to 30 min of cardiac ischemia and 14 days of reperfusion. Metformin treatment (5 mg/kg/day, i.p.) started at 15 min of post-reperfusion and continued for 14 days. Scale bar is 25 μM. **(B)**. Quantification of cell size from **(A)**. **(C)**. qRT-PCR analysis of the expression level of the hypertrophic marker BNP. Data are presented as mean ± SEM. Statistical analysis was carried out by one-way ANOVA: $^{*}P < 0.05$, $^{**}P < 0.01$, $^{***}P < 0.001$ between indicated conditions.

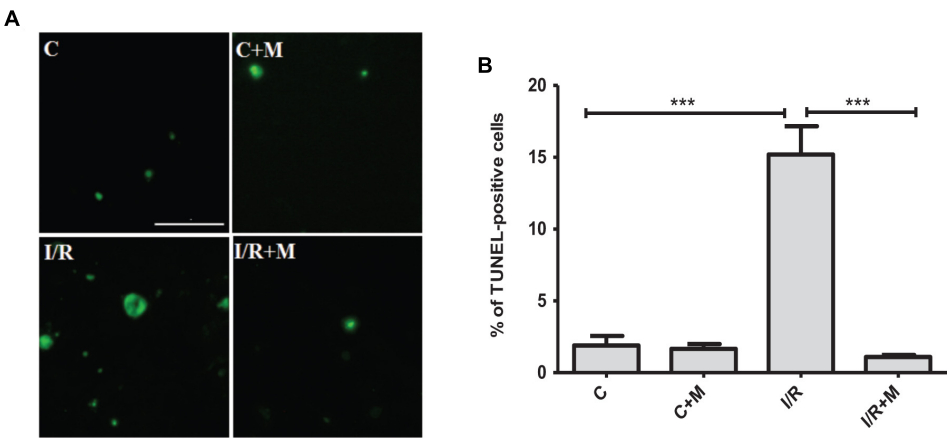

FIGURE 8 | Metformin treatment protects against cardiac apoptosis in I/R-challenged hearts. **(A)**. TUNEL staining of cardiac tissue from vehicle- or metformin-treated mice subjected to 30 min of cardiac ischemia and 14 days of reperfusion. Metformin treatment (5 mg/kg/day, i.p.) started at 15 min of post-reperfusion and continued for 14 days. Scale bar is 100 μM. **(B)**. Quantification of apoptotic cells from **(A)**. Data are presented as mean ± SEM. Statistical analysis was carried out by one-way ANOVA: $^{***}P < 0.001$ between indicated conditions.

organs. Further studies are necessary to explore the potential mechanisms of action and biological effects of metformin in non-metabolic disorders.

In conclusion, metformin prevented cardiac hypertrophy, and ultimately abolished myocardial apoptosis through FoxO1 pathway. These findings provide new insights into the role of hypertrophic and apoptotic remodeling in the failing heart and deepen our understanding of how metformin regulates cardiac cell decisions in response to stress. Altogether, these data suggest that metformin could have cardiovascular benefit for diabetic patients.

AUTHOR CONTRIBUTIONS

HL, FB, HT, MC, and SK carried out the experiments. OO and MK supervised the project. OK conceived the original idea and supervised the project.

FUNDING

This work was supported by the INSERM, Région Midi-Pyrénées and ERASMUS + project.

REFERENCES

Accili, D., and Arden, K. C. (2004). FoxOs at the crossroads of cellular metabolism, differentiation, and transformation. *Cell* 117, 421–426.

American Diabetes Association. (2018). Pharmacologic approaches to glycemic treatment: standards of medical care in diabetes 2018. *Diabetes Care* 41(Suppl. 1), 73–85.

Aneja, A., Tang, W. W., Bansilal, S., Garcia, M. J., and Farkouh, M. E. (2008). Diabetic cardiomyopathy: insights into pathogenesis, diagnostic challenges, and therapeutic options. *Am. J. Med.* 121, 748–757. doi: 10.1016/j.amjmed.2008.03.046

Arunachalam, G., Samuel, S. M., Marei, I., Ding, H., and Triggle, C. R. (2014). Metformin modulates hyperglycaemia-induced endothelial senescence and apoptosis through SIRT1. *Br. J. Pharmacol.* 171, 523–535. doi: 10.1111/bph.12496

Boal, F., Timotin, A., Roumegoux, J., Alfarano, C., Calise, D., Anesia, R., et al. (2016). Apelin-13 administration protects against ischaemia/reperfusion-mediated apoptosis through the FoxO1 pathway in high-fat diet-induced obesity. *Br. J. Pharmacol.* 173, 1850–1863. doi: 10.1111/bph.13485

Borner, C., and Monney, L. (1999). Apoptosis without caspases: an inefficient molecular guillotine? *Cell Death Differ.* 6, 497–507. doi: 10.1038/sj.cdd.4400525

Bugger, H., and Abel, E. D. (2014). Molecular mechanisms of diabetic cardiomyopathy. *Diabetologia* 57, 660–671. doi: 10.1007/s00125-014-3171-6

Clerk, A., Cole, S. M., Cullingford, T. E., Harrison, J. G., Jormakka, M., and Valks, D. M. (2003). Regulation of cardiac myocyte cell death. *Pharmacol. Ther.* 97, 223–261.

Dorn, G. W., Robbins, J., and Sugden, P. H. (2003). Phenotyping hypertrophy: eschew obfuscation. *Circ. Res.* 92, 1171–1175. doi: 10.1161/01.RES.0000077012.11088.BC

Eguchi, M., Kim, Y. H., Kang, K. W., Shim, C. Y., Jang, Y., Dorval, T., et al. (2012). Ischemia-reperfusion injury leads to distinct temporal cardiac emodeling in normal versus diabetic mice. *PLoS One* 7:e30450. doi: 10.1371/journal.pone.0030450

Eijkelenboom, A., and Burgering, B. M. (2013). FOXOs: signalling integrators for homeostasis maintenance. *Nat. Rev. Mol. Cell Biol.* 14, 83–97. doi: 10.1038/nrm3507

Frey, N., Katus, H. A., Olson, E. N., and Hill, J. A. (2004). Hypertrophy of the heart: a new therapeutic target? *Circulation* 109, 1580–1589. doi: 10.1161/01.cir.0000120390.68287.bb

Gundewar, S., Calvert, J. W., Jha, S., Toedt-Pingel, I., Ji, S. Y., Nunez, et al. (2009). Activation of AMP-activated protein kinase by metformin improves left ventricular function and survival in heart failure. *Circ. Res.* 104, 403–411. doi: 10.1161/CIRCRESAHA.108.190918

Hescheler, J., Meyer, R., Plant, S., Krautwurst, D., Rosenthal, W., and Schultz, G. (1991). Morphological, biochemical, and electrophysiologicalcharacterization of a clonal cell (H9c2) linefrom rat heart. *Circ. Res.* 69, 1476–1486.

Holman, R. R., Paul, S. K., Bethel, M. A., Matthews, D. R., and Neil, H. A. W. (2008). 10-year follow-up of intensive glucose control in type 2 diabetes. *N. Engl. J. Med.* 359, 1577–1589. doi: 10.1056/NEJMoa0806470

Huang, H., and Tindall, D. J. (2007). Dynamic FoxO transcription factors. *J. Cell Sci.* 120, 2479–2487. doi: 10.1242/jcs.001222

Hunter, J. J., and Chien, K. R. (1999). Signaling pathways for cardiac hypertrophy and failure. *N. Engl. J. Med.* 341, 1276–1283. doi: 10.1056/NEJM199910213411706

Kannel, W. B., and McGee, D. L. (1979). Diabetes and cardiovascular disease: the Framingham study. *JAMA* 241, 2035–2038. doi: 10.1001/jama.1979.03290450033020

Kharroubi, A. T., and Darwish, H. M. (2015). Diabetes mellitus: the epidemic of the century. *World J. Diabetes.* 6:850. doi: 10.4239/wjd.v6.i6.850

King, P., Peacock, I., and Donnelly, R. (1999). The UK prospective diabetes study (UKPDS): clinical and therapeutic implications for type 2 diabetes. *Br. J. Clin. Pharmacol.* 48, 643–648.

Kirpichnikov, D., McFarlane, S. I., and Sowers, J. R. (2002). Metformin: an update. *Ann. Intern. Med.* 137, 25–33. doi: 10.7326/0003-4819-137-1-200207020-00009

Li, J., Gui, Y., Ren, J., Liu, X., Feng, Y., Zeng, Z., et al. (2016). Metformin protects against cisplatin-induced tubular cell apoptosis and acute kidney injury via AMPKα-regulated autophagy induction. *Sci. Rep.* 6:23975. doi: 10.1038/srep23975

Li, X., Kover, K. L., Heruth, D. P., Watkins, D. J., Moore, W. V., Jackson, K., et al. (2015). New insight into metformin action: regulation of ChREBP and FOXO1 activities in endothelial cells. *Mol. Endocrinol.* 29, 1184–1194. doi: 10.1210/ME.2015-1090

Liu, P., Cheng, G. C., Ye, Q. H., Deng, Y. Z., and Wu, L. (2016). LKB1/AMPK pathway mediates resistin-induced cardiomyocyte hypertrophy in H9c2 embryonic rat cardiomyocytes. *Biomed. Rep.* 4, 387–391. doi: 10.3892/br.2016.593

Narula, J., Haider, N., Virmani, R., DiSalvo, T. G., Kolodgie, F. D., Hajjar, R. J., et al. (1996). Apoptosis in myocytes in end-stage heart failure. *N. Engl. J. Med.* 335, 1182–1189. doi: 10.1056/NEJM199610173351603

Ni, Y. G., Berenji, K., Wang, N., Oh, M., Sachan, N., Dey, A., et al. (2006). Foxo transcription factors blunt cardiac hypertrophy by inhibiting calcineurin signaling. *Circulation* 114, 1159–1168. doi: 10.1161/CIRCULATIONAHA.106.637124

O'Connor, R., and Barr, F. G. (2009). FOXO1 (Forkhead box O1). *Atlas Genet. Cytogenet. Oncol. Haematol.* 13, 268–272. doi: 10.4267/2042/44448

Olivetti, G., Abbi, R., Quaini, F., Kajstura, J., Cheng, W., Nitahara, J. A., et al. (1997). Apoptosis in the failing human heart. *N. Engl. J. Med.* 336, 1131–1141. doi: 10.1056/NEJM199704173361603

Paiva, M. A., Gonçalves, L. M., Providência, L. A., Davidson, S. M., Yellon, D. M., and Mocanu, M. M. (2010). Transitory activation of AMPK at reperfusion protects the ischaemic-reperfused rat myocardium against infarction. *Cardiovasc. Drugs Ther.* 24, 25–32. doi: 10.1007/s10557-010-6222-3

Saraste, A., Pulkki, K., Kallajoki, M., Henriksen, K., Parvinen, M., and Voipio-Pulkki, L. M. (1997). Apoptosis in human acute myocardial infarction. *Circulation* 95, 320–323. doi: 10.1161/01.CIR.95.2.320

Sasaki, H., Asanuma, H., Fujita, M., Takahama, H., Wakeno, M., Ito, S., et al. (2009). Metformin prevents progression of heart failure in dogs: role of AMP-activated protein kinase. *Circulation* 119, 2568–2577. doi: 10.1161/CIRCULATIONAHA.108.798561

Townsend, N., Wilson, L., Bhatnagar, P., Wickramasinghe, K., Rayner, M., and Nichols, M. (2016). Cardiovascular disease in Europe: epidemiological update 2016. *Eur. Heart J.* 37, 3232–3245. doi: 10.1093/eurheartj/ehw334

UK Prospective Diabetes Study [Ukpds] Group. (1998). Effect of intensive blood-glucose control with metformin on complications in overweight patients with type 2 diabetes (UKPDS 34). *Lancet* 352, 854–865. doi: 10.7326/ACPJC-1999-130-1-003

Watkins, S. J., Borthwick, G. M., and Arthur, H. M. (2011). The H9C2 cell line and primary neonatal cardiomyocyte cells show similar hypertrophic responses in vitro. *Cell Dev. Biol. Anim.* 47, 125–131. doi: 10.1007/s11626-010-9368-1

Wynn, T. A., and Ramalingam, T. R. (2012). Mechanisms of fibrosis: therapeutic translation for fibrotic disease. *Nat. Med.* 18, 1028–1040. doi: 10.1038/nm.2807

Xu, X., Lu, Z., Fassett, J., Zhang, P., Hu, X., Liu, X., et al. (2014). Metformin Protects Against Systolic Overload–Induced Heart Failure Independent of AMP-Activated Protein Kinase α2. *Hypertension* 63, 723–728. doi: 10.1161/HYPERTENSIONAHA.113.02619

Zinman, B., Wanner, C., Lachin, J. M., Fitchett, D., Bluhmki, E., Hantel, S., et al. (2015). Empagliflozin, cardiovascular outcomes, and mortality in type 2 diabetes. *N. Engl. J. Med.* 373, 2117–2128. doi: 10.1056/NEJMoa1504720

Conflict of Interest Statement: The authors declare that the research was conducted in the absence of any commercial or financial relationships that could be construed as a potential conflict of interest.

frontiers in Pharmacology

ORIGINAL RESEARCH
published: 22 March 2019
doi: 10.3389/fphar.2019.00221

Rolipram, a PDE4 Inhibitor, Enhances the Inotropic Effect of Rat Heart by Activating SERCA2a

Huili Huang[1†], Ming Xie[1†], Li Gao[1], Wenhui Zhang[1], Xiaojia Zhu[1], Yuwei Wang[1], Wei Li[1], Rongrong Wang[2,3], Kesu Chen[4], Mohamed Boutjdir[5,6,7] and Long Chen[1,8]*

[1]National Standard Laboratory of Pharmacology for Chinese Materia Medica, School of Pharmacy, Nanjing University of Chinese Medicine, Nanjing, China, [2]Dalian Institute of Chemical Physics, Dalian, China, [3]Chinese Academy of Sciences Biomedical Innovation Institute of China Medical City, Taizhou, China, [4]Department of Respiratory, Inpatient Wards for Senior Cadres, Nanjing General Hospital of Nanjing Military Command Region, Nanjing, China, [5]VA New York Harbor Healthcare System, New York, NY, United States, [6]State University of New York Downstate Medical Center, New York, NY, United States, [7]NYU School of Medicine, New York, NY, United States, [8]Institute of Chinese Medicine of Taizhou China Medical City, Taizhou, China

OPEN ACCESS

Edited by:
Ioanna Andreadou,
National and Kapodistrian University of Athens, Greece

Reviewed by:
Carla Cicala,
University of Naples Federico II, Italy
Scott M. MacDonnell,
Regeneron Pharmaceuticals, Inc., United States

***Correspondence:**
Long Chen
longchen@njucm.edu.cn

[†]These authors have contributed equally to this work

Specialty section:
This article was submitted to Experimental Pharmacology and Drug Discovery, a section of the journal Frontiers in Pharmacology

Received: 20 November 2018
Accepted: 22 February 2019
Published: 22 March 2019

Citation:
Huang H, Xie M, Gao L, Zhang W, Zhu X, Wang Y, Li W, Wang R, Chen K, Boutjdir M and Chen L (2019) Rolipram, a PDE4 Inhibitor, Enhances the Inotropic Effect of Rat Heart by Activating SERCA2a. Front. Pharmacol. 10:221. doi: 10.3389/fphar.2019.00221

This study was designed to investigate the hemodynamic effect of rolipram, a phosphodiesterase type 4 (PDE4) inhibitor, in normal rat hearts both *in vivo* and *in vitro* and its underlying mechanism. The pressure-volume loop, isolated heart, and Ca^{2+} transients triggered by field stimulation or caffeine were used to analyze the hemodynamic mechanism of rolipram. The results demonstrated that rolipram (3 mg/kg, ip) significantly increased the *in vivo* rat heart contractility by enhancing stroke work, cardiac output, stroke volume, end-systolic volume, end-diastolic volume, end-systolic pressure, heart rate, ejection fraction, peak rate of rise of left pressure ($+dp/dt_{max}$), the slopes of end-systolic pressure-volume relationship (slope of ESPVR) named as left ventricular end-systolic elastance, and reduced the slopes of end-diastolic pressure-volume relationship (slope of EDPVR). Meanwhile, the systolic blood pressure, diastolic blood pressure, and pulse pressure were significantly enhanced by rolipram. Also, rolipram deviated normal ventricular-arterial coupling without changing the arterial elastance. Furthermore, rolipram (0.1, 1, 10 μM) also exerted positive inotropic effect in isolated rat hearts by increasing the left ventricular development pressure, and $+dp/dt_{max}$ in non-paced and paced modes. Rolipram (10 μM) increased the SERCA2a activity, Ca^{2+} content, and Ca^{2+} leak rate without changing diastolic Ca^{2+} level. Rolipram had significant positive inotropic effect with less effect on peripheral vascular elastance and its underlying mechanism was mediated by increasing SERCA2a activity. PDE4 inhibition by rolipram resulted in a positive inotropic effect and might serve as a target for developing agents for the treatment of heart failure in clinical settings.

Keywords: PDE4, rolipram, P-V loop, Ca^{2+} transient, SERCA2a

INTRODUCTION

Over 60 cyclic nucleotide phosphodiesterase (PDE) isozymes have been grouped into 11 classes based on their hydrolysis substrates and biochemical features (Knight and Yan, 2012). Of the 11 PDE families, at least 7 members, which are PDE1, 2, 3, 4, 5, 8, and 9, appear to be expressed in the myocardium (Kim and Kass, 2017). PDE1, 2, and 3 hydrolyze both cAMP and cGMP, PDE4 and 8 hydrolyze cAMP only, and PDE5 and 9 only hydrolyze cGMP (Knight and Yan, 2012). Except PDE9, all other six members involve the cardiac physiological and pathological activities (Miller and Yan, 2010). PDE3 inhibitors which further stimulate the force or frequency of the heart have been serving as inotropic agents for treating acute heart failure (Miller and Yan, 2010). With an increased risk of mortality for the chronic use of PDE3 inhibitors, the interest for developing the PDE inhibitors as the treatment of chronic heart failure has been reduced in the mid-1990s (Eschenhagen, 2013). However, due to the many more PDE subtypes and their inhibitors that have been discovered, the interests for developing potential drugs targeting PDEs have been reignited (Eschenhagen, 2013). Specifically, the selective PDE5 inhibitors have been used for the treatment of erectile dysfunction and pulmonary hypertension, and a selective PDE4 inhibitor (roflumilast) was recently licensed for the treatment of chronic obstructive lung disease (Maurice et al., 2014). All these diseases treated by the selective PDE5 or PDE4 inhibitors are associated with increased cardiovascular risk (Eschenhagen, 2013). Meanwhile, the clinical and basic studies for treating heart failure based on targets of selective PDEs are still ongoing.

The small, highly diffusible molecule, cAMP exerts multiple, discrete receptor-specific responses in the same cells (Fertig and Baillie, 2018). Such multiple responses of cAMP are based on compartmentalization of cAMP signaling by restricting the number and identity of PKA-phosphorylated substrates (Zaccolo and Pozzan, 2002) and the fine control by the subcellular localization of PDEs that degrade cAMP (Fertig and Baillie, 2018). Among the six PDE families which are expressed in the myocardium, PDE4 appears to be predominantly in the heart (Eschenhagen, 2013). More than 20 isoforms belong to four different PDE4 genes, PDE4A, 4B, 4C, and 4D, with PDE4A, 4B, and 4D detected in the hearts (Kostic et al., 1997), with PDE4 and D5 interacting with β-arrestin (Bolger et al., 2003), PDE4B and 4D with the cardiac L-type Ca^{2+} channel (Leroy et al., 2011), PDE4B with ryanodine receptor (RyR) (Fertig and Baillie, 2018), PDE4D with SERCA2a (Beca et al., 2011), PDE4D3 with slow delayed rectifier potassium current I_{KS} channel (Terrenoire et al., 2009; Parks et al., 2014). The cellular integrated function of PDE4 is based on the distribution of the localized PDE4 subtypes and cAMP levels which are affected by adrenergic stimulation (Fertig and Baillie, 2018). Therefore, the functions of PDE4 in the myocardium may differ by sex (Parks et al., 2014), age (Park et al., 2012), species (Richter et al., 2011), cell types (Molina et al., 2014), and pathological status (Zheng et al., 2014).

The studies on cellular, biochemical, molecular, and structural changes in the heart tissue induced by PDE4 inhibitors have been extensively performed (Kim and Kass, 2017). The studies of non-selective PDE4 inhibitor on cardiac hemodynamics both *in vivo* and *in vitro* are still lacking. This study aimed at investigating the effects of rolipram, a PDE4 inhibitor, on the hemodynamics from both *in vivo* and isolated heart and the underlying cellular Ca^{2+} handling mechanism. In addition, the present study addresses the potential clinical benefit of PDE4 inhibitor for the treatment of heart failure and provides additional information for understanding the precise regulation of subtypes of PDE4 in the heart.

MATERIALS AND METHODS

Chemicals

Rolipram with a purity of more than 99.56% was purchased from MedChemExpress (MCE) in Shanghai (China) with the catalog number of HY-16900. All other chemicals were purchased from Sigma-Aldrich (USA). Rolipram was dissolved in DMSO at room temperature and used on the same day.

In vivo Left Ventricular and Arterial Hemodynamic Parameters Recording

The investigation conformed to the Guide for the Care and Use of Laboratory Animals published by the US National Institutes of Health (NIH publication No. 85-23, revised 1996). Male Sprague Dawley rats (300–350 g) (from the laboratory animal center of Nanjing University of Chinese Medicine) were used in this study. Experiments were performed as previously described (Li et al., 2017). Briefly, the rats were anesthetized by 20% urethane (5 ml/kg, ip) and their right carotid arteries were inserted with two pressure and volume microsensors' catheter (MILLAR, SPR-901, 840-8,188, Houston, USA) connected to a PowerLab 4/30 data acquisition system (AD Instruments, PowerLab4/30, Australia). The two pressure sensors at the microtip of catheter were placed in the aorta or left ventricle for each and used to measure the pressures of arterial or left ventricular pressures simultaneously. Rolipram (3 mg/kg) dissolved in DMSO less than 0.5 ml was injected intraperitoneally. DMSO (0.5 ml) had no measurable effects on the hemodynamic parameters studied. The control values were recorded after the hemodynamic parameters remained constant and before injection of rolipram. Rolipram's effects were recorded after all parameters reached constant values with usually longer than 30 min. The pressure and volume sensors in the left ventricle were set to analyze the pressure-volume relationship (P-V loop). The hemodynamic parameters were analyzed with Labchart 8 from AD Instruments including stroke work, cardiac output, heart rate, stroke volume, end-systolic volume, end-diastolic volume, end-systolic pressure, end-diastolic pressure, ejection fraction, and $+dp/dt_{max}$ (peak rate of rise of left ventricular pressure), Slope of linear regression' ESPVR (end-systolic pressure-volume relationship) which is also named as left ventricular end-systolic elastance, Slope of linear regression' EDPVR (end-diastolic

pressure-volume relationship). Furthermore, the systolic blood pressure, diastolic blood pressure, pulse pressure, arterial elastance which is the ratio of end-systolic pressure to stroke volume, and ventricular-arterial coupling were analyzed.

In vitro Intraventricular Pressure Recording From Isolated Rat Hearts

The selection and anesthesia of rats for *ex vivo* experiments were the same as that of *in vivo* experiment described above and the methods used were described previously (Li et al., 2017). Briefly, the hearts were then perfused in the Langendorff non-recirculating mode, at a perfusion pressure of 80 mmHg, with a perfusion solution (37°C) containing (in mM): NaCl 117, KCl 5.7, $CaCl_2$ 1.8, $MgCl_2$ 1.7, $NaHCO_3$ 4.4, NaH_2PO_4 1.5, HEPES 20, Glucose 11 gassed with 95% O_2 plus 5% CO_2 (pH 7.4 with NaOH). Rolipram was dissolved in DMSO and then transferred to perfusion solutions to reach the final concentrations of 0.1, 1, and 10 μM, respectively. The control perfusion solutions contained the same concentrations of DMSO as that in rolipram groups. During the experiments, these different concentrations of rolipram from low to high concentration order were added to the perfusion solution and infused *via* retrograde perfusion of the coronary artery. The hemodynamic parameters of control or rolipram (0.1, 1, 10 μM) were recorded when isolated heart contraction reached constant level with rolipram perfusions longer than 10 min for each concentration. Their intraventricular pressures under non-isovolumic condition of contraction were measured by a pressure and volume microtip catheter (MILLAR, SPR-901, 840-8,188, Houston, USA) inserted into the left ventricle *via* the left atrium. The hearts were beating spontaneously (non-paced) or stimulated at a rate of 4 Hz (paced). The paced isolated hearts were stimulated between left and right atrium at 5 V. Left ventricular developed pressure was calculated as the difference between the peak systolic pressure and end-diastolic pressure. Also, the heart rate only in non-paced setting and + dp/dt_{max} were calculated.

Ca^{2+} Transient Recording of Adult Rat Left Ventricular Myocytes Triggered by Field Stimulation

For isolation of adult rat left ventricular myocytes, the rat ventricular myocytes were obtained by enzymatic dissociation as previously described (Li et al., 2017). The excised whole heart was first perfused at 37°C with a perfusion solution (37°C) containing (in mM): NaCl 117, KCl 5.7, $CaCl_2$ 1.8, $MgCl_2$ 1.7, $NaHCO_3$ 4.4, NaH_2PO_4 1.5, HEPES 20, Glucose 11 gassed with 95% O_2 plus 5% CO_2 (pH 7.4 with NaOH). The heart was then perfused with the same buffer with the addition of 2.0 mg/ml collagenase type II and 0.1 mg/ml Protease Type for 50 min. Following removal of both atria and the right ventricle, the left ventricular myocytes were gently separated with forceps in the buffer without collagenase. Rod-shaped non-contracting cells with clear striations were used.

For Ca^{2+} transient recording triggered by field stimulation, adult rat left ventricular myocytes were loaded with the membrane-permeable acetoxymethyl ester form of the fluorescent Ca^{2+} indicator Fluo-4 AM (5 μM) for 30 min at 37°C. Fluo-4 was excited at 488 nm (Lambda DG-4, Sutter instruments, USA) and emitted fluorescence measured with a 515-nm-long pass filter. The region of interest was restricted to a single cell with the aid of an adjustable window. The Ca^{2+} transient amplitudes were calculated as a difference of the peak and diastolic fluorescent values. Background fluorescence levels were used to correct raw fluorescence data. Ca^{2+} spark fluorescent intensity of Fluo-4 loaded in myocytes was recorded at imaging frequency of 100 Hz during electrical pacing (1 Hz, 15 V, alternating polarities) with two platinum electrodes. The extracellular solution contained (in mM): NaCl 117, KCl 5.7, $NaHCO_3$ 4.4, $MgCl_2$ 1.7, HEPES 20, Glucose 20, Taurine 20, $CaCl_2$ 1.8, pH 7.4 with NaOH. After the constant imaging of control was recorded, rolipram (10 μM) in the extracellular solution was perfused for longer than 5 min and then its constant Ca^{2+} transient effect was recorded. Images were recorded with an ANDOR ZYLA-5.5-CL3 CCD camera (AndorTechnologe, EU) connected to an inverted microscope (Olympus IX53, Olympus, Tokyo, Japan) that was synchronized by a real-time analog-digital processor unit and Meta fluor acquisition software (64-bit, version 7.8.10.0, Molecular Device, USA).

The decaying phase of Ca^{2+} transient involves two components, which are a fast component dominated by sarcoplasmic reticulum (SR) Ca^{2+}-ATPase type 2a (SERCA2a) and slow component dominated mainly by Na^+/Ca^{2+} exchanger (NCX) and sarcolemmal Ca^{2+}-ATPase (PMCA). Isolation of two components was analyzed by the theory and method of plasma concentration-time curve with two exponential fitting following intravenous administration of a drug in human.

Functional Isolations of Na^+/Ca^{2+} Exchanger (NCX) and Sarcolemmal Ca^{2+}-ATPase (PMCA) From the Decaying Phase of Caffeine-Evoked Ca^{2+} Transients

The decaying phase of Ca^{2+} transient by field stimulation is mediated mainly by SERCA2a, NCX, and PMCA. The NCX and PMCA control the decaying phase of caffeine-evoked Ca^{2+} transient in normal Tyrode's solution (NT) in which caffeine prevents the effect of SERCA2a on SR Ca^{2+} concentration gradient formation by widely opening RyR2. Also, PMCA function can be isolated from decaying phase of the caffeine-evoked Ca^{2+} transient in the condition of Na^+, Ca^{2+}-free solution which deactivates NCX activity. The rate constants of decline of caffeine-evoked Ca^{2+} transient in normal Tyrode's solution and Na^+, Ca^{2+}-free solution were used to analyze the functions of mixed NCX plus PMCA and PMCA alone. The detailed methods were previously described (Choi and Eisner, 1999; Maczewski and Mackiewicz, 2008; Schulte et al., 2016). Briefly, immediately after stopping the field stimulation when the steady Ca^{2+} transient was obtained, caffeine (20 mM) was perfused to myocytes in normal Tyrode's solution to obtain the decaying rate constant of combined activity of NCX and PMCA. To

calculate the decaying rate constant of PMCA alone, Ca^{2+} leak rate, and Ca^{2+} content, Na^+,Ca^{2+}-free solution was perfused before caffeine (20 mM) perfusion. The normal Tyrode's solution contained (in mM): NaCl 134, KCl 4, $MgCl_2$ 1, HEPES 10, Glucose 11, $CaCl_2$ 1, adjusted to pH 7·4 with NaOH. The Na^+, Ca^{2+}-free solution contained (in mM): LiCl 130, HEPES 10, Glucose 11, $MgCl_2$ 1, KCl 4, adjusted to pH 7.4 with KOH. For control experiment, normal Tyrode's solution was used to record functional isolations of NCX and PMCA. Rolipram (10 μM) was added to recording chamber for at least 10 minutes to maximize its effects on NCX and PMCA. The effects of control or rolipram on combined function of NCX plus PMCA or PMCA only were performed in different group cells and *t*-test was used to analyze significant differences.

Statistical Analyses

All values are expressed as mean ± SEM. *t*-test and one-way ANOVA were used as appropriate and data analysis was performed using SPSS 11.0. Differences with $p < 0.05$ were deemed statistically significant.

TABLE 1 | Pressure-volume relationship analysis in normal and rolipram (3 mg/kg) treated anesthetized rats.

Kinetic parameters	Control	Rolipram
Stroke work (mmHg μl)	5,970 ± 168.2	9,664 ± 214.4*
Cardiac output (μl/min)	20,260 ± 538.6	32,442 ± 819.2*
Stroke volume (μl)	68 ± 0.7	88 ± 1.0*
end-systolic volume (μl)	79 ± 1.3	46 ± 2.7*
end-diastolic volume (μl)	147 ± 1.7	133 ± 3.7*
end-systolic pressure (mmHg)	88 ± 2.0	110 ± 2.5*
end-diastolic pressure (mmHg)	2.8 ± 0.1	2.5 ± 0.3
Heart rate (bpm)	298 ± 6.9	370 ± 5.8*
Ejection fraction (%)	46 ± 0.4	66 ± 1.1*
$+dP/dt_{max}$ (mmHg/s)	4,306 ± 327.8	9,005 ± 756.7*
Slope of ESPVR (Ees)	1.246 ± 0.030	1.699 ± 0.031*
Slope of EDPVR	0.108 ± 0.010	0.080 ± 0.008*

*$+dp/dt_{max}$, Peak rate of rise of left pressure; Slope of ESPVR, the slopes of end-systolic pressure-volume relationship or left ventricular end-systolic elastance (Ees); Slope of EDPVR, the slopes of end-diastolic pressure-volume relationship; mean ± SEM, n = 6. *p < 0.05 vs respective control. All parameters for rolipram were under condition of intraperitoneal injection except Ees and slope of EDPVR for rolipram by intravenous injection.*

RESULTS

Rolipram Increased Left Ventricular Inotropy of Rat Heart *in vivo*

To examine the hemodynamic effects of rolipram on the rat heart and peripheral vessels, the pressure-volume loop (P-V loop) technique was used to measure the left ventricular pressure-volume and aortic pressure simultaneously. Rolipram (3 mg/kg, ip) significantly enhanced the stroke work, cardiac output, stroke volume, end-systolic pressure, heart rate, ejection fraction, and $+dp/dt_{max}$, and decreased the end-systolic volumes, end-diastolic volume compared with control ($p < 0.05$, $n = 6$) without significantly changing end-diastolic pressure. Also, the slope of ESPVR (Ees) was increased and the slope of EDPVR was reduced as shown in **Table 1**. **Figure 1** shows the representative original simultaneous recordings of the left ventricular pressure, volume, and aortic pressure and the derivative relationship of P-V loop. The higher and wider P-V loop induced by rolipram indicates increased left ventricular pressure and stroke volume. Moreover, the steeper slope of ESPVR (Ees) induced by rolipram indicates the increased contractile function which is independent of preload. The smoother slope of EDPVR reflects decreased diastolic stiffness compared with control as shown in **Figure 2**. The arterial hemodynamic effective changes indicated that rolipram increased the systolic blood pressure, diastolic blood pressure, and pulse pressure as shown in **Table 2**. Moreover, rolipram decreased the ventricular-arterial coupling, indicating rolipram had inotropic effect without significant arterial elastance change. **Figure 3**

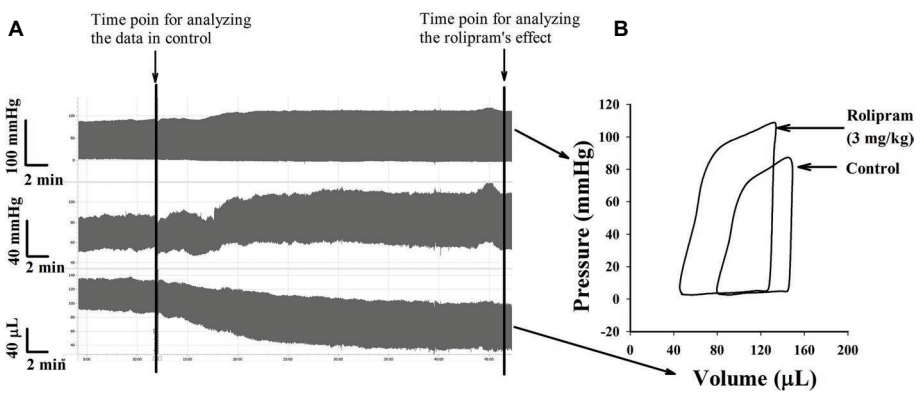

FIGURE 1 | (A) Original simultaneous recordings of left ventricular pressure, aortic blood pressure and left ventricular volume versus time before and after rolipram (3 mg/kg, ip) to an anesthetized rat. **(B)** The derivative steady-state P-V loops of left ventricular pressure versus its volume before and after rolipram (3 mg/kg, ip) at marked time points.

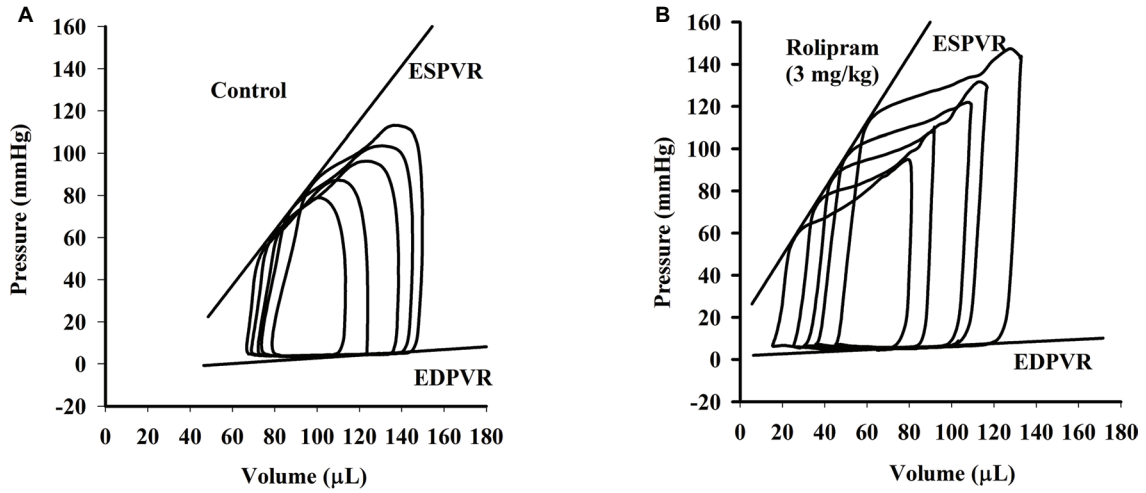

FIGURE 2 | The continuous multi P-V loops' recordings when the rat inferior vena cava was blocked before **(A)** and after **(B)** intravenous injection of rolipram (3 mg/kg) to an anesthetized rat. The slope of ESPVR is formatted by linear regression of multi end-systolic pressures and the slope of EDPVR by linear regression of multi end-diastolic pressures.

TABLE 2 | Effects of rolipram (3 mg/kg, ip)on aortic blood pressure and ventricular-arterial coupling in anesthetized rats.

Kinetic parameters	Control	Rolipram
Systolic blood pressure (mmHg)	90 ± 2.4	116 ± 1.8*
Diastolic blood pressure (mmHg)	48 ± 1.4	61 ± 3.3*
Pulse pressure (mmHg)	42 ± 2.6	55 ± 2.3*
Ea (mmHg/μl)	1.292 ± 0.027	1.264 ± 0.036
Ea/Ees	1.041 ± 0.037	0.746 ± 0.032*

Ea, arterial elastance; Ea/Ees: Ventricular-arterial coupling; mean ± SEM, n = 6.
**p < 0.05 vs respective control.*

shows the simultaneous recordings of rat left ventricular and aortic pressure versus time course.

Rolipram Increased Left Ventricular Inotropy of Isolated Rat Hearts

To further investigate the direct effect of rolipram on the heart, the isolated non-paced and paced rat hearts were used to analyze the inotropic and chronotropic effects of rolipram. The pacing was used to rule out the frequency-induced inotropic effect and 4-Hz pacing was chosen to match the non-paced heart rate as shown in **Figure 4**. As documented in **Table 3**,

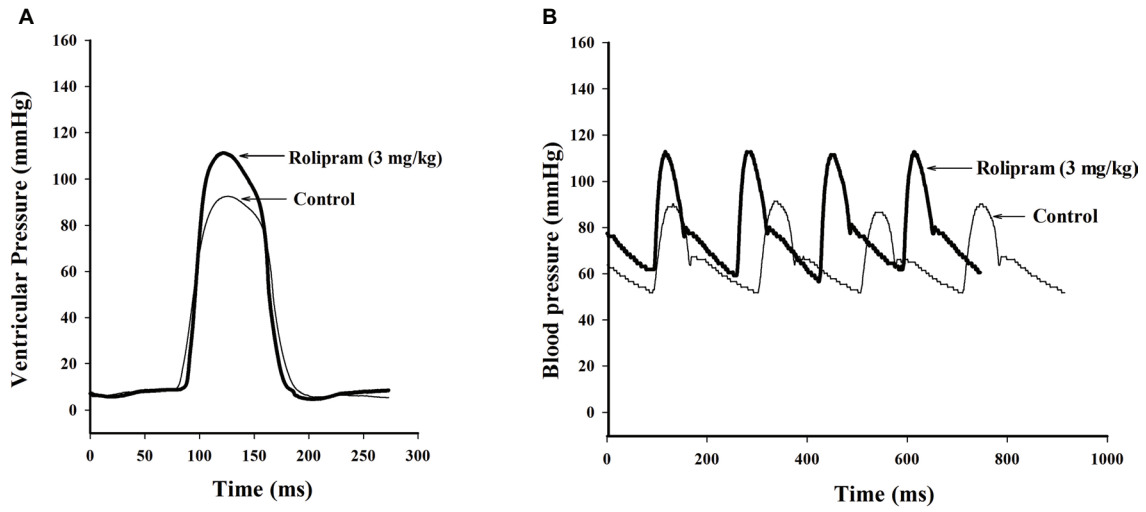

FIGURE 3 | Original simultaneous recordings of left ventricular pressures **(A)** and aortic blood pressures **(B)** versus time course before and after rolipram (3 mg/kg, ip) to an anesthetized rat.

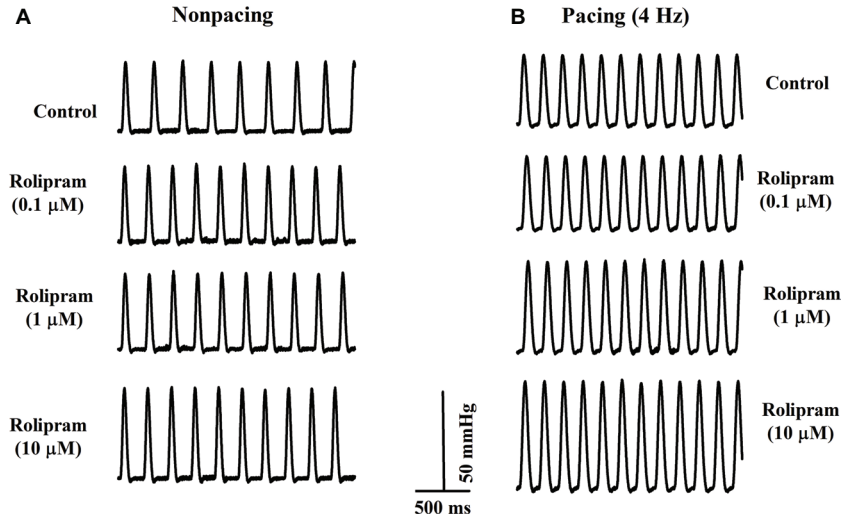

FIGURE 4 | Representative rat left ventricular pressure curves from the isolated rats in non-paced **(A)** and paced modes **(B)** before and after perfusion of rolipram (0.1, 1, 10 μM) with the same concentrations of DMSO.

TABLE 3 | Effects of rolipram in isolated rat hearts in the conditions of nonpacing and pacing modes.

	Nonpacing			Pacing (4 Hz)		
	LVDP (mmHg)	HR (bpm)	+dp/dt$_{max}$ (mmHg/s)	LVDP (mmHg)	HR (bpm)	+dp/dt$_{max}$ (mmHg/s)
Control	39 ± 2.3	177 ± 3.6	991 ± 21.0	38 ± 2.4	240	1,230 ± 24.7
Rolipram (0.1 μM)	42 ± 2.1*	189 ± 4.1*	1,027 ± 35.8	44 ± 2.6*	240	1,308 ± 34.4*
Rolipram (1 μM)	42 ± 2.3*	192 ± 3.8*	1,061 ± 34.9*	48 ± 2.4*#	240	1,465 ± 26.4*#
Rolipram (10 μM)	47 ± 2.9*#△	200 ± 4.1*#△	1,132 ± 35.8*#△	52 ± 2.2*#	240	1,655 ± 28.5*#△

*LVDP: left ventricular developed pressure; HR: heart rate; +dP/dt$_{max}$: peak rate of rise of left ventricular pressure. Rolipram was dissolved in DMSO before reaching the desired concentrations and control perfusion solution also contained the same concentration of DMSO as that in rolipram groups. Data are expressed as Mean ± SEM, n = 6. *p < 0.05 vs control; #p < 0.05 vs 0.1 μM groups; △p < 0.05 vs 1 μM groups in non-paced and paced modes respectively.*

TABLE 4 | Kinetic analysis of rolipram's effecton Ca^{2+} transient induced by field stimulation in left ventricular myocytes.

Kinetic parameters	Control	Rolipram (10 μM)
$I_{baseline}$ (%)	100 ± 3.5	102 ± 1.3
$\Delta I_{amplitude}$ (%)	100 ± 6.0	112 ± 2.9*
α	5.20 ± 0.32	6.35 ± 0.83*
β	0.30 ± 0.03	0.26 ± 0.03*

*$I_{baseline}$(%): Normalized baseline fluorescence intensity of Ca^{2+} transient as 100% in control; $\Delta I_{amplitude}$ (%); Normalized fluorescence intensity amplitude of Ca^{2+} transient as 100% in control; α: rate constants of fast component mediated by SERCA2a activityin decaying phase of Ca^{2+} transient; β: rate constants of slow component mediated by NCX and PMCA activities in decaying phase of Ca^{2+} transient. Data are expressed as Mean ± SEM, Paired t-test was used, *p < 0.05 compared with their respective controls, n = 6.*

rolipram (0.1, 1, 10 μM) increased the left ventricular developed pressure, heart rate, and +dp/dt$_{max}$ in non-paced mode in a concentration-dependent manner. In paced mode, rolipram (0.1, 1, 10 μM) also increased in a concentration-dependent manner the left ventricular developed pressure and +dp/dt$_{max}$ with a fixed heart rate of 240 beats per min.

Rolipram Enhanced the Ca^{2+} Uptake of Field Stimulation-Induced Ca^{2+} Transient by Facilitating SERCA2a Activity

Rolipram (10 μM) significantly enhanced the amplitude of Ca^{2+} transient from rat left ventricular myocytes without changing the diastolic baseline fluorescence intensity (proportional to cytoplasmic Ca^{2+} level) as shown in **Table 4**. The separated decaying phases were fitted by two exponential equations according to method of plasma concentration-time curve fitting following intravenous administration of a drug in human. The representative fitting curves with fast and slow components are presented in **Figure 5**. Rolipram (10 μM) remarkably enhanced the fast component rate constant (α) and decreased the slow component rate constant (β) as shown in **Table 4**, indicating that rolipram enhanced SERCA2a activity and reduced the combined activity of NCX and PMCA.

Rolipram Had No Direct Effects on Combined NCX and PMCA Activities in Caffeine-Induced Ca^{2+} Transient

To further analyze the decreased rate constant of NCX and PMCA activities in field stimulation-induced Ca^{2+} transient,

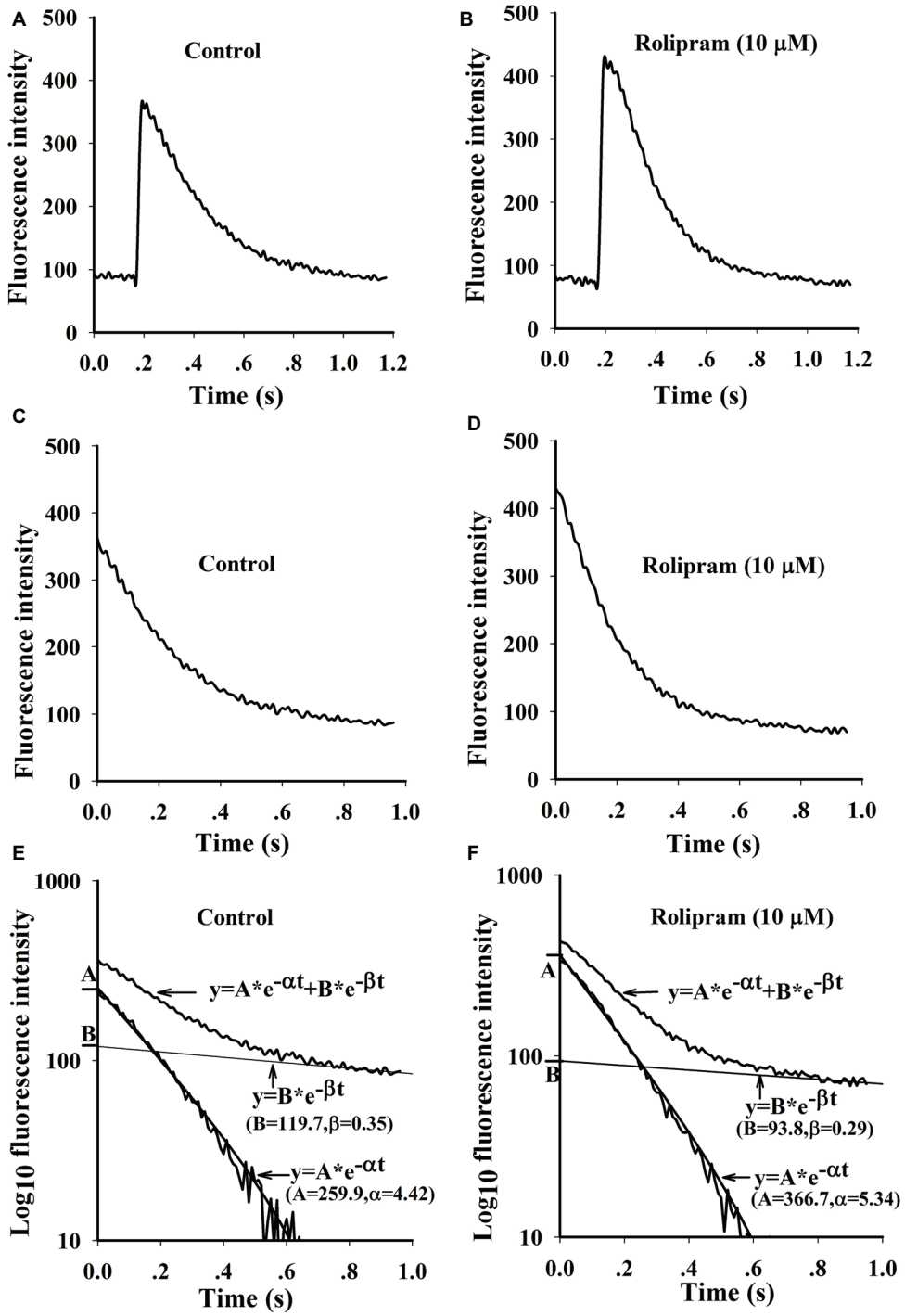

FIGURE 5 | Representative curves of Ca^{2+} transients induced by field stimulation and the fittings by two exponential equations. **(A** and **B)** are original Ca^{2+} transient curves triggered by field stimulation before and after rolipram (10 μM). **(C** and **D)** are decaying phase curves of Ca^{2+} transients by deleting the fast rise phase before and after rolipram (10 μM). The decay phase curves and fittings are presented as the relationships of timing of ms in X axis to the $\log_{10}$ fluorescence intensities in Y axis before **(E)** and after rolipram (10 μM) **(F)**. The decaying phases are expressed as an equation of $y = A^*e^{-\alpha t} + B^*e^{-\beta t}$. The equation in fast component is described as $y = A^*e^{-\alpha t}$ and slow one as $y = B^*e^{-\beta t}$.

caffeine-induced Ca^{2+} transient experiment was performed. In this condition, SERCA2a activity was abolished due to the opening of RyR2 by caffeine and the decaying phase mainly was mediated by NCX and PMCA. The result in **Figure 6A** shows that rolipram (10 μM) did not significantly change the rate constant of combined activity of NCX and PMCA ($r_{NCX + PMCA}$)

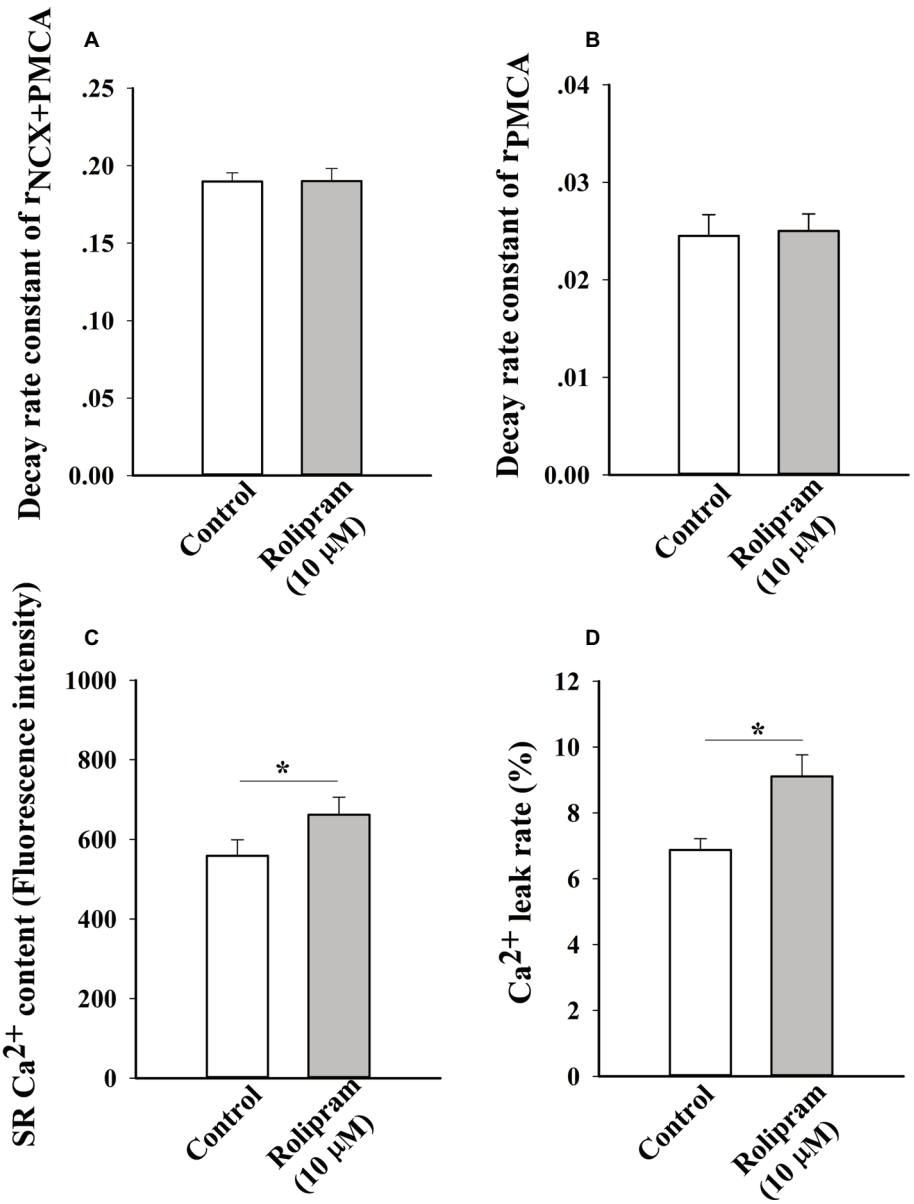

FIGURE 6 | The histograms show the statistical results of decaying rate constants of Ca^{2+} extrusion by combined activity of NCX and PMCA **(A)**, PMCA alone **(B)**, Ca^{2+} contents **(C)** and Ca^{2+} leak rates of real leak value to Ca^{2+} content **(D)**. The *t*-test was used to analyze the data in control and rolipram-treated rat left ventricular myocytes. *$p < 0.05$ vs respective control, $n = 11$ for all groups.

from 0.190 ± 0.006 in control to 0.190 ± 0.008 ($p < 0.05$, $n = 11$). The representative curves of caffeine-induced Ca^{2+} transients in normal Tyrode's solution before and after rolipram (10 μM) injection are shown in **Figure 7**.

Rolipram Increased the Diastolic Ca^{2+} Leak Rate and SR Ca^{2+} Content Without Direct Effect on PMCA Activity in Caffeine-Induced Ca^{2+} Transient

To further isolate the activity of PMCA by rolipram from combined activity of NCX and PMCA, the Na^+ and Ca^{2+}-free extracellular solution was used to block the activity of NCX. In this condition, the Ca^{2+} transient decaying phase is mainly mediated by PMCA. Rolipram (10 μM) had no effect on PMCA activity based on insignificant rate constant (r_{PMCA}) change from 0.025 ± 0.002 in control to 0.025 ± 0.002 ($p < 0.05$, $n = 11$) as shown in **Figure 6B**. However, rolipram (10 μM) significantly increased SR Ca^{2+} content from 559.0 ± 40.2 in control to 662.0 ± 44.2 (**Figure 6C**) ($p < 0.05$, $n = 11$) and enhanced the diastolic Ca^{2+} leak rate from 6.9% ± 0.3 in control to 9.1% ± 0.7 (**Figure 6D**) ($p < 0.05$, $n = 11$). The representative Ca^{2+} transient curves induced by caffeine in Na^+ and Ca^{2+}-free extracellular solution are presented in **Figure 8**.

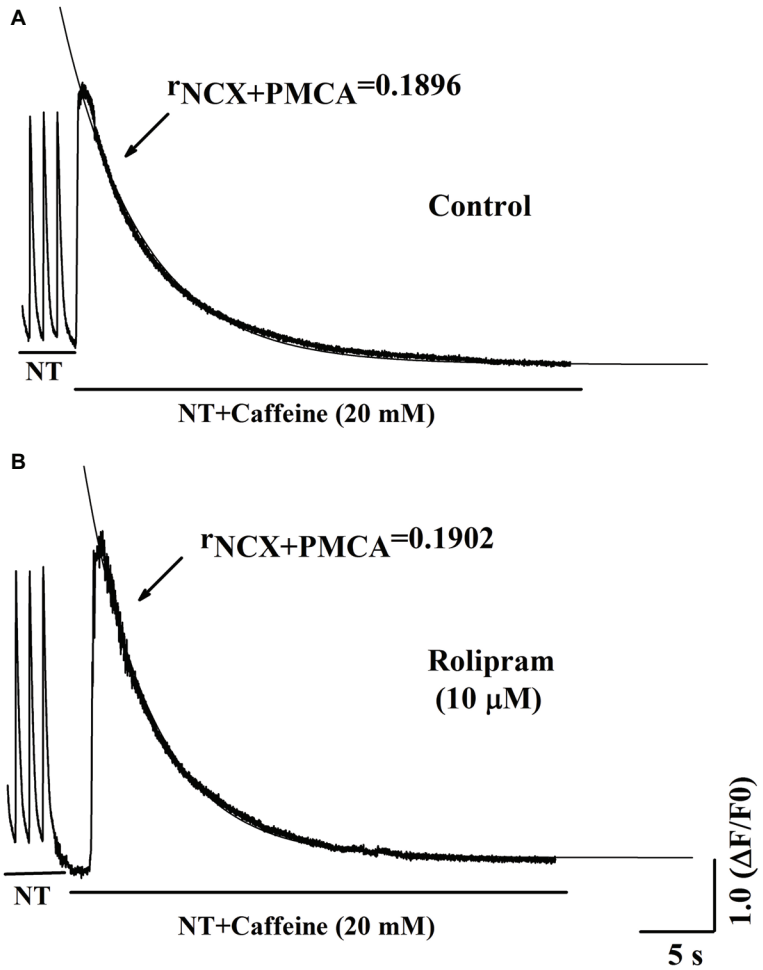

FIGURE 7 | Representative curves of Ca^{2+} transient induced by caffeine in normal Tyrode's solution (NT) before **(A)** and after **(B)** rolipram (10 μM). The $r_{NCX+PMCA}$ is presented as decaying phase rate constant which is dominated by combined activity of NCX and PMCA to extrude Ca^{2+} to outside cell.

DISCUSSION

Three subtypes of PDE4 (PDE4A, B, D) are expressed in rat heart (Fertig and Baillie, 2018). Although their fundamental mechanism involving hydrolysis of cAMP is clear, their functions, especially *in vivo*, are not dissected due to their differential compartment distribution and basal level of hydrolysis substrates (Miller and Yan, 2010). In this P-V loop study, we underlined that rolipram, a PDE4 inhibitor, significantly increased the rat heart rate and contractility based on its enhanced end-systolic left ventricular pressure, stroke volume, cardiac output, ejection fraction, slope of ESPVR, and reduced end-systolic volume. Meanwhile, rolipram increased the systolic, diastolic blood pressure and pulse pressure without changing the arterial elastance which is proportional to the peripheral vascular resistance. Rolipram mismatched the rat normal ventricular-arterial coupling by reducing the normal value in control to the low level indicating that rolipram exerted positive inotropy with insignificant vascular effect in normal rats. However, the decreased effect on ventricular-arterial coupling by rolipram might be beneficial in heart failure of rats which have higher value of ventricular-arterial coupling (Cheng et al., 2008; Ky et al., 2013).

The *in vivo* positive inotropic effect of rolipram is under the condition of basal β-adrenergic tension by neurohumoral regulation. To elucidate whether this positive inotropic effect is independent of basal β-adrenergic stimulation, the isolated rat heart perfusion experiment was used. The results demonstrated that rolipram significantly enhanced rat left ventricular developed pressure, heart rate, and $+dp/dt_{max}$ *in vitro* in a concentration-dependent manner. This effect occurred in both non-paced and paced models, and was independent of heart rate as reported (Beca et al., 2011). The increased inotropy by rolipram indicated that there is intrinsic cAMP content which exists in subcellular compartmentation independent of β-adrenergic stimulation.

To investigate the mechanism underlying the positive inotropic effect, the Ca^{2+} transient recording of rat left ventricular myocyte was used to analyze the effect of rolipram on Ca^{2+} handling. Ca^{2+} transient is composed of a fast rise phase mediated by Ca^{2+} release from SR to cytoplasm *via* RyR2 and a recovery

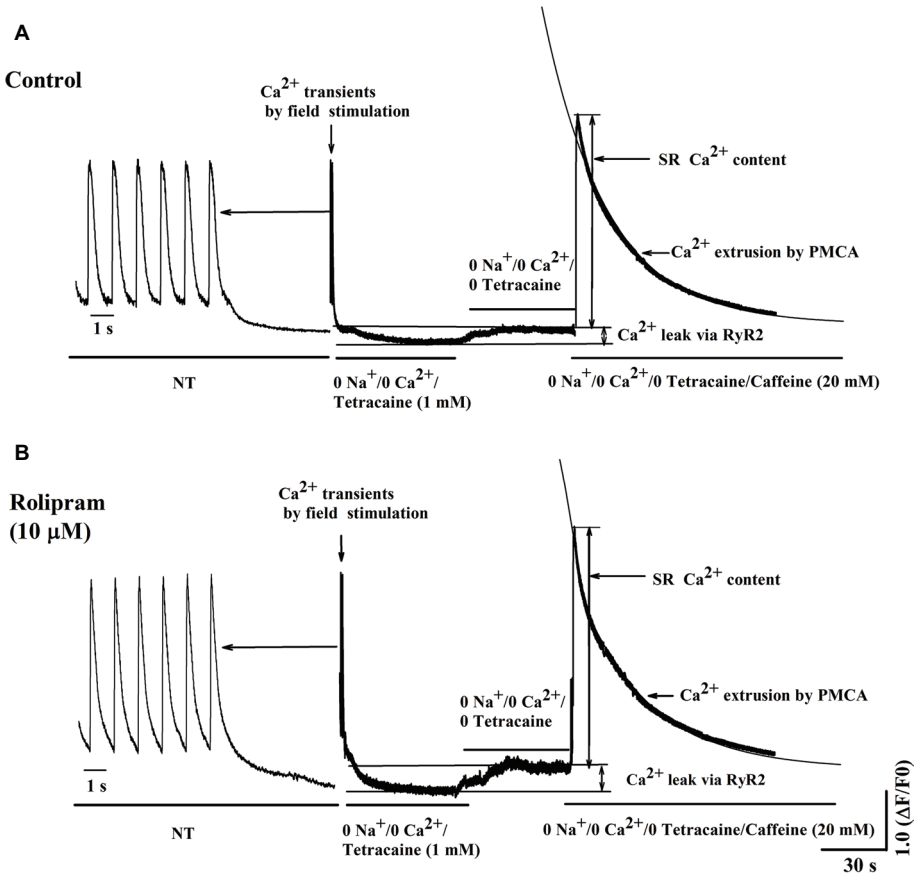

FIGURE 8 | Representative curves of Ca^{2+} leak, SR Ca^{2+} content, and Ca^{2+} transient induced by caffeine before **(A)** and after **(B)** rolipram (10 μM) in the conditions of Na^{+} and Ca^{2+}-free extracellular solution following steady field stimulation-induced Ca^{2+} transient in normal Tyrode's solution (NT). The r_{PMCA} is presented as decaying phase rate constant which is dominated by activity of PMCA alone to extrude Ca^{2+} to outside cell.

phase or decaying phase by mainly re-uptaking Ca^{2+} from cytoplasm to SR *via* SERCA2a and extruding Ca^{2+} from cytoplasm to outside cell *via* NCX and PMCA. Rolipram increased the amplitude of Ca^{2+} transient induced by field stimulation without changing the diastolic Ca^{2+} level. The shape and amplitude of Ca^{2+} transient are determined mainly by RyR2, SERCA2a, NCX, and PMCA. First, the decaying phase was fitted by two exponential equations of type $y = A^{*}e^{-\alpha t} + B^{*}e^{-\beta t}$, which follows the method of concentration-time curve fitting following intravenous administration of a drug in human. The decaying phase fast component rate constant of "α" represents the activity of SERCA2a and slow one of "β" represents the activity of combined NCX and PMCA. Rolipram significantly increased the SERCA2a activity and decreased the combined NCX and PMCA activity based on their decaying rate constants' changes. Second, to isolate the decreased activities of NCX and PMCA by rolipram in field stimulation-induced Ca^{2+} transient, caffeine-induced Ca^{2+} transient experiments which inactivate SERCA2a activity were used in conditions of normal Tyrode's solution or Na^{+} and Ca^{2+}-free extracellular solution. The results indicated that rolipram failed to change the rate constants of activities of combined NCX and PMCA or PMCA alone. This result apparently differed from the fitting data in field stimulation-induced Ca^{2+} transient experiment in which rolipram reduced the combined activities of NCX and PMCA. The discrepancy might be due to that the robust increased SERCA2a activity compressed the abilities of NCX and PMCA to extrude the Ca^{2+} to outside cell during the relaxation in field stimulation-induced Ca^{2+} transient and the direct effect of rolipram on activities of NCX and PMCA in caffeine-induced Ca^{2+} transient remained unchanged. This explanation also helps to understand the mechanism underlying the increased SR Ca^{2+} content by rolipram, in which SERCA2a re-uptaked more Ca^{2+} into to SR by rolipram and passively reduced Ca^{2+} extrusion to outside cell *via* NCX and PMCA by reducing cytoplasmic diastolic Ca^{2+} concentration without enhancing Ca^{2+} entry from outside cell *via* L-type Ca^{2+} channel (Kerfant et al., 2007; Beca et al., 2011). Third, rolipram enhanced the Ca^{2+} leak rate in the caffeine-induced Ca^{2+} transient experiment. However, diastolic Ca^{2+} level was not changed in field stimulation-induced Ca^{2+} transient experiment. The balancing effects by enhanced re-uptaking function of SERCA2a and increased Ca^{2+} leak might explain these data. The Ca^{2+} leak occurs during the relaxation period and is easily measured by caffeine-induced Ca^{2+} transient experiment in the condition of inactivating SERCA2a (caffeine widely opens RyR2 and make SR membrane has no effect on

building Ca^{2+} concentration gradient) and NCX (0 Na^+ and 0 Ca^{2+} were added to external solution to abolish NCX activity). However, RyR2 activity which mediates the Ca^{2+} transient rise phase was not analyzed due to the limitation in this study with slow sampling of 10 ms. Even though, the peak shape of field stimulation induced-Ca^{2+} transient demonstrated that there was a sharp peak in control and a blunt one in rolipram-treated groups (data was not shown). The peak shape is determined by decay "tail" RyR2 Ca^{2+} release, Ca^{2+} leak, and start of SERCA2a activity. The underlying mechanism still needs further investigation. Many studies have reported that PDE4 inhibition increased the PLB phosphorylation which enhances the activity of SERCA2a and RyR2 phosphorylation level (Kerfant et al., 2007). Moreover, the inhibition of PDE4 by rolipram increased the NCX current which was used to determine the Ca^{2+} content of cytoplasm (Kerfant et al., 2007; Beca et al., 2011). In our study, we measured the combined rate constant of NCX and PMCA activities and not NCX current. Furthermore, the direct effect of rolipram on NCX might be not equal to one in the global effect with the involvement of SERCA2a.

Although this study addressed the inotropic effects of rolipram both in *in vivo* and *in vitro* and its underlying mechanism was mediated by enhancing the SERCA2a activity, however, there are still a few limitations in this study. First, PDE4 constitutes a large fraction of the total PDE activity in rodent heart than in human heart (Eschenhagen, 2013), suggesting the data in this study should be applied to humans cautiously. Secondly, the mechanism of enhanced SERCA2a activity by rolipram still needs to be further explored, such as involvement with p-phospholamban mediated by PKA, CaMKII, protein phosphatase, etc.

In conclusion, rolipram, a PDE4 inhibitor, exerted positive inotropic effect both *in vivo* and *in vitro* without insignificant peripheral arterial elastance, which resulted in the mismatched ventricular-arterial coupling in normal rats. The inotropic effect was mediated by Ca^{2+} handling in which rolipram enhanced SERCA2a activity and Ca^{2+} leak and reduced NCX and PMCA activities. However, rolipram had no direct effects on rate constants of NCX and PMCA. These results indicated that this PDE4 inhibitor may serve as a potential positive inotropic agent for the treatment of heart failure.

DATA AVAILABILITY

This manuscript contains previously unpublished data. The name of the repository and accession number are not available.

AUTHOR CONTRIBUTIONS

LC, HH, and MX contributed to study design. WL, RW, and KC carried out literature research. HH, MX, LG, WZ, XZ, and YW performed experiments. HH and MX contributed to data analysis and photographs analysis. LC contributed to manuscript preparation, and MB contributed to manuscript revision.

FUNDING

This study was supported by "113 Talent Project" of the Fourth Round High Level Innovation Program in Taizhou China Medical City (2016024), and National Natural Science Foundation of China (81573304).

REFERENCES

Beca, S., Helli, P. B., Simpson, J. A., Zhao, D., Farman, G. P., Jones, P., et al. (2011). Phosphodiesterase 4D regulates baseline sarcoplasmic reticulum Ca^{2+} release and cardiaccontractility, independently of L-type Ca^{2+} current. *Circ Res.* 109, 1024–1030. doi: 10.1161/CIRCRESAHA.111.250464

Bolger, G. B., McCahill, A., Huston, E., Cheung, Y. F., McSorley, T., Baillie, G. S., et al. (2003). The unique amino-terminal region of the PDE4D5 cAMP phosphodiesterase isoform confers preferential interaction with beta-arrestins. *J. Biol. Chem.* 278, 49230–49238. doi: 10.1074/jbc.M303772200

Cheng, H. M., Yu, W. C., Sung, S. H., Wang, K. L., Chuang, S. Y., and Chen, C. H. (2008). Usefulness of systolic time intervals in the identification of abnormal ventriculo-arterial coupling in stable heart failure patients. *Eur. J. Heart Fail.* 10, 1192–1200. doi: 10.1016/j.ejheart.2008.09.003

Choi, H. S., and Eisner, D. A. (1999). The role of sarcolemmal Ca^{2+}-ATPase in the regulation of resting calcium concentration in rat ventricular myocytes. *J. Physiol.* 515, 109–118. doi: 10.1111/j.1469-7793.1999.109ad.x

Eschenhagen, T. (2013). PDE4 in the human heart–major player or little helper? *Br. J. Pharmacol.* 169, 524–527. doi: 10.1111/bph.12168

Fertig, B. A., and Baillie, G. S. (2018). PDE4-mediated cAMP signalling. *J. Cardiovasc. Dev. Dis.* 5:E8. doi: 10.3390/jcdd5010008

Kerfant, B. G., Zhao, D., Lorenzen-Schmidt, I., Wilson, L. S., Cai, S., Chen, S. R., et al. (2007). PI3K gamma is required for PDE4, not PDE3, activity in subcellular microdomains containing the sarcoplasmic reticular calcium ATPase in cardiomyocytes. *Circ. Res.* 101, 400–408. doi: 10.1161/CIRCRESAHA.107.156422

Kim, G. E., and Kass, D. A. (2017). Cardiac phosphodiesterases and their modulation for treating heart disease. *Handb. Exp. Pharmacol.* 243, 249–269. doi: 10.1007/164_2016_82

Knight, W. E., and Yan, C. (2012). Cardiac cyclic nucleotide phosphodiesterases: function, regulation, and therapeutic prospects. *Horm. Metab. Res.* 44, 766–775. doi: 10.1055/s-0032-1321870

Kostic, M. M., Erdogan, S., Rena, G., Borchert, G., Hoch, B., Bartel, S., et al. (1997). Altered expression of PDE1 and PDE4 cyclic nucleotide phosphodiesterase isoforms in 7-oxo-prostacyclin-preconditioned rat heart. *J. Mol. Cell. Cardiol.* 29, 3135–3146. doi: 10.1006/jmcc.1997.0544

Ky, B., French, B., May Khan, A., Plappert, T., Wang, A., Chirinos, J. A., et al. (2013). Ventricular-arterial coupling, remodeling, and prognosis in chronic heart failure. *J. Am. Coll. Cardiol.* 62, 1165–1172. doi: 10.1200/JOP.18.00027

Leroy, J., Richter, W., Mika, D., Castro, L. R., Abi-Gerges, A., Xie, M., et al. (2011). Phosphodiesterase 4B in the cardiac L-type Ca^{2+} channel complex regulates Ca^{2+} current and protects against ventricular arrhythmias in mice. *J. Clin. Invest.* 121, 265126–265161. doi: 10.1172/JCI44747

Li, S., Huang, H., Zhang, M., Wang, W., Xue, S., Gao, Y., et al. (2017). Liguzinediol enhances the inotropic effect of rat hearts via inhibition of protein phosphatase (PP1 and PP2A) activities. *J. Cardiovasc. Pharmacol.* 69, 236–244. doi: 10.1097/FJC.0000000000000467

Maczewski, M., and Mackiewicz, U. (2008). Effect of metoprolol and ivabradine on left ventricular remodeling and Ca^{2+} handling in the post-infarction rat heart. *Cardiovasc. Res.* 79, 42–51. doi: 10.1093/cvr/cvn057

Maurice, D. H., Ke, H., Ahmad, F., Wang, Y., Chung, J., and Manganiello, V. C. (2014). Advances in targeting cyclic nucleotide phosphodiesterases. *Nat. Rev. Drug Discov.* 13, 290–314. doi: 10.1038/nrd4228

Miller, C. L., and Yan, C. (2010). Targeting cyclic nucleotide phosphodiesterase in the heart: therapeutic implications. *J. Cardiovasc. Transl. Res.* 3, 507–515. doi: 10.1038/nrd4228

Molina, C. E., Johnson, D. M., Mehel, H., Spätjens, R. L., Mika, D., Algalarrondo, V., et al. (2014). Interventricular differences in β-adrenergic responses in

the canine heart: role of phosphodiesterases. *J. Am. Heart Assoc.* 3:e000858. doi: 10.1161/JAHA.114.000858

Park, S. J., Ahmad, F., Philp, A., Baar, K., Williams, T., Luo, H., et al. (2012). Resveratrol ameliorates aging-related metabolic phenotypes by inhibiting cAMP phosphodiesterases. *Cell* 148, 421–433. doi: 10.1016/j.cell.2012.01.017

Parks, R. J., Ray, G., Bienvenu, L. A., Rose, R. A., and Howlett, S. E. (2014). Sex differences in SR Ca^{2+} release in murine ventricular myocytes are regulated by the cAMP/PKA pathway. *J. Mol. Cell. Cardiol.* 75, 162–173. doi: 10.1016/j.yjmcc.2014.07.006

Richter, W., Xie, M., Scheitrum, C., Krall, J., Movsesian, M. A., and Conti, M. (2011). Conserved expression and functions of PDE4 in rodent and human heart. *Basic Res. Cardiol.* 106, 249–262. doi: 10.1007/s00395-010-0138-8

Schulte, J. S., Fehrmann, E., Tekook, M. A., Kranick, D., Fels, B., Li, N., et al. (2016). Cardiac expression of the CREM repressor isoform CREM-IbΔC-X in mice leads to arrhythmogenic alterations in ventricular cardiomyocytes. *Basic Res. Cardiol.* 111:15. doi: 10.1007/s00395-016-0532-y

Terrenoire, C., Houslay, M. D., Baillie, G. S., and Kass, R. S. (2009). The cardiac I_{Ks} potassium channel macromolecular complex includes the phosphodiesterase PDE4D3. *J. Biol. Chem.* 284, 9140–9146. doi: 10.1074/jbc.M805366200

Zaccolo, M., and Pozzan, T. (2002). Discrete microdomains with high concentration of cAMP in stimulatedrat neonatal cardiac myocytes. *Science* 295, 1711–1715. doi: 10.1126/science.1069982

Zheng, X., Zu, L., Becker, L., and Cai, Z. P. (2014). Ischemic preconditioning inhibits mitochondrial permeability transition pore opening through the PTEN/PDE4 signaling pathway. *Cardiology* 129, 163–173. doi: 10.1159/000363646

Conflict of Interest Statement: The authors declare that the research was conducted in the absence of any commercial or financial relationships that could be construed as a potential conflict of interest.

frontiers in Pharmacology

REVIEW
published: 27 March 2019
doi: 10.3389/fphar.2019.00308

Glucocorticoid-Induced Leucine Zipper: A Novel Anti-inflammatory Molecule

*Oxana Bereshchenko[1], Graziella Migliorati[2], Stefano Bruscoli[2] and Carlo Riccardi[2]**

[1] Department of Surgery and Biomedical Sciences, University of Perugia, Perugia, Italy, [2] Section of Pharmacology, Department of Medicine, University of Perugia, Perugia, Italy

Glucocorticoids (GCs) are the most commonly used drugs for treatment of autoimmune and inflammatory diseases. Their efficacy is due to their ability to bind cytoplasmic receptors (glucocorticoid receptors, GR) and other cytoplasmic proteins, thus regulating gene expression. Although GCs are potent life-saving drugs, their therapeutic effects are transitory and chronic use of GCs is accompanied by serious side effects. Therefore, new drugs are needed to replace GCs. We have identified a gene, glucocorticoid-induced leucine zipper (GILZ or tsc22d3), that is rapidly and invariably induced by GCs. Human GILZ is a 135-amino acid protein that mediates many GC effects, including inhibition of the NF-κB and MAPK pathways. Similar to GCs, GILZ exerts anti-inflammatory activity in experimental disease models, including inflammatory bowel diseases and arthritis. While transgenic mice that overexpress GILZ are more resistant, GILZ knockout mice develop worse inflammatory diseases. Moreover, the anti-inflammatory effect of GCs is attenuated in GILZ-deficient mice. Importantly, *in vivo* delivery of recombinant GILZ protein cured colitis and facilitated resolution of lipopolysaccharide-induced inflammation without apparent toxic effects. A synthetic GILZ-derived peptide, corresponding to the GILZ region that interacts with NF-κB, was able to suppress experimental autoimmune encephalomyelitis. Collectively, these findings indicate that GILZ is an anti-inflammatory molecule that may serve as the basis for designing new therapeutic approaches to inflammatory diseases.

Keywords: glucocorticoid-induced leucine zipper, recombinant GILZ protein, GILZ, GILZ-derived peptide, anti-inflammatory molecules

OPEN ACCESS

Edited by:
Arianna Carolina Rosa, University of Turin, Italy

Reviewed by:
Mythily Srinivasan, Indiana University Bloomington, United States
Brendan E. Russ, Monash University, Australia
Taylah Bennett, Monash University, Melbourne, Australia, in collaboration with BR

****Correspondence:***
Carlo Riccardi
carlo.riccardi@unipg.it

Specialty section:
This article was submitted to Experimental Pharmacology and Drug Discovery, a section of the journal Frontiers in Pharmacology

Received: *07 December 2018*
Accepted: *12 March 2019*
Published: *27 March 2019*

Citation:
Bereshchenko O, Migliorati G, Bruscoli S and Riccardi C (2019) Glucocorticoid-Induced Leucine Zipper: A Novel Anti-inflammatory Molecule. Front. Pharmacol. 10:308. doi: 10.3389/fphar.2019.00308

INTRODUCTION: GLUCOCORTICOID-INDUCED LEUCINE ZIPPER (GILZ) IS A GLUCOCORTICOID (GC)-INDUCIBLE GENE

Glucocorticoids (GCs) are important hormones able to regulate homeostasis of virtually all organs and tissues of the human body. GCs act mainly as regulators of transcriptional activity of a large number of genes, but also by control of epigenetic mechanisms (Cain and Cidlowski, 2017; Zannas and Chrousos, 2017). GCs have anti-inflammatory and immunosuppressive activities that involve nearly all arms of the inflammatory response. Accordingly, GCs are widely used for therapy. However, although GCs are potent anti-inflammatory drugs, their clinical effects are transitory and chronic use of GCs is accompanied by serious side effects, such as hypertension, hyperglycemia, osteoporosis, mood disorders and Cushing's syndrome, that lead to discontinuation of therapy

(Ayroldi et al., 2014). Therefore, new drugs that can substitute for GCs may provide a critical aid in suppressing inflammation. Most of the effects mediated by GCs, at physiological and pharmacological concentrations, are mediated by interactions with the glucocorticoid receptor (GR) (De Bosscher et al., 2003). GR is predominantly located in the cytoplasm as a multiprotein complex called the receptosome. After GC/GR interaction and consequent conformational changes, GR dissociates from the complex and translocates into the nucleus, where, as a dimer, it interacts with other transcription and coactivator factors and binds to specific DNA sequences, called glucocorticoid recognition elements (GREs). Almost all the effects of GCs, therapeutic and unwanted, are mediated by GR activity. Extensive efforts to separate beneficial from harmful gene activation by modulating GR activity have not yielded any success and GC toxicity is still a big issue in clinical practice. Since GC-induced effects are mostly due to the modulation of target gene expression, we initiated studies aimed at identifying proteins induced by GC treatment that mediate the anti-inflammatory effects, but not the side effects, of GCs. This is an emerging approach in drug design and is based on the development of peptide and mimetic drugs with decreased toxicity and enhanced specificity compared with conventional anti-inflammatory molecules.

Glucocorticoid-induced leucine zipper (GILZ, or tsc22d3) was discovered in our laboratory as a gene rapidly induced by dexamethasone (DEX), a synthetic GC (D'Adamio et al., 1997; Cannarile et al., 2001). *In silico* and mutational analyses of the GILZ promoter showed that at least three canonical GREs are present in the proximal region of the GILZ transcriptional start site (Asselin-Labat et al., 2004; Wang et al., 2004). More than 100 papers have been published showing that GILZ is one of the earliest transcriptional targets of GR, thus indicating that it is a good candidate as a downstream GC-induced effector molecule. GC signaling can also induce epigenetic modifications, such as changes in histone methylation and acetylation (Vockley et al., 2016). We have observed that GILZ binds and inhibits histone deacetylases in myoblasts, suggesting GILZ may also be involved in the effect of epigenetic changes induced by GCs (Bruscoli et al., 2010).

Of note, responsiveness of GC-inducible genes to activated GR may also be dependent on chromatin accessibility of the regulatory regions (enhancers and promoters) that may be influenced and affected by environmental stimuli. These epigenetic changes might influence expression of GC-induced genes, including GILZ (John et al., 2011; Stavreva et al., 2015). On the other hand, the secretion of GCs itself is a classic endocrine response to environmental exposures, including stress. Consequently, GILZ, induced by GCs, is produced in response to stressful events such as tissue damage, infection, anxiety or depression. Notably, it has been shown that major depressive disorder (MDD) patients with reduced GILZ expression in the hippocampus and amygdala showed a smaller hippocampal volume, suggesting the involvement of GILZ in stress-related disorders such as depression and anxiety (Frodl et al., 2012).

In this review, we describe experimental evidence suggesting that GILZ mediates the anti-inflammatory effects of GCs and that GILZ-based molecules have anti-inflammatory properties.

GILZ MEDIATES THE ANTI-INFLAMMATORY ACTIVITY OF GCs

In recent years, several laboratories including our own have produced a large amount of experimental evidence that supports the role of GILZ as a mediator of the anti-inflammatory activity of GCs (**Figure 1**) (Ayroldi et al., 2014; Ronchetti et al., 2015). GILZ is involved in the modulation of the same signaling immune responses and inflammation-related pathways implicated in GC-induced anti-inflammatory and immunosuppressive activities (**Figure 1**), suggesting that targeting GILZ can constitute a new approach to the treatment of inflammatory/autoimmune diseases.

Glucocorticoid-induced leucine zipper was initially cloned in 1997 by comparing gene expression profiles of DEX-treated versus untreated murine T cells in differential display assays (D'Adamio et al., 1997). In this work, D'Adamio et al. (1997) showed that GILZ is involved in the regulation of T cell apoptosis. GILZ expression protects T cells from activated induced cell death through inhibition of Fas and FasL expression. The discovery of a human GILZ ortholog by Cannarile et al. (2001) indicated that GILZ is expressed and is induced by GCs in all peripheral blood cells, including T lymphocytes, monocytes and granulocytes. GILZ is also expressed in several other non-lymphoid tissues, and is ubiquitously upregulated by GCs (Cari et al., 2015). Much experimental evidence shows that GILZ interacts with several transcription factors and cellular signaling pathways (**Table 1**). Among those, GILZ physically interacts with essential factors in the control of inflammatory processes, including subunit p65 of nuclear factor kappa-light-chain-enhancer of activated B cells (NF-κB), c-Jun/c-Fos heterodimer (named Activator protein-1, AP-1), Raf-1, Ras, and CCAAT-enhancer-binding proteins (CEBPs) (**Figure 2**), as discussed in detail in the following sections, suggesting it has a remarkable central role in the control of inflammation.

GILZ INTERACTION WITH NF-κB and MAPK/ERK PATHWAYS IN INFLAMMATION

So far, the most relevant evidence of anti-inflammatory GILZ activities is related to interference with the NF-κB and Mitogen-Activated Protein Kinase (MAPK)/extracellular signal–regulated kinases (ERK) pathways. NF-κB is a transcription factor essential for the modulation of inflammatory and immune responses by controlling cytokine and chemokine production. Although NF-κB plays an essential, beneficial role in normal physiology, inappropriate regulation of NF-κB activity has been implicated in the pathogenesis of diseases including rheumatoid arthritis (RA), inflammatory bowel diseases (IBDs), osteoarthritis, atherosclerosis, asthma, multiple sclerosis (MS), and cancer (Barnes and Karin, 1997; Dai et al., 2009; Lawrence, 2009; Ben-Neriah and Karin, 2011).

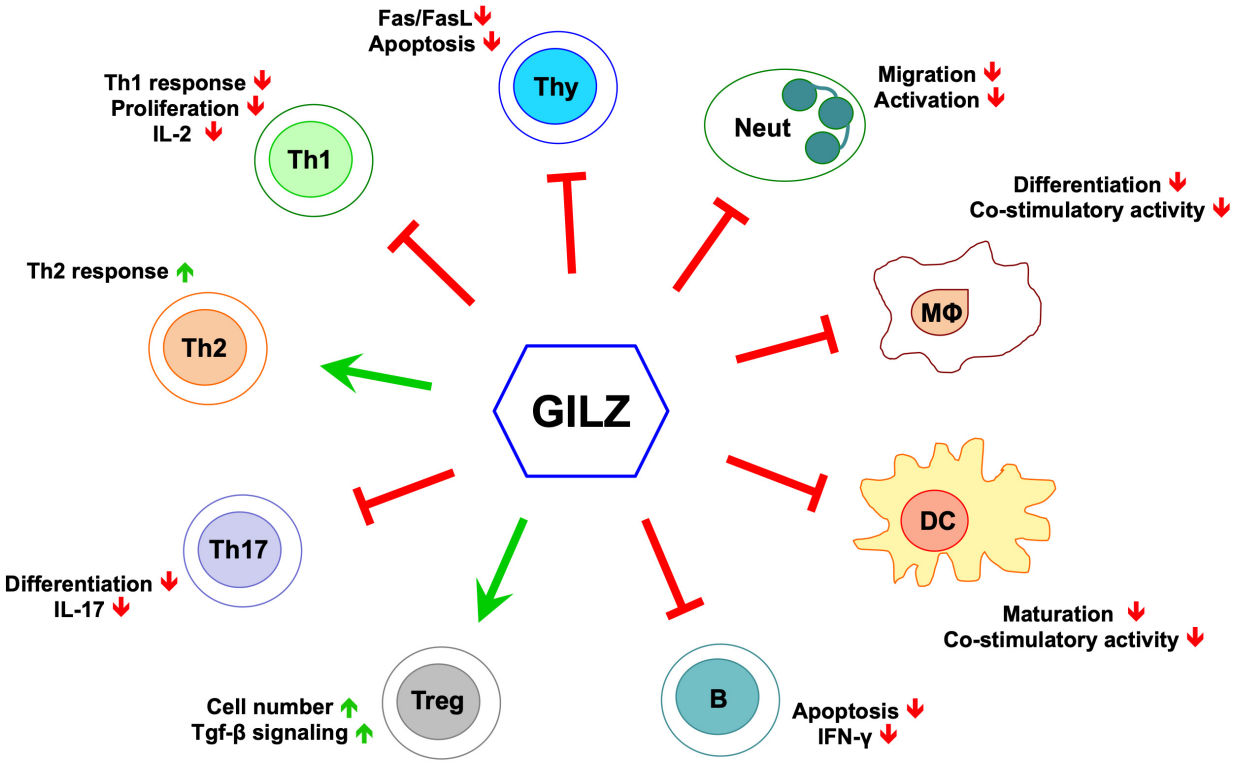

FIGURE 1 | GILZ's effects in cells of the immune system. Green arrows indicate positive regulation, red lines indicate negative regulation. Neut, neutrophils; Mϕ, monocytes/macrophages; DC, dendritic cells; B, B cells; Treg, T regulatory cells; Th17, T helper Type-17 cells; Th2, T helper Type-2 cells; Th1, T helper Type-1 cells; Thy, thymocytes.

Interference with NF-κB transcriptional activity by GCs in monocytes, macrophages, neutrophils, dendritic cells (DCs) and T lymphocytes is very important for the inhibition of the inflammatory response. We proposed that GILZ up-regulation induced by GCs is another way in which GCs control the activation of NF-κB. Ayroldi et al. (2001) demonstrated that GILZ directly binds to NF-κB and inhibits its activation (**Figure 2**). They showed that GILZ overexpression blocks nuclear translocation of the NF-κB/p65 subunit and it prevents the induction of pro-inflammatory NF-κB target genes in thymocytes, for example Interleukin-2 (IL-2) (Ayroldi et al., 2001; Di Marco et al., 2007). GILZ also mimics the effects of GCs on the differentiation of mature T cells, since GILZ overexpression in T cells of GILZ transgenic mice induces downregulation of the T helper (Th)-1 response and upregulation of the Th-2 response (Cannarile et al., 2006). The shift toward a Th2 response correlates with inhibition of NF-κB nuclear translocation in CD4+ T lymphocytes of intestinal lamina propria, and as a consequence, GILZ transgenic mice are less susceptible to Th1-mediated colitis.

Subsequent experimental evidence, obtained using several *in vitro* and *in vivo* models, further supported the link between anti-inflammatory activity of GILZ and inhibition of NF-κB. Berrebi et al. (2003) showed that GC inhibition of macrophage activation is at least in part achieved by GILZ-mediated inhibition of NF-κB. GILZ is constitutively expressed in mouse and human macrophages and in human monocytes, and is upregulated by GCs (Cannarile et al., 2001; Berrebi et al., 2003). In the THP-1 macrophage cell line, GILZ binds to the p65/NF-κB subunit and inhibits the expression of costimulatory molecules CD80 and CD86 and the production of chemokines Regulated on Activation, Normal T Cell Expressed and Secreted (RANTES) and Macrophage inflammatory protein 1 (MIP-1), thus mimicking the effect of GC treatment on macrophages (Berrebi et al., 2003). It has also been shown that GILZ mediates immunosuppressive effects in DCs. Overexpression of GILZ led to a tolerogenic effect of DCs in mediating T-cell activation by interfering with the NF-κB pathway (Cohen et al., 2006; Benkhoucha et al., 2014).

Beside the reported functions on cells of the immune system, GILZ has also been implicated in regulation of epithelial and endothelial inflammatory response. Indeed, GILZ silencing in human alveolar macrophages led to increased pro-inflammatory response and NF-κB activity (Hoppstadter et al., 2012). GILZ is also expressed in epithelial cells and GILZ peptide in human airway epithelial BEAS-2B cell line suppressed NF-κB activation (Eddleston et al., 2007). Furthermore, GILZ is expressed in synovial endothelial cells in RA, where it has been suggested to modulate inflammatory leukocyte recruitment via NF-κB. GILZ overexpression inhibits endothelial cell adhesive function through decreased expression of *E*-selectin, Intercellular Adhesion Molecule 1 (ICAM-1), C-C Motif

TABLE 1 | GILZ protein binding partners.

Gene name	Experimental system	Reference	PubMed ID
JUN	*In vitro* binding assay	Mittelstadt and Ashwell, 2001	11397794
FOS	*In vitro* binding assay	Mittelstadt and Ashwell, 2001	11397794
NFKB2 (p52)	Affinity Capture-Western	Ayroldi et al., 2001	11468175
NFKB1 (p65)	Affinity Capture-Western	Ayroldi et al., 2001	11468175
RAF1	Affinity Capture-Western	Ayroldi et al., 2002	12391160
RAS	Affinity Capture-Western	Ayroldi et al., 2007	17492054
SCNN1B	Affinity Capture-Western	Soundararajan et al., 2009	19380724
MYOD1	Affinity Capture-Western	Bruscoli et al., 2010	20124407
HDAC2	Affinity Capture-Western	Bruscoli et al., 2010	20124407
HDAC1	Affinity Capture-Western	Bruscoli et al., 2010	20124407
UBE2I	*In vitro* binding assay	Delfino et al., 2011	20671745
SUMO1	*In vitro* binding assay	Delfino et al., 2011	20671745
CASP8	Affinity Capture-Western	Delfino et al., 2011	20671745
SGK1	Affinity Capture-Western	Soundararajan et al., 2009	20947508
RAS	*In vitro* binding assay	Venanzi et al., 2014	24993177
TP53	*In vitro* binding assay	Ayroldi et al., 2014	25168242
TP53	Affinity Capture-Western	Ayroldi et al., 2014	25168242
MDM2	Affinity Capture-Western	Ayroldi et al., 2014	25168242
PU.1	Affinity Capture-Western	Ricci et al., 2017	28373208

Chemokine Ligand 2 (CCL2), C-X-C Motif Chemokine Ligand 8 (CXCL8), and Interleukin-6 (IL-6) and inhibition of Tumor Necrosis Factor (TNF)-stimulated leukocyte rolling, adhesion, and transmigration. Moreover, GILZ is downregulated in human umbilical vein endothelial cells by pro-inflammatory TNFα. Again, the anti-inflammatory effect of GILZ on endothelial cells involves the inhibition of NF-κB (Hahn et al., 2014). Moreover, GILZ-mediated inhibition of NF-κB nuclear translocation diminishes Cyclooxygenase 2 (COX-2) expression in bone marrow mesenchymal stem cells (MSCs) that were implicated in the pathogenesis and progression of RA (Chen and Tuan, 2008). GILZ expression was detected in the synovium of patients with RA and of mice with collagen-induced arthritis (CIA), and the severity of the disease was enhanced by GILZ silencing (Beaulieu et al., 2010; Ayroldi et al., 2014). The role of GILZ in the anti-inflammatory effect of MSCs in RA involves modulation of Th17 response toward a regulatory phenotype (Luz-Crawford et al., 2015). Another study confirmed that GILZ acts as a negative regulator of IL-17 production by T cells (Jones et al., 2015). GILZ expression in salivary gland is decreased in a mouse model of Sjögren's syndrome, and GILZ overexpression inhibits production of IL-17 in salivary gland cells, suggesting that GILZ represents a potential target for diagnosis and treatment of Sjögren's syndrome (Qin et al., 2015). Biological functions of Th17 cells are usually associated with pro-inflammatory activity implicated in the pathogenesis of autoimmune diseases. Yosef et al. (2013) proposed a dynamic regulatory network that comprises distinct Th17 cells with pro-inflammatory or regulatory activities. They indicated GILZ as a potential marker of Th17 cells with a non-pathogenic status (Yosef et al., 2013).

It has also been shown that GILZ dampens the pro-inflammatory effects of TNFα in human adipocytes by inhibiting p65/NF-κB nuclear translocation (Lee et al., 2016).

We have also shown that GILZ plays an important role in the homeostasis of B-cells (Bruscoli et al., 2015, 2018). GILZ deficiency leads to increased B-cell survival through elevated NF-κB activity and B-Cell CLL/Lymphoma 2 (Bcl-2) overexpression. B lymphocytosis observed in gilz deficient mice suggests that GILZ could be implicated in the pathogenesis of B-cell disorders such as hematological and/or autoimmune/inflammatory diseases. In this regard, a recent study reports a reduced GILZ expression in B cells of patients with systemic lupus erythematosus (SLE) (Jones et al., 2016).

The influence of GILZ on the expression of Bcl-2 family members is consistent with observations indicating that GILZ overexpression inhibits apoptosis in T lymphocytes through down-regulation of Bcl-2 Interacting Mediator Of Cell Death (Bim), a pro-apoptotic member of the Bcl-2 family (Asselin-Labat et al., 2004). GILZ also inhibits apoptosis in cardiomyocytes, where the pro-survival isoform of Bcl-XL protein is overexpressed when GILZ is overexpressed (Aguilar et al., 2014).

Interestingly, it has been shown that a GILZ-based peptide inhibits p65/NF-kB activation in lipopolysaccharide (LPS)-stimulated THP-1 myeloid cell line (Srinivasan et al., 2014). More recently, another study showed that a peptide corresponding to the 98–134 amino acids of GILZ inhibits LPS-induced p65/NF-kB nuclear translocation in retinal Müller cells (Gu et al., 2018a).

Collectively, these findings suggest that GILZ or GILZ-based peptides mimic the effect of GCs on NF-κB inhibition and GILZ expression is sufficient to achieve efficacious suppression of NF-κB-induced inflammation (Ngo et al., 2013; Ayroldi et al., 2014).

Many anti-inflammatory effects of GCs depend on cross-talk with the MAPK signaling pathway. We have shown that GILZ interacts with the MAPK pathway by binding to Raf-1 and Ras (**Figure 2**) (Ayroldi et al., 2002, 2007). GILZ interaction with activated Ras results in inhibition of both the Phosphoinositide 3-kinase (PI3K)/Akt and ERK pathways, thus dampening cell growth (including tumor cell growth) and differentiation. Also, GILZ mediates DEX-induced inhibition of the MAPK/ERK pathway in human airway epithelial cells (Liu et al., 2013). Specific genetic ablation of GILZ in myeloid cells resulted in an increased susceptibility to LPS-induced macrophage activation through hyperactivity of the MAPK/ERK pathway (Hoppstadter et al., 2015). Furthermore, in cooperation with Annexin-1, another mediator of anti-inflammatory effects of GCs, GILZ inhibits LPS-induced macrophage activation by enhancement of the ERK and JUN N-Terminal Kinase (JNK) MAPK pathways (Yang et al., 2009), and neutrophil migration into inflamed tissues (Ricci et al., 2017). In addition, GILZ also inhibits neutrophil activation in a mouse model of C. albicans infection (Ricci et al., 2019).

Inhibition of oncoprotein Ras affects both the MAPK and PI3k/Akt pathways that are involved in cell survival and activation of immune responses. Forkhead family (Fox) transcription factors are mediators in the PI3K/Akt pathway

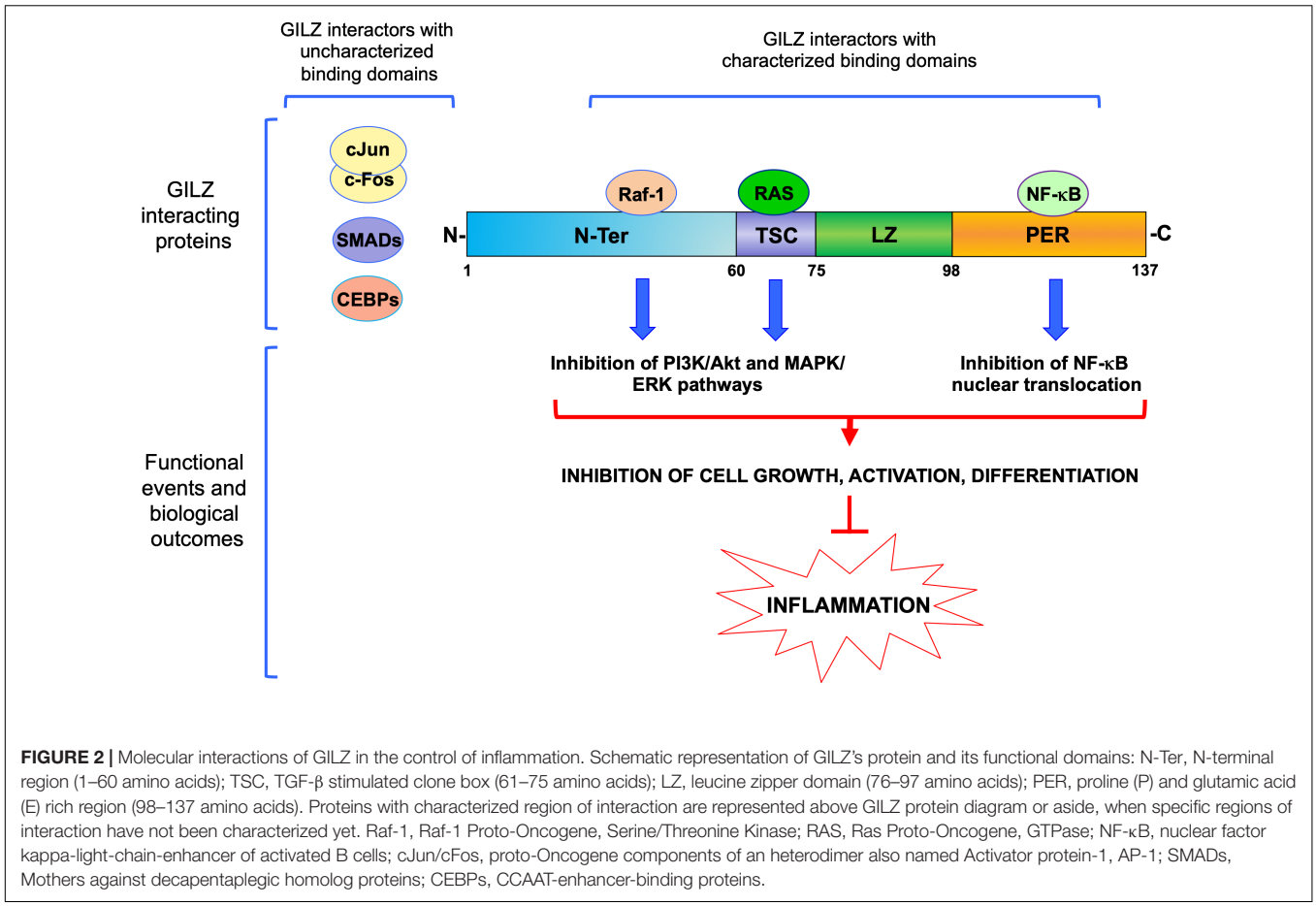

FIGURE 2 | Molecular interactions of GILZ in the control of inflammation. Schematic representation of GILZ's protein and its functional domains: N-Ter, N-terminal region (1–60 amino acids); TSC, TGF-β stimulated clone box (61–75 amino acids); LZ, leucine zipper domain (76–97 amino acids); PER, proline (P) and glutamic acid (E) rich region (98–137 amino acids). Proteins with characterized region of interaction are represented above GILZ protein diagram or aside, when specific regions of interaction have not been characterized yet. Raf-1, Raf-1 Proto-Oncogene, Serine/Threonine Kinase; RAS, Ras Proto-Oncogene, GTPase; NF-κB, nuclear factor kappa-light-chain-enhancer of activated B cells; cJun/cFos, proto-Oncogene components of an heterodimer also named Activator protein-1, AP-1; SMADs, Mothers against decapentaplegic homolog proteins; CEBPs, CCAAT-enhancer-binding proteins.

in the homeostasis of immune cells, including T lymphocytes (Peng, 2008). Among these factors, FoxO3 is phosphorylated and inactivated by activated Akt. It has been shown that GILZ inhibits FoxO3 activity and is part of a PI3K/Akt-FoxO3 signaling pathway that controls cell proliferation (Latre de Late et al., 2010).

A recent interesting report by Hoppstadter et al. (2016) showed that GILZ is induced in macrophages by curcumin, a natural product with anti-inflammatory properties. Hoppstadter et al. (2016) showed that curcumin inhibits inflammatory activities of the NF-κB and MAPK/Erk pathways and subsequent TNFα production via GILZ (Hoppstadter et al., 2016).

GILZ AND OTHER INFLAMMATORY SIGNALING PATHWAYS

GILZ is able to inhibit the function of AP-1, a transcription factor pivotal for activation of immune cells during inflammation (Schonthaler et al., 2011). GILZ heterodimerizes with components of AP-1, c-Fos and c-jun (Mittelstadt and Ashwell, 2001), and GILZ overexpression inhibits production of IL-2, a cytokine that plays a central role in T-cell homeostasis and activation (Ayroldi et al., 2001; Mittelstadt and Ashwell, 2001; Di Marco et al., 2007). T-cell activation, also through IL-2 production, suppresses GILZ expression (D'Adamio et al., 1997; Ayroldi et al., 2001; Asselin-Labat et al., 2004). This reciprocal inhibitory activity between T-cell activation and GILZ expression indicates that GILZ is important to maintain T-cell anergy, thus suggesting that modifications of GILZ expression and/or functions may have relevant effects in the control of inflammatory processes. Recently, we demonstrated that in GILZ-deficient mice, interferon-γ (IFNγ) production by B cells is increased, depending at least in part on enhanced AP-1 transcriptional activity. GILZ binds AP-1, inhibits its nuclear translocation and hence dampens AP-1-mediated transcriptional activation of IFNγ promoter, thus regulating B cell activities and the development of inflammatory diseases (Bruscoli et al., 2018).

As already mentioned, GILZ, like GCs, supports T cell differentiation toward the Th2 phenotype (Cannarile et al., 2006). An appropriate balance between inflammatory and anti-inflammatory signals is dependent on the regulated activity of different T cell subpopulations and the ability of tissue to regulate the immune response (Hall et al., 2011). In particular, T regulatory (Treg) cells participate in modulation of inflammatory response and their deregulation has been shown to be involved in many inflammatory diseases (Rudensky, 2011). It is now clear that Treg induction is important for GC-induced therapeutic effects. GCs are able to synergize with Transforming growth factor beta (TGF-β) in regulating the expression of Foxp-3, a transcription factor essential for Treg

generation (Rudensky, 2011; Bereshchenko et al., 2014). Foxp-3 expression is in fact induced by TGF-β pathway activation that is due to Mothers against decapentaplegic homolog (SMAD) protein phosphorylation; interaction of TGF-β with specific receptors induces SMAD phosphorylation and consequently increases Foxp-3 expression. Bereshchenko et al. (2014) showed that GILZ is necessary for GC-mediated Treg cell induction. This effect is due to GILZ interaction with SMAD proteins, thus synergizing with the TGF-β activity in enhancing FoxP3 expression (Bereshchenko et al., 2014). Notably, the therapeutic effect of GCs was lacking in a colitis model in GILZ knockout mice (Bereshchenko et al., 2014).

CEBPs are leucine zipper (LZ) transcription factors involved in diverse cellular responses including cell proliferation and differentiation, and also in inflammatory processes. There are several studies indicating a role for CEBP members in mediating GC effects (Roos and Nord, 2012). CEBPs are transcription factors that hetero-dimerize with many other proteins, including GC-target proteins such as MAPK phosphatase 1(MKP1)/dual specificity phosphatase 1 (DUSP1) (Kassel et al., 2001).

It has been shown that GILZ binds CEBPδ and inhibits peroxisome proliferator-activator receptor (PPAR)-gamma 2 expression, thus resulting in inhibition of differentiation adipogenesis in MSCs (Shi et al., 2003). Moreover, GILZ overexpression inhibits CEBPα expression and function, thus promoting osteogenesis in MSCs (Zhang et al., 2008). Although there is no direct evidence that GILZ is involved in the control of immunoregulatory molecules produced by MSCs, as GCs do, the aforementioned evidence supports the idea that GCs also affect CEBP activity through GILZ expression. Thus, more studies are warranted to understand the interplay between GILZ and CEPBs in mediating the anti-inflammatory effects of GCs in MSCs.

Serum/Glucocorticoid Regulated Kinase 1 (SGK1) is another important kinase that participates in the control of inflammation. Aberrant SGK1 expression is observed in a wide variety of diseases, including lung fibrosis, diabetic nephropathy, glomerulonephritis, obstructive nephropathy, liver cirrhosis, pancreatitis, and Crohn's disease (Artunc and Lang, 2014). Pharmacologic inhibition of SGK1 or suppression by small interfering RNA enhances pro-inflammatory cytokine production (including TNF, IL-12, and IL-6) in Toll Like Receptor (TLR)-activated monocytes. Lack of SGK1 results in increased phosphorylation of inhibitor of NF-kB kinase (IKK) and inhibitor of NF-kB Alpha (IκBα), and consequent increased NF-κB/p65 transcriptional activity in LPS-stimulated cells (Zhou et al., 2015). Interestingly, both SGK-1 and GILZ are up-regulated by aldosterone in the kidney and regulate the activity of Epithelial Na(+) Channel (ENaC), a sodium transport channel (Bhalla et al., 2006). More recently, it has been reported that reduced SGK-1 and GILZ expression was concomitant with increased IL-6 expression in patients with MDD (Frodl et al., 2012). These indications suggest a possible cooperation of SGK-1 and GILZ in the control of inflammatory response pathways.

Many members of the nuclear receptor superfamily are involved in the modulation of inflammation. In particular, the PPARs, like GR, have anti-inflammatory properties because they reduce expression of several pro-inflammatory cytokines, chemokines and cell adhesion molecules. Three isoforms, PPAR-α, PPAR-β/δ, and PPAR-γ, form heterodimers with retinoic acid receptors. Deficiency of PPAR-α in mice impairs DEX-induced inhibition of NF-κB, TNF-α production, cell migration, and COX-2 production. Moreover, PPAR-α contributes to the transcriptional up-regulation of GILZ by GCs (Cuzzocrea et al., 2008). GILZ over-expression inhibits PPAR-γ2 expression and blocks adipocyte differentiation (Zhang et al., 2008). The interplay between PPARs, GCs and GILZ is still not well characterized, and further studies are warranted to clarify whether GILZ also affects PPAR functions in inflammatory processes.

Estrogen receptor (ER), another member of the nuclear receptor superfamily, regulates GILZ expression. Tynan et al. (2004) showed that estrogens modulate GILZ expression in MCF-7 human breast cancer cells. Again, crosstalk between the GR and ER nuclear receptor members in inflammation might be therapeutically relevant and anti-inflammatory activity of GILZ may play a relevant role in this interplay (Cuzzocrea et al., 2007).

Together, these studies indicate that GILZ acts as a factor necessary for the maintenance of quiescence of immune cells. GILZ is downregulated upon activation of many cell types, including T and B lymphocytes, macrophages and DCs (D'Adamio et al., 1997; Lebson et al., 2011; Bruscoli et al., 2018; Hoppstadter et al., 2019), and is required for their proper activation, maturation and differentiation.

GILZ STRUCTURE-BASED DESIGN OF PUTATIVE ANTI-INFLAMMATORY MOLECULES

The mouse GILZ gene encodes a 137-amino acid (aa) LZ protein (D'Adamio et al., 1997). Human GILZ is a 135-aa protein, almost identical to its murine homologue (97% identity) (Cannarile et al., 2001). GILZ is composed of three domains—a TGF-β-stimulated clone (TSC) box (aa positions 40–75), a central LZ domain (aa 76–97), and a C-terminal domain endowed with a proline and glutamic acid rich (PER) region (aa 98–137). We also characterized a transcriptional variant, named long (L)-GILZ, that shares with GILZ all the conserved domains including the TSC box, LZ, and PER region, but differs in the N-terminal domain, and is encoded by an upstream alternative exon 1 (Bruscoli et al., 2012). Unlike most LZ proteins, which are usually transcription factors, GILZ isoforms do not contain a basic-rich region, and so far there has been no formal demonstration of direct binding to DNA; GILZ is mostly located in the cytoplasm, although it may also be present in the nucleus (Shi et al., 2003).

Different domains have been identified as essential for direct protein–protein binding interactions with different molecules. For example, the TSC-box domain is important for binding with Ras, while Raf-1 binds the N-terminal portion of GILZ. Both Raf-1 and Ras are activators of MAPK/ERK and PI3K/Akt pathways and GILZ expression negatively modulates both pathways (Ayroldi et al., 2002, 2007; Asselin-Labat et al., 2004; Venanzi et al., 2014). Interestingly, both c-Fos and c-Jun, proteins containing LZ domains and components of the transcription

factor AP-1, are efficiently retained by the GILZ N-terminal portion (aa 1–60), which lacks the LZ domain necessary for homo-dimerization, indicating that the LZ domain is not necessary for GILZ to bind AP-1 components (Di Marco et al., 2007). This evidence opens an interesting question about the role of the LZ domain in GILZ. Usually, a LZ region is a protein–protein interaction motif in which there is a leucine every seventh residue in an α-helix over a short stretch of protein, forming a stable coiled-coil structure. This motif is important for homo- and heterodimerization with a similar motif to promote specific DNA binding by a basic region adjacent to the LZ motif. The LZ model was originally proposed on the basis of the leucine distribution in LZ regions of proteins. It is now known to be common to over 40 proteins, including C/EBPs, Myc, Fos, Jun, and cAMP Responsive Element Binding Protein (CREB), involved in stress responses and the regulation of cell survival and proliferation (Jindrich and Degnan, 2016). LZ proteins can also associate with non-identical partners to form heterodimers composed of two different subunits, thus greatly expanding the repertoire of functions that these proteins can display. Although the LZ domain of GILZ is highly conserved, it has not yet been demonstrated to be necessary for hetero-dimerization with other LZ proteins. It is possible that the presence of the TSC-box domain, close to the LZ domain, limits the capacity of the GILZ LZ domain to bind other LZ family proteins. Interestingly, GILZ also binds to other LZ proteins such as CEBPα, CEBPβ and CEBPγ, but the region responsible for direct binding has not yet been identified (Shi et al., 2003; Pan et al., 2014).

Importantly, much experimental evidence reporting GILZ overexpression in mice, as well as *in vivo* delivery of recombinant GILZ protein, suggests that GILZ mimics some of the anti-inflammatory effects of GCs, including inhibition of T cell activation/differentiation and macrophage activation (D'Adamio et al., 1997; Ayroldi et al., 2001; Berrebi et al., 2003; Cannarile et al., 2009; Pinheiro et al., 2013; Bereshchenko et al., 2014; Hoppstadter et al., 2015), thus supporting the idea that GILZ protein may serve as a basis for rational drug design to achieve similar anti-inflammatory effects to GCs but with reduced side effects.

The first demonstration that recombinant GILZ protein has anti-inflammatory effects was by Cannarile et al. (2009), when a transactivator of transcription (TAT)–GILZ fusion protein, injected subcutaneously in a mouse model of Dinitrobenzene sulfonic acid (DNBS)-induced colitis, was found efficacious in ameliorating signs of colon inflammation (Cannarile et al., 2009). It has also been demonstrated that hydrodynamic delivery of GILZ-expressing vectors containing the TAT–GILZ sequence was sufficient to prevent LPS-induced lethal inflammation (shock) (Pinheiro et al., 2013). In addition, Vago et al. (2015) have shown that TAT–GILZ fusion protein efficiently induces a pro-apoptotic program *in vivo* that promotes resolution of neutrophilic inflammation induced by LPS. Recently, it was shown that *in vivo* administration of TAT–GILZ fusion protein in a mouse model of acute kidney injury exerts protective effects by promoting neutrophil and T cell polarization toward an anti-inflammatory phenotype (Baban et al., 2018).

The use of GILZ-derived peptides containing the critical aa 120–123 necessary for GILZ interaction with NF-κB (Di Marco et al., 2007) has been shown to effectively counteract neuroinflammation in a mouse model of MS (Srinivasan and Janardhanam, 2011). Recently, an *in vivo* injection of GILZ-based peptide prevented light-induced photoreceptor apoptosis and protected the retina from degeneration in Sprague Dawley rats, thus demonstrating the therapeutic efficacy of GILZ-based peptide in degenerative retinal diseases (Gu et al., 2018b).

The inhibitory effect on neuroinflammation was also reported in a study where transgenic mice overexpressing GILZ showed reduced damage and inflammation upon spinal cord injury (SCI) compared with wild-type controls (Esposito et al., 2012). Interestingly, a different study showed that, in the same SCI model, genetic ablation of GILZ in T lymphocytes led to reduced lesions and inflammation, suggesting that GILZ is involved in inflammatory processes upon SCI (Mazzon et al., 2014). This apparent contradiction is probably because, apart from its direct immunomodulatory role on T cells (D'Adamio et al., 1997; Ronchetti et al., 2015) GILZ is also expressed in neurons and may have functions in cells involved in neuronal damage (Srinivasan and Lahiri, 2017). Further studies are warranted to define the role of GILZ in the central nervous system.

Finally, forced GILZ overexpression in endothelial cells inhibits their activation and production of chemoattractant molecules, through NF-κB inhibition, thus reducing leukocyte recruitment to the site of inflammation (Cheng et al., 2013).

CONCLUSION

Data indicate that GILZ protein and GILZ-based molecules have therapeutic efficacy and are non-toxic to cells and mice. Therefore, novel drugs in the area of "inflammatory/autoimmune" diseases, including chronic, acute and lethal inflammation (shock), can be developed based on GILZ and its molecular interactions. Moreover, those drugs will be of interest for many inflammation-based degenerative diseases and possibly cancer. In the near future, we propose to identify novel anti-inflammatory drugs designed on the basis of the GILZ protein structure and described molecular interactions of GILZ that have been characterized in recent years. The efficacy, toxicity and molecular effects of these drugs will be evaluated in cellular systems and in established *in vivo* models of IBD and RA. A combination of experimental and computational techniques, together with a deep knowledge of the determinants of protein–protein and protein–ligand interactions, is necessary for the successful design of small compounds based on GILZ that will be efficacious for the treatment of inflammatory and autoimmune diseases.

AUTHOR CONTRIBUTIONS

OB, GM, and CR conceived the manuscript. OB and SB wrote the manuscript. SB designed the table and the figures. All authors approved the final version of the manuscript.

FUNDING

This work was supported by the Italian Ministry of Education and Research, grants PRIN2015ZT9HXY to CR and RBFR13BN6Y to OB, by the Fondazione Cassa Risparmio Perugia Grant 2018.0410 021 and by University Funding for Basic Research – Assignment 2018 to GM.

REFERENCES

Aguilar, D., Strom, J., and Chen, Q. M. (2014). Glucocorticoid induced leucine zipper inhibits apoptosis of cardiomyocytes by doxorubicin. *Toxicol. Appl. Pharmacol.* 276, 55–62. doi: 10.1016/j.taap.2014.01.013

Artunc, F., and Lang, F. (2014). Mineralocorticoid and SGK1-sensitive inflammation and tissue fibrosis. *Nephron. Physiol.* 128, 35–39. doi: 10.1159/000368267

Asselin-Labat, M. L., David, M., Biola-Vidamment, A., Lecoeuche, D., Zennaro, M. C., Bertoglio, J., et al. (2004). GILZ, a new target for the transcription factor FoxO3, protects T lymphocytes from interleukin-2 withdrawal-induced apoptosis. *Blood* 104, 215–223. doi: 10.1182/blood-2003-12-4295

Ayroldi, E., Macchiarulo, A., and Riccardi, C. (2014). Targeting glucocorticoid side effects: selective glucocorticoid receptor modulator or glucocorticoid-induced leucine zipper? A perspective. *FASEB J.* 28, 5055–5070. doi: 10.1096/fj.14-254755

Ayroldi, E., Migliorati, G., Bruscoli, S., Marchetti, C., Zollo, O., Cannarile, L., et al. (2001). Modulation of T-cell activation by the glucocorticoid-induced leucine zipper factor via inhibition of nuclear factor kappaB. *Blood* 98, 743–753. doi: 10.1182/blood.V98.3.743

Ayroldi, E., Zollo, O., Bastianelli, A., Marchetti, C., Agostini, M., Di Virgilio, R., et al. (2007). GILZ mediates the antiproliferative activity of glucocorticoids by negative regulation of Ras signaling. *J. Clin. Invest.* 117, 1605–1615. doi: 10.1172/JCI30724

Ayroldi, E., Zollo, O., Macchiarulo, A., Di Marco, B., Marchetti, C., and Riccardi, C. (2002). Glucocorticoid-induced leucine zipper inhibits the Raf-extracellular signal-regulated kinase pathway by binding to Raf-1. *Mol. Cell. Biol.* 22, 7929–7941. doi: 10.1128/MCB.22.22.7929-7941.2002

Baban, B., Marchetti, C., Khodadadi, H., Malik, A., Emami, G., Lin, P. C., et al. (2018). Glucocorticoid-induced leucine zipper promotes neutrophil and T-cell polarization with protective effects in acute kidney injury. *J. Pharmacol. Exp. Ther.* 367, 483–493. doi: 10.1124/jpet.118.251371

Barnes, P. J., and Karin, M. (1997). Nuclear factor-kappaB: a pivotal transcription factor in chronic inflammatory diseases. *N. Engl. J. Med.* 336, 1066–1071. doi: 10.1056/NEJM199704103361506

Beaulieu, E., Ngo, D., Santos, L., Yang, Y. H., Smith, M., Jorgensen, C., et al. (2010). Glucocorticoid-induced leucine zipper is an endogenous antiinflammatory mediator in arthritis. *Arthritis Rheum.* 62, 2651–2661. doi: 10.1002/art.27566

Benkhoucha, M., Molnarfi, N., Dunand-Sauthier, I., Merkler, D., Schneiter, G., Bruscoli, S., et al. (2014). Hepatocyte growth factor limits autoimmune neuroinflammation via glucocorticoid-induced leucine zipper expression in dendritic cells. *J. Immunol.* 193, 2743–2752. doi: 10.4049/jimmunol.1302338

Ben-Neriah, Y., and Karin, M. (2011). Inflammation meets cancer, with NF-kappaB as the matchmaker. *Nat. Immunol.* 12, 715–723. doi: 10.1038/ni.2060

Bereshchenko, O., Coppo, M., Bruscoli, S., Biagioli, M., Cimino, M., Frammartino, T., et al. (2014). GILZ promotes production of peripherally induced Treg cells and mediates the crosstalk between glucocorticoids and TGF-beta signaling. *Cell Rep.* 7, 464–475. doi: 10.1016/j.celrep.2014.03.004

Berrebi, D., Bruscoli, S., Cohen, N., Foussat, A., Migliorati, G., Bouchet-Delbos, L., et al. (2003). Synthesis of glucocorticoid-induced leucine zipper (GILZ) by macrophages: an anti-inflammatory and immunosuppressive mechanism shared by glucocorticoids and IL-10. *Blood* 101, 729–738. doi: 10.1182/blood-2002-02-0538

Bhalla, V., Soundararajan, R., Pao, A. C., Li, H., and Pearce, D. (2006). Disinhibitory pathways for control of sodium transport: regulation of ENaC by SGK1 and GILZ. *Am. J. Physiol. Renal Physiol.* 291, F714–F721. doi: 10.1152/ajprenal.00061.2006

Bruscoli, S., Biagioli, M., Sorcini, D., Frammartino, T., Cimino, M., Sportoletti, P., et al. (2015). Lack of glucocorticoid-induced leucine zipper (GILZ) deregulates B-cell survival and results in B-cell lymphocytosis in mice. *Blood* 126, 1790–1801. doi: 10.1182/blood-2015-03-631580

Bruscoli, S., Donato, V., Velardi, E., Di Sante, M., Migliorati, G., Donato, R., et al. (2010). Glucocorticoid-induced leucine zipper (GILZ) and long GILZ inhibit myogenic differentiation and mediate anti-myogenic effects of glucocorticoids. *J. Biol. Chem.* 285, 10385–10396. doi: 10.1074/jbc.M109.070136

Bruscoli, S., Sorcini, D., Flamini, S., Gagliardi, A., Adamo, F., Ronchetti, S., et al. (2018). Glucocorticoid-Induced Leucine Zipper Inhibits Interferon-Gamma Production in B Cells and Suppresses Colitis in Mice. *Front. Immunol.* 9:120. doi: 10.3389/fimmu.2018.01720

Bruscoli, S., Velardi, E., Di Sante, M., Bereshchenko, O., Venanzi, A., Coppo, M., et al. (2012). Long glucocorticoid-induced leucine zipper (L-GILZ) protein interacts with ras protein pathway and contributes to spermatogenesis control. *J. Biol. Chem.* 287, 1242–1251. doi: 10.1074/jbc.M111.316372

Cain, D. W., and Cidlowski, J. A. (2017). Immune regulation by glucocorticoids. *Nat. Rev. Immunol.* 17, 233–247. doi: 10.1038/nri.2017.1

Cannarile, L., Cuzzocrea, S., Santucci, L., Agostini, M., Mazzon, E., Esposito, E., et al. (2009). Glucocorticoid-induced leucine zipper is protective in Th1-mediated models of colitis. *Gastroenterology* 136, 530–541. doi: 10.1053/j.gastro.2008.09.024

Cannarile, L., Fallarino, F., Agostini, M., Cuzzocrea, S., Mazzon, E., Vacca, C., et al. (2006). Increased GILZ expression in transgenic mice up-regulates Th-2 lymphokines. *Blood* 107, 1039–1047. doi: 10.1182/blood-2005-05-2183

Cannarile, L., Zollo, O., D'Adamio, F., Ayroldi, E., Marchetti, C., Tabilio, A., et al. (2001). Cloning, chromosomal assignment and tissue distribution of human GILZ, a glucocorticoid hormone-induced gene. *Cell Death. Differ.* 8, 201–203. doi: 10.1038/sj.cdd.4400798

Cari, L., Ricci, E., Gentili, M., Petrillo, M. G., Ayroldi, E., Ronchetti, S., et al. (2015). A focused Real Time PCR strategy to determine GILZ expression in mouse tissues. *Results Immunol.* 5, 37–42. doi: 10.1016/j.rinim.2015.10.003

Chen, F. H., and Tuan, R. S. (2008). Mesenchymal stem cells in arthritic diseases. *Arthritis Res. Ther.* 10:223. doi: 10.1186/ar2514

Cheng, Q., Fan, H., Ngo, D., Beaulieu, E., Leung, P., Lo, C. Y., et al. (2013). GILZ overexpression inhibits endothelial cell adhesive function through regulation of NF-kappaB and MAPK activity. *J. Immunol.* 191, 424–433. doi: 10.4049/jimmunol.1202662

Cohen, N., Mouly, E., Hamdi, H., Maillot, M. C., Pallardy, M., Godot, V., et al. (2006). GILZ expression in human dendritic cells redirects their maturation and prevents antigen-specific T lymphocyte response. *Blood* 107, 2037–2044. doi: 10.1182/blood-2005-07-2760

Cuzzocrea, S., Bruscoli, S., Crisafulli, C., Mazzon, E., Agostini, M., Muia, C., et al. (2007). Estrogen receptor antagonist fulvestrant (ICI 182,780) inhibits the anti-inflammatory effect of glucocorticoids. *Mol. Pharmacol.* 71, 132–144. doi: 10.1124/mol.106.029629

Cuzzocrea, S., Bruscoli, S., Mazzon, E., Crisafulli, C., Donato, V., Di Paola, R., et al. (2008). Peroxisome proliferator-activated receptor-alpha contributes to the anti-inflammatory activity of glucocorticoids. *Mol. Pharmacol.* 73, 323–337. doi: 10.1124/mol.107.041475

D'Adamio, F., Zollo, O., Moraca, R., Ayroldi, E., Bruscoli, S., Bartoli, A., et al. (1997). A new dexamethasone-induced gene of the leucine zipper family protects T lymphocytes from TCR/CD3-activated cell death. *Immunity* 7, 803–812. doi: 10.1016/S1074-7613(00)80398-2

Dai, Y., Lawrence, T. S., and Xu, L. (2009). Overcoming cancer therapy resistance by targeting inhibitors of apoptosis proteins and nuclear factor-kappa B. *Am. J. Transl. Res.* 1, 1–15.

De Bosscher, K., Vanden Berghe, W., and Haegeman, G. (2003). The interplay between the glucocorticoid receptor and nuclear factor-kappaB or activator protein-1: molecular mechanisms for gene repression. *Endocr. Rev.* 24, 488–522. doi: 10.1210/er.2002-0006

Delfino, D. V., Spinicelli, S., Pozzesi, N., Pierangeli, S., Velardi, E., Bruscoli, S., et al. (2011). Glucocorticoid-induced activation of caspase-8 protects the

glucocorticoid-induced protein Gilz from proteasomal degradation and induces its binding to SUMO-1 in murine thymocytes. *Cell Death Differ.* 18, 183–190. doi: 10.1038/cdd.2010.86

Di Marco, B., Massetti, M., Bruscoli, S., Macchiarulo, A., Di Virgilio, R., Velardi, E., et al. (2007). Glucocorticoid-induced leucine zipper (GILZ)/NF-kappaB interaction: role of GILZ homo-dimerization and C-terminal domain. *Nucleic Acids Res.* 35, 517–528. doi: 10.1093/nar/gkl1080

Eddleston, J., Herschbach, J., Wagelie-Steffen, A. L., Christiansen, S. C., and Zuraw, B. L. (2007). The anti-inflammatory effect of glucocorticoids is mediated by glucocorticoid-induced leucine zipper in epithelial cells. *J. Allergy Clin. Immunol.* 119, 115–122. doi: 10.1016/j.jaci.2006.08.027

Esposito, E., Bruscoli, S., Mazzon, E., Paterniti, I., Coppo, M., Velardi, E., et al. (2012). Glucocorticoid-induced leucine zipper (GILZ) over-expression in T lymphocytes inhibits inflammation and tissue damage in spinal cord injury. *Neurotherapeutics* 9, 210–225. doi: 10.1007/s13311-011-0084-7

Frodl, T., Carballedo, A., Hughes, M. M., Saleh, K., Fagan, A., Skokauskas, N., et al. (2012). Reduced expression of glucocorticoid-inducible genes GILZ and SGK-1: high IL-6 levels are associated with reduced hippocampal volumes in major depressive disorder. *Transl. Psychiatry* 2:e88. doi: 10.1038/tp.2012.14

Gu, R., Ding, X., Tang, W., Lei, B., Jiang, C., and Xu, G. (2018a). A synthesized glucocorticoid- induced leucine zipper peptide inhibits retinal muller cell gliosis. *Front. Pharmacol.* 9:331. doi: 10.3389/fphar.2018.00331

Gu, R., Tang, W., Lei, B., Jiang, C., Song, F., and Xu, G. (2018b). Synthesized glucocorticoid-induced leucine zipper peptide inhibits photoreceptor apoptosis and protects retinal function in light-induced retinal degeneration model. *Clin. Exp. Ophthalmol.* doi: 10.1111/ceo.13452 [Epub ahead of print].

Hahn, R. T., Hoppstadter, J., Hirschfelder, K., Hachenthal, N., Diesel, B., Kessler, S. M., et al. (2014). Downregulation of the glucocorticoid-induced leucine zipper (GILZ) promotes vascular inflammation. *Atherosclerosis* 234, 391–400. doi: 10.1016/j.atherosclerosis.2014.03.028

Hall, B. M., Verma, N. D., Tran, G. T., and Hodgkinson, S. J. (2011). Distinct regulatory CD4+T cell subsets; differences between naive and antigen specific T regulatory cells. *Curr. Opin. Immunol.* 23, 641–647. doi: 10.1016/j.coi.2011.07.012

Hoppstadter, J., Diesel, B., Eifler, L. K., Schmid, T., Brune, B., and Kiemer, A. K. (2012). Glucocorticoid-induced leucine zipper is downregulated in human alveolar macrophages upon Toll-like receptor activation. *Eur. J. Immunol.* 42, 1282–1293. doi: 10.1002/eji.201142081

Hoppstadter, J., Diesel, B., Linnenberger, R., Hachenthal, N., Flamini, S., Minet, M., et al. (2019). Amplified Host Defense by Toll-Like Receptor-Mediated Downregulation of the Glucocorticoid-Induced Leucine Zipper (GILZ) in Macrophages. *Front. Immunol.* 9:3111. doi: 10.3389/fimmu.2018.03111

Hoppstadter, J., Hachenthal, N., Valbuena-Perez, J. V., Lampe, S., Astanina, K., Kunze, M. M., et al. (2016). Induction of glucocorticoid-induced leucine zipper (GILZ) contributes to anti-inflammatory effects of the natural product curcumin in macrophages. *J. Biol. Chem.* 291, 22949–22960. doi: 10.1074/jbc.M116.733253

Hoppstadter, J., Kessler, S. M., Bruscoli, S., Huwer, H., Riccardi, C., and Kiemer, A. K. (2015). Glucocorticoid-induced leucine zipper: a critical factor in macrophage endotoxin tolerance. *J. Immunol.* 194, 6057–6067. doi: 10.4049/jimmunol.1403207

Jindrich, K., and Degnan, B. M. (2016). The diversification of the basic leucine zipper family in eukaryotes correlates with the evolution of multicellularity. *BMC Evol. Biol.* 16:28. doi: 10.1186/s12862-016-0598-z

John, S., Sabo, P. J., Thurman, R. E., Sung, M. H., Biddie, S. C., Johnson, T. A., et al. (2011). Chromatin accessibility pre-determines glucocorticoid receptor binding patterns. *Nat. Genet.* 43, 264–268. doi: 10.1038/ng.759

Jones, S. A., Perera, D. N., Fan, H., Russ, B. E., Harris, J., and Morand, E. F. (2015). GILZ regulates Th17 responses and restrains IL-17-mediated skin inflammation. *J. Autoimmun.* 61, 73–80. doi: 10.1016/j.jaut.2015.05.010

Jones, S. A., Toh, A. E., Odobasic, D., Oudin, M. A., Cheng, Q., Lee, J. P., et al. (2016). Glucocorticoid-induced leucine zipper (GILZ) inhibits B cell activation in systemic lupus erythematosus. *Ann. Rheum. Dis.* 75, 739–747. doi: 10.1136/annrheumdis-2015-207744

Kassel, O., Sancono, A., Kratzschmar, J., Kreft, B., Stassen, M., and Cato, A. C. (2001). Glucocorticoids inhibit MAP kinase via increased expression and decreased degradation of MKP-1. *EMBO J.* 20, 7108–7116. doi: 10.1093/emboj/20.24.7108

Latre de Late, P., Pepin, A., Assaf-Vandecasteele, H., Espinasse, C., Nicolas, V., Asselin-Labat, M. L., et al. (2010). Glucocorticoid-induced leucine zipper (GILZ) promotes the nuclear exclusion of FOXO3 in a Crm1-dependent manner. *J. Biol. Chem.* 285, 5594–5605. doi: 10.1074/jbc.M109.068346

Lawrence, T. (2009). The nuclear factor NF-kappaB pathway in inflammation. *Cold Spring Harb. Perspect. Biol.* 1:a001651. doi: 10.1101/cshperspect.a001651

Lebson, L., Wang, T., Jiang, Q., and Whartenby, K. A. (2011). Induction of the glucocorticoid-induced leucine zipper gene limits the efficacy of dendritic cell vaccines. *Cancer Gene Ther.* 18, 563–570. doi: 10.1038/cgt.2011.23

Lee, M. J., Yang, R. Z., Karastergiou, K., Smith, S. R., Chang, J. R., Gong, D. W., et al. (2016). Low expression of the GILZ may contribute to adipose inflammation and altered adipokine production in human obesity. *J. Lipid Res.* 57, 1256–1263. doi: 10.1194/jlr.M067728

Liu, J., Zhang, M., Niu, C., Luo, Z., Dai, J., Wang, L., et al. (2013). Dexamethasone inhibits repair of human airway epithelial cells mediated by glucocorticoid-induced leucine zipper (GILZ). *PLoS One* 8:e60705. doi: 10.1371/journal.pone.0060705

Luz-Crawford, P., Tejedor, G., Mausset-Bonnefont, A. L., Beaulieu, E., Morand, E. F., Jorgensen, C., et al. (2015). Glucocorticoid-induced leucine zipper governs the therapeutic potential of mesenchymal stem cells by inducing a switch from pathogenic to regulatory Th17 cells in a mouse model of collagen-induced arthritis. *Arthritis Rheumatol.* 67, 1514–1524. doi: 10.1002/art.39069

Mazzon, E., Bruscoli, S., Galuppo, M., Biagioli, M., Sorcini, D., Bereshchenko, O., et al. (2014). Glucocorticoid-induced leucine zipper (GILZ) controls inflammation and tissue damage after spinal cord injury. *CNS Neurosci. Ther.* 20, 973–981. doi: 10.1111/cns.12315

Mittelstadt, P. R., and Ashwell, J. D. (2001). Inhibition of AP-1 by the glucocorticoid-inducible protein GILZ. *J. Biol. Chem.* 276, 29603–29610. doi: 10.1074/jbc.M101522200

Ngo, D., Beaulieu, E., Gu, R., Leaney, A., Santos, L., Fan, H., et al. (2013). Divergent effects of endogenous and exogenous glucocorticoid-induced leucine zipper in animal models of inflammation and arthritis. *Arthritis Rheum.* 65, 1203–1212. doi: 10.1002/art.37858

Pan, G., Cao, J., Yang, N., Ding, K., Fan, C., Xiong, W. C., et al. (2014). Role of glucocorticoid-induced leucine zipper (GILZ) in bone acquisition. *J. Biol. Chem.* 289, 19373–19382. doi: 10.1074/jbc.M113.535237

Peng, S. L. (2008). Foxo in the immune system. *Oncogene* 27, 2337–2344. doi: 10.1038/onc.2008.26

Pinheiro, I., Dejager, L., Petta, I., Vandevyver, S., Puimege, L., Mahieu, T., et al. (2013). LPS resistance of SPRET/Ei mice is mediated by Gilz, encoded by the Tsc22d3 gene on the X chromosome. *EMBO Mol. Med.* 5, 456–470. doi: 10.1002/emmm.201201683

Qin, X., Liu, J. Y., Abdelsayed, R., Shi, X., Yu, J. C., Mozaffari, M. S., et al. (2015). The status of glucocorticoid-induced leucine zipper protein in the salivary glands in Sjogren's syndrome: predictive and prognostic potentials. *EPMA J.* 7:3. doi: 10.1186/s13167-016-0052-8

Ricci, E., Ronchetti, S., Gabrielli, E., Pericolini, E., Gentili, M., Roselletti, E., et al. (2019). GILZ restrains neutrophil activation by inhibiting the MAPK pathway. *J. Leukoc. Biol.* 105, 187–194. doi: 10.1002/JLB.3AB0718-255R

Ricci, E., Ronchetti, S., Pericolini, E., Gabrielli, E., Cari, L., Gentili, M., et al. (2017). Role of the glucocorticoid-induced leucine zipper gene in dexamethasone-induced inhibition of mouse neutrophil migration via control of annexin A1 expression. *FASEB J.* 31, 3054–3065. doi: 10.1096/fj.201601315R

Ronchetti, S., Migliorati, G., and Riccardi, C. (2015). GILZ as a Mediator of the Anti-Inflammatory Effects of Glucocorticoids. *Front. Endocrinol.* 6:170. doi: 10.3389/fendo.2015.00170

Roos, A. B., and Nord, M. (2012). The emerging role of C/EBPs in glucocorticoid signaling: lessons from the lung. *J. Endocrinol.* 212, 291–305. doi: 10.1530/JOE-11-0369

Rudensky, A. Y. (2011). Regulatory T cells and Foxp3. *Immunol. Rev.* 241, 260–268. doi: 10.1111/j.1600-065X.2011.01018.x

Schonthaler, H. B., Guinea-Viniegra, J., and Wagner, E. F. (2011). Targeting inflammation by modulating the Jun/AP-1 pathway. *Ann. Rheum. Dis.* 70(Suppl. 1), i109–i112. doi: 10.1136/ard.2010.140533

Shi, X., Shi, W., Li, Q., Song, B., Wan, M., Bai, S., et al. (2003). A glucocorticoid-induced leucine-zipper protein, GILZ, inhibits adipogenesis of mesenchymal cells. *EMBO Rep.* 4, 374–380. doi: 10.1038/sj.embor.embor805

Soundararajan, R., Melters, D., Shih, I.-C., Wang, J., and Pearce, D. (2009). Epithelial sodium channel regulated by differential composition of a signaling complex. *Proc. Natl. Acad. Sci. U.S.A.* 106, 7804–7809. doi: 10.1073/pnas.0809892106

Srinivasan, M., Blackburn, C., and Lahiri, D. K. (2014). Functional characterization of a competitive peptide antagonist of p65 in human macrophage-like cells suggests therapeutic potential for chronic inflammation. *Drug Des. Devel. Ther.* 8, 2409–2421. doi: 10.2147/DDDT.S59722

Srinivasan, M., and Janardhanam, S. (2011). Novel p65 binding glucocorticoid-induced leucine zipper peptide suppresses experimental autoimmune encephalomyelitis. *J. Biol. Chem.* 286, 44799–44810. doi: 10.1074/jbc.M111.279257

Srinivasan, M., and Lahiri, D. K. (2017). Glucocorticoid-Induced Leucine Zipper in Central Nervous System Health and Disease. *Mol. Neurobiol.* 54, 8063–8070. doi: 10.1007/s12035-016-0277-5

Stavreva, D. A., Coulon, A., Baek, S., Sung, M. H., John, S., Stixova, L., et al. (2015). Dynamics of chromatin accessibility and long-range interactions in response to glucocorticoid pulsing. *Genome Res.* 25, 845–857. doi: 10.1101/gr.184168.114

Tynan, S. H., Lundeen, S. G., and Allan, G. F. (2004). Cell type-specific bidirectional regulation of the glucocorticoid-induced leucine zipper (GILZ) gene by estrogen. *J. Steroid Biochem. Mol. Biol.* 91, 225–239. doi: 10.1016/j.jsbmb.2004.05.002

Vago, J. P., Tavares, L. P., Garcia, C. C., Lima, K. M., Perucci, L. O., Vieira, E. L., et al. (2015). The role and effects of glucocorticoid-induced leucine zipper in the context of inflammation resolution. *J. Immunol.* 194, 4940–4950. doi: 10.4049/jimmunol.1401722

Venanzi, A., Di Sante, M., Bruscoli, S., Biagioli, M., Sorcini, D., Cimino, M., et al. (2014). Recombinant long-glucocorticoid-induced leucine zipper (L-GILZ) protein restores the control of proliferation in gilz KO spermatogonia. *Eur. J. Pharm. Sci.* 63, 22–28. doi: 10.1016/j.ejps.2014.06.013

Vockley, C. M., D'Ippolito, A. M., McDowell, I. C., Majoros, W. H., Safi, A., Song, L., et al. (2016). Direct GR Binding Sites Potentiate Clusters of TF Binding across the Human Genome. *Cell* 166:1269-1281.e19. doi: 10.1016/j.cell.2016.07.049

Wang, J. C., Derynck, M. K., Nonaka, D. F., Khodabakhsh, D. B., Haqq, C., and Yamamoto, K. R. (2004). Chromatin immunoprecipitation (ChIP) scanning identifies primary glucocorticoid receptor target genes. *Proc. Natl. Acad. Sci. U.S.A.* 101, 15603–15608. doi: 10.1073/pnas.0407008101

Yang, Y. H., Aeberli, D., Dacumos, A., Xue, J. R., and Morand, E. F. (2009). Annexin-1 regulates macrophage IL-6 and TNF via glucocorticoid-induced leucine zipper. *J. Immunol.* 183, 1435–1445. doi: 10.4049/jimmunol.0804000

Yosef, N., Shalek, A. K., Gaublomme, J. T., Jin, H., Lee, Y., Awasthi, A., et al. (2013). Dynamic regulatory network controlling TH17 cell differentiation. *Nature* 496, 461–468. doi: 10.1038/nature11981

Zannas, A. S., and Chrousos, G. P. (2017). Epigenetic programming by stress and glucocorticoids along the human lifespan. *Mol. Psychiatry* 22, 640–646. doi: 10.1038/mp.2017.35

Zhang, W., Yang, N., and Shi, X. M. (2008). Regulation of mesenchymal stem cell osteogenic differentiation by glucocorticoid-induced leucine zipper (GILZ). *J. Biol. Chem.* 283, 4723–4729. doi: 10.1074/jbc.M704147200

Zhou, H., Gao, S., Duan, X., Liang, S., Scott, D. A., Lamont, R. J., et al. (2015). Inhibition of serum- and glucocorticoid-inducible kinase 1 enhances TLR-mediated inflammation and promotes endotoxin-driven organ failure. *FASEB J.* 29, 3737–3749. doi: 10.1096/fj.15-270462

Conflict of Interest Statement: The authors declare that the research was conducted in the absence of any commercial or financial relationships that could be construed as a potential conflict of interest.

frontiers in Pharmacology

ORIGINAL RESEARCH
published: 27 March 2019
doi: 10.3389/fphar.2019.00303

Transcriptome-Wide Effects of Sphingosine Kinases Knockdown in Metastatic Prostate and Breast Cancer Cells: Implications for Therapeutic Targeting

Heba Alshaker[1,2], Qi Wang[1], Daniel Brewer[1,3] and Dmitri Pchejetski[1]**

[1] School of Medicine, University of East Anglia, Norwich, United Kingdom, [2] Department of Pharmacology and Biomedical Sciences, Faculty of Pharmacy and Medical Sciences, University of Petra, Amman, Jordan, [3] Earlham Institute, Norwich, United Kingdom

OPEN ACCESS

Edited by:
Vadim V. Sumbayev, University of Kent, United Kingdom

Reviewed by:
Bernhard F. Gibbs, University of Oldenburg, Germany
Salvatore Salomone, Università degli Studi di Catania, Italy

***Correspondence:**
Heba Alshaker
h.alshaker@uea.ac.uk
Dmitri Pchejetski
d.pshezhetskiy@uea.ac.uk

Specialty section:
This article was submitted to Experimental Pharmacology and Drug Discovery, a section of the journal Frontiers in Pharmacology

Received: *13 December 2018*
Accepted: *11 March 2019*
Published: *27 March 2019*

Citation:
Alshaker H, Wang Q, Brewer D and Pchejetski D (2019) Transcriptome-Wide Effects of Sphingosine Kinases Knockdown in Metastatic Prostate and Breast Cancer Cells: Implications for Therapeutic Targeting. Front. Pharmacol. 10:303. doi: 10.3389/fphar.2019.00303

Sphingosine kinases 1 and 2 (SK1 and SK2) are proto-oncogenic isozymes expressed in many human tumors and associated with chemoresistance and poor prognosis. They are well-recognized therapy targets and their inhibition was shown to induce tumor volume reduction and chemosensitization in multiple cancer models. Oncogenic signaling is extremely complex and often cross-regulated. Designing molecular therapies and their combinations requires rational approaches to avoid redundant targeting or developing resistance. In this study, we have performed RNA transcriptome microarray analysis of two breast and two prostate metastatic cancer cell lines treated with siRNAs targeting SK1 or SK2. In prostate cancer cell lines SK1 knockdown (KD) has significantly changed expression of several genes including downregulation of *NSUN2*, *G3BP2* and upregulation of ETS1. SK2 KD also affected expression of multiple genes including downregulation of *CAPZA1 NSUN3* and *ADPGK* and upregulation of *VDAC1*, *IBTK*, *ETS1*, and *MKNK2*. Similarly, in breast cancer cells SK1 KD led to downregulation of *NSUN2*, *NFATC3*, *CDK2*, and *G3BP2* and upregulation of *GTF2B*, *TTC17*, and *RAB23*. SK2 KD in breast cancer cells has decreased expression of *ITGAV* and *CAPZA1* and increased expression of *GTF2B* and *ST13*. Gene-set enrichment analysis of known biochemical pathways showed that in prostate and breast cell lines SKs KD have altered multiple pathways. SK1 KD altered chromatin assembly, regulation of G1/S transition and mitosis, Wnt and MAP kinase signaling and cell motility. SK2 KD altered RAS protein signal transduction, regulation of MAP kinase and serine/threonine kinase activity, cell motility, small GTPase mediated signal transduction and phosphatidylinositol 3-kinase (PI3K) signaling. Through genome-wide microarray analysis, we have identified important molecular pathways affected by SK1 and SK2 KD. It appears that while KD of both genes leads to a decrease in individual pro-tumorigenic genes, there is a universal cellular response resulting in upregulation of several known

pro-survival and pro-tumorigenic pathways such as MAPK, RAS, and PI3K, which may mediate cancer resistance to anti-SKs therapies. Our data point out to the potential advantage of certain molecular therapy combinations in targeting prostate and breast cancer. Further signaling studies are required to confirm the individual involvement of identified pathways.

Keywords: sphingosine kinase, gene knockdown, DNA microarray, transcriptome, breast cancer, prostate cancer, molecular targets, targeted therapy

INTRODUCTION

Sphingosine kinases 1 and 2 (SK1 and SK2) are proto-oncogenic enzymes expressed in multiple human tumors (Alshaker et al., 2013). They convert proapoptotic lipid second messenger sphingosine to anti-apoptotic sphingosine-1-phosphate. SKs display different subcellular localization and tissue expression patterns. SK1 is a constitutively active cytosolic enzyme, that translocates to the plasma membrane upon phosphorylation at Ser225. SK2 is localized mainly in the nucleus where it has a role in DNA synthesis and histone H3 acetylation (Song et al., 2018).

There is compelling evidence that SK1 activation contributes to cancer progression and leads to oncogenic transformation, increased tumor growth and impairment of apoptosis (reviewed in Alshaker et al., 2013; White et al., 2016). SK1 is a tumor-associated enzyme: high levels of SK1 expression have been shown in various human tumors such as brain, breast, colon, lung, ovary, stomach, uterus, kidney, rectum, and small intestine, where they enhance tumor neovascularization and metastatic potential by promoting motility and invasion of cancer cells (Cuvillier, 2007; Shida et al., 2008; Pyne et al., 2012). High levels of SK1 expression or activity are associated with a poor prognosis in several human cancers, making it a key pathway in the search for targeted therapies (Pyne et al., 2012). SK2 is predominantly localized to cell organelles and its role in cell proliferation/apoptosis is less well studied. However, several studies showed a critical role of SK2 for epidermal growth factor-stimulated migration of breast cancer cells, growth of tumor xenografts and lung cancer chemoresistance (Song et al., 2018).

Multiple SK1 and SK2 inhibitors have been synthesized and assayed in different biological systems. Selective SK1 inhibitors such as SK1-I or SK-F have been demonstrated to efficiently induce apoptosis in cancer cells (Paugh et al., 2008; Alshaker et al., 2018). A sphingosine analog FTY720 was shown to inhibit SK1 and induce cancer cell apoptosis (Wang et al., 1999; Permpongkosol et al., 2002), chemo- and radiosensitization (Pchejetski et al., 2010; Alshaker et al., 2017; Wang et al., 2017). Several studies have indicated an anti-tumorigenic role of a specific SK2 inhibitor ABC294640 (Antoon et al., 2011; Beljanski et al., 2011; Song et al., 2018).

Oncogenic signaling pathways are complex. Intervention with a single pathway usually leads to multiple pathways being affected due to cross-regulation. Based on this rationale, identifying signaling "hubs" has become popular in molecular therapy design, hoping that by targeting one key molecule, multiple signaling pathways can be regulated. This, however, can lead to undesirable side effects. Furthermore, targeting only one pathway does not always lead to desired effects due to the presence of parallel signaling pathways leading to the same end-point, prompting the use of combined therapies. Care should be taken in the creation of combined therapeutic interventions utilizing compounds that could target independent or compensatory pathways and therefore have synergistic effects. The rationale for such combinations could be derived from studying the gene expression and pathways regulation.

In this study, we have used for the first time RNA transcriptome microarray technology to investigate the transcriptome-wide effects of SK1 and SK2 downregulation. This approach mimics the therapeutic targeting of SKs by inhibitors and allows mapping the affected/unaffected signaling cascades. Our data provide useful insight for creating more robust therapeutic combinations for cancer targeting.

MATERIALS AND METHODS

Cell Culture and Reagents

Human breast cancer cell lines MDA-MB-231 and BT-549 and human prostate cancer cells lines PC-3 and DU145 were purchased from ATCC (Manassas, VA, United States), and maintained in RPMI with 10% FCS, 50 U/ml penicillin, 50 μg/ml streptomycin and 2 mM glutamine (Sigma-Aldrich, St. Louis, MO, United States). Cell lines were kept in culture for up to 30 passages. Cells were seeded to reach 70–80% confluence by the end of the treatment. All chemicals unless specified were from Sigma Aldrich (Poole, United Kingdom).

RNA Interference

Cells were seeded at a density to reach 30–50% confluence by the day of transfection. Cells were transfected as described previously (Alshaker et al., 2014, 2015) using siRNA directed against SK1 and SK2 as pooled four independent sequences and non-targeting siRNA as a negative control combined with HiPerFect (Qiagen, West Sussex, United Kingdom). Optimal knockdown (KD) was obtained 72 h post-transfection and verified by qRT-PCR.

RNA Extraction, cDNA Synthesis and qRT-PCR

Isolation of total RNA from cancer cells was performed using the RNeasy Mini kit (Qiagen, Valencia, CA, United States) as per manufacturer's instructions. RNA quantity and purity

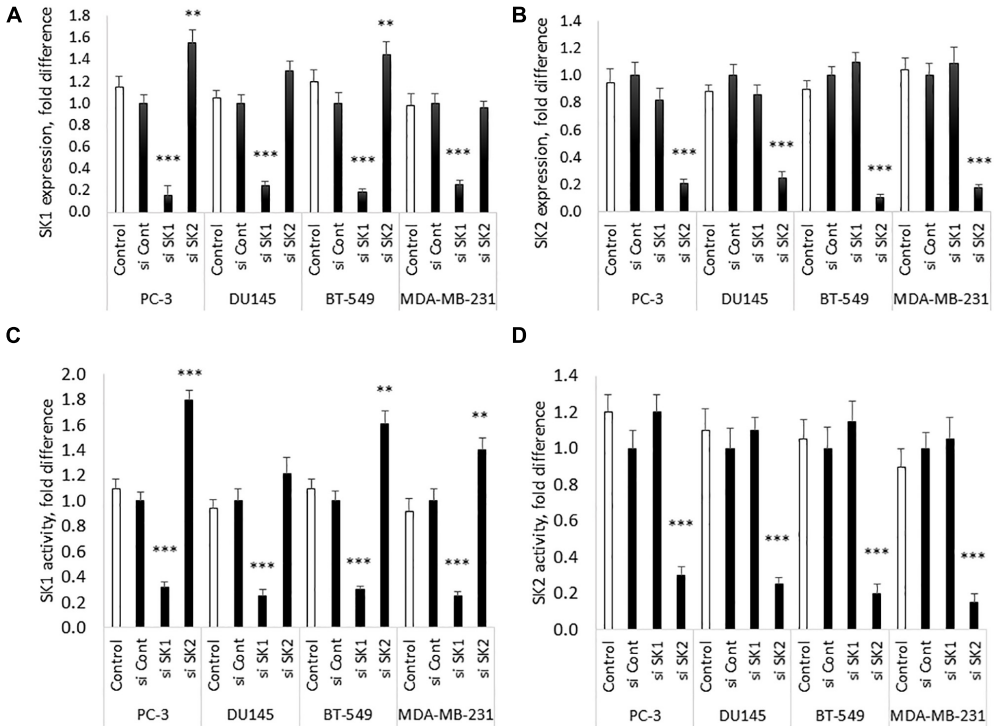

FIGURE 1 | SK1/SK2 knockdown in prostate and breast cancer cell lines. Human breast cancer cell lines MDA-MB-231 and BT-549 and human prostate cancer cells lines PC-3 and DU145 were transfected with SK1 and SK2 siRNA and gene knockdown was assessed by qRT-PCR **(A,B)**. SK1 and SK2 activity was assessed using radiolabeling assay **(C,D)**. Data mean values of at least three independent experiments normalized to control ± SEM. $^{**}p < 0.01$, $^{***}p < 0.001$.

was measured using a NanoDrop 2000c Spectrophotometer (Thermo Fisher Scientific, Loughborough, United Kingdom). Reverse transcription was performed using Precision nanoScript^{TM} Reverse transcription kit (PrimerDesign Ltd., Southampton, United Kingdom). qRT-PCR was done as already described (Alshaker et al., 2014, 2017). Ct values were exported and analyzed using qbase software (Biogazelle NV, Zwijnaarde, Belgium).

RNA Microarray

RNA was normalized to an input amount of 99.9 ng and underwent reverse transcription. sscDNA was purified using magnetic beads and fragmented using UDG. Fragmented sample was hybridized to Affymetrix Clariom S human arrays at 45°C overnight. Stained arrays are scanned to generate intensity data. All reagent kits and arrays were purchased from Thermo Fisher Scientific, Loughborough, United Kingdom.

Sphingosine Kinase Activity

Sphingosine kinases 1 and 2 assay was performed using radiolabeling as previously described (Pchejetski et al., 2011; Alshaker et al., 2014, 2015), in conditions favoring either SK1 or SK2 activity (Liu et al., 2000).

Statistical Analysis

qRT-PCR data are presented as the mean values of at least three independent experiments normalized to control ± standard error of the mean (SEM) calculated using GraphPad Prism. Statistical significance between two groups was conducted by unpaired Student's *t*-test. *P*-value of <0.05 is considered statistically significant.

DNA microarray analyses were performed in R version 3.4.3. Gene-level signal estimates were derived from CEL files generated from Affymetrix Clariom S human arrays using the multi-array analysis (RMA) algorithm (Irizarry et al., 2003) implemented in Bioconductor package oligo version 1.42.0 (Carvalho and Irizarry, 2010). Differential expression analysis was performed using the *limma* version 3.34.4: linear models were determined for each transcript cluster (gene) and an estimate for the global variance calculated by an empirical Bayes approach (Smyth, 2004). A moderated *t*-statistic was computed for each transcript cluster with the resulting *p*-values adjusted for multiple testing using Benjamini and Hochberg's method to control the false discovery rate. Those transcript clusters with an adjusted *p*-value less than 0.05 were considered to be significantly differentially expressed between the two groups.

Gene ontology biological process and hallmarks of cancer gene sets were tested in gene set enrichment analysis using the clusterProfiler package, version 3.6 (Yu et al., 2012). The *t*-statistic generated in the differential expression analyses was used as the metric, with all entrez genes as the background and a cut-off *p*-value of 0.05 after multiple testing using the false discovery rate.

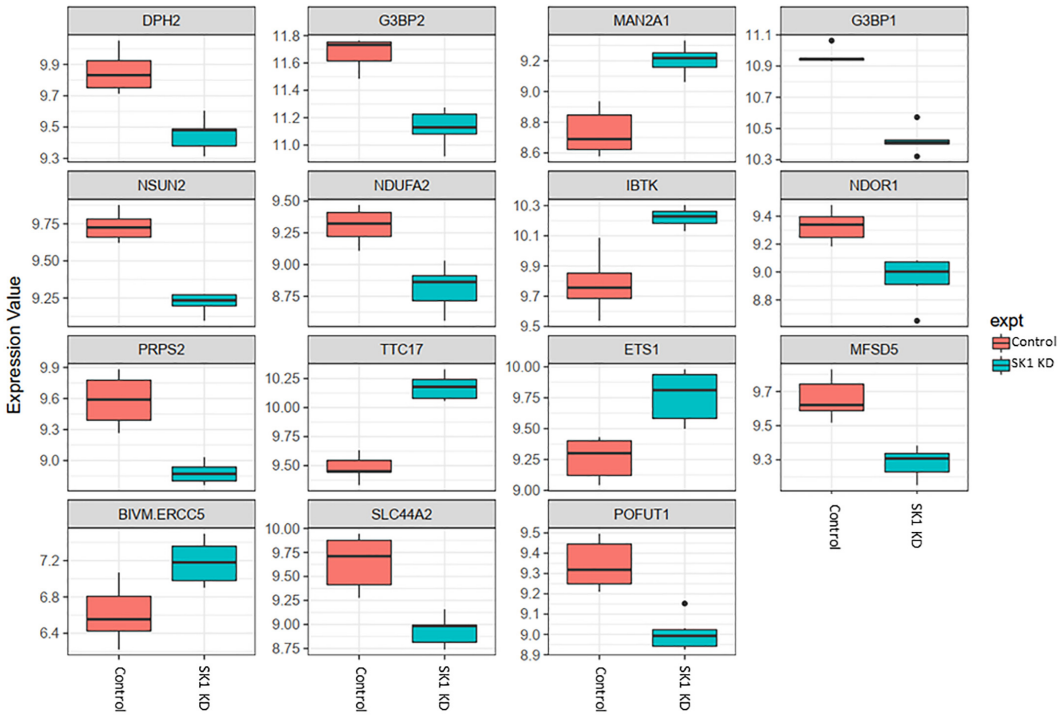

FIGURE 2 | Altered gene expression in response to SK1 knockdown (KD) in prostate cancer cell lines. Human prostate cancer cells lines PC-3 and DU145 were transfected with SK1 siRNA and Affymetrix Clariom S human array was performed as described in materials and methods. Differential expression analysis was performed using the *limma* version 3.34.4: linear models were determined for each transcript cluster (gene) and an estimate for the global variance calculated by an empirical Bayes approach. A moderated *t*-statistic was computed for each transcript cluster with the resulting *p*-values adjusted for multiple testing using Benjamini and Hochberg's method to control the false discovery rate. Those transcript clusters with an adjusted *p*-value less than 0.05 were considered to be significantly differentially expressed between the two groups; *bars*, SEM.

RESULTS

Chemotherapy and molecular therapy are currently used in treatment of locally advanced and metastatic prostate and breast cancers. Among those cancers, androgen-independent prostate tumors and triple negative breast tumors are considered the most aggressive form of the disease. As a model of those diseases, we have chosen two metastatic androgen-insensitive prostate cancer cells lines PC-3 and DU145 and two metastatic triple negative breast cancer cell lines MBA-MB-231 and BT-549. SK1 and SK2 downregulation was achieved by transfection with four pooled sequences siRNA (Qiagen) for 72 h and verified using qRT-PCR (**Figure 1**). It is interesting to note that in PC-3 and BT-549 cells KD of SK1 caused a significant increase in SK2 expression (55 and 45%, respectively), however this effect was not present in MDA-MB-231 and DU145 cells (**Figure 1**). These results were confirmed on the enzyme level using SK1 and SK2 activity (**Figure 1**).

DNA CHIP analysis was performed on all samples in triplicate using Affymetrix Clariom S microarray. Genes were determined to be significantly differentially expressed using a moderated *t*-test (p (0.05; Benjamin Hochberg multiple testing correction applied). SK1 and SK2 regulated genes exhibited tissue specific differences. As expected, SK1 and SK2 were shown to be down-regulated by respective siRNA pools (for clarity, these effects are not shown in **Figures 2–5**).

In prostate cancer cells SK1 KD induced downregulation of expression of ten genes and upregulation of five genes (**Figure 2**, only genes identically regulated in both cell lines are shown). Among the genes downregulated by SK1 were G3BP stress granule assembly factors G3BP1 and G3BP2 [involved in nuclear factor kappa B (NFκB), RAS and Wnt signaling], phosphoribosyl pyrophosphate synthetase 2 (PRPS2), involved in multiple biosynthesis pathways like purine synthesis, NOP2/Sun RNA methyltransferase family member 2 (NSUN2) which regulates mRNA translation and NADH:ubiquinone oxidoreductase subunit A2 (NDUFA2), a subunit of complex I of the respiratory chain. SK1 KD increased expression of IBTK (inhibitor of Bruton tyrosine kinase) and notably ETS1 (ETS proto-oncogene 1, transcription factor).

In breast cancer cells SK1 KD (**Figure 3**) has decreased the expression of E2F5 (E2F transcription factor 5), NSUN2, nuclear factor of activated T-cells 3 (NFATC3) which regulates transcription, PRPS2, cyclin dependent kinase 2 (CDK2), known regulator in the cell cycle, G3BP stress granule assembly factors G3BP1 and G3BP2, vesicle-associated membrane-protein-associated protein B (VAPB) involved in vesicle trafficking and N-acetylglucosamine kinase (NAGK), involved in metabolism.

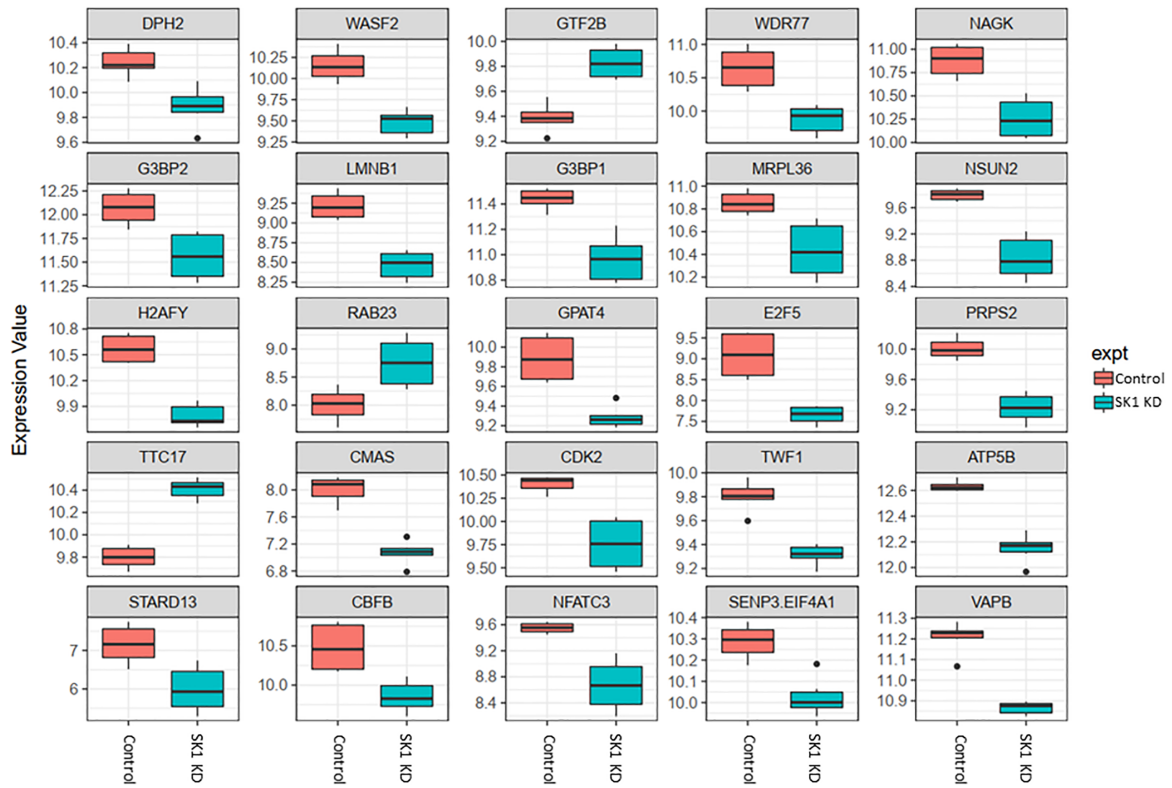

FIGURE 3 | Altered gene expression in response to SK1 knockdown (KD) in breast cancer cell lines. Human breast cancer cell lines MDA-MB-231 and BT-549 were transfected with SK1 siRNA and Affymetrix Clariom S human array was performed as described in materials and methods. Differential expression analysis was performed using the *limma* version 3.34.4: linear models were determined for each transcript cluster (gene) and an estimate for the global variance calculated by an empirical Bayes approach. A moderated *t*-statistic was computed for each transcript cluster with the resulting *p*-values adjusted for multiple testing using Benjamini and Hochberg's method to control the false discovery rate. Those transcript clusters with an adjusted *p*-value less than 0.05 were considered to be significantly differentially expressed between the two groups; *bars*, SEM.

SK1 KD has notably increased expression of RAB23 (encodes a small GTPase of the RAS oncogene superfamily).

In prostate cells, SK2 KD affected expression of 25 genes (**Figure 4**) including downregulation of capping actin protein of muscle Z-line alpha subunit 1 (CAPZA1), involved in inhibition of autophagy and epithelial-mesenchymal transition (EMT), NSUN3 (NOP2/Sun RNA methyltransferase family member 3, mRNA translation), ADP dependent glucokinase (ADPGK), involved in EMT in cancer cells and kelch domain containing 10 (KLHDC10), which regulates oxidative stress. SK2 KD increased expression of voltage dependent anion channel 1 (VDAC1) oncogene, regulator of mammalian target of rapamycin (mTOR), inhibitor of Bruton tyrosine kinase (IBTK), antiproliferative, ataxin 10 (ATXN10) which activates the RAS-MAP kinase pathway, ETS proto-oncogene 1 (ETS1), transcription factor, ubiquitin conjugating enzyme E2 R2 (UBE2R2) involved in ubiquitination and cell differentiation, MAP kinase interacting serine/threonine kinase 2 (MKNK2), protein phosphatase 2 regulatory subunit B′alpha (PPP2R5A) and WEE1 G2 checkpoint kinase (WEE1), cell cycle regulator.

On the other hand, SK2 KD in breast cancer (**Figure 5**) has downregulated expression of integrin subunit alpha V (ITGAV), belongs to the integrin alpha chain family which may regulate angiogenesis and cancer progression and capping actin protein of muscle Z-line alpha subunit 1 (CAPZA1), regulates growth of the actin filament and increased expression of general transcription factor IIB (GTF2B), zinc finger DHHC-type containing 20 (ZDHHC20) and ST13, Hsp70 interacting protein, involved in the assembly process of glucocorticoid receptor.

We have then performed a functional analysis of identified genes for the gene-set enrichment of known biochemical pathways upon SK1 and 2 KD. We have investigated the changes for gene ontology biological process pathways (**Figure 6** and **Supplementary Tables S1–S4**) and hallmarks of cancer gene sets (**Tables 1–4**). SK1 and SK2 KD had different effect on pathway enrichment which was also cell line dependent, although there were several common pathways shared between both cell lines and both SKs. Gene-set enrichment analysis of gene ontology biological process enrichment pathways showed that in prostate cancer cells SK1 KD has induced downregulation of pathways linked with DNA conformation change, chromatin assembly and regulation of G1/S transition of mitotic cell cycle and notably

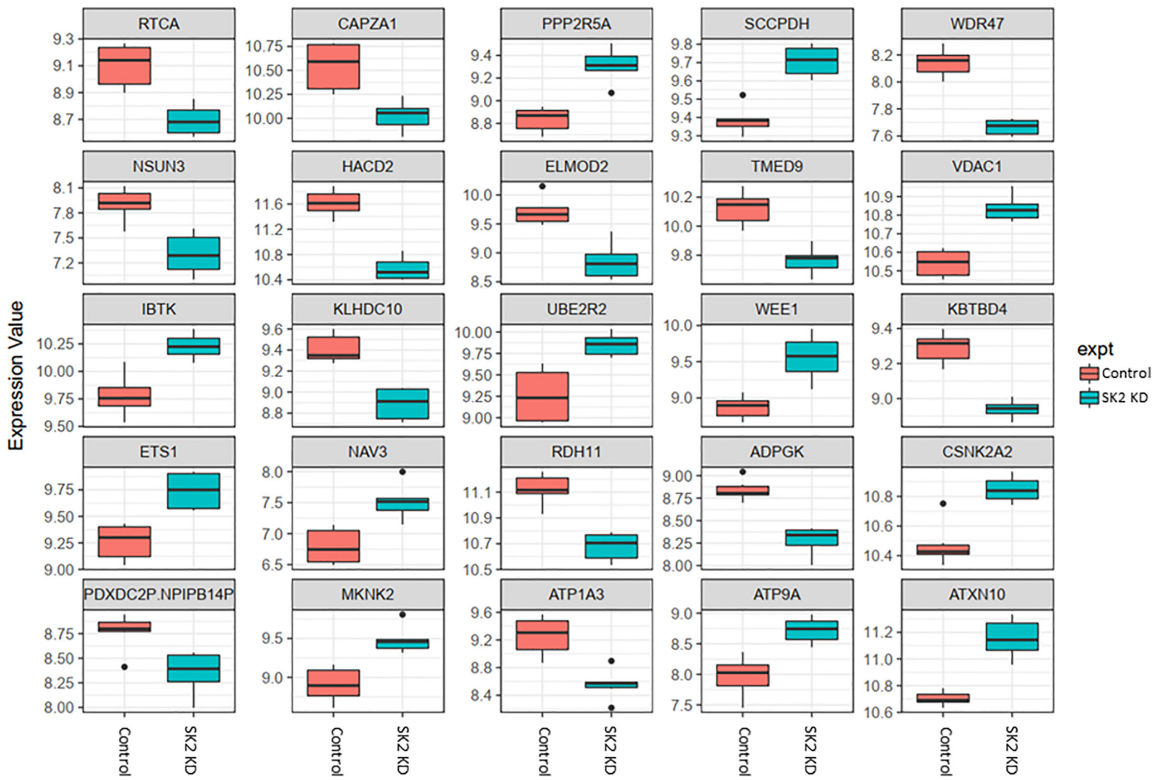

FIGURE 4 | Altered gene expression in response to SK2 knockdown (KD) in prostate cancer cell lines. Human prostate cancer cells lines PC-3 and DU145 were transfected with SK2 siRNA and Affymetrix Clariom S human array was performed as described in materials and methods. Differential expression analysis was performed using the *limma* version 3.34.4: linear models were determined for each transcript cluster (gene) and an estimate for the global variance calculated by an empirical Bayes approach. A moderated *t*-statistic was computed for each transcript cluster with the resulting *p*-values adjusted for multiple testing using Benjamini and Hochberg's method to control the false discovery rate. Those transcript clusters with an adjusted *p*-value less than 0.05 were considered to be significantly differentially expressed between the two groups; *bars*, SEM.

enrichment of Wnt signaling pathway, cell motility and MAP kinase activity (**Supplementary Table S1**, examples of linked pathways shown in **Figure 6**). In breast cancer cells SK1 KD has induced a downregulation of pathways responsible for DNA replication and repair, cell cycle (G1/S), p53, enrichment in Wnt signaling and vesicle-mediated transport pathways (**Supplementary Table S2**, examples of linked pathways shown in **Figure 6**). In prostate cancer cells, SK2 KD has enriched RAS protein signal transduction, MAP kinase, protein serine/threonine kinase, cell motility, small GTPase and phosphatidylinositol 3-kinase signaling pathways (**Supplementary Table S3**, examples of linked pathways shown in **Figure 6**) while in breast cancer cells it induced Wnt signaling, small GTPase mediated signal transduction, MAP kinase, endosomal transport and RAS protein signal transduction pathways and downregulated DNA repair pathway (**Supplementary Table S4**, examples of linked pathways shown in **Figure 6**).

Gene-set enrichment analysis of hallmarks of cancer pathways has shown several important pathways regulated by SK1/SK2 KD. SK1 KD in breast cancer cell lines downregulated Myc, G2/M cell cycle and E2F pathways (**Table 1**) and upregulated KRAS, IL2/signal transducer and activator of transcription (STAT)5 and tumor necrosis factor (TNF)/NFκB pathways. Prostate cancer cell lines similarly had G2/M, E2F and additionally p53 pathways downregulated, and KRAS, IL2/STAT5, TNF/NFκB and additionally EMT pathways upregulated by SK1 KD (**Table 2**).

Sphingosine kinase 2 KD had similar effects to SK1 in breast cancer cells downregulating KRAS, G2/M and E2F pathways and upregulating EMT and p53 pathways (**Table 3**). On the contrary, in prostate cancer cells SK2 KD has upregulated G2/M and E2F pathways (**Table 4**).

DISCUSSION

In the last decade SK inhibitors have shown significant potential for cancer treatment. There are dozens of papers proving their antitumour efficacy *in vitro* and *in vivo* (reviewed in Alshaker et al., 2013) and two molecules are already in clinical trials: SK1 inhibitor phenoxodiol (Veyonda) for prostate cancer, non-small cell lung cancer and sarcoma; and SK2 inhibitor ABC294640 (opaganib) for advanced solid tumors and multiple myeloma. These inhibitors are often proposed to be used as "sensitisers" to chemo- and radiotherapy and can be used as

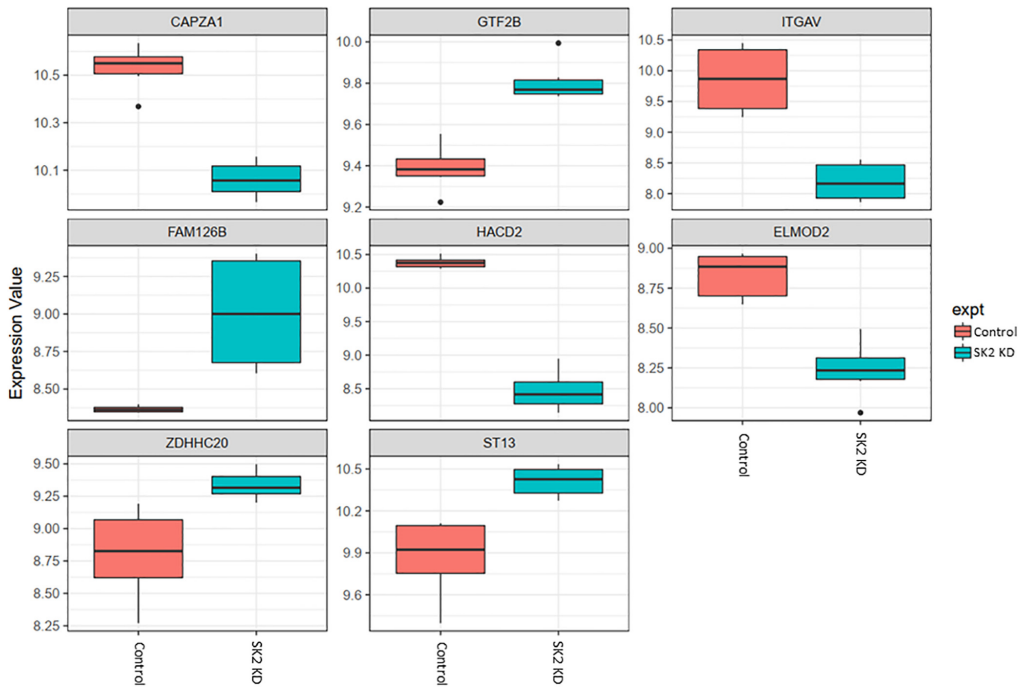

FIGURE 5 | Altered gene expression in response to SK2 knockdown (KD) in breast cancer cell lines. Human breast cancer cell lines MDA-MB-231 and BT-549 were transfected with SK2 siRNA and Affymetrix Clariom S human array was performed as described in materials and methods. Differential expression analysis was performed using the *limma* version 3.34.4: linear models were determined for each transcript cluster (gene) and an estimate for the global variance calculated by an empirical Bayes approach. A moderated *t*-statistic was computed for each transcript cluster with the resulting *p*-values adjusted for multiple testing using Benjamini and Hochberg's method to control the false discovery rate. Those transcript clusters with an adjusted *p*-value less than 0.05 were considered to be significantly differentially expressed between the two groups; *bars*, SEM.

free drugs or in nanoparticle settings (Alshaker et al., 2017; Wang et al., 2017; Yee et al., 2017). Their specificity has significantly increased with the recent discovery of SK1 structure (Wang et al., 2013) and the use of computer modeling methods (Alshaker et al., 2018).

Cancer progression is mediated by multiple mutations and involves activation of a wide variety of signaling pathways, many of which are cross-regulated or lead to similar downstream events (reviewed in Garland, 2017). For example, in cancer cell, a mutation in receptor tyrosine kinase can activate multiple signaling pathways and subsequent transcription factors leading to gene expression, while each of these pathways can be also mutated or activated independently, creating a highly complex web of signaling. The typical molecular targeting therapy approach is to block these pathways (e.g., tyrosine kinases, mTOR, MAPK, PARP, CDK, etc.) with specific inhibitors. Aside from few cases (such as BCR-Abl), where one major mutation is responsible for cancer progression, it appears that switching off one pathway is usually insufficient to completely block cancer cell growth and induce cell death. Ordinarily, targeted cancer monotherapy can end up with bypass mechanisms. Resistant clones of cancer cells evolve that can compensate for the switched off pathway by upregulating other independent pathways.

Several approaches can be used to circumvent this phenomenon. First, improved drug delivery may allow achieving higher drug concentrations in the tumor leading to higher efficacy. Second, the employment of several combined targeted or non-targeted therapies or agents that interfere with multiple cell-signaling pathways may allow making multiple hits on the cell proliferation machinery. Finally, a combination of these approaches can possibly provide a significant benefit both in terms of efficacy and reducing side effects (Alshaker et al., 2017; Wang et al., 2017).

When designing the successful drug combinations, one may consider which pathways are implicated in proliferation and chemoresistance in the target system, as well as the known crosstalk between these pathways. For example, if a pro-survival pathway A activates a pro-survival pathway B, but doesn't affect the pro-survival pathway C, targeting both A and B is redundant while targeting A and C may have synergistic therapeutic effect.

We have conducted this study to identify which signaling pathways are universally or tissue specifically regulated by SK1 and SK2 in prostate and breast cancers. More importantly, we questioned which common cell proliferation pathways are upregulated as compensatory mechanisms and may be responsible for resistance to anti-SK therapies. Considering that SK inhibitors may reach clinic in near future, this knowledge would allow us to hypothesize which combinational therapies may have synergistic effects.

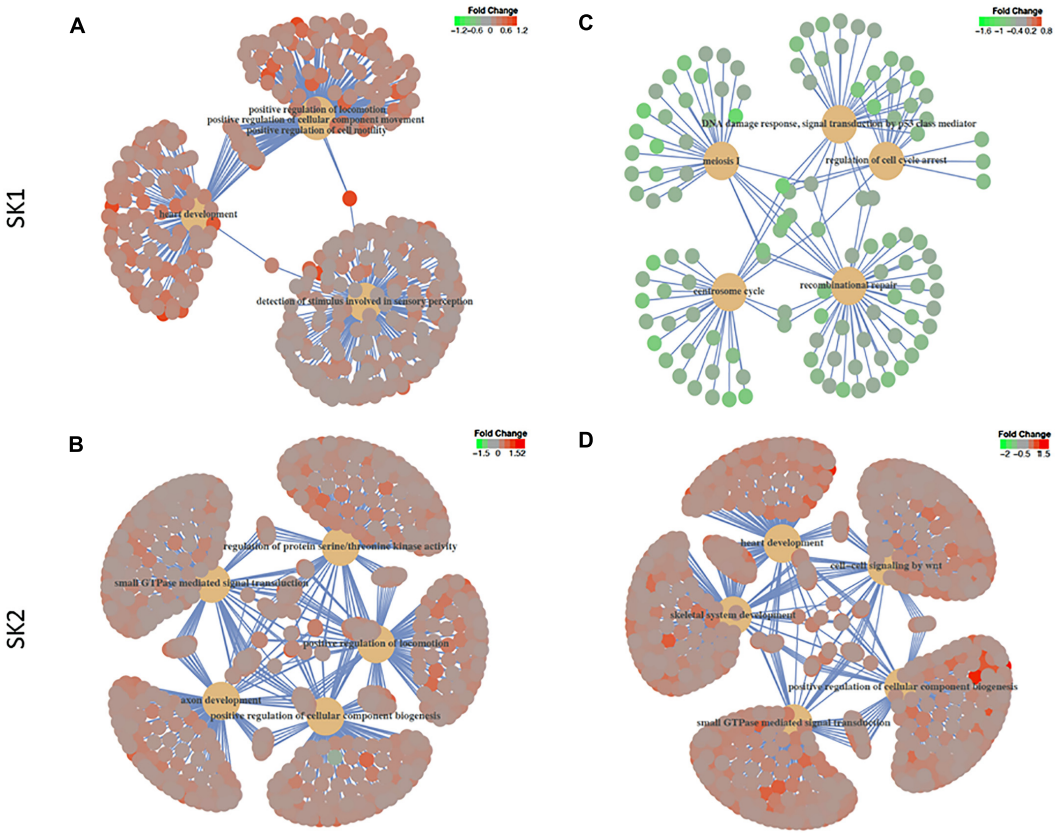

FIGURE 6 | Gene-set enrichment analysis of gene ontology biological process enrichment pathways. Human prostate cancer cells lines PC-3 and DU145 **(A,B)** and human breast cancer cell lines MDA-MB-231 and BT-549 **(C,D)** were transfected with SK1 **(A,C)** and SK2 **(B,D)** siRNA and Affymetrix Clariom S human array was performed as described in materials and methods. Gene ontology biological process and hallmarks of cancer gene sets were tested in gene set enrichment analysis using the clusterProfiler package, version 3.6. The *t*-statistic generated in the differential expression analyses was used as the metric, with all Entrez Genes as the background and a cut-off *p*-value of 0.05 after multiple testing using the false discovery rate.

Across all four cell lines investigated SK1 KD downregulated expression of NSUN2 (mRNA translation), PRPS2 (purine synthesis) and G3BP1,2 (NFκB, RAS, and Wnt signaling) (**Figures 2**, **3**). Other notable genes decreased by SK1 KD were NDUFA2 in prostate and E2F5, NAGK, VAPB, NFATC3, CDK2 in breast cancer cell lines. SK2 KD universally downregulated expression of CAPZA1 (inhibition of autophagy and EMT) and also decreased expression of NSUN3, ADPGK and KLHDC10 in prostate and ITGAV in breast cancer cell lines (**Figures 4**, **5**). From these data it appears that SK targeting carries a significant antiproliferative effect through downregulation of expression of several genes which are relevant for cell survival and division. However, individually SK1 and SK2 KD have led to upregulation of multiple genes (IBTK, GTF2B, VDAC1, GTF2B, ETS1, TTC17, IBTK, ZDHHC20, RAB23, ATXN10, ST13, ETS1, PPP2R5A, MKNK2, UBE2R2, WEE1) that regulate transcription, cell cycle, EMT, cell motility, serine/threonine kinases, small GTPases, phosphatidylinositol 3-kinase (PI3K), HSP70, Wnt, mTOR, RAS and MAPK signaling pathways (Jiang-Hua et al., 2014; Hu et al., 2018; Liu et al., 2018). It is very likely that these pathways represent a cellular "compensatory" response and may be potentially contributing to SK-inhibitor resistance.

Sphingosine kinases 1 and 2 KD has up- and downregulated a significant number of genes in individual cell lines (**Supplementary Table S5**). This number was reduced to 15 and 25 genes for SK1 and SK2 KD, respectively, in prostate cells and 25 and 8 genes for SK1 and SK2 KD, respectively, in breast cancer cells (**Figures 2**–**5**, **7**). There was some concordance of SK-regulated genes between the tissues. Five genes (DPH2 G3BP1, G3BP2, NSUN2, and TTC17) were similarly regulated by SK1 KD in prostate and breast cancer cells (**Figure 7**). SK2 KD has regulated CAPZA1, ELMOD2, and HACD2 in a similar fashion across all four cell lines (**Figure 7**). There was no overlap between SK1 and SK2 regulated genes.

While individual genes may provide insight into altered signaling, gene-set enrichment analysis may demonstrate a bigger picture of significant pathways modulated by SK KD. Gene-set enrichment pathway analysis showed that in all cell lines SK1 KD decreased DNA conformation and replication pathways, while SK2 KD did not decrease any major pro-proliferative pathways. In contrast, there is a clear concordance in pathways upregulated in response to SK KD. SK2 KD has upregulated RAS, MAPK and small GTPase pathways, while

TABLE 1 | Gene-set enrichment analysis of hallmark of cancer enrichment pathways in response to SK1 KD in breast cancer cells.

Description	Enrichment score	*p*-value
HALLMARK_E2F_TARGETS	−0.58603	0.001923
HALLMARK_G2M_CHECKPOINT	−0.45283	0.001905
HALLMARK_MYC_TARGETS_V1	−0.40462	0.001923
HALLMARK_UV_RESPONSE_UP -0.32927	0.012121	
HALLMARK_INFLAMMATORY_ RESPONSE	0.285129	0.026971
HALLMARK_KRAS_SIGNALING_UP	0.287628	0.024896
HALLMARK_IL2_STAT5_SIGNALING	0.296696	0.010526
HALLMARK_APOPTOSIS	0.300881	0.026
HALLMARK_GLYCOLYSIS	0.30635	0.004149
HALLMARK_TNFA_SIGNALING_VIA_ NFKB	0.314365	0.004211
HALLMARK_COMPLEMENT	0.32964	0.004211
HALLMARK_APICAL_JUNCTION	0.340443	0.002075
HALLMARK_MYOGENESIS	0.34409	0.002105
HALLMARK_P53_PATHWAY	0.354588	0.002096
HALLMARK_HYPOXIA	0.355858	0.002105
HALLMARK_FATTY_ACID_ METABOLISM	0.373058	0.003984
HALLMARK_XENOBIOTIC_ METABOLISM	0.374965	0.002075
HALLMARK_ADIPOGENESIS	0.381432	0.002105
HALLMARK_COAGULATION	0.404393	0.001996
HALLMARK_INTERFERON_GAMMA_ RESPONSE	0.4096	0.00211
HALLMARK_EPITHELIAL_ MESENCHYMAL_TRANSITION	0.414758	0.002105
HALLMARK_UV_RESPONSE_DN	0.437977	0.001976

TABLE 2 | Gene-set enrichment analysis of hallmark of cancer enrichment pathways in response to SK1 KD in prostate cancer cells.

Description	Enrichment score	*p*-value
HALLMARK_UV_RESPONSE_UP	−0.402737052	0.0027
HALLMARK_E2F_TARGETS	−0.382852104	0.0028
HALLMARK_G2M_CHECKPOINT	0.373919221	0.0028
HALLMARK_P53_PATHWAY	−0.311816056	0.0028
HALLMARK_XENOBIOTIC_METABOLISM	−0.31162798	0.0028
HALLMARK_INTERFERON_GAMMA_ RESPONSE	−0.308977776	0.0028
HALLMARK_FATTY_ACID_METABOLISM	−0.290319736	0.0134
HALLMARK_ADIPOGENESIS	−0.290165971	0.0057
HALLMARK_OXIDATIVE_ PHOSPHORYLATION	−0.273082408	0.0113
HALLMARK_COMPLEMENT	0.283316334	0.0246
HALLMARK_HYPOXIA	0.291083127	0.0185
HALLMARK_IL2_STAT5_SIGNALING	0.295293643	0.0154
HALLMARK_TNFA_SIGNALING_VIA_ NFKB	0.317881573	0.0077
HALLMARK_MITOTIC_SPINDLE	0.333397383	0.0046
HALLMARK_KRAS_SIGNALING_UP	0.367158279	0.0015
HALLMARK_EPITHELIAL_ MESENCHYMAL_TRANSITION	0.440097468	0.0015

TABLE 3 | Gene-set enrichment analysis of hallmark of cancer enrichment pathways in response to SK2 KD in breast cancer cells.

Description	Enrichment score	*p*-value
HALLMARK_INTERFERON_GAMMA_ RESPONSE	−0.389698297	0.0043
HALLMARK_ALLOGRAFT_REJECTION	−0.339536274	0.0043
HALLMARK_KRAS_SIGNALING_DN	−0.28487173	0.0042
HALLMARK_E2F_TARGETS	−0.278165758	0.0085
HALLMARK_G2M_CHECKPOINT	−0.270306348	0.0129
HALLMARK_GLYCOLYSIS	0.317865223	0.0222
HALLMARK_FATTY_ACID_METABOLISM	0.326776858	0.0214
HALLMARK_MITOTIC_SPINDLE	0.348623881	0.0052
HALLMARK_XENOBIOTIC_METABOLISM	0.356201125	0.0013
HALLMARK_HYPOXIA	0.356508267	0.0013
HALLMARK_APICAL_JUNCTION	0.356988995	0.0013
HALLMARK_EPITHELIAL_ MESENCHYMAL_TRANSITION	0.373510215	0.0013
HALLMARK_ADIPOGENESIS	0.382867908	0.0013
HALLMARK_HEME_METABOLISM	0.390882683	0.0013
HALLMARK_P53_PATHWAY	0.424168593	0.0013
HALLMARK_MYOGENESIS	0.429404077	0.0013
HALLMARK_UV_RESPONSE_DN	0.445254468	0.0014

TABLE 4 | Gene-set enrichment analysis of hallmark of cancer enrichment pathways in response to SK2 KD in prostate cancer cells.

Description	Enrichment score	*p*-value
HALLMARK_INTERFERON_GAMMA_ RESPONSE	−0.45775	0.003021148
HALLMARK_UV_RESPONSE_UP	−0.35239	0.002881844
HALLMARK_FATTY_ACID_ METABOLISM	−0.30608	0.00877193
HALLMARK_HEME_METABOLISM	0.3308	0.004470939
HALLMARK_E2F_TARGETS	0.33106	0.004451039
HALLMARK_G2M_CHECKPOINT	0.34475	0.001501502
HALLMARK_UV_RESPONSE_DN	0.3727	0.003120125
HALLMARK_MITOTIC_SPINDLE	0.47889	0.00148368

SK1 KD has increased Wnt signaling in all four cell lines (**Supplementary Tables S1–S4**). In tissue specific manner, SK1 and SK2 KD individually have also increased cell motility, vesicular transport, cell motility, Rho, PI3K and serine/threonine kinase pathways. Similar to individual genes, these pathways are likely to represent the "compensatory" response of cancer cells to SKs KD and may contribute to developing resistance for anti SK therapies.

Gene-set enrichment analysis of hallmarks of cancer pathways has shown that several important pathways are upregulated in response to SK1/SK2 KD, most notably KRAS, IL2/STAT5, EMT and TNF/NFκB (SK1 KD) and EMT, G2/M and E2F (SK2 KD) (**Tables 1–4**). Interestingly, several well-known pathways implicated in cancer progression or apoptosis were unaffected by SK KD (such as BCL2, PARP, or many transcription factors). These pathways are also therapeutic targets and concurrent

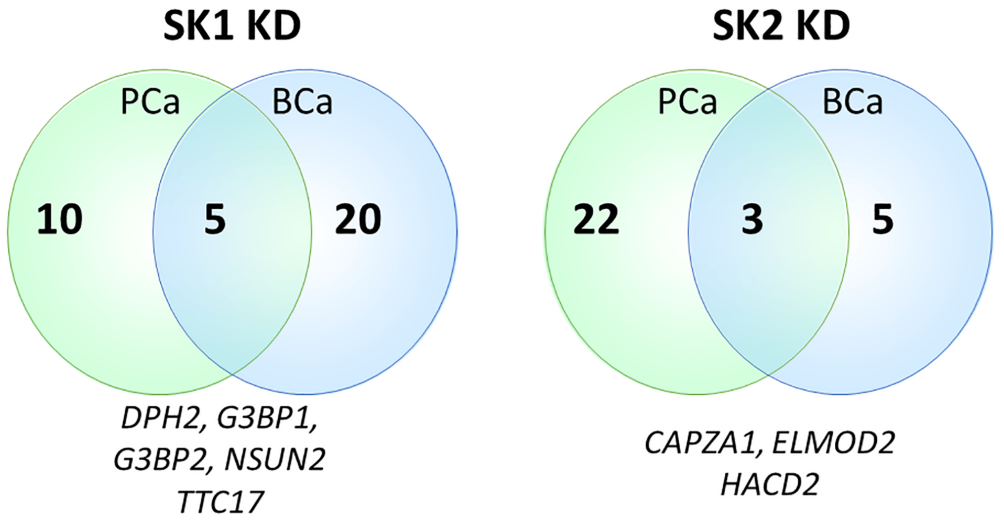

FIGURE 7 | Venn diagram of genes regulated by SK1/SK2 knockdown (KD) in prostate and breast cell lines. Human breast cancer cell lines MDA-MB-231 and BT-549 and prostate cancer cells lines PC-3 and DU145 were transfected with SK1 or SK2 siRNA and Affymetrix Clariom S human array was performed as described in materials and methods. Numbers of significantly regulated genes common to prostate or breast cell lines are shown in outer semicircles and the number of genes universally regulated by SK1 or SK2 KD in all cell lines is shown in the middle. These universal genes are listed below the circles.

use of their inhibitors and SK inhibitors may have therapeutic advantage. For example, if one were to use SK1 inhibitor in prostate cancer, adding PI3K inhibitor may be of particular benefit as SK1 KD is upregulating PI3K pathway which may mediate resistance. Same goes for e.g., Ras pathway and SK2 in both prostate and breast cancer cells. Conversely G1/S and G2/M are both significantly inhibited by SK1 KD in breast cancer cells, therefore adding cell cycle inhibitors may be of no additional benefit.

There were no previous studies investigating transcriptome in response to SK1 KD. An opposite study was performed by Pham et al. (2014), who have transfected NIH3T3 cells with SK1 and analyzed transcriptome identifying multiple genes regulated by artificially increased SK1. There, however, may be significant difference between genes regulated by baseline SK1 activity or its absence (as in our case) and artificial SK1 overexpression. From comparison of both studies it is also clear that SK1-regulated genes are tissue and cell line specific. Angerer et al. (2018) have described transcriptome profiling of peripheral blood immune cell populations in multiple sclerosis patients before and during treatment with a sphingosine-1-phosphate receptor modulator fingolimod (also an SK1 inhibitor in higher doses) identifying *QGAP2*, *MYBL1*, and *PTPN12* that were consistently expressed at significantly higher transcript levels in response to continued administration of fingolimod in $CD8^+$, $CD4^+$ and $CD19^+$ cells. Fingolimod has S1P receptor affinity at nanomolar range but requires micromolar levels to inhibit SK1 (Pchejetski et al., 2010), and it is unlikely that such levels were achieved in human patients. In addition to designing combined therapies, our data may also provide an insight into the potential side effects of therapeutic SKs inhibition. Many of the identified pathways are linked with tissue development, DNA repair, apoptosis and many other pivotal physiological processes.

As any pharmacological compounds, most SK inhibitors are not uniquely targeting SKs. Some of them have higher affinity toward SK1 (e.g., SK1-I) or SK2 (e.g., ABC294640), while others inhibit both SKs (e.g., SKI-II). They may also affect activity of other kinases. We therefore focused on using a "clean method" of SKs downregulation. It is, however, possible that siRNAs may have different effect on gene expression than pharmacological inhibitors.

CONCLUSION

Through genome-wide microarray, we have identified important molecular pathways affected and not affected by SK1 and SK2 signaling. Multiple pathways such RAS, MAPK, small GTPase, Wnt and PI3K were upregulated in response to SK KD. Additionally, several well-known pathways implicated in cancer progression or apoptosis were unaffected by SK KD (such as BCL2, PARP). Co-targeting of these pathways may present a viable therapeutic option to overcome SK inhibitor resistance in prostate and breast cancer. Further signaling studies are required to confirm the individual involvement of the identified pathways.

AUTHOR CONTRIBUTIONS

HA developed the idea, performed the experiments, interpreted the data, edited figures and wrote the manuscript. QW provided assistance and materials. DB analyzed and interpreted data and prepared the figures. DP developed the idea, supervised

experiments, interpreted the data, and wrote the manuscript. All authors reviewed the manuscript and agreed the final version of the manuscript for publication.

FUNDING

Funding for the project was generously provided by Research Innovation Fund, University of East Anglia (DP) and by the Deanship of Scientific Research, University of Petra, Amman, Jordan (HA).

SUPPLEMENTARY MATERIAL

The Supplementary Material for this article can be found online at: https://www.frontiersin.org/articles/10.3389/fphar.2019.00303/full#supplementary-material

REFERENCES

Alshaker, H., Krell, J., Frampton, A. E., Waxman, J., Blyuss, O., Zaikin, A., et al. (2014). Leptin induces upregulation of sphingosine kinase 1 in oestrogen receptor-negative breast cancer via Src family kinase-mediated, janus kinase 2-independent pathway. *Breast Cancer Res.* 16:426. doi: 10.1186/s13058-014-0426-6

Alshaker, H., Sauer, L., Monteil, D., Ottaviani, S., Srivats, S., Bohler, T., et al. (2013). Therapeutic potential of targeting SK1 in human cancers. *Adv. Cancer Res.* 117, 143–200. doi: 10.1016/B978-0-12-394274-6.00006-6

Alshaker, H., Srivats, S., Monteil, D., Wang, Q., Low, C. M. R., and Pchejetski, D. (2018). Field template-based design and biological evaluation of new sphingosine kinase 1 inhibitors. *Breast Cancer Res. Treat.* 172, 33–43. doi: 10.1007/s10549-018-4900-1

Alshaker, H., Wang, Q., Frampton, A. E., Krell, J., Waxman, J., Winkler, M., et al. (2015). Sphingosine kinase 1 contributes to leptin-induced STAT3 phosphorylation through IL-6/gp130 transactivation in oestrogen receptor-negative breast cancer. *Breast Cancer Res. Treat.* 149, 59–67. doi: 10.1007/s10549-014-3228-8

Alshaker, H., Wang, Q., Srivats, S., Chao, Y., Cooper, C., and Pchejetski, D. (2017). New FTY720-docetaxel nanoparticle therapy overcomes FTY720-induced lymphopenia and inhibits metastatic breast tumour growth. *Breast Cancer Res. Treat.* 165, 531–543. doi: 10.1007/s10549-017-4380-8

Angerer, I. C., Hecker, M., Koczan, D., Roch, L., Friess, J., Ruge, A., et al. (2018). Transcriptome profiling of peripheral blood immune cell populations in multiple sclerosis patients before and during treatment with a sphingosine-1-phosphate receptor modulator. *CNS Neurosci. Ther.* 24, 193–201. doi: 10.1111/cns.12793

Antoon, J. W., White, M. D., Slaughter, E. M., Davis, J. L., Khalili, H. S., Elliott, S., et al. (2011). Targeting NF-kB mediated breast cancer chemoresistance through selective inhibition of sphingosine kinase-2. *Cancer Biol. Ther.* 11, 678–689. doi: 10.4161/cbt.11.7.14903

Beljanski, V., Lewis, C. S., and Smith, C. D. (2011). Antitumor activity of Sphingosine kinase 2 inhibitor ABC294640 and sorafenib in hepatocellular carcinoma xenografts. *Cancer Biol. Ther.* 11, 524–534. doi: 10.4161/cbt.11.5.14677

Carvalho, B. S., and Irizarry, R. A. (2010). A framework for oligonucleotide microarray preprocessing. *Bioinformatics* 26, 2363–2367. doi: 10.1093/bioinformatics/btq431

Cuvillier, O. (2007). Sphingosine kinase-1–a potential therapeutic target in cancer. *Anticancer Drugs* 18, 105–110. doi: 10.1097/CAD.0b013e328011334d

Garland, J. (2017). Unravelling the complexity of signalling networks in cancer: a review of the increasing role for computational modelling. *Crit. Rev. Oncol. Hematol.* 117, 73–113. doi: 10.1016/j.critrevonc.2017.06.004

Hu, P., Liang, Y., Hu, Q., Wang, H., Cai, Z., He, J., et al. (2018). SNX6 predicts poor prognosis and contributes to the metastasis of pancreatic cancer cells via activating epithelial-mesenchymal transition. *Acta Biochim. Biophys. Sin.* 50, 1075–1084. doi: 10.1093/abbs/gmy110

Irizarry, R. A., Bolstad, B. M., Collin, F., Cope, L. M., Hobbs, B., and Speed, T. P. (2003). Summaries of Affymetrix GeneChip probe level data. *Nucleic Acids Res.* 31:e15. doi: 10.1093/nar/gng015

Jiang-Hua, Q., De-Chuang, J., Zhen-Duo, L., Shu-de, C., and Zhenzhen, L. (2014). Association of methylenetetrahydrofolate reductase and methionine synthase polymorphisms with breast cancer risk and interaction with folate, vitamin B6, and vitamin B 12 intakes. *Tumour Biol.* 35, 11895–11901. doi: 10.1007/s13277-014-2456-1

Liu, H., Sugiura, M., Nava, V. E., Edsall, L. C., Kono, K., Poulton, S., et al. (2000). Molecular cloning and functional characterization of a novel mammalian sphingosine kinase type 2 isoform. *J. Biol. Chem.* 275, 19513–19520. doi: 10.1074/jbc.M002759200

Liu, X., He, B., Xu, T., Pan, Y., Hu, X., Chen, X., et al. (2018). MiR-490-3p functions as a tumor suppressor by inhibiting oncogene VDAC1 expression in colorectal cancer. *J. Cancer* 9, 1218–1230. doi: 10.7150/jca.23662

Paugh, S. W., Paugh, B. S., Rahmani, M., Kapitonov, D., Almenara, J. A., Kordula, T., et al. (2008). A selective sphingosine kinase 1 inhibitor integrates multiple molecular therapeutic targets in human leukemia. *Blood* 112, 1382–1391. doi: 10.1182/blood-2008-02-138958

Pchejetski, D., Bohler, T., Brizuela, L., Sauer, L., Doumerc, N., Golzio, M., et al. (2010). FTY720 (fingolimod) sensitizes prostate cancer cells to radiotherapy by inhibition of sphingosine kinase-1. *Cancer Res.* 70, 8651–8661. doi: 10.1158/0008-5472.CAN-10-1388

Pchejetski, D., Nunes, J., Coughlan, K., Lall, H., Pitson, S. M., Waxman, J., et al. (2011). The involvement of sphingosine kinase 1 in LPS-induced Toll-like receptor 4-mediated accumulation of HIF-1alpha protein, activation of ASK1 and production of the pro-inflammatory cytokine IL-6. *Immunol. Cell Biol.* 89, 268–274. doi: 10.1038/icb.2010.91

Permpongkosol, S., Wang, J. D., Takahara, S., Matsumiya, K., Nonomura, N., Nishimura, K., et al. (2002). Anticarcinogenic effect of FTY720 in human prostate carcinoma DU145 cells: modulation of mitogenic signaling, FAK, cell-cycle entry and apoptosis. *Int. J. Cancer* 98, 167–172. doi: 10.1002/ijc.10178

Pham, D. H., Powell, J. A., Gliddon, B. L., Moretti, P. A., Tsykin, A., Van der Hoek, M., et al. (2014). Enhanced expression of transferrin receptor 1 contributes to oncogenic signalling by sphingosine kinase 1. *Oncogene* 33, 5559–5568. doi: 10.1038/onc.2013.502

Pyne, N. J., Tonelli, F., Lim, K. G., Long, J., Edwards, J., and Pyne, S. (2012). Targeting sphingosine kinase 1 in cancer. *Adv. Biol. Regul.* 52, 31–38. doi: 10.1016/j.advenzreg.2011.07.001

Shida, D., Takabe, K., Kapitonov, D., Milstien, S., and Spiegel, S. (2008). Targeting SphK1 as a new strategy against cancer. *Curr. Drug Targets* 9, 662–673. doi: 10.2174/138945008785132402

Smyth, G. K. (2004). Linear models and empirical bayes methods for assessing differential expression in microarray experiments. *Stat. Appl. Genet. Mol. Biol.* 3:Article3. doi: 10.2202/1544-6115.1027

Song, D. D., Zhou, J. H., and Sheng, R. (2018). Regulation and function of sphingosine kinase 2 in diseases. *Histol. Histopathol.* 33, 433–445. doi: 10.14670/HH-11-939

Wang, J. D., Takahara, S., Nonomura, N., Ichimaru, N., Toki, K., Azuma, H., et al. (1999). Early induction of apoptosis in androgen-independent prostate cancer cell line by FTY720 requires caspase-3 activation. *Prostate* 40, 50–55. doi: 10.1002/(SICI)1097-0045(19990615)40:1<50::AID-PROS6>3.0.CO;2-N

Wang, Q., Alshaker, H., Bohler, T., Srivats, S., Chao, Y., Cooper, C., et al. (2017). Core shell lipid-polymer hybrid nanoparticles with combined docetaxel and molecular targeted therapy for the treatment of metastatic prostate cancer. *Sci Rep.* 7:5901. doi: 10.1038/s41598-017-06142-x

Wang, Z., Min, X., Xiao, S. H., Johnstone, S., Romanow, W., Meininger, D., et al. (2013). Molecular basis of sphingosine kinase 1 substrate recognition and catalysis. *Structure* 21, 798–809. doi: 10.1016/j.str.2013.02.025

White, C., Alshaker, H., Cooper, C., Winkler, M., and Pchejetski, D. (2016). The emerging role of FTY720 (Fingolimod) in cancer treatment. *Oncotarget* 7, 23106–23127. doi: 10.18632/oncotarget.7145

Yee, E. M., Hook, J. M., Bhadbhade, M. M., Vittorio, O., Kuchel, R. P., Brandl, M. B., et al. (2017). Preparation, characterization and in vitro biological evaluation of (1:2) phenoxodiol-beta-cyclodextrin complex. *Carbohydr. Polym.* 165, 444–454. doi: 10.1016/j.carbpol.2017.02.081

Yu, G., Wang, L. G., Han, Y., and He, Q. Y. (2012). clusterProfiler: an R package for comparing biological themes among gene clusters. *OMICS* 16, 284–287. doi: 10.1089/omi.2011.0118

Conflict of Interest Statement: The authors declare that the research was conducted in the absence of any commercial or financial relationships that could be construed as a potential conflict of interest.

frontiers in Pharmacology

BRIEF RESEARCH REPORT
published: 29 March 2019
doi: 10.3389/fphar.2019.00333

Targeting of Basophil and Mast Cell Pro-Allergic Reactivity Using Functionalised Gold Nanoparticles

Inna M. Yasinska[1], Luigi Calzolai[2], Ulrike Raap[3], Rohanah Hussain[4], Giuliano Siligardi[4], Vadim V. Sumbayev[1] and Bernhard F. Gibbs[1,3]**

[1] Medway School of Pharmacy, Universities of Kent and Greenwich, Chatham Maritime, United Kingdom, [2] European Commission, Joint Research Centre, Ispra, Italy, [3] Division of Experimental Allergology and Immunodermatology, University of Oldenburg, Oldenburg, Germany, [4] Beamline B23, Diamond Light Source, Didcot, United Kingdom

OPEN ACCESS

Edited by:
José das Neves,
Instituto de Investigação e Inovação em Saúde, Portugal

Reviewed by:
Fiorentina Roviezzo,
University of Naples Federico II, Italy
Marco Aurélio Martins,
Fundação Oswaldo Cruz (Fiocruz), Brazil
Glenn Cruse,
North Carolina State University, United States

***Correspondence:**
Inna M. Yasinska
I.Yasinska-24@kent.ac.uk
Bernhard F. Gibbs
bernhard.gibbs@uni-oldenburg.de

Specialty section:
This article was submitted to Experimental Pharmacology and Drug Discovery, a section of the journal Frontiers in Pharmacology

Received: 07 December 2018
Accepted: 19 March 2019
Published: 29 March 2019

Citation:
Yasinska IM, Calzolai L, Raap U, Hussain R, Siligardi G, Sumbayev VV and Gibbs BF (2019) Targeting of Basophil and Mast Cell Pro-Allergic Reactivity Using Functionalised Gold Nanoparticles. Front. Pharmacol. 10:333. doi: 10.3389/fphar.2019.00333

Calcineurin inhibitors potentially prevent pro-allergic mediator release from basophils and mast cells but are rarely used systemically due to ubiquitous expressions of target signaling proteins. However, specific targeting of allergic effector cells with these inhibitors could circumvent unwanted side effects. We recently demonstrated the biocompatibility of gold nanoparticles (AuNPs) as a platform for non-toxic delivery of signaling inhibitors due to unique physicochemical properties of these nanomaterials. Since AuNPs can be conjugated with both anti-allergic drugs and antibodies or other proteins that specifically recognize basophils and mast cells, our aims were to assess specific targeting of allergic effector cell function using AuNPs conjugated with the calcineurin inhibitor ascomycin. Purified human basophils and LAD2 human mast cells were used for investigations with AuNPs conjugated either to CD203c antibodies or containing stem cell factor (SCF), respectively, which were amine-coupled to acidic groups of reduced glutathione (GSH). GSH was also used as a spacer for immobilization of ascomycin on the gold surface. AuNPs conjugated with anti-CD203c and ascomycin strikingly blocked IgE-dependent degranulation of both purified basophils and those present in mixed leukocyte preparations, suggesting specific targeting of these cells. In contrast, LAD2 mast cell responses were not inhibited using anti-CD203c-containing nanoconjugates but were when the conjugates contained SCF. Successful targeting of allergic effector cells using gold nanoconjugates indicates that this technology may have therapeutic potential for the treatment of allergies by specifically delivering highly effective signaling inhibitors with reduced side effects.

Keywords: gold nanoconjugates, basophils, mast cells, ascomycin, IgE, CD203c, stem cell factor

INTRODUCTION

Inflammatory mediator release, (e.g., histamine) from basophils and mast cells plays a major role in contributing to the symptoms of allergic reactions and these cells may also support the underlying tendency for an individual's immune system to respond in a pro-allergic manner (reviewed in Varricchi et al., 2018). In terms of anti-allergic therapy, it is therefore desirable to target these cells and limit their ability to release inflammatory and immunomodulatory

mediators. Several pharmacological inhibitors of intracellular signaling, (e.g., Syk and calcineurin inhibitors) have been shown to substantially reduce the ability of mast cells and basophils to release allergic mediators following stimulation of the high-affinity IgE receptor (FcεRI) (Oliver et al., 1994; Zuberbier et al., 2001; Plath et al., 2003; Matsubara et al., 2006; Rossi et al., 2006; Harrison et al., 2007). However, due to the ubiquitous expressions of intracellular signals systemic clinical use of these inhibitors is problematical in terms of potential side effects and adverse drug reactions. It is therefore desirable to be able to specifically target effector cells involved in human allergy with drugs that are known to prevent allergen-induced cell activation and the release of pro-inflammatory mediators.

We recently reported the proof-of-principle that gold nanoparticles (AuNPs) could be used to specifically target basophils and other cell types with certain signal transduction inhibitors (Gibbs et al., 2014; Yasinska et al., 2018). Furthermore, compared to most other nanomaterials, AuNPs are relatively non-toxic (Deng et al., 2011; Pissuwan et al., 2011) and are easily conjugated with pharmacological agents and antibodies/antigen-binding peptides (Ma et al., 2010; Gibbs et al., 2014; Yasinska et al., 2018). Moreover, we observed that AuNPs display inherent anti-inflammatory properties themselves by neutralizing the effects of IL-1β (Sumbayev et al., 2013), a cytokine that contributes to allergic inflammation, particularly in asthma.

As a specific marker for mast cells and basophils, we chose CD203c [the ectonucleotide pyrophosphatase/phosphodiesterase family member 3 (ENPP-3)] since it is currently the only known membrane-associated protein that is almost exclusively expressed on both human mast cells and basophils (Bühring et al., 2001; Ghannadan et al., 2002). This marker has been employed in flow cytometric assays for clinical diagnostics regarding basophil activation (Boumiza et al., 2003; Kleine-Tebbe et al., 2006). Its biological function in these cells is not clear but its surface expression is upregulated by priming factors involved in allergic diseases, such as IL-3, and during allergic responses of these cells (Hauswirth et al., 2007; Ono et al., 2010).

Given the above statements, our main aim was to specifically target and inhibit the function of primary human basophils and LAD2 mast cells using AuNPs conjugated to anti-CD203c and ascomycin. Furthermore, we characterized our AuNP-based nanoconjugates (NCJ) using synchrotron radiation circular dichroism (SRCD) spectroscopy. We also compared the effects of NCJ containing anti-CD203c to those conjugated to stem cell factor (SCF). This may allow mast cell-selective targeting since SCF binds to KIT, a receptor that is highly expressed in mature mast cells (other cells include immature haemopoietic stem cells, melanocytes and interstitial cells of the Cajal).

METHODS

Generation and Characterization of NCJ

Synthesis of 5 nm AuNPs was performed essentially as described previously (Sumbayev et al., 2013; Gibbs et al., 2014; Yasinska et al., 2018). Briefly, 5 ml of aqueous gold (III) chloride trihydrate (10 mM) and 2.5 ml of aqueous sodium citrate (100 mM) were added to 95 ml of milliQ-water in a round bottom flask equipped with a magnetic stirrer. The solution (which has a pale yellow appearance) was cooled down to 1–2°C. Under vigorous stirring 1 ml of aqueous sodium borohydride (4°C, 0.1 M) was added and the solution (which should have a dark red appearance) was then stirred for further 10 min on an ice bath before being allowed to warm up to room temperature. NCJ were generated as described before using glutathione as a linker to immobilize one molecule of anti-CD203c antibody or SCF per 1 nanoparticle. The rest of the surface was covered by glutathiolated (through –COOH group) ascomycin (maximum 1,000 molecules per nanoparticle) (Gibbs et al., 2014; Yasinska et al., 2018). The same principle was adopted for the generation of SCF-containing NCJ (where SCF was employed instead of anti-CD203c). Nanomaterials were characterized using SRCD spectroscopy as described previously (Yasinska et al., 2018).

Briefly, SRCD measurements were conducted using 10 cm path length cell with 3 mm aperture diameter and capacity of 800 μl using the Module B with a 1 nm increment, 1s integration time and 1.2 nm bandwidth at 23°C (Hussain et al., 2012; Yasinska et al., 2018). The results obtained were analyzed using CDAPPs program (Hussain et al., 2012, 2015) and Origin software (OriginLab^{TM}).

Basophil Isolation and Purification

Basophils, were isolated from buffy coat blood (purchased from the NHS Blood and Transplant service following ethics approval (NHS REC 12/WM/0319) by Ficoll-density centrifugation and purified further (to >90%) by immunomagnetic cell sorting using commercial kits, as previously described (Gibbs et al., 2008). Basophil purities were determined by alcian blue staining.

LAD2 Mast Cells

LAD2 cells were generously provided to us by Dr. A. Kirshenbaum and Prof. D. Metcalfe (NIH, Bethesda, United States) and cultured in Stem-Pro-34 serum-free media in the presence of 100 ng/ml SCF as previously reported (Kirshenbaum et al., 2003). Human SCF protein was produced in *Escherichia Coli* and purified following established protocols (Wang et al., 2008). Cells were sensitized with 100 ng/ml polyclonal IgE (Amsbio, Abingdon, United Kingdom) 24 h before the experiments.

Cell Stimulation and Histamine Release Assay

Cells were re-suspended in HEPES-buffered Tyrode's solution (containing 1 mM $CaCl_2$) and pre-incubated with or without either NCJ or ascomycin alone (5 or 100 nM) for 15 min at 37° before stimulation (either anti-IgE (1 μg/ml), fMLP (100 nM) or buffer alone) for 30 min. Following centrifugation, histamine content were determined in the supernatants and lysed cell pellets by spectrofluorometric analysis based on the method described by Shore et al. (1959). Histamine releases were calculated by dividing histamine content in respective supernatants by that present in equivalent cell lysates × 100%.

Net histamine releases were then calculated by subtracting spontaneous secretions and the results then presented as percentage inhibitions of net histamine release caused by the stimulus alone.

Statistical Analysis

Each experiment was performed at least three times. When comparing two events at a time we used a two-tailed Student's *t*-test. Multiple comparisons were performed by ANOVA test and *post hoc* Bonferroni correction was applied. Statistical probabilities (p) were shown in the figures as * for $p < 0.05$; ** for $p < 0.01$ and *** for $p < 0.001$.

RESULTS

Our first objective was to characterize the NCJs using far-UV CD spectra of the components, the materials and compounds comprising the anti-CD203c- and ascomycin-conjugated AuNPs (**Figures 1A–F**) by use of SRCD spectroscopy (**Figure 1G**). Our observations confirmed that immobilization of both antibody and the drug was successful.

Next, we compared the effects of NCJs and ascomycin alone on histamine release from purified human basophils stimulated either with anti-IgE (**Figures 2A,B** and **Supplementary Figures 1A,B**) or the N-formylated tripeptide fMLP (**Figure 2C** and **Supplementary Figures 1C,D**). In agreement with our previous observations (Gibbs et al., 2014) NCJs containing ascomycin and anti-CD203c substantially inhibited IgE-dependent basophil histamine release and this level of inhibition was similar to that seen with 100 nM ascomycin alone. Our current results also include the effects of NCJs without ascomycin, which did not show any inhibitory properties. In contrast, NCJs were less effective at inhibiting histamine release from basophils induced by fMLP, although the inhibitory effects with NCJs were still significantly greater than those seen with ascomycin alone at the highest concentration (**Figure 2C**).

We next asked whether the striking inhibitory properties of NCJs regarding the abrogation of IgE-dependent histamine release from purified basophils were matched in unpurified basophil preparations. Indeed, NCJs had similar inhibitory effects in both preps, while ascomycin alone was less effective (especially at the lower, 5 nM, concentration), presumably due to specific basophil targeting by the NCJs and greater distribution of the free drug between basophils and contaminating peripheral blood mononuclear cells (**Figure 2D** and **Supplementary Figure 2**).

Surprisingly, NCJs containing anti-CD203c were not effective at inhibiting anti-IgE-induced histamine release from LAD2 mast cells (**Figures 2E,F** and **Supplementary Figure 3**). The effects of ascomycin alone were also less effective than previously observed for basophils, possibly owing to requiring longer preincubation periods than for basophils. Non-etheless, anti-CD203c-containing NCJ were even less effective at inhibiting histamine release from LAD2 mast cells than the moderate inhibition seen with ascomycin alone. In contrast, when coupled to SCF, the inhibitory actions of NCJ were restored to levels greater than seen for ascomycin alone. We also observed that SCF-containing NCJs were moderately (though significantly) effective at inhibiting basophil-derived histamine release, though the inhibitory properties were considerably less compared to anti-CD203c-containing NCJs (**Figure 2G**).

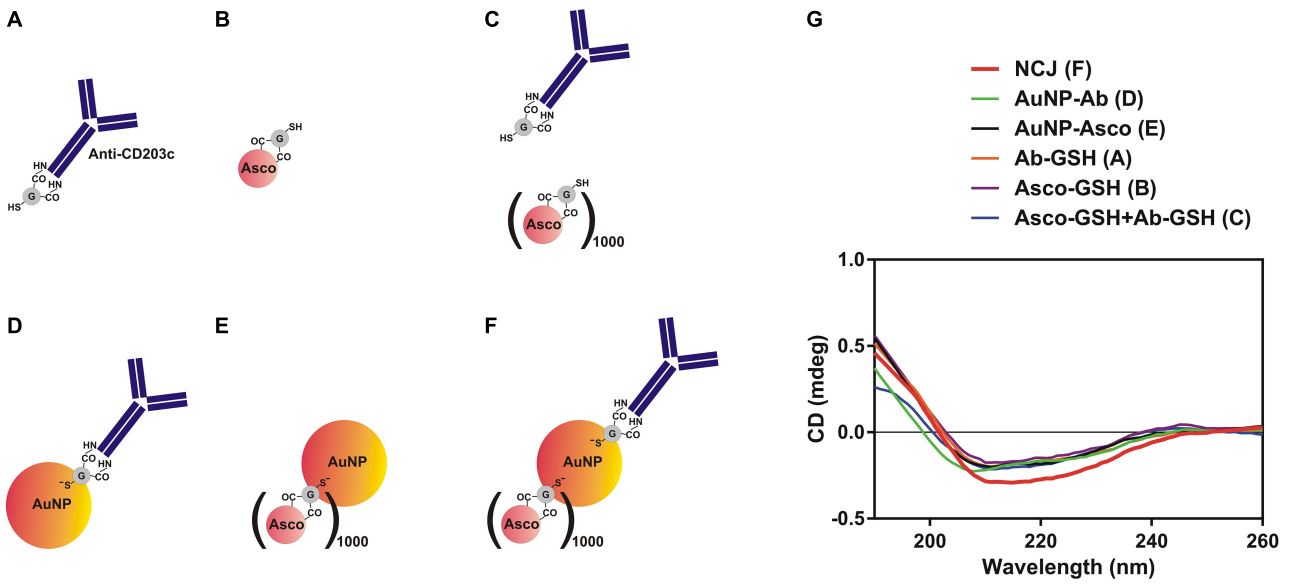

FIGURE 1 | Characterization of nanoconjugates using synchrotron radiation circular dichroism (SRCD) spectroscopy. **(A–F)** Nanomaterials and compounds which were analyzed using SRCD spectroscopy. **(G)** Observed far-UV spectra of anti-CD203c antibody, ascomycin and all possible types of functionalised gold nanoparticles. Data are the mean values of four independent experiments.

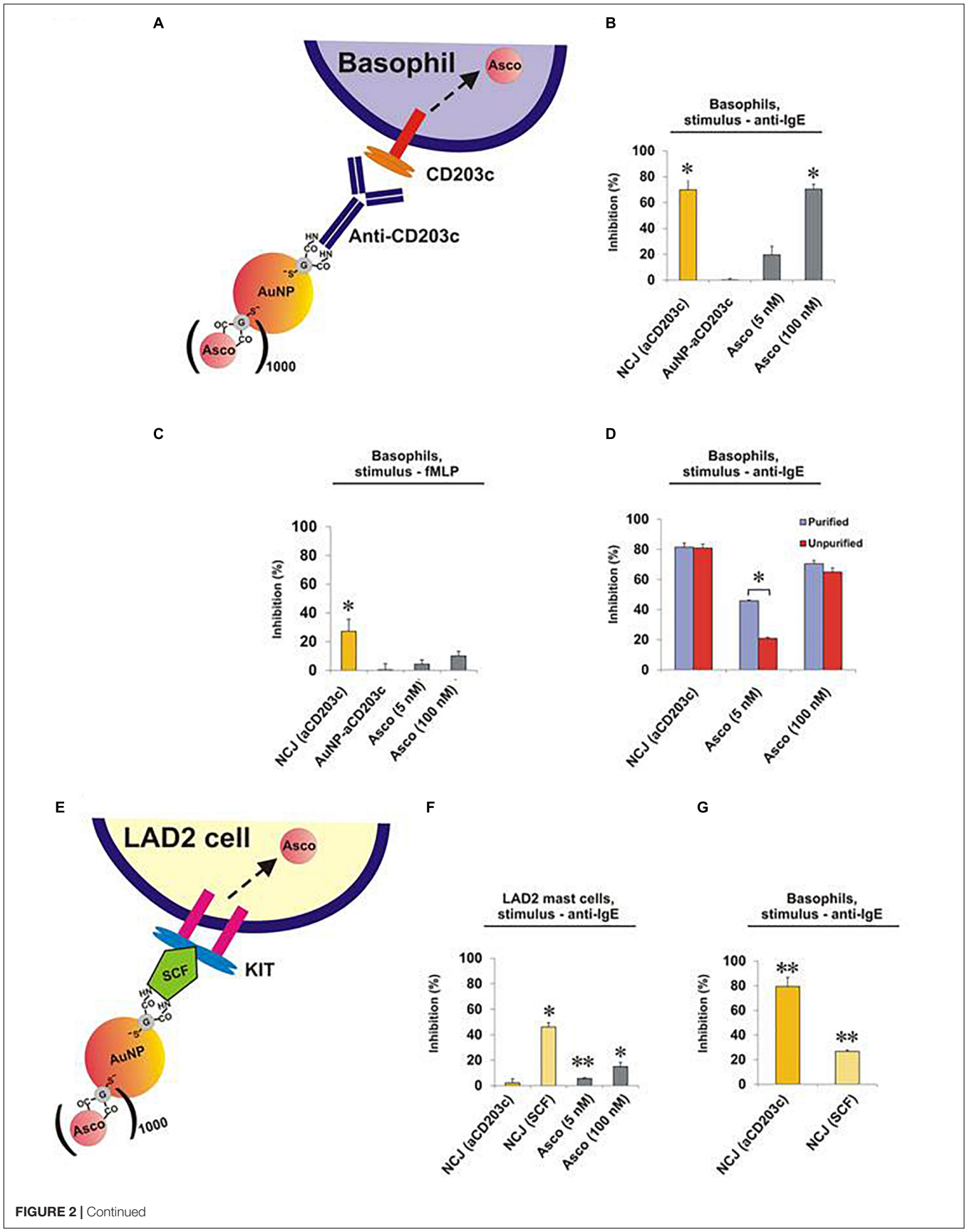

FIGURE 2 | Continued

FIGURE 2 | Effect of NCJs on histamine release from human basophils and LAD2 mast cells. Cells were preincubated for 15 min either with NCJs, ascomycin or buffer alone before stimulation for 30 min, after which histamine releases were assessed. All results are shown as percentage inhibition of histamine release ± SEM. * and ** denote significant differences from control using a paired Student's *t*-test ($p < 0.05$ or $p < 0.01$, respectively). Panel **A** Scheme illustrating the interaction of a NCJ containing anti-CD203c with a human basophil and subsequent ascomycin delivery. Panel **B** Basophils stimulated with anti-IgE ($n = 4$). Results were first corrected from spontaneous releases (5.4 ± 1.1%) and percentage inhibition calculated from net anti-IgE-induced release in the absence of NCJs or inhibitors (25.3 ± 4.1%). Panel **C** Basophils stimulated with fMLP ($n = 4$). Results were first corrected from spontaneous releases (4.2 ± 1.2%) and percentage inhibition calculated from net fMLP-induced release in the absence of NCJs or inhibitors (31.6 ± 4.0%). Panel **D** Comparison of the inhibitory effects of NCJs and ascomycin alone in purified (>90% pure) and unpurified (<2% pure) human basophils stimulated with anti-IgE. Spontaneous histamine releases (4.6 ± 0.5% for purified basophils, 3.2 ± 0.7% for unpurified basophils) were first subtracted and the results expressed as percentage inhibition of histamine release caused by anti-IgE alone (net releases were 14 ± 2.7% for purified basophils, 14.2 ± 2.5% for unpurified basophils) ($n = 8$). Panel **E** Scheme illustrating interaction of a NCJ containing SCF with LAD2 mast cell and subsequent ascomycin delivery. Panel **F** Effect of NJCs on histamine release from LAD2 cells stimulated with anti-IgE ($n = 6$). Results were first corrected from spontaneous releases (15.7 ± 0.5%) and percentage inhibition calculated from net anti-IgE-induced release in the absence of NCJs or inhibitors (15.9 ± 0.7%). Panel **G** Effect of different NJCs on histamine release from purified human basophils stimulated with anti-IgE. Results were first corrected from spontaneous releases (4.0 ± 0.3%) and percentage inhibition calculated from net anti-IgE-induced release in the absence of NCJs or inhibitors (10.6 ± 1.0%).

DISCUSSION

Our SRCD spectroscopy results demonstrate that immobilization of ascomycin and anti-CD203c on the gold surface of AuNPs doesn't affect the antibody secondary structure, based on unchanged shape of the respective SRCD spectrum curves (**Figure 1G**; successful immobilizations of targeting agents on AuNPs is shown in **Supplementary Figure 4**). This explains preserved biochemical activity of the antibody upon its immobilization on the gold surface. This is confirmed by the functional activities of the NCJs in terms of targeting and inhibiting histamine release from allergic effector cells. For basophils, this inhibitory action was clearly due to the presence of ascomycin on the NCJs, since no effects were observed using NCJs without ascomycin conjugation. Furthermore, the inhibitory actions of ascomycin were more pronounced in terms of inhibiting IgE-dependent histamine release compared to fMLP. As a result, ascomycin-containing NCJs were also less effective at inhibiting fMLP-induced basophil histamine release.

The concentration of ascomycin delivered into basophils within the NCJs was maximally 5 nM, based on stoicheometrical calculations on the number of ascomycin molecules fused to each nanoparticle and the number of nanoparticles incubated with basophils (Gibbs et al., 2014). The increased inhibitory effect of these NCJs compared to incubation with 5 nM ascomycin alone supports that the NCJs facilitate specific cellular targeting. Furthermore, we obtained the same results with the NCJs in both pure and unpure basophils preparations, whereas 5 nM ascomycin alone displayed less inhibitory effects on unpure basophils than pure basophils. This suggests that ascomycin, which is a relatively lipophilic molecule, would otherwise disperse into various cell populations *in vivo*, lowering its effective concentration in basophils and increasing the likelihood of side effects (thus emphasizing the need for cell-specific targeting using NCJs).

In terms of the effects of NCJs on LAD2 mast cells, anti-CD203c conjugation surprisingly failed to target these cells, where no significant inhibition of IgE-dependent histamine release was observed in contrast to ascomycin alone. Indeed, we observed that LAD2 cells expressed barely detectable levels of CD203c (**Supplementary Figure 5A**). This suggests that CD203c may be absent in certain aberrant mast cell disorders although it is be widely expressed both on a variety of human primary mast cells as well as *in vitro* cultured mast cells and other human mast cell lines (Ghannadan et al., 2002; Andersen et al., 2008; Cop et al., 2017). The LAD2 cell line is derived from a patient with mast cell leukemia/sarcoma (Kirshenbaum et al., 2003). However, neoplastic mast cells from systemic mastocytosis patients have, in contrast to our observations with LAD2 cells, been shown to overexpress CD203c (Hauswirth et al., 2008). This would advocate the use of NCJs containing anti-CD203c (or single chain antibodies/peptides against this protein) to target most other human mast cells and highlights the limitations of LAD2 mast cells in these particular studies.

An alternative mast cell-specific marker is CD117 (KIT), which binds SCF. Our results clearly showed, in contrast to anti-CD203c-containing NCJs, that NCJs containing SCF significantly inhibited LAD2 cell histamine release much more than ascomycin alone. This verifies the concept of specific drug delivery into mast cells using NCJs and shows that CD117 could be used to specifically target mast cells in tissues where other KIT-positive cells (present mainly in the bone marrow) are absent. We assumed that basophils could not be targeted with SCF-containing NCJs since, other than during development, they are generally considered to be CD117/KIT negative (Han et al., 2008). Indeed, Western blot analysis of LAD2 and basophil lysates clearly demonstrated high KIT expression in LAD2 mast cells whereas it was undetectable in basophils (**Supplementary Figure 5B**). However, SCF-containing NCJs still gave rise to a moderate inhibition of histamine release from basophils. This suggests that SCF may non-specifically interact with some of the basophil cell surface-based receptors or have a moderate affinity to some of them. The second scenario is more likely given that SCF is known to stimulate chemotaxis and the survival of peripheral blood basophils (Heinemann et al., 2005).

We conclude that AuNP-based NCJs are highly effective both at targeting human allergic effector cells and substantially

blocking their function by delivering anti-allergic agents. However, expensive stability as well as *in vivo* safety testing will need to be conducted in before this technology can be developed further as a new therapeutic approach in a clinical setting.

DATA AVAILABILITY

The datasets generated for this study are available on request to the corresponding author.

AUTHOR CONTRIBUTIONS

BG conceived the work, together with VS, and conducted the experiments on basophils and LAD2 mast cells together with IY. LC provided and characterized the gold nanoparticles. VS, IY, and BG designed the nanoconjugates. RH, GS, IY, and VS characterized the NCJs using SRCD spectroscopy. UR contributed to analysis and interpretation of the data and critical evaluation of the manuscript content. All authors contributed to writing the manuscript.

ACKNOWLEDGMENTS

We would like to thank the Daphne Jackson Trust for providing a research fellowship to IY to support her contribution to this study. We are grateful to Diamond Light Source for providing access to B23 beamline (SM12578). We also thank Dr. Luca Varani (Institute for Research in Biomedicine, Bellinzona, Switzerland) for generously providing us with purified SCF. We also thank Dr. A. Kirshenbaum and Prof. D. Metcalfe (NIH, Bethesda, MD, United States) for kindly providing us with LAD2 cells.

SUPPLEMENTARY MATERIAL

The Supplementary Material for this article can be found online at: https://www.frontiersin.org/articles/10.3389/fphar.2019.00333/full#supplementary-material

REFERENCES

Andersen, H. B., Holm, M., Hetland, T. E., Dahl, C., Junker, S., Schiøtz, P. O., et al. (2008). Comparison of short term in vitro cultured human mast cells from different progenitors - peripheral blood-derived progenitors generate highly mature and functional mast cells. *J. Immunol. Methods* 336, 166–174. doi: 10.1016/j.jim.2008.04.016

Boumiza, R., Monneret, G., Forissier, M. F., Savoye, J., Gutowski, M. C., Powell, W. S., et al. (2003). Marked improvement of the basophil activation test by detecting CD203c instead of CD63. *Clin. Exp. Allergy* 33, 259–265. doi: 10.1046/j.1365-2222.2003.01594.x

Bühring, H. J., Seiffert, M., Giesert, C., Marxer, A., Kanz, L., Valent, P., et al. (2001). The basophil activation marker defined by antibody 97A6 is identical to the ectonucleotide pyrophosphatase/phosphodiesterase 3. *Blood* 97, 3303–3305. doi: 10.1182/blood.V97.10.3303

Cop, N., Decuyper, I. I., Faber, M. A., Sabato, V., Bridts, C. H., Hagendorens, M. M., et al. (2017). Phenotypic and functional characterization of in vitro cultured human mast cells. *Cytometry B Clin. Cytom.* 92, 348–354. doi: 10.1002/cyto.b.21399

Deng, Z. J., Liang, M., Monteiro, M., Toth, I., and Minchin, R. F. (2011). Nanoparticle-induced unfolding of fibrinogen promotes Mac-1 receptor activation and inflammation. *Nat. Nanotechnol.* 6, 39–44. doi: 10.1038/nnano.2010.250

Ghannadan, M., Hauswirth, A. W., Schernthaner, G. H., Müller, M. R., Klepetko, W., Schatzl, G., et al. (2002). Detection of novel CD antigens on the surface of human mast cells and basophils. *Int. Arch. Allergy Immunol.* 127, 299–307. doi: 10.1159/000057747

Gibbs, B. F., Papenfuss, K., and Falcone, F. H. (2008). A rapid two-step procedure for the purification of human peripheral blood basophils to near homogeneity. *Clin. Exp. Allergy* 38, 480–485. doi: 10.1111/j.1365-2222.2007.02919.x

Gibbs, B. F., Yasinska, I. M., Calzolai, L., Gilliland, D., and Sumbayev, V. V. (2014). Highly specific targeting of human leukocytes using gold nanoparticle-based biologically active conjugates. *J. Biomed. Nanotechnol.* 10, 1259–1266. doi: 10.1166/jbn.2014.1807

Han, X., Jorgensen, J. L., Brahmandam, A., Schlette, E., Huh, Y. O., Shi, Y., et al. (2008). Immunophenotypic study of basophils by multiparameter flow cytometry. *Arch. Pathol. Lab. Med.* 132, 813–819. doi: 10.1043/1543-21652008132

Harrison, C. A., Bastan, R., Peirce, M. J., Munday, M. R., and Peachell, P. T. (2007). Role of calcineurin in the regulation of human lung mast cell and basophil function by cyclosporine and FK506. *Br. J. Pharmacol.* 150, 509–518. doi: 10.1038/sj.bjp.0707002

Hauswirth, A. W., Escribano, L., Prados, A., Nuñez, R., Mirkina, I., Kneidinger, M., et al. (2008). CD203c is overexpressed on neoplastic mast cells in systemic mastocytosis and is upregulated upon IgE receptor cross-linking. *Int. J. Immunopathol. Pharmacol.* 21, 797–806. doi: 10.1177/039463200802100404

Hauswirth, A. W., Sonneck, K., Florian, S., Krauth, M. T., Bohm, A., Sperr, W. R., et al. (2007). Interleukin-3 promotes the expression of E-NPP3/CD203C on human blood basophils in healthy subjects and in patients with birch pollen allergy. *Int. J. Immunopathol. Pharmacol.* 20, 267–278. doi: 10.1177/039463200702000207

Heinemann, A., Sturm, G. J., Ofner, M., Sturm, E. M., Weller, C., Peskar, B. A., et al. (2005). Stem cell factor stimulates the chemotaxis, integrin upregulation, and survival of human basophils. *J. Allergy Clin. Immunol.* 116, 820–826. doi: 10.1016/j.jaci.2005.06.008

Hussain, R., Benning, K., Javorfi, T., Longo, E., Rudd, T. R., Pulford, B., et al. (2015). CDApps: integrated software for experimental planning and data processing at beamline B23, Diamond Light Source. *J. Synchrotron Radiat.* 22, 465–468. doi: 10.1107/S1600577514028161

Hussain, R., Javorfi, T., and Siligardi, G. (2012). Circular dichroism beamline B23 at the diamond light source. *J. Synchrotron Radiat.* 19, 132–135. doi: 10.1107/S0909049511038982

Kirshenbaum, A. S., Akin, C., Wu, Y., Rottem, M., Goff, J. P., Beaven, M. A., et al. (2003). Characterization of novel stem cell factor responsive human mast cell lines LAD 1 and 2 established from a patient with mast cell sarcoma/leukemia; activation following aggregation of FcepsilonRI or FcgammaRI. *Leuk. Res.* 27, 677–682. doi: 10.1016/S0145-2126(02)00343-0

Kleine-Tebbe, J., Erdmann, S., Knol, E. F., MacGlashan, D. W. Jr., Poulsen, L. K., and Gibbs, B. F. (2006). Diagnostic tests based on human basophils: potentials, pitfalls and perspectives. *Int. Arch. Allergy Immunol.* 141, 79–90. doi: 10.1159/000094495

Ma, J. S., Kim, W. J., Kim, J. J., Kim, T. J., Ye, S. K., Song, M. D., et al. (2010). Gold nanoparticles attenuate LPS-induced NO production through the inhibition of NF-kappaB and IFN-beta/STAT1 pathways in RAW264.7 cells. *Nitric Oxide* 23, 214–219. doi: 10.1016/j.niox.2010.06.005

Matsubara, S., Li, G., Takeda, K., Loader, J. E., Pine, P., Masuda, E. S., et al. (2006). Inhibition of spleen tyrosine kinase prevents mast cell activation

and airway hyperresponsiveness. *Am. J. Respir. Crit. Care Med.* 173, 56–63. doi: 10.1164/rccm.200503-361OC

Oliver, J. M., Burg, D. L., Wilson, B. S., McLaughlin, J. L., and Geahlen, R. L. (1994). Inhibition of mast cell Fc epsilon R1-mediated signaling and effector function by the Syk-selective inhibitor, piceatannol. *J. Biol. Chem.* 269, 29697–29703.

Ono, E., Taniguchi, M., Higashi, N., Mita, H., Kajiwara, K., Yamaguchi, H., et al. (2010). CD203c expression on human basophils is associated with asthma exacerbation. *J. Allergy Clin. Immunol.* 125, 483–489. doi: 10.1016/j.jaci.2009.10.074

Pissuwan, D., Niidome, T., and Cortie, M. B. (2011). The forthcoming applications of gold nanoparticles in drug and gene delivery systems. *J. Control Release* 149, 65–71. doi: 10.1016/j.jconrel.2009.12.006

Plath, K. E., Grabbe, J., and Gibbs, B. F. (2003). Calcineurin antagonists differentially affect mediator secretion, p38 mitogen-activated protein kinase and extracellular signal-regulated kinases from immunologically activated human basophils. *Clin. Exp. Allergy* 33, 342–350. doi: 10.1046/j.1365-2222.2003.01610.x

Rossi, A. B., Herlaar, E., Braselmann, S., Huynh, S., Taylor, V., Frances, R., et al. (2006). Identification of the syk kinase inhibitor R112 by a human mast cell screen. *J. Allergy Clin. Immunol.* 118, 749–755. doi: 10.1016/j.jaci.2006.05.023

Shore, P. A., Burkhalter, A., and Cohn, V. H. (1959). A method for the fluorometric assay of histamine in tissues. *J. Pharmacol. Exp. Ther.* 127, 182–186.

Sumbayev, V. V., Yasinska, I. M., Garcia, C. P., Gilliland, D., Lall, G. S., Gibbs, B. F., et al. (2013). Gold nanoparticles downregulate interleukin-1β-induced pro-inflammatory responses. *Small* 9, 472–477. doi: 10.1002/smll.201201528

Varricchi, G., Raap, U., Rivellese, F., Marone, G., and Gibbs, B. F. (2018). Human mast cells and basophils - how are they similar how are they different? *Immunol. Rev.* 282, 8–34. doi: 10.1111/imr.12627

Wang, C., Liu, J., Wang, L., and Geng, X. (2008). Solubilization and refolding with simultaneous purification of recombinant human stem cell factor. *Appl. Biochem. Biotechnol.* 144, 181–189. doi: 10.1007/s12010-007-8112-0

Yasinska, I. M., Ceccone, G., Ojea-Jimenez, I., Ponti, J., Hussain, R., Siligardi, G., et al. (2018). Highly specific targeting of human acute myeloid leukaemia cells using pharmacologically active nanoconjugates. *Nanoscale* 10, 5827–5833. doi: 10.1039/c7nr09436a

Zuberbier, T., Chong, S. U., Grunow, K., Guhl, S., Welker, P., Grassberger, M., et al. (2001). The ascomycin macrolactam pimecrolimus (Elidel, SDZ ASM 981) is a potent inhibitor of mediator release from human dermal mast cells and peripheral blood basophils. *J. Allergy Clin. Immunol.* 108, 275–280. doi: 10.1067/mai.2001.116865

Conflict of Interest Statement: The authors declare that the research was conducted in the absence of any commercial or financial relationships that could be construed as a potential conflict of interest.

frontiers in Pharmacology

RESEARCH SNAPSHOT
published: 05 April 2019
doi: 10.3389/fphar.2019.00342

Mitochondrial Defunctionalization Supresses Tim-3-Galectin-9 Secretory Pathway in Human Colorectal Cancer Cells and Thus Can Possibly Affect Tumor Immune Escape

Svetlana S. Sakhnevych[1], *Inna M. Yasinska*[1], *Elizaveta Fasler-Kan*[2,3]* and *Vadim V. Sumbayev*[1]*

[1] Medway School of Pharmacy, Universities of Kent and Greenwich, Chatham, United Kingdom, [2] Department of Pediatric Surgery and Department of Biomedical Research, Children's Hospital, Inselspital, University of Bern, Bern, Switzerland, [3] Department of Biomedicine, University Hospital Basel and University of Basel, Basel, Switzerland

OPEN ACCESS

Edited by:
Chiranjib Chakraborty, Galgotias University, India

Reviewed by:
Raghvendra Mohan Srivastava, Memorial Sloan Kettering Cancer Center, United States
Emerson Soares Bernardes, Instituto de Pesquisas Energéticas e Nucleares (CNEN), Brazil

***Correspondence:**
Elizaveta Fasler-Kan
elizaveta.fasler@insel.ch
Vadim V. Sumbayev
V.Sumbayev@kent.ac.uk

Specialty section:
This article was submitted to Experimental Pharmacology and Drug Discovery, a section of the journal Frontiers in Pharmacology

Received: 15 December 2018
Accepted: 19 March 2019
Published: 05 April 2019

Citation:
Sakhnevych SS, Yasinska IM, Fasler-Kan E and Sumbayev VV (2019) Mitochondrial Defunctionalization Supresses Tim-3-Galectin-9 Secretory Pathway in Human Colorectal Cancer Cells and Thus Can Possibly Affect Tumor Immune Escape. Front. Pharmacol. 10:342. doi: 10.3389/fphar.2019.00342

The Tim-3-galectin-9 secretory pathway is known to protect various types of cancer cells against host immune surveillance. We found that pharmacologically induced mitochondrial dysfunction leads to a reduced galectin-9 expression/exocytosis in human colorectal cancer cells and re-distribution of this protein (the effect described for various cellular proteins) into mitochondria.

Keywords: galectin-9, Tim-3, immune surveillance, mitochondria, colorectal cancer

RESULTS

It has recently been discovered that the immune receptor Tim-3 (T cell immunoglobulin and mucin domain-containing protein 3) and it's ligand galectin-9 determines the capability of various types of malignant cells [e.g., acute myeloid leukemia (AML), colorectal cancer] to escape host immune surveillance (Kang et al., 2015; Gonçalves Silva et al., 2017; Sakhnevych et al., 2018; Yasinska et al., 2018b). Also, some of the galectin family members (for example galectin-3) were found to be able to protect AML and colorectal cancer cells against apoptosis through mitochondrial stabilization in a B cell lymphoma protein (Bcl) 2-dependent manner (Lee et al., 2013; Ruvolo, 2016). We asked whether galectin-9 has the same intracellular anti-apoptotic activity in addition to its extracellular immunosuppressive role. We used a pharmacological inhibitor 5-[(4-bromophenyl)methylene]-a-(1-methylethyl)-4-oxo-2-thioxo-3-thiazolidineacetic acid (BH3I-1, **Figure 1A**), a synthetic cell permeable Bcl-X_L antagonist, which induces apoptosis via inhibition of interactions between the BH3 domain and Bcl-X_L thus defunctionalyzing mitochondria. We found that BH3I-1 was capable of inducing apoptosis in Colo 205 colorectal adenocarcinoma cells of epithelial origin (based on increased caspase-3 activity and decreased viability of the cells, **Figure 1A**). Silencing either galectin-9 or its receptor and possible trafficker Tim-3 did not affect the pro-apoptotic activity of BH3I-1 suggesting that galectin-9 is unlikely to display anti-apoptotic activity in this case. Interestingly, the action of BH3I-1 did not affect the activity of mammalian target of rapamycin (mTOR) translational pathway as seen from its capability to phosphorylate eukaryotic initiation

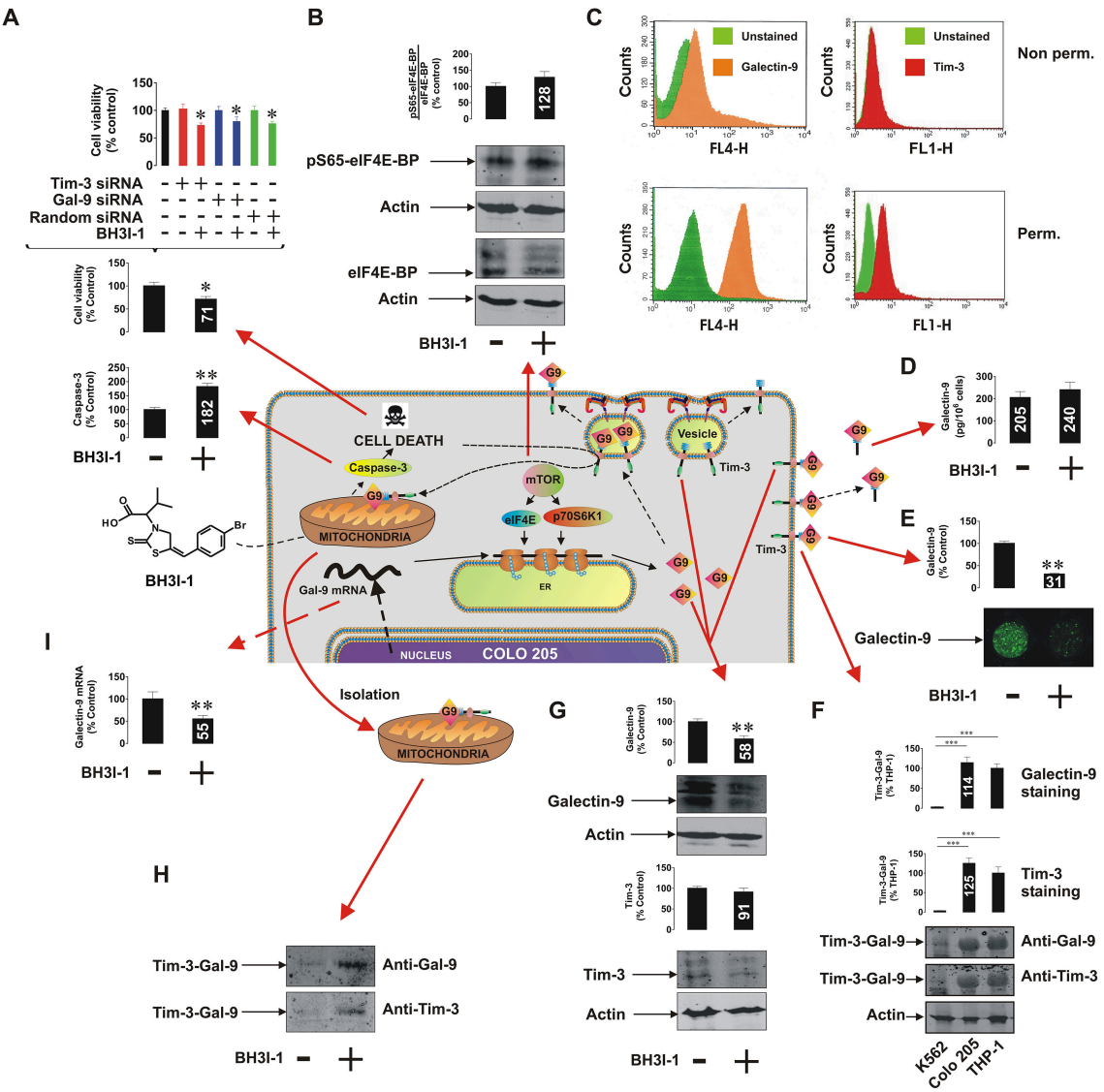

FIGURE 1 | Pro-apoptotic defunctionalization of mitochondria reduces galectin-9 expression and leads to its redistribution in human Colo 205 colorectal adenocarcinoma cells. Colo 205 cells were exposed to 100 μM BH3I-1 for 24 h followed by **(A)** detection of cell viability using an MTS test and colorimetric assay of caspase-3 activity. Cell viability was also tested for normal and Tim-3 or galectin-9 knockdown Colo 205 cells. **(B)** Following 24 h of exposure to BH3I-1 S65-phosphorylation levels of eIF4E-BP were analyzed by Western blot. **(C)** Surface presence and total cellular levels of Tim-3 and galectin-9 were analyzed in Colo 205 cells using FACS. **(D)** Secreted levels of galectin-9 were analyzed in Colo 205 cells following 24 h of exposure to BH3I-1 by ELISA. **(E)** Surface levels of galectin-9 in non-treated and BH3I-1-stimulated Colo 205 cells were compared using an on-cell assay. **(F)** The presence of Tim-3-galectin-9 complex in Colo 205 cells was confirmed using Western blot analysis (bands were appearing at around 70 KDa, better detectable when temperature denaturation is not applied). THP-1 cells were used as a positive and K562 as a negative control. **(G)** Levels of Tim-3 and galectin-9 were analyzed in Colo 205 lysates following 24 h of exposure to BH3I-1 by Western blot. **(H)** Mitochondrial extracts were obtained from non-treated and BH3I-1-stimulated Colo 205 cells and subjected to Western blot analysis to detect Tim-3 and galectin-9. Total protein levels were measured using a Bradford assay and equal protein amounts were loaded onto the gels. **(I)** Galectin-9 mRNA levels were analyzed in non-treated Colo 205 cells and those exposed to BH3I-1 using qRT-PCR. In the scheme galectin-9 is abbreviated as G9. Quantitative results are shown as mean values (crucial mean values are written inside respective bars) ± SEM of 3–6 independent experiments. $^{*}p < 0.05$; $^{**}p < 0.01$; $^{***}p < 0.001$ vs. control. The scheme in the centre of the figure is based on our work on Tim-3-galectin-9 secretory pathway (Gonçalves Silva et al., 2017).

factor-4E-binding protein (eIF4E-BP, **Figure 1B**). Obviously, one could suggest that Colo 205 cells accumulate galectin-9 on their surface and inside the cells based on FACS analysis (**Figure 1C**). Reduced levels of surface-based Tim-3 might indicate its masking by galectin-9 (Yasinska et al., 2018a). BH3I-1 does not affect the ability of Colo 205 cells to secrete galectin-9 (**Figure 1D**) but significantly reduces its surface presence (**Figure 1E**) as measured by on-cell assay. Colo 205 cells accumulate the Tim-3-galectin-9 complex (**Figure 1F**) at a level comparable to THP-1 AML cells (K562 chronic ML cells expressing traces

of galectin-9 were used as a negative control). Both proteins are also clearly detectable in Colo 205 cells by Western blot (**Figure 1G**) and treatment with BH3I-1 reduces intracellular levels of galectin-9. Importantly, Western blot analysis of Colo 205 mitochondrial extracts showed that the Tim-3-galectin-9 complex is accumulated in mitochondria upon stimulation with BH3I-1 (**Figure 1H**). The intracellular levels of galectin-9 mRNA were significantly reduced upon stimulation with BH3I-1, as detected by quantitative real-time PCR (qRT-PCR, **Figure 1I**).

Interestingly, the ability of Colo 205 cells to secrete galectin-9 is lower compared to THP-1 AML cells and the levels of secretion in both cell types are proportional to cellular Tim-3 levels (**Supplementary Figure 1**). This further supports conclusion regarding the involvement of Tim-3 in galectin-9 secretion (Gonçalves Silva et al., 2017).

We have also investigated two other types of epithelial cells—non-malignant human kidney RC-124 and malignant human HepG2 hepatoma cells. Both cell types have abundant mitochondria, however they are often [especially non-malignant, like RC-124—confirmed by a direct chemical measurement as described of the drug-associated bromine (Sollo et al., 1971) uptake in these cells, data not shown] less permeable for inhibitors of this type compared to colorectal cancer and AML cells. Therefore, 6 h of exposure to 1 mM H_2O_2 was used in order to defunctionalize mitochondria (Nicholas et al., 2011). We found that galectin-9 levels were significantly reduced in both cell types but the Tim-3-galectin-9 complex was only accumulated in the mitochondria of HepG2 and not RC-124 cells (**Supplementary Figure 2**).

MATERIALS AND METHODS

Commercially available Colo 205, RC-124, HepG2, THP-1, and K562, accompanied by authentication certificates, were used in this study. Mitochondria isolation, Western blot, on-cell assays, qRT-PCR, ELISA, and FACS analysis were performed as described before (Nicholas et al., 2011; Gonçalves Silva et al., 2016, 2017; Yasinska et al., 2018a). Detailed description of materials and methods used is provided in **Supplementary Information**.

DISCUSSION

Our results indicate that colorectal cancer cells operate the Tim-3-galectin-9 secretory pathway, where Tim-3 acts as a galectin-9 binding partner and possible trafficker. Pro-apoptotic mitochondrial dysfunction leads to a decreased transcription of galectin-9 mRNA leading to its reduced translation. However, exocytosis of galectin-9 is affected by mitochondrial defunctionalization leading to a re-distribution of the Tim-3-galectin-9 complex into mitochondria where galectin-9 could possibly interact with mitochondrial glycoproteins. The physiological relevance of this process is unclear but may well be a part of the regulated cell suicide programme which might involve transfer of galectin-9 into mitochondria so that it can't be involved in protection of a dying cell thus allowing its smooth elimination. Our further studies indicate that this phenomenon might be applicable mainly to malignant epithelial cells (**Figure 1**, **Supplementary Figure 2**). Importantly, targeted defunctionalization of mitochondria in malignant cells may be a novel strategy for anti-cancer immunotherapy since it reduces cell surface presence of galectin-9 capable of suppressing anti-cancer activity of cytotoxic lymphoid cells.

AUTHOR CONTRIBUTIONS

SS performed majority of the experiments reported in the **Figure 1** and significant number of experiments reported in **Supplementary Figures 1**, **2**, analyzed the data and contributed to manuscript writing. IY performed analysis of Tim-3-galectin-9 interactions and significant amount of experiments reported in **Supplementary Figure 2**, contributed to data analysis and manuscript writing. EF-K contributed to study design, performed FACS analysis, contributed to data analysis, and manuscript writing. VS designed the study, supervised the whole project, put the data together, wrote the manuscript.

SUPPLEMENTARY MATERIAL

The Supplementary Material for this article can be found online at: https://www.frontiersin.org/articles/10.3389/fphar.2019.00342/full#supplementary-material

REFERENCES

Gonçalves Silva, I., Ruegg, L., Gibbs, B. F., Bardelli, M., Fruewirth, A., Varani, L., et al. (2016). The immune receptor Tim-3 acts as a trafficker in a Tim-3/galectin-9 autocrine loop in human myeloid leukaemia cells. *Oncoimmunology* 5:e1195535. doi: 10.1080/2162402X.2016.1195535

Gonçalves Silva, I., Yasinska, I. M., Sakhnevych, S. S., Fiedler, W., Wellbrock, J., Bardelli, M., et al. (2017). The Tim-3-galectin-9 secretory pathway is involved in the immune escape of human acute myeloid leukemia cells. *EBio Med.* 22, 44–57. doi: 10.1016/j.ebiom.2017.07.018

Kang, C. W., Dutta, A., Chang, L. Y., Mahalingam, J., Lin, Y. C., Chiang, J. M., et al. (2015). Apoptosis of tumor infiltrating effector TIM-3+CD8+ T cells in colon cancer. *Sci. Rep.* 5:15659. doi: 10.1038/srep15659

Lee, Y. K., Lin, T. H., Chang, C. F., and Lo, Y. L. (2013). Galectin-3 silencing inhibits epirubicin-induced ATP binding cassette transporters and activates the mitochondrial apoptosis pathway via beta-catenin/GSK-3beta modulation in colorectal carcinoma. *PLoS ONE* 8:e82478. doi: 10.1371/journal.pone.0082478

Nicholas, S. A., Coughlan, K., Yasinska, I., Lall, G. S., Gibbs, B. F., Calzolai, L., et al. (2011). Dysfunctional mitochondria contain endogenous high-affinity human Toll-like receptor 4 (TLR4) ligands and induce TLR4-mediated inflammatory reactions. *Int. J. Biochem. Cell Biol.* 43, 674–681. doi: 10.1016/j.biocel.2011.01.012

Ruvolo, P. P. (2016). Galectin 3 as a guardian of the tumor microenvironment. *Biochim. Biophys. Acta* 1863, 427–437. doi: 10.1016/j.bbamcr.2015.08.008

Sakhnevych, S. S., Yasinska, I. M., Bratt, A. M., Benlaouer, O., Gonçalves Silva, I., Hussain, R., et al. (2018). Cortisol facilitates the immune escape of human

acute myeloid leukemia cells by inducing latrophilin 1 expression. *Cell. Mol. Immunol.* 15, 994–997. doi: 10.1038/s41423-018-0053-8

Sollo, F. W., Larson, T. E., and McGurk, F. F. (1971). Coloimetric methods for bromine. *Environ. Sci. Technol.* 5, 240–246. doi: 10.1021/es60050a009

Yasinska, I. M., Ceccone, G., Ojea-Jimenez, I., Ponti, J., Hussain, R., and Siligardi, G. (2018a). Highly specific targeting of human acute myeloid leukaemia cells using pharmacologically active nanoconjugates. *Nanoscale* 10, 5827–5833. doi: 10.1039/C7NR09436A

Yasinska, I. M., Gonzalves Silva, I., Sakhnevych, S. S., Ruegg, L., Hussain, R., Siligardi, G., et al. (2018b). High mobility group box 1 (HMGB1) acts as an "alarmin" to promote acute myeloid leukaemia progression. *Oncoimmunology* 7:e1438109. doi: 10.1080/2162402X.2018.1438109

Conflict of Interest Statement: The authors declare that the research was conducted in the absence of any commercial or financial relationships that could be construed as a potential conflict of interest.

frontiers in Pharmacology

MINI REVIEW
published: 09 April 2019
doi: 10.3389/fphar.2019.00299

Histamine and Delirium: Current Opinion

Paul L. Chazot[1], Laura Johnston[1], Edel Mcauley[2] and Stephen Bonner[2]*

[1] Department of Biosciences, Durham University, Durham, United Kingdom, [2] Intensive Care, South Tees Hospitals NHS Foundation Trust, The James Cook University Hospital, Middlesbrough, United Kingdom

Delirium is a very common, but refractory clinical state, notably present in intensive care and in the growing aging community. It is characterized by fluctuating disturbances in a number of key behavioral features, namely cognition, mood, attention, arousal, and self-awareness. Histamine is arguably the most pleotropic neurotransmitter in the human brain, and this review provides a rationale, and proposes that this neuroactive amine plays a role in modulating the characteristic features of delirium. While centrally permeable H_1 and H_2 histamine receptor antagonists have pro-delirium potential, we propose that centrally permeable H_3 histamine receptor antagonists may provide an exciting new strategy to combat delirium. The Histamine H_4 receptor may also have an indirect inflammatory neuroglial role which requires further exploration.

Keywords: histamine, H3 receptor, delirium, CNS, autoreceptor, heteroreceptor

INTRODUCTION

What Is Delirium?

Delirium is a very common, but refractory clinical state, notably commonly present in intensive care and in the growing aging community, with occurrence rates ranging from 14 to 56%, and hospital mortality rates ranging from 25 to 33% (Leslie and Inouye, 2011). It is characterized by fluctuating disturbances in arousal, attention, cognition, mood, and self-awareness, which can arise acutely, either in the absence of prior intellectual impairment or superimposed on chronic intellectual impairment in the growing aging population. The rise and development of delirium has been associated with increased morbidity, persistent functional decline, increased nursing time, higher hospital costs, increased length of hospital stay, and higher rates of nursing car home placement. Worryingly, delirium is a common, serious, and refractory source of mortality in intensive and community care across the age range, but is only recently being addressed in the United Kingdom, Europe and worldwide (Leslie and Inouye, 2011). Delirium in older hospitalized patients is of particular concern because patients aged 65 years and over currently account for more than half of all days spent in hospital care.

Delirium is a neurobehavioral syndrome caused by dysregulation of neuronal activity often secondary to serious systemic disturbances. Over time, a number of theories have been proposed in an attempt to explain the processes leading to the development of delirium (Maldonado, 2015; Herling et al., 2018). Each proposed complementary theory has focused on combinations of specific mechanisms or pathological processes (e.g., dopamine excess or acetylcholine deficiency, inflammatory responses), observational qualitative evidence (e.g., sleep deprivation, aging), or empirical scientific data (e.g., specific pharmacological agents such as opioids) or intraoperative hypoxia state association with postoperative delirium) (Maldonado, 2013; Egberts et al., 2018). The literature suggests that many factors or mechanisms included in these theories lead to a final common outcome associated with an alteration in neurotransmitter synthesis, function, and/or availability that triggers the complex behavioral and cognitive changes reported in delirium. In general,

OPEN ACCESS

Edited by:
Mitsunobu Mio,
Shujitsu University, Japan

Reviewed by:
Estefanía Moreno,
University of Barcelona, Spain
Enric I. Canela,
University of Barcelona, Spain

****Correspondence:***
Paul L. Chazot
paul.chazot@durham.ac.uk

Specialty section:
This article was submitted to Experimental Pharmacology and Drug Discovery, a section of the journal Frontiers in Pharmacology

Received: *17 January 2019*
Accepted: *11 March 2019*
Published: *09 April 2019*

Citation:
Chazot PL, Johnston L, Mcauley E and Bonner S (2019) Histamine and Delirium: Current Opinion. Front. Pharmacol. 10:299. doi: 10.3389/fphar.2019.00299

the most commonly described neurochemical changes associated with delirium include deficiencies in acetylcholine and/or melatonin, together with excess in glutamate and monoamines dopamine and noradrenalin, and bi-directional activity alterations (e.g., decreased or increased activity, depending on delirium presentation and trigger) in serotonin, γ-aminobutyric acid (GABA) and/or, importantly, histamine (Maldonado, 2013). The unknown nature of etiology for most types of delirium and the complete lack of placebo-controlled Randomized Controlled drug Trials, the lack of any FDA-approved drug treatment for delirium and the wide ranging nature of drugs with multiple chemical neurotransmitter pathways affected (variable across NHS Trust hospitals) used to treat it is clearly a major problem. Furthermore the lack of effective non-pharmacological approaches is also problematical (Wade et al., 2015, 2019; Richards-Belle et al., 2018) Without understanding more about the underlying nature of the pathways involved how can we hope to effectively and rationally treat it?

In this short commentary, we offer a rationale for a new pharmacological strategy to combat delirium. We propose that central histamine is a significant player in all of the clinical features of delirium; while H_1 and H_2 histamine-targeted antihistamines should be treated with care, a centrally acting histamine H_3 receptor antagonist, with appropriate diurnal pharmacokinetic properties, may provide a novel and effective strategy for preventing or combatting delirium. We discuss the key evidence base and potential mechanisms underpinning these proposals and clinical implications.

HISTAMINE AND ANATOMICAL FRAMEWORK RELEVANCE TO DELIRIUM COGNITION, MOOD AND WAKEFULLNESS

Arousal stems from the wakefulness of a person and awareness is the individual's ability to perceive his/her environment. In both these behavioral states, histamine has a primary role to play. Diminished alertness, delayed reaction times, and somnolence are common manifestations of allergy treatments with use of classic first-generation (CNS-permeant) anti-histamines, thus evidencing that histamine is required for arousal/wakefulness and awareness/attention. The evidence became stronger with the report that histidine decarboxylase (HDC) knockout mice, which lack histamine, display increased paradoxical sleep, sleep-wake cycle modifications, and are unable to remain awake under diurnal high vigilance (narcolepsy) (Parmentier et al., 2002). The mammalian, including human, waking state is maintained by continual activation of neuromodulatory aminergic neurotransmitters [dopamine, noradrenaline (NA), acetylcholine and notably histamine], hypocretin/orexinergic (Oxergic), and selective excitatory glutamatergic and inhibitory GABAergic pathways (Korotkova et al., 2005; Yu et al., 2018). Cortical activation is one of the physiological signs of wakefulness and requires robust cholinergic, noradrenergic, serotonergic and, importantly, histaminergic tones. Histamine controls these features through the extensive influence of ascending branches from the tuberomammillary nucleus (TMN) in the hypothalamus to all parts of the brain, including the prefrontal cerebral cortex, various limbic regions and the basal ganglia (Yu et al., 2018). Monoaminergic neurons comprising noradrenergic (locus coeruleus: LC), serotonergic (raphe nuclei, RN) and histaminergic (TMN) neurons project to the cerebrocortex, thalamus and brainstem are known together as the center of sleep regulation (Oh et al., 2018; Yu et al., 2018). Furthermore, Oxergic cell bodies in the hypothalamus densely project to LC, TM and RN, which suggests a strong link between monoaminergic and Oxergic neurons, again in the control of wakefulness. It is well established that the Oxergic wake-active neurons provide a major excitatory drive onto TMN histamine neurons (Lin et al., 2011), and this could be a key way that orexin promotes arousal, through amplifying its effects via the histaminergic system. During the wake state, TMN histamine/GABA-ergic neurons are co-active in parallel and their ascending histamine/GABA fibers release histamine and GABA into the prefrontal cortex (PFC), neocortex (Ctx) and striatum (Str) (Lin et al., 2011). Glutamatergic pyramidal neurons in the PFC send excitatory projections back to the histamine neurons in the TMN, reinforce wakefulness, attention and consciousness (Lin et al., 2011). The Histamine-GABA-ergic neurons are silenced during Non-REM sleep by preoptic GABAergic neurons. Histamine-only projections from the TMN also excite cholinergic neurons into the basal forebrain, and the axons of these excited cholinergic neurons release acetylcholine throughout the cortex (the fundamental basis for high attention together with productive cognitive function). We suggest that when the brain is exposed to these neuromodulators appropriately, we are wakeful, attentive and conscious, importantly, *without* delirium. This this overall neuronal anatomical framework provides the mechanistic basis for the influence of histamine upon delirium, through auto- and hetero-presynaptic and postsynaptic functions, respectively.

HISTAMINE RECEPTOR SUBTYPE-DEPENDENT EFFECTS

Histamine elicits its physiological action via four G-protein couple receptor (GPCR subtypes, namely H_1, H_2, H_3, and H_4 receptors, expressed widely and differentially throughout the body, including the CNS (reviewed in Panula et al., 2015). In terms of the brain, H_1, H_2, H_3 receptors play clear roles in neuronal function, post- and pre-synaptically, and, interestingly, the H_4R appears to influence neuronal function indirectly through modulating activated microglia (Zhou et al., 2018). Histamine driven H_1 and H_2 receptor-mediated actions are mostly excitatory, while H_3 receptors act as inhibitory auto- and heteroreceptors (Panula et al., 2015). Histamine-mediated excitation was blocked by a CNS-permeable H_1 receptor antagonist, mepyramine, in 78% of cells and by cimetidine, a CNS-permeable H_2 receptor antagonist, in 42% of cells (Korotkova et al., 2005). Histamine H_3 heteroreceptor function modulates cholinergic, GABA-ergic, as well as noradrenergic function (Panula et al., 2015) (**Figure 1**).

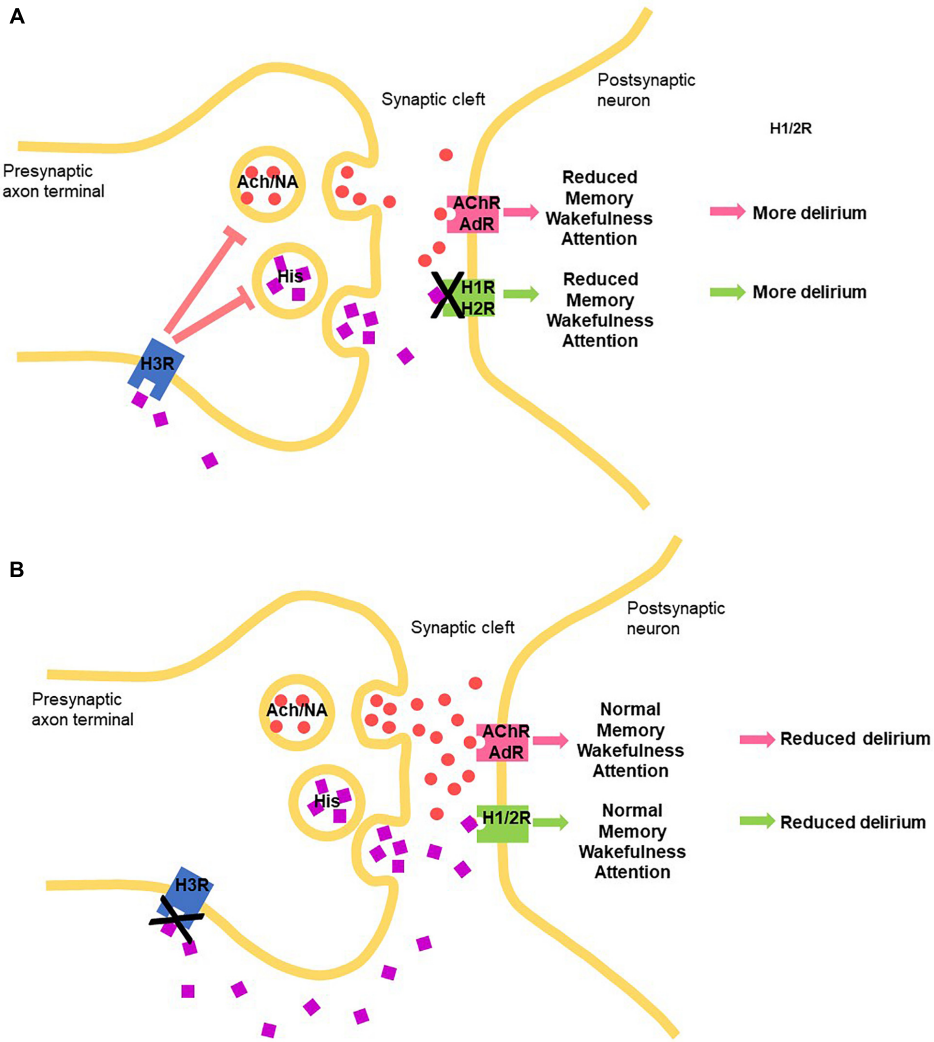

FIGURE 1 | Schematic how manipulating the central histaminergic system by blocking the histamine receptors can potentially modify delirium symptom induction and maintenance through manipulating levels of histamine (HIS) through autoreceptors, acetylcholine (Ach) and noradrenalin (NA), through heteroreceptors binding to histamine receptors, acetylcholine receptor (AChR) and AdR (adrenergic receptors, respectively. **(A)** H_1 and H_2 histamine receptor antagonists. **(B)** H_3 receptor antagonists.

HISTAMINE H_1 RECEPTOR CNS PHYSIOLOGY

Histamine H_1 receptors occur throughout the CNS, with particular high densities in regions involved in arousal and waking, notably the thalamus and cortex, and neurochemically the cholinergic, noradrenergic, dopaminergic, and serotonergic nuclei. H_1 receptor activation causes excitation in many brain regions (brain stem, thalamus, hypothalamus, cortex, amygdala, striatum) through G_{q11} protein and direct block of leak K^+ conductance or phospholipase C, inositol trisphosphate (IP_3), and diacylglycerol (DAG) mediation (discussed in Obara et al., 2019). IP_3 releases Ca^{2+} from internal stores and activates a number of Ca^{2+}-dependent processes, including the opening of a cation channel of the transient receptor potential canonical (TRPC) type or stimulation of a Na^+–Ca^{2+}-exchanger. Furthermore, the elevated intracellular Ca^{2+} can stimulate NO synthase and, consequently, guanylate cyclase. On the other hand, Ca^{2+}-dependent K^+ channels can be opened, leading to hyperpolarization and inhibition, for instance, in hippocampal pyramidal neurons.

H_2 HISTAMINE RECEPTOR CNS PHYSIOLOGY

Histamine H_2 receptors are also widely distributed in the mammalian brain (reviewed in Panula et al., 2015). The highest densities of histamine H_2 receptors are found in the basal ganglia, hippocampus, amygdala and cerebral cortex, with

modest expression levels in the cerebellum and hypothalamus (Panula et al., 2015; Monczor and Fernandez, 2016). A similar distribution of the histamine H_2 receptor occurs in the brain of humans and rodents. H_2 histamine receptor antagonists decreased significantly the hypothalamic NA content by 21–32%. Activation of the histamine H_2 receptor in the brain inhibits nerve cells and blocks long-lasting afterhyperpolarization and accommodation of firing in cortical and thalamic neurons (Haas and Reiner, 1988). However, if this afterhyperpolarization block continues for an protracted period, it can lead to potentiation of excitation in rodent and in human brain, resulting in enhanced synaptic plasticity (Brown et al., 1995). Therefore, H_2 receptor antagonism can suppress plasticity. RT-PCR revealed that while mRNA for the H_1 receptor was expressed in 77% of isolated LC neurons, mRNA for the H_2 receptor was in 41% and H_3 receptors in 29% of LC neurons. These findings underline the coordination between aminergic systems and suggest that the arousal induced by the histamine system could involve excitation of noradrenergic neurons in the LC (Korotkova et al., 2005).

H_3 RECEPTORS CNS PHYSIOLOGY

H_3 receptors, pre-synaptic inhibitory GPCRs, inhibit voltage-activated Ca^{2+} channels, on the terminals of histaminergic axons themselves (as an autoreceptor) and many types of neurons (heteroreceptor), which leads to reduced transmitter release of histamine, and acetylcholine, noradrenalin, serotonin, GABA, glutamate (heteroreceptors), respectively (reviewed in Panula et al., 2015). Despite H_3 receptors being predominantly presynaptic receptors, regulating the release of neurotransmitters such as acetylcholine and histamine in most areas of the brain, in a particular part of the brain, namely the striatum, the vast majority of these receptors are actually postsynaptic, affecting signaling throughout the basal ganglia. Because the basal ganglia are centrally involved in several major neurological and psychiatric disorders, this aspect requires consideration. Constitutive activity *in vivo* and the possibility of dimerization shown *in vitro* for the H_3 receptor has been reported (summarized in Panula et al., 2015), but relevance to physiological function of these functional and structural features and, therefore, to modulating delirium, is unclear.

H_4 RECEPTORS CNS PHYSIOLOGY

A number of recent experimental studies suggest that systemic inflammation contributes to the pathophysiology of delirium in both elderly and post-trauma delirium. A common raised inflammatory cytokine linked to delirium in these studies is IL-6. Histamine via the histamine H_4 receptor is known to play a key role in activating systemic inflammation through activation of microglia, mast cells and immune dendritic cells, with consequent production of proinflammatory factors TNF-α and, notably, IL-6 (Desai and Thurmond, 2011; Simon et al., 2011; Vasunilashorn et al., 2015; Ngo et al., 2017; Zhou et al., 2018). A rise in microglia H_4R has been implicated in Parkinson's disease, in which delirium has been a recently recognized feature. This offers a possible role for the H_4R in the neuroinflammatory components of delirium.

HISTAMINE RECEPTOR SUBTYPE CONNECTIONS IN THE DELIRIUM CLINICAL SETTING AND WAKEFULLNESS

Histamine H_1 and H_2 Receptors

Drug-induced delirium is often seen in clinical practice. Even before it was discovered that histamine was a transmitter in the brain, first generation anti-histamines (i.e., H_1 receptor antagonists) were noted historically to be sedatives (eg., Monnier et al., 1967). Interestingly, H_1 receptor antagonists, for example, doxepin (at low concentrations), are making a comeback to treat primary insomnia (Yeung et al., 2015). Histamine and H_1Rs are involved in maintaining arousal and cognition in humans, and that the severity of clinical symptoms is correlated to the amount of antihistamine that has penetrated into the brain (Tashiro et al., 2002). It was noted, as far back as the 1980s, that delirium was a rare side-effect of both H_1 and H_2 antagonists (reviewed in Yanai et al., 2017) (**Table 1**). First generation H_1 anti-histamines significantly increased daytime sleepiness and nocturnal sleep quality. Some, including cetirizine and hydroxyzine, seemed to also have negative influences on mood states. Outpatients who received cetirizine and hydroxyzine treatments reported higher scores on the depression, anxiety, and fatigue sub-scales compared to those who received desloratadine, levocetirizine, and rupatadine (Clegg and Young, 2011). The sedating antihistamines are non-specific in their actions and often have marked anticholinergic effects. Features of overdose include tachycardia, blood pressure disturbances, dry mouth, ataxia, psychosis, convulsion and, notably, agitation (Clegg and Young, 2011).

The second generation CNS-sparing H_1 antihistamine, betahistine is not normally known to induce delirium, but an investigation in a side-effects databases did reveal several cases in which delirium may have been present, even though the term, delirium, was not actually used. In this case, delirium was potentially due to the combination of an elevated betahistine plasma level and, significantly, a damaged blood-brain barrier due to cerebral infarctions, confirmed both by computed tomography (CT) and Magnetic resonance imaging (MRI) scans (Hoenders and Wilterdink, 2004). It is noted that caution is often required when prescribing antihistamine H_1 antagonists for people at risk of delirium and considered individual patient assessment is recommended. In contrast, a small, recent study showed cyproheptadine, a first generation anti-H_1 antihistamine, with its range of diverse effects was proposed to be a potential option for prevention of postoperative delirium. In this pilot study, cyproheptadine significantly decreased the incidence, but not severity of postoperative delirium (this may relate to its central-permeability). In contrast, the main negative feature of promethazine (another first generation H_1 antihistamine) is

TABLE 1 | The implication of histaminergic system and drugs to delirium.

Drug	Selectivity	CNS-permeable?	Effects on delirium?	Reference
Doxepin	H_1	Yes	unknown	Yeung et al., 2015
Cetirizine	H_1	Yes	possible	Clegg and Young, 2011
Hydroxyzine	H_1	Yes	possible	Clegg and Young, 2011
Desloratadine	H_1	No	No	Clegg and Young, 2011
Levocetirizine	H_1	No	No	Clegg and Young, 2011
Rupatadine	H_1	No	No	Clegg and Young, 2011
Betahistine	H_1	No	Mixed data	Hoenders and Wilterdink, 2004
Cyproheptadine	H_1	Yes	Decreased incidence but not severity	Page et al., 2009
Cimetidine	H_2	Yes	Possible	Cantú and Korek, 1991
Cimetidine	H_2	Yes	Yes	Nowak, 1980
Cimetidine	H_2	Yes	Yes	Fujii et al., 2012
Ranitidine	H_2	No	Unusual	Mauran et al., 2016

delirium, the probability of which can be predicted from the dose ingested by the individual (Page et al., 2009).

Studies on the association between CNS negative symptoms (psychosis, agitation, hallucinations, mental status changes, disorientation, confusion, irritability, a greatly reduced level of consciousness or hostility all underpinning delirium) and H_2 blockers have been explored previously. These reactions generally occur during the first 2 weeks of therapy and resolve within 3 days of drug withdrawal, although long term use in critical care or the community may prove problematical. The estimated incidence of CNS negative symptoms is 0.2% or less in outpatients, but significantly higher, 1.6 to 80% in long-term hospitalized patients.

CNS side effects such as mental confusion (major facet of delirium) develop in elderly patients and in patients with severe renal or hepatic impairment. Cimetidine is CNS-permeable in the elderly and critically ill patients (with compromised blood-brain barrier). Cimetidine is frequently associated with these "delirium" reactions; however, no clear evidence exists that one H_2 blocker is more likely than another to cause such a reaction (Cantú and Korek, 1991). It has been noted that for people at risk of delirium, certain drug combinations are to be prescribed with care. Caution is also required when prescribing antihistamine H_2 antagonists for people at risk of delirium and a considered individual patient assessment is advocated. Many case studies have been reported to support this policy. One example was a "serious" case of severe mania leading to hospitalization in a 42-year-old alcohol-dependent 4 days after ranitidine introduction (Mauran et al., 2016). Histamine H_2 receptor antagonists may also cause acute or chronic cognitive impairment. These effects are often associated with some of the H_2-histamine receptor antagonists, eg., cimetidine (Tagamet) again, but are unusual with ranitidine (Zantac), potentially again due to their respective CNS permeability (Mauran et al., 2016). An old study showed that that a large dose of H_2-receptor antagonists (50–259 micrograms ivt) decreased hypothalamic NA content (Nowak, 1980). A comparison was made between two groups of patients in a small study who were treated with H_2 antagonists or proton pump inhibitors (PPI group) for anastomotic ulcer prevention following surgical treatment of esophageal cancer. It was noted that the incidence of delirium was significantly lower in the PPI group than in the H_2 group. Significantly, in the 11 patients from the H_2 group who developed delirium, discontinuation of H_2 antagonists resulted in a significant reduction in the delirium rate score. This study indicated that switch from H_2 blockers to PPIs reduced delirium and, thus, providing an appropriate strategy to combat drug-induced delirium using antiulcer drugs (Fujii et al., 2012). The ventrolateral preoptic nucleus is a sleep-promoting nucleus located in the basal forebrain. A commonly used intravenous anesthetic, propofol, had been reported to induce sleep and augment the firing rate of neurons in ventrolateral GABAergic preoptic nucleus, but the underlining mechanism is yet to be clearly determined. Interestingly, the propofol-induced inhibition of inhibitory postsynaptic currents on noradrenalin-inhibited neurons have been shown to be mediated by histaminergic H_1 and H_2 receptors (Liu et al., 2017).

Opioids and Histamine Interactions

An interaction between histaminergic and opioidergic systems within the CNS was proposed three decades ago, suggesting that analgesia produced by opioids may be associated with release of histamine and the stimulation of histamine receptors at the supraspinal (central) level (Nishibori et al., 1985). Many more recent studies have shown that histamine receptor antagonists can modulate the analgesic action of opioids, however, the site and mode of action of this interaction differs between the spinal or supraspinal level, and depends on the subtype of histamine receptor (Mobarakeh et al., 2002, 2006, 2009; Stein et al., 2016). A series of studies have also shown than in H_1R and H_2R KO mice, morphine-induced antinociception was significantly augmented when compared to the wild-type controls in models of acute pain. Therefore, anti-histamines should be prescribed with caution in people at risk of delirium, but this should be tempered by the observation that untreated severe pain can itself trigger delirium.

Rationale for Use of H_3 Antagonists for Future Development?

Cortical activation (EEG desynchronization) is one of the salient signs of wakefulness, attention and enhanced cognitive function, and requires high histaminergic, and cholinergic, noradrenergic, and serotonergic tones, controlled by H_3 auto- and heteroreceptor action, respectively. Arousal induced by the histamine system through the H_3 histamine heteroreceptor blockade is believed to largely involve excitation of noradrenergic neurons in the LC. As discussed above, the Histamine H_3 receptor is expressed on and controls a population of the TM histamine/GABA-ergic neurons which are co-active in parallel and their ascending histamine/GABA fibers release histamine

and GABA onto the PFC. Glutamatergic pyramidal neurons in the PFC send excitatory projections back to the histamine neurons in the TMN, reinforcing wakefulness, attention and consciousness. Selective blockade of the H_3-autoreceptor with an H_3 receptor antagonist would be predictive to drive this positive reinforcement.

Histamine promotes wakefulness by tonic control over sleep-generating mechanisms in the preoptic/anterior hypothalamus, and cholinergic neurons seem to be implicated. The role of histamine indicates that the histaminergic system also influences attention and learning and memory performance by modulating the release of ACh, although some cognitive effects of histamine and histaminergic agents occur independent of ACh. H_3R antagonists are well known to enhance cognition and rescue cognitive deficits in preclinical models and modulate neurotransmission (Chazot, 2010), through, in particular, acetylcholine (ACh) release in the cortex and hippocampus, two key brain areas involved in memory processing. It has been recently shown that histamine H_3 receptor antagonist/inverse agonists require the integrity of brain histamine system to successfully elicit physiological and procognitive effects in the mouse (Provensi et al., 2016). Perfusion of the TMN with the H_3 inverse agonist/antagonist (ABT-239) differentially increased histamine release from the TMN, NBM, and PFC, but not from the STR or NAcc. When administered locally, ABT-239 (H_3 receptor antagonist) again increased histamine release from the NBM, but not from the NAcc. As defined by their sensitivity to ABT-239, histaminergic neurons establish distinct pathways according to their terminal projections, and can differentially modulate neurotransmitter release in a brain region-specific manner (Munari et al., 2013; Provensi et al., 2016). This implies independent functions of subsets of histamine neurons according to their terminal projections, with relevant consequences for the development of specific compounds that affect only subsets of histamine neurones, thus increasing target specificity. The selective mode of action is currently believed to be due to the respective levels of presynaptic H_3Rs expressed on the TMN and cholinergic neurons (Giannoni et al., 2009). This requires formal confirmation. Overall, we provide an anatomical, pharmacological and physiological rationale for developing a CNS-permeable H_3 histamine receptor antagonist/inverse agonist as a strategy for combatting the range of components of delirium.

AUTHOR CONTRIBUTIONS

All authors listed have made a substantial, direct and intellectual contribution to the work, and approved it for publication.

REFERENCES

Brown, R. E., Fedorov, N. B., Haas, H. L., and Reymann, K. G. (1995). Histaminergic modulation of synaptic plasticity in area CA1 of rat hippocampal slices. *Neuropharmacology* 34, 181–190. doi: 10.1016/0028-3908(94)00138-I

Cantú, T. G., and Korek, J. S. (1991). Central nervous system reactions to histamine-2 receptor blockers. *Ann. Intern. Med.* 114, 1027–1034. doi: 10.7326/0003-4819-114-12-1027

Chazot, P. L. (2010). Therapeutic potential of histamine H3 receptor antagonists in dementias. *Drug News Perspect.* 23, 99–103. doi: 10.1358/dnp.2010.23.2.1475899

Clegg, A., and Young, J. B. (2011). Which medications to avoid in people at risk of delirium: a systematic review. *Age Ageing* 40, 23–29. doi: 10.1093/ageing/afq140

Desai, P., and Thurmond, R. L. (2011). Histamine H4 receptor activation enhances LPS-induced IL-6 production in mast cells via ERK and PI3K activation. *Eur. J. Immunol.* 41, 1764–1773. doi: 10.1002/eji.201040932

Egberts, A., Wijnbeld, E. H., Fekkes, D., van der Ploeg, M. A., Ziere, G., Hooijkaas, H., et al. (2018). Neopterin: a potential biomarker for delirium in elderly patients. *Front. Neural Circuits* 12:4.

Fujii, S., Tanimukai, H., and Kashiwagi, Y. (2012). Comparison, and analysis of delirium induced by histamine H_2 receptor antagonists and proton pump inhibitors in cancer patients. *Case Rep. Oncol.* 5, 409–412. doi: 10.1159/000341873

Giannoni, P., Passani, M. B., Nosi, D., Chazot, P. L., Shenton, F. C., Medhurst, A. D., et al. (2009). Heterogeneity of histaminergic neurons in the tuberomammillary nucleus of the rat. *Eur. J. Neurosci.* 29, 2363–2374. doi: 10.1111/j.1460-9568.2009.06765.x

Haas, H. L., and Reiner, P. B. (1988). Membrane properties of histaminergic tuberomammillary neurones of the rat hypothalamus in vitro. *J. Physiol.* 399, 633–646. doi: 10.1113/jphysiol.1988.sp017100

Herling, S. F., Greve, I. E., Vasilevskis, E. E., Egerod, I., Bekker Mortensen, C., Møller, A. M., et al. (2018). Interventions for preventing Intensive care unit delirium in adults. *Cochrane Database Syst. Rev.* 11:CD009783. doi: 10.1002/14651858.CD009783.pub2

Hoenders, H. J., and Wilterdink, J. (2004). Delirium in a 73-year-old man after many years of unwise use of betahistine. *Ned. Tijdschr. Geneeskd.* 148, 2338–2341.

Korotkova, T. M., Sergeeva, O. A., Ponomarenko, A. A., and Haas, H. L. (2005). Histamine excites noradrenergic neurons in locus coeruleus in rats. *Neuropharmacology* 49, 129–134. doi: 10.1016/j.neuropharm.2005.03.001

Leslie, D. L., and Inouye, S. K. (2011). The importance of delirium: economic and societal costs. *MPH J. Am. Geriatr. Soc.* 59(Suppl. 2), S241–S243. doi: 10.1111/j.1532-5415.2011.03671.x

Lin, J. S., Anaclet, C., Sergeeva, O. A., and Haas, H. L. (2011). The waking brain: an update. *Cell Mol. Life Sci.* 68, 2499–2512. doi: 10.1007/s00018-011-0631-8

Liu, Y., Zhang, Y., Qian, K., Zhang, L., and Yu, T. (2017). Histaminergic H1 and H2 receptors mediate the effects of propofol on the noradrenalin-inhibited neurons in rat ventrolateral preoptic nucleus. *Neurochem. Res.* 42, 1387–1393. doi: 10.1007/s11064-017-2187-y

Maldonado, J. R. (2013). Neuropathogenesis of delirium: review of current etiologic theories and common pathways. *Am. J. Geriatr. Psychiatry* 21, 1190–1222. doi: 10.1016/j.jagp.2013.09.005

Maldonado, J. R. (2015). "Delirium," in *Handbook of Consultation-Liaison Psychiatry*, 2nd Edn, eds H. Leigh and J. Streltzer (New York, NY: Springer International Publishing), 157–187.

Mauran, A., Goze, T., Abadie, D., Bondon-Guitton, E., Chevrel, P., Schmitt, L., et al. (2016). Mania associated with ranitidine: a case report and review of literature. *Fundam. Clin. Pharmacol.* 30, 294–296. doi: 10.1111/fcp.12201

Mobarakeh, J. I., Sakurada, S., Hayashi, T., Orito, T., Okuyama, K., Sakurada, T., et al. (2002). Enhanced antinociception by intrathecally-administered morphine in histamine H1 receptor gene knockout mice. *Neuropharmacology* 42, 1079–1088. doi: 10.1016/S0028-3908(02)00058-8

Mobarakeh, J. I., Takahashi, K., Sakurada, S., Kuramasu, A., and Yanai, K. (2006). Enhanced antinociceptive effects of morphine in histamine H2 receptor gene knockout mice. *Neuropharmacology* 51, 612–622. doi: 10.1016/j.neuropharm.2006.05.003

Mobarakeh, J. I., Takahashi, K., and Yanai, K. (2009). Enhanced morphine-induced antinociception in histamine H3 receptor gene knockout mice. *Neuropharmacology* 57, 409–414. doi: 10.1016/j.neuropharm.2009.06.036

Monczor, F., and Fernandez, N. (2016). Current knowledge and perspectives on histamine H1 and H2 receptor pharmacology: functional selectivity, receptor crosstalk, and repositioning of classic histaminergic ligands. *Mol. Pharmacol.* 90, 640–648. doi: 10.1124/mol.116.105981

Monnier, M., Fallert, M., and Battacharya, I. C. (1967). The waking action of histamine. *Experientia* 23, 21–22. doi: 10.1007/BF02142244

Munari, L., Provensi, G., Passani, M. B., and Blandina, P. (2013). Selective brain region activation by histamine H3 receptor antagonist/inverse agonist ABT-239 enhances acetylcholine and histamine release and increases c-Fos expression. *Neuropharmacology* 70, 131–140. doi: 10.1016/j.neuropharm.2013.01.021

Ngo, L. H., Inouye, S. K., Jones, R. N., Travison, T. G., Libermann, T. A., Dillon, S. T., et al. (2017). Methodologic considerations in the design and analysis of nested case-control studies: association between cytokines and postoperative delirium. *BMC Med. Res. Methodol.* 17:88. doi: 10.1186/s12874-017-0359-8

Nishibori, M., Oishi, R., Itoh, Y., and Saeki, K. (1985). Morphine-induced changes in histamine dynamics in mouse brain. *Neurochem. J.* 45, 719–724. doi: 10.1111/j.1471-4159.1985.tb04051.x

Nowak, J. Z. (1980). Effects of histamine H1- and H2-receptor antagonists on dopamine, noradrenaline and serotonin systems in rat brain. *Pol. J. Pharmacol. Pharm.* 32, 451–461.

Obara, I., Telezhkin, V., Alrashdi, I., and Chazot, P. L. (2019). Histamine receptors and neuropathic pain relief. *BJP* (in press).

Oh, J., Petersen, C., Walsh, C. M., Bittencourt, J. C., Neylan, T. C., and Grinberg, L. T. (2018). The role of co-neurotransmitters in sleep and wake regulation. *Mol. Psychiatry* doi: 10.1038/s41380-018-0291-2 [Epub ahead of print].

Page, C. B., Duffull, S. B., Whyte, I. M., and Isbister, G. K. (2009). Promethazine overdose: clinical effects, predicting delirium and the effect of charcoal. *QJM* 102, 123–131. doi: 10.1093/qjmed/hcn153

Panula, P., Chazot, P. L., Cowart, M., Gutzmer, R., Leurs, R., Liu, W. L., et al. (2015). International union of basic and clinical pharmacology. XCVIII. Histamine receptors. *Pharmacol. Rev.* 67, 601–655. doi: 10.1124/pr.114.010249

Parmentier, R., Ohtsu, H., Djebbara-Hannas, Z., Valatx, J. L., Watanabe, T., and Lin, J. S. (2002). Anatomical, physiological, and pharmacological characteristics of histidine decarboxylase knock-out mice: evidence for the role of brain histamine in behavioral and sleep-wake control. *J. Neurosci.* 22, 7695–7711. doi: 10.1523/JNEUROSCI.22-17-07695.2002

Provensi, G., Costa, A., Passani, M. B., and Blandina, P. (2016). Donepezil, an acetylcholine esterase inhibitor, and ABT-239, a histamine H3 receptor antagonist/inverse agonist, require the integrity of brain histamine system to exert biochemical and procognitive effects in the mouse. *Neuropharmacology* 70, 131–140. doi: 10.1016/j.neuropharm.2013.01.021

Richards-Belle, A., Mouncey, P. R., Wade, D., Brewin, C. R., Emerson, L. M., Grieve, R., et al. (2018). Psychological outcomes following a nurse-led preventative psychological intervention for critically ill patients (POPPI): protocol for a cluster-randomised clinical trial of a complex intervention. *BMJ Open* 8:e020908. doi: 10.1136/bmjopen-2017-020908

Simon, T., Laszlo, V., Lang, O., Buzas, E., and Falus, A. (2011). Histamine regulates relevant murine dendritic cell functions via H4 receptor. *Front. Biosci.* 3:1414–1424. doi: 10.2741/e343

Stein, T., Souza-Silva, E., Mascarin, L., Eto, C., Fin, F. E., and Tonussi, C. R. (2016). Histaminergic pharmacology modulates the analgesic and anti-dematogenic effects of spinally injected morphine. *Anesth. Analg.* 123, 238–243. doi: 10.1213/ANE.0000000000001326

Tashiro, M., Mochizuki, H., Iwabuchi, K., Sakurada, Y., Itoh, M., Watanabe, T., et al. (2002). Roles of histamine in regulation of arousal and cognition: functional neuroimaging of histamine H1 receptors in human brain. *Life Sci.* 72, 409–414. doi: 10.1016/S0024-3205(02)02276-2

Vasunilashorn, S. M., Ngo, L., Inouye, S. K., Libermann, T. A., Jones, R. N., Alsop, D. C., et al. (2015). Cytokines and postoperative delirium in older patients undergoing major elective surgery. *Dement Geriatr. Cogn. Disord.* 39, 116–124.

Wade, D. M., Moon, Z., Windgassen, S., Harrison, A., Morris, L., and Weinman, J. (2015). Non-pharmacological interventions to reduce ICU-related psychological distress: a systematic review. *Minerva Anestesiol.* 82, 465–478.

Wade, D. M., Mouncey, P. R., Richards-Belle, A., Wulff, J., Harrison, D. A., Sadique, M. Z., et al. (2019). Effect of a nurse-led preventive psychological intervention on symptoms of posttraumatic stress disorder among critically ill patients: a randomized clinical trial. *JAMA* 321, 665–675. doi: 10.1001/jama.2019.0073

Yanai, K., Yoshikawa, T., Yanai, A., Nakamura, T., Iida, T., Leurs, R., et al. (2017). The clinical pharmacology of non-sedating antihistamines. *Pharmacol. Ther.* 178, 148–156. doi: 10.1016/j.pharmthera.2017.04.004

Yeung, W. F., Chung, K. F., Yung, K. P., and Ng, T. H. (2015). Doxepin for insomnia: a systematic review of randomized placebo-controlled trials. *Sleep Med. Rev.* 19, 75–83. doi: 10.1016/j.smrv.2014.06.001

Yu, X., Franks, N. P., and Wisden, W. (2018). Sleep and sedative states induced by targeting the histamine and noradrenergic systems. *Front. Neural Circuits.* 12:4. doi: 10.3389/fncir.2018.00004

Zhou, P., Homberg, J. R., Fang, Q., Wang, J., Li, W., Meng, X., et al. (2018). Histamine-4 receptor antagonist JNJ7777120 inhibits pro-inflammatory microglia and prevents the progression of Parkinson-like pathology and behaviour in a rat model. *Brain Behav. Immun.* 76, 61–73. doi: 10.1016/j.bbi.2018.11.006

Conflict of Interest Statement: The authors declare that the research was conducted in the absence of any commercial or financial relationships that could be construed as a potential conflict of interest.

frontiers in Pharmacology

ORIGINAL RESEARCH
published: 10 April 2019
doi: 10.3389/fphar.2019.00367

Inhibitory Effect of KP-A038 on Osteoclastogenesis and Inflammatory Bone Loss Is Associated With Downregulation of Blimp1

Hye Jung Ihn[1†], Taeho Lee[2†], Doohyun Lee[2], Jong-Sup Bae[2], Sang-Hyun Kim[3], Il Ho Jang[4], Yong Chul Bae[5], Hong-In Shin[6] and Eui Kyun Park[6]*

[1] Institute for Hard Tissue and Bio-tooth Regeneration, Kyungpook National University, Daegu, South Korea, [2] College of Pharmacy, Research Institute of Pharmaceutical Sciences, Kyungpook National University, Daegu, South Korea, [3] Department of Pharmacology, School of Medicine, Kyungpook National University, Daegu, South Korea, [4] Department of Oral Biochemistry and Molecular Biology, School of Dentistry, Pusan National University, Yangsan, South Korea, [5] Department of Oral Anatomy and Neurobiology, School of Dentistry, Kyungpook National University, Daegu, South Korea, [6] Department of Oral Pathology and Regenerative Medicine, School of Dentistry, Institute for Hard Tissue and Bio-tooth Regeneration, Kyungpook National University, Daegu, South Korea

OPEN ACCESS

Edited by:
Vadim V. Sumbayev, University of Kent, United Kingdom

Reviewed by:
Luca Vanella, Università degli Studi di Catania, Italy
Michael Danilenko, Ben-Gurion University of the Negev, Israel

***Correspondence:**
Eui Kyun Park
epark@knu.ac.kr

[†] These authors have contributed equally to this work

Specialty section:
This article was submitted to Experimental Pharmacology and Drug Discovery, a section of the journal Frontiers in Pharmacology

Received: *17 December 2018*
Accepted: *25 March 2019*
Published: *10 April 2019*

Citation:
Ihn HJ, Lee T, Lee D, Bae J-S, Kim S-H, Jang IH, Bae YC, Shin H-I and Park EK (2019) Inhibitory Effect of KP-A038 on Osteoclastogenesis and Inflammatory Bone Loss Is Associated With Downregulation of Blimp1. Front. Pharmacol. 10:367. doi: 10.3389/fphar.2019.00367

Excessive osteoclastic activity results in pathological bone resorptive diseases, such as osteoporosis, periodontitis, and rheumatoid arthritis. As imidazole-containing compounds possess extensive therapeutic potential for the management of diverse diseases, we synthesized a series of imidazole derivatives and investigated their effects on osteoclast differentiation and function. In the present study, we found that a novel imidazole derivative, KP-A038, suppressed receptor activator of nuclear factor-κB ligand (RANKL)-mediated osteoclastogenesis and bone-resorbing activity *in vitro* and attenuated lipopolysaccharide (LPS)-induced bone destruction *in vivo*. KP-A038 significantly inhibited the induction of nuclear factor of activated T-cells, cytoplasmic 1 (NFATc1) and the expression of its target genes, including tartrate-resistant acid phosphatase (*Acp5*), cathepsin K (*Ctsk*), dendritic cell-specific transmembrane protein (*Dcstamp*), and matrix metallopeptidase 9 (*Mmp9*). KP-A038 upregulated the expression of negative regulators of osteoclast differentiation, such as interferon regulatory factor-8 (*Irf8*) and B-cell lymphoma 6 (*Bcl6*). Consistently, KP-A038 downregulated the expression of B lymphocyte-induced maturation protein-1 (Blimp1 encoded by *Prdm1*), a repressor for *Irf8* and *Bcl6*. Moreover, administration of KP-A038 reduced LPS-induced bone erosion by suppressing osteoclast formation *in vivo*. Thus, our findings suggest that KP-A038 may serve as an effective therapeutic agent for the treatment and/or prevention of bone loss in pathological bone diseases, including osteoporosis and periodontitis.

Keywords: imidazole, KP-A038, osteoclast, differentiation, bone resorption

INTRODUCTION

Bone remodeling comprises of resorption of aged or damaged tissue by osteoclasts and replacement of new bone by osteoblasts, which is delicately regulated in a steady physiological state. This process occurs continuously to maintain skeletal integrity and strength and mineral homeostasis. Enhanced osteoclast differentiation and resorbing activity lead to loss of bone mass and architectural deterioration of bone tissue, which is mainly responsible for osteolytic bone diseases, including osteoporosis, periodontitis, and rheumatoid arthritis (Manolagas and Jilka, 1995; Sato and Takayanagi, 2006; Bartold et al., 2010). Therefore, various studies have focused on the development of novel treatments targeting osteoclast formation and activation to prevent and treat osteolytic lesions.

Osteoclasts, the only cells capable of degrading the bone matrix, are formed through multiple steps, including proliferation, differentiation of monocyte/macrophage lineage progenitors into mononuclear preosteoclasts, fusion of preosteoclasts, and activation to break down bone (Chambers, 2000; Teitelbaum, 2000). Mature osteoclasts exhibit unique morphological characteristics, including a ruffled border membrane and an actin ring structure (Teitelbaum, 2011). Osteoclast differentiation and function are governed by two essential factors: macrophage-colony stimulating factor (M-CSF), required for the survival and proliferation of progenitor cells, and receptor activator of nuclear factor-κB ligand (RANKL), primarily involved in differentiation to osteoclasts (Feng and Teitelbaum, 2013). Upon binding of RANKL to its receptor RANK, intracellular signaling pathways, such as mitogen-activated protein kinases (MAPKs) and nuclear factor-kappa B (NF-κB), are activated, which eventually lead to the induction of nuclear factor of activated T-cells cytoplasmic 1 (NFATc1), a key regulator of osteoclast differentiation (Wong et al., 1998; Lee and Kim, 2003). The transcriptional activity of NFATc1 is repressed by several negative regulators, such as interferon regulatory factor-8 (IRF-8), v-Maf musculoaponeurotic fibrosarcoma oncogene family member protein B (MafB), and B-cell lymphoma 6 (Bcl6) (Kim et al., 2007; Zhao et al., 2009; Park-Min et al., 2013). During osteoclast differentiation, RANKL-induced B lymphocyte-induced maturation protein-1 (Blimp1, encoded by *Prdm1*) upregulation acts as a transcriptional repressor of these anti-osteoclastogenic transcription factors (Nishikawa et al., 2010).

Imidazole is a heterocyclic ring compound with molecular formula $C_3H_4N_2$ and is a major constituent of various biological molecules, such as histidine, vitamin B12, and biotin (De Luca, 2006). Imidazole derivatives have been reported to exhibit a broad spectrum of biological and pharmacological effects, including anti-inflammatory, antiviral, antitumor, antifungal, and antimycobacterial activity, and numerous commercial drugs, like cimetidine, azithromycin, and metronidazole, contain imidazole nucleus in their structure (Fukui et al., 1982; el-Feky and Abd el-Samii, 1995; Johnson et al., 1999; Banfi et al., 2006). Due to these favorable and beneficial activities, studies have focused on the development of imidazole-based drugs in the pharmaceutical field (De Luca, 2006). Previous studies related to bone metabolism have revealed that imidazole and its analogs could suppress bone resorption, and a substituted imidazole, 4-nitroimidazole derivative, could inhibit RANKL-mediated osteoclast differentiation (Heersche and Jez, 1981; Chen et al., 2006). In addition, zoledronic acid, a potent third-generation bisphosphonate, contains an imidazole ring in the side chain (Paiva-Fonseca et al., 2014). However, it can induce unwanted adverse effects ranging from common to rare (Lambrinoudaki et al., 2008).

In order to develop a novel antiresorptive agent, we synthesized a series of imidazole derivatives and investigated their effects on osteoclastogenesis and bone-resorbing activity. In the present study, we demonstrated that KP-A038 significantly suppressed RANKL-mediated osteoclastogenesis *in vitro* and reduced lipopolysaccharide (LPS)-induced inflammatory bone erosion *in vivo*.

MATERIALS AND METHODS

Antibodies and Reagents

Antibodies against phospho-p38, phospho-JNK, phospho-ERK, and phospho-IκBα were purchased from Cell Signaling Technology (Danvers, MA, United States). Anti-NFATc1 antibody was purchased from BD Pharmingen™ (San Diego, CA, United States), and antibody against IRF8 was obtained from Santa Cruz Biotechnology. Recombinant M-CSF and RANKL were obtained from R&D Systems (Minneapolis, MN, United States). Fetal bovine serum (FBS) and α-minimum essential medium (α-MEM) were obtained from Gibco BRL (Grand Island, NY, United States). KP-A038 is the imidazobenzimidazole compound of in-house chemical library and the chemical name of KP-A038 is (2-([1,1′-biphenyl]-4-yl)-1-(2-(piperidin-1-yl)ethyl)-1*H*-benzo[*d*]imidazo[1,2-*a*]imidazole (**Figure 1**). KP-A038 was synthesized as described previously (**Supplementary Figure S1**; Kim et al., 2014), and dissolved in DMSO for further experiments.

In vitro Osteoclast Differentiation

Mouse bone marrow cells isolated from the tibiae and femora of 6–8 week-old male C57/B6L mice (Dae Han Bio

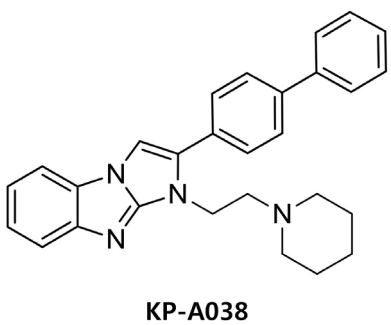

KP-A038

FIGURE 1 | Chemical structures of KP-A038.

Link Co., LTD., Chungbuk, South Korea) were incubated in α-MEM supplemented with 10% FBS (Ihn et al., 2017; Yoon et al., 2018). After 24 h, non-adherent cells were collected and cultured in α-MEM containing 10% FBS and M-CSF (30 ng/mL) for 3 days to generate bone marrow-derived macrophages (BMMs). BMMs were plated in 96-well plates and incubated in osteoclast-inducing media containing 20 ng/mL RANKL and 10 ng/mL M-CSF with or without various concentrations of KP-A038. The media were changed every 2 days until mature osteoclasts were formed. The cells were fixed in 4% paraformaldehyde, and formation of osteoclasts was determined using an Acid Phosphatase, Leukocyte (TRAP) staining kit (Sigma-Aldrich, St. Louis, MO, United States). TRAP-positive multinucleated cells (MNCs) with more than three nuclei were scored as osteoclast-like cells.

Cell Viability Assay

The cytotoxic effect of KP-A038 on cell viability was determined using Cell Counting Kit-8 (CCK-8; Dojindo Molecular Technologies Inc., Rockville, MD, United States) following the manufacturer's instructions. BMMs seeded in 96-well plates (3×10^3 cells/well) were cultured in α-MEM containing 10% FBS and M-CSF (10 ng/mL) in the presence or absence of various doses of KP-A038 for 3 days. The media were replaced with fresh medium containing 10% CCK-8, and the cells were incubated at 37°C for 2 h. The absorbance at 450 nm was measured using a 96-well microplate reader (Bio-Rad Laboratories, Hercules, CA, United States).

Quantitative Real-Time PCR

Bone marrow-derived macrophages were cultured in 6-well plates with or without 5 μM KP-A038 in osteoclast-inducing media. Total RNA was extracted using TRI-solution (Bioscience, Seoul, South Korea) according to the manufacturer's instructions. cDNA was synthesized using SuperScript II Reverse Transcriptase (Invitrogen, Carlsbad, CA, United States). Real-time PCR was performed using a LightCycler 1.5 real-time PCR system (Roche Diagnostics, Basel, Switzerland) and the SYBR Premix Ex Taq (Takara Bio Inc., Shiga, Japan) (Ihn et al., 2018). The primer sequences used in real-time PCR analysis were: *Acp5*, 5′-TCCCCAATGCCCCATTC-3′ and 5′-CGGTTCTGGCGATCTCTTTG-3′; *Ctsk*, 5′-GGCTGTGGAG GCGGCTAT-3′ and 5′-AGAGTCAATGCCTCCGTTCTG-3′; *Mmp9*, 5′-AAAGACCTGAAAACCTCCAACCT-3′ and 5′-GCCCGGGTGTAACCATAGC-3′; *Dcstamp*, 5′-CTTC CGTGGGCCAGAAGTT-3′ and 5′-AGGCCAGTGC TGACTAGGATGA-3′; *Nfatc1*, 5′-ACCACCTTTCCGCAACCA-3′ and 5′-TTCCGTTTCCCGTTGCA-3′; *Irf8*, 5′-GA TCGAACAGATCGACAGCA-3′ and 5′-AGCACAGCGTAA CCTCGTCT-3′; *Bcl6*, 5′-ATGAGATTGCCCTGCATTTC-3′ and 5′-TTCTTCCAGTTGCAGGCTTT-3′; *Ifng*, 5′-TCAAGT GGCATAGATGTGGAAGAA-3′ and 5′-TGGCTCTGCAGGATT TTCATG-3′; *Prdm1*, 5′-TTCTTGTGTGGTATTGTCGGG ACTT-3′ and 5′-TTGGGGACACTCTTTGGGTAGAGTT-3′.

Immunoblotting

Cells were lysed with RIPA buffer containing protease and phosphatase inhibitors. Equal volume of cell lysates (25 μg of protein) was loaded onto 10% sodium dodecyl sulfate-polyacrylamide gels, followed by transfer to nitrocellulose membranes (Whatman Inc., Florham Park, NJ, United States). The membranes were placed in a blocking solution [3% non-fat dry milk in TBS-T (25 mM Tris–HCl, pH 7.4, 150 mM NaCl, and 0.2% Tween 20)] for 1 h. After blocking, the membranes were incubated with specific primary antibodies (1:1000) at 4°C overnight. Following incubation with secondary antibodies, protein signals were detected using WesternBright ECL (Advansta, Menlo Park, CA, United States), and imaged with an X-ray film or by using chemiluminescence imager (Azure Biosystems, Inc., Dublin, CA, Unites States).

Staining of Actin Rings

Bone marrow-derived macrophages grown on glass coverslips were cultured with 10 ng/mL M-CSF and 20 ng/mL RANKL in the presence or absence of 5 μM KP-A038. The cells were washed with phosphate buffered saline, fixed with 4% paraformaldehyde, and permeabilized with 0.1% Triton X-100. F-actin was stained with rhodamine conjugated phalloidin (Cytoskeleton, Denver, CO, United States), and 4',6-diamidino-2-phenylindole dihydrochloride (Santa Cruz Biotechnology, Santa Cruz, CA, United States) was used for nuclei staining. The images were acquired using a BX51 Fluorescent Microscope (Olympus, Tokyo, Japan).

Resorption Pit Assay

Bone marrow-derived macrophages were placed on bone slices (IDS Nordic Bioscience, Herlev, Denmark) and incubated with M-CSF (10 ng/mL) and RANKL (20 ng/mL) to induce differentiation of BMMs into multinucleated osteoclasts. After 3 days, the cells were treated with vehicle or 5 μM KP-A038 for 2 days. The cells removed with 1 N NaOH for 20 min, followed by staining with hematoxylin to identify the areas of resorption pits. The resorbed areas were measured using the i-Solution image analysis program (IMT i-Solution, Daejeon, South Korea).

In vivo LPS-Induced Bone Loss

All animal experiments were approved by the Animal Care and Use Committee at Kyungpook National University and were conducted in accordance with the guidelines for the care and use of laboratory animals. To study the effect of KP-A038 on *in vivo* bone destruction, 8-week-old C57/B6L mice were intraperitoneally injected with KP-A038 (30 mg/kg) or vehicle daily for 9 days, and LPS (5 mg/kg) was intraperitoneally administered to the mice on days 2 and 6, as previously described (Ihn et al., 2015a). On day 10, the mice were euthanized by cervical dislocation under anesthesia with avertin. The femurs were isolated and fixed in 4% paraformaldehyde for 18 h.

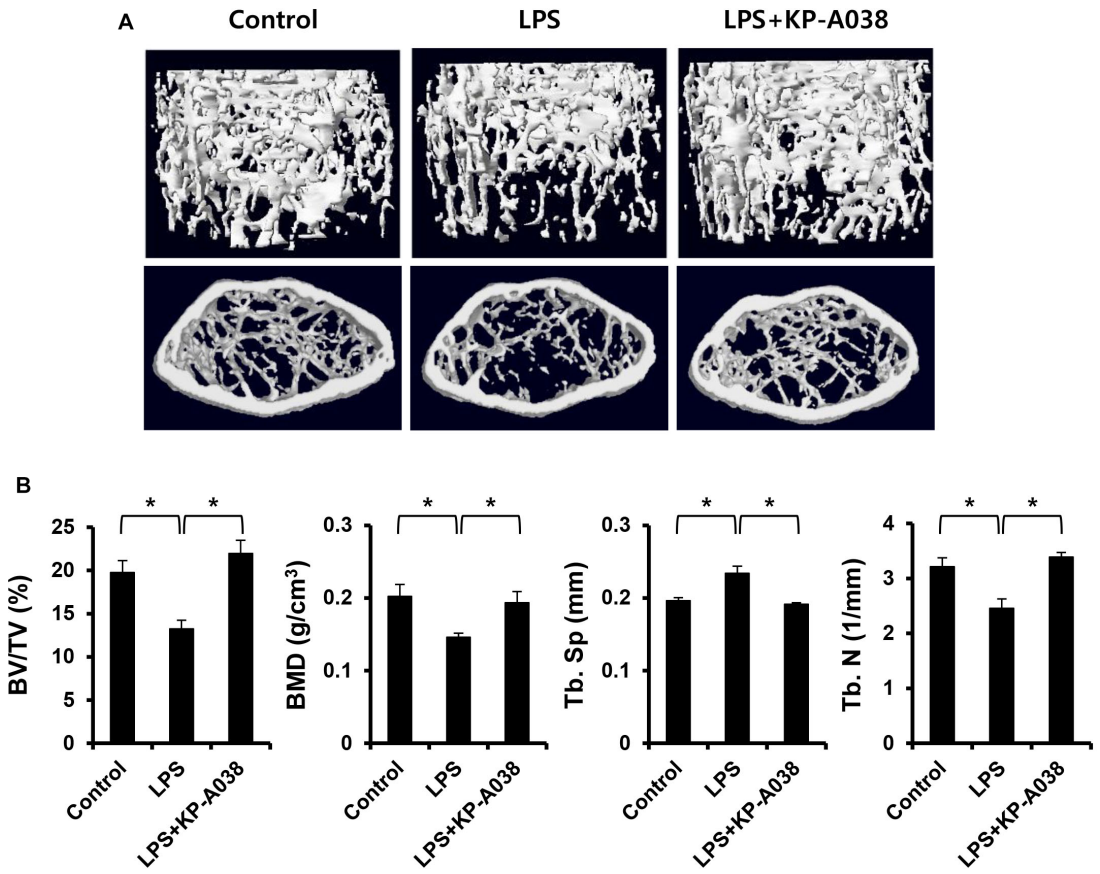

FIGURE 2 | KP-A038 mitigated femoral bone loss induced by LPS *in vivo*. **(A)** Representative micro-CT images of distal femurs of three groups. **(B)** Quantification of bone volume per tissue volume (BV/TV), bone mineral density (BMD), trabecular separation (Tb. Sp), and trabecular number (Tb. N) from each group. $n = 5$ (10 legs) in each group. $^*p < 0.05$.

Micro-CT and Histomorphometric Analysis

The fixed femurs were scanned using high-resolution μCT (Skyscan 1272; Kontich, Belgium) with a source voltage of 60 kV, current of 166 μA, and resolution of 14 μm. Bone morphometric parameters, including bone volume per total volume (BV/TV), bone mineral density (BMD), trabecular separation (Tb. Sp.), and trabecular number (Tb. N.) were analyzed using CTAn software (Bruker; Kontich, Belgium). Micro-CT 3D images of trabecular bones in the distal femurs were generated using CTAn/CTVol software (Bruker; Kontich, Belgium).

For histology, the fixed femurs were decalcified in 12% EDTA and embedded in paraffin, and the histological tissue sections were stained with hematoxylin and eosin and TRAP.

Statistics

Experiments were conducted three times, and all data are presented as mean±standard deviation (SD). Statistical significance was evaluated by the two-tailed Student's *t*-test or one-way analysis of variance (ANOVA) with Tukey's multiple comparison *post hoc* test. $p < 0.05$ or $p < 0.01$ was considered statistically significant.

RESULTS

KP-A038 Prevents LPS-Induced Bone Resorption *in vivo*

To examine the *in vivo* efficacy of KP-A038 in osteoclast formation and bone resorption, we used an LPS-induced bone erosion model. Mice were intraperitoneally administered with LPS on days 2 and 6 and received vehicle or KP-A038 daily for 9 days. Injection of KP-A038 alone did not cause adverse events, including death, abnormal behavior, sickness, and distress or change bone parameters (**Supplementary Figure S2**). Administration of LPS led to a reduction in trabecular bone mass of femurs, and this LPS-mediated bone loss was suppressed by co-injection with KP-A038 (**Figure 2A**). Three-dimensional morphometric analysis of distal femurs showed that BV/TV, BMD, and Tb. N were significantly reduced in LPS-treated group (**Figure 2B**). Such reduction in bone parameters was attenuated by KP-A038 treatment (**Figure 2B**). In correlation with μCT images and analysis of bone parameters, the histological sections stained with hematoxylin and eosin or TRAP showed that KP-A038 effectively suppressed LPS-induced osteoclast formation and subsequent bone loss *in vivo* (**Figure 3**).

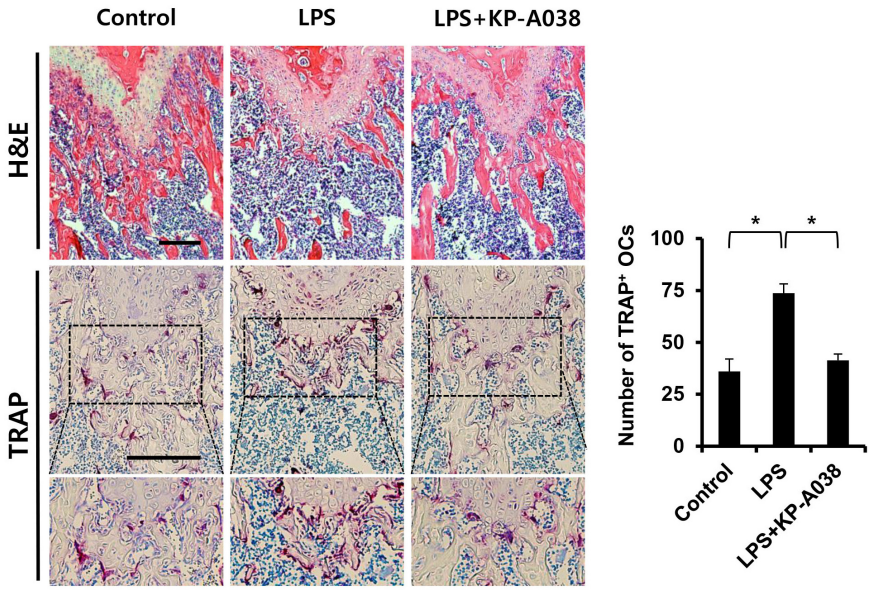

FIGURE 3 | Histological analysis of the effect of KP-A038 on LPS-mediated bone destruction. Fixed femurs were decalcified and sectioned. The sections were stained with hematoxylin and eosin (upper panel) and tartrate-resistant acid phosphatase (TRAP, middle and lower panel). The number of osteoclasts was analyzed in the TRAP-stained slices (right graph). $n = 5$ (10 legs) in each group. $^{*}p < 0.05$.

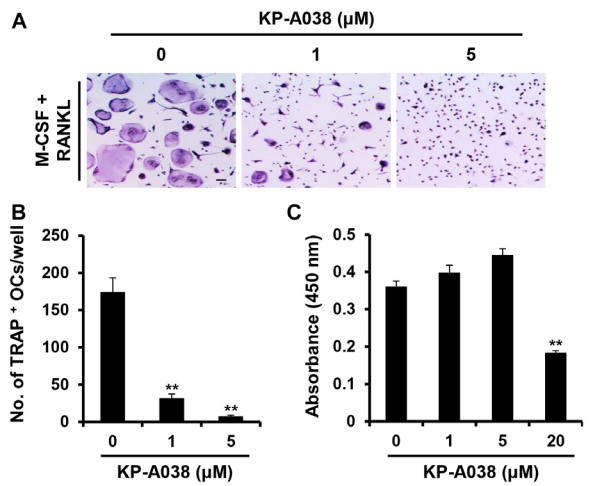

FIGURE 4 | KP-A038 inhibited RANKL-mediated osteoclastogenesis without cytotoxicity. **(A)** BMMs were incubated in osteoclastogenic medium supplemented with M-CSF (10 ng/mL) and RANKL (20 ng/mL) in the presence of KP-A038 or vehicle. The cells were stained to evaluate TRAP activity. **(B)** The number of osteoclast-like cells was quantified. **(C)** BMMs were cultured with M-CSF (10 ng/mL) and various doses of KP-A038 for 3 days. Cell viability was assessed by CCK-8 assay. $^{**}p < 0.01$.

KP-A038 Inhibits RANKL-Induced Osteoclast Formation *in vitro*

To clarify whether KP-A038 affects the viability of osteoclast progenitors, CCK-8 assay was performed using primary BMMs cultured with M-CSF and various doses of KP-A038 for 3 days. As shown in **Figure 4C**, KP-A038 at concentrations of up to 5 μM did not decrease the rate of proliferation and survival of BMMs. Hence, 5 μM KP-A038 was chosen for subsequent *in vitro* studies. As primary BMMs are capable of differentiating into multinucleated osteoclasts in response to M-CSF and RANKL, we first examined the effect of KP-A038 on osteoclast formation in BMMs. Primary cultured BMMs were treated with KP-A038 (1 μM or 5 μM) in osteoclast-inducing media supplemented with M-CSF and RANKL. RANKL promoted the formation of osteoclasts (TRAP-positive MNCs) from progenitors (BMMs) in the vehicle-treated control group, whereas treatment with KP-A038 markedly suppressed osteoclast formation in a concentration-dependent manner (**Figure 4A**). In the presence of 5 μM KP-A038, the number of TRAP-positive MNCs was reduced by 96% (**Figure 4B**).

KP-A038 Attenuates the Expression of Osteoclast-Specific Markers as Well as the Formation of Actin Rings

We next evaluated the mRNA and protein expression levels of osteoclast-specific markers during RANKL-induced osteoclast differentiation via real-time PCR and western blotting to further determine its inhibitory role in osteoclastogenesis. Consistent with the decreased osteoclast formation, treatment with KP-A038 (5 μM) downregulated the mRNA levels of *Acp5*, *Ctsk*, *Dcstamp*, *Mmp9*, and *Nfatc1*, which are required for osteoclast formation and/or bone resorption (**Figures 5A,B**). In addition, the induction of both cathepsin K (Ctsk) and NFATc1 proteins and the nuclear expression of NFATc1 were decreased by treatment with 5 μM KP-A038 (**Figures 5C,F**).

An essential step in the generation of multinucleated osteoclasts is cell-cell fusion, and DC-STAMP is a key regulator

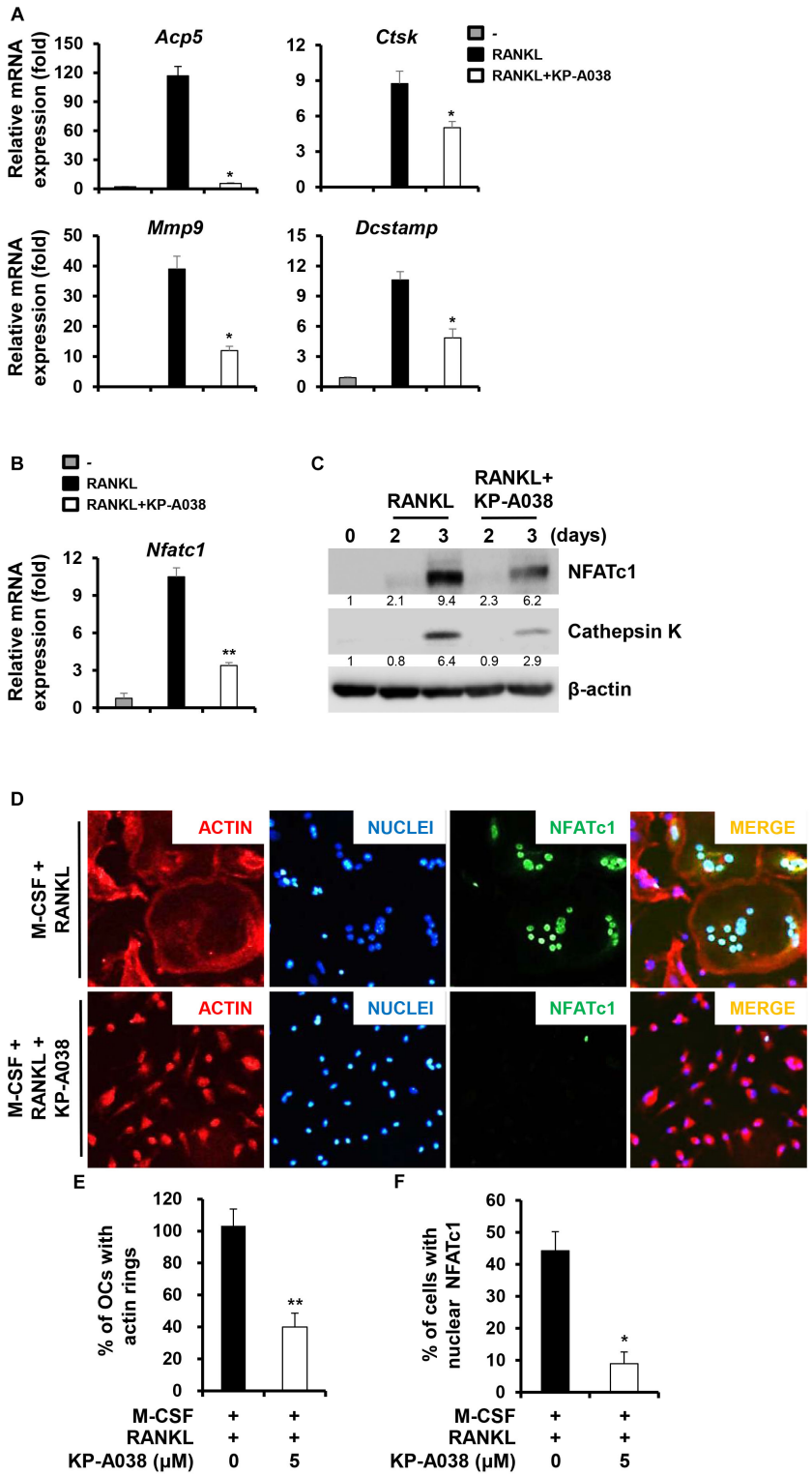

FIGURE 5 | KP-A038 suppressed the expression of osteoclast-specific markers and the formation of actin rings. **(A–C)** BMMs were incubated in osteoclastogenic medium with KP-A038 (5 μM) or vehicle for the indicated times. The mRNA **(A,B)** and protein **(C)** expression levels of markers were evaluated by real-time PCR and western blot analysis, respectively. **(D)** BMMs were seeded on glass coverslips and cultured with M-CSF (10 ng/mL) and RANKL (20 ng/mL) in the presence or absence of 5 μM KP-A038. Cells were fixed, and F-actin structures and nuclei were visualized by staining with rhodamine-conjugated phalloidin and 4',6-diamidino-2-phenylindole dihydrochloride, respectively. Quantification of the percentage of **(E)** osteoclasts with actin rings and **(F)** cells with nuclear NFATc1. $^{*}p < 0.05$, $^{**}p < 0.01$.

of this process (Yagi et al., 2005). In accordance with the decreased induction of *Dcstamp*, we found that the number of multinucleated giant cells with actin ring structure was significantly decreased by KP-A038 treatment (**Figures 5D,E**).

KP-A038 Impairs the Bone-Resorbing Function of Osteoclasts

We next examined if KP-A038 affects the bone-resorbing activity of osteoclasts. BMMs were plated on bone slices in osteoclastogenic media to generate multinucleated osteoclast-like cells. Then, the cells were treated with vehicle or 5 μM KP-A038 in osteoclast-inducing media for 2 days. Analysis of resorption pit showed that KP-A038 treatment significantly reduced the formation of resorption pits compared to vehicle treatment, which resulted in formation of larger resorbed areas. Addition of KP-A038 resulted in an 87% reduction of the resorbed area (**Figure 6A**), thereby suggesting that KP-A038 directly attenuates the bone-resorbing function of osteoclasts.

KP-A038 Inhibits the Repression of Negative Regulators of Osteoclast Differentiation

To understand the molecular mechanism of the inhibitory action of KP-A038 in osteoclast differentiation and function, the effect

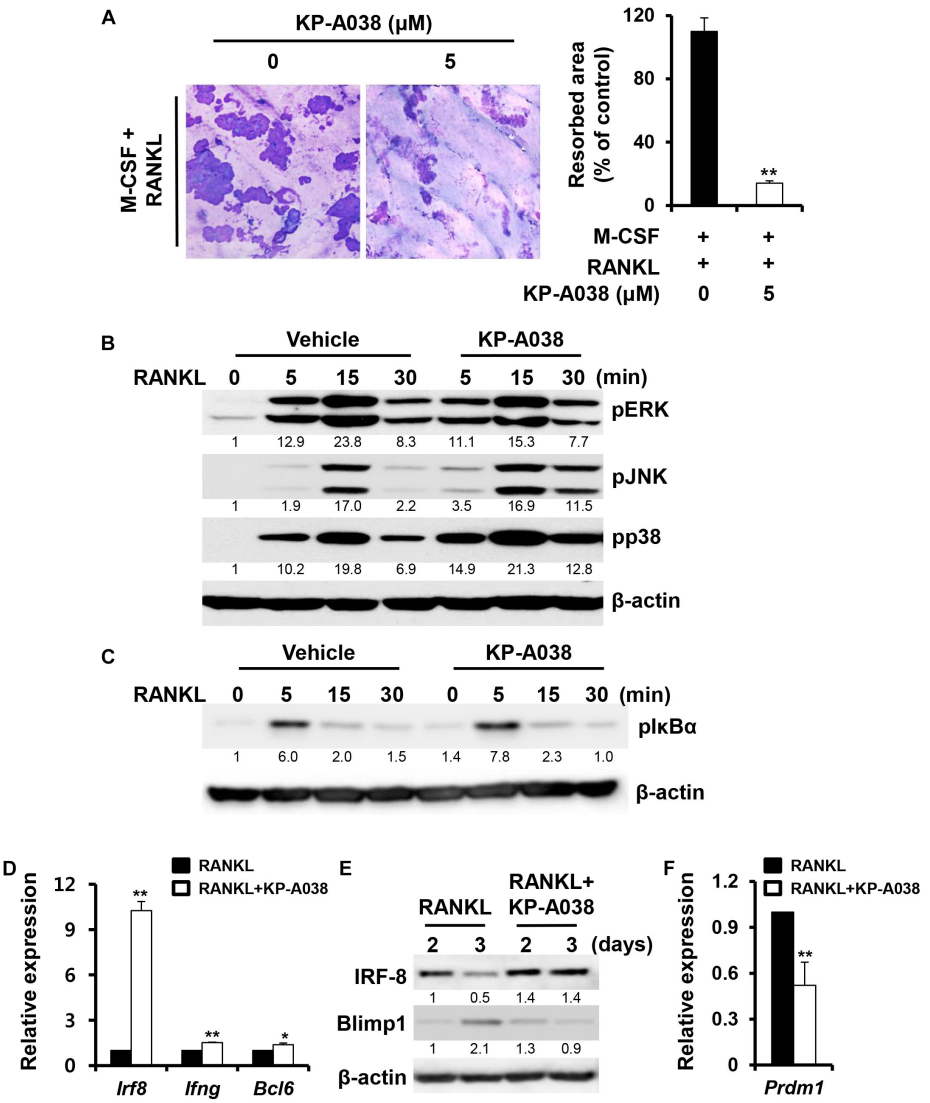

FIGURE 6 | KP-A038 attenuated osteoclastic resorption activity and modulated the expression of negative regulators of osteoclastogenesis. **(A)** BMMs were seeded on bone slices and incubated in osteoclast- inducing medium. After 3 days, vehicle or 5 μM KP-A038 was added to the cell culture for 24 h and the resorptive areas were quantified using the i-Solution program (right graph). **(B,C)** BMMs were pretreated with vehicle or KP-A038 (5 μM) for 1 h followed by stimulation with RANKL (50 ng/mL) for indicated periods. Phosphorylation of ERK, JNK, p38, and IκBα was assessed by western blot analysis. β-actin was used as the loading control. **(D,F)** The mRNA expression of *Irf8*, *Ifng*, *Bcl6*, and *Prdm1* was analyzed by real-time PCR. **(E)** BMMs were cultured with M-CSF (10 ng/mL) and RANKL (20 ng/mL) in the presence or absence of 5 μM KP-A038 for indicated times. The protein expression of IRF-8 and Blimp1 was evaluated by immunoblotting. $^{*}p < 0.05$, $^{**}p < 0.01$.

of KP-A038 on RANKL-stimulated MAPK and NF-κB signaling pathways was examined. Serum-starved BMMs were stimulated with RANKL after pretreatment with vehicle or 5 μM KP-A038 for 1 h. Stimulation with RANKL led to activation of MAPKs (ERK, p38, and JNK) and IκBα within 15 min in control cells, and pretreatment with KP-A038 had no effect on the phosphorylation levels of MAPKs and IκBα, indicating that KP-A038 does not affect the MAPK and NF-κB signaling pathways (**Figures 6B,C**).

RANKL-RANK signaling pathways ultimately converge on the induction of NFATc1, which is the main transcriptional regulator of osteoclastogenesis, and its activity is negatively regulated by IRF-8 and Bcl6 during osteoclast differentiation (Zhao et al., 2009; Miyauchi et al., 2010). Hence, we examined the expression levels of anti-osteoclastogenic genes, such as *Irf8*, *Ifng*, and *Bcl6*. While the mRNA expression of *Irf8*, *Ifng*, and *Bcl6* was downregulated by RANKL stimulation in vehicle-treated control group, such downregulation was blocked in the presence of 5 μM KP-A038 (**Figure 6D**). As shown in **Figure 6E**, IRF-8 protein expression was similarly upregulated in a time-dependent manner. Blimp1 (encoded by *Prdm1*) is known to function as a transcriptional repressor of IRF-8 and Bcl6, and Blimp1-mediated *Irf8,* and *Bcl6* suppression is critical for osteoclast differentiation (Zhao et al., 2009; Miyauchi et al., 2010). Consistent with increased *Irf8* and *Bcl6* expression, Blimp1 mRNA and protein levels were reduced in the presence of KP-A038 (**Figures 6E,F**).

DISCUSSION

Although the bone is remodeled through coordinated destruction and deposition, and the remodeling process is strictly regulated, abnormal bone remodeling can arise due to various causes, inducing skeletal diseases ranging from mild to severe. In particular, enhanced osteoclastogenesis and resorbing activity of mature osteoclasts causes destructive bone diseases. Therefore, the suppression of osteoclast differentiation and bone-resorbing function of mature osteoclasts is an important aspect for preventing and treating osteolytic diseases. In the current study, we observed that KP-A038, a novel imidazole compound, possessed anti-osteoclastogenic activity via downregulation of NFATc1 and modulation of the expression of negative regulators of osteoclast differentiation. Consistent with the suppression of osteoclast differentiation *in vitro*, results from the *in vivo* LPS-induced bone destruction study demonstrated that KP-A038 protected against bone loss by attenuation of osteoclast formation.

RANKL-RANK signaling ultimately causes the induction of NFATc1, which acts as a key transcription factor of osteoclastogenesis. Even though RANKL signaling is required for osteoclast differentiation, embryonic stem cells lacking NFATc1 fail to undergo osteoclast differentiation even in the presence of RANKL (Takayanagi et al., 2002). Furthermore, ectopic expression of NFATc1 in BMMs leads to osteoclast differentiation without RANKL signaling (Takayanagi et al., 2002). Overexpression of NFATc1 in osteoclast precursors lacking c-Fos, a pivotal regulator of early activation of NFATc1, rescues osteoclast differentiation *in vitro* (Matsuo et al., 2004). Aliprantis et al. (2008) reported that osteoclast-specific NFATc1 deficiency causes osteopetrosis due to impaired osteoclast differentiation. These *in vivo* and *in vitro* studies have established the essential role of NFATc1 in osteoclast formation and function. We demonstrated that KP-A038 treatment markedly downregulated both mRNA and protein levels of NFATc1, resulting in inhibition of osteoclastogenesis (**Figures 5B,C**). As expected, downregulation of NFATc1 by KP-A038 treatment attenuated the expression of direct transcriptional target genes, including *Acp5*, *Ctsk*, *Dcstamp*, and *Mmp9* (**Figure 5A**). Among them, DC-STAMP is essential for cell-to-cell fusion, which is a critical process to generate MNCs and reorganize the actin cytoskeleton during osteoclast differentiation (Yagi et al., 2005). Due to the reduced *Dcstamp* levels, KP-A038 treatment suppressed the formation of actin rings (**Figure 5D**). Our study suggested that KP-A038 might target NFATc1 leading to inhibition of osteoclast differentiation and impairment of cellular fusion.

The activation of signaling molecules, like MAPKs and NF-κB involved in the RANKL/RANK signaling pathway, is an early cellular event of osteoclast differentiation, eventually leading to the induction NFATc1 (Iotsova et al., 1997; Mizukami et al., 2002). To understand the molecular mechanisms of inhibition of osteoclast differentiation and bone-resorbing function, we analyzed the extent of phosphorylation of the signaling molecules. Although our studies showed that KP-A038 definitely reduced the expression of NFATc1 and its target genes, KP-A038 treatment did not inhibit the activation of RANKL-mediated MAPKs and NF-κB (**Figures 6B,C**). Previously we screened and identified several chemicals from our in-house chemical library that exerted inhibitory effects on osteoclast differentiation and bone resorption. Although those compounds exhibited anti-osteoclastogenic and antiresorptive activities with a similar inhibitory concentration, the inhibitory mechanism and chemical structure of the compounds were quite distinct one another (Ihn et al., 2015a,b, 2017, 2018). In particular, unlike our previous compounds, KP-A038 did not inhibit an early RANKL-RANK signaling pathways (**Figures 6B,C**), suggesting different mode of action of KP-A038 from our previous chemicals. RANKL/RANK signaling has also been shown to downregulate various transcriptional repressors, including MafB, IRF-8, and Bcl6, which act as anti-osteoclastogenic factors via downregulating NFATc1 expression (Kim et al., 2007; Zhao et al., 2009; Miyauchi et al., 2010). Nishikawa et al. found that a transcriptional repressor of the negative regulators of NFATc1, Blimp 1 (*Prdm1*), is induced by RANKL stimulation, and Blimp 1-mediated suppression of anti-osteoclastogenic factors is necessary for osteoclastogenesis (Nishikawa et al., 2010). Therefore, forced expression of the negative regulators leads to impaired osteoclast differentiation. Among them, IRF-8 suppresses NFATc1 autoamplification and its transcriptional activity, and Bcl6 inhibits the expression of NFATc1 and its target genes associated with osteoclastogenesis and bone resorption (Zhao and Ivashkiv, 2011). In our study, KP-A038 prevented the downregulation of negative regulators of osteoclastogenesis, and in particular, the mRNA and protein expression of IRF-8 was strongly induced in the presence of KP-A038

(**Figures 6D,E**). Consistently, KP-A038 suppressed both mRNA and protein levels of Blimp1 (Prdm1) (**Figures 6E,F**). These results indicated that the inhibitory effect of KP-A038 on osteoclastogenesis might be in part mediated by the failure of repression of negative regulators. Further studies would be necessary to identify the primary target (s) for KP-A038.

The major role of osteoclasts is to break down the bone matrix, which is termed as bone resorption. Various antiresorptive drugs, such as bisphosphonates and selective estrogen receptor modulators have been clinically used for preventing further loss of bone density (Migliaccio et al., 2007). Therefore, we evaluated the effect of KP-A038 on bone-resorbing function by resorption pit assay. KP-A038, at a concentration that inhibited osteoclast differentiation, considerably suppressed the ability of osteoclasts to degrade the calcified bone matrix (**Figure 6A**), indicating that KP-A038 exhibits not only anti-osteoclastogenic but also antiresorptive activity.

Lipopolysaccharide is a structural constituent of the outer membrane of gram-negative bacteria and it functions as a potent stimulator of bone loss. The production of inflammatory cytokines in response to LPS is increased, which directly and indirectly contributes to stimulation of osteoclastogenesis and inflammatory bone loss (Wada et al., 2004; Islam et al., 2007). Especially, alveolar bone destruction mediated by inflammatory responses in the oral cavity can lead to tooth loss (Pihlstrom et al., 2005). For that reason, it is critical to prevent the balance of two opposing activities (bone formation and bone resorption) from breaking for maintenance and regeneration of alveolar bone and supporting tissue (Larsson et al., 2016). Consistent with its inhibitory effect on osteoclast differentiation and function *in vitro*, KP-A038 attenuated the femoral bone destruction induced by LPS (**Figure 2**). Administration of KP-A038 decreased the numbers of TRAP-positive osteoclasts as well as bone resorption *in vivo* (**Figure 3**), indicating that KP-A038 may have the potential to not only protect from the risk of inflammatory bone loss in periodontitis but also to contribute to bone regeneration in the oral cavity.

CONCLUSION

Developing alternative agents that modulate excessive osteoclast formation and bone resorption is an important and urgent task. The results of this study demonstrated that KP-A038 exhibited anti-osteoclastogenic and antiresorptive properties by inhibiting the induction of NFATc1 via modulating the expression of negative regulators of osteoclastogenesis. Furthermore, KP-A038 protected against LPS-induced femoral bone loss *in vivo*. Our results suggest that KP-A038 might serve as a novel antiresorptive agent for osteoclast-related diseases.

ETHICS STATEMENT

All animal experiments were approved by the Animal Care and Use Committee at Kyungpook National University and were conducted in accordance with the guidelines for the care and use of laboratory animals.

AUTHOR CONTRIBUTIONS

HI, TL, and EP designed the research and wrote the manuscript. HI and DL performed the research and collected the data. J-SB, S-HK, IJ, YB, and H-IS analyzed the data and clarified the manuscript.

FUNDING

This work was supported by the National Research Foundation of Korea (NRF) grant funded by the Korean government (MSIT; NRF-2017R1A2B1005409 and NRF-2017R1A5A2015391) and the Bio & Medical Technology Development Program of the NRF, which was funded by the Government of South Korea (MSIT; NRF-2017M3A9E4047244).

SUPPLEMENTARY MATERIAL

The Supplementary Material for this article can be found online at: https://www.frontiersin.org/articles/10.3389/fphar.2019.00367/full#supplementary-material

REFERENCES

Aliprantis, A. O., Ueki, Y., Sulyanto, R., Park, A., Sigrist, K. S., Sharma, S. M., et al. (2008). NFATc1 in mice represses osteoprotegerin during osteoclastogenesis and dissociates systemic osteopenia from inflammation in cherubism. *J. Clin. Invest.* 118, 3775–3789. doi: 10.1172/JCI35711

Banfi, E., Scialino, G., Zampieri, D., Mamolo, M. G., Vio, L., Ferrone, M., et al. (2006). Antifungal and antimycobacterial activity of new imidazole and triazole derivatives. A combined experimental and computational approach. *J. Antimicrob. Chemother.* 58, 76–84. doi: 10.1093/jac/dkl182

Bartold, P. M., Cantley, M. D., and Haynes, D. R. (2010). Mechanisms and control of pathologic bone loss in periodontitis. *Periodontology* 2000, 55–69. doi: 10.1111/j.1600-0757.2010.00347.x

Chambers, T. J. (2000). Regulation of the differentiation and function of osteoclasts. *J. Pathol.* 192, 4–13. doi: 10.1002/1096-9896(2000)9999:9999<::AID-PATH645>3.0.CO;2-Q

Chen, T., Knapp, A. C., Wu, Y., Huang, J., Lynch, J. S., Dickson, J. K., et al. (2006). High throughput screening identified a substituted imidazole as a novel RANK pathway-selective osteoclastogenesis inhibitor. *Assay Drug Dev. Technol.* 4, 387–396. doi: 10.1089/adt.2006.4.387

De Luca, L. (2006). Naturally occurring and synthetic imidazoles: their chemistry and their biological activities. *Curr. Med. Chem.* 13, 1–23.

el-Feky, S. A., and Abd el-Samii, Z. K. (1995). Synthesis and antiinflammatory properties of some novel thiazolidinones and imidazolidinones derived from 4-(3-phenyl-4(3H)-quinazolinon-2-yl)-3-thiosemicarbazone. *Pharmazie* 50, 341–343. doi: 10.1002/chin.199537188

Feng, X., and Teitelbaum, S. L. (2013). Osteoclasts: new insights. *Bone Res.* 1, 11–26. doi: 10.4248/BR201301003

Fukui, M., Inaba, M., Tsukagoshi, S., and Sakurai, Y. (1982). New antitumor imidazole derivative, 5-carbamoyl-1H-imidazol-4-yl piperonylate, as an inhibitor of purine synthesis and its activation by adenine phosphoribosyltransferase. *Cancer Res.* 42, 1098–1102.

Heersche, J. N., and Jez, D. H. (1981). The effect of imidazole-analogues on bone resorption in vitro: a suggested role for thromboxane A2. *Prostaglandins* 21, 401–411. doi: 10.1016/0090-6980(81)90085-X

Ihn, H. J., Lee, D., Lee, T., Kim, S. H., Shin, H. I., Bae, Y. C., et al. (2015a). Inhibitory effects of KP-A159, a thiazolopyridine derivative, on osteoclast differentiation, function, and inflammatory bone loss via suppression of RANKL-induced MAP kinase signaling pathway. *PLoS One* 10:e0142201. doi: 10.1371/journal.pone.0142201

Ihn, H. J., Lee, D., Lee, T., Shin, H. I., Bae, Y. C., Kim, S. H., et al. (2015b). The 1,2,3-triazole derivative KP-A021 suppresses osteoclast differentiation and function by inhibiting RANKL-mediated MEK-ERK signaling pathway. *Exp. Biol. Med.* 240, 1690–1697. doi: 10.1177/1535370215576310

Ihn, H. J., Lee, T., Kim, J. A., Lee, D., Kim, N. D., Shin, H. I., et al. (2017). OCLI-023, a novel pyrimidine compound, suppresses osteoclastogenesis in vitro and alveolar bone resorption in vivo. *PLoS One* 12:e0170159. doi: 10.1371/journal.pone.0170159

Ihn, H. J., Lee, T., Lee, D., Kim, J. A., Kim, K., Lim, S., et al. (2018). A novel benzamide derivative protects ligature-induced alveolar bone erosion by inhibiting NFATc1-mediated osteoclastogenesis. *Toxicol. Appl. Pharmacol.* 355, 9–17. doi: 10.1016/j.taap.2018.06.017

Iotsova, V., Caamano, J., Loy, J., Yang, Y., Lewin, A., and Bravo, R. (1997). Osteopetrosis in mice lacking NF-kappaB1 and NF-kappaB2. *Nat. Med.* 3, 1285–1289. doi: 10.1038/nm1197-1285

Islam, S., Hassan, F., Tumurkhuu, G., Dagvadorj, J., Koide, N., Naiki, Y., et al. (2007). Bacterial lipopolysaccharide induces osteoclast formation in RAW 264.7 macrophage cells. *Biochem. Biophys. Res. Commun.* 360, 346–351. doi: 10.1016/j.bbrc.2007.06.023

Johnson, R. A., Huong, S. M., and Huang, E. S. (1999). Inhibitory effect of 4-(4-fluorophenyl)-2-(4-hydroxyphenyl)-5-(4-pyridyl)1H - imidazole on HCMV DNA replication and permissive infection. *Antiviral Res.* 41, 101–111. doi: 10.1016/S0166-3542(99)00002-9

Kim, K., Kim, J. H., Lee, J., Jin, H. M., Kook, H., Kim, K. K., et al. (2007). MafB negatively regulates RANKL-mediated osteoclast differentiation. *Blood* 109, 3253–3259. doi: 10.1182/blood-2006-09-048249

Kim, S. Y., Lee, S. H., Shin, J. S., Lee, D., Lee, T., Park, K. C., et al. (2014). A derivative of imidazobenzimidazole, ML106, inhibits melanin synthesis via p38 MAPK activation. *Pharmazie* 69, 353–357. doi: 10.1691/ph.2014.3868

Lambrinoudaki, I., Vlachou, S., Galapi, F., Papadimitriou, D., and Papadias, K. (2008). Once-yearly zoledronic acid in the prevention of osteoporotic bone fractures in postmenopausal women. *Clin. Interv. Aging* 3, 445–451. doi: 10.2147/CIA.S2046

Larsson, L., Decker, A. M., Nibali, L., Pilipchuk, S. P., Berglundh, T., and Giannobile, W. V. (2016). Regenerative medicine for periodontal and peri-implant diseases. *J. Dent. Res.* 95, 255–266. doi: 10.1177/0022034515618887

Lee, Z. H., and Kim, H. H. (2003). Signal transduction by receptor activator of nuclear factor kappa B in osteoclasts. *Biochem. Biophys. Res. Commun.* 305, 211–214. doi: 10.1016/S0006-291X(03)00695-8

Manolagas, S. C., and Jilka, R. L. (1995). Bone marrow, cytokines, and bone remodeling. Emerging insights into the pathophysiology of osteoporosis. *N. Engl. J. Med.* 332, 305–311. doi: 10.1056/NEJM199502023320506

Matsuo, K., Galson, D. L., Zhao, C., Peng, L., Laplace, C., Wang, K. Z., et al. (2004). Nuclear factor of activated T-cells (NFAT) rescues osteoclastogenesis in precursors lacking c-Fos. *J. Biol. Chem.* 279, 26475–26480. doi: 10.1074/jbc.M313973200

Migliaccio, S., Brama, M., and Spera, G. (2007). The differential effects of bisphosphonates, SERMS (selective estrogen receptor modulators), and parathyroid hormone on bone remodeling in osteoporosis. *Clin. Interv. Aging* 2, 55–64. doi: 10.2147/ciia.2007.2.1.55

Miyauchi, Y., Ninomiya, K., Miyamoto, H., Sakamoto, A., Iwasaki, R., Hoshi, H., et al. (2010). The Blimp1-Bcl6 axis is critical to regulate osteoclast differentiation and bone homeostasis. *J. Exp. Med.* 207, 751–762. doi: 10.1084/jem.20091957

Mizukami, J., Takaesu, G., Akatsuka, H., Sakurai, H., Ninomiya-Tsuji, J., Matsumoto, K., et al. (2002). Receptor activator of NF-kappaB ligand (RANKL) activates TAK1 mitogen-activated protein kinase kinase kinase through a signaling complex containing RANK, TAB2, and TRAF6. *Mol. Cell Biol.* 22, 992–1000. doi: 10.1128/MCB.22.4.992-1000.2002

Nishikawa, K., Nakashima, T., Hayashi, M., Fukunaga, T., Kato, S., Kodama, T., et al. (2010). Blimp1-mediated repression of negative regulators is required for osteoclast differentiation. *Proc. Natl. Acad. Sci. U.S.A.* 107, 3117–3122. doi: 10.1073/pnas.0912779107

Paiva-Fonseca, F., Santos-Silva, A. R., Della-Coletta, R., Vargas, P. A., and Lopes, M. A. (2014). Alendronate-associated osteonecrosis of the jaws: a review of the main topics. *Med. Oral Patol. Oral Cir. Bucal* 19, e106–e111. doi: 10.4317/medoral.19094

Park-Min, K. H., Lee, E. Y., Moskowitz, N. K., Lim, E., Lee, S. K., Lorenzo, J. A., et al. (2013). Negative regulation of osteoclast precursor differentiation by CD11b and beta2 integrin-B-cell lymphoma 6 signaling. *J. Bone Miner. Res.* 28, 135–149. doi: 10.1002/jbmr.1739

Pihlstrom, B. L., Michalowicz, B. S., and Johnson, N. W. (2005). Periodontal diseases. *Lancet* 366, 1809–1820. doi: 10.1016/S0140-6736(05)67728-8

Sato, K., and Takayanagi, H. (2006). Osteoclasts, rheumatoid arthritis, and osteoimmunology. *Curr. Opin. Rheumatol.* 18, 419–426. doi: 10.1097/01.bor.0000231912.24740.a5

Takayanagi, H., Kim, S., Koga, T., Nishina, H., Isshiki, M., Yoshida, H., et al. (2002). Induction and activation of the transcription factor NFATc1 (NFAT2) integrate RANKL signaling in terminal differentiation of osteoclasts. *Dev. Cell* 3, 889–901. doi: 10.1016/S1534-5807(02)00369-6

Teitelbaum, S. L. (2000). Bone resorption by osteoclasts. *Science* 289, 1504–1508. doi: 10.1126/science.289.5484.1504

Teitelbaum, S. L. (2011). The osteoclast and its unique cytoskeleton. *Ann. N. Y. Acad. Sci.* 1240, 14–17. doi: 10.1111/j.1749-6632.2011.06283.x

Wada, N., Maeda, H., Yoshimine, Y., and Akamine, A. (2004). Lipopolysaccharide stimulates expression of osteoprotegerin and receptor activator of NF-kappa B ligand in periodontal ligament fibroblasts through the induction of interleukin-1 beta and tumor necrosis factor-alpha. *Bone* 35, 629–635. doi: 10.1016/j.bone.2004.04.023

Wong, B. R., Josien, R., Lee, S. Y., Vologodskaia, M., Steinman, R. M., and Choi, Y. (1998). The TRAF family of signal transducers mediates NF-kappaB activation by the TRANCE receptor. *J. Biol. Chem.* 273, 28355–28359. doi: 10.1074/jbc.273.43.28355

Yagi, M., Miyamoto, T., Sawatani, Y., Iwamoto, K., Hosogane, N., Fujita, N., et al. (2005). DC-STAMP is essential for cell-cell fusion in osteoclasts and foreign body giant cells. *J. Exp. Med.* 202, 345–351. doi: 10.1084/jem.20050645

Yoon, J. Y., Baek, C. W., Kim, H. J., Kim, E. J., Byeon, G. J., and Yoon, J. U. (2018). Remifentanil negatively regulates RANKL-induced osteoclast differentiation and bone resorption by inhibiting c-Fos/NFATc1 expression. *Tissue Eng. Regen. Med.* 15, 333–340. doi: 10.1007/s13770-018-0116-z

Zhao, B., and Ivashkiv, L. B. (2011). Negative regulation of osteoclastogenesis and bone resorption by cytokines and transcriptional repressors. *Arthr. Res. Ther.* 13:234. doi: 10.1186/ar3379

Zhao, B., Takami, M., Yamada, A., Wang, X., Koga, T., Hu, X., et al. (2009). Interferon regulatory factor-8 regulates bone metabolism by suppressing osteoclastogenesis. *Nat. Med.* 15, 1066–1071. doi: 10.1038/nm.2007

Conflict of Interest Statement: The authors declare that the research was conducted in the absence of any commercial or financial relationships that could be construed as a potential conflict of interest.

frontiers in Pharmacology

ORIGINAL RESEARCH
published: 17 April 2019
doi: 10.3389/fphar.2019.00315

Embelin Prevents Seizure and Associated Cognitive Impairments in a Pentylenetetrazole-Induced Kindling Zebrafish Model

*Uday Praful Kundap[1,2], Yam Nath Paudel[1], Yatinesh Kumari[1], Iekshan Othman[1] and Mohd. Farooq Shaikh[1]**

[1]Neuropharmacology Research Laboratory, Jeffrey Cheah School of Medicine and Health Sciences, Monash University Malaysia, Bandar Sunway, Malaysia, [2]University of Montreal Hospital Centre (CRCHUM), Montreal, QC, Canada

Epilepsy is a neuronal disorder associated with several neurological and behavioral alterations characterized by recurrent spontaneous epileptic seizures. Despite having more than 20 anti-epileptic drugs (AEDs), they only provide a symptomatic treatment. As well as, currently available AEDs also displayed cognitive alterations in addition to retarding seizure. This leads to the need for exploring new molecules that not only retard seizure but also improve cognitive impairment. Embelin (EMB) is a benzoquinone derivative which has already demonstrated its pharmacological potentials against arrays of neurological conditions. The current study developed a chronic kindling model in adult zebrafish by using repeated administration of small doses of pentylenetetrazole (PTZ) and a single dose of Kainic acid (KA) to investigate the associated memory impairment. This has been done by using the three-axis maze which is a conventional method to test the learning ability and egocentric memory in zebrafish. As well as, the ameliorative potential of EMB has been evaluated against chronic epilepsy-related memory alterations. Moreover the expression level of pro-inflammatory genes such as C-C motif ligand 2 (CCL2), toll-like receptor-4 (TLR4), tumor necrosis factor-α (TNF-α), interleukin-1 (IL-1) and interferon-γ (IFN-γ) were evaluated. The level of several neurotransmitters such as γ-aminobutyric acid (GABA), acetylcholine (Ach) and glutamate (Glu) was evaluated by liquid chromatography-mass spectrometry (LC-MS). The results showed that daily dose of PTZ 80 mg/kg for 10 days successfully induces a kindling effect in zebrafish, whereas the single dose of KA did not. As compared to control, the PTZ and KA group demonstrates impairment in memory as demonstrated by the three-axis maze. The PTZ group treated with a series of EMB doses (ranging from 0.156 to 0.625 mg/kg) was found to have retarded seizure as well as significantly reduces epilepsy-induced memory alteration. In addition, EMB treatment reduces the expression of inflammatory markers implicating its anti-inflammatory potential. Moreover, levels of GABA, Ach, and glutamate are increased in EMB administered group as compared to the PTZ administered group. Overall, findings demonstrate that EMB might be a potential candidate against chronic epilepsy-related cognitive dysfunction as EMB prevents the seizures, so we expect it to prevent the associated neuroinflammation and learning deficit.

Keywords: chronic epilepsy, zebrafish, three-axis maze, cognition, behavior

OPEN ACCESS

Edited by:
Ioanna Andreadou, National and Kapodistrian University of Athens, Greece

Reviewed by:
Tamara Amstislavskaya, State Scientific-Research Institute of Physiology and Basic Medicine, Russia
Barbara Dotto Fontana, University of Portsmouth, United Kingdom

****Correspondence:***
Mohd. Farooq Shaikh
farooq.shaikh@monash.edu

Specialty section:
This article was submitted to Experimental Pharmacology and Drug Discovery, a section of the journal Frontiers in Pharmacology

Received: *25 January 2019*
Accepted: *14 March 2019*
Published: *17 April 2019*

Citation:
Kundap UP, Paudel YN, Kumari Y, Othman I and Shaikh MF (2019) Embelin Prevents Seizure and Associated Cognitive Impairments in a Pentylenetetrazole-Induced Kindling Zebrafish Model. Front. Pharmacol. 10:315. doi: 10.3389/fphar.2019.00315

HIGHLIGHTS

- A repeated small dose of PTZ (80 mg/kg) (kindling) for 10 days produces chronic epilepsy like condition in adult zebrafish.
- EMB was reported to reduce epileptic seizures and improve long term memory as evidenced by a three-axis maze test.
- EMB demonstrated an anti-inflammatory effect *via* downregulating several inflammatory markers (CCL2, TLR4, IL-1, and IFN-γ) in the epileptic brain.
- EMB might be a potential candidate against chronic epilepsy and related cognitive dysfunction as well as can overcome the limitations of mainstream AEDs.

INTRODUCTION

Epilepsy is a neurologic disorder affecting more than 70 million people worldwide (Singh and Trevick, 2016). Epilepsy is mainly characterized by the occurrence of spontaneous recurrent seizures (SRS) and high prevalence of comorbidities, such as cognitive impairments, depression, and anxiety, affecting the lives of individuals (Keezer et al., 2016). Chronic epilepsy is characterized by repeated unpredictable seizures, impairing memory in 30–40% of patients under long-term anti-epileptic drugs (AEDs) treatment, so epilepsy and AEDs both are responsible for memory problems (Helmstaedter, 2002; Canevini et al., 2010; Zhang et al., 2017). Despite there being more than 20 mainstream AEDs, they only provide symptomatic treatment rather than interfering with the disease's mechanism, and 30% of patients do not respond to current AEDs (Remy and Beck, 2005; Chen et al., 2018). These data indicate the pressing need to develop novel and innovative therapy that can reduce seizures and maintain good memory status. Despite recent advances in research, the underlying pathomechanism of epilepsy is still less known. However, findings are emerging that implicate the role of inflammation in epilepsy (Vezzani, 2005; van Vliet et al., 2018; Paudel et al., 2018b). High mobility group box 1 (HMGB1) protein is an initiator and amplifier of neuroinflammation and has been implicated in seizures *via* activating toll-like receptor 4 (TLR4) (Ravizza et al., 2017; Paudel et al., 2018a). Moreover, C-C motif ligand 2 (CCL2), tumor necrosis factor-α (TNF-α), interleukin-1 (IL-1) and interferon-γ (IFN-γ) have been implicated in seizure generation as well as found to be up-regulated during a seizure (Marchi et al., 2014; Dey et al., 2016).

Local or systemic administration of kainate in rodents leads to repetitive limbic seizures and status epilepticus (SE), lasting for several hours. It is a useful model of temporal lobe epilepsy (TLE) in rodents (Dal-Pizzol et al., 2000). Kainic acid (KA) is an epileptogenic and the neuroexcitotoxic agent acting on specific kainate receptors (KARs) in the central nervous system (CNS) (Zheng et al., 2011). The complete seizure characterization of KA-induced epilepsy is studied in zebrafish and it produces continuous seizures with neuronal toxicity (Alfaro et al., 2011; Menezes et al., 2014; Mussulini et al., 2018). Traditional models like the maximal electroshock seizure (MES) and pentylenetetrazole (PTZ) seizure models have been instrumental for pre-clinical screening for a long time, however, these models have limited themselves in identifying novel compounds with improved efficacy against different chronic disorders (Löscher, 2011). A PTZ induced acute seizure model has been already developed in adult zebrafish and recapitulates all the clinical phenotypes of seizure (Mussulini et al., 2013; Kundap et al., 2017). Kindling is a chronic animal model of epilepsy that has been extensively studied to understand the underlying mechanism of epileptogenesis (Kandratavicius et al., 2014). In addition, kindling is a phenomenon where a sub-convulsive stimulus (either chemical or electrical), if applied repetitively and intermittently, will ultimately lead to the generation of full-blown convulsions (Dhir, 2012a). The study was conducted by using PTZ kindling discusses detail methodology to execute a chemical induced kindling in mice (Dhir, 2012a). A number of different promising models which fulfill this criterion have been developed over recent years, but has not been modeled in zebrafish (Wilcox et al., 2013). Moreover, the understanding of the molecular involvement underlying such diseases is still under study and it is preventing adequate therapeutic outcomes (Samarut et al., 2016). Various numbers of pre-clinical models have been studied to investigate the role of different brain functions and understand the structure of disease development (Samarut, 2016).

In recent days, zebrafish disease models has received increased attention due to its genetic similarity to humans, economic value, and its suitability as an alternative for a human disease model and for large-scale drug screenings (Shams et al., 2018). Zebrafish has rapid embryonic development as compared to rodents, as well as easy cellular observation and phenotypic analysis, which makes it a better model to study the neurological aspect of a brain disorder.

The three-axis maze is a method to evaluate learning ability and egocentric memory in zebrafish. In a three-axis maze, fish are required to navigate a route based on x (forward/backward), y (horizontal) and z (vertical) axes (Nasir et al., 2012). Egocentric navigation is an evidence-based process, where fish navigate to the feeding ring independent of environmental cues and deals directly with the spatial relationship between subject and reward goal (Nasir et al., 2012).

Embelin (EMB) (2,5-dihydroxy-3-undecyl-1,4 benzoquinone) is the main component in the red berry fruits produced by *Embelia ribes* (Dubéarnès et al., 2015). EMB has been studied extensively using various in-vitro and in-vivo animal models and have exhibited strong anti-convulsant, anxiolytic and anti-depressant properties as well as improving conditions such as sickness behavior, Huntington's disease (HD), multiple sclerosis (MS), cerebral ischemia and traumatic brain injury (TBI) (Mahendran et al., 2011; Poojari, 2014). Moreover, earlier findings reported that EMB significantly inhibited seizures induced by electroshock and PTZ in a dose-dependent manner (Shankar et al., 2012). In spite of the huge pharmacological significance of EMB, no study has earlier reported the ameliorative potential of EMB against PTZ kindling induced chronic epilepsy and related cognitive alterations using zebrafish as an animal model.

The current investigation developed a protocol of PTZ kindling in an adult zebrafish. A small amount of proconvulsant drug (PTZ) was administered for a period of 10 days in order to produce progressive chronic epilepsy like behavior. To KA-treated fish, as per rodent model, we tried to induce chronic epilepsy by administrating a single dose of KA-3 mg/kg the day before the start of the experiment. The seizure scores were calculated, and the three-axis maze trial was performed in order to check the memory status and seizure progression on a daily basis. The same procedure was employed in the fish pretreated with EMB and the effect of EMB was analyzed. In addition, fold change of neuroinflammatory genes and neurotransmitter levels were quantified in order to confirm the positive effect of EMB against chronic epilepsy induced cognitive dysfunction model in adult zebrafish.

MATERIALS AND METHODS

Experimental Equipment and Chemicals List

All analytical grade reagents were used unless specified otherwise. Water was purified and filtered with a specific liquid chromatography-mass spectrometry (LC-MS) filter using a Milli-Q system from Millipore (Bedford, MA, USA). Glutamate, γ-aminobutyric acid (GABA), KA, and PTZ were purchased from Sigma Aldrich (USA). The pure form of plant extract of EMB was purchased from YUCCA Enterprises, Mumbai, India. Ethanol 95% (EtOH) was purchased from Kolin Chemicals Co. Ltd, Korea, methanol (MeOH), chloroform (CHCl3), isopropanol (IPA), and formic acid (FA) was purchased from Friedemann Schmidt Chemicals, Parkwood 6147, Western Australia.

Zebrafish Maintenance and Housing Conditions

Adult zebrafish (*Danio rerio*) of heterozygous wild-type-AB stock (standard short-fin phenotype) were obtained from the Institute of Molecular and Cell Biology (IMCB), 61 Bioplis Drive Proteos, Singapore 138673. All fish were kept in the Monash University Malaysia fish facility at 28°C, with a 10/14 h dark/light cycle (white incident light off at 10 pm, white incident light on at 8 am) under standard aquarium conditions. Care was taken to maintain system water pH between 6.8–7.1 by using an electronic pH pen (Classic PH Pen Tester, Yi Hu Fish Farm Trading, Singapore 698950) and intensity of light was maintained at 250 Lux to get the uniform light all over the housing area. Fish were fed, thrice a day to ensure a constant source of nourishment. Nutrition for fish was maintained by Tropical TetraMin® Flakes and live brine shrimps Artemia from Bio-Marine (Aquafauna, Inc. United States). Circulating water system with zebrafish tank which is equipped with constant aeration having (36 × 26 × 22 cm) tank dimensions (Kundap et al., 2017). Monash Animal Research Platform (MARP), Australia, approved all the zebrafish experimental procedures (MUM-2017-03) (MARP-2017-003).

During the experimental procedure the animals were housed individually in each tank of 3 L in size. The animals were not fed in the home tank as they received the food a reward during each trial daily. The fish that did not reach the feeding ring (goal chamber) were fed once in the home tank. To avoid the encounter of aggressive behavior with each other and to individually track the behavior of each fish individually, the fish were housed separately in each tank (Parker et al., 2012). The water temperature of 28°C was maintained the same as the system water, with 7.2 pH, the light–dark cycle of 14/10 h, and intensity of light was maintained at 250 Lux to get uniform lighting all over the housing area.

Animal Grouping/Randomization and Treatment

Groups of animals exposed to drug treatment were divided as follows. Animals selected for testing were randomized as per the groups with $n = 12$. The experiment was not blinded as videos were recorded and then manually analyzed and checked by two investigators individually for confirmation. The fish were pre-treated with embelin and then exposed to PTZ before the start of the three-axis maze trial. The behavior recording for an epilepsy seizure score and transfer latency was recorded daily for the period of 10 days for each fish. Animal treated with embelin were observed for its epilepsy behavior, cognitive performance in three-axis maze and biochemical changes. Later on, the zebrafish brains were isolated for LC-MS/MS studies and gene expression analysis. For experimental procedure and drug administration follow **Figure 1**.

Set 1: Development of chronic epilepsy induced cognitive problems in zebrafish.

Group I: Vehicle control; **Group II:** PTZ 80 mg/kg; **Group III:** KA 3 mg/kg.

Set 2: Elucidating the therapeutic potential of EMB against chronic epilepsy induced cognitive dysfunction.

EMB and PTZ were dissolved in 10% DMSO.

Group I: Vehicle control (10% DMSO); **Group II:** Pentylenetetrazole (PTZ)–80 mg/kg; **Group III:** Embelin (EMB)–0.156 mg/kg + PTZ; **Group IV:** Embelin (EMB)–0.312 mg/kg + PTZ; Group V: **Embelin (EMB)**–0.625 mg/kg + PTZ.

Software and Equipment

The Smart V3.0.05 tracking software (Pan Lab, Harvard Apparatus), the Sony (Handycam HDR-PJ340E) video camera and Sony Camcorder stands were used for the automated tracking of zebrafish swimming patterns and locomotion parameters. The Applied Biosystems StepOnePlusTM Real-Time PCR System was used for the gene expression study. The MilliQ system from Millipore (Bedford, MA, United States) was used to produce pure water for the experiment purpose. The equipment used for quantifying brain neurotransmitters was the Agilent 1,290 Infinity UHPLC, coupled with the Agilent 6410 Triple, Quad LC/MS. Fish tank –10 liters capacity (PETCO-Pet keeper, Malaysia), The syringe used for intraperitoneal injection was Hamilton syringe 700–702 series 25 µl along with BD disposable needle–30G (Becton Dickinson, USA).

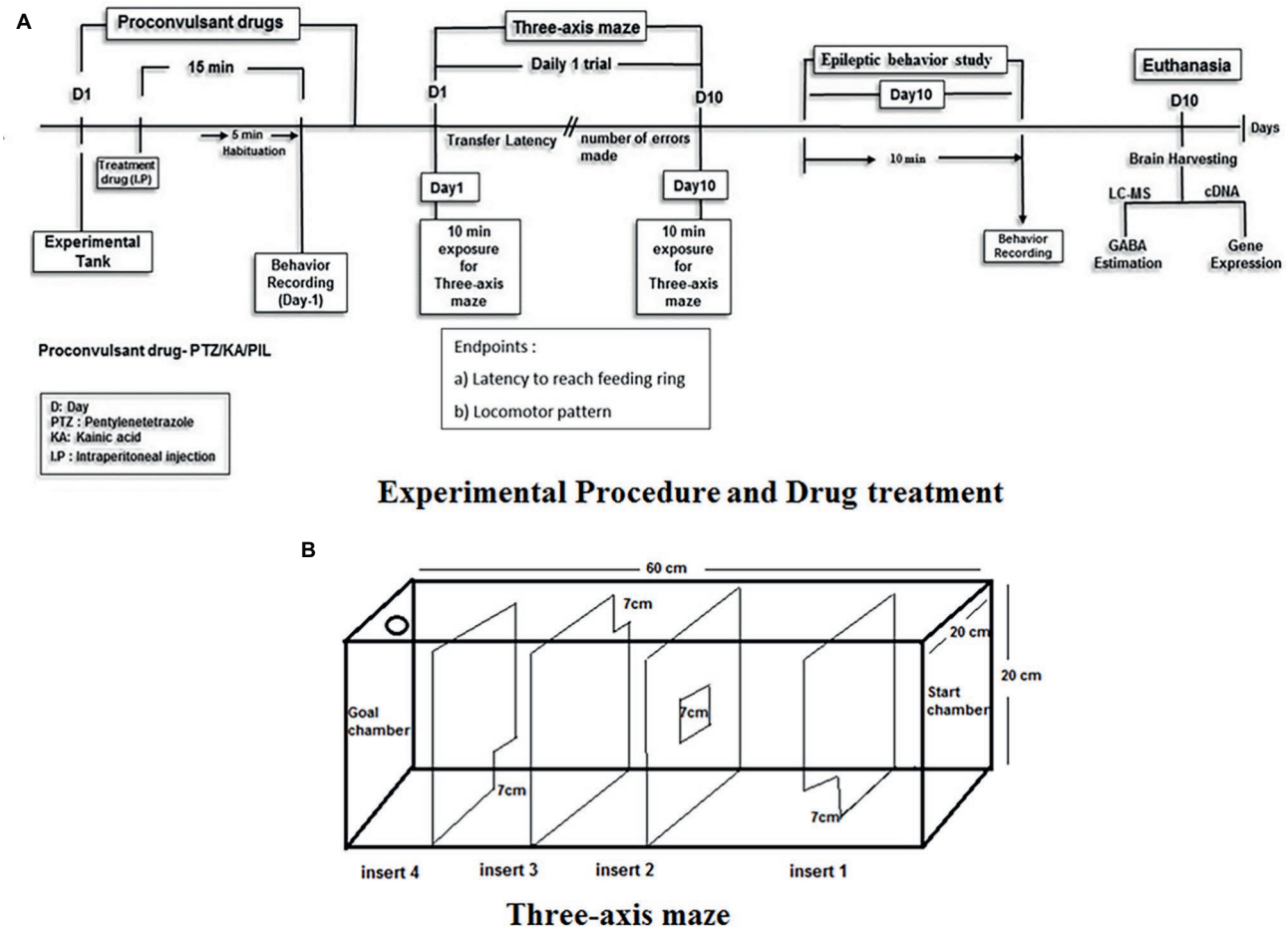

FIGURE 1 | Experimental setup and design procedure. **(A)** Represents the flowchart represents the scheme for EMB treatment, PTZ administration and behavior recording for epilepsy and three-axis maze used in the study. **(B)** Acrylic white experimental box of Three-axis maze with different openings from start chamber to goal chamber (feeding ring).

Procedure for Zebrafish Anesthesia and Intraperitoneal Injection

PTZ and the EMB were intraperitoneally infused into the zebrafish as indicated by the convention given by Kundap et al. (2017) and is given beneath. At the point when different intraperitoneal infusions were required, the infusions were given at alternating lateral ends, instead of the midline between the pelvic fins. Each zebrafish was caught individually utilizing a fish holding net, and after that moved into an anesthesia arrangement (30 mg/L Benzocaine). The fish were kept into the anesthesia water for 30 s until they stop moving. The zebrafish was taken out once anesthetized and weighed afterward to calculate the dose and subsequently the infusion volume. A delicate sponge roughly 20 mm in stature was soaked with water and set inside a 60 mm Petri dish. A cut between 10 and 15 mm inside and out was made in the sponge to control and hold the fish for the intraperitoneal infusion. The intraperitoneal infusion was given while utilizing a dismembering magnifying lens by embeddings the needle into the midline between the pelvic fins. An appropriate volume was then injected into the zebrafish, after considering the body weight of the zebrafish.

All intraperitoneal infusions were administered into the stomach pit at an area back to the pelvic support, utilizing a 10 µl Hamilton syringe (700 arrangement, Hamilton 80400) (Stewart et al., 2011). The experiment was performed in a separate behavior room with the room temperature kept between 26 and 30°C and humidity between 50 and 60%. All zebrafish were acclimatized in the said behavior room for 2 h prior to the experiment for minimizing any novel tank response. Other precautions taken include using a small injection volume of 10 µl per gram of fish and using a 30-gauge needle. The zebrafish were restrained in water saturated sponge under benzocaine anesthesia to reduce the distress inflicted on the zebrafish (Barbosa et al., 2012). This intraperitoneal injection technique was found to be effective in zebrafish (Kundap et al., 2017) and did not cause any mortality throughout the experiment. After the intraperitoneal injection, the zebrafish was immediately transferred to an observation tank.

Seizure Score Analysis

PTZ-Induced Seizure Score

PTZ is a proconvulsant drug. As per earlier reported studies, PTZ at 220–250 mg/kg dose produces full-blown seizures in zebrafish (Banote et al., 2013). In order to produce kindling effect, PTZ at lower doses (80 mg/kg) was administered daily for 10 days which was almost 1/3 of the actual dose reported earlier. Kindling is a process by which a seizure or other brain event is initiated and its recurrence is made more likely (Dhir, 2012). The PTZ Kindling model is well established in rodents and in other animals so in accordance to those animal model the dose of PTZ administration is calculated for zebrafish (80 mg/kg dose/10 days) (Ohno et al., 2010). After the fish was prone to seizures for at least 10 days it was observed for its locomotor behavior, three-axis maze memory analysis, and other biochemical alterations. For the EMB treated group fish were pre-treated with a single dose of EMB dissolved in 10% DMSO prior to daily PTZ administration. However, in the control group fish were pre-treated with 10% DMSO and the distilled water was administered to maintain the same number of injection in all the groups.

PTZ injected zebrafish displays unique seizure characters, intensities and latency in generating the different seizure scores. PTZ induced seizure behavior will remain around 10 min after the PTZ administration and gradually decrease with time. The PTZ injected adult zebrafish were then transferred to the observation tank water for behavior and the three-axis maze test. The behavior of the zebrafish was then recorded for 10 min after recovery from anesthesia and the video was later viewed using a computer to determine the highest seizure score during the 10 min. The zebrafish seizure score was recorded as per the earlier scoring protocol (Banote et al., 2013; Mussulini et al., 2013; Kundap et al., 2017) and is given below.

Score 1–Short swim mainly at the bottom of the tank.

Score 2–Increased swimming activity and high frequency of opercula movement.

Score 3–Burst swimming, left and right movements as well as the erratic movements.

Score 4–Circular movements.

Score 5–Clonic–tonic full body system rhythmic contractions.

Score 6–Fall at the bottom of the tank.

Score 7–Death

KA-Induced Seizure Score

Throughout the time of pre-exposure to KA, the behavior of the zebrafish was monitored for 10 min after the fish was fully recovered from anesthesia. The seizure behavior for KA-induced seizure was modified from the earlier findings (Menezes et al., 2014) and described below.

Score 1–Rigidity and hyperventilation of the animal.

Score 2–Whirlpool-like swimming behavior.

Score 3–Rapid muscular uncontrol movements from right to left.

Score 4–Abnormal and spasmodic muscular contractions.

Score 5–Rapid whole-body clonus-like convulsions.

Score 6–Sinking to the bottom of the tank and spasms for several minutes.

Score 7–Death.

Under the directives of the Monash Animal Research Platform (MARP)-Australia, the PTZ dose was standardized at 80 mg/kg of zebrafish body weight in order to produce the kindling seizure progression. The dose of KA-3 mg/kg (single dose) (Alfaro et al., 2011) was titrated in order to produce the maximum survival of zebrafish in a group for more than 48 h until day-10. The highest observed seizure score was the highest seizure score noted within the entire 10 min duration of the recording. The zebrafish swimming pattern and locomotion parameters were determined *via* analysis using the Smart tracking software.

Three-Axis Maze Test and Behavior Analysis

In the three-axis maze (**Figure 1**) fish are required to navigate a route based on x (forward/backward), y (lateral) and z (depth) axes and is designed as a measure of spatial memory. The maze is constructed from white 0.25″ acrylic held together with acrylic epoxy and sealed with aquarium sealant. The maze consists of a 20 × 20 × 60-cm tank divided into five 12 × 20 × 20-cm chambers with a 7 × 7-cm window cut into the corner or center of each insert as shown in **Figure 1**. A floating NutraFin Max feeding ring (PetCo, Inc.) was attached to the end of the maze in the goal chamber. The walls and inserts of the maze are constructed of white acrylic to minimize any external visual cues that could be used by the fish as markers. In addition, the maze was uniformly illuminated from above to minimize shadows and visual cues external to the maze. With the inserts in place, fish swim from one chamber to another through the windows in the inserts to reach a food reward in the goal chamber. The order of inserts in the maze was constant throughout the experiment, to allow the route to remain constant until the feeding ring as shown in **Figure 1**.

The detailed specifications regarding the maze were as per the given standard protocol (Nasir et al., 2012). Transfer latencies (TL) were recorded from day-1 to day-10 post-PTZ administration. An inflexion ratio (IR–day-1) = (TL0-TL1)/(TL1), (IR-day-2) = (TL0-TL2)/(TL2) rest as follows was calculated, where TL0 is the initial latency(s) at day-0 and TL1 and TL2 is the latency(s) at the Day-1 and day-2 trial respectively. The IR was calculated as compared to day-0 to measure the amount of memory increase each day with the progression of days/ treatment. The behavior recordings during seizure activity and the three-maze test were analyzed to track the locomotor patterns. Tracking of the locomotor pattern was done by using the computer software SMART v3.4-Panlab Harvard Apparatus®.

Training

The fish were food-deprived for 1 day prior to the start of both the training and testing periods and are not fed outside of the maze throughout the duration of the experiment. Training consisted of two back-to-back trials on the day before testing. During training, the inserts were removed from the maze; the fish were netted from their home tank and placed at the

end of the maze opposite the feeding ring. A small amount of Tetramin flakes was placed in the feeding ring, and fish were trained to swim the length of the maze to receive food. The fish were permitted to feed for more than 30 s up to maximum 1 min before being netted and returned to their home tank. Training allows the fish to acclimatize to the testing apparatus and to learn the location of the feeding ring at the opposite end of the tank. Food-deprived fish learn to associate the testing apparatus with food and actively search for the feeding ring when the inserts will be present. Training is necessary in order to avoid novel tank anxiety effect in fish during the actual testing period. Food deprivation is part of the experimental procedure. The reason behind food-deprivation is that fish learn to associate the testing apparatus with food and actively search for the feeding ring when the inserts are present. After repeated trials fish learn the task to reach the feeding ring and eat the food (Nasir et al., 2012).

Testing

Testing consists of one trial per day for 10 consecutive days. Vehicle control animals will be administered I.P with vehicle agent first and then administered with distilled water before placing it in the maze. For the PTZ treated group, each fish was administered with an 80 mg/kg dose I.P daily prior to the testing period. The fish were habituated for 10 min after PTZ administration to check the memory test in the three-axis maze. For the KA-treated group, each fish was administered with 3 mg/kg dose at the start of the experiment on day-1. For the EMB treated group, the fish was pre-treated with EMB (0.156/0.312/0.625 mg/kg) daily prior to the administration of PTZ. After specific treatment, the fish are placed in the start chamber and the response latency to reach the feeding ring in the last chamber is recorded. Fish will be allowed to feed for more than 30 s maximum up to 1 min before being returned to their home tanks. If fish failed to complete the maze within 10 min, they are fed and returned back to the home tank.

Gene Expression

Gene expression studies were carried out to determine the expression level of several inflammatory genes such as CCL2, HMGB1, TLR4, IFN- γ, TNF-α and IL-1. All the brain samples were collected in ice-cold 200 µl TRIzol® reagent (Invitrogen, Carlsbad, CA, USA) and immediately stored at −80°C until further usage. The study was divided into three steps such as isolation of mRNA, synthesis of cDNA strand and then real-time PCR to estimate the level of genes expressed.

Isolation of RNA and First Strand cDNA Synthesis

The mRNA was isolated by following the manufacturer's protocol. In brief, brain tissue was properly homogenized in TRIzol® reagent, mixed with chloroform and centrifuged at 13,500 rpm (revolutions per minute) for 15 min at 4°C. The upper aqueous supernatant was transferred into new tubes and isopropanol was added, mixed and was incubated for 10 min at room temperature and later centrifuged for 10 min at 13,500 rpm at 4°C. The supernatant was discarded, and the pellets were subjected to rinsing with 75% ethanol. Then, the pellets were left for air drying between 5 and 8 min of air drying. Finally, nuclease-free water was added to each tube to dissolve the mRNA pellet. The concentration and purity of the isolated mRNA were measured by using a NanoDrop Spectrophotometer. The mRNA samples were converted into cDNA using Omniscript Reverse-transcription Kit (QIAGEN) according to the manufacturer's protocol.

All the primer sets were provided by Qiagen (NL).

CCL2: Dr_ccl2_1_SG QuantiTect Primer Assay (Cat no: QT02205763) TLR4: Dr_tlr4ba_va. 1_SG QuantiTect Primer Assay (Cat no: QT02198539).

IFN-G: Dr_ifng1-2_1_SG QuantiTect Primer Assay (Cat no: QT02064328).

TNF-α: Dr_tnf_1_SG QuantiTect Primer Assay (Cat no.QT02097655).

IL-1: Dr_il1rapl1a_1_SG QuantiTect Primer Assay (Cat no.QT02131850).

eef1a1b: Dr_eef1a1b_2_SG QuantiTect Primer Assay (Cat no.QT02042684).

Estimation of Neurotransmitters by LC/MS-MS

Glutamate, GABA, and Ach are significant neurotransmitters to study epilepsy and cognition. These neurotransmitters were analyzed using the LC-MS/MS technique. All the standard neurotransmitters were prepared in methanol (0.1% formic acid) as a stock solution of 1 mg/ml and were kept at 4°C until use. Standards for calibration were prepared from the original stock solution. Serial dilution from 100–2000 ppb was used for calibration. The brain was homogenized in 200 µl of ice-cold methanol (0.1% formic acid). The homogenate was vortex-mixed for 1 min and then centrifuged at 18,000*g* for 10 min at 4°C. Finally, the supernatant was pipetted and placed into vials for LC-MS/MS analysis.

LC-MS/MS was run on an Agilent 1,290 Infinity UHPLC, coupled with Agilent 6,410 Triple, Quad LC/MS, ZORBAX Eclipse plus C18 RRHD 2.1 × 150 mm, 1.8-micron (P/N 959759–902) auto-sampler system (Agilent Technologies, Santa Clara, CA, USA). The samples were separated on a SMol-RRHD-Eclipse-C18-8 (15) UHPLC-160129-00011-Pos-DMRM used at 30°C. The mobile phase consisting of 0.1% formic acid in water (Solvent A) and acetonitrile with 0.1% formic acid (Solvent B) was used with a gradient elution: 0–3 min, 50% B; 3–6 min, 95% B; 06–07 min, 95% B at a flow rate of 0.1 ml/min. ESI-MS/MS Conditions were set as follows: ESI ion source, positive ion polarity, gas temperature 325°C, drying gas flow 9.0 L/min, nebulizer pressure 45 psi, Vcap 4,000 V. MS acquisition of GABA, Glu, ACh was performed in electrospray positive ionization multiple reaction monitoring (MRM) mode.

Statistical Analysis

The data were analyzed by GraphPad Prism v.7.02 (San Diego, CA) with repeated measure (mixed model) two-way ANOVA followed by Bonferroni post-test to compare replicated means by row. Data are presented as means and standard errors of the mean (SEM) to assess the differences in seizure, latency and inflexion ratio. The results acquired for neurotransmitter

levels and gene expression between treatments and control were analyzed by one-way ANOVA and subsequent Dunnett's multiple comparison tests. A p of <0.05 indicates statistical significance.

RESULTS

Daily Administration of PTZ Induces Chronic Epilepsy in Adult Zebrafish

Daily administration of small doses of PTZ for 10 days induced full-blown seizures in zebrafish. It was observed that 80 mg/kg dose of PTZ cause a gradual increase in seizure scores from day-4 until day-10. Seizure score increase from score 1.5 to score 5 from day-1 to day-10. In addition, a single dose of KA-induced epileptic seizures, however, it was not able to maintain a high seizure score on daily observation and the score was eventually reduced from score 5 at day-1 to no seizure to score 1 at day-10 (**Figure 2AI**).

Moreover, in the three-axis maze, it was observed that all the fish from the control group showed a significant decrease in time taken to reach the feeding ring (goal chamber) from day-1 to day-10 and it was less than 100 s (**Figure 2AII**). However, all the fish from PTZ and KA-treated group found to worsen the cognitive function in zebrafish on observation of three-axis maze study. Indeed, the latency to reach the feeding chamber was high in PTZ and KA-treated fish when compared to the control group (**Figure 2AII**). It was observed that PTZ treated fish took more than 450 s to reach the feeding ring until day-10. However, the time was increased to 250 s in KA-treated fish when compared to the control group as shown in **Figure 2AII**.

Daily Administration of EMB Ameliorates PTZ Seizures and Memory Decline

PTZ at 80 mg/kg, when administrated daily for 10 days, produces kindling like behavior with a continuous unprovoked seizure. Fish, when treated with EMB, ameliorates the gradual increase in seizure generated due to PTZ kindling (**Figure 3AI**). It was found that EMB-0.156 mg/kg to EMB-0.625 reversed chronic epilepsy induced due to PTZ kindling and maintained a low seizure score from day-1 to day-10. All the animals from PTZ treated group demonstrated disruption in cognitive functions when analyzed on the three-axis maze model (**Figure 3AII**). Due to the alteration in cognitive functions induced due to PTZ kindling, fish get lost in the maze compartment of the three-axis maze. The tracking pattern of PTZ administered fish demonstrated complex behavior patterns, as well as not being able to analyze the path towards the feeding ring and hence spending more time in each compartment. As seen in **Figure 2**, the time is taken, and distance traveled by PTZ kindled fish to reach the feeding ring was higher as compared to the control group. Simple and straight tracking pattern was observed in the control group which might be due to the continuous daily trial of control fish in the three axis maze for 10 days. As the fish was treated daily with a single dose of EMB prior to PTZ administration, EMB ameliorated the epileptic seizure generated from PTZ kindling and improved the locomotor tracking pattern. EMB pre-treated fish with a dose ranging from 0.156 to 0.625 mg/kg demonstrated simple and improved tracking patterns similar to the control group on the 10th day of three-maze trial shown in **Figure 3**. Due to PTZ kindling effects, epileptic fish exhibited loss in memory function which is detrimental for egocentric navigation. EMB (0.156–0.625 mg/kg) significantly improved maze navigation times and reduced performance errors in the three-axis maze with P-value significant $^{*}p \leq 0.05$, $^{**}p \leq 0.01$, and $^{***}p \leq 0.001$.

Estimation of Neurotransmitters by LC/MS-MS

Neurotransmitter analysis was performed to check the amount of chemical change in the brain after chronic epilepsy treatment. Neurotransmitter analysis by LC/MS-MS demonstrated a significant reduction ($^{*}p < 0.05$) in the level of GABA in the PTZ administered group when compared to the control groups. Significant elevation in the level of GABA was observed on the EMB (0.156 mg/kg) ($^{**}p < 0.01$) and the EMB (0.625 mg/kg) ($^{*}p < 0.05$) administered groups when compared to the PTZ group (**Figure 4**). The level of glutamate was non-significantly different between the control group and the PTZ treated group. However, there was a significant elevation in EMB (0.156 mg/kg) ($^{**}p < 0.01$), EMB (0.312 mg/kg) ($^{*}p < 0.05$) and the EMB (0.625 mg/kg) ($^{**}p < 0.01$), administered group when compared to PTZ injected group. However, the brain Ach level was significantly decreased on the PTZ administered group as compared to the control group. In addition, there was significant upregulation in the level of Ach in EMB (0.156 mg/kg) ($^{***}p < 0.001$) and the EMB (0.625 mg/kg) ($^{***}p < 0.001$) treated group when compared to the PTZ treated group shown in **Figure 4**.

EMB Pre-treatment, Reverse Epilepsy That Affects Expression Levels of Several Inflammatory Genes

CCL2 mRNA expression level was non-significantly upregulated in the PTZ treated group when compared with the control group. However, CCL2 mRNA expression level was significantly down-regulated in EMB (0.156 mg/kg) ($^{*}p < 0.05$) and the EMB (0.312 mg/kg) ($^{*}p < 0.05$) treated group as compared to the PTZ administered group. In addition, there was non-significant downregulation in the CCL2 mRNA expression level on EMB (0.625 mg/kg) treated group when compared to the PTZ treated the group as shown in **Figure 5A**.

TLR4 mRNA expression was significantly ($^{***}p < 0.001$) decreased in the control group when compared to the PTZ treated group. When compared to the PTZ administered group, TLR4 mRNA expression level was decreased in EMB (0.312 mg/kg) ($^{*}p < 0.05$) and the EMB (0.625 mg/kg) ($^{**}p < 0.01$). However, non-significant downregulation of TLR4 mRNA expression level was observed in the EMB (0.156 mg/kg) treated group when compared to the PTZ treated group as shown in **Figure 5B**.

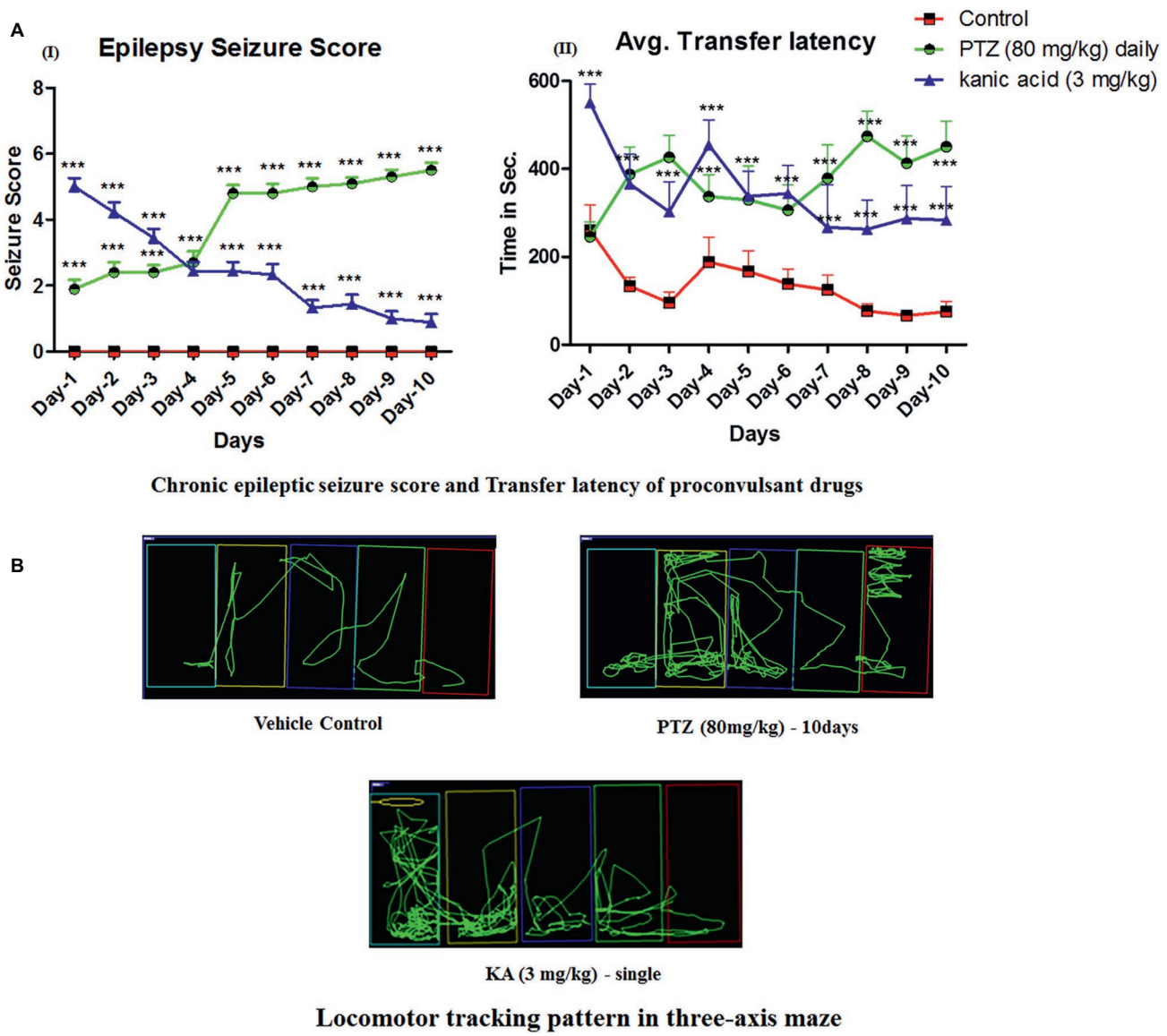

FIGURE 2 | Daily administration of PTZ induces chronic epilepsy in adult zebrafish. **(AI)** Represents the seizure progression pattern of PTZ and KA from day-1 to day-10 with *F*-value of 413.7, DF-18 and mean square–19.41; **(AII)** represents transfer latency, the time taken by PTZ and KA-treated fish against a control group. PTZ (80 mg/kg) and KA–3 mg/kg significantly increase the time taken to reach the feeding ring. The data were analyzed by GraphPad Prism v.7.02 (San Diego, CA) with repeated measure (mixed model) Two-way ANOVA followed by Bonferroni post-test to compare replicated means by row. Data are presented as means and standard errors of the mean (SEM) to assess the differences in seizure, latency, and inflexion ratio: with *F*-value of 22.24, DF-18 and mean square–70,622 $*p \leq 0.05$; $**p \leq 0.01$; $***p \leq 0.001$. **(B)** Locomotor tracking pattern of a single representative fish in a treated group with the proconvulsant drug at day-10 in three-axis maze.

TNF-α mRNA expression was non-significantly upregulated in the control group as compared to the PTZ treated group. However, no significant difference was observed in the TNF-α expression levels in all the EMB (0.156, 0.312 and 0.625 mg/kg) treated group when compared to PTZ treated group as shown in **Figure 5C**.

IL-1 mRNA expression was found to be significantly ($***p < 0.001$) down-regulated in the control group when compared with the PTZ administered group. An IL-1 mRNA expression level was significantly ($***p < 0.001$) down-regulated in the EMB (0.156 and 0.312 mg/kg) treated group as compared to the PTZ treated group. However, non-significant downregulation of the IL-1 mRNA expression level was observed in EMB (0.625 mg/kg) treated group when compared to the PTZ treated the group as shown in **Figure 5D**.

Significant ($*p < 0.05$) downregulation in the level of INF-γ mRNA expression was observed in the control group as compared to the PTZ treated group. However, INF-γ mRNA expression was found to be significantly downregulated in EMB (0.156 mg/kg) ($*p < 0.05$) and in the EMB (0.312 mg/kg) ($**p < 0.01$) the treated group as compared to the PTZ treated

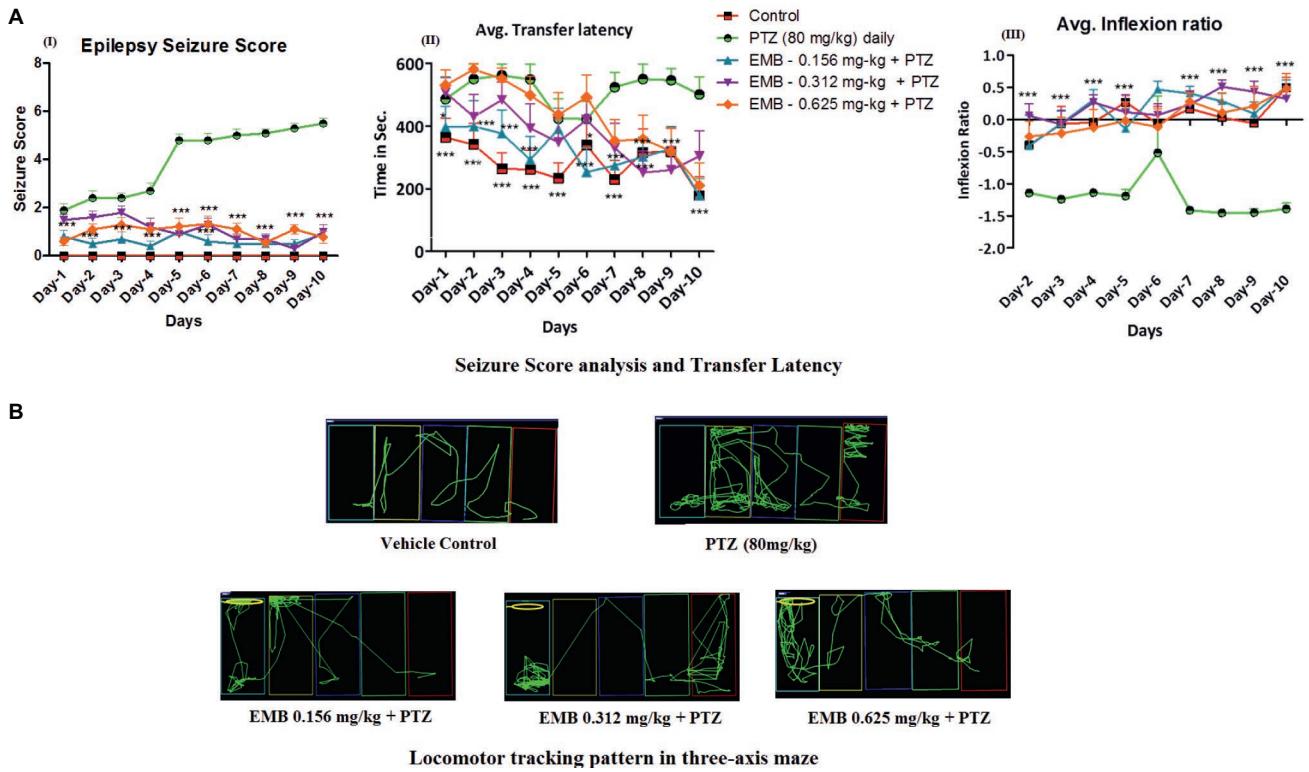

FIGURE 3 | Daily administration of EMB ameliorates PTZ seizures and memory decline. **(AI)** Represents the seizure progression pattern of EMB against PTZ kindling from day-1 to day-10 with *F*-value of 106.4, DF-36 and mean square–5.489. **(AII)** Represents transfer latency, the time taken by EMB treated fish against PTZ treated fish. **(AIII)** Represents the inflexion ratio of EMB treated group compared to the PTZ treated group. The data were analyzed by GraphPad Prism v.7.02 (San Diego, CA) with repeated measure (mixed model) Two-way ANOVA followed by Bonferroni post-test to compare replicated means by row. Data are presented as means and standard errors of the mean (SEM) to assess the differences in seizure, latency and inflexion ratio with *F*value of 9.850, DF-36 and mean square–41,046, $^{*}p \leq 0.05$; $^{**}p \leq 0.01$; $^{***}p \leq 0.001$. **(B)** Locomotor tracking pattern a single representative fish in a treated group with EMB against PTZ treated, control and PTZ negative control at day-10 in a three-axis maze.

group. In comparison with the PTZ administered group, non-significant downregulation in INF-γ mRNA expression levels was observed in the EMB (0.635 mg/kg) treated group as shown in **Figure 5E**.

DISCUSSION

The development of new drug treatment for chronic epilepsy induced cognitive dysfunction has largely stalled with very minor advances over the past few decades (Witt and Helmstaedter, 2017). In fact, in addition to minimizing seizures, the currently available AEDs produces cognitive alterations in around one-third of the epileptic patients (Witt and Helmstaedter, 2017). Herein, current study utilizes multifaceted approach and for the very first time develop PTZ kindling induced chronic epilepsy which significantly altered memory as compared to KA. We also evaluated the therapeutic potential of EMB against PTZ kindled chronic epilepsy and related cognitive alterations. In addition to that, modulation of several neurotransmitters and inflammatory genes by EMB treatment of varying doses (0.156, 0.312 and 0.612 mg/kg) has opened new therapeutic approach to deal with epilepsy and related memory problems (van Vliet et al., 2018).

Chronic epilepsy is a complex brain disorder exhibiting multiple underlying known and unknown causes with poorly understood mechanisms (Staley, 2015). Impairment of learning and memory is frequently observed in long-term epileptic patients and chronic epilepsy (Paudel et al., 2018b). To the best of our knowledge, current options to treat epilepsy only help with seizures and do not help to improve cognitive impairment, or standard AEDs contribute to impaired memory in patients with epilepsy (Santulli et al., 2016). In relation to that, current investigation shed light on the development of natural product-based novel therapy of using pro-inflammatory targets that can ameliorate chronic seizure as well as associated cognitive alterations (Barker-Haliski et al., 2017).

In spite of growing interest of utilizing zebrafish as an experimental model, much more remained to learned about the spatial cognitive abilities of zebrafish in the epileptic condition as compared to more widely used mammalian species (Meshalkina et al., 2017a). Zebrafish is one of the most emerging model systems to study neurologically related disorders and memory function (Fontana et al., 2018).

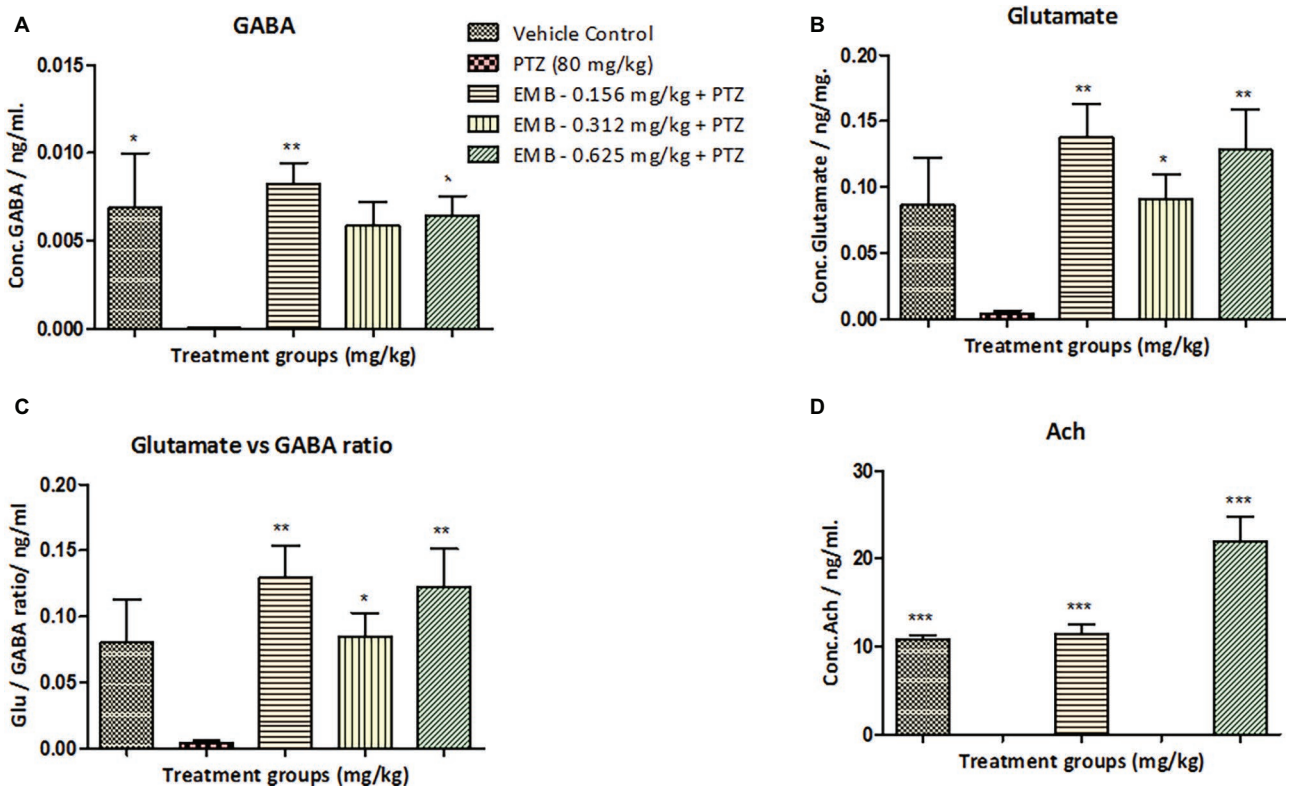

FIGURE 4 | Neurotransmitters analysis in zebrafish brain after 10 days of three-axis maze trial. **(A)** Represents the concentration of GABA in the zebrafish brain. **(B)** Represents concentration of glutamate in the zebrafish brain with *F*-value = 3.976, R-square = 0.4429, $p = 0.0156$. **(C)** Represents the ratio of glutamate over GABA showing a significant increase in glutamate levels against PTZ treated group with *F*-value = 5.5.4, R-square = 0.5240, $p = 0.0037$. **(D)** Represents concentration of acetylcholine (Ach) in the zebrafish brain with *F*-value = 41.86, R-square = 0.9331, $p = 0.0001$. In each neurotransmitter analysis, all the control and EMB treated groups are compared with negative control PTZ treated group. Data are represented as mean ± SEM, $n = 5$ and statistically analyzed by one-way ANOVA followed by Dunnett's test $^{*}p \leq 0.05$, $^{**}p \leq 0.01$, and $^{***}p \leq 0.001$.

Use of zebrafish as a model system is considered to be one of the most highly productive animal models with low cost, ease in doing an in-vivo pharmacodynamic study and easy tracking analysis of behavior study (Khan et al., 2017). Recently, a large number of studies related to PTZ-kindling are conducted on rodents which have high cost and is a time-consuming procedure (Kumar et al., 2016; Shimada and Yamagata, 2018). It is also known that once the rodents and large animals are epileptic they become difficult to handle, which is exactly opposite to zebrafish model (Meshalkina et al., 2017b). Zebrafish are easy to handle and inject, they are cost-effective, easy to maintain and feed, can adapt to new conditions quickly and produce a robust accurate result (Kearney, 2018). Moreover, zebrafish as an experimental model has been significantly important in the investigation elucidating epilepsy-related cognitive alterations (Stewart and Kalueff, 2012; Kundap et al., 2017).

Seizure-like behavioral and neurophysiological responses can be evoked in adult zebrafish by various genetic modifications and pro-convulsive chemicals that collectively strengthen the growing utility of this model for studying epilepsy (Kalueff et al., 2014). Moreover, learning and memory function can be tested in the zebrafish using various types of mazes like the T or Y axis maze, light/color preference test and three-axis maze (Nasir et al., 2012). In the neurological translational research, many advances have been made in understanding CNS and epilepsy-related problems, but there is still a lack of an animal model that can fully recapitulate the clinical phenotypes of human epilepsy-related cognitive dysfunction. In this regard, there is an increased understanding about the usability of zebrafish as an animal model in epilepsy research and has been demonstrated the features of human epilepsy (Mussulini et al., 2013, 2018).

PTZ (80 mg/kg) kindling acts *via* $GABA_A$ receptor induces epileptic seizures and disrupts the cognitive function for 10 days in adult zebrafish as observed on the three-axis maze test. Repeated administration of PTZ produces a chronic epilepsy-like condition in zebrafish along with the significant loss of cognitive performance in one of the three-axis mazes which is considered to be one of a complex maze. Repeated administration of small doses of PTZ (80 mg/kg) successfully induces a chronic epilepsy-like condition at least for 10 days as evidenced by increased seizure score. These findings were in agreement with an earlier reported study conducted using

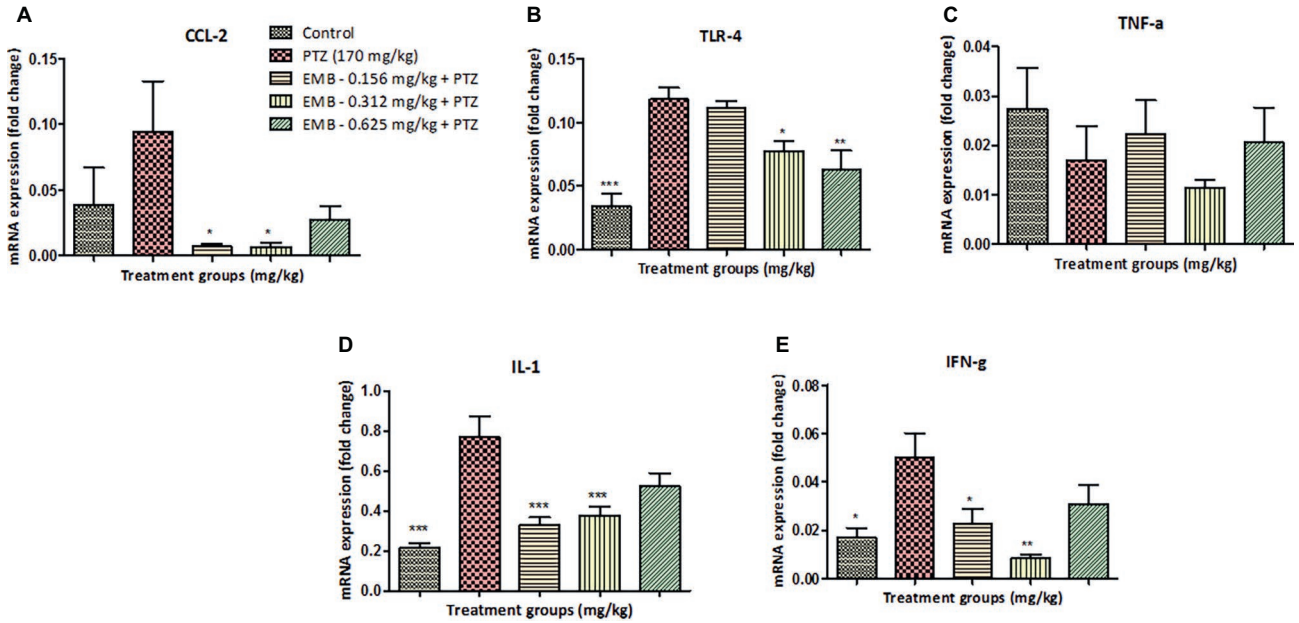

FIGURE 5 | EMB pre-treatment, reverse epilepsy that affects expression levels of several inflammatory genes. **(A)** Represents graph plot for CCL2 mRNA expression in the zebrafish brain with *F*-value = 3.564, R-square = 0.4712, $p = 0.0292$. **(B)** Represents graph plot of TLR-4 mRNA expression in the zebrafish brain with *F*-value = 12.98, R-square = 0.7644, $p = 0.0001$. **(C)** Represents graph plot for INF-γ mRNA expression in the zebrafish brain with *F*-value = 5.414, R-square = 0.5751, $p = 0.0059$. **(D)** Represents graph plot of IL-1 mRNA expression levels in the zebrafish brain with *F*-value = 12.4, R-square = 0.7121, $p = 0.0001$. **(E)** Represents graph plot of TNF-α mRNA expression in the zebrafish brain with *F*-value = 1.127, R-square = 0.2198, $p = 0.3788$. In each gene, all the control and EMB treated groups are compared with negative control PTZ treated group. Data are represented as mean ± SEM, $n = 5$ and statistically analyzed by one-way ANOVA followed by Dunnett's test $^{*}p \leq 0.05$, $^{**}p \leq 0.01$, and $^{***}p \leq 0.001$.

PTZ in a rat model reporting impaired memory and epileptic seizures (Golechha et al., 2010). Similar findings were reported earlier regarding PTZ kindling in rodents, where administration of PTZ resulted in a progressive increase in sensitivity of epileptic seizures (Löscher, 2017). Similarly, in the present study, a single dose of KA (3 mg/kg) failed to maintain the progressive increase in seizure sensitivity throughout the experiment. This finding was different from the findings from rodents where a single high dose of KA produces full-blown seizure (Demars et al., 2018). This might be due to the virtue (ability of excellence or performance) of zebrafish and its regenerative property which regenerates the damaged neurons and makes the fish less sensitive (Ceci et al., 2018). These findings implicate that a single dose of KA (3 mg/kg) lack (reduced in sensitivity or less sensitive) produce long term sensitivity in zebrafish for epileptic seizures.

The cognitive behavior of PTZ treated fish showed that latency to reach the feeding ring was high in PTZ treated fish as compared to the control group. It might be because PTZ treated fish could not find their way to the feeding ring and get repeatedly lost and backtrack to the previous compartment instead of moving forward to the feeding ring. This implies that PTZ kindling impairs memory in adult zebrafish. Interestingly, latency to reach the feeding ring in KA-treated fish was less than the PTZ treated group but was higher than the control group. This implies that though a single dose of KA (3 mg/kg) does not maintain a chronic epilepsy-like stage for 10 days, it still manages to disrupt the memory function for 10 days. All these findings are in agreement with the earlier findings reporting cognitive alteration in epileptic conditions (Black et al., 2010; Leeman-Markowski and Schachter, 2016). We observed that pre-treatment with different EMB doses rescued the fish from the epileptic stage as well as ameliorating its cognitive function. In addition, pre-treatment also reduces seizure scores and seizure intensity until day 10 as compared to PTZ treated fish. This finding strengthens the usability of EMB against chronic seizure-induced cognitive disruptions. However, evaluating the ameliorative potential of EMB against a range of seizure models and related cognitive impairments would further verify this statement.

Neurotransmitters play a crucial role in regulating neuronal excitation and maintaining normal behavior of the cognitive function (Moavero et al., 2017). Hypoactivity GABA leads to the increase in higher dopamine release, causing dopaminergic neurons to influence the GABAergic system to shut down through the $GABA_A$ receptor (Werner and Coveñas, 2011). Moreover, glutamate hyperactivity is influenced by n-methyl-D-aspartate (NMDA) receptor, inhibiting serotonin release *via* postsynaptic glutaminergic receptors, which can induce epileptic seizures (Lewerenz and Maher, 2015). In the

current investigation, in the EMB treated group the level of GABA was found to be significantly rescued back to control level as compared to the PTZ treated group, implicating the release of dopamine causing epileptic seizures. Also, an increase in the level of GABA in EMB treated group helps in controlling epileptic seizures. On the other hand, the level of glutamate was found to be elevated in the EMB treated group in comparison to the PTZ treated group, however, it does not affect epileptic behavior because the inhibitory GABA was controlling the hyperexcitation of neurons from glutamate (Medrihan et al., 2014). Ach has a crucial role in regulating attention, learning and short-term memory (Klinkenberg et al., 2011). Moreover, Ach has been implicated in controlling the release of glutamate in the brain during epileptic activity (Belousov et al., 2001). The current study documented the increased level of Ach in the EMB treated group compared to the PTZ treated group and reported a similar line of neurotransmitter levels as observed in our earlier studies after PTZ administration (Kundap et al., 2017).

The alteration of neurotransmitter is closely associated during the epileptic event. Many studies have shown the drastic increase in the level of inhibitory neurotransmitters like GABA in the epileptic brain (Swaminathan et al., 2018). The study suggests that proinflammatory biomarkers contribute to regulation of epilepsy-associated biochemical changes CNS. The neuroinflammatory markers like IL-1 TNF-α and INF-ϒ play an important role in regulating GABA expression and transportation of extracellular GABA in the brain (Su et al., 2015). The TLR-4 and RAGE inflammatory pathway is stimulated by one of the most important pro-inflammatory cytokines knows as HMGB1, which is responsible for the release of glutamate and causing hyperexcitability of the brain during epilepsy (Paudel et al., 2019).

There is an increased understanding of the role of inflammation in epileptic seizure (Vezzani and Granata, 2005; Vezzani et al., 2013). Inflammatory mediators are produced by glia, neurons, endothelial cells of the blood-brain barrier (BBB), and peripheral immune cells and might contribute to the onset and perpetuation of seizures in various types of epilepsy (Liu and Huang, 2011). Induction of recurrent seizures or single prolonged seizures by chemoconvulsants or electrical stimulation triggers rapid induction of inflammatory mediators in brain regions and upregulates CCL2 expression (Vezzani et al., 2011). Moreover, findings are emerging implicating the same inflammatory pathways in epilepsy and related neurobehavioral comorbidities including cognitive dysfunctions (Mazarati et al., 2017; Paudel et al., 2018b). Current study reported an increased level of CCL2 in PTZ kindled group. These findings are in corroboration with earlier findings reporting upregulation of CCL2 in the epileptic brain (Bozzi and Caleo, 2016). Interestingly, EMB treatment reduces the expression level of CCL2 as compared to the PTZ treated group. These findings are in agreement with the earlier findings reporting anti-inflammatory activities of EMB (Lee et al., 2018). These results are in line with the recent finding of anti-inflammatory activity of EMB in A549 cells and epithelial cell line (Ahmed, 2017).

TLR4 is the principal receptor for HMGB1 and has been implicated in seizure generation (Iori et al., 2017). The contribution of TLR4 in seizure generation is more than that of RAGE (Iori et al., 2013). This makes TLR4 worth exploring against several seizure models in order to elucidate the contribution of TLR4 in seizure generation. Similar to earlier findings (Maroso et al., 2010), we observed an increased level of TLR4 in the PTZ administered group suggesting its role in a seizure. EMB pre-treatment reduces the expression level of TLR4 which might be due to the prevention of epileptic seizure by EMB pre-treatment. The increased level of HMGB1 and TLR4 after pro-convulsant administration in current investigation supports the notion that HMGB1-TLR4 signaling may contribute to generating and perpetuating seizures (Maroso et al., 2010).

The effect of TNF-α on seizures depends mainly on its endogenous brain levels and the receptor subtypes predominantly stimulated by this cytokine (Vezzani and Granata, 2005). Few studies have reported the seizure inhibiting activity of TNF-α mainly *via* p75 receptors. Generally, the levels of TNF-α found to be elevated in seizure conditions, either in rodents (Ashhab et al., 2013) or in adult zebrafish (Choo et al., 2018). Surprisingly, we currently observed a non-significant decrease in the level of TNF-α after PTZ administration. However, this finding is in corroboration with the earlier reported study, reporting a decrease in TNF-α levels even after the pro-convulsant (pilocarpine) administration in rats (Marchi et al., 2007).

It was reported that IL-1 mediates upregulation of NMDA receptor in PTZ induced seizures causing epileptogenesis in the rat model (Yi et al., 2017). In an experimental model of status epilepticus (SE) triggered by electrical stimulation, brain mRNA expression level of IL-1 has been elevated (De Simoni et al., 2000). In a similar line, brain mRNA expression level of IL-1 was upregulated after PTZ administration. On the other side, EMB pre-treatment reduced the brain mRNA expression level of IL-1 suggesting its plausible anti-inflammatory potential.

IFN-γ plays an important role in the development of the brain's excitatory seizure pathways, and it has been associated with the development of limbic seizures (Borham et al., 2016). IFN-γ has been implicated in the seizure generation; this makes IFN-γ worth exploring in the current investigation. We observed an increased level of IFN-γ after PTZ administration, which is in support of an earlier study reporting elevated IFN-γ level in epileptic condition (Mao et al., 2013). Interestingly, EMB pre-treatment decreases the level of IFN-γ which might be since EMB pre-treatment prevents the epileptic seizure which in turn helps in preventing neuroinflammation. These overall findings from the current study suggest the possible anti-inflammatory potential of EMB in addition to seizure retarding and related memory improving potential. More studies describing the fact that embelin in the absence of PTZ or seizures can reduce neuroinflammation can be the point of interest for further researchers.

CONCLUSION

Herein, we conclude that EMB suppresses seizure-like behavior and improves cognitive function altered due to a chronic epilepsy

condition. EMB significantly modulates inflammatory genes affected by seizure and also affects neurotransmitter levels, which eventually improves the cognitive status of the animals. Moreover, behavioral observation, neurotransmitter analysis and gene expression results suggest that EMB can reverse learning and memory dysfunction associated with chronic epilepsy in a zebrafish model. Though we developed a KA-induced seizure model, we did not assess the ameliorative effect of embelin against KA-induced seizure and related cognitive alterations as a single KA dose did not produce chronic epilepsy like behavior similar to PTZ kindling. We acknowledge this part as a limitation of the current study. However, overall findings suggest that EMB has potential therapeutic value for the management of epilepsy and related cognitive alterations in experimental studies. However, further work is highly recommended to evaluate the therapeutic effects of EMB against genetic models and to compare its efficacy with current AEDs.

ETHICS STATEMENT

The experimental protocol was approved by the MARP Animal Ethics Committee, Monash University, Australia (MUM/2017/03 and MARP/2017/003).

AUTHOR CONTRIBUTIONS

UK performed the experiment, analysis of the results and writing of the manuscript. YP contributed to manuscript writing, result analysis and proofreading. YK contributed to the gene expression study and result analysis. IO contributed to LC-MS/MS study and result analysis. MS conceptualized the idea, contributed in the designing of the study, result interpretation & analysis, editing and proofreading of the manuscript. All authors have approved the final version of the manuscript.

FUNDING

This research work was supported by the eScience Fund of Ministry of Science, Technology, and Innovation (MOSTI), Malaysia (Grant No. 06-02-10-SF0250).

ACKNOWLEDGMENTS

We would like to thank Dr. Eric Samarut and Mr. Brandon Choo for the proofreading of the manuscript.

REFERENCES

Ahmed, R. (2017). Antiepileptic drugs and developmental neuroendocrine dysfunction: every why has A wherefore. *Arch. Med.* 9, 1–4. doi: 10.21767/1989-5216.1000244

Alfaro, J. M., Ripoll-Gómez, J., and Burgos, J. S. (2011). Kainate administered to adult zebrafish causes seizures similar to those in rodent models. *Eur. J. Neurosci.* 33, 1252–1255. doi: 10.1111/j.1460-9568.2011.07622.x

Ashhab, M. U., Omran, A., Kong, H., Gan, N., He, F., Peng, J., et al. (2013). Expressions of tumor necrosis factor alpha and microRNA-155 in an immature rat model of status epilepticus and children with mesial temporal lobe epilepsy. *J. Mol. Neurosci.* 51, 950–958. doi: 10.1007/s12031-013-0013-9

Banote, R. K., Koutarapu, S., Chennubhotla, K. S., Chatti, K., and Kulkarni, P. (2013). Oral gabapentin suppresses pentylenetetrazole-induced seizure-like behavior and cephalic field potential in adult zebrafish. *Epilepsy Behav.* 27, 212–219. doi: 10.1016/j.yebeh.2013.01.018

Barker-Haliski, M. L., Löscher, W., White, H. S., and Galanopoulou, A. S. (2017). Neuroinflammation in epileptogenesis: insights and translational perspectives from new models of epilepsy. *Epilepsia* 58, 39–47. doi: 10.1111/epi.13785

Barbosa, A., Maximino, C., Pereira, A. D. S. F., Wolkers, C. P. B., Alves, F. L., Ide, L. M., et al. (2012). "Rapid method for acute intracerebroventricular injection in adult zebrafish" in *Zebrafish Protocols for Neurobehavioral Research*. (Totowa, NJ: Humana Press), 323–330.

Belousov, A. B., O'hara, B. F., and Denisova, J. V. (2001). Acetylcholine becomes the major excitatory neurotransmitter in the hypothalamus in vitro in the absence of glutamate excitation. *J. Neurosci.* 21, 2015–2027. doi: 10.1523/JNEUROSCI.21-06-02015.2001

Black, L. C., Schefft, B. K., Howe, S. R., Szaflarski, J. P., Yeh, H.-S., and Privitera, M. D. (2010). The effect of seizures on working memory and executive functioning performance. *Epilepsy Behav.* 17, 412–419. doi: 10.1016/j.yebeh.2010.01.006

Borham, L. E., Mahfoz, A. M., Ibrahim, I. A., Shahzad, N., Alrefai, A. A., Labib, A. A., et al. (2016). The effect of some immunomodulatory and anti-inflammatory drugs on Li-pilocarpine-induced epileptic disorders in Wistar rats. *Brain Res.* 1648, 418–424. doi: 10.1016/j.brainres.2016.07.046

Bozzi, Y., and Caleo, M. (2016). Epilepsy, seizures, and inflammation: the role of the CC motif ligand 2 chemokine. *DNA Cell Biol.* 35, 257–260. doi: 10.1089/dna.2016.3345

Canevini, M. P., De Sarro, G., Galimberti, C. A., Gatti, G., Licchetta, L., Malerba, A., et al. (2010). The relationship between adverse effects of antiepileptic drugs, number of coprescribed drugs, and drug load in a large cohort of consecutive patients with drug-refractory epilepsy. *Epilepsia* 51, 797–804. doi: 10.1111/j.1528-1167.2010.02520.x

Ceci, M., Mariano, V., and Romano, N. (2018). Zebrafish as a translational regeneration model to study the activation of neural stem cells and the role of their environment. *Rev. Neurosci.* 30. doi: 10.1515/revneuro-2018-0020

Chen, Z., Brodie, M. J., Liew, D., and Kwan, P. (2018). Treatment outcomes in patients with newly diagnosed epilepsy treated with established and new antiepileptic drugs: a 30-year longitudinal cohort study. *JAMA Neurol.* 75, 279–286. doi: 10.1001/jamaneurol.2017.3949

Choo, B. K. M., Kundap, U. P., Kumari, Y., Hue, S.-M., Othman, I., and Shaikh, M. F. (2018). Orthosiphon stamineus leaf extract affects TNF-α and seizures in a zebrafish model. *Front. Pharmacol.* 9:139. doi: 10.3389/fphar.2018.00139

Dal-Pizzol, F., Klamt, F., Vianna, M. M., Schroder, N., Quevedo, J., Benfato, M. S., et al. (2000). Lipid peroxidation in hippocampus early and late after status epilepticus induced by pilocarpine or kainic acid in Wistar rats. *Neurosci. Lett.* 291, 179–182. doi: 10.1016/S0304-3940(00)01409-9

De Simoni, M. G., Perego, C., Ravizza, T., Moneta, D., Conti, M., Marchesi, F., et al. (2000). Inflammatory cytokines and related genes are induced in the rat hippocampus by limbic status epilepticus. *Eur. J. Neurosci.* 12, 2623–2633. doi: 10.1046/j.1460-9568.2000.00140.x

Demars, F., Clark, K., Wyeth, M. S., Abrams, E., and Buckmaster, P. S. (2018). A single subconvulsant dose of domoic acid at mid-gestation does not cause temporal lobe epilepsy in mice. *Neurotoxicology* 66, 128–137. doi: 10.1016/j.neuro.2018.04.001

Dey, A., Kang, X., Qiu, J., Du, Y., and Jiang, J. (2016). Anti-inflammatory small molecules to treat seizures and epilepsy: from bench to bedside. *Trends Pharmacol. Sci.* 37, 463–484. doi: 10.1016/j.tips.2016.03.001

Dhir, A. (2012). Pentylenetetrazol (PTZ) kindling model of epilepsy. *Curr. Protoc. Neurosci.* 58, 9.37.1–9.37.12. doi: 10.1002/0471142301.ns0937s58

Dubéarnès, A., Julius, A., and Utteridge, T. M. (2015). A synopsis of the genus Embelia in Peninsular Malaysia and Singapore. Studies in Malaysian Myrsinaceae III. *Kew Bull.* 70, 1–33.

Fontana, B. D., Mezzomo, N. J., Kalueff, A. V., and Rosemberg, D. B. (2018). The developing utility of zebrafish models of neurological and neuropsychiatric disorders: a critical review. *Exp. Neurol.* 299, 157–171. doi: 10.1016/j.expneurol.2017.10.004

Golechha, M., Bhatia, J., and Arya, D. S. (2010). Hydroalcoholic extract of Emblica officinalis Gaertn. affords protection against PTZ-induced seizures, oxidative stress and cognitive impairment in rats.

Helmstaedter, C. (2002). Effects of chronic epilepsy on declarative memory systems. *Prog. Brain Res.* 135, 439–453. doi: 10.1016/S0079-6123(02)35041-6

Iori, V., Iyer, A. M., Ravizza, T., Beltrame, L., Paracchini, L., Marchini, S., et al. (2017). Blockade of the IL-1R1/TLR4 pathway mediates disease-modification therapeutic effects in a model of acquired epilepsy. *Neurobiol. Dis.* 99, 12–23. doi: 10.1016/j.nbd.2016.12.007

Iori, V., Maroso, M., Rizzi, M., Iyer, A. M., Vertemara, R., Carli, M., et al. (2013). Receptor for advanced Glycation endproducts is upregulated in temporal lobe epilepsy and contributes to experimental seizures. *Neurobiol. Dis.* 58, 102–114. doi: 10.1016/j.nbd.2013.03.006

Kalueff, A. V., Stewart, A. M., and Gerlai, R. (2014). Zebrafish as an emerging model for studying complex brain disorders. *Trends Pharmacol. Sci.* 35, 63–75. doi: 10.1016/j.tips.2013.12.002

Kandratavicius, L., Balista, P. A., Lopes-Aguiar, C., Ruggiero, R. N., Umeoka, E. H., Garcia-Cairasco, N., et al. (2014). Animal models of epilepsy: use and limitations. *Neuropsychiatr. Dis. Treat.* 10:1693. doi: 10.2147/NDT.S50371

Kearney, J. A. (2018). Expanding the Zebrafish toolkit for epilepsy research. *Epilepsy Curr.* 18, 56–58. doi: 10.5698/1535-7597.18.1.56

Keezer, M. R., Sisodiya, S. M., and Sander, J. W. (2016). Comorbidities of epilepsy: current concepts and future perspectives. *Lancet Neurol.* 15, 106–115. doi: 10.1016/S1474-4422(15)00225-2

Khan, K. M., Collier, A. D., Meshalkina, D. A., Kysil, E. V., Khatsko, S. L., Kolesnikova, T., et al. (2017). Zebrafish models in neuropsychopharmacology and CNS drug discovery. *Br. J. Pharmacol.* 174, 1925–1944. doi: 10.1111/bph.13754

Klinkenberg, I., Sambeth, A., and Blokland, A. (2011). Acetylcholine and attention. *Behav. Brain Res.* 221, 430–442. doi: 10.1016/j.bbr.2010.11.033

Kumar, A., Nidhi, S., Manveen, B., and Sumitra, S. (2016). A review on chemical induced kindling models of epilepsy. *J. Vet. Med. Res.* 3, 1–6.

Kundap, U. P., Kumari, Y., Othman, I., and Shaikh, M. F. (2017). Zebrafish as a model for epilepsy-induced cognitive dysfunction: a pharmacological, biochemical and behavioral approach. *Front. Pharmacol.* 8:515. doi: 10.3389/fphar.2017.00515

Lee, I.-S., Cho, D.-H., Kim, K.-S., Kim, K.-H., Park, J., Kim, Y., et al. (2018). Anti-inflammatory effects of embelin in A549 cells and human asthmatic airway epithelial tissues. *Immunopharmacol. Immunotoxicol.* 40, 83–90. doi: 10.1080/08923973.2017.1414836

Leeman-Markowski, B. A., and Schachter, S. C. (2016). Treatment of cognitive deficits in epilepsy. *Neurol. Clin.* 34, 183–204. doi: 10.1016/j.ncl.2015.08.008

Lewerenz, J., and Maher, P. (2015). Chronic glutamate toxicity in neurodegenerative diseases—what is the evidence? *Front. Neurosci.* 9:469. doi: 10.3389/fnins.2015.00469

Liu, G.-J., and Huang, R.-Y. (2011). Inflammation and epilepsy. *Med. Rec.* 24:004.

Löscher, W. (2011). Critical review of current animal models of seizures and epilepsy used in the discovery and development of new antiepileptic drugs. *Seizure* 20, 359–368. doi: 10.1016/j.seizure.2011.01.003

Löscher, W. (2017). Animal models of seizures and epilepsy: past, present, and future role for the discovery of antiseizure drugs. *Neurochem. Res.* 42, 1873–1888. doi: 10.1007/s11064-017-2222-z

Mahendran, S., Thippeswamy, B., Veerapur, V., and Badami, S. (2011). Anticonvulsant activity of embelin isolated from Embelia ribes. *Phytomedicine* 18, 186–188. doi: 10.1016/j.phymed.2010.04.002

Mao, L. Y., Ding, J., Peng, W. F., Ma, Y., Zhang, Y. H., Fan, W., et al. (2013). Interictal interleukin-17 A levels are elevated and correlate with seizure severity of epilepsy patients. *Epilepsia* 54, e142–e145. doi: 10.1111/epi.12337

Marchi, N., Granata, T., and Janigro, D. (2014). Inflammatory pathways of seizure disorders. *Trends Neurosci.* 37, 55–65. doi: 10.1016/j.tins.2013.11.002

Marchi, N., Oby, E., Batra, A., Uva, L., De Curtis, M., Hernandez, N., et al. (2007). In vivo and in vitro effects of pilocarpine: relevance to ictogenesis. *Epilepsia* 48, 1934–1946. doi: 10.1111/j.1528-1167.2007.01185.x

Maroso, M., Balosso, S., Ravizza, T., Liu, J., Aronica, E., Iyer, A. M., et al. (2010). Toll-like receptor 4 and high-mobility group box-1 are involved in ictogenesis and can be targeted to reduce seizures. *Nat. Med.* 16:413. doi: 10.1038/nm.2127

Mazarati, A. M., Lewis, M. L., and Pittman, Q. J. (2017). Neurobehavioral comorbidities of epilepsy: role of inflammation. *Epilepsia* 58, 48–56. doi: 10.1111/epi.13786

Medrihan, L., Ferrea, E., Greco, B., Baldelli, P., and Benfenati, F. (2014). Asynchronous GABA release is a key determinant of tonic inhibition and controls neuronal excitability: a study in the Synapsin II–/– mouse. *Cereb. Cortex* 25, 3356–3368. doi: 10.1093/cercor/bhu141

Menezes, F. P., Rico, E. P., and Da Silva, R. S. (2014). Tolerance to seizure induced by kainic acid is produced in a specific period of zebrafish development. *Prog. Neuro-Psychopharmacol. Biol. Psychiatry* 55, 109–112. doi: 10.1016/j.pnpbp.2014.04.004

Meshalkina, D. A., Kizlyk, M. N., Kysil, E. V., Collier, A. D., Echevarria, D. J., Abreu, M. S., et al. (2017a). Understanding zebrafish cognition. *Behav. Process.* 141, 229–241. doi: 10.1016/j.beproc.2016.11.020

Meshalkina, D. A., Song, C., and Kalueff, A. V. (2017b). Better lab animal models for translational neuroscience research and CNS drug development. *Lab Anim.* 46:91. doi: 10.1038/laban.1236

Moavero, R., Santarone, M. E., Galasso, C., and Curatolo, P. (2017). Cognitive and behavioral effects of new antiepileptic drugs in pediatric epilepsy. *Brain Dev.* 39, 464–469. doi: 10.1016/j.braindev.2017.01.006

Mussulini, B. H. M., Leite, C. E., Zenki, K. C., Moro, L., Baggio, S., Rico, E. P., et al. (2013). Seizures induced by pentylenetetrazole in the adult zebrafish: a detailed behavioral characterization. *PLoS One* 8:e54515. doi: 10.1371/journal.pone.0054515

Mussulini, B. H. M., Vizuete, A. F. K., Braga, M., Moro, L., Baggio, S., Santos, E., et al. (2018). Forebrain glutamate uptake and behavioral parameters are altered in adult zebrafish after the induction of status Epilepticus by kainic acid. *Neurotoxicology*. 67, 305–312. doi: 10.1016/j.neuro.2018.04.007

Nasir, R., Choezom, T., Cunningham, J., Bajaj, B., Rubi, C., Butler, J., et al. (2012). "Measuring effects of psychostimulants on egocentric spatial learning and memory in adult zebrafish" in *Zebrafish protocols for neurobehavioral research* (Totowa, NJ: Springer), 247–256.

Ohno, Y., Ishihara, S., Terada, R., Serikawa, T., and Sasa, M. (2010). Antiepileptogenic and anticonvulsive actions of levetiracetam in a pentylenetetrazole kindling model. *Epilepsy Res.* 89, 360–364. doi: 10.1016/j.eplepsyres.2010.01.011

Parker, M. O., Millington, M. E., Combe, F. J., and Brennan, C. H. (2012). Housing conditions differentially affect physiological and behavioural stress responses of zebrafish, as well as the response to anxiolytics. *PLoS One* 7:e34992. doi: 10.1371/journal.pone.0034992

Paudel, Y. N., Semple, B. D., Jones, N. C., Othman, I., and Shaikh, M. F. (2019). High mobility group box 1 (HMGB 1) as a novel frontier in epileptogenesis: from pathogenesis to therapeutic approaches. *J. Neurochem.* doi: 10.1111/jnc.14663

Paudel, Y. N., Shaikh, M., Serrano, Á. A., Kumari, Y., Aleksovska, K., Alvim, M. K. M., et al. (2018a). HMGB1: a common biomarker and potential target for TBI, neuroinflammation, epilepsy and cognitive dysfunction. *Front. Neurosci.* 12, 1–19. doi: 10.3389/fnins.2018.00628

Paudel, Y. N., Shaikh, M. F., Shah, S., Kumari, Y., and Othman, I. (2018b). Role of inflammation in epilepsy and neurobehavioral comorbidities: implication for therapy. *Eur. J. Pharmacol.* 837, 145–155. doi: 10.1016/j.ejphar.2018.08.020

Poojari, R. (2014). Embelin–a drug of antiquity: shifting the paradigm towards modern medicine. *Expert Opin. Investig. Drugs* 23, 427–444. doi: 10.1517/13543784.2014.867016

Ravizza, T., Terrone, G., Salamone, A., Frigerio, F., Balosso, S., Antoine, D. J., et al. (2017). High mobility group box 1 is a novel pathogenic factor and a mechanistic biomarker for epilepsy. *Brain Behav. Immun.* 14–21. doi: 10.1016/j.bbi.2017.10.008

Remy, S., and Beck, H. (2005). Molecular and cellular mechanisms of pharmacoresistance in epilepsy. *Brain* 129, 18–35. doi: 10.1093/brain/awh682

Samarut, É. (2016). Zebrafish embryos as in vivo test tubes to unravel cell-specific mechanisms of neurogenesis during neurodevelopment and in diseases. *Neurogenesis* 3:e1232678. doi: 10.1080/23262133.2016.1232678

Samarut, É., Lissouba, A., and Drapeau, P. (2016). A simplified method for identifying early CRISPR-induced indels in zebrafish embryos using high

resolution melting analysis. *BMC Genomics* 17:547. doi: 10.1186/s12864-016-2881-1

Santulli, L., Coppola, A., Balestrini, S., and Striano, S. (2016). The challenges of treating epilepsy with 25 antiepileptic drugs. *Pharmacol. Res.* 107, 211–219. doi: 10.1016/j.phrs.2016.03.016

Shams, S., Rihel, J., Ortiz, J. G., and Gerlai, R. (2018). The zebrafish as a promising tool for modeling human brain disorders: a review based upon an IBNS symposium. *Neurosci. Biobehav. Rev.* 85, 176–190. doi: 10.1016/j.neubiorev.2017.09.002

Shankar, R., Lavekar, G., Deb, S., Sharma, B., and Rawat, M. (2012). Distribution, conservation and folk uses of Vaibidang (*Embelia ribes* Burm. f.). *Int. J. Biodiversity Conserv.* 4, 525–529. doi: 10.5897IJBC12.046

Shimada, T., and Yamagata, K. (2018). Pentylenetetrazole-induced kindling mouse model. *J. Vis. Exp.* e56573. doi: 10.3791/56573

Singh, A., and Trevick, S. (2016). The epidemiology of global epilepsy. *Neurol. Clin.* 34, 837–847. doi: 10.1016/j.ncl.2016.06.015

Staley, K. (2015). Molecular mechanisms of epilepsy. *Nat. Neurosci.* 18:367. doi: 10.1038/nn.3947

Stewart, A., Cachat, J. M., Suciu, C., Hart, P. C., Gaikwad, S., Utterback, E., et al. (2011). "Intraperitoneal injection as a method of psychotropic drug delivery in adult zebrafish" in *Zebrafish neurobehavioral protocols* (Humana Press), Vol. 51, 169–179.

Stewart, A. M., and Kalueff, A. V. (2012). The developing utility of zebrafish models for cognitive enhancers research. *Curr. Neuropharmacol.* 10, 263–271. doi: 10.2174/157015912803217323

Su, J., Yin, J., Qin, W., Sha, S., Xu, J., and Jiang, C. (2015). Role for pro-inflammatory cytokines in regulating expression of GABA transporter type 1 and 3 in specific brain regions of kainic acid-induced status epilepticus. *Neurochem. Res.* 40, 621–627. doi: 10.1007/s11064-014-1504-y

Swaminathan, A., Hassan-Abdi, R., Renault, S., Siekierska, A., Riché, R., Liao, M., et al. (2018). Non-canonical mTOR-independent role of DEPDC5 in regulating GABAergic network development. *Curr. Biol.* 28, 1924–1937.e5 doi: 10.1016/j.cub.2018.04.061

van Vliet, E. A., Aronica, E., Vezzani, A., and Ravizza, T. (2018). Neuroinflammatory pathways as treatment targets and biomarker candidates in epilepsy: emerging evidence from preclinical and clinical studies. *Neuropathol. Appl. Neurobiol.* 44, 91–111. doi: 10.1111/nan.12444

Vezzani, A. (2005). Inflammation and epilepsy. *Epilepsy Curr.* 5, 1–6. doi: 10.1111/j.1535-7597.2005.05101.x

Vezzani, A., Aronica, E., Mazarati, A., and Pittman, Q. J. (2013). Epilepsy and brain inflammation. *Exp. Neurol.* 244, 11–21. doi: 10.1016/j.expneurol.2011.09.033

Vezzani, A., French, J., Bartfai, T., and Baram, T. Z. (2011). The role of inflammation in epilepsy. *Nat. Rev. Neurol.* 7:31. doi: 10.1038/nrneurol.2010.178

Vezzani, A., and Granata, T. (2005). Brain inflammation in epilepsy: experimental and clinical evidence. *Epilepsia* 46, 1724–1743. doi: 10.1111/j.1528-1167.2005.00298.x

Werner, F.-M., and Coveñas, R. (2011). Classical neurotransmitters and neuropeptides involved in generalized epilepsy: a focus on antiepileptic drugs. *Curr. Med. Chem.* 18, 4933–4948. doi: 10.2174/092986711797535191

Wilcox, K. S., Dixon-Salazar, T., Sills, G. J., Ben-Menachem, E., Steve White, H., Porter, R. J., et al. (2013). Issues related to development of new antiseizure treatments. *Epilepsia* 54, 24–34. doi: 10.1111/epi.12296

Witt, J.-A., and Helmstaedter, C. (2017). Cognition in epilepsy: current clinical issues of interest. *Curr. Opin. Neurol.* 30, 174–179. doi: 10.1097/WCO.0000000000000430

Yi, P.-L., Chou, Y.-J., and Chang, F.-C. (2017). IL-1 signal and NMDA receptor in PTZ-induced epilepsy and sleep disruption. *Sleep Med.* 40:e355. doi: 10.1016/j.sleep.2017.11.1047

Zhang, B., Zhang, J. W., Wang, W. P., Dong, R. F., Tian, S., and Zhang, C. (2017). Effect of lamotrigine on epilepsy-induced cognitive impairment and hippocampal neuronal apoptosis in pentylenetetrazole-kindled animal model. *Synapse* 71:e21945. doi: 10.1002/syn.21945

Zheng, X. Y., Zhang, H. L., Luo, Q., and Zhu, J. (2011). Kainic acid-induced neurodegenerative model: potentials and limitations. *J. Biomed. Biotechnol.* 2011:457079. doi: 10.1155/2011/457079

Conflict of Interest Statement: The authors declare that the research was conducted in the absence of any commercial or financial relationships that could be construed as a potential conflict of interest.

frontiers in Pharmacology

ORIGINAL RESEARCH
published: 24 April 2019
doi: 10.3389/fphar.2019.00385

DNMT Inhibitors Increase Methylation in the Cancer Genome

Anil K. Giri[1]* *and Tero Aittokallio*[1,2,3]*

[1] Institute for Molecular Medicine Finland, University of Helsinki, Helsinki, Finland, [2] Helsinki Institute for Information Technology, Department of Computer Science, Aalto University, Espoo, Finland, [3] Department of Mathematics and Statistics, University of Turku, Turku, Finland

DNA methyltransferase inhibitors (DNMTi) decitabine and azacytidine are approved therapies for myelodysplastic syndrome and acute myeloid leukemia, and their combinations with other anticancer agents are being tested as therapeutic options for multiple solid cancers such as colon, ovarian, and lung cancer. However, the current therapeutic challenges of DNMTis include development of resistance, severe side effects and no or partial treatment responses, as observed in more than half of the patients. Therefore, there is a critical need to better understand the mechanisms of action of these drugs. In order to discover molecular targets of DNMTi therapy, we identified 638 novel CpGs with an increased methylation in response to decitabine treatment in HCT116 cell lines and validated the findings in multiple cancer types (e.g., bladder, ovarian, breast, and lymphoma) cell lines, bone marrow mononuclear cells from primary leukemia patients, as well as peripheral blood mononuclear cells and ascites from platinum resistance epithelial ovarian cancer patients. Azacytidine treatment also increased methylation of these CpGs in colon, ovarian, breast, and lymphoma cancer cell lines. Methylation at 166 identified CpGs strongly correlated ($|r| \geq 0.80$) with corresponding gene expression in HCT116 cell line. Differences in methylation at some of the identified CpGs and expression changes of the corresponding genes was observed in TCGA colon cancer tissue as compared to adjacent healthy tissue. Our analysis revealed that hypermethylated CpGs are involved in cancer cell proliferation and apoptosis by P53 and olfactory receptor pathways, hence influencing DNMTi responses. In conclusion, we showed hypermethylation of CpGs as a novel mechanism of action for DNMTi agents and identified 638 hypermethylated molecular targets (CpGs) common to decitabine and azacytidine therapy. These novel results suggest that hypermethylation of CpGs should be considered when predicting the DNMTi responses and side effects in cancer patients.

Keywords: DNA methyltransferase inhibitors, decitabine, azacytidine, anticancer treatment, olfactory receptor pathway, alternative splicing

OPEN ACCESS

Edited by:
Ioanna Andreadou, National and Kapodistrian University of Athens, Greece

Reviewed by:
Giuseppe Toffoli, Centro di Riferimento Oncologico di Aviano (IRCCS), Italy
Tiziana Bonaldi, Istituto Europeo di Oncologia s.r.l., Italy

***Correspondence:**
Anil K. Giri
anil.kumar@helsinki.fi
Tero Aittokallio
tero.aittokallio@helsinki.fi

Specialty section:
This article was submitted to Experimental Pharmacology and Drug Discovery, a section of the journal Frontiers in Pharmacology

Received: *19 November 2018*
Accepted: *27 March 2019*
Published: *24 April 2019*

Citation:
Giri AK and Aittokallio T (2019) DNMT Inhibitors Increase Methylation in the Cancer Genome. Front. Pharmacol. 10:385. doi: 10.3389/fphar.2019.00385

INTRODUCTION

DNA methyltransferase inhibitors (DNMTi) are widely used as chemical tools for hypomethylating the genome, with an aim to understand the role of DNA methylation in multiple processes (e.g., X-chromosome inactivation and DNA imprinting) and as an anti-cancer therapy (Minkovsky et al., 2015; Ramos M.P. et al., 2015; Bohl et al., 2018). At present, two DNMTi drugs, decitabine and

azacytidine, have been approved for treating patients with myelodysplastic syndrome (MDS) and acute myeloid leukemia (AML) (Döhner et al., 2017; Bohl et al., 2018), and are also being tested as therapeutic options in multiple solid cancers (Fu et al., 2011; Singal et al., 2015; Lee et al., 2018). However, treatment response rates have remained very low in both solid and hematological cancers patients (Derissen et al., 2013; Nervi et al., 2015; Koch et al., 2018). At the same time, DNMTi treatment incurs considerable side effects (e.g., bleeding, anemia, and joint pain). Attempts are being made to improve treatment efficacy (e.g., by testing combinations of DNMTis with other anticancer agents) and safety (e.g., by stratifying cancer patients into DNMTi responders and non-responders) (Nervi et al., 2015) of the drugs. However, the precise prediction of drugs that show synergy with DNMTi in combination as well as distinguishing the drug responders from the non-responders are challenging tasks and are currently compromised by our incomplete knowledge of the drug mechanisms of action in various cancer-types (Ramos F. et al., 2015; Wang et al., 2018).

Hypomethylation of the genome is one of the principal mechanisms behind the therapeutic benefit of DNMTi treatment and hypomethylated targets of the drugs (e.g., CpGs, genes, genomic region, pathways) have been functionally well-characterized in multiple cancer cell lines and other model systems (Sarkar et al., 2013; Tobiasson et al., 2017; Koch et al., 2018). However, DNMTi induced hypomethylation of the genome is not sufficient to clearly understand DNMTis' response and side effects (Ramos F. et al., 2015; Wang et al., 2018), suggesting presence of additional mechanisms by which DNMTis' may modulate their responses. Therefore, there is a critical need to better understand the mechanism of action of DNMTis' in more details, including their molecular targets in various cancer cells. Only a few studies indicated that DNMTi treatment can also lead to DNA hypermethylations in specific cell types, probably due to an increased expression of DNA methylating enzymes (Broday et al., 1999; Kastl et al., 2010; Chowdhury et al., 2015). For example, Kastl et al. (2010) reported an increase in the mRNA level of DNMT1, DNMT3a, and DNMT3b genes in docetaxel-resistant MCF7 cells, as compared to drug-sensitive cells when treated with decitabine. However, we currently lack the information of the genomic location and function of molecular targets in the cancer genome that can resist the DNA demethylation and show hypermethylation in response to DNMTi treatment.

In the present work, we hypothesized that DNMTi treatment causes hypermethylation in the genome, and therefore we systematically investigated the extent of hypermethylated CpGs, their location, and biological role by analyzing cell line and primary tumor data. Since colon cancer tissue has revealed silencing of various tumor suppressor genes due to hypermethylation (Huidobro et al., 2012), and especially the HCT116 cell line has widely been utilized to study DNA methylation and its role in regulating gene expression in colon cancer (De Carvalho et al., 2012; Yang et al., 2014), we selected HCT116 cell line as our primary disease model to discover novel hypermethylated CpGs. We validated the findings in a panel of 53 other cancer cell lines (e.g., lymphoma, colon, ovarian, and breast cancer), as well as in bone marrow cells of 2 primary leukemia patients, 2 PBMCs and 2 ascites samples of ovarian cancer patients. There was a significant correlation in the methylation of a fraction of identified CpGs and corresponding genes' expression in HCT116 cell line indicating that the identified hypermethylated CpGs are clinically functional. Our work aims at initiating the search of hypermethylation in the response to DNMTi treatment in cancer cells and tissues as a novel mechanism by which one could predict in future the therapeutic and adverse effects of DNMTis in multiple cancer sub-types (i.e., stratified medicine), or even in individual cancer patients (i.e., personalized medicine).

MATERIALS AND METHODS

Processing of Published Methylation Data

To identify CpGs with increased methylation after decitabine treatment, we re-analyzed the DNA methylation (Illumina 450K platform, GSE51810) data from the study of Yang et al. (2014), where colon cancer HCT116 cells were treated with decitabine (0.3 mM) for 72 h. Cells were maintained in McCoy's 5A medium, supplemented with 10% fetal bovine serum along with 1% penicillin/streptomycin after drug treatment, and followed through 5, 14, 24, 42, and 68 days. The increase in DNA methylation in HCT116 cells were validated using methylation data from the study of Han et al. (2013) (Illumina 450K, GSE41525), where HCT116 and T24 bladder cancer cell lines were treated with 0.3 and 1 μM of decitabine, respectively, for 24 h, and Illumina 450K assay was performed for both untreated and decitabine-treated cells. We also tested the increase in DNA methylation of identified CpGs using DMSO (as mock treatment) and decitabine-treated (0.06 μM for 72 h) MCF7 breast cancer cells using data generated by Leadem et al. (2018) (Illumina 450K platform, GSE97483). These cells were cultured in Minimum Essential Medium (MEM) with 10% fetal bovine serum).

Further, we validated our findings identified in cell lines using DNA methylation data from primary bone marrow mononuclear cells (Illumina 450K platform, GSE20945-GPL13534) from two freshly diagnosed acute myelogenous leukemia patients (IDs 1107 and 1307) and one healthy control (BM) (Tsai et al., 2012). The frozen primary cells were thawed and cultured in Poietics HPGM supplemented with 50 ng/ML human thrombopoietin, 25 ng/mL stem cell factor, 50 ng/mL Flt-3 ligand, 10 ng/mL recombinant human IL-3, 10 ng/mL recombinant human IL-6, 10 ng/mL recombinant human GM-CSF and 1 ng/mL recombinant human G-CSF, as specified in Tsai et al. (2012). These cells have been treated with 10 nM of decitabine or PBS (control) for 72 h with daily medium change. DNA methylation for patient 1307 was assessed at day 3 as well as day 14 and for patient 1107 at day 7. We also analyzed genome wide DNA methylation (Illumina Infinium 27K Beadchip, GSE31826) profile of 14 peripheral blood mononuclear cells (PBMC), 8 tumor biopsies and 6 ascites samples from recurrent, platinum resistant epithelial ovarian cancer patients, before and after treatment with decitabine (Matei et al., 2012). Patients have been treated with decitabine (Eisai) at

10 mg/m^2 given intravenously daily for 5 days. The methylation for each sample was measured before treatment at day 1 (control) and after decitabine treatment at day 8 (treated). The comparison of treated and control samples was done using the paired Wilcoxon non-parametric test on the basis of 16 common CpGs (out of 638) with hypermethylation.

We extended our discovery analyses also to another DNMTi inhibitor, azacytidine, by re-analyzing DNA methylation data (Illumina 450K, GSE45707) for untreated and azacytidine-treated (5 mM for 72 h) lymphoma U937 cell line. We further re-analyzed additional methylation (Illumina 450K platform, GSE57342) and gene expression data (GSE57343) from 26 breast cancer cell lines (MDA231, SKBR3, HCC38, ZR7530, HCC1937, CAMA1, MDA415, HCC1500, BT474, EFM192A, MDA175, MDA468, MDA361, HCC1954, BT20, ZR751, HCC1569, EFM19, T47D, MDA453, MCF7, HCC1187, HCC1419, MDA436, SUM149, and SUM159), 12 colorectal cancer cell lines (SW48, HCT116, HT29, RKO, SW480, Colo320, Colo205, SW620, SNUC-1, CACO-2, SK-CO1, and Colo201), and 13 ovarian cancer cell lines (TykNu, CAOV3, OAW28, OV2008, ES2, EF27, Kuramochi, OVKATE, Hey, A2780, OVCAR3, OVCAR5, and SKOV3) measured after mock treatment and 0.5 μM azacytidine treatment for 72 h (Li et al., 2014). The cells were cultured and maintained under recommended conditions for each cell line (Li et al., 2014).

To investigate the alteration in methylation status of identified probes in cancerous tissue and their role in gene expression regulation, TCGA level 3 HumanMethylation 450K data and normalized RNA-seq gene expression profiles for colon adenocarcinoma (COAD) patients (both tumor and adjacent healthy tissue samples) were downloaded using the FireBrowse tool[1].

In all the analysis, methylation status at a CpG site was measured as beta value (β), which is the ratio of the methylated probe intensity and the overall intensity (sum of methylated and unmethylated probe intensities designed for a particular CpG in 450K beadchip). β ranges from 0 to 1, indicating no methylation (β = 0) to complete methylation of the CpGs (β = 1). We performed appropriate quality control of the published data before their downstream analysis as described previously (Giri et al., 2017). As a part of quality control, we removed all the CpGs with missing values and CpGs assessed by probes that have a tendency of cross-hybridization, as specified in the supplementary file of Chen et al. (2013). To remove any possible bias due to design differences in the type of probes (the type I and type II probes) present in the Illumina 450K platform, we performed BMIQ normalization (Teschendorff et al., 2013) to the DNA methylation data from the TCGA samples before correlation and differential methylation analysis. All other data processing was done using local inbuilt commands in R.

Identification of Probes With Increased Methylation in HCT116 Cell Line

We calculated the difference in methylation level of CpGs before and after treatment with decitabine in HCT116 cell line at day 5 in data from Yang et al. (2014) (GSE51810). CpG that showed an increase in β-value of greater than or equal to 0.10 ($\Delta\beta \geq 0.10$) between untreated control and decitabine treated HCT116 cells were identified as hypermethylated CpGs. The population doubling time reported by Yang et al. (2014) was used for correlation analysis with methylation level of identified CpGs. We estimated population doubling time as 24 h for untreated cells and 34, 38, 31, 28, 26, and 25.5 h for treated cells at time points of 5, 14, 24, 42, and 68 days.

Gene Expression Data Analysis

We downloaded gene expression profiles of untreated control and decitabine treated HCT116 cell lines at 5, 14, 24, and 42 days (GSE51811, Illumina HumanHT-12 V4.0 expression beadchip) from the same study of Yang et al. (2014). The downloaded data were $\log_2$-transformed and normalized using robust spline normalization (RSN) method as implemented in the lumi package in R (Du et al., 2008). Pearson correlation between methylation and gene expression across different time points in HCT116 cell line was assessed using the cor.test function of R.

Normalized RNA-seq data of TCGA colon adenocarcinoma patients downloaded from FireBrowse tool[1] were further normalized using voom function in the limma package (Ritchie et al., 2015), and these data were Z-transformed before the differential and correlation analyses. Wilcoxon non-parametric test was used to identify differentially methylated and differentially expressed genes between TCGA adenocarcinoma tumors and adjacent healthy tissue samples (FDR < 0.05). Only those adenocarcinoma samples that had both DNA methylation and gene expression information were used for the correlation analyses.

In order to find the possible reasons for absence of hypermethylation by low dose treatment with azacytidine in breast cancer cell lines, we extracted and compared the gene expression DNMT3A, DNMT3B, DNMT1, and DNMTL across 26 breast cancer, 12 colorectal cancer, and 13 ovarian cancer cell lines at day 3 (after azacytidine treatment) using gene expression data from Li et al. (2014) (GSE57343). We downloaded the processed gene expression data of azacytidine treated cells normalized to mock treated respective controls and compared across cell lines of different tissue types.

Gene Annotation and Pathway Enrichment Analysis

Identified CpGs were annotated for their location in the genome based on annotation file provided by Illumina[2]. Gene ontology and pathway enrichment analysis of the genes corresponding to CpGs with hypermethylation were done using GeneCodis (Tabas-Madrid et al., 2012). Statistical enrichment was assessed by FDR corrected *p*-values from hypergeometric test for separate ontology terms and pathways. GENEMANIA (Zuberi et al., 2013) was used to construct and visualize the interaction network between genes and the transcription factor regulating them.

[1] http://gdac.broadinstitute.org/

[2] ftp://ussd-ftp.illumina.com/downloads/ProductFiles/HumanMethylation450/HumanMethylation450_15017482_v1-2.csv

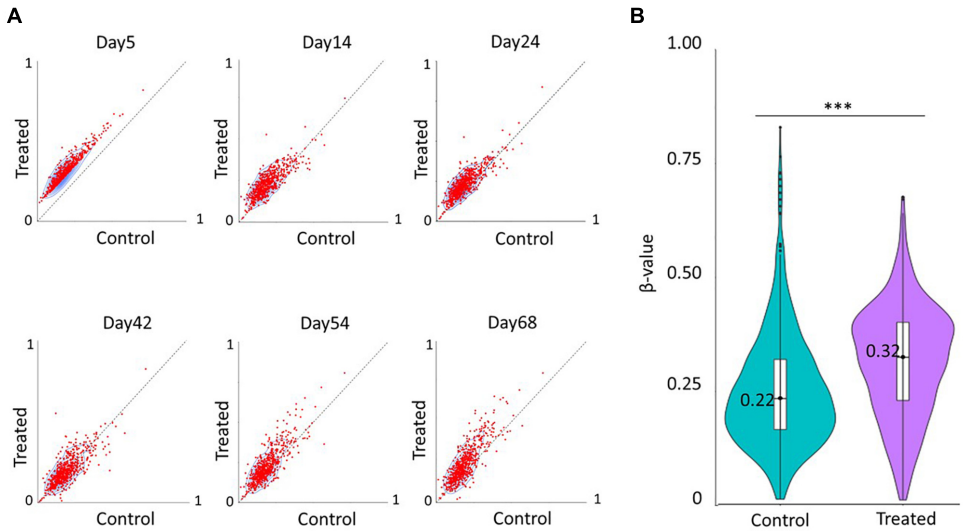

FIGURE 1 | Decitabine treatment increases DNA methylation levels of a subset of CpGs. **(A)** Scatter plots showing DNA methylation patterns of 638 differentially methylated CpGs between untreated control cells (x-axis) and decitabine-treated cells (y-axis) at various time points in the study of Yang et al. (2014). **(B)** Violin plot showing the median methylation level (horizontal line) and distribution patterns (density and IQR) of the identified 583 CpGs in untreated and 0.3 μM decitabine-treated HCT116 cells after 24 h in the study of Han et al. (2013). The statistical significance was assessed using the non-parametric Wilcoxon test. ***$p < 0.0005$.

Key term enrichment analysis for the genes corresponding to CpGs was done using DAVID (Huang Da et al., 2009).

RESULTS

DNMTi Treatment Increases Methylation of a Small Portion of the CpGs

After quality control, we re-analyzed a total of 369886 CpGs across the genome of HCT116 colon cancer cells from Yang et al. (2014), and identified hypermethylation ($\Delta\beta \geq 0.10$) of 638 CpGs in 393 unique genes after 5 days of decitabine treatment (0.3 mM for 72 h), as compared to untreated cells (**Figure 1A**). Most of the loci were hypomethylated in the genome (median $\beta = 0.18$), and after decitabine treatment, a median increase of 0.12 ($\Delta\beta = 0.12$, $p < 0.0005$) in methylation level was observed for these sites. The detailed list of the identified CpGs is provided in **Supplementary Table 1**. Change in methylation at 34 of the identified CpGs were strongly correlated (Pearson correlation coefficient > 0.80, FDR <0.05) with the population doubling time of HCT116 cell lines after decitabine treatment (**Supplementary Table 2**), indicating that methylation at a fraction of identified CpGs affects proliferation and growth of cancer cells. However, most of the identified sites loss their hypermethylation by day 10 (**Figure 1**) suggesting that the observed hypermethylation is transient. Re-analysis of another methylation data for HCT116 cell line from the Han et al. (2013) study validated our finding, as we found a corresponding increase in methylation level (median $\Delta\beta = 0.09$) at 583 common CpGs after decitabine treatment (0.3 μM for 24 h) (**Figure 1B**). These results indicate that the increase in DNA methylation at most of the identified sites starts as early as 24 h after the DNMTi treatment and lasts up to at least day 5. The result suggests that there are CpGs that not only resist the demethylation in response to DNMTi but also show transient hypermethylation.

Further, we also tested the effect of decitabine on identified differentially methylated CpGs in a bladder cancer cell line (T24). An increase in median DNA methylation levels (median $\Delta\beta = 0.14$, $p < 0.0005$) at 616 common CpGs was observed after the drug treatment (1 μM for 24 h) in T24 cells (**Figure 2A**) in contrast to a significant decrease in the methylation level of other CpGs present in the 450K beadchip (median $\Delta\beta = -0.14$) as shown in **Supplementary Figure 1**. However, we did not observe any increase in methylation level of 590 common identified CpGs (median $\Delta\beta = -0.01$, $p < 0.0005$) in breast cancer MCF7 cell line treated with 0.06 μM of decitabine for 72 h (**Figure 2B**). Replication of the results in multiple cancer cell lines indicates that hypermethylation in the cancer genome is a common effect of decitabine treatment that can contribute to DNMTis' response.

To study the effect of another DNMT inhibitor, azacytidine, on methylation of identified CpGs, we next re-analyzed 450K data from 52 pan-cancer cell lines. We found a significant increase in methylation of identified CpGs in 9 out of 13 ovarian cancer cell lines (median $\Delta\beta > 0.03$), 3 out of 26 breast cancer cell lines (median $\Delta\beta > 0.01$), and in 9 out of 12 colon cancer cell lines (median $\Delta\beta > 0.02$), and in 1 lymphoma cell line (U937, median $\Delta\beta > 0.06$) after azacytidine treatment (**Figures 3A–D**). Validation of the observed hypermethylation at identified target CpGs in multiple cancer types (bladder, ovarian, breast, and lymphoma cancer cell lines) suggests that hypermethylation in the genome is a shared phenomenon in response to multiple DNMTi agents and that the degree of the hypermethylation is cancer- and cell line-specific.

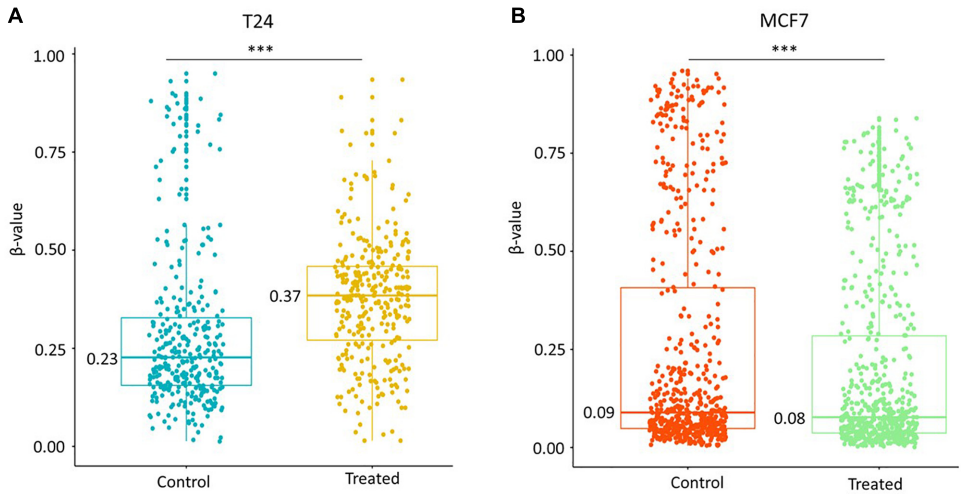

FIGURE 2 | Increase in methylation of identified CpGs is cell line-specific. **(A)** Methylation level of 616 identified probes common in untreated and decitabine-treated (1 μM for 24 h) bladder cancer T24 cell line. An increase in median DNA methylation levels (median $\Delta\beta = 0.14$) at 616 common CpGs was observed after the drug treatment. **(B)** Methylation level of 590 identified probes common in mock (DMSO) and decitabine-treated (0.06 μM for 72 h) breast cancer MCF7 cell line. We observed a smaller decrease in methylation level (median $\Delta\beta = -0.01$, $p < 0.005$) when the cells were treated with lower dose (0.06 μM) of decitabine in MCF7 cell lines. The statistical significance was assessed using the non-parametric Wilcoxon test. ***$p < 0.0005$.

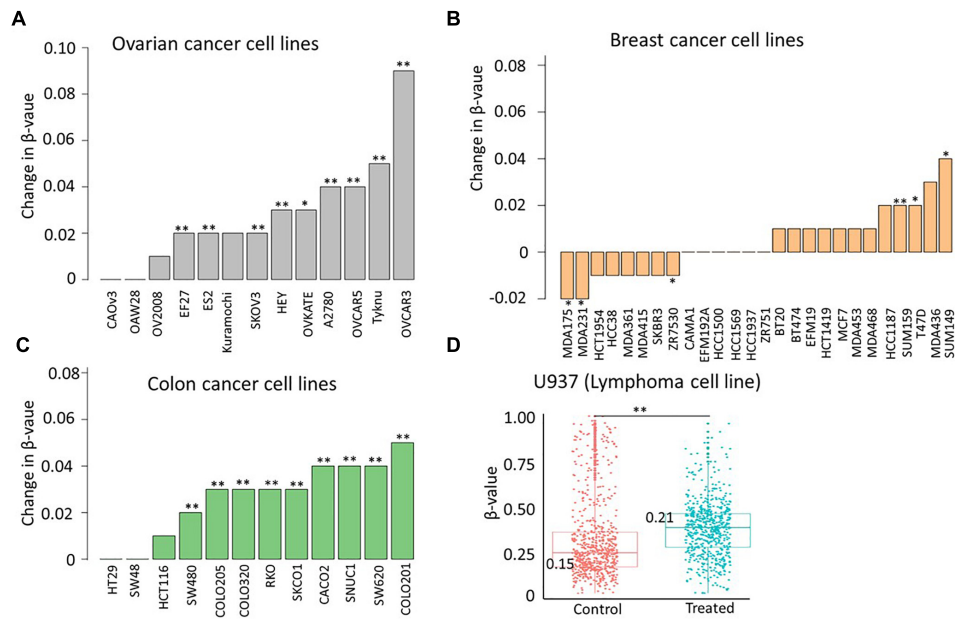

FIGURE 3 | Azacytidine treatment increases methylation of identified sites in a subset of cell lines. Change in median methylation level of identified CpGs in **(A)** 13 ovarian cancer cell lines **(B)** 26 breast cancer cell lines, and **(C)** 12 colon cancer cell lines. The bar plot represents the difference in the median methylation level of identified CpGs between cells treated with 0. 5 μM azacytidine (test group) or carboplatin (mock group) after 72 h. **(D)** Scatter plot showing the distribution of methylation level of identified probes in untreated (control) and treated cells (5 mM of azacytidine for 72 h) in U937 lymphoma cell lines. The statistical significance was assessed using the non-parametric Wilcoxon test. *$p < 0.05$, **$p < 0.005$.

Identified CpGs Show Trend of Hypermethylation in AML and Ovarian Cancer Primary Cells

To investigate the CpGs identified in the HCT116 colon cancer cells in primary patient samples, we analyzed hypermethylation of identified CpGs in mononuclear cells from bone marrow sample of two primary AML patients (**Figure 4**). Increase in DNA methylation ($\Delta\beta = 0.06$, $p = 4.68 \times 10^{-7}$ at day 7) was observed at the identified CpGs after decitabine treatment in the bone marrow mononuclear cells of one patient (ID 1107) but not of the healthy control (median $\Delta\beta = -0.02$, $p = 0.26$

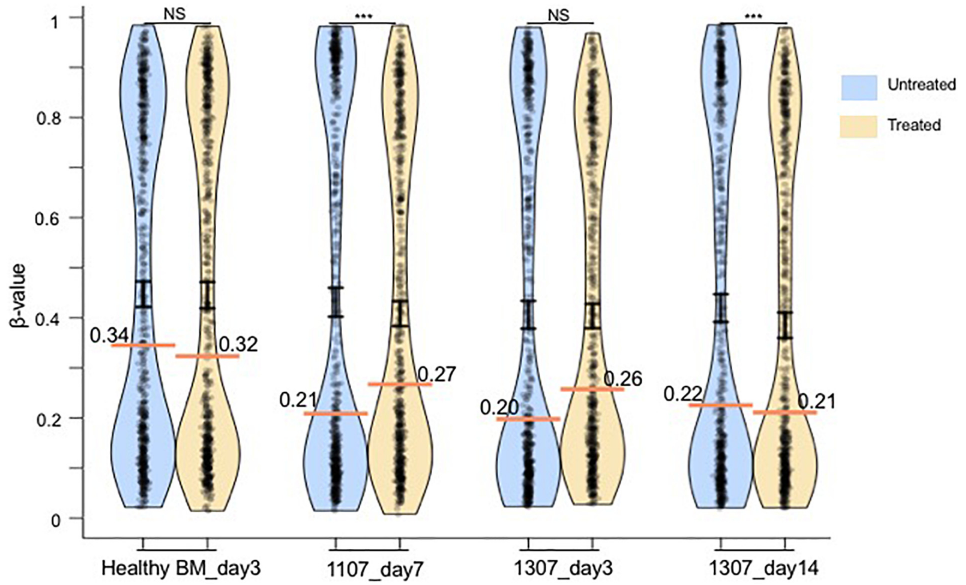

FIGURE 4 | Pirate plot show the median methylation level (horizontal colored line) and distribution pattern (mean ± standard error as vertical black line) of the identified 638 CpGs in untreated and treated (10 nM of decitabine) mononuclear cells from a healthy bone marrow (BM) sample and two primary leukemia patient samples (IDs 1307 and 1107), based on the data from the study of Tsai et al. (2012). DNA methylation assay for the patient 1307 was performed at days 3 and 14. For the patient 1107, the assay was performed only at day 7. The median methylation level is indicated in each plot. The statistical significance was assessed using the paired non-parametric Wilcoxon test. NS, not significant. ***$p < 0.0005$.

at day 3), suggesting that hypermethylation in response to DNMTi might be specific to cancerous cells but not to healthy cells (**Figure 4**). We also observed trend of hypermethylation at identified CpGs (median $\Delta\beta = 0.06$, $p = 0.76$) at day 3 in another primary leukemia patient (ID 1307) that was lost by day 14 (median $\Delta\beta = -0.01$, $p = 2.13 \times 10^{-35}$) (**Figure 4**). This result again suggests that hypermethylation at identified sites after DNMTi treatment is transient also in primary leukemia cancer cells, similarly as was observed in the HCT116 cell line model. Further, significant hypermethylation was observed in 2 out of 14 PBMCs (P2 and P3) and 2 out of 6 ascites (A1 and A2) samples of platinum resistant epithelial ovarian cancer patients treated with decitabine as compared to untreated paired samples (**Supplementary Figure 2**). Validation of the hypermethylation at identified CpGs in the PBMCs and ascites samples treated with clinically used dose of decitabine (10 nM) further confirm our findings. We did not either observe hypermethylation in any of the eight tumor biopsy samples (**Supplementary Figure 2**) from the ovarian cancer patients which might be because of the requirement of higher dose of drug to result in the same effect in solid cancer as compared to PBMC and ascites samples.

The Methylation of Identified CpGs Correlates With Expression of Corresponding Genes

To discover the functional role of methylation in differentially methylated CpGs, we correlated DNA methylation level of identified CpGs and expression levels of the corresponding genes at multiple time points (0, 5, 14, 24, and 42 days) measured in HCT116 cell line after decitabine treatment. The distribution of correlation coefficients for 130 CpGs in promoter and 200 CpGs in gene body area has been shown in **Figure 5A**. A strong correlation ($|r| \geq 0.80$) between the gene expression and DNA methylation profiles was observed at 27% of loci (166 CpGs in 153 genes) in HCT116 cells, out of them, 47 CpGs corresponding to 44 genes were nominally significant ($p < 0.05$) (**Supplementary Table 3**) indicating that observed hypermethylations affect cellular function by altering gene expression in cancer cell lines. The correlation between gene expression and DNA methylation suggests that the increase in DNA methylation is functional and causes transcriptional changes that affects cellular processes (e.g., cell proliferation).

Genes Corresponding to the Identified CpGs Show Differential Expression in Cancerous Tissue

We further investigated the pathological relevance of the increased methylation at identified CpGs using DNA methylation and gene expression profile of normal and cancerous tissue from TCGA colon adenocarcinoma patients. Out of 638 CpGs discovered in HCT116 cell line, we extensively investigated the methylation of CpGs in promoter and gene body area in TCGA data as methylations at these locations have a major effect on gene expression (Yang et al., 2014; Koch et al., 2018). We selected 53 promoter CpGs and 78 gene body CpGs showing a strong methylation-expression correlation ($|r| \geq 0.8$) in HCT116 cell lines and their methylation levels were compared between cancerous ($n = 273$) and adjacent healthy tissues ($n = 19$)

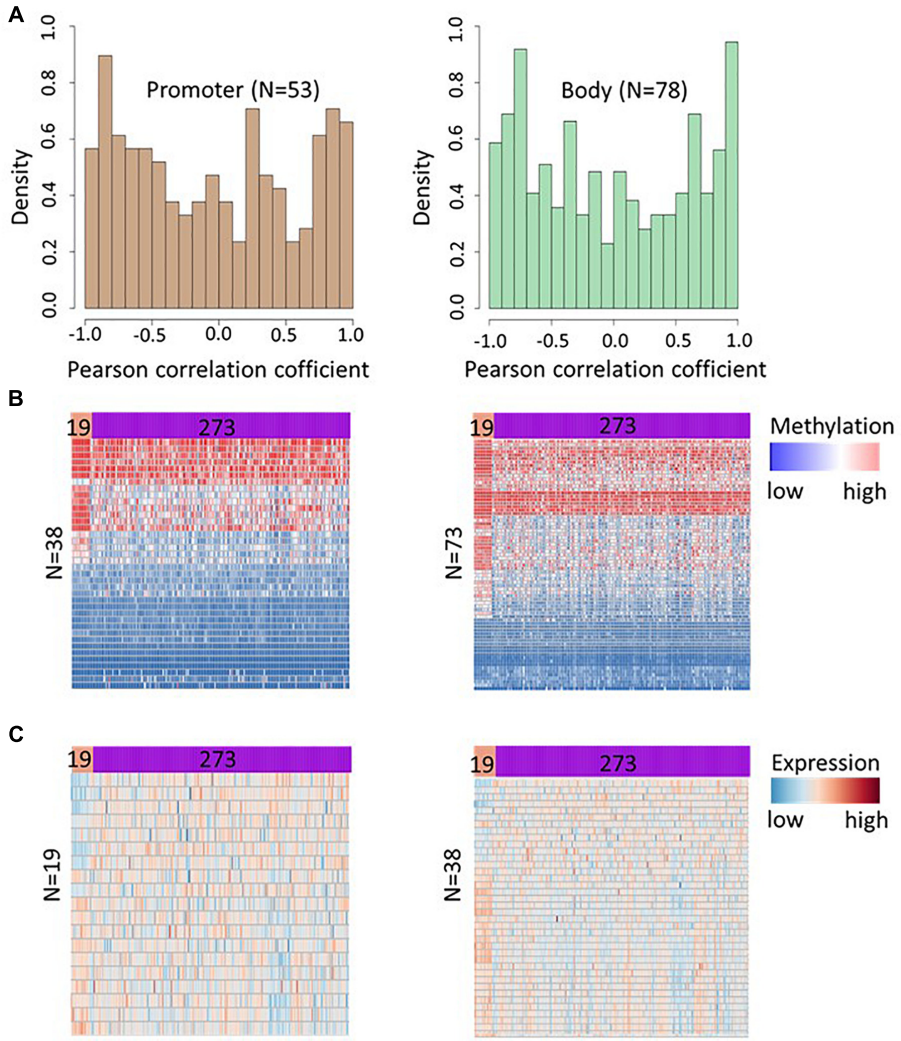

FIGURE 5 | DNA methylation at hypermethylated sites affects gene expression in HCT116 cell lines and TCGA colon adenocarcinoma samples. **(A)** Histogram depicts density of Pearson correlation coefficients (PCCs) between DNA methylation and gene expression for 130 CpGs in promoter region (left panel) and 200 CpGs in gene body area (right panel). The PCCs were calculated using DNA methylation of a CpGs and the expression level of corresponding genes at day 0 (untreated cells), 5, 14, 24, and 42 days after decitabine treatment. Further, 53 promoter CpGs and 78 gene body CpGs showing a strong methylation-expression correlation ($|r| \geq 0.8$) in HCT116 cell lines were selected and their methylation levels were compared between cancerous ($n = 273$) and adjacent healthy tissues ($n = 19$) samples in TCGA colon cancer data. A significant difference in methylation level (FDR < 0.05) was observed at 38 promoter and 73 gene body CpGs. **(B)** Heatmap showing the methylation level of these 38 promoters (left panel) and 73 gene body (right panel) CpGs in healthy tissue and colon cancer tissue. Subsequently, the expression level of genes corresponding to CpGs showing significant methylation differences in TCGA colon cancer data were compared and 19 genes corresponding to significant CpGs in promoter region, and 38 genes corresponding to the significant CpGs in gene body region were found differentially expressed (FDR < 0.05). **(C)** Heatmap showing the expression profile of genes with significant differences in adjacent healthy tissue ($n = 19$) and colon cancer samples ($n = 273$).

samples in TCGA colon cancer data. This analysis revealed differential methylation of 38 promoter CpGs and 73 gene body CpGs in cancer tissue (**Figure 5B** and **Supplementary Table 4**). Subsequently, the expression level of genes corresponding to CpGs showing significant methylation differences in TCGA colon cancer data were compared and the analysis revealed significant difference (FDR < 0.05) in expression of 19 and 38 genes corresponding to differentially methylated CpGs at promoter and gene body area in colon cancer tissue respectively (**Figure 5C** and **Supplementary Table 5**). The analysis suggests that DNMTi treatment increases methylation at CpGs that involved in the pathology of cancer and hence such alteration can contribute to the therapeutic response of the drugs.

Genes With Increased Methylation Are Enriched in Cancer-Related Pathways and Are NFAT, LEF1, and MAZ-Regulated

We next investigated the functions of the genes corresponding to the identified CpGs using the GeneCodis (v2) gene set enrichment analysis tool. Gene ontology enrichment analysis revealed that five out of the 10 (50%) most significant

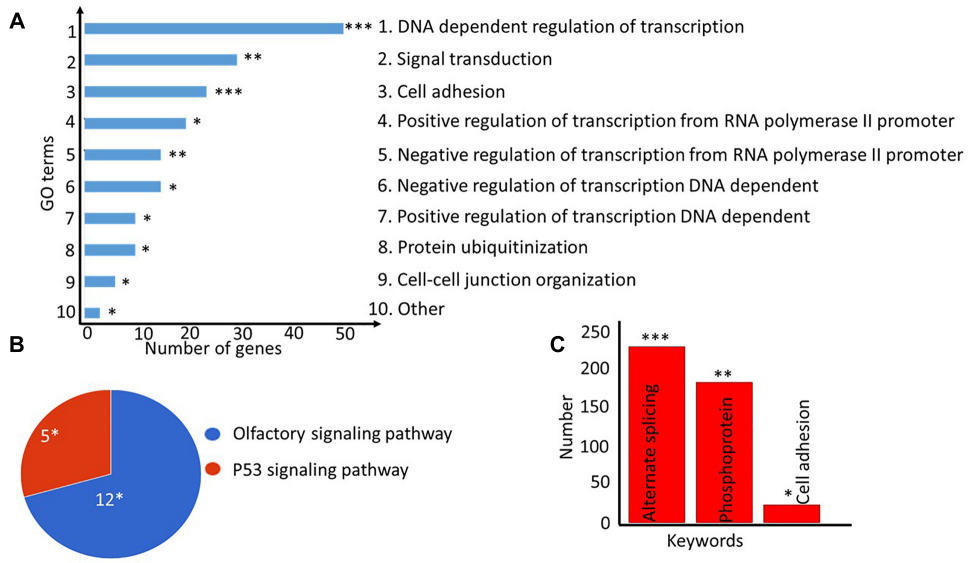

FIGURE 6 | Gene ontology (GO) and pathway enrichment analyses of genes corresponding to differentially methylated CpGs. **(A)** Top-10 most significantly enriched cellular processes are shown as a bar plot. The lengths of the bars denote the number of genes present in each of the top GO categories. **(B)** Pie-chart showing the significantly enriched pathways for the genes. The number of genes present in each pathway group is shown along with the hypergeometric test *p*-value corrected for multiple testing as implemented in the DAVID tool. **(C)** The keywords enrichment analysis for the genes is shown as a bar chart. The length of the bar represents the number of genes enriched for each keyword, the FDR-corrected *p*-value is shown at the top. *FDR < 0.05; **FDR < 0.005; ***FDR < 0.0005.

TABLE 1 | Top five transcription factor enriched in gene set corresponding to identified 638 CpGs and its regulated genes.

Transcription factor	Genes (*N*)	FDR	Regulated genes
NFATC1	47	1.48×10^{-8}	SLIT3, RORA, SYT10, CNTNAP2, SCN3A, MRPL28, ADAMTSL1, CTNND2, ESR1, PPM1B, PDE4D, RARB, OPCML, SNX15, PRKD2, ID3, PTPRO, ADCY2, CUL3, DMD, ITM2C, KLF12, BCOR, CTNND1, SGCD, ACACA, HDAC6, POGK, AUTS2, PAX3, DLG2, SLC6A5, SOX5, DLC1, ANTXR1, NGFRAP1, LSAMP, GRM8, CACNA2D3, ETS1, S100A10, ADAMTS17, KCNH5, ARHGAP6, KCNMA1, MAP7, KCNN2
LEF1	59	2.10×10^{-8}	PDCD10, NRXN1, SLIT3, RORA, YWHAZ, COX7B, SYNPR, SCN3A, SORCS1, TMSB4X, ADAMTSL1, NXN, CLSTN2, ZNF8, CNTN6, MAGED2, WHSC1L1, GMPR2, PDE4D, ABCF2, RARB, CNKSR2, TIA1, SMARCA1, SFRP2, OPCML, WDFY3, MBTD1, CACNA1E, PTPRO, MCTS1, DMD, KLF12, CTNND1, SGCD, ACACA, POGK, OXCT1, TAF1, PAX3, SLC6A5, SOX5, 1, SIX4, GPC6, DLC1, GTF2A2, TLE3, GAB2, TMSL3, CACNA2D3, ETS1, BZW1, ADAMTS12, CD160, TCERG1L, KCNH5, ARHGAP6, NR2F1
MAZ	51	4.07×10^{-8}	PDCD10, SLIT3, SV2B, RORA, YWHAZ, CNTNAP2, SORCS1, PRKCI, CTNND2, ACCN2, ESR1, MAGED2, HRK, FKBP2, RARB, CNKSR2, SSR1, SMARCA1, SFRP2, PRKD2, UBE2L3, PTPRF, ID3, DMD, ITM2C, KLF12, P4HA1, BCOR, RGS7, CTNND1, DUSP6, POGK, TAF1, LYPLA2, AUTS2, DLG2, SOX5, SIX4, DLC1, TLE3, PRDM16, NGFRAP1, POLR1D, ARVCF, BZW1, THRAP3, TRRAP, ZNRF1, KCNH5, KCNMA1, NR2F1
OCT1	16	1.49×10^{-7}	NRXN1, NR2C2, SCN3A, PDE4D, RARB, DMD, KLF12, DUSP6, SOX5, DLC1, TLE3, GAB2, TMSL3, TCERG1L, IRX2, NR2F1
MEF2	27	2.32×10^{-7}	HIPK1, CTNNA1, NRXN3, ESR1, PPM1B, SLC12A1, SMARCA1, OPCML, WBP5, ADCY2, CUL3, DMD, KLF12, P4HA1, CTNND1, SGCD, DLG2, SOX5, GLG1, NELL2, GRM8, CACNA2D3, ETS1, CIAO1, ADAMTS12, AGTPBP1, NR2F1

FDR-corrected p-values from the hypergeometric test are shown in the table.

GO processes (FDR = 0.05) were related to transcription regulation, which is one of the key functional role of DNA methylation in order to control gene expression (**Figure 6A**). Notably, the list of enriched genes included well-known oncogenes, such as AFF3, CTNND2, ELK4, ESR1, PAX3, TRRAP, and WHSC1L1. The pathway enrichment analysis revealed that olfactory transduction and p53 signaling pathway were overrepresented (FDR = 0.05) in the gene set with increased methylation (**Figure 6B**), and alternating splicing was enriched as the major keyword (fold enrichment = 1.27, FDR = 0.000132, **Figure 6C**). Identified CpGs were also enriched in the enhancer region ($p = 3.36 \times 10^{-4}$) of the genomes (**Supplementary Figure 3**).

Furthermore, enrichment analysis among the transcription factors regulating these identified genes revealed that 59 genes were regulated by lymphoid enhancer-binding factor 1 (LEF1) ($p = 2.1 \times 10^{-8}$, **Table 1** and **Supplementary Figure 4A**), 51 genes by MYC Associated Zinc Finger Protein

(MAZ) ($p = 4.07 \times 10^{-8}$, **Table 1** and **Supplementary Figure 4B**) and 47 of genes were regulated by the nuclear factor of activated T-cells (NFATC1, $p = 1.48 \times 10^{-8}$, **Supplementary Figure 4C**). Enrichment of genes in cancer-related pathways, especially in the p53 tumor suppressor pathway and the olfactory pathway, suggests that hypermethylation in the identified sites affects cancer cell proliferation and apoptosis.

DISCUSSION

Our study indicates that a clinically feasible dose of decitabine (0.3 to 300 μM) treatment causes a transient increase in DNA methylation level of a small fraction of CpGs in the colon cancer genome. The use of 3-day exposure with such doses *in vitro* produces a quick increase in DNA methylation that may reflect the immediate response of cells to external stimuli. The transient increase in methylation (that vanishes 10 days after treatment) at identified targets also suggests that the response is mainly a temporary alteration of transcript level of certain genes, rather than permanent shut down or enhancement of their expression.

The further study of the hypermethylation in primary bone marrow mononuclear cells from AML patients, peripheral blood cells and ascites from epithelial ovarian cancer patients indicated that hypermethylation of subsets of the identified CpGs is an important mechanism behind DNMTi effects against primary cancer cells, which, as expected, varies across patients and cancer types. Additionally, the absence of hypermethylation in normal bone marrow mononuclear cells indicates that the hypermethylation is limited to cancerous tissues and cell lines. However, a future study exploring hypermethylation at identified CpGs in pre- and post-treated cancerous tissue types (e.g., kidney, skin, brain), in comparison to corresponding healthy cells, is needed to detail the tissue-specificity of the hypermethylation at the identified CpGs.

We did not observe hypermethylation in case of breast cancer MCF7 cell lines treated with low dose (0.06 μM) of decitabine, nor in 20 out of 26 breast cancer cell lines treated with 5 mM of azacytidine (low dose), even though the same dose of azacytidine was sufficient to hypermethylate the CpGs in colon and ovarian cancer cell lines. It suggests that lower doses of DNMTi agents are not sufficient to hypermethylate the identified CpGs in all the cancer cell lines, which could be because of their molecular peculiarities. For example, lower change in expression level of DNA methylating enzymes DNMT3A was observed in breast cancer cell lines 3 days after azacytidine treatment, as compared to colon and ovarian cancer cell lines (**Supplementary Figure 5**). DNMT3A is a *de novo* methylating enzyme and have been associated with CpGs hypermethylation phenotype in AML (Spencer et al., 2017). Further, the expression level of DNMT3A and DNMT3B have been associated with sensitivity to decitabine cytotoxic response in embryonic cells (Oka et al., 2005), testicular germ cell tumor (Beyrouthy et al., 2009) and have also shown to be predictive of decitabine treatment response in patient-derived xenograft model for triple negative breast cancer (Yu et al., 2018). Differences in expression of DNMT enzymes, together other molecular differences (e.g., genetic mutations or epigenetic differences) may resists breast cancer cells against the hypermethylation in response to DNMTi at a lower dose. However, a detailed mechanistic study will be needed to understand the absence of hypermethylation in breast cancer cells in relation with DNMT3A or DNMT3B levels and other molecular heterogeneity.

Additionally, genes associated with identified CpGs were enriched among olfactory receptor and p53 pathways. P53 pathway regulates DNA repair and apoptosis in HCT116 cells (Li et al., 2015), and there is growing evidence for the involvement of olfactory receptor pathway in cancers of non-olfactory tissues such as prostate (Neuhaus et al., 2009), lung (Giandomenico et al., 2013; Kalbe et al., 2017), and colon cancers (Morita et al., 2016). For instance, olfactory receptor OR51B4 is highly expressed in colon cancer HCT116 cells and the activation of the receptor by its ligand (Troenan) inhibited cell proliferation and apoptosis by phosphorylation of p38, mTOR, and Akt kinases (Weber et al., 2017). The available literature therefore suggests that identified hypermethylation can affect colon cancer cells proliferation and apoptosis through olfactory receptor pathway. However, a detailed mechanistic study is warranted to decipher the exact role of hypermethylation at identified CpGs in cellular growth through p53 and olfactory receptor pathways.

Further, enriched transcription factor LEF1 is implicated in tumorigenesis and cancer cell proliferation, migration, invasion, and stemness in multiple cancer (e.g., colorectal cancer, AML, oral squamous cell carcinoma) (Santiago et al., 2017). Moreover, the methylation at a fraction of CpGs was positively correlated with the population doubling time of HCT116 cells indicating the role of identified CpGs in cell division, and proliferation. Enrichment of genes among the cancer-related pathways involved in cell proliferation and apoptosis suggests a non-random selection of CpGs for hypermethylation in order to alter the cellular dynamics (e.g., population doubling time). We consider that increased in methylation at identified CpGs can contribute to the drug response in multiple cancer types partly by altering the cell division rate. The methylation levels at identified CpGs could be useful to design better treatment strategies (e.g., predicting the DNMTi responders and non-responders), and to understand side effects due to higher drug dose (e.g., the increase in DNA methylation at identified CpGs could be an indicator for degree of possible toxic effect). These novel findings therefore warrant further analyses in a number of cancer types using either pre-clinical animal studies or clinical treatment data from cancer patients with baseline molecular profiles available.

There are multiple reasons to suggest that at least one key mechanism underlying the anti-tumor responses to DNMTi treatment may involve hypermethylation of specific genes in cancer cells. First, we showed an increase in DNA methylation at identified CpGs in more than one type of cancer cells. Second, as defined for an epigenetic change, these sustained

changes persist for significant periods of time (at least more than 5 days) after a transient, subsequently withdrawn, drug exposure (in this case 72 h). Third, the expression patterns for a subset of the genes are different between cancer and normal tissue types. Importantly, these changes are induced by drug doses that do not acutely kill cells and, thus, allow the transient alterations in gene methylation patterns to act on emerging molecular changes to cells after DNMTi therapy.

In summary, our findings suggest that DNMTi mediates its therapeutic effect through a complex mechanism of action, and therefore a generalized pattern for the activity is challenging to find as DNMTi treatment causes hypermethylation at certain loci and hypomethylation at others. Hence, the effects of DNMTi on cancer tissues should be analyzed at the individual gene level, rather than at the entire genomic level, and separately for each tissue type and even for each cancer patient. Further, any attempt to predict DNMTi response should also incorporate the hypermethylated targets of the drugs along with the hypomethylated targets of the drugs. However, a functional mechanistic study in more advanced model systems and several human tissue types will be required for further revealing how the increase in methylation at identified loci alters treatment response and the pathological burden of disease. We hope that these identified targets associated with hypermethylation have broad implications for further research on DNMTi response mechanisms in multiple cancer types.

AUTHOR CONTRIBUTIONS

AG conceptualized, analyzed the data, and wrote the manuscript. TA critically revised and edited the manuscript.

FUNDING

This work was funded by the Academy of Finland (Grant Nos. 269862, 292611, 310507, and 313267), Cancer Society of Finland, and the Sigrid Juselius Foundation.

ACKNOWLEDGMENTS

This study is an independent analysis of existing data available in the public domain and does not involve any animal or human samples that have been collected by the authors themselves. The preprint of the manuscript has been published in bioRxiv (https://www.biorxiv.org/content/early/2018/08/25/395467).

SUPPLEMENTARY MATERIAL

The Supplementary Material for this article can be found online at: https://www.frontiersin.org/articles/10.3389/fphar.2019.00385/full#supplementary-material

REFERENCES

Beyrouthy, M. J., Garner, K. M., Hever, M. P., Freemantle, S. J., Eastman, A., Dmitrovsky, E., et al. (2009). High DNA methyltransferase 3B expression mediates 5-aza-deoxycytidine hypersensitivity in testicular germ cell tumors. *Cancer Res.* 69, 9360–9366. doi: 10.1158/0008-5472.CAN-09-1490

Bohl, S. R., Bullinger, L., and Rucker, F. G. (2018). Epigenetic therapy: azacytidine and decitabine in acute myeloid leukemia. *Expert. Rev. Hematol.* 11, 361–371. doi: 10.1080/17474086.2018.1453802

Broday, L., Lee, Y. W., and Costa, M. (1999). 5-azacytidine induces transgene silencing by DNA methylation in Chinese hamster cells. *Mol. Cell. Biol.* 19, 3198–3204. doi: 10.1128/MCB.19.4.3198

Chen, Y. A., Lemire, M., Choufani, S., Butcher, D. T., Grafodatskaya, D., and Zanke, B. W. (2013). Discovery of cross-reactive probes and polymorphic CpGs in the illumina infinium humanMethylation450 microarray. *Epigenetics* 8, 203–209. doi: 10.4161/epi.23470

Chowdhury, B., Mcgovern, A., Cui, Y., Choudhury, S. R., Cho, I. H., Cooper, B., et al. (2015). The hypomethylating agent decitabine causes a paradoxical increase in 5-hydroxymethylcytosine in human leukemia cells. *Sci. Rep.* 5:9281. doi: 10.1038/srep09281

De Carvalho, D. D., Sharma, S., You, J. S., Su, S. F., Taberlay, P. C., Kelly, T. K., et al. (2012). DNA methylation screening identifies driver epigenetic events of cancer cell survival. *Cancer Cell* 21, 655–667. doi: 10.1016/j.ccr.2012.03.045

Derissen, E. J., Beijnen, J. H., and Schellens, J. H. (2013). Concise drug review: azacitidine and decitabine. *Oncologist* 18, 619–624. doi: 10.1634/theoncologist.2012-0465

Döhner, H., Estey, E., Grimwade, D., Amadori, S., Appelbaum, F. R., Büchner, T., et al. (2017). Diagnosis and management of AML in adults: 2017 ELN recommendations from an international expert panel. *Blood* 129, 424–447. doi: 10.1182/blood-2016-08-733196

Du, P., Kibbe, W. A., and Lin, S. M. (2008). lumi: a pipeline for processing Illumina microarray. *Bioinformatics* 24, 1547–1548. doi: 10.1093/bioinformatics/btn224

Fu, S., Hu, W., Iyer, R., Kavanagh, J. J., Coleman, R. L., Levenback, C. F., et al. (2011). Phase 1b2a study to reverse platinum resistance through use of a hypomethylating agent, azacitidine, in patients with platinum-resistant or platinum-refractory epithelial ovarian cancer. *Cancer* 117, 1661–1669. doi: 10.1002/cncr.25701

Giandomenico, V., Cui, T., Grimelius, L., Öberg, K., Pelosi, G., and Tsolakis, A. V. (2013). Olfactory receptor 51E1 as a novel target for diagnosis in somatostatin receptor-negative lung carcinoids. *J. Mol. Endocrinol.* 51, 277–286. doi: 10.1530/JME-13-0144

Giri, A. K., Bharadwaj, S., Banerjee, P., Chakraborty, S., Parekatt, V., Rajashekar, D., et al. (2017). DNA methylation profiling reveals the presence of population-specific signatures correlating with phenotypic characteristics. *Mol. Genet. Genomics* 292, 655–662. doi: 10.1007/s00438-017-1298-0

Han, H., Yang, X., Pandiyan, K., and Liang, G. (2013). Synergistic re-activation of epigenetically silenced genes by combinatorial inhibition of DNMTs and LSD1 in cancer cells. *PLoS One* 8:e75136. doi: 10.1371/journal.pone.0075136

Huang Da, W., Sherman, B. T., and Lempicki, R. A. (2009). Systematic and integrative analysis of large gene lists using DAVID bioinformatics resources. *Nat. Protoc.* 4, 44–57. doi: 10.1038/nprot.2008.211

Huidobro, C., Urdinguio, R. G., Rodriguez, R. M., Mangas, C., Calvanese, V., Martinez-Camblor, P., et al. (2012). A DNA methylation signature associated with aberrant promoter DNA hypermethylation of DNMT3B in human colorectal cancer. *Eur. J. Cancer* 48, 2270–2281. doi: 10.1016/j.ejca.2011.12.019

Kalbe, B., Schulz, V. M., Schlimm, M., Philippou, S., Jovancevic, N., Jansen, F., et al. (2017). Helional-induced activation of human olfactory receptor 2J3 promotes apoptosis and inhibits proliferation in a non-small-cell lung cancer cell line. *Eur. J. Cell Biol.* 96, 34–46. doi: 10.1016/j.ejcb.2016.11.004

Kastl, L., Brown, I., and Schofield, A. C. (2010). Altered DNA methylation is associated with docetaxel resistance in human breast cancer cells. *Int. J. Oncol.* 36, 1235–1241.

Koch, A., Joosten, S. C., Feng, Z., De Ruijter, T. C., Draht, M. X., Melotte, V., et al. (2018). Analysis of DNA methylation in cancer: location revisited. *Nat. Rev. Clin. Oncol.* 15, 459–466. doi: 10.1038/s41571-018-0004-4

Leadem, B. R., Kagiampakis, I., Wilson, C., Cheung, T. K., Arnott, D., Trojer, P., et al. (2018). A KDM5 inhibitor increases global H3K4 trimethylation occupancy and enhances the biological efficacy of 5-Aza-2'-deoxycytidine. *Cancer Res.* 78, 1127–1139. doi: 10.1158/0008-5472.CAN-17-1453

Lee, V., Wang, J. S., Zahurak, M. L., Gootjes, E. C., Verheul, H. M. W., Parkinson, R. M., et al. (2018). A phase I trial of a guadecitabine (SGI-110) and irinotecan in metastatic colorectal cancer patients previously exposed to irinotecan. *Clin. Cancer Res.* 24, 6160–6167. doi: 10.1158/1078-0432.CCR-18-0421

Li, H., Chiappinelli, K. B., Guzzetta, A. A., Easwaran, H., Yen, R. W., Vatapalli, R., et al. (2014). Immune regulation by low doses of the DNA methyltransferase inhibitor 5-azacitidine in common human epithelial cancers. *Oncotarget* 5, 587–598. doi: 10.18632/oncotarget.1782

Li, X. L., Zhou, J., Chen, Z. R., and Chng, W. J. (2015). P53 mutations in colorectal cancer - molecular pathogenesis and pharmacological reactivation. *World J. Gastroenterol.* 21, 84–93. doi: 10.3748/wjg.v21.i1.84

Matei, D., Fang, F., Shen, C., Schilder, J., Arnold, A., Zeng, Y., et al. (2012). Epigenetic resensitization to platinum in ovarian cancer. *Cancer Res.* 72, 2197–2205. doi: 10.1158/0008-5472.CAN-11-3909

Minkovsky, A., Sahakyan, A., Bonora, G., Damoiseaux, R., Dimitrova, E., Rubbi, L., et al. (2015). A high-throughput screen of inactive X chromosome reactivation identifies the enhancement of DNA demethylation by 5-aza-2'-dC upon inhibition of ribonucleotide reductase. *Epigenet. Chrom.* 8:42. doi: 10.1186/s13072-015-0034-4

Morita, R., Hirohashi, Y., Torigoe, T., Ito-Inoda, S., Takahashi, A., Mariya, T., et al. (2016). Olfactory receptor family 7 subfamily C member 1 is a novel marker of colon cancer-initiating cells and is a potent target of immunotherapy. *Clin. Cancer Res* 22, 3298–3309. doi: 10.1158/1078-0432.CCR-15-1709

Nervi, C., De Marinis, E., and Codacci-Pisanelli, G. (2015). Epigenetic treatment of solid tumours: a review of clinical trials. *Clin. Epigenet.* 7:127. doi: 10.1186/s13148-015-0157-2

Neuhaus, E. M., Zhang, W., Gelis, L., Deng, Y., Noldus, J., and Hatt, H. (2009). Activation of an olfactory receptor inhibits proliferation of prostate cancer cells. *J. Biol. Chem.* 284, 16218–16225. doi: 10.1074/jbc.M109.012096

Oka, M., Meacham, A. M., Hamazaki, T., Rodiæ, N., Chang, L. J., and Terada, N. (2005). De novo DNA methyltransferases Dnmt3a and Dnmt3b primarily mediate the cytotoxic effect of 5-aza-2'-deoxycytidine. *Oncogene* 24, 3091–3099. doi: 10.1038/sj.onc.1208540

Ramos, F., Thépot, S., Pleyer, L., Maurillo, L., Itzykson, R., Bargay, J., et al. (2015). Azacitidine frontline therapy for unfit acute myeloid leukemia patients: clinical use and outcome prediction. *Leuk. Res.* 2015, 296–306. doi: 10.1016/j.leukres.2014.12.013

Ramos, M. P., Wijetunga, N. A., Mclellan, A. S., Suzuki, M., and Greally, J. M. (2015). DNA demethylation by 5-aza-2'-deoxycytidine is imprinted, targeted to euchromatin, and has limited transcriptional consequences. *Epigenet. Chrom.* 8:11. doi: 10.1186/s13072-015-0004-x

Ritchie, M. E., Phipson, B., Wu, D., Hu, Y., Law, C. W., Shi, W., et al. (2015). limma powers differential expression analyses for RNA-sequencing and microarray studies. *Nucleic Acids Res.* 43:e47. doi: 10.1093/nar/gkv007

Santiago, L., Daniels, G., Wang, D., Deng, F. M., and Lee, P. (2017). Wnt signaling pathway protein LEF1 in cancer, as a biomarker for prognosis and a target for treatment. *Am. J. Cancer Res.* 7, 1389–1406.

Sarkar, S., Goldger, S., Byler, S., Rosenthal, S., and Heerboth, S. (2013). Demethylation and re-expression of epigenetically silenced tumor suppressor genes: sensitization of cancer cells by combination therapy. *Epigenomics* 5, 87–94. doi: 10.2217/epi.12.68

Singal, R., Ramachandran, K., Gordian, E., Quintero, C., Zhao, W., and Reis, I. M. (2015). Phase I/II study of azacitidine, docetaxel, and prednisone in patients with metastatic castration-resistant prostate cancer previously treated with docetaxel-based therapy. *Clin. Genitourin. Cancer* 13, 22–31. doi: 10.1016/j.clgc.2014.07.008

Spencer, D. H., Russler-Germain, D. A., Ketkar, S., Helton, N. M., Lamprecht, T. L., Fulton, R. S., et al. (2017). CpG island hypermethylation mediated by DNMT3A is a consequence of AML progression. *Cell* 168, 801–816. doi: 10.1016/j.cell.2017.01.021

Tabas-Madrid, D., Nogales-Cadenas, R., and Pascual-Montano, A. (2012). GeneCodis3: a non-redundant and modular enrichment analysis tool for functional genomics. *Nucleic Acids Res.* 40, W478–W483. doi: 10.1093/nar/gks402

Teschendorff, A. E., Marabita, F., Lechner, M., Bartlett, T., Tegner, J., Gomez-Cabrero, D., et al. (2013). A beta-mixture quantile normalization method for correcting probe design bias in Illumina infinium 450 k DNA methylation data. *Bioinformatics* 29, 189–196. doi: 10.1093/bioinformatics/bts680

Tobiasson, M., Abdulkadir, H., Lennartsson, A., Katayama, S., Marabita, F., De Paepe, A., et al. (2017). Comprehensive mapping of the effects of azacitidine on DNA methylation, repressive/permissive histone marks and gene expression in primary cells from patients with MDS and MDS-related disease. *Oncotarget* 8, 28812–28825. doi: 10.18632/oncotarget.15807

Tsai, H. C., Li, H., Van Neste, L., Cai, Y., Robert, C., Rasool, F. V., et al. (2012). Transient low doses of DNA-demethylating agents exert durable antitumor effects on hematological and epithelial tumor cells. *Cancer Cell* 21, 430–446. doi: 10.1016/j.ccr.2011.12.029

Wang, H., Li, Y., Lv, N., Li, Y., Wang, L., and Yu, L. (2018). Predictors of clinical responses to hypomethylating agents in acute myeloid leukemia or myelodysplastic syndromes. *Ann. Hematol.* 97, 2025–2038. doi: 10.1007/s00277-018-3464-9

Weber, L., Al-Refae, K., Ebbert, J., Jagers, P., Altmuller, J., Becker, C., et al. (2017). Activation of odorant receptor in colorectal cancer cells leads to inhibition of cell proliferation and apoptosis. *PLoS One* 12:e0172491. doi: 10.1371/journal.pone.0172491

Yang, X., Han, H., De Carvalho, D. D., Lay, F. D., Jones, P. A., and Liang, G. (2014). Gene body methylation can alter gene expression and is a therapeutic target in cancer. *Cancer Cell* 26, 577–590. doi: 10.1016/j.ccr.2014.07.028

Yu, J., Qin, B., Moyer, A. M., Nowsheen, S., Liu, T., Qin, S., et al. (2018). DNA methyltransferase expression in triple-negative breast cancer predicts sensitivity to decitabine. *J. Clin. Invest.* 128, 2376–2388. doi: 10.1172/JCI97924

Zuberi, K., Franz, M., Rodriguez, H., Montojo, J., Lopes, C. T., Bader, G. D., et al. (2013). GeneMANIA prediction server 2013 update. *Nucleic Acids Res.* 41, W115–W122. doi: 10.1093/nar/gkt533

Conflict of Interest Statement: The authors declare that the research was conducted in the absence of any commercial or financial relationships that could be construed as a potential conflict of interest.

frontiers in Pharmacology

BRIEF RESEARCH REPORT
published: 24 April 2019
doi: 10.3389/fphar.2019.00436

Non-linear Dose Response of Lymphocyte Cell Lines to Microtubule Inhibitors

Daria M. Potashnikova[1,2], Aleena A. Saidova[1,3], Anna V. Tvorogova[3,4], Eugene V. Sheval[4] and Ivan A. Vorobjev[1,4,5]*

[1] Department of Cell Biology and Histology, School of Biology, M.V. Lomonosov Moscow State University, Moscow, Russia, [2] Laboratory of Atherothrombosis, Moscow State University of Medicine and Dentistry, Moscow, Russia, [3] Department of Cell Biotechnology, Center of Experimental Embryology and Reproductive Biotechnology, Moscow, Russia, [4] A.N. Belozersky Institute of Physico-Chemical Biology, M.V. Lomonosov Moscow State University, Moscow, Russia, [5] Department of Biology, School of Science and Technology, Nazarbayev University, Astana, Kazakhstan

Microtubule (MT) inhibitors show anti-cancer activity in a wide range of tumors *in vitro* and demonstrate high clinical efficacy. To date they are routinely included into many chemotherapeutic regimens. While the mechanisms of MT inhibitors' interactions with tubulin have been well-established, the relationship between their concentration and effect on neoplastic cells is not completely understood. The common notion is that tumor cells are most vulnerable during division and all MT inhibitors block them in mitosis and induce mitotic checkpoint-associated cell death. At the same time multiple evidence of more subtle effects of lower doses of MT inhibitors on cell physiology exist. The extent of efficacy of the low-dose MT inhibitor treatment and the mechanisms of resulting cell death currently present a critical issue in oncology. The prospect of MT inhibitor dose reduction is promising as protocols at higher concentration have multiple side effects. We assessed cell cycle changes and cell death induced by MT inhibitors (paclitaxel, nocodazole, and vinorelbine) on human lymphoid B-cell lines in a broad concentration range. All inhibitors had similar accumulation effects and demonstrated "trigger" concentrations that induce cell accumulation in G2/M phase. Concentrations slightly below the "trigger" promoted cell accumulation in sub-G1 phase. Multi-label analysis of live cells showed that the sub-G1 population is heterogeneous and may include cells that are still viable after 24 h of treatment. Effects observed were similar for cells expressing Tat-protein. Thus cell cycle progression and cell death are differentially affected by high and low MT inhibitor concentrations.

Keywords: cell cycle, cell death, microtubule inhibitors, paclitaxel, nocodazole, vinorelbine, B-lymphocytes, RPMI8866

OPEN ACCESS

Edited by:
Vadim V. Sumbayev, University of Kent, United Kingdom

Reviewed by:
Martin Degen, Universität Bern, Switzerland
John Holmes Miller, Victoria University of Wellington, New Zealand

****Correspondence:***
Daria M. Potashnikova
dpotashnikova@gmail.com

Specialty section:
This article was submitted to Experimental Pharmacology and Drug Discovery, a section of the journal Frontiers in Pharmacology

Received: *08 February 2019*
Accepted: *05 April 2019*
Published: *24 April 2019*

Citation:
Potashnikova DM, Saidova AA, Tvorogova AV, Sheval EV and Vorobjev IA (2019) Non-linear Dose Response of Lymphocyte Cell Lines to Microtubule Inhibitors. Front. Pharmacol. 10:436. doi: 10.3389/fphar.2019.00436

INTRODUCTION

The importance of microtubule (MT) dynamics for cell motility (Liao et al., 1995), migration (Kaverina and Straube, 2011), and division (Jordan et al., 1993) has been well-established. The multi-aspect effect of suppressed microtubule dynamics makes MT inhibitors an important part of most anti-cancer chemotherapeutic regimens by inhibiting tumor growth (antimitotic effect) and metastasis (antimigration effect) (Dumontet and Jordan, 2010).

Microtubule inhibitors encompass several classes of compounds with varying mechanisms of interactions with tubulin (Perez, 2009) that disrupt MT dynamics by either stabilizing or de-stabilizing them. MT inhibitors of the first generation widely used in clinics (taxanes, vinca alkaloid derivatives) have certain drawbacks, including neurotoxic effects (Windebank, 1999), neutropenia (Donehower and Rowinsky, 1993) and loss of efficacy against advanced forms of some cancers (Sève et al., 2008). Clinical limitations in treatment of solid tumors and hematologic malignancies prompted further research for analogs with improved clinical characteristics, recently introducing vinflunine, epothilones, indibulin, and many other (Bennouna et al., 2008; Cortes and Vidal, 2012).

Varying effects of high and low MT inhibitor concentrations on different aspects of cell physiology have been described for a number of cell models (Grigoriev et al., 1999; Yang et al., 2010). The first meta-analysis focused on efficacy and toxicity of low-dose versus conventional-dose chemotherapies has been published recently (Xie et al., 2017) and provided data on low-dose chemotherapy advantages.

Microtubule inhibitors are integrated into a variety of chemotherapy schemes for B-cell malignancies, including the curative regimens of non-Hodgkin lymphomas (Bates et al., 2016). Their anti-cancer effects extend beyond their ability arrest mitosis and include their potential to induce apoptosis at all cell cycle phases (Bates and Eastman, 2017). The physiological consequences of MT dynamics inhibition are still poorly understood; the elucidation of its pleiotropic effects on cell death and cell cycle will provide novel therapeutic strategies. In this study we sought to determine the lowest efficient concentration of several MT inhibitors and tested their dose-dependent effects on cell death and mitotic arrest on B-cell lines RPMI8866 and its Tat-expressing modification RPMI8866-Tat-GFP. B-cell lymphomas (Burkitt lymphoma, DLBCL, and B-CLL) are one of the most common comorbid conditions for HIV-infected patients (Gopal et al., 2013). B-cell oncogenesis in HIV patients is related to Tat viral protein that enters B-lymphocytes, acts as a transcription factor in oncogenic cascades (Vendrame et al., 2014; Musinova et al., 2016) but also has cytoplasmic targets including MTs (de Mareuil et al., 2005). To our knowledge, no current research describes the effect of MT inhibitors on Tat-expressing B-cells.

MATERIALS AND METHODS

Cell Lines and Microtubule Inhibitors

Human B-cell [RPMI8866 and Tat-GFP expressing RPMI8866 (RPMI8866-Tat-GFP)] and T-cell (Jurkat) lines were used in the study. Cells were maintained in EX-CELL Medium (SAFC Biosciences, United States) supplemented with L-glutamine and 10% FBS (Paneco, Russia). The effects of three MT inhibitors on cell cycle and cell death were evaluated in the study: paclitaxel (taxol; Sigma, United States), nocodazole (Biochem, United States) and vinorelbine (Sigma, United States). MT inhibitors were added to the medium 24 h prior to analysis at final concentrations of 3; 10; 30; 100; 300; and 1000 nM.

Fluorescence Staining

Propidium iodide for DNA staining: The protocol for cell cycle analysis in suspension cells was published previously (Potashnikova et al., 2018).

Anti-caspase 3 immunostaining kit: PE-conjugated antibodies against active caspase 3 (BD, United States) were used to assess percentages of apoptotic cells. Cell fixation, permeabilization and staining were performed using supplied buffers based on the manufacturer's instructions.

Multi-label cell cycle and apoptosis staining: live cell suspensions of RPMI8866 and RPMI8866-Tat-GFP were simultaneously stained with tetramethyl-rhodamine ethyl ester (TMRE) for membrane potential, Hoechst33342 for DNA and annexin V-Alexa Fluor 647 (all Thermo Fisher Scientific, United States) for phosphatidylserine externalization. RPMI8866 cells were also stained with CellEvent fluorescent caspase 3/7 substrate (Thermo Fisher Scientific, United States): RPMI8866-Tat-GFP cells were not stained with CellEvent to avoid fluorescence signal conflict. The staining protocol was published previously (Vorobjev and Barteneva, 2016).

Flow Cytometry

Cells were analyzed using a FACSAria SORP cell sorter at Ex.407 nm/Em.425–475 nm for Hoechst33342, Ex.488 nm/Em.515–535 nm for CellEvent, Ex.561 nm/Em.575–590 nm for TMRE, PI and anti-caspase3-PE and Ex.640 nm/Em.663–677 nm for annexin V-Alexa Fluor 647. Flow cytometry data were acquired and analyzed using FACS Diva v.6.1.3 software (BD, United States). Each measurement was performed at least in triplicate.

Fluorescence Microscopy

Cell suspensions simultaneously stained with TMRE, Hoechst33342, CellEvent and annexin V-Alexa Fluor 647 were analyzed using a Nikon Ti Eclipse microscope under PlanApo 60×/1.4 objective. Images were recorded by Hamamatsu ORCA FLASH2 digital camera, using the following filter sets: Ex.450–490 nm/Em.510–540 nm; Ex.340–380 nm/Em.435–485 nm; Ex.530–560 nm/Em.573–640 nm and Ex.595–645 nm/Em.665–715 nm.

Statistical Analysis

Data from biological repeats were calculated as mean and standard deviation and plotted in GraphPad Prism software (United States). Unpaired *t*-test (95% confidence interval) was used as significance test.

Electron Microscopy

Cells were fixed in 4% glutaraldehyde (Ted Pella, United States) in 0.1 M Sørensen phosphate buffer for 2 h, post-fixed with 1% osmium tetroxide (Sigma, United States) for 1 h, dehydrated in ethanol and propylene oxide and embedded in Spi-pon 812 epoxy resin (SPI Inc., United States). Ultrathin sections were cut using an LKB III ultramicrotome (LKB), stained with uranyl acetate

and lead citrate, and photographed using a JEM-1400 electron microscope (Jeol, Japan)[1].

RESULTS

The Mitostatic Response to Various MT Inhibitor Concentrations Is Non-linear

We tested the mitostatic effect of three common stabilizing (paclitaxel) and depolymerizing (nocodazole, vinorelbine) MT inhibitors, on RPMI8866, RPMI8866-Tat-GFP (B-lymphocytes) and Jurkat (T-lymphocytes) cell lines. Linear gates were set to determine cell percentages at different cell cycle stages on DNA content curves (**Figures 1A–C**).

Microtubule inhibitors uniformly prompted cell accumulation in G2/M in a non-linear fashion: we found "trigger" concentrations sufficient to accumulate cells in G2/M phase that fell into 10–100 nM range for all inhibitors and cell lines. Concentrations below the "trigger" retained cell cycle distribution close to normal. For example, for 3 nM paclitaxel we observed 46% cells in G0/G1, 22% cells in S, and 18% in G2/M for RPMI8866 cells compared to 53% cells in G0/G1, 20% cells in S, and 18% in G2/M in control (**Figure 1D**). Concentrations above the "trigger" increased the G2/M population peak with a subsequent decrease of the G1 peak (**Figures 1B,C** and **Supplementary Figure S1**). Similar response patterns were achieved for every MT inhibitor; however, paclitaxel graphs were chosen as most representative.

The Sub-G1 Population on DNA Content Curves Likely Represents Apoptotic Cells but Its Percentage Does Not Correlate With Percentages of Caspase-3 Positive Cells

The number of cells with sub-G1 DNA content increased significantly in every MT inhibitor concentration compared to untreated control ($p < 0.05$, unpaired t-test) (**Figures 1A–C** and **Supplementary Figure S1**). Hypodiploid amounts of DNA can be explained by nucleic acid degradation in late apoptosis. Intriguingly, the largest sub-G1 populations did not correspond

[1]For Original Research articles, please note that the Material and Methods section can be placed in any of the following ways: before Results, before Discussion or after Discussion.

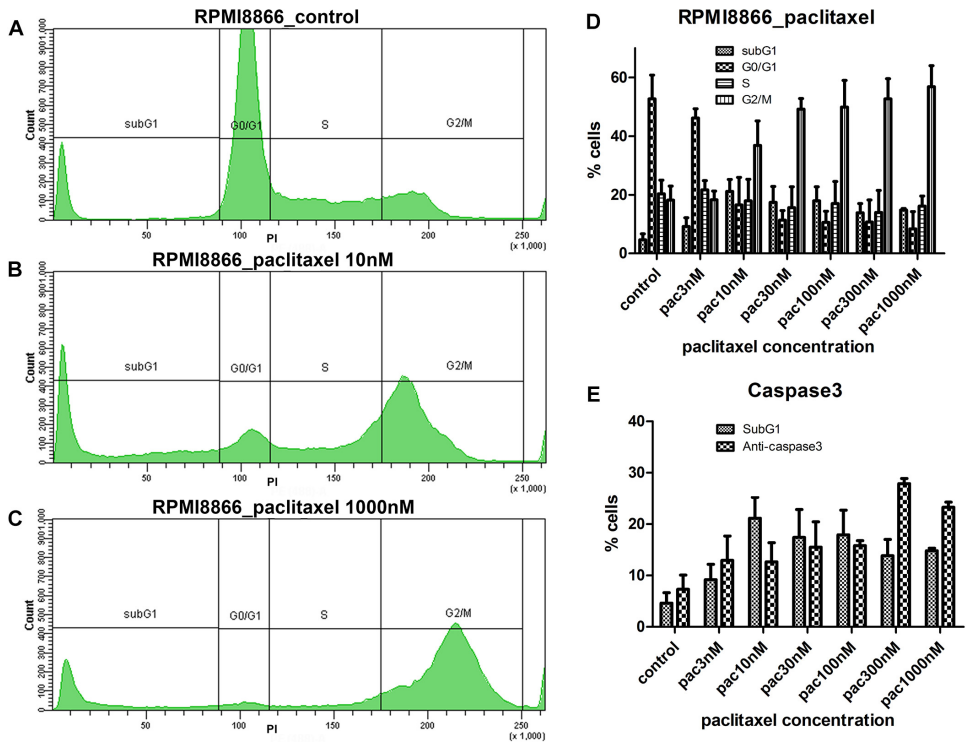

FIGURE 1 | RPMI8866 B-lymphocytes untreated (control) and treated with paclitaxel (concentration range 3, 10, 30, 100, 300, and 1000 nM) for 24 h. **(A–C)** DNA content curves in individual samples assessed by flow cytometry after propidium iodide staining and linear gates set to determine sub-G1, G0/G1, S, and G2/M cell cycle populations. 50 000 events were analyzed per sample. **(A)** Normal cell cycle distribution in control cells; G2/M comprises 19% cells, sub-G1 comprises 5% cells. **(B)** G2/M accumulation after 10 nM paclitaxel treatment; G2/M comprises 38% cells, sub-G1 comprises 25% cells. **(C)** G2/M accumulation after 1000 nM paclitaxel treatment; G2/M comprises 63% cells, sub-G1 comprises 15% cells. **(D)** Data from biological repeats on sub-G1, G0/G1, S, and G2/M population distributions were presented as mean percentages with *SD* on a histogram. Each measurement was performed at least in triplicate. **(E)** Miscorrelation of sub-G1 population numbers and caspase 3-positive cell numbers after paclitaxel treatment. The largest sub-G1 peak is observed at 10 nM paclitaxel while the largest caspase 3-positive population is observed at 300 nM paclitaxel.

to the highest MT inhibitor concentrations. Sub-G1 cell percentages did not significantly differ at "trigger," sub-"trigger" and high MT inhibitor concentrations. The only significant difference was obtained for paclitaxel: the highest percentage of cells in sub-G1 (21%) was present in 10 nM paclitaxel; that was significantly increased compared to 3, 300, and 1000 nM paclitaxel and insignificantly different from 30 to 100 nM paclitaxel ($p < 0.05$, unpaired t-test). To assess apoptosis levels, cells were immunostained for active caspase 3. Lack of correlation between sub-G1 and caspase 3-positive cell percentages was observed (**Figure 1E**) as the number of caspase 3-positive cells at 10 nM paclitaxel (13%) was similar to the numbers of caspase 3-positive cells in the range of 3–100 nM paclitaxel. To further investigate the apparent contradiction between the results obtained by DNA content analysis and anti-caspase 3 staining a novel protocol for live cell analysis was developed and tested on B-lymphocytes.

Live Cell Staining With Hoechst33342 Provides Similar Results to PI Staining and Allows a Simultaneous Multi-Parameter Apoptosis Assessment

Live cell suspensions of RPMI8866 and RPMI8866-Tat-GFP were simultaneously stained with TMRE, Hoechst33342, CellEvent fluorescent caspase 3/7 substrate and annexin V-Alexa Fluor 647. Combined DNA content and apoptotic marker cell labeling was visualized using flow cytometry and fluorescence microscopy. Hoechst33342-based DNA content analysis provided a dose response pattern similar to PI staining with G2/M peak shift at "trigger" concentrations (**Supplementary Figure S2**). Dying cells exhibit the typical pattern of apoptotic events (Vorobjev and Barteneva, 2015): the gradual TMRE fluorescence decrease corresponding to mitochondrial membrane potential (MMP) loss, CellEvent fluorescence corresponding to caspase 3 activation and annexin V surface staining corresponding to phosphatidylserine externalization (**Figures 2D–I**). This result was confirmed by electron microscopy (**Figures 2J–N**): multiple apoptotic cells were detected in the paclitaxel-treated specimen. Early stages were characterized by chromatin marginalization; at later stages, cell volume decreased markedly, accompanied by cytoplasm condensation. Dead cells had destroyed plasma membranes and cytoplasmic organelles, but inside them the residuals of nuclei were still distinguishable.

Sub-G1 cell accumulation was observed at various rates upon MT inhibitor treatment and was most prominent in 10 nM paclitaxel (26%) (**Figures 2A–C**). The sub-G1 population was heterogeneous and contained cell debris with apoptotic markers and low MMP and cells with no apoptotic markers, hypodiploid DNA content and a two-fold decreased MMP compared to live cells with normal ploidy. Median TMRE fluorescence intensity was 976 a.u. for cell debris, 22380 a.u. for hypodiploid cells and 48265 a.u. for normal live cells (**Figures 2F–G**). Differences were statistically significant ($p < 0.05$). Fluorescence microscopy revealed live cells, apoptotic cells, cell debris and a fraction of small-sized live cells, often with micronuclei and dim mitochondria, in all MT inhibitor-treated specimens (**Supplementary Figure S3**).

DISCUSSION

It was shown that MT inhibitor concentrations sufficient for cell motility suppression can be lower than those needed for mitotic arrest (Kapoor and Panda, 2012; Molina et al., 2013). One of the thrilling questions is whether cytotoxic effects can be exerted at low concentrations of MT inhibitors. To answer this, we opted for a multi-parameter simultaneous cell cycle and cell death assessment. The proposed approach was derived from the two protocols described previously (Vorobjev and Barteneva, 2016; Potashnikova et al., 2018). It provides an easy and robust way to separately estimate the cytotoxic and mitostatic effects of microtubule inhibitors. The staining is suitable for high-throughput flow cytometry and imaging flow cytometry, as well as for microscopic evaluation of apoptosis kinetics in heterogeneous cell populations after chemotherapeutic treatment.

Using such an approach we described the non-linear dose response to an array of MT inhibitors, which seems to be universal. The "trigger" concentrations fall between 10–30 nM for paclitaxel, 30–100 nM for nocodazole and 10–30 nM for vinorelbine. Increasing dosages do not significantly alter G2/M accumulation. Despite the controversial data on B-cell responses to various types of MT inhibitors (Beswick et al., 2006; Frezzato et al., 2014) in our experiments the pattern of response to all compounds was similar for all cell lines. Our data on cell cycle accumulation and cell death percentages after MT inhibitor treatment correspond to the published data on adherent cells (Di Cesare et al., 2017).

Cells accumulated in G2/M phase die via apoptosis, exhibiting mitochondrial membrane potential (MMP) decrease, caspase activation and phosphatidylserine externalization. A sub-G1 population on DNA content curves includes late apoptotic cells and cell debris. However, at low paclitaxel concentrations this population also includes particularly large numbers of cells with MMP decreased only two-fold compared to normal cells and no markers of apoptosis. This explains the miscorrelation between sub-G1 and caspase 3-positive cell percentages observed in a range of paclitaxel concentrations. Such addition biases the interpretation of sub-G1 population as homogeneous and invariably apoptotic. Sub-G1 cells were described in other cell models as potentially non-viable products of aberrant mitosis (Demidenko et al., 2008) resulting from MT inhibition. Using fluorescence microscopy we visualized cells with smaller nuclei, often with micronuclei, and dim TMRE staining that fit the description of such cells. While their viability has to be further investigated, they present a distinctly different pattern of response to MT inhibitors compared to standard G2/M-accumulating cells that has to be accounted for.

Interestingly, MT inhibitors had the same effect on Tat-expressing B-lymphocytes (**Supplementary Figures S1**, **S2**).

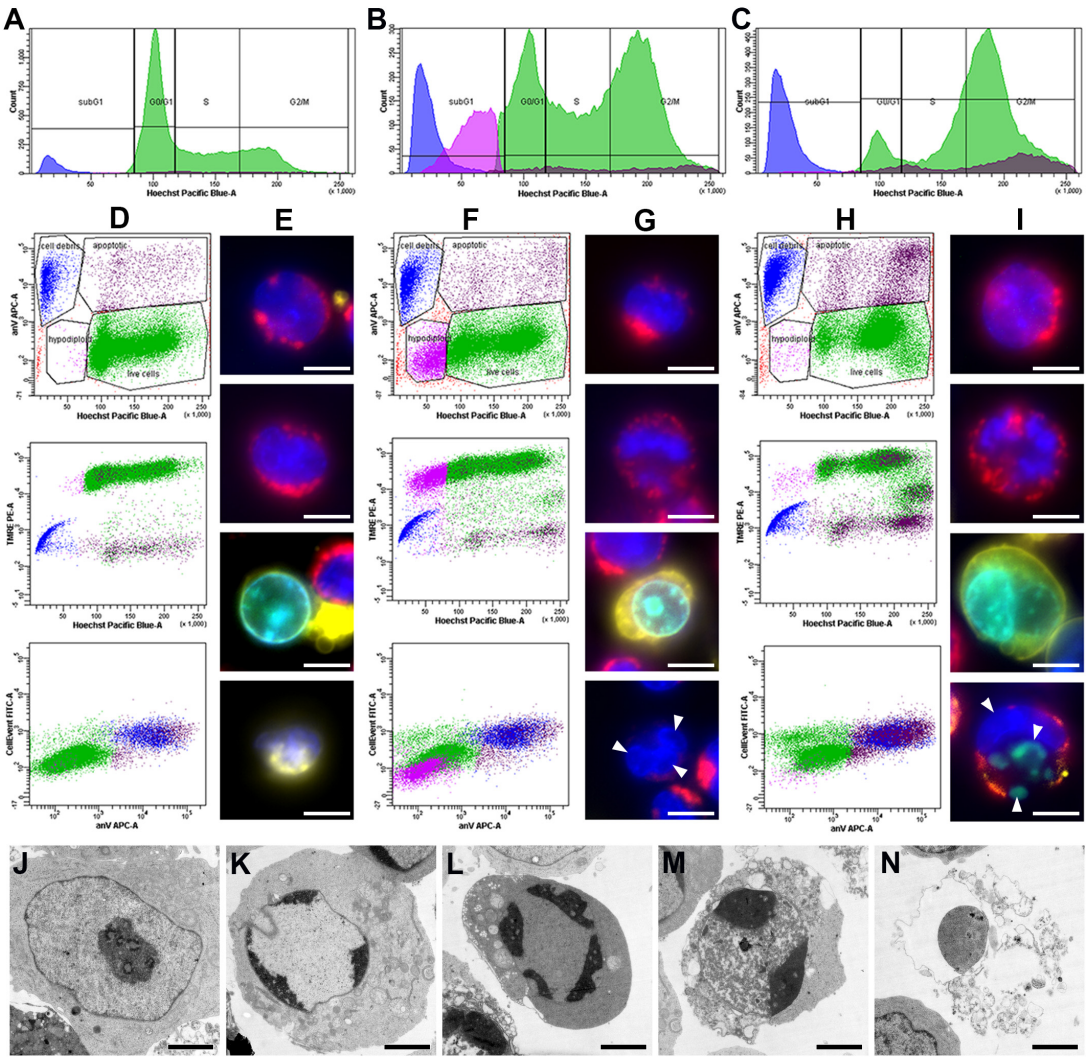

FIGURE 2 | RPMI8866 B-lymphocytes untreated (control) and treated with paclitaxel (10 and 1000 nM) for 24 h. **(A–C)** DNA content curves in individual samples assessed by flow cytometry after Hoechst33342 staining and linear gates set to determine sub-G1, G0/G1, S, and G2/M cell cycle populations [colored subpopulations correspond to live cells (green), apoptotic cells (brown), hypodiploid cells (purple) and cell debris (blue) as gated on dot plots **(D–F)**]. 50 000 events were analyzed per sample. **(A)** Normal cell cycle distribution in control cells; G2/M comprises 18% cells, sub-G1 comprises 6% cells. **(B)** G2/M accumulation after 10 nM paclitaxel treatment; G2/M comprises 30% cells, sub-G1 comprises 26% cells. **(C)** G2/M accumulation after 1000 nM paclitaxel treatment; G2/M comprises 49% cells, sub-G1 comprises 19% cells. **(D,F,H)** Dot plots representing simultaneous staining of RPMI8866 B-lymphocytes with Hoechst33342, TMRE, annexin V-Alexa Fluor 647, and CellEvent. Region gates are set to determine live cells (green), apoptotic cells (brown), hypodiploid cells (purple) and cell debris (blue) based on Hoechst33342 vs. annexin V staining. **(D)** Normal apoptosis rate in control cells. Region gates are set to live cells (green) – 89.4%, apoptotic cells (brown) – 3.2%, hypodiploid cells (purple) – 0.6% and cell debris (blue) – 6.8% based on Hoechst33342 vs. annexin V staining. The colors of the gated populations remain the same in the TMRE vs. Hoechst33342 and CellEvent vs. annexin V graphs. **(F)** G2/M and sub-G1 accumulation after 10 nM paclitaxel treatment. Region gates are set to live cells (green) – 69.0%, apoptotic cells (brown) – 4.9%, hypodiploid cells (purple) – 13.5% and cell debris (blue) – 12.6% based on Hoechst33342 vs. annexin V staining. The colors of the gated populations remain the same in the TMRE vs. Hoechst33342 and CellEvent vs. annexin V graphs. **(H)** G2/M accumulation after 1000 nM paclitaxel treatment. Region gates are set to live cells (green) – 67.0%, apoptotic cells (brown) – 13.3%, hypodiploid cells (purple) – 1.6% and cell debris (blue) – 18.1% based on Hoechst33342 vs. annexin V staining. The colors of the gated populations remain the same in the TMRE vs. Hoechst33342 and CellEvent vs. annexin V graphs. **(E,G,I)** Fluorescence images of cells untreated (control) and treated with paclitaxel (10 and 1000 nM) for 24 h. Simultaneous staining of RPMI8866 B-lymphocytes with Hoechst33342 (blue), TMRE (red), annexin V-Alexa 647 (yellow), and CellEvent (green). Scale bar – 10 μm. **(E)** Control cells; top two images correspond to live cells with bright nuclear Hoechst33342 and mitochondrial TMRE fluorescence, bottom two images correspond to an apoptotic cell with CellEvent staining in the nucleus and surface annexin V and cell debris with a dim nucleus and surface annexin V. **(G)** 10 nM paclitaxel treatment; top two images correspond to live cells with bright nuclear Hoechst33342 and mitochondrial TMRE fluorescence, third image corresponds to an apoptotic cell with CellEvent staining in the nucleus and surface annexin V, bottom image corresponds to aneuploid (hypodiploid) cell with dim mitochondrial TMRE fluorescence and micronuclei. White arrowheads indicate micronuclei. **(I)** 1000 nM paclitaxel treatment; top two images correspond to live cells with bright nuclear Hoechst33342 and mitochondrial TMRE fluorescence, bottom two images correspond to apoptotic cells with CellEvent staining in the nucleus and surface annexin V with/without micronuclei. White arrowheads indicate micronuclei. **(J–N)** Electron microscopy of cells at various stages of apoptosis after 10 nM paclitaxel treatment. Scale bar – 2 μm. **(J)** Normal cell with typical RPMI8866 lymphocyte morphology. **(K)** Chromatin marginalization. **(L)** Decrease of cell volume and condensation of cytoplasm (cell shrinkage). **(M)** Early stage of cell destruction (secondary necrosis). **(N)** Cellular debris inside which the residual chromatin and cytoplasmic organelles can be distinguished.

Despite some evidence of Tat protein interactions with microtubules (de Mareuil et al., 2005) RPMI8866-Tat-GFP cells do not differ from normal RPMI8866 lymphocytes in their MT inhibitor responses. The relevance of our findings for HIV-associated non-Hodgkin's lymphoma model is important for treating such patients.

Thus cell cycle arrest and cell death may be differentially affected by high and low doses of MT inhibitors which has a big therapeutic potential in oncology.

AUTHOR CONTRIBUTIONS

DP and AS conceived and performed the experiments, analyzed the data, and wrote the manuscript. AT performed the experiments and analyzed the data. ES and IV conceived and performed the experiments, analyzed the data, and edited the manuscript.

FUNDING

The project was funded by Russian Science Foundation Grant #18-75-00033.

ACKNOWLEDGMENTS

The authors acknowledge support from the MSU Program of Development (FACSAria SORP facility).

SUPPLEMENTARY MATERIAL

The Supplementary Material for this article can be found online at: https://www.frontiersin.org/articles/10.3389/fphar.2019.00436/full#supplementary-material

FIGURE S1 | Lymphocytes treated with MT inhibitors (concentration range 3, 10, 30, 100, 300, and 1000 nM) for 24 h and stained for DNA content with propidium iodide. Data from biological repeats on sub-G1, G0/G1, S, and G2/M population distributions presented as mean percentages with *SD* on a histogram. Graphs in columns represent RPMI8866 B-lymphocytes, RPMI8866-Tat-GFP B-lymphocytes and Jurkat T-lymphocytes, respectively. Graphs in rows represent paclitaxel, nocodazole and vinorelbine, respectively. Jurkat cells were previously known to respond to MT inhibitors and were therefore used as control.

FIGURE S2 | Lymphocytes treated with MT inhibitors (concentration range 3, 10, 30, 100, 300, and 1000 nM) for 24 h and stained for DNA content with Hoechst33342. Data from biological repeats on sub-G1, G0/G1, S, and G2/M population distributions presented as mean percentages with *SD* on a histogram. Graphs in columns represent RPMI8866 B-lymphocytes and RPMI8866-Tat-GFP B-lymphocytes, respectively. Graphs in rows represent paclitaxel, nocodazole and vinorelbine, respectively.

FIGURE S3 | Fluorescence image galleries of RPMI8866 B-lymphocytes treated with a low dose of MT inhibitor 10 nM paclitaxel for 24 h. Simultaneous staining with Hoechst33342 (blue), TMRE (red), annexin V-Alexa 647 (yellow), and CellEvent (green). Scale bar – 10 μm. **(A)** Live cells with normal morphology have bright round nuclei, bright mitochondrial TMRE fluorescence and bear no apoptotic markers. **(B)** Apoptotic cells have TMRE-negative mitochondria, CellEvent caspase substrate staining co-localized with nuclear staining and surface-bound annexin V indicating phosphatidylserine externalization. **(C)** Cell debris and late apoptotic cells have smaller size, irregular shape, TMRE-negative mitochondria, deformed nuclei, often with CellEvent staining, and surface-bound annexin V indicating phosphatidylserine externalization. **(D)** small-sized cells with small nuclei, micronuclei, few TMRE-dim mitochondria, and no apoptotic markers. White arrowheads indicate micronuclei.

REFERENCES

Bates, D., and Eastman, A. (2017). Microtubule destabilising agents: far more than just antimitotic anticancer drugs. *Br. J. Clin. Pharmacol.* 83, 255–268. doi: 10.1111/bcp.13126

Bates, D., Feris, E. J., Danilov, A. V., and Eastman, A. (2016). Rapid induction of apoptosis in chronic lymphocytic leukemia cells by the microtubule disrupting agent BNC105. *Cancer Biol. Ther.* 17, 291–299. doi: 10.1080/15384047.2016.1139245

Bennouna, J., Delord, J.-P., Campone, M., and Nguyen, L. (2008). Vinflunine: a new microtubule inhibitor agent. *Clin. Cancer Res.* 14, 1625–1632. doi: 10.1158/1078-0432.CCR-07-2219

Beswick, R. W., Ambrose, H. E., and Wagner, S. D. (2006). Nocodazole, a microtubule de-polymerising agent, induces apoptosis of chronic lymphocytic leukaemia cells associated with changes in Bcl-2 phosphorylation and expression. *Leuk Res.* 30, 427–436.

Cortes, J., and Vidal, M. (2012). Beyond taxanes: the next generation of microtubule targeting agents. *Breast Cancer Res. Treat.* 133, 821–830. doi: 10.1007/s10549-011-1875-6

de Mareuil, J., Carre, M., Barbier, P., Campbell, G. R., Lancelot, S., Opi, S., et al. (2005). HIV-1 Tat protein enhances microtubule polymerization. *Retrovirology* 2:5.

Demidenko, Z. N., Kalurupalle, S., Hanko, C., Lim, C. U., Broude, E., and Blagosklonny, M. V. (2008). Mechanism of G1-like arrest by low concentrations of paclitaxel: next cell cycle p53-dependent arrest with sub G1 DNA content mediated by prolonged mitosis. *Oncogene* 27, 4402–4410. doi: 10.1038/onc.2008.82

Di Cesare, E., Verrico, A., Miele, A., Guibettini, M., Rovella, P., Coluccia, A., et al. (2017). Mitotic cell death induction by targeting the mitotic spindle with tubulin-inhibitory indole derivative molecules. *Oncotarget* 8, 19738–19759. doi: 10.18632/oncotarget.14980

Donehower, R. C., and Rowinsky, E. K. (1993). An overview of experience with TAXOL (paclitaxel) in the U.S.A. *Cancer Treat. Rev.* 19(Suppl. C), 63–78.

Dumontet, C., and Jordan, M. A. (2010). Microtubule-binding agents: a dynamic field of cancer therapeutics. *Nat. Rev. Drug Discov.* 10, 790–803. doi: 10.1038/nrd3253

Frezzato, F., Trimarco, V., Martini, V., Gattazzo, C., Ave, E., Visentin, A., et al. (2014). Leukaemic cells from chronic lymphocytic leukaemia patients undergo apoptosis following microtubule depolymerization and Lyn inhibition by nocodazole. *Br. J. Haematol.* 165, 659–672. doi: 10.1111/bjh.12815

Gopal, S., Patel, M. R., Yanik, E. L., Cole, S. R., Achenbach, C. J., Napravnik, S., et al. (2013). Temporal trends in presentation and survival for HIV-associated lymphoma in the antiretroviral therapy era. *J. Natl. Cancer Inst.* 105, 1221–1229. doi: 10.1093/jnci/djt158

Grigoriev, I. S., Chernobelskaya, A. A., and Vorobjev, I. A. (1999). Nocodazole, vinblastine and taxol at low concentrations affect fibroblast locomotion and saltatory movements of organelles. *Membr. Cell Biol.* 13, 23–48.

Jordan, M. A., Toso, R. J., Thrower, D., and Wilson, L. (1993). Mechanism of mitotic block and inhibition of cell proliferation by taxol at low concentrations. *Proc. Natl. Acad. Sci. U.S.A.* 90, 9552–9556.

Kapoor, S., and Panda, D. (2012). Kinetic stabilization of microtubule dynamics by indanocine perturbs EB1 localization, induces defects in cell polarity and inhibits migration of MDA-MB-231 cells. *Biochem. Pharmacol.* 83, 1495–1506. doi: 10.1016/j.bcp.2012.02.012

Kaverina, I., and Straube, A. (2011). Regulation of cell migration by dynamic microtubules. *Semin. Cell Dev. Biol.* 22, 968–974. doi: 10.1016/j.semcdb.2011.09.017

Liao, G., Nagasaki, T., and Gundersen, G. G. (1995). Low concentrations of nocodazole interfere with fibroblast locomotion without significantly affecting

microtubule level: implications for the role of dynamic microtubules in cell locomotion. *J. Cell Sci.* 108, 3473–3483.

Molina, A., Velot, L., Ghouinem, L., Abdelkarim, M., Bouchet, B. P., Luissint, A. C., et al. (2013). ATIP3, a novel prognostic marker of breast cancer patient survival, limits cancer cell migration and slows metastatic progression by regulating microtubule dynamics. *Cancer Res.* 73, 2905–2915. doi: 10.1158/0008-5472.CAN-12-3565

Musinova, Y. R., Sheval, E. V., Dib, C., Germini, D., and Vassetzky, Y. S. (2016). Functional roles of HIV-1 tat protein in the nucleus. *Cell. Mol. Life Sci.* 73, 589–601. doi: 10.1007/s00018-015-2077-x

Perez, E. A. (2009). Microtubule inhibitors: differentiating tubulin-inhibiting agents based on mechanisms of action, clinical activity, and resistance. *Mol. Cancer Ther.* 8, 2086–2095. doi: 10.1158/1535-7163.MCT-09-0366

Potashnikova, D., Golyshev, S., Penin, A., Logacheva, M., Klepikova, A., Zharikova, A., et al. (2018). FACS isolation of viable cells in different cell cycle stages from asynchronous culture for RNA sequencing. *Methods Mol. Biol.* 1745, 315–335. doi: 10.1007/978-1-4939-7680-5_18

Sève, P., Reiman, T., Isaac, S., Trillet-Lenoir, V., Lafanéchère, L., Sawyer, M., et al. (2008). Protein abundance of class III beta-tubulin but not Delta2-alpha-tubulin or tau is related to paclitaxel response in carcinomas of unknown primary site. *Anticancer Res.* 28, 1161–1167.

Vendrame, E., Hussain, S. K., Breen, E. C., Magpantay, L. I., Widney, D. P., Jacobson, L. P., et al. (2014). Serum levels of cytokines and biomarkers for inflammation and immune activation, and HIV-associated non-Hodgkin B-cell lymphoma risk. *Cancer Epidemiol. Biomarkers Prev.* 23, 343–349. doi: 10.1158/1055-9965.EPI-13-0714

Vorobjev, I., and Barteneva, N. (2016). Temporal heterogeneity in apoptosis determined by imaging flow cytometry. *Methods Mol. Biol.* 1389, 221–233. doi: 10.1007/978-1-4939-3302-0_16

Vorobjev, I., and Barteneva, N. S. (2015). Temporal heterogeneity metrics in apoptosis induced by anticancer drugs. *J. Histochem. Cytochem.* 63, 494–510. doi: 10.1369/0022155415583534

Windebank, A. J. (1999). Chemotherapeutic neuropathy. *Curr. Opin. Neurol.* 12, 565–571.

Xie, X., Wu, Y., Luo, S., Yang, H., Li, L., Zhou, S., et al. (2017). Efficacy and toxicity of low-dose versus conventional-dose chemotherapy for malignant tumors: a meta-analysis of 6 randomized controlled trials. *Asian Pac. J. Cancer Prev.* 18, 479–484.

Yang, H., Ganguly, A., and Cabral, F. (2010). Inhibition of cell migration and cell division correlates with distinct effects of microtubule inhibiting drugs. *J. Biol. Chem.* 285, 32242–32250. doi: 10.1074/jbc.M110.160820

Conflict of Interest Statement: The authors declare that the research was conducted in the absence of any commercial or financial relationships that could be construed as a potential conflict of interest.

frontiers in Pharmacology

BRIEF RESEARCH REPORT
published: 09 May 2019
doi: 10.3389/fphar.2019.00507

Synergistic Cytotoxicity of Methyl 4-Hydroxycinnamate and Carnosic Acid to Acute Myeloid Leukemia Cells *via* Calcium-Dependent Apoptosis Induction

Aviram Trachtenberg[1]*, *Suchismita Muduli*[1], *Katarzyna Sidoryk*[2], *Marcin Cybulski*[2] and *Michael Danilenko*[1]

[1] Department of Clinical Biochemistry and Pharmacology, Ben-Gurion University of the Negev, Beer Sheva, Israel, [2] Chemistry Department, Pharmaceutical Research Institute, Warsaw, Poland

OPEN ACCESS

Edited by:
Vadim V. Sumbayev,
University of Kent, United Kingdom

Reviewed by:
Elvira V. Grigorieva,
Institute of Molecular Biology and Biophysics (RAS), Russia
Michael Milyavsky,
Tel Aviv University, Israel
Xi Zheng,
Rutgers, The State University of New Jersey, Newark, United States

***Correspondence:**
Aviram Trachtenberg
aviramtr@post.bgu.ac.il

Specialty section:
This article was submitted to Experimental Pharmacology and Drug Discovery, a section of the journal Frontiers in Pharmacology

Received: 12 February 2019
Accepted: 24 April 2019
Published: 09 May 2019

Citation:
Trachtenberg A, Muduli S, Sidoryk K, Cybulski M and Danilenko M (2019) Synergistic Cytotoxicity of Methyl 4-Hydroxycinnamate and Carnosic Acid to Acute Myeloid Leukemia Cells via Calcium-Dependent Apoptosis Induction. Front. Pharmacol. 10:507. doi: 10.3389/fphar.2019.00507

Acute myeloid leukemia (AML) is a malignant hematopoietic disease with poor prognosis for most patients. Conventional chemotherapy has been the standard treatment approach for AML in the past 40 years with limited success. Although, several targeted drugs were recently approved, their long-term impact on survival of patients with AML is yet to be determined. Thus, it is still necessary to develop alternative therapeutic approaches for this disease. We have previously shown a marked synergistic anti-leukemic effect of two polyphenols, curcumin (CUR) and carnosic acid (CA), on AML cells *in-vitro* and *in-vivo*. In this study, we identified another phenolic compound, methyl 4-hydroxycinnamate (MHC), which among several tested phytochemicals could uniquely cooperate with CA in killing AML cells, but not normal peripheral blood mononuclear cells. Notably, our data revealed striking phenotypical and mechanistic similarities in the apoptotic effects of MHC+CA and CUR+CA on AML cells. Yet, we show that MHC is a non-fluorescent molecule, which is an important technical advantage over CUR that can interfere in various fluorescence-based assays. Collectively, we demonstrated for the first time the antileukemic activity of MHC in combination with another phenolic compound. This type of synergistically acting combinations may represent prototypes for novel antileukemic therapy.

Keywords: acute myeloid leukemia, curcumin, carnosic acid, methyl 4-hydroxycinnamate, calcium-dependent apoptosis

INTRODUCTION

Acute myeloid leukemia (AML) is a devastating hematological malignancy characterized by poor survival, particularly for older patients, and high relapse rate. In the past four decades, there have been no major changes in the standard AML chemotherapy regimen. Although in 2017–2018 eight new promising AML drugs were approved by the U.S. Food and Drug Administration (FDA) (Stone, 2017; Rowe, 2018), their impact on long-term patient survival is yet to be determined. Various natural and synthetic phenolic compounds have

been shown to possess anti-leukemic potential in preclinical models (De Martino et al., 2011), curcumin (CUR) being one of the most studied polyphenols (Kelkel et al., 2010). However, the majority of *in vitro* studies employed high supraphysiological concentrations of CUR (Lin et al., 2008; Zhang et al., 2017; Martínez-Castillo et al., 2018) which induced generalized cellular stress events leading to cell death, such as oxidative stress (Lin et al., 2008; Yoon et al., 2012), ER stress (Lin et al., 2008; Cao et al., 2013), or mitochondrial damage (Yoon et al., 2012; Cao et al., 2013; Xu et al., 2015). We have previously shown that CUR combined with another polyphenol, carnosic acid (CA), at noncytotoxic concentrations of each agent synergistically and selectively killed AML cells by inducing massive apoptosis both *in vitro* and *in vivo* (Pesakhov et al., 2010, 2016). This synergistic effect was not accompanied by cellular stress and was specifically mediated by cytosolic calcium ($[Ca^{2+}]_{cyt}$) overload (Pesakhov et al., 2010, 2016).

In the current study, we examined whether in addition to CUR some other phytochemicals are capable of synergizing with CA against AML cells. Thus, following screening of several phenolic compounds and a sesquiterpene lactone we identified another synergistically acting combination comprised of the phenolic acid derivative methyl 4-hydroxycinnamate (MHC) and CA. MHC is found in several plants, such as green onion (*Allium cepa*) (Xiao and Parkin, 2007) or noni (*Morinda citrifolia* L.) leaves (Zhang et al., 2016), and has potential chemopreventive activity (Xiao and Parkin, 2007). To the best of our knowledge, MHC has not been previously tested as an antileukemic agent. Here, we report that the cytotoxic effect of the MHC+CA combination is very similar to that of CUR+CA, both phenomenologically and mechanistically. Furthermore, in contrast to CUR, which is highly fluorescent, and thus is known to interfere with fluorescence-based assays (Nelson et al., 2017), MHC had no detectable fluorescence when tested by flow cytometry in a wide range of wavelengths (FL1–FL10).

MATERIALS AND METHODS

Materials

Curcumin (≥90%) and carnosic acid (98%) were purchased from Cayman Chemicals (Ann Arbor, MI, USA) and Chemlin UK (Nanjing, China), respectively. Methyl 4-hydroxycinnamate (96%) was synthesized by Dr. Katarzyna Sidoryk (Chemistry Department, Pharmaceutical Research Institute, Poland), as described previously (Sidoryk et al., 2018). zVAD-fmk was purchased from AdooQ BioScience (Irvine, CA, USA). Propidium iodide (PI), 2-aminoethoxydiphenyl borate (2-APB), Arabinosylcytosine (Ara-C), and staurosporine (STS) were purchased from Sigma (Rehovot, Israel). Annexin V-APC was obtained from BioLegend (San Diego, CA, USA). Fluo-3/AM, 2′,7′-dichlorofluorescein-diacetate (DCFH-DA), dihydrorhodamine 123 (DHR) and tetramethylrhodamine methyl ester (TMRE) were purchased from Santa Cruz Biotechnology (Dallas, TX, USA). RPMI 1640 medium and heat-inactivated fetal bovine serum (FBS) were purchased from Gibco-Invitrogen (Carlsbad, CA, USA). Hank's buffered salt solution (HBSS), Ca^{2+}/Mg^{2+}-free phosphate buffered saline (PBS), penicillin, streptomycin, and HEPES were purchased from Biological Industries (Beit Haemek, Israel). Stock solutions of curcumin (5 mM) and carnosic acid (10 mM) were prepared in absolute ethanol and methyl 4-hydroxycinnamate (50 mM) in DMSO.

Cell Culture and Enumeration

Human AML cell lines, such as KG-1a stem-like cells (CCL-246.1) and HL60 myoblastic cells (CCL-240), were purchased from American Type Culture Collection (Rockville, MD). Cells were cultured in RPMI 1640 medium supplemented with 10% FBS, penicillin (100 U/ml), streptomycin (0.1 mg/ml), and 10 mM HEPES (pH = 7.4) in a humidified atmosphere of 95% air and 5% CO_2, at 37°C. Cells were enumerated in Vi-Cell XR cell viability analyzer (Beckman Coulter Inc., Fullerton, CA) using an automatic trypan blue exclusion assay. The number of viable (trypan blue-impermeable) cells was counted directly, and cell viability was calculated as the percentage of viable cells relative to the total (viable + dead) cell count.

Acridine Orange and Ethidium Bromide Staining

Cells were collected by centrifugation and double stained with 14 μg/ml acridine orange and 14 μg/ml ethidium bromide, as described previously (Pesakhov et al., 2010). Nuclear morphology of stained cells was examined by fluorescent microscopy at a magnification of 400x.

Annexin V/Propidium Iodide Assay

Cells were washed with PBS then stained with annexin V-APC and PI, as described previously (Pesakhov et al., 2016). Percentages of apoptotic cells were determined by flow cytometry in a Gallios instrument (Beckman Coulter, Miami, FL). For each analysis 10,000 events were recorded, and the data were processed using Kaluza software, version 2.1 (Beckman Coulter).

Determination of Intracellular Levels of Reactive Oxygen Species (ROS)

The intracellular ROS levels were determined as described previously (Pesakhov et al., 2010) using the oxidation-sensitive fluorescent probes DCFH-DA and DHR. Cells were harvested, washed with HEPES-supplemented HBSS (pH = 7.3) and loaded with 5 μM DCFH-DA or DHR. Cells were then incubated in a shaking water bath at 37°C, for 15 min in the dark. Fluorescence intensity was analyzed by flow cytometry, as described above.

Determination of Mitochondrial Membrane Potential

Cells were harvested, washed with HEPES-supplemented HBSS (pH = 7.3) and loaded with

Abbreviations: 2-APB, 2-aminoethoxydiphenyl borate; Ara-C, arabinosylcytosine (Cytarabine); DCF, 2′,7′-dichlorofluorescein; DCFH-DA, 2′,7′-dichlorofluorescein-diacetate; DHR, dihydrorhodamine 123; FCCP, carbonyl cyanide-4-(trifluoromethoxy)phenylhydrazone; IP_3R, inositol trisphosphate receptor; PARP, poly(ADP-ribose) polymerase; PBMC, peripheral blood mononuclear cells; PI, propidium iodide; STS, staurosporine; TMRE, tetramethylrhodamine methyl ester.

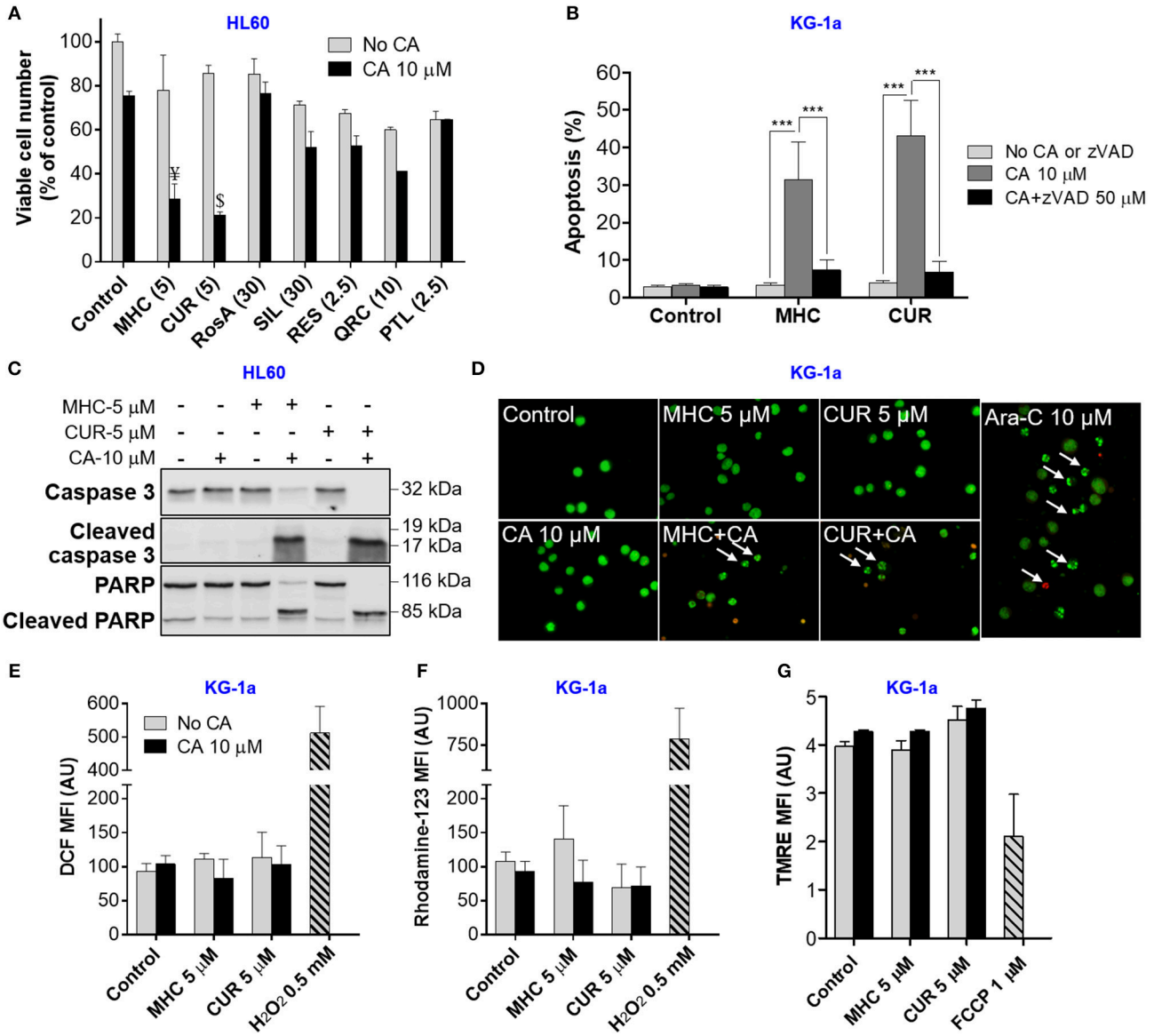

FIGURE 1 | MHC is similar to CUR in the ability to synergize with CA in inducting anti-leukemic effects on AML cells. **(A)** Changes in viable cell numbers. HL60 cells were treated with different phenolic compounds (in μM): CUR, MHC, rosmarinic acid (RosA), silibinin (SIL), resveratrol (RES), quercetin (QRC), parthenolide (PTL) and/or 10 μM CA, for 72 h. Viable cell numbers were determined by the trypan blue exclusion assay. The data are the means ± SD ($n = 3$). **(B)** Apoptosis induction. KG1a cells were treated for 8 h in the presence or absence of zVAD (50 μM). The extent of apoptosis was determined by the annexin V/PI binding assay. **(C)** Western blot analysis of caspase-3 and PARP cleavage in HL60 cells treated with MHC or CUR with or without CA, for 24 h. **(D)** Changes in nuclear morphology. KG-1a cells were treated with the indicated compounds, for 8 h, followed by staining with acridine orange (green fluorescence) and ethidium bromide (red fluorescence). Stained cells were examined under fluorescence microscope at 400x magnification. Cells treated with 10 μM Ara-C, for 8 h, were used as the positive control. Arrows indicate late apoptotic cells and/or apoptotic bodies. **(E,F)** Assessment of the intracellular ROS. KG-1a cells were treated with the indicated compounds, for 4 h, followed by loading with $DCFH_2$-DA **(E)** or DHR **(F).** DCF and rhodamine-123 fluorescence was measured by flow cytometry. Averaged geometric means of fluorescence intensities (MFI) ± SD from three independent experiments are shown. H_2O_2 (0.5 mM) was used as the positive control. **(G)** Assessment of the mitochondrial membrane potential. KG-1a cells were treated with the indicated compounds, for 2 h, followed by loading with TMRE. Averaged MFI ± SD were measured in 3 independent experiments. The uncoupler FCCP (1 μM, 10 min) was used as the positive control. Synergistic effect (AB>A+B): ¥, $p < 0.05$; $, $p < 0.01$; Student's *t*-test. AU, arbitrary units. **(B)** ***$p < 0.001$; one-way ANOVA with Tukey multiple comparison *post-hoc* analysis.

TMRE (100 nM), for 30 min in the dark, washed and resuspended in serum-free medium. Changes in mitochondrial membrane potential were assessed by flow cytometry.

Measurement of Cytosolic Calcium Levels ($[Ca^{2+}]_{cyt}$)

To evaluate changes in steady-state $[Ca^{2+}]_{cyt}$, cells were harvested, washed and incubated with 2.5 μM Fluo-3/AM

in calcium (2 mM)-supplemented Ringer's solution (Levin-Gromiko et al., 2014; Pesakhov et al., 2016) at room temperature for 30 min in the dark. Cells were then washed, resuspended in Ca^{2+}-free Ringer's solution and analyzed by flow cytometry.

Western Blot Analysis

Western blotting was performed using whole cell extracts, as described before (Pesakhov et al., 2016). The following primary antibodies were used: caspase-3 from Santa Cruz Biotechnology (sc-7272; 1:500); cleaved caspase-3 from Cell Signaling Technology (#9661; 1:1,000) and poly(ADP-ribose) polymerase (PARP) from Enzo (BML-SA253; 1:5,000).

Statistical Analysis

All experiments were conducted at least three times. Statistically significant differences between two experimental groups were estimated by unpaired two-tailed Student's *t*-test. The significance of the differences between the means of several subgroups was assessed by one-way ANOVA with Tukey multiple comparison *post-hoc* analysis. A $P < 0.05$ was considered statistically significant. The synergy between the effects of two compounds was determined as described previously (Danilenko et al., 2001; Pesakhov et al., 2010). Briefly, two compounds (A and B) were considered to show enhancement in the particular experiment if the effect of their combination (AB) was larger than the sum of their individual effects (AB>A+B), the data being compared after subtraction of the respective control values from A, B, and AB. Detailed analysis of the interaction between two compounds was performed by the combination index (CI) method (see **Supplementary Material**). The statistical analyses were performed using GraphPad Prism 6.0 software (Graph-Pad Software, San Diego, CA).

RESULTS

MHC and CUR, but Not Other Tested Phytochemicals, Similarly Synergize With CA to Induce Apoptotic Cell Death in AML Cells

We first performed pilot experiments in HL60 cells to determine the maximal non-cytotoxic concentrations (MNC) of several phytochemicals (**Supplemental Figure S1**) for further screening of these compounds for the ability to cooperate with CA in inducing AML cell death. **Figure 1A** demonstrates that, when applied alone at the MNC for 72 h, the phenolic compounds MHC, CA, rosmarinic acid (RosA), silibinin (SIL), resveratrol (RES), quercetin (QRC), and the sesquiterpene lactone parthenolide (PTL) reduced HL60 viable cell numbers to a varying extent (by 10–40%), without significantly affecting cell viability (**Supplemental Figure S1**). However, besides CUR, only MHC could strongly synergize with CA in reducing viable cell numbers, as determined in KG-1a, HL60, and U937 AML cells (**Figure 1A** and **Supplemental Figures S2A,D**). The analysis of interaction between MHC and CA in KG-1a cells shows a strong synergy at different concentrations of the two compounds, as indicated by very low (<<1) Combination Index values (**Supplemental Figures S2B,C**). A synergistic decrease in cell viability, i.e., in the percentage of viable cells relative to the total cell count, was observed only in samples treated with MHC+CA or CUR+CA (**Supplemental Figure S1**), though this effect was less pronounced compared to a decrease in viable cell numbers (**Figure 1A**). This may be due to inhibition of cell proliferation in addition to cytotoxicity. Furthermore, some of the cells can be completely destroyed following combined treatments, a phenomenon not uncommon in cell culture studies. Thus, the proportion of dead cells in cultures remaining after CUR+CA and MHC+CA treatments (**Figure 1A**) might be underestimated when using trypan blue exclusion assay (**Supplemental Figure S1**).

In analogy with the previously characterized CUR+CA combination (Pesakhov et al., 2010, 2016), MHC+CA-induced cytotoxicity was accompanied by an induction of caspase-dependent apoptosis (**Figure 1B** and **Supplemental Figure S3B**) that was manifested by a rapid zVAD-inhibitable cleavage of caspase 3 and PARP (**Figure 1C** and **Supplemental Figures S2E, S3A**). Notably, although the combinations were cytotoxic to all three cell lines tested (**Figure 1A** and **Supplemental Figures S2A,D)**, KG-1a cells were the most sensitive, as demonstrated by a more rapid cleavage of caspase-3 or PARP (8 h; **Supplemental Figure S3A)** than in HL60 and U937 cells (24 h; **Figure 1C** and **Supplemental Figure S2E**). In contrast, neither combination significantly affected cell death in PBMC samples. This was evidenced both by the annexin V/PI assay (**Supplemental Figure S4A**) and by continuous real-time monitoring for the appearance of low-area (shrunk) cells in the IncuCyte Live-Cell Analysis System (**Supplemental Figures S2F, S4B,C**). U937 cells treated with MHC+CA and PBMCs treated with staurosporine, a known apoptosis inducer, exhibited a marked time-dependent increase in the proportion of low-area cells (**Supplemental Figures S2F, S4B,C** and **Supplemental Videos**) which are considered apoptotic/dead (Majno and Joris, 1995).

As expected, apoptosis of AML cells was accompanied by shrinkage and fragmentation of the nuclei and chromatin condensation (**Figure 1D**). On the other hand, we have not observed the signs of necrotic cell death, such as uniformly stained (in orange) nuclei of regular size or larger, which usually exhibit normal morphology. Importantly, the induction of apoptosis was not preceded by intracellular ROS accumulation (**Figures 1E,F**) or changes in the mitochondrial membrane potential (**Figure 1G**).

A Synergistic Induction of Apoptosis by the MHC+CA Combination Is Mediated by Intracellular Calcium Accumulation

Since CUR+CA-induced apoptosis was previously found to be mediated by a sustained $[Ca^{2+}]_{cyt}$ overload, we next

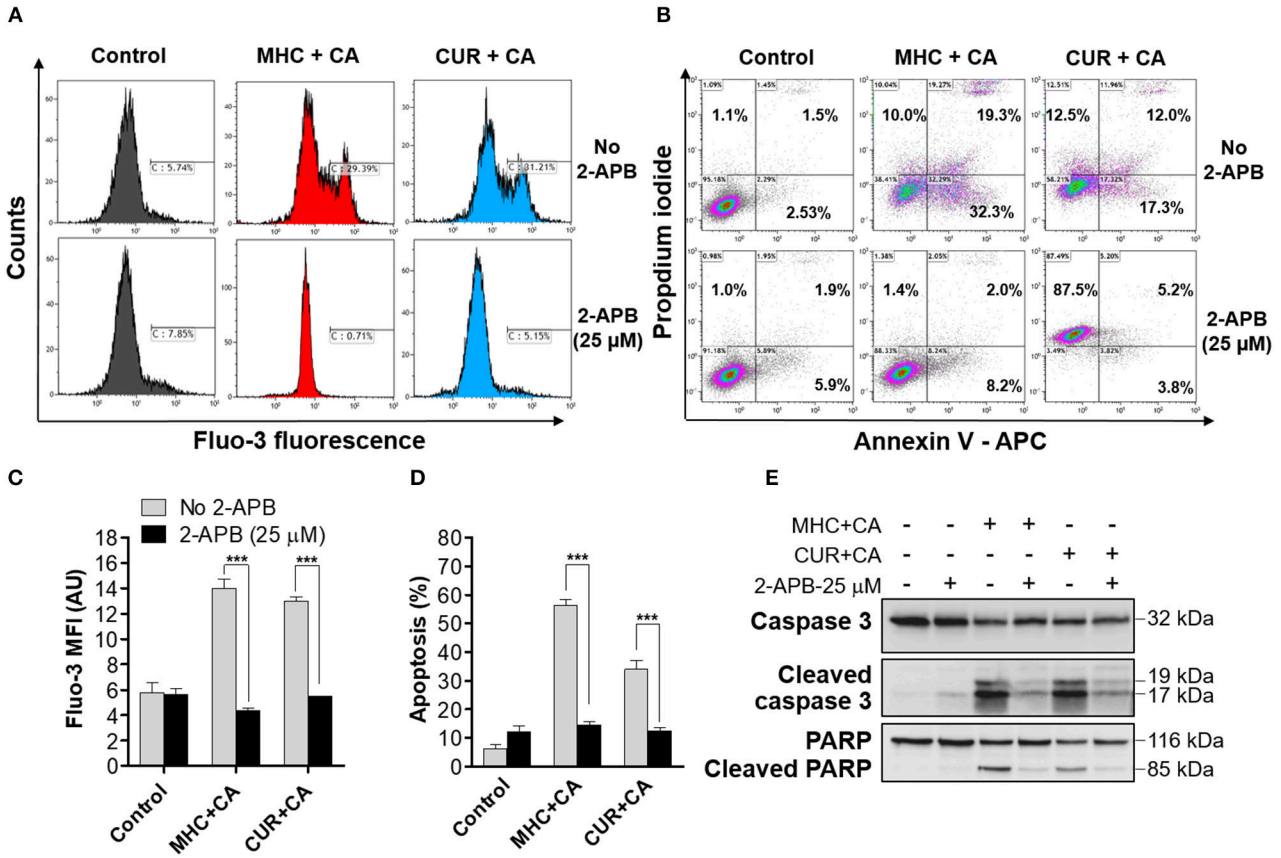

FIGURE 2 | Similar to CUR+CA, the MHC+CA combination induces calcium-dependent apoptosis in the KG-1a cell line. Cells were treated with MHC+CA or CUR+CA in the presence or absence of 2-APB (25 μM). **(A,C)** Steady-state cytosolic calcium levels were measured after 4 h of incubation. **(A)** Typical histograms obtained from Fluo-3 loaded cells in a representative experiment. **(C)** Averaged Fluo-3 MFI ± SD from three independent experiments. **(B,D,E)** The extent of apoptosis was determined by the annexin V/PI binding assay, after 8 h of incubation. **(B)** Typical flow cytometric data obtained in a representative experiment. The data were analyzed after setting threshold for CUR+CA auto-fluorescence. **(D)** Averaged percentages of apoptotic cells ± SD ($n = 3$). **(E)** Representative Western blots showing caspase-3 and PARP cleavage ($n = 3$). ***$p < 0.001$; one-way ANOVA with Tukey multiple comparison *post-hoc* analysis.

examined whether MHC+CA also kills AML cells by a Ca^{2+}-dependent mechanism (Pesakhov et al., 2016). Indeed, using the cytosolic Ca^{2+} indicator Fluo-3 we found that, similar to CUR+CA, the MHC+CA combination applied to KG-1a cells caused a sustained elevation of $[Ca^{2+}]_{cyt}$ and that this effect was prevented by 2-APB known to antagonize inositol trisphosphate receptors (IP_3R) and store-operated Ca^{2+} channels (**Figures 2A,C**) (Dobrydneva and Blackmore, 2001; Yanamandra et al., 2011; Littlechild et al., 2015). Likewise, 2-APB abrogated the induction of apoptosis in MHC+CA-treated cells (**Figures 2B,D**). The latter inhibitory effect was associated with an almost complete block of MHC+CA-induced caspase-3 and PARP cleavage by 2-APB (**Figure 2E**).

Fluorescence Properties of CUR and MHC

CUR is known as a fluorescent molecule and is considered a pan-assay interference compound (PAINS) (Nelson et al., 2017). Furthermore, CUR is unstable in aqueous solutions (Wang et al., 1997) and various antioxidants, including phenolic compounds, have been shown to stabilize CUR in buffers and to increase its plasma levels in animals (Nimiya et al., 2016; Nelson et al., 2017). Screening of CUR-treated and otherwise unstained AML cell samples over the entire standard set of flow cytometer channels (FL1–FL10) revealed noticeable CUR fluorescence in half of these channels, FL1–FL3 and FL9–FL10 (**Supplemental Figures S5A,B**). Furthermore, CUR fluorescence was found to increase in the presence of the antioxidant CA (**Supplemental Figure S5C**). This made it necessary to utilize fluorophores, which can be detected in the "CUR-insensitive" range of wavelengths, or, if not possible, to set threshold fluorescence parameters using unstained CUR ± CA-treated cells. For instance, in the annexin V/PI assay we utilized allophycocyanin (APC)-labeled annexin V (e.g., **Figure 2B** and **Supplemental Figure S3B**) for measurements in FL6, instead of the most commonly used fluorescein isothiocyanate (FITC)-labeled annexin V which has green fluorescence detected in FL1. Threshold for orange CUR+CA fluorescence in the propidium iodide (FL3) channel was set as described above (**Figure 2B** and **Supplemental Figure S3B**). Interestingly, we found that 2-APB strongly enhanced CUR+CA fluorescence in PI-stained

cells (**Figure 2B**). In contrast to CUR, MHC did not exhibit auto-fluorescence under any experimental conditions of this study (**Figure 2B**, **Supplemental Figures S3B**, **S5**), and thus did not require any adjustments in fluorescence-based assays.

DISCUSSION

The major novel finding of this study is that, similar to CUR (Pesakhov et al., 2016), MHC is capable of synergistically cooperating with another phenolic compound, CA, at low concentrations of each agent in inducing profound cytotoxicity to AML cells, but not to normal PBMCs (**Supplemental Figure S4)** *in vitro*. This similarity was evidenced by a comparable ability of the two combinations to induce caspase- and calcium-dependent apoptosis (**Figures 1B**, **2B,D** and **Supplemental Figures S2E, S3**) which was not associated with increased generation of ROS (**Figures 1E,F**) or reduction in the mitochondrial membrane potential (**Figure 1G**). Interestingly, no such cooperation was observed between MHC and CUR (data not shown) or between CA and other phytochemicals tested here (**Figure 1A** and **Supplemental Figure S1**). These findings suggest that comparable apoptosis-inducing activities of MHC+CA and CUR+CA may be due to certain structural similarities between MHC and CUR molecules, such as the presence of the 4-hydroxyl group at the aromatic ring and the α,β-unsaturated carbonyl group (**Supplemental Figure S6**). Apart from the above similarities, we found that MHC is a non-fluorescent molecule (**Supplemental Figure S5**) which made it technically superior to CUR, a widely recognized PAINS compound (Nelson et al., 2017). Further mechanistic and translational studies are needed to evaluate the therapeutic potential of the MHC+CA combination. This and similar combinations of synergistically acting natural or synthetic phenolic compounds may represent molecular prototypes for the design of novel modalities in AML therapy and/or prevention.

DATA AVAILABILITY

All datasets generated for this study are included in the manuscript and/or the **Supplementary Files**.

AUTHOR CONTRIBUTIONS

MD, AT, and KS conceived the concept. AT and MD designed experiments and wrote the manuscript. AT and SM performed experiments. KS and MC provided reagents.

FUNDING

This work is supported by the Israel Science Foundation grant 226/16.

SUPPLEMENTARY MATERIAL

The Supplementary Material for this article can be found online at: https://www.frontiersin.org/articles/10.3389/fphar.2019.00507/full#supplementary-material

REFERENCES

Cao, A., Li, Q., Yin, P., Dong, Y., Shi, H., Wang, L., et al. (2013). Curcumin induces apoptosis in human gastric carcinoma AGS cells and colon carcinoma HT-29 cells through mitochondrial dysfunction and endoplasmic reticulum stress. *Apoptosis* 18, 1391–1402. doi: 10.1007/s10495-013-0871-1

Danilenko, M., Wang, X., and Studzinski, G. P. (2001). Carnosic acid and promotion of monocytic differentiation of HL60-G cells initiated by other agents. *J. Natl. Cancer Inst.* 93, 1224–1233. doi: 10.1093/jnci/93.16.1224

De Martino, L., D'Arena, G., Filosa, R., Peduto, A., Zeppa, R., and De Feo, V. (2011). Natural compounds in anti-leukaemic therapy: a review. *Mini Rev. Med. Chem.* 11, 492–502. doi: 10.2174/138955711795843284

Dobrydneva, Y., and Blackmore, P. (2001). 2-Aminoethoxydiphenyl borate directly inhibits store-operated calcium entry channels in human platelets. *Mol. Pharmacol.* 60, 541–552.

Kelkel, M., Jacob, C., Dicato, M., and Diederich, M. (2010). Potential of the dietary antioxidants resveratrol and curcumin in prevention and treatment of hematologic malignancies. *Molecules* 15, 7035–7074. doi: 10.3390/molecules15107035

Levin-Gromiko, U., Koshelev, V., Kushnir, P., Fedida-Metula, S., Voronov, E., and Fishman, D. (2014). Amplified lipid rafts of malignant cells constitute a target for inhibition of aberrantly active NFAT and melanoma tumor growth by the aminobisphosphonate zoledronic acid. *Carcinogenesis* 35, 2555–2566. doi: 10.1093/carcin/bgu178

Lin, S. S., Huang, H. P., Yang, J. S., Wu, J. Y., Hsia, T. C., Lin, C. C., et al. (2008). DNA damage and endoplasmic reticulum stress mediated curcumin-induced cell cycle arrest and apoptosis in human lung carcinoma A-549 cells through the activation caspases cascade- and mitochondrial-dependent pathway. *Cancer Lett.* 272, 77–90. doi: 10.1016/j.canlet.2008.06.031

Littlechild, R., Zaidman, N., Khodaverdi, D., and Mason, M. J. (2015). Inhibition of KCa3.1 by depolarisation and 2-aminoethoxydiphenyl borate (2-APB) during Ca^{2+} release activated Ca^{2+} (CRAC) entry in human erythroleukemia (HEL) cells: implications for the interpretation of 2-APB inhibition of CRAC entry. *Cell Calcium* 57, 76–88. doi: 10.1016/j.ceca.2014.12.009

Majno, G., and Joris, I. (1995). Apoptosis, oncosis, and necrosis. An overview of cell death. *Am. J. Pathol.* 146, 3–15.

Martínez-Castillo, M., Villegas-Sepúlveda, N., Meraz-Rios, M. A., Hernández-Zavala, A., Berumen, J., Coleman, M. A., et al. (2018). Curcumin differentially affects cell cycle and cell death in acute and chronic myeloid leukemia cells. *Oncol. Lett.* 15, 6777–6783. doi: 10.3892/ol.2018.8112

Nelson, K. M., Dahlin, J. L., Bisson, J., Graham, J., Pauli, G. F., and Walters, M. A. (2017). The essential medicinal chemistry of curcumin. *J. Med. Chem.* 60, 1620–1637. doi: 10.1021/acs.jmedchem.6b00975

Nimiya, Y., Wang, W., Du, Z., Sukamtoh, E., Zhu, J., Decker, E., et al. (2016). Redox modulation of curcumin stability: redox active antioxidants increase chemical stability of curcumin. *Mol. Nutr. Food Res.* 60, 487–494. doi: 10.1002/mnfr.201500681

Pesakhov, S., Khanin, M., Studzinski, G. P., and Danilenko, M. (2010). Distinct combinatorial effects of the plant polyphenols curcumin, carnosic acid, and silibinin on proliferation and apoptosis in acute myeloid leukemia cells. *Nutr. Cancer* 62, 811–824. doi: 10.1080/01635581003693082

Pesakhov, S., Nachliely, M., Barvish, Z., Aqaqe, N., Schwartzman, B., Voronov, E., et al. (2016). Cancer-selective cytotoxic Ca^{2+} overload in acute myeloid leukemia cells and attenuation of disease progression in mice by synergistically acting polyphenols curcumin and carnosic acid. *Oncotarget* 7, 31847–31861. doi: 10.18632/oncotarget.7240

Rowe, J. M. (2018). Progress and predictions: AML in 2018. *Best Pract. Res. Clin. Haematol.* 31, 337–340. doi: 10.1016/j.beha.2018.09.002

Sidoryk, K., Jaromin, A., Filipczak, N., Cmoch, P., and Cybulski, M. (2018). Synthesis and antioxidant activity of caffeic acid derivatives. *Molecules* 23:E2199. doi: 10.3390/molecules23092199

Stone, R. M. (2017). Which new agents will be incorporated into frontline therapy in acute myeloid leukemia? *Best Pract. Res. Clin. Haematol.* 30, 312–316. doi: 10.1016/j.beha.2017.09.006

Wang, Y. J., Pan, M. H., Cheng, A. L., Lin, L. I., Ho, Y. S., Hsieh, C. Y., et al. (1997). Stability of curcumin in buffer solutions and characterization of its degradation products. *J. Pharm. Biomed. Anal.* 15, 1867–1876. doi: 10.1016/S0731-7085(96)02024-9

Xiao, H., and Parkin, K. L. (2007). Isolation and identification of potential cancer chemopreventive agents from methanolic extracts of green onion (Allium cepa). *Phytochemistry* 68, 1059–1067. doi: 10.1016/j.phytochem.2007.01.021

Xu, X., Chen, D., Ye, B., Zhong, F., and Chen, G. (2015). Curcumin induces the apoptosis of non-small cell lung cancer cells through a calcium signaling pathway. *Int. J. Mol. Med.* 35, 1610–1616. doi: 10.3892/ijmm.2015.2167

Yanamandra, N., Buzzeo, R. W., Gabriel, M., Hazlehurst, L. A., Mari, Y., Beaupre, D. M., et al. (2011). Tipifarnib-induced apoptosis in acute myeloid leukemia and multiple myeloma cells depends on Ca^{2+} influx through plasma membrane Ca^{2+} channels. *J. Pharmacol. Exp. Ther.* 337, 636–643. doi: 10.1124/jpet.110.172809

Yoon, M. J., Kim, E. H., Kwon, T. K., Park, S. A., and Choi, K. S. (2012). Simultaneous mitochondrial Ca^{2+} overload and proteasomal inhibition are responsible for the induction of paraptosis in malignant breast cancer cells. *Cancer Lett.* 324, 197–209. doi: 10.1016/j.canlet.2012.05.018

Zhang, W. M., Wang, W., Zhang, J. J., Wang, Z. R., Wang, Y., Hao, W. J., et al. (2016). Antibacterial constituents of hainan *Morinda citrifolia* (Noni) leaves. *J. Food Sci.* 81, M1192–M1196. doi: 10.1111/1750-3841.13302

Zhang, Y., Kong, Y., Liu, S., Zeng, L., Wan, L., and Zhang, Z. (2017). Curcumin induces apoptosis in human leukemic cell lines through an IFIT2-dependent pathway. *Cancer Biol. Ther.* 18, 43–50. doi: 10.1080/15384047.2016.1276129

Conflict of Interest Statement: The authors declare that the research was conducted in the absence of any commercial or financial relationships that could be construed as a potential conflict of interest.

frontiers in Pharmacology

ORIGINAL RESEARCH
published: 16 May 2019
doi: 10.3389/fphar.2019.00525

Effects of PARP-1 Deficiency and Histamine H_4 Receptor Inhibition in an Inflammatory Model of Lung Fibrosis in Mice

*Mariaconcetta Durante[1], Silvia Sgambellone[1], Cecilia Lanzi[2], Patrizia Nardini[3], Alessandro Pini[3], Flavio Moroni[1], Emanuela Masini[1] and Laura Lucarini[1]**

[1]Section of Pharmacology, Department of Neurosciences, Psychology, Drug Research and Child Health (NEUROFARBA), University of Florence, Florence, Italy, [2]Medical Toxicology Unit, Careggi-University Hospital (AOUC), Florence, Italy, [3]Section of Histology, Department of Clinical and Experimental Medicine, University of Florence, Florence, Italy

Pulmonary fibrosis is the most frequent form of interstitial lung disease. Effective therapies are not yet available; novel therapeutic approaches are needed for counteracting fibrosis. Poly(ADP-ribose) polymerases are enzymes, involved in DNA repair and cell apoptosis. PARP-1 deficient mice exhibited reduced lung fibrosis in response to bleomycin treatment compared to wild-type controls. Histamine H_4 receptors (H_4Rs) have been recognized as a new target for inflammatory and immune diseases, and H_4R ligands reduced inflammation and oxidative stress in lung tissue. The aim of the study was to evaluate the cross-talk between PARP-1 and H_4R in a model of bleomycin-induced lung fibrosis in PARP-$1^{-/-}$ and WT mice. Animals were treated with bleomycin or saline by intra-tracheal injection. JNJ7777120, an H_4R antagonist, or VUF8430, an H_4R agonist, were administered i.p for 21 days. Airway resistance to inflation was evaluated, and lung tissues were processed for PARylated protein content, oxidative stress evaluation, and histology of small bronchi. The levels of pro-inflammatory (IL-1β and TNF-α), regulatory (IL-10), and pro-fibrotic (TGF-β) cytokines were evaluated. The deposition of αSMA was determined by immunofluorescence analysis. The results indicate that JNJ7777120 reduces PARylated protein production, decreases oxidative stress damage, and MPO, a marker for leukocyte tissue infiltration, in PARP-$1^{-/-}$ mice. A significant decrease in the production of both IL-1β and TNF-α and a significant increase in IL-10 levels are observed in mice treated with H_4R antagonist, suggesting a crucial anti-inflammatory activity of JNJ7777120. The smooth muscle layer thickness, the goblet cell relative number, and collagen deposition decreased following JNJ7777120 administration. The H_4R antagonist treatment also reduces TGF-β production and αSMA deposition, suggesting an important role of JNJ7777120 in airway remodeling. Our results show that PARylation is essential for the pathogenesis of pulmonary fibrosis and propose that PARP-1 and H_4Rs are both involved in inflammatory and fibrotic responses. JNJ7777120 treatment, in a condition of PARP-1 inhibition, exerts anti-inflammatory and anti-fibrotic effects, reducing airway remodeling and bronchoconstriction. Therefore, selective inhibition of H_4Rs together with non-toxic doses of selective PARP-1 inhibitors could have clinical relevance for the treatment of idiopathic pulmonary fibrosis.

Keywords: histamine H_4 receptors, poly(ADP-ribose) polymerase 1, pulmonary fibrosis, inflammation, oxidative stress, cytokines

OPEN ACCESS

Edited by:
Ioanna Andreadou, National and Kapodistrian University of Athens, Greece

Reviewed by:
Manfred Kietzmann, University of Veterinary Medicine Hannover, Germany
Longshuang Huang, University of Illinois at Chicago, United States

****Correspondence:***
Laura Lucarini
laura.lucarini@unifi.it

Specialty section:
This article was submitted to Experimental Pharmacology and Drug Discovery, a section of the journal Frontiers in Pharmacology

Received: *07 February 2019*
Accepted: *26 April 2019*
Published: *16 May 2019*

Citation:
Durante M, Sgambellone S, Lanzi C, Nardini P, Pini A, Moroni F, Masini E and Lucarini L (2019) Effects of PARP-1 Deficiency and Histamine H_4 Receptor Inhibition in an Inflammatory Model of Lung Fibrosis in Mice. Front. Pharmacol. 10:525. doi: 10.3389/fphar.2019.00525

INTRODUCTION

Idiopathic pulmonary fibrosis (IPF) is a severe and progressive lung disease with approximately 3 years of median survival from the time of diagnosis and great associated morbidity, with wide-ranging negative effects on quality of life (Swigris et al., 2005). Despite recent advances in understanding the disease pathobiology, IPF remains a disease with a poor prognosis and an incompletely understood pathogenesis. In the last few years, the European Medicines Agency and the Food and Drug Administration (FDA) approved the use of nintedanib and pirfenidone as new safe drugs for IPF treatment. However, effective treatments are not available, and new therapeutic strategies are needed as alternative options when the standards of care are not sufficient or effective (Wynn, 2007; Paz and Shoenfeld, 2010).

Despite an unknown etiology, many studies identified a significant genetic risk associated with the development of IPF, such as SFTPC, MUC5B, and telomerase mutations; however, mechanisms by which genetic risk factors promoting IPF remain unclear (Allen et al., 2017). It has been proposed that pulmonary fibrosis is due to an augmented proliferation of fibroblasts with massive formation and accumulation of extracellular matrix (ECM) proteins (e.g., vimentin, collagen, and fibronectin) that eventually damage lung function (Wilson and Wynn, 2009). Deposition of "scar" tissue in the *interstitium* of the lung causes an alteration in the homeostatic cross-talk between epithelial and mesenchymal cells. Epithelial cells secrete anti-fibrotic mediators like prostaglandin E_2 (PGE_2) (Lama et al., 2002); thus, the loss of epithelial cells results in lower levels of PGE_2, which in turn, can allow resident fibroblasts to proliferate and differentiate into alpha-smooth muscle actin (αSMA) positive myofibroblasts (Kolodsick et al., 2003). Additionally, the release of the transforming growth factor-β (TGF-β), the most potent pro-fibrotic growth factor, promotes apoptosis of epithelial cells while simultaneously prevents apoptosis in lung fibroblasts (Thannickal and Horowitz, 2006). The apoptosis paradox allows resident fibroblasts to accumulate and become myofibroblasts. Myofibroblasts, organized into agglomerations of cells known as fibroblastic foci, are highly secretory cells producing an excessive tissue matrix, especially collagen, and highly contractile cells causing distortion of the alveolar architecture. When the synthesis of new collagen by myofibroblasts overcomes its degradation rate, pulmonary fibrosis occurs leading to the accumulation of collagen (Wynn, 2008), the common pathological hallmark of fibrotic disorders. This process results in multiple alterations in the lung structure, with progressive thickening of the air-blood membrane and airway stiffening; these lesions impair both gas diffusion and ventilation/perfusion relationship, with reduction or loss of gas exchange capacity (Plantier et al., 2018).

Abbreviations: αSMA, Alpha-smooth muscle actin; ECM, Extracellular matrix; 8-OHdG, 8-Hydroxy-deoxy-guanosine; H_4R, Histamine H_4 receptor; IL-10, Interleukin-10; IL-1β, Interleukin-1β; i.p., Intra-peritoneal; IPF, Idiopathic pulmonary fibrosis; JNJ, JNJ7777120; MPO, Myeloperoxidase; OD, Optical density; PARP, Poly(ADP-ribose) polymerase; PAO, Pressure at the airway opening; PAS, Periodic acid-Schiff; PGE_2, Prostaglandin E_2; TGF-β, Transforming growth factor-β; TNF-α, Tumor necrosis factor-α; WT, Wild-type; VUF, VUF8430.

Poly(ADP-ribose) polymerases (PARPs) are enzymes, involved in DNA repair and apoptosis. PARP-1 is the most abundant member of the PARP family and the most widely studied enzyme of this class. PARP-1 is activated upon binding to single- and double-strand DNA breaks *via* its N-terminal zinc finger domains (Ali et al., 2012; Langelier et al., 2012). Once activated by DNA damage, PARP-1 widely poly(ADP-ribosyl) ates itself and promotes the enrollment of DNA repair proteins that are required for lesion processing and repair. However, when DNA damage is severe, PARP-1 becomes over-activated leading to excessive consumption of NAD^+ and consequently to depletion of ATP that results in cellular dysfunction and necrotic cell death.

It has been reported that PARP activation characterizes a key pathway in many pathophysiological conditions associated with inflammation and oxidative stress. Interestingly, genes targeting approaches and the use of non-selective inhibitors have shown that PARP-1 is involved in a number of fibrotic diseases affecting the heart (Pacher et al., 2002), liver (Mukhopadhyay et al., 2014), vessels (Abdallah et al., 2007), and lungs (Genovese et al., 2005). Moreover, recent studies demonstrated that genetic depletion and pharmacological inhibition of PARP-1 reduced pulmonary fibrosis in an animal model of bleomycin-induced lung injury (Hu et al., 2013; Lucarini et al., 2017), suggesting that PARylation is important for myofibroblast differentiation and for the pathogenesis of the disease.

Histamine H_4 receptor (H_4R) has been identified as a novel target for inflammatory and immune disorders (Gschwandtner et al., 2013). Recent studies demonstrated that H_4Rs are involved in the prevention of fibronectin-induced lung fibroblast migration, suggesting these receptors as new targets for the treatment of lung fibrosis (Kohyama et al., 2010). Moreover, H_4R antagonists significantly reduce goblet cell hyperplasia and collagen deposition in a model of allergic asthma (Masini et al., 2013) and decrease inflammation and oxidative stress in a bleomycin-induced lung injury model (Rosa et al., 2014; Lucarini et al., 2017).

However, the cellular mechanism underlying the beneficial effects of H_4R antagonists in lung diseases are not completely understood, and this topic needs to be investigated in details.

The aim of the present study is to evaluate a possible involvement of PARP-1 in the H_4R antagonists' beneficial effects in reducing airway inflammation and remodeling. For this purpose, we evaluated the effects of the H_4R-selective antagonist, JNJ7777120, and of the H_4R agonist, VUF8430, in an *in vivo* model of bleomycin-induced lung fibrosis, in PARP-1 *knock-out* and in *wild-type* mice.

MATERIALS AND METHODS

Drugs and Reagents

Compound JNJ7777120 (JNJ; 1-[(5-chloro-1H-indol-2-yl) carbonyl]-4-methylpiperazine), a potent and selective H_4R antagonist, has been used at a concentration of 2.5 mg/kg of body weight (b.wt.). This compound was kindly provided by

Dr. Robin Thurmond (Janssen Research & Development, USA). Compound VUF8430, (VUF; 2-[(aminoiminomethyl)amino] ethyl carbamodithioic acid ester, S-(2-guanidylethyl)-isothiourea), an H_4R agonist, (Sigma-Aldrich, San Louis, MO, USA), was used at a concentration of 2 mg/kg b.wt. Bleomycin (Merck-Millipore, Burlington, MA, USA) was used at a concentration of 0.05 IU for each mouse and dissolved in 50 µl of saline, in order to obtain the bleomycin-induced model of lung fibrosis. The drug doses and frequency of administrations were selected according to previous papers (Rosa et al., 2014; Lucarini et al., 2016).

Animals

Male wild-type (WT) C57BL/6 mice, approximately weighing 25–30 g and 8–9 weeks old, purchased from a commercial dealer (Harlan, Udine, Italy), and male C57BL/6 PARP-1 deficient mice (PARP-$1^{-/-}$) (Wang et al., 1995), comparable in mice strain, age, and weight with WT mice, were used for the experiments. All the animals were fed with standard diet and water at libitum and housed under a 12 h light/dark photoperiod at 22°C for at least 48 h before the experiments.

The study protocol complied with the recommendations of the European Economic Community (86/609/CEE) and the Declaration of Helsinki on animal experimentation and was approved by the animal Ethical and Care Committee of the University of Florence (Florence, Italy) and by the Italian Health Ministry (Authorization n 874/2017-PR). Experiments were performed at the Centre for Laboratory Animal Housing and Experimentation (CeSAL) at the University of Florence. The ARRIVE guidelines were considered (McGrath et al., 2010).

Surgery and Treatments

Seventy mice (30 WT and 40 PARP-$1^{-/-}$) were anesthetized with zolazepam/tiletamine (Zoletil, 50/50 mg/ml, Virbac Srl, Milan, Italy; 50 µg/g, in 100 µl of saline, i.p.); 50 of them (20 WT and 30 PARP-$1^{-/-}$) were intra-tracheally treated with bleomycin (0.05 IU in 50 µl of saline), and the other 20 (10 WT and 10 PARP-$1^{-/-}$) were intra-tracheally treated with 50 µl of saline (referred to as non-fibrotic negative controls, Naive).

Ten bleomycin-treated WT and 10 bleomycin-treated PARP-1 deficient mice received two daily intra-peritoneal (i.p.) injections of 100 µl of JNJ solution (2.5 mg/kg; i.p.), after bleomycin administration and for the next 21 days. These are referred to as Bleomycin+JNJ treated groups. Ten bleomycin treated PARP-$1^{-/-}$ mice received two daily intra-peritoneal injection of 100 µl of VUF solution (2 mg/kg; i.p.), after bleomycin administration and for the next 21 days. These are referred to as Bleomycin+VUF treated group. Ten WT mice and 10 PARP-$1^{-/-}$ mice were treated only with vehicle (PBS) and referred to as fibrotic positive controls (Bleomycin+Vehicle).

Functional Assay of Fibrosis

At the end of the treatment period, all mice were subjected to the measurement of airway resistance to inflation and static lung compliance, functional parameters for fibrosis-induced lung stiffness. The measurement is performed using a constant volume mechanical ventilation method with constant number of breaths in a minute; the static compliance determination is performed applying a positive end-expiratory pressure of 3 cm H_2O, to mimic spontaneous ventilation (Pini et al., 2010, 2012; Manni et al., 2016). Briefly, a 22-gauge cannula (Venflon 2; Viggo Spectramed, Windlesham, UK, 0.8 mm diameter) was inserted into the trachea of the anesthetized mouse. The animal was ventilated with a small-animal respirator (Ugo Basile, Comerio, Italy) adjusted to deliver a tidal volume of 0.8 ml at a rate of 20 strokes/min. A high-sensitivity pressure transducer (settings: gain 1, chart speed 25 mm/sec.; P75 type 379; Harvard Apparatus Inc., Holliston, MA, USA) connected to a polygraph (Harvard Apparatus Inc. Edenbridge, UK; settings: gain 1, chart speed 25 mm/s) was used to register the changes in lung resistance to inflation, defined as the pressure at airway opening (PAO). Changes in lung resistance to inflation, expressed as millimeters on the chart and registered for at least 3 min, were carried out not less than 40 consecutive tracings of respiratory strokes and then averaged. For static lung compliance determination, multiple linear regression was used to fit pressure and volume in each individual mouse to the linear model of the lung (Manni et al., 2016).

Lung Tissue Sampling

After PAO measurements, the animals were killed with lethal dose of anesthetic drugs. The whole left lungs were removed and fixed with 4% paraformaldehyde in PBS for histological analysis. The right lungs were weighed, quickly frozen, and stored at −80°C. For biochemical measurements, the samples were thawed at 4°C, homogenized on ice in 50 mM Tris-HCl buffer (180 mM KCl and 10 mM EDTA, pH 7.4), and then centrifuged for 30 min at 10,000 g at 4°C, unless otherwise reported. The homogenized supernatants were collected.

Histology and Assessment of Collagen Deposition, Goblet Cell Hyperplasia, and Smooth Muscle Layer Thickness

Six µm thick histological sections were cut from the paraffin-embedded lung samples. In order to minimize artefactual differences in the staining process, all sections were stained in a single session. A digital camera connected to a light microscope equipped with an ×20 objective was used to randomly take photomicrographs of the histological slides. Computer-aided densitometry was performed to obtain quantitative assessment of the stained sections. The free-share ImageJ 1.33 image analysis program[1] was used to measure optical density (OD) and surface area. For each measured parameter, values are means ± SEM of the OD measurements (arbitrary units) of individual mouse (five images each) from every experimental groups (tested blind).

The assessment of lung collagen was obtained by staining the histological sections with a simplified Azan method for collagen fibers (Smolle et al., 1996), omitting azocarminium and orange G to reduce parenchymal tissue background. OD measurements of the aniline blue-stained collagen fibers were

[1]http://rsb.info.nih.gov/ij

performed after selection of a correct threshold to eliminate aerial air spaces and bronchial/alveolar epithelium (Formigli et al., 2007). To confirm the assessment of lung collagen, the Picrosirius red staining was carried out; the sections were stained in 0.1% Direct Red 80/Sirius Red F3B (Sigma-Aldrich) in saturated picric acid at room temperature for 1 h, and then they were differentiated in 0.5% acetic acid, prior to dehydration, clearing, and mounting (Lattouf et al., 2014; Marcos-Garcés et al., 2017).

Moreover, lung tissue sections were stained with hematoxylin and eosin or with periodic acid-Schiff (PAS) staining for mucins in order to obtain morphometry of smooth muscle layer thickness and bronchial goblet cell number, respectively, both key markers of airway remodeling. Digital microphotographs of small-sized bronchi were taken randomly. The thickness of the bronchial smooth muscle layer was measured on the digitized images using the above-mentioned software. Total bronchial epithelial cells and PAS-stained goblet cells were counted on bronchial cross-section profiles, and the percentage of goblet cells was calculated.

Western Blot Analysis of PARylated Protein Content

For determination of PARylated protein content in the lung, tissues were homogenized in RIPA buffer plus a cocktail of protease inhibitors and centrifuged at 12,000 g for 5 min. Supernatants were collected, and total protein levels were measured using Micro BCA Protein Assay (ThermoFisher Scientific, Waltham, MA, USA). Thirty μg of proteins were used for Western blot analysis, with a mouse monoclonal anti-PAR(10H) antibody (Alexis Biochemicals, Florence, Italy) diluted 1:1,000 in PBS-T containing 5% non-fat dry milk. The PAR(10H) monoclonal antibody recognizes poly(ADP-ribose) synthesized by PARP enzymes. A suitable peroxidase-conjugated secondary antibody (diluted 1:5,000 in PBS-T containing 5% non-fat dry milk) was used to determine the binding of the primary antibody. The loading transfer of equal amounts of proteins was controlled by reblotting the membrane with an anti-β-actin antibody (diluted 1:20,000 in 5% non-fat dry milk-PBS-T, Sigma-Aldrich). Bands were visualized by enhanced chemiluminescence (Luminata Crescendo Western HRP substrate, Merck Millipore) and quantified by densitometric analysis with the ImageJ software.

Determination of Transforming Growth Factor-β (TGF-β), Interleukin-1β (IL-1β), Tumor Necrosis Factor-α (TNF-α), and Interleukin-10 (IL-10)

The levels of TGF-β, the main profibrotic cytokine involved in fibroblast activation, and two pro-inflammatory cytokines, IL-1β and TNF-α, were measured on aliquots (20 μl) of lung samples homogenated in PBS by using the FlowCytomix assay (Bender Medsystems GmbH, Vienna, Austria), following the protocol provided by the manufacturer. Briefly, suspensions of anti-TGF-β, IL-1β or TNF-α-coated beads were incubated with the supernatant samples and then with biotin-conjugated secondary antibodies and streptavidin-phycoerythrin. Fluorescence was read with a cytofluorimeter (CyFlow® Space, Partec, Carate Brianza, MB, Italy).

The levels of the anti-inflammatory cytokine IL-10 were measured on aliquots (100 μl) of lung homogenate supernatants by using the mouse IL-10 ELISA Ready-SET&Go!® assay (eBioscience, San Diego, USA), following the protocol provided by the manufacturer. Values are indicated as means ± SEM of 10 individual mice from each group and expressed as pg/μg of total proteins determined over an albumin standard curve.

Determination of αSMA Deposition

Immunofluorescence analysis was performed as previously described (Lucarini et al., 2014). Briefly, histological sections of 5 μm thick were deparaffinized and boiled for 10 min in sodium citrate buffer (10 mM, pH 6.0, Bio-Optica, Milan, Italy) for antigen retrieval. A pre-incubation in 1.5% bovine serum albumin (BSA) in PBS, pH 7.4 for 20 min at RT was necessary to minimize the unspecific binding; whereupon, the sections were incubated overnight at 4°C with rabbit monoclonal anti-αSMA antibody (1:200 ABCAM, USA) followed by goat anti-rabbit Alexa Fluor 488-conjugated IgG (1:300 Invitrogen, San Diego, CA, USA) for 2 h in the dark at RT. Negative controls were performed with non-immune rabbit serum substituted for the primary antibody. The counterstaining of nuclei was obtained with 4′,6-diamidino-2-phenylindole (DAPI). Representative images were acquired with an Olympus BX63 microscope coupled to CellSens Dimension Imaging Software version 1.6 (Olympus, Milan, Italy). αSMA expression was quantified by densitometric analysis of fluorescence signal intensity, measured on digitized images using ImageJ software[2]. Twenty regions of interest (ROI) were evaluated for each sample. Values are expressed as mean ± SEM of the OD measurements (arbitrary units) of individual mouse from the different experimental groups.

Determination of 8-Hydroxy-Deoxyguanosine (8-OHdG)

Lung DNA isolation was performed as previously described (Lodovici et al., 2000) with minor modifications. In brief, lung samples were homogenized in 1 ml of 10 mM PBS, pH 7.4, sonicated on ice for 1 min, added to 1 ml of 10 mM Tris-HCl buffer, pH 8, containing 10 mM EDTA, 10 mM NaCl, and 0.5% SDS, and incubated for 1 h at 37°C with 20 μg/ml RNase 1 (Sigma-Aldrich). Samples were incubated at 37°C overnight in the presence of 100 μg/ml proteinase K (Sigma-Aldrich). The mixture was extracted with chloroform/isoamyl alcohol (10:2, v/v). DNA was precipitated from the aqueous phase with 0.2 volumes of 10 M ammonium acetate, solubilized in 200 μl of 20 mM acetate buffer, pH 5.3, and denatured at 90°C for 3 min. The extract was supplemented with 10 IU of P1 nuclease (Sigma-Aldrich) in 10 μl and incubated for 1 h at 37°C with 5 IU of alkaline phosphatase (Sigma-Aldrich) in 0.4 M phosphate buffer, pH 8.8. All the procedures were

[2]http://rsbweb.nih.gov/ij

performed in the dark. The mixture was filtered by an Amicon Micropure-EZ filter (Merck-Millipore), and 100 µl of each sample were used for 8-OHdG determination by using an ELISA kit (JalCA, Shizuoka, Japan), following the instructions provided by the manufacturer. The absorbance of the chromogenic product was measured at 450 nm. The results were calculated from a standard curve based on an 8-OHdG solution and expressed as ng of 8-OHdG/ng of total DNA.

Determination of Myeloperoxidase Activity (MPO)

Frozen lung samples were weighed and homogenized (10 µl/mg of tissue) in 0.2 M phosphate buffer solution (PBS), pH 6, supplemented with protease inhibitors (1 mM PMSF, 20 µg/ml leupeptin, 1 µg/ml pepstatin, 1 mg/ml Pefabloc SC, and 2.5 µg/ml aprotinin, Sigma-Aldrich) and were centrifuged at 10,000 g at 4°C for 30 min. MPO was measured in the supernatants with a specific immunoassay kit (CardioMPO; PrognostiX, Cleveland, OH), according to the manufacturer's instructions (Pini et al., 2010). Total protein concentration in the lung tissue samples was determined over an albumin standard curve. The results are expressed as picomoles/mg of protein. Values are means ± SEM of individual mice from different experimental groups.

Statistical Analysis

Data were reported as mean values (±SEM) of individual average measures of the different animals per group, for each assay. Significance of differences among the groups was evaluated by one-way ANOVA followed by Newman-Keuls *post hoc* test for multiple comparisons. Calculations were made with Prism 5 statistical software (GraphPad Software, Inc., USA). A probability value $p < 0.05$ was considered significant.

RESULTS

Functional Assay of Fibrosis (PAO)

Intra-tracheal administration of bleomycin causes an increase in airway stiffness leading to a clear-cut elevation of the pressure in airway opening (PAO) (Masini et al., 2005). Intra-tracheal delivery of bleomycin to rodents results in an intense inflammatory reaction within the first week, followed by the development of fibrosis by day 14, with maximal responses at day 21. Therefore, bleomycin administration caused a significant increase in airway stiffness, as judged by the elevation of PAO in the fibrotic positive controls (Bleomycin+Vehicle) compared with the non-fibrotic negative ones (Naïve), both in WT and PARP-1$^{-/-}$ mice (**Figure 1**).

After 21 days, the treatment with JNJ significantly reduces PAO both in WT and in PARP-1$^{-/-}$ mice, in comparison to the relative group of animals treated with Vehicle; while VUF treatment seems to be not significantly effective in reducing the bleomycin-induced airway stiffness (**Figure 1**). The selected doses were based on previous papers (Pini et al., 2012; Lucarini et al., 2016). These results confirm our previous observation that H_4R ligands could have beneficial effects in decreasing lung fibrosis in WT (Lucarini et al., 2016) and in PARP-1$^{-/-}$ animals, indicating that the treatment with H_4R antagonists exerts its beneficial effects also in situation of PARP-1 deletion.

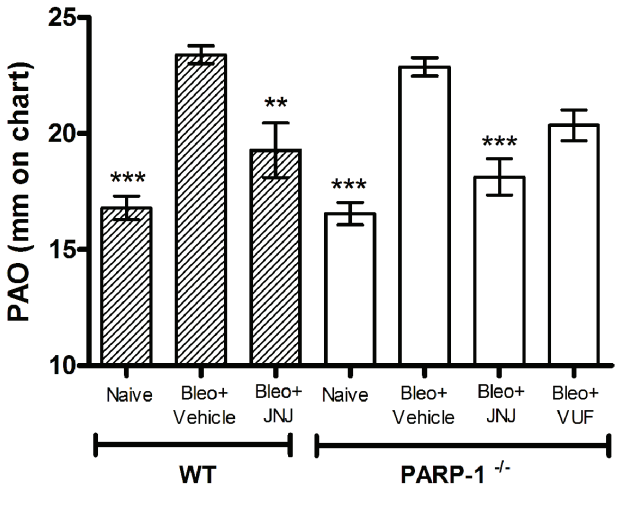

FIGURE 1 | Spirometric evaluation. Bar graph and statistical analysis of differences in PAO values (means ± SEM) between different experimental groups (n = 10 animals per group). $^{**}p < 0.01$ and $^{***}p < 0.001$ *vs.* Bleo+Vehicle of each related group WT or PARP$^{-/-}$ (Bleo = Bleomycin).

Changes in PARP-1 Activity

It has been demonstrated that bleomycin administration increases PARP activity in mouse lung tissues (Genovese et al., 2005). Moreover, previous studies provided evidence that PARylated protein levels, the major products of PARP activity, are significantly increased in lung homogenates of WT mice treated with bleomycin, while the treatment with HYDAMTIQ, a potent PARP-1/2 inhibitor, dose-dependently, prevents this PARylation (Lucarini et al., 2017).

To evaluate the effects of intra-tracheal administration of bleomycin on PARP activity, we investigated the formation of polyADP ribose (PAR) polymers in mouse lung tissues in WT and PARP-1$^{-/-}$ mice. As shown in **Figure 2** and in **Supplementary Figure 1**, Western blot analysis with anti-PAR antibodies report an increase in PARylated protein content in lung homogenates of WT and in PARP-1$^{-/-}$ mice treated with bleomycin (Vehicle), compared to non-fibrotic controls (Naïve). Treatment with the H_4R antagonist reduces the PARylated protein content in WT animals. Interestingly, our results indicate a reduction of PARylated protein levels in the lung tissues of PARP-1$^{-/-}$ mice treated with JNJ, compared to those treated with VUF, suggesting a positive role of H_4R antagonism in suppressing catalytic activity of PARP enzymes different from PARP-1.

Histological and Morphometric Analysis

Acute inflammatory events and deposition of collagen fibers cause a pathological remodeling of the parenchyma of the lungs. Morphological observation and computer-aided densitometry

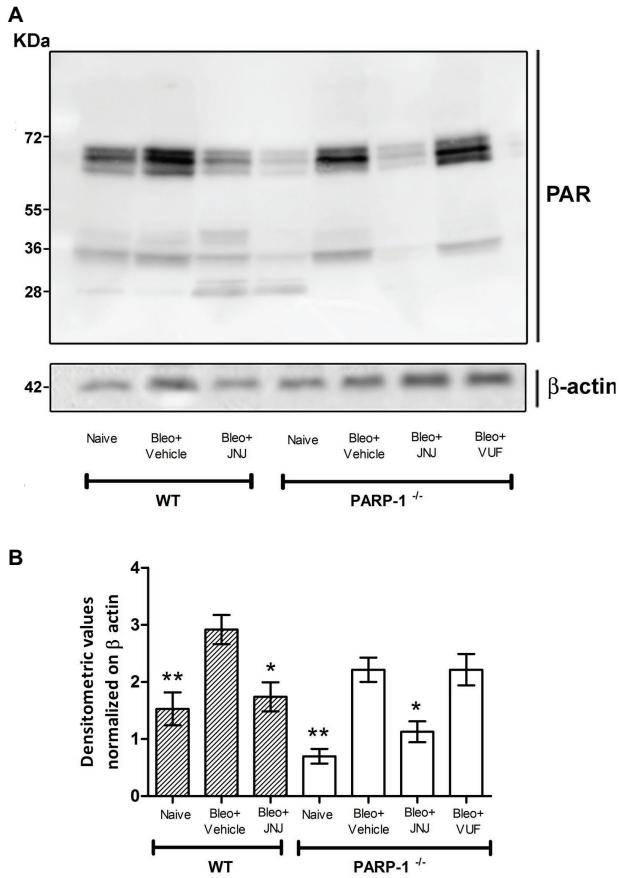

FIGURE 2 | PARP activity. **(A)** Western blot analysis of PARylated protein content in lung samples from each experimental group. **(B)** Densitometric analysis was normalized on β-actin (n = 10 animals per group). *$p < 0.05$ and **$p < 0.01$ *vs.* Bleo+Vehicle of each related group WT or PARP$^{-/-}$ (Bleo = Bleomycin).

on Azan-stained sections (**Figure 3A**) reveal a significant increase in collagen deposition in the lungs of all bleomycin-treated animals (Vehicle) compared to the non-fibrotic negative controls (Naïve). As already published, in WT animals, H_4R antagonists reduce the deposition of collagen fibers in lungs compared to Vehicle (Rosa et al., 2014; Lucarini et al., 2016). The treatment with JNJ causes an important and significant reduction of the amount of lung collagen fibers in PARP-1$^{-/-}$ mice compared to Vehicle group. A slight effect is reported in VUF treated mice. To confirm the assessment of lung collagen, the Picrosirius red was used as second staining method; this specific staining for collagen (Lattouf et al., 2014; Marcos-Garcés et al., 2017) confirms the results obtained with Azan staining (**Figure 3B**).

We also evaluated the bronchial remodeling by measuring the number of goblet cells and the thickness of the smooth muscle layer, key histological parameters of inflammation-induced adverse airway remodeling (Bai and Knight, 2005). These two parameters are increased after intra-tracheal injection of bleomycin, both in WT and PARP-1 deficient mice. The treatment with JNJ significantly reduces the percentage of PAS-positive goblet cells over bronchial epithelial cells (**Figure 4A**), as well as the thickness of the airway smooth muscle layer (**Figure 4B**). On the contrary, VUF administration has no effect on both histological parameters, confirming our previous published results that on the effect of H_4R antagonists on goblet cells and thickness of the smooth muscle layer in lungs, (Rosa et al., 2014; Lucarini et al., 2016).

TGF-β Signaling Pathway

An increased TGF-β expression and an amplified TGF-β signaling through Smad pathways contribute to the establishment and development of pulmonary fibrosis (Leask and Abraham, 2004; Chen et al., 2013; Chitra et al., 2015). Our results clearly indicate that TGF-β, a major pro-fibrotic cytokine, is increased in the vehicle groups, both in WT and PARP-1$^{-/-}$ mice. Systemic administration of JNJ causes a significant decrease of the levels of TGF-β in WT as well as PARP-1$^{-/-}$ animals, while the treatment with the H_4R agonist has no effect on the production of this cytokine (**Figure 5A**). These results demonstrate the anti-fibrotic activity of JNJ both in WT and in PARP-1$^{-/-}$ mice.

Fibroblast Activation

Transforming growth factor-β signaling has been reported to regulate the expression of αSMA, a marker of fibroblast activation, and myofibroblasts differentiation (Martin et al., 2007; Conte et al., 2014). To investigate the expression of αSMA during the fibrotic process, we performed immunofluorescence analysis in mouse lung tissues. Our results show a significant increase of αSMA levels in bleomycin-exposed PARP-1$^{-/-}$ animals (**Figures 5B,C**). Treatment with JNJ significantly reduces αSMA levels in lung tissue of PARP-1$^{-/-}$ mice compared to the vehicle group. Systemic administration of the H_4R agonist provides no changes in αSMA lung levels. These results indicate that the use of an H_4R antagonist, in the absence of PARP-1 enzyme, reduces the activation of fibroblasts and myofibroblasts differentiation and consequently the development of progressive fibrotic disease in bleomycin-exposed animals.

Effects of H_4R Ligands on Pro-Inflammatory Cytokine Production

Chronic inflammation is determined by pathological wound-healing response, resulting in the accumulation of permanent scar tissue at the site of injury and consequently in the development of progressive fibrotic disease (Wynn and Ramalingam, 2012). Based on this evidence, we evaluated the late (21 days after challenge) inflammatory response to bleomycin by measuring the pro-inflammatory cytokines IL-1β and TNF-α, in lung homogenates of WT and PARP-1$^{-/-}$ mice. Bleomycin treatment increases the levels of IL-1β and TNF-α both in WT and PARP-1$^{-/-}$ mice; of note, in PARP-1$^{-/-}$ mice, this increase is less pronounced in comparison to WT mice. The systemic administration of JNJ significantly reduces the increase in both groups of animals, but in PARP-1$^{-/-}$ mice, this reduction is more evident. The treatment with VUF is not effective in the reduction of inflammatory cytokine production (**Figures 6A,B**).

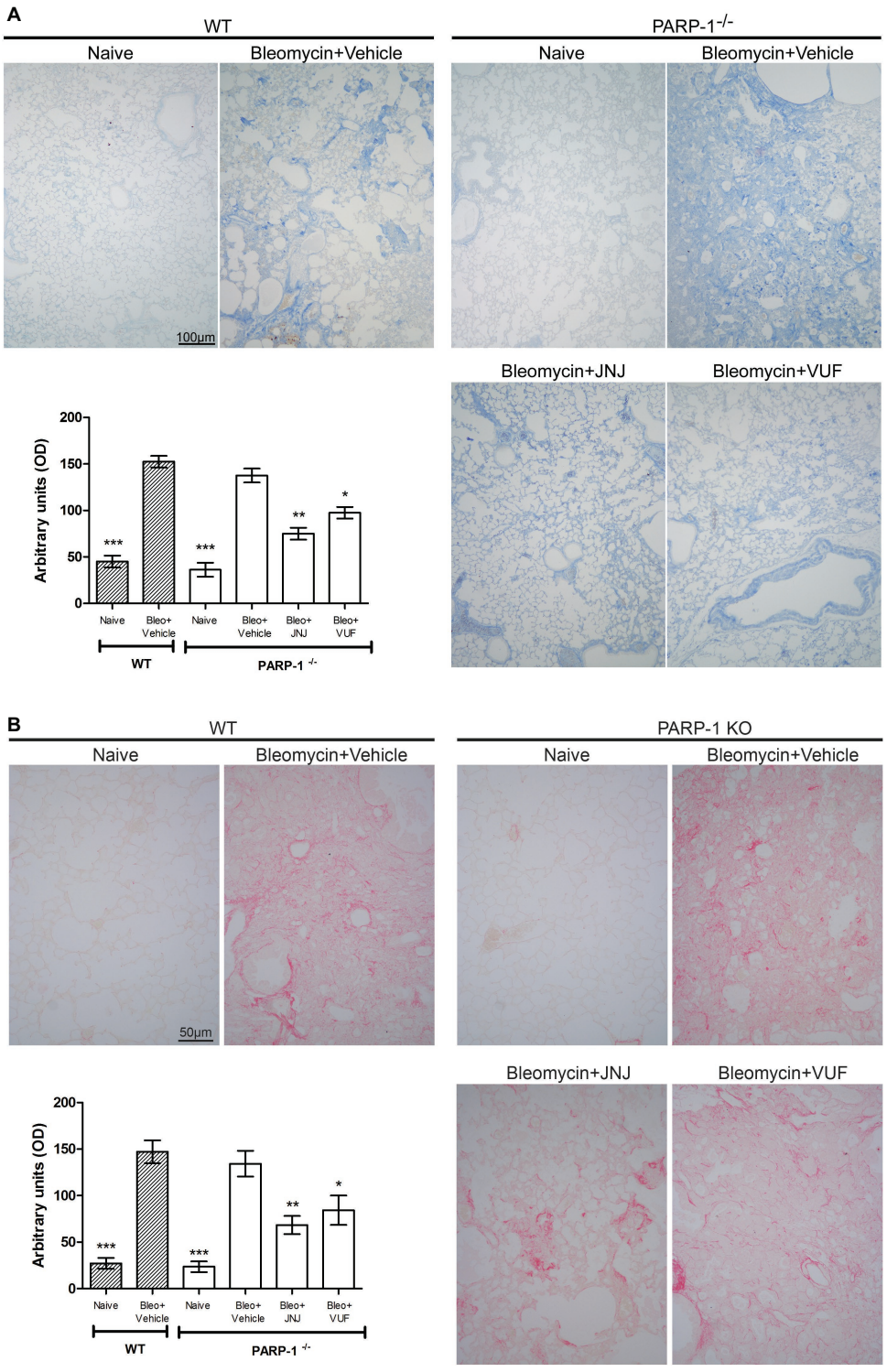

FIGURE 3 | Evaluation of lung fibrosis. **(A)** Representative micrographs of Azan-stained sections from mice of the different experimental groups. Collagen fibers are stained deep blue. The lung from fibrotic controls treated with vehicle show marked fibrosis in peribronchial stroma, which is absent in non-fibrotic negative control lungs (Naïve) and reduced in JNJ treated animals. Bar graph showing the optical density (OD) (means ± SEM) of Azan-stained collagen fibers of the different experimental groups (n = 10 animals per group). *$p < 0.05$, **$p < 0.01$, and ***$p < 0.001$ *vs.* Bleomycin+Vehicle of each related group. **(B)** Representative micrographs of Picrosirius red-stained sections from mice of the different experimental groups. Collagen fibers are stained in red. Bar graph showing the optical density (OD) (means ± SEM) of Picrosirius red-stained collagen fibers of the different experimental groups (n = 10 animals per group). *$p < 0.05$, **$p < 0.01$, and ***$p < 0.001$ *vs*. Bleomycin+Vehicle of each related group.

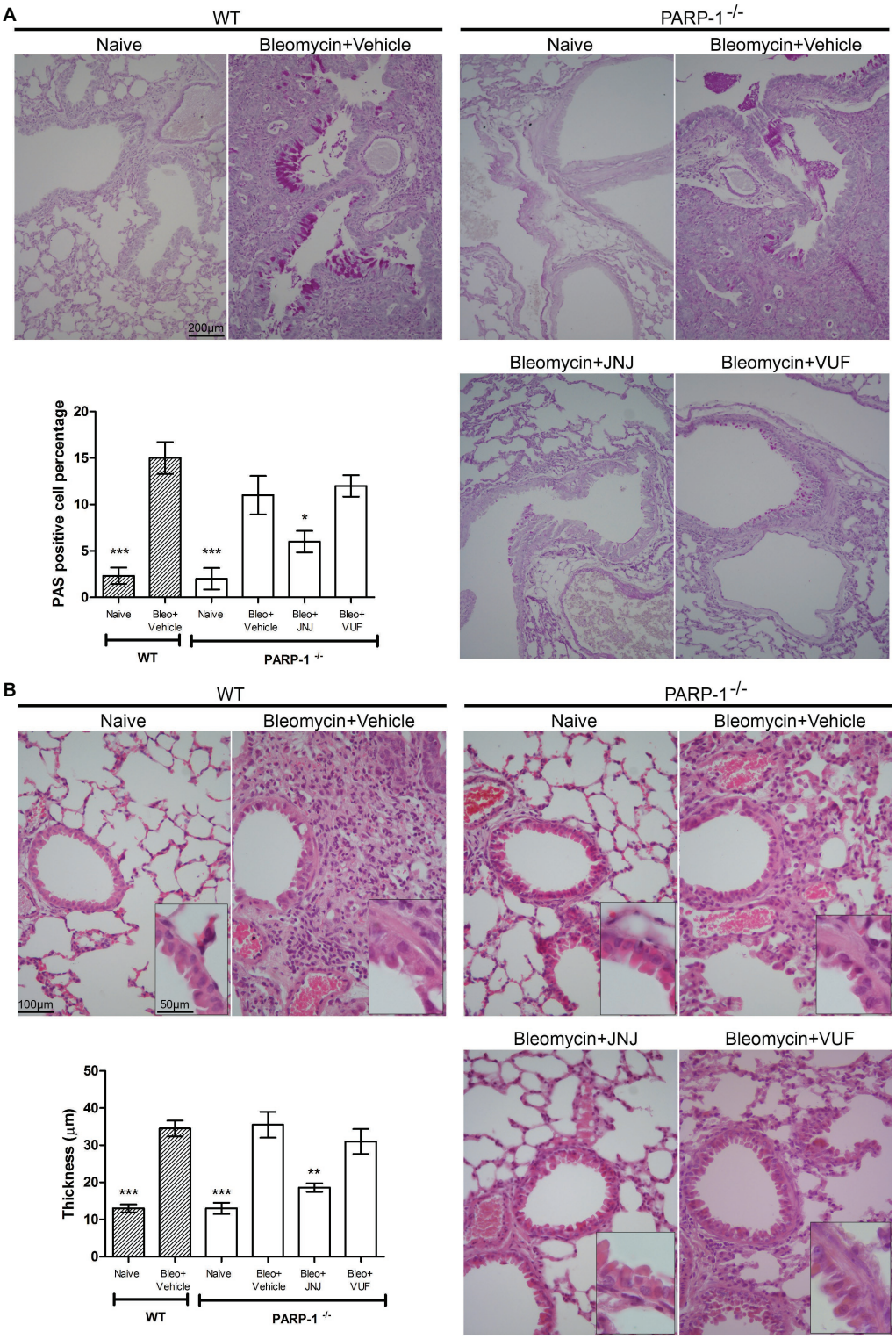

FIGURE 4 | (A) Goblet cell hyperplasia. Representative micrographs of PAS-stained sections. Bar graph showing fraction of goblet cells (% means ± SEM) in the different experimental groups (n = 10 animals per group). *$p < 0.05$ and ***$p < 0.001$ of *vs.* Bleo+Vehicle of each related group. **(B)** Evaluation of muscular remodeling. Smooth muscle thickness was assessed by computer aided morphometry on H&E-stained lung sections. Representative micrographs of the sections. Bar graph showing the thickness of the muscular fiber (means ± SEM) in the different experimental groups (n = 10 animals per group). **$p < 0.01$ and ***$p < 0.001$ *vs.* Bleo+Vehicle of each related group.

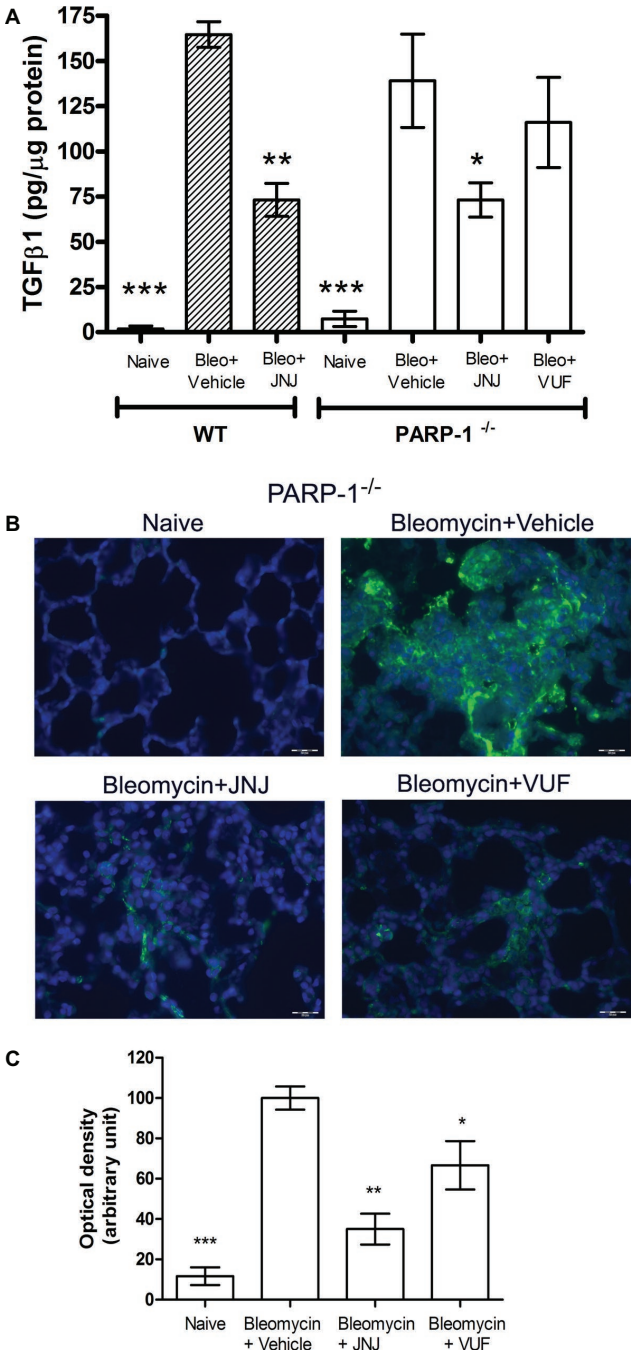

FIGURE 5 | (A) Evaluation of TGF-β1 production. Bar graph showing lung tissue levels of the profibrotic cytokine TGFβ1 (means ± SEM) of the different experimental groups (n = 10 animals per group). *$p < 0.05$, **$p < 0.01$, and ***$p < 0.001$ *vs.* Bleo+Vehicle of each related group. **(B)** Evaluation of fibroblast activation. Immunofluorescence staining of lung tissue sections labeled with alpha smooth muscle actin (αSMA) (green) and nuclei (blue) counterstained with DAPI (20×). Images in the panels show the inhibition of αSMA expression, a marker of the transformation of fibroblasts into myofibroblasts (n = 10 animals/group). **(C)** Bar graph shows the optical density (means ± SEM) in the different experimental groups (n = 10 animals per group). *$p < 0.05$ and **$p < 0.01$ *vs.* Bleo+Vehicle. (Bleo = Bleomycin).

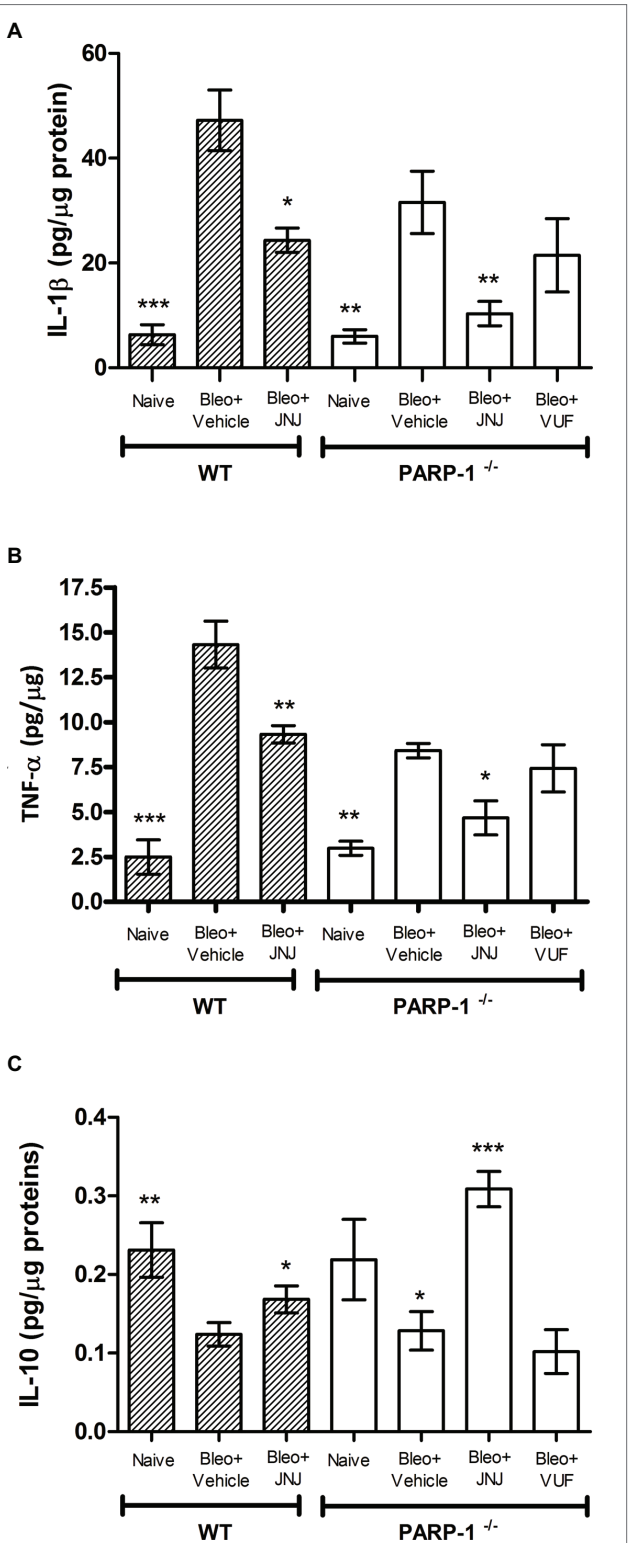

FIGURE 6 | Determination of IL-1β **(A)**, TNF-α **(B)**, and IL-10 **(C)** levels in the supernatant of lung tissue homogenates. The values are expressed as pg/μg of total proteins (n = 10 animals per group). Values are mean ± SEM. *$p < 0.05$, **$p < 0.01$, and ***$p < 0.001$ *vs.* Bleo+Vehicle of each related group (Bleo = Bleomycin).

In order to confirm the anti-inflammatory activity of the H_4R antagonist, we evaluated the levels of interleukin-10 (IL-10), the most potent anti-inflammatory cytokine involved in resolution of different acute and chronic inflammatory diseases (Ajuebor et al., 1999). Our results report a significant increase in the production of IL-10 in WT and PARP-$1^{-/-}$ mice treated with JNJ in comparison to PARP-$1^{-/-}$ mice treated with vehicle or VUF (**Figure 6C**).

Our findings support the hypothesis that H_4R antagonism exerts anti-inflammatory and anti-fibrotic effects in a model of bleomycin-induced lung fibrosis.

Determination of Leukocyte Lung Infiltration and of Oxidative Stress Marker

Lung MPO is a peroxidase enzyme abundantly expressed in neutrophils and monocytes/macrophages granules, and it is considered a reliable marker for leukocyte accumulation in inflamed tissues (Mullane et al., 1985). Levels of MPO were very low in the Naïve groups of both WT and PARP$^{-/-}$ mice; MPO levels increased significantly in the bleomycin-treated mice (Vehicle groups of WT and PARP$^{-/-}$ mice). A significant decrease in MPO was demonstrated after treatment with JNJ in WT and PARP$^{-/-}$ groups of animals in comparison to Vehicle; treatment with VUF has some non-significant effects (**Figure 7A**).

The determination of 8-OHdG, a biological marker of DNA damage under oxidative stress, demonstrates that it is significantly increased in bleomycin-exposed animals (Vehicle), compared with non-fibrotic negative ones (Naïve). Interestingly, our results show a significant reduction of 8-OHdG levels in WT and PARP-$1^{-/-}$ animals treated with JNJ (**Figure 7B**), but not with VUF.

DISCUSSION

Pulmonary fibrosis is an unmet medical need with a median survival of ~3 years since diagnosis. It is often severe and difficult to manage, resulting in a chronic condition that negatively affects the quality of life. The pharmacological therapy of pulmonary fibrosis is challenging, and for many patients, effective treatment is lacking. Therefore, novel therapeutic strategies are required (Wynn, 2007; Paz and Shoenfeld, 2010).

Recent studies demonstrated the involvement of PARP enzymes in modulating airway inflammation and fibrosis. Particularly, PARP-1 inhibition improves functional, biochemical, and morphometric parameters in an *in vivo* allergen-induced asthma-like reaction model (Lucarini et al., 2014) and in a bleomycin-induced pulmonary fibrosis model (Lucarini et al., 2017).

Histamine H_4 receptor (H_4R), the last discovered histamine receptor subtype, is functionally expressed and distributed in white blood cells, mast cells, eosinophils, dendritic cells, and T cells (Gutzmer et al., 2009). Recent evidence strongly suggests that H_4R ligands might be exploited as potential therapeutics in modulating allergy, inflammation, autoimmune disorders, and possibly cancer. In an animal model of allergic airway inflammation, H_4R-*knockout* mice present lower inflammation, reduced pulmonary infiltrate of lymphocytes and eosinophils, and an attenuated Th_2 response (Dunford et al., 2006). Moreover, blocking H_4R in a model of pulmonary fibrosis alleviates the inflammatory response, reducing COX-2 expression and activity, leukocyte infiltration, TGF-β production, and collagen deposition (Lucarini et al., 2016).

Although these findings suggest a promising therapeutic use for H_4R antagonists in the modulation of chronic lung

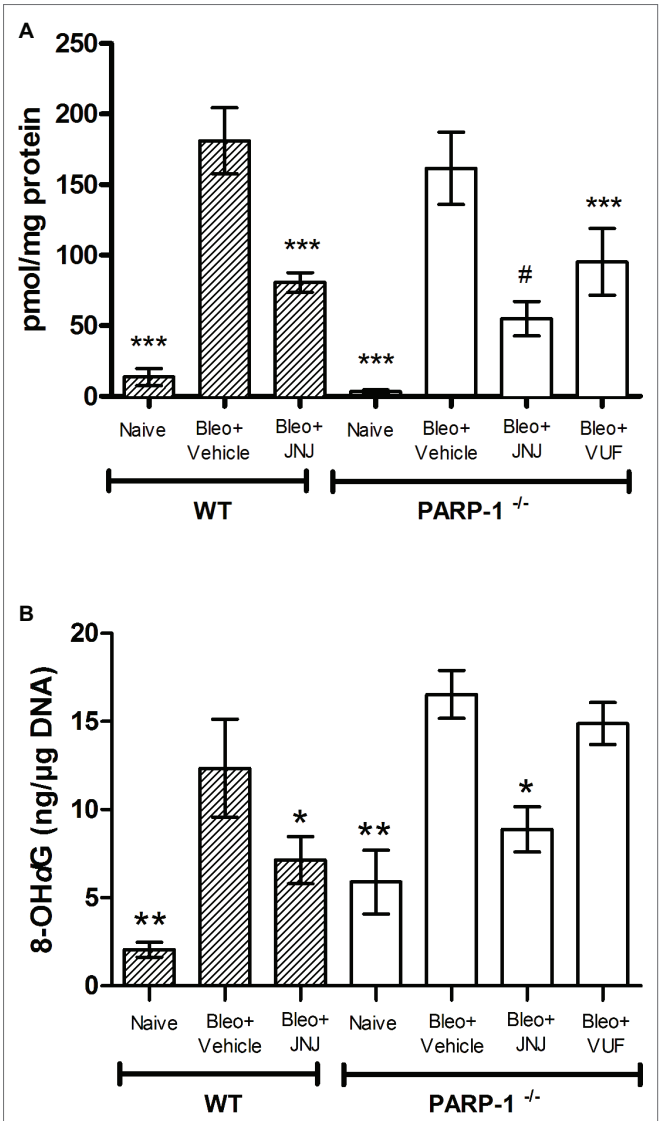

FIGURE 7 | (A) MPO levels, a marker for leukocyte infiltration, are shown in the histogram. Values are expressed as mean ± SEM, expressed as picomoles per milligram of lung tissue protein (n = 10 animals per group) ***$p < 0.001$ *vs.* Bleo+Vehicle of each related group (Bleo = Bleomycin); #$p < 0.05$ *vs.* Bleo+VUF. **(B)** Evaluation of oxidative stress parameter in lung tissue. Bar graph shows the levels of 8-OHdG, a marker of free radicals-induced by DNA damage, (mean ± SEM) in the different experimental groups (n = 10 animals per group). *$p < 0.05$, **$p < 0.01$ *vs.* Bleo+Vehicle of each related group (Bleo = Bleomycin).

diseases, the biochemical basis underlying the protective and beneficial effects of these drugs are unknown and need to be further elucidated.

Here, we tested the possible role that PARP-1 may have in the mechanism of action of H_4R antagonists. Briefly, we demonstrate that JNJ, a selective antagonist of the histamine H_4R, exerts its anti-inflammatory and anti-fibrotic properties independently of PARP-1 signaling pathway, in an *in vivo* mouse model of bleomycin-induced lung fibrosis.

Chronic inflammation is determined by pathological wound-healing response, resulting in the accumulation of scar tissue and consequently in the development of progressive fibrotic disease (Wynn and Ramalingam, 2012). Our model of pulmonary fibrosis is well described and widely accepted and includes an acute inflammatory phase (7–9 days), followed by a chronic inflammatory infiltrate and fibrotic process in the next 2 weeks, with maximal responses at day 21 (Moore and Hogaboam, 2008).

Therefore, we evaluated the inflammatory response to bleomycin in lung homogenates of WT and PARP-$1^{-/-}$ mice. The results show that the treatment with JNJ significantly reduces the production of IL-1β and TNF-α pro-inflammatory cytokines and the activity of MPO, as well as the levels of 8-OHdG, a reliable marker of oxidative stress, in WT and in PARP-$1^{-/-}$ mice. Collectively, our results demonstrate that H_4R antagonist's anti-inflammatory and anti-fibrotic effects are not dependent on PARP-1 expression, thus adding further evidence on the role of H_4R in controlling leukocyte trafficking and pro-inflammatory responses (Zampeli and Tiligada, 2009).

Previous data demonstrated a role for histamine and H_4R in the production of TGF-β, the major pro-fibrotic cytokine, and in fibroblast activation (Cowden et al., 2010). The cytokine TGF-β has been proposed to play a key role in lung fibrosis (Tatler and Jenkins, 2012), and drugs able to control TGF-β expression and/or signaling seem to be active in reducing fibroblast activation and clinical progression of the disease (Bonniaud et al., 2005). The TGF-β overexpression has been repeatedly associated to lung fibrosis (Sime et al., 1997), and the administration of TGF-β neutralizing antibodies was able to prevent the disease.

Here, we report the positive effects of the H_4R antagonist on the lung TGF-β pathway, showing that the treatment with JNJ significantly reduces TGF-β levels also in PARP-$1^{-/-}$ mice. Thus, our results indicate that H_4R antagonists can ameliorate lung fibrosis independently of PARP-1 expression. To further confirm the effects of the H_4R antagonist JNJ, we performed experiments also with VUF8430, introduced as a selective H_4R agonist. Surprisingly, in our model, VUF has some unexpected effects in reducing features of lung injury, in functional assay as well as α-SMA and collagen deposition. This discrepancy could be explained because this H_4R agonist with minor modification on imidazole moiety has affinity also for H_3R (Lim et al., 2009), thus reducing the endogenous release of histamine and H_4R activation.

PARP-1 activity contributes to lung fibroblast activation and induces their proliferation with increased expression of αSMA, which plays a pivotal role in lung fibrosis (Hu et al., 2013). In order to confirm the above results, we demonstrate a significant reduction of αSMA levels in PARP-$1^{-/-}$ mice treated with JNJ, suggesting that the use of an H_4R antagonist, in the absence of PARP-1 enzyme, strongly reduces the activation of fibroblasts and the differentiation of myofibroblasts, consequently blocking the development of progressive fibrotic disease.

Overall, these findings suggest that PARylation is a key factor for the pathogenesis of pulmonary fibrosis and provide evidence that PARP-1 and H_4R are independently involved in the signaling pathways activated during inflammatory and fibrotic processes. The association of PARP-1 deficiency and H_4R antagonist treatment exerts a cross-talk response with anti-inflammatory and anti-fibrotic effects, decreasing bronchoconstriction and airway inflammation, as also shown by the reduction of the percentage number of goblet cells and the thickness of the smooth muscle layer, key parameters of inflammation-induced adverse airway remodeling.

Actually, the treatment of idiopathic pulmonary fibrosis is based on the use of either pirfenidone, a drug able to reduce the production of fibrogenic mediators, such as TGF-β, and inflammatory mediators, such as TNFα and IL-1β (Inomata et al., 2015), or nintedanib, a tyrosine kinase inhibitor able to reduce the transduction pathway of growth factor receptors, such as platelet-derived growth factor receptor, fibroblast growth factor receptor, and vascular endothelial growth factor receptor, and to reduce the transduction pathways leading to cell activation and proliferation (Nanthakumar et al., 2015). Both agents have recently been introduced into clinical practice showing their ability to ameliorate lung fibrotic processes; however, it is still not clear whether these agents have a clinically meaningful efficacy in long-term patient survival (Karimi-Shah and Chowdhury, 2015). Effective therapies to contrast airway inflammation and remodeling are not available, and novel therapeutic strategies are needed as alternative options when the standards of care are not enough.

In this study, we showed that the beneficial effects of H_4R antagonists in reducing progressive pulmonary fibrosis are not dependent upon PARP-1.

In conclusion, the therapeutic potential of the combination of H_4R antagonists with non-toxic doses of selective PARP-1 inhibitors could significantly reduce the development of pulmonary fibrosis. Although JNJ itself is emerging as a promising therapeutic agent in lung inflammation, the combination with PARP inhibitors could have an advantage over the single drug for the potentiating effect on the inhibition of inflammatory and pro-fibrotic parameters.

ETHICS STATEMENT

The study protocol complied with the Declaration of Helsinki and the recommendations of the European Economic Community (86/609/CEE) on animal experimentation and was approved by the animal Ethical and Care Committee of the University of Florence (Florence, Italy) and by the Health Ministry (Authorization n 874/2017-PR). Experiments were

carried out at the Centre for Laboratory Animal Housing and Experimentation (CeSAL), University of Florence. All studies involving animals are reported in accordance with the ARRIVE guidelines for reporting experiments involving animals (McGrath et al., 2010).

AUTHOR CONTRIBUTIONS

LL, MD, CL, and EM designed the research study. LL, MD, CL, SS, PN, and AP performed the research. AP and LL analyzed the data. LL, MD, and EM wrote the paper. FM revised the scientific content of the manuscript.

ACKNOWLEDGMENTS

We thank Prof. Alberto Chiarugi, University of Florence, for providing us with PARP-$1^{-/-}$ mice, and Dr. Robin Thurmond (Janssen Research & Development, USA) for supplying the compound JNJ7777120.

SUPPLEMENTARY MATERIAL

The Supplementary Material for this article can be found online at: https://www.frontiersin.org/article/10.3389/fphar.2019.00525/full#supplementary-material

REFERENCES

Abdallah, Y., Gligorievski, D., Kasseckert, S. A., Dieterich, L., Schäfer, M., Kuhlmann, C. R., et al. (2007). The role of poly(ADP-ribose) polymerase (PARP) in the autonomous proliferative response of endothelial cells to hypoxia. *Cardiovasc. Res.* 73, 568–574. doi: 10.1016/j.cardiores.2006.11.027

Ajuebor, M. N., Das, A. M., Virág, L., Flower, R. J., Szabó, C., and Perretti, M. (1999). Role of resident peritoneal macrophages and mast cells in chemokine production and neutrophil migration in acute inflammation: evidence for an inhibitory loop involving endogenous IL-10. *J. Immunol.* 162, 1685–1691. Available at: http://www.ncbi.nlm.nih.gov/pubmed/9973430 [Accessed January 14, 2019]

Ali, A. A. E., Timinszky, G., Arribas-Bosacoma, R., Kozlowski, M., Hassa, P. O., Hassler, M., et al. (2012). The zinc-finger domains of PARP1 cooperate to recognize DNA strand breaks. *Nat. Struct. Mol. Biol.* 19, 685–692. doi: 10.1038/nsmb.2335

Allen, R. J., Porte, J., Braybrooke, R., Flores, C., Fingerlin, T. E., Oldham, J. M., et al. (2017). Genetic variants associated with susceptibility to idiopathic pulmonary fibrosis in people of European ancestry: a genome-wide association study. *Lancet Respir. Med.* 5, 869–880. doi: 10.1016/S2213-2600(17)30387-9

Bai, T. R., and Knight, D. A. (2005). Structural changes in the airways in asthma: observations and consequences. *Clin. Sci.* 108, 463–477. doi: 10.1042/CS20040342

Bonniaud, P., Margetts, P. J., Ask, K., Flanders, K., Gauldie, J., and Kolb, M. (2005). TGF-beta and Smad3 signaling link inflammation to chronic fibrogenesis. *J. Immunol.* 175, 5390–5395. doi: 10.4049/jimmunol.175.8.5390

Chen, Y.-L., Zhang, X., Bai, J., Gai, L., Ye, X.-L., Zhang, L., et al. (2013). Sorafenib ameliorates bleomycin-induced pulmonary fibrosis: potential roles in the inhibition of epithelial–mesenchymal transition and fibroblast activation. *Cell Death Dis.* 4:e665. doi: 10.1038/cddis.2013.154

Chitra, P., Saiprasad, G., Manikandan, R., and Sudhandiran, G. (2015). Berberine inhibits Smad and non-Smad signaling cascades and enhances autophagy against pulmonary fibrosis. *J. Mol. Med.* 93, 1015–1031. doi: 10.1007/s00109-015-1283-1

Conte, E., Gili, E., Fagone, E., Fruciano, M., Iemmolo, M., and Vancheri, C. (2014). Effect of pirfenidone on proliferation, TGF-b-induced myofibroblast differentiation and fibrogenic activity of primary human lung fibroblasts. *Eur. J. Pharm. Sci.* 58, 13–19. doi: 10.1016/j.ejps.2014.02.014

Cowden, J. M., Riley, J. P., Ma, J. Y., Thurmond, R. L., and Dunford, P. J. (2010). Histamine H4 receptor antagonism diminishes existing airway inflammation and dysfunction via modulation of Th2 cytokines. *Respir. Res.* 11:86. doi: 10.1186/1465-9921-11-86

Dunford, P. J., O'Donnell, N., Riley, J. P., Williams, K. N., Karlsson, L., and Thurmond, R. L. (2006). The histamine H4 receptor mediates allergic airway inflammation by regulating the activation of CD4+ T cells. *J. Immunol.* 176, 7062–7070. doi: 10.4049/jimmunol.176.11.7062

Formigli, L., Perna, A. M., Meacci, E., Cinci, L., Margheri, M., Nistri, S., et al. (2007). Paracrine effects of transplanted myoblasts and relaxin on post-infarction heart remodelling: In Focus. *J. Cell. Mol. Med.* 11, 1087–1100. doi: 10.1111/j.1582-4934.2007.00111.x

Genovese, T., Mazzon, E., Di Paola, R., Muià, C., Threadgill, M. D., Caputi, A. P., et al. (2005). Inhibitors of poly(ADP-ribose) polymerase modulate signal transduction pathways and the development of bleomycin-induced lung injury. *J. Pharmacol. Exp. Ther.* 313, 529–538. doi: 10.1124/jpet.104.080705

Gschwandtner, M., Koether, B., Werfel, T., Stark, H., and Gutzmer, R. (2013). Profiling of histamine H_4 receptor agonists in native human monocytes. *Br. J. Pharmacol.* 170, 136–143. doi: 10.1111/bph.12237

Gutzmer, R., Mommert, S., Gschwandtner, M., Zwingmann, K., Stark, H., and Werfel, T. (2009). The histamine H4 receptor is functionally expressed on TH2 cells. *J. Allergy Clin. Immunol.* 123, 619–625. doi: 10.1016/j.jaci.2008.12.1110

Hu, B., Wu, Z., Hergert, P., Henke, C. A., Bitterman, P. B., and Phan, S. H. (2013). Regulation of myofibroblast differentiation by poly(ADP-ribose) polymerase 1. *Am. J. Pathol.* 182, 71–83. doi: 10.1016/j.ajpath.2012.09.004

Inomata, M., Nishioka, Y., and Azuma, A. (2015). Nintedanib: evidence for its therapeutic potential in idiopathic pulmonary fibrosis. *Core Evid.* 10, 89–98. doi: 10.2147/CE.S82905

Karimi-Shah, B. A., and Chowdhury, B. A. (2015). Forced vital capacity in idiopathic pulmonary fibrosis—FDA review of pirfenidone and nintedanib. *N. Engl. J. Med.* 372, 1187–1189. doi: 10.1056/NEJMp1414949

Kohyama, T., Yamauchi, Y., Takizawa, H., Kamitani, S., Kawasaki, S., and Nagase, T. (2010). Histamine stimulates human lung fibroblast migration. *Mol. Cell. Biochem.* 337, 77–81. doi: 10.1007/s11010-009-0287-y

Kolodsick, J. E., Peters-Golden, M., Larios, J., Toews, G. B., Thannickal, V. J., and Moore, B. B. (2003). Prostaglandin E2 inhibits fibroblast to myofibroblast transition via E. prostanoid receptor 2 signaling and cyclic adenosine monophosphate elevation. *Am. J. Respir. Cell Mol. Biol.* 29, 537–544. doi: 10.1165/rcmb.2002-0243OC

Lama, V., Moore, B. B., Christensen, P., Toews, G. B., and Peters-Golden, M. (2002). Prostaglandin E_2 synthesis and suppression of fibroblast proliferation by alveolar epithelial cells is cyclooxygenase-2–dependent. *Am. J. Respir. Cell Mol. Biol.* 27, 752–758. doi: 10.1165/rcmb.4857

Langelier, M.-F., Planck, J. L., Roy, S., and Pascal, J. M. (2012). Structural basis for DNA damage-dependent poly(ADP-ribosyl)ation by human PARP-1. *Science* 336, 728–732. doi: 10.1126/science.1216338

Lattouf, R., Younes, R., Lutomski, D., Naaman, N., Godeau, G., Senni, K., et al. (2014). Picrosirius red staining: a useful tool to appraise collagen networks in normal and pathological tissues. *J. Histochem. Cytochem.* 62, 751–758. doi: 10.1369/0022155414545787

Leask, A., and Abraham, D. J. (2004). TGF-beta signaling and the fibrotic response. *FASEB J.* 18, 816–827. doi: 10.1096/fj.03-1273rev

Lim, H. D., Adami, M., Guaita, E., Werfel, T., Smits, R. A., de Esch, I. J. P., et al. (2009). Pharmacological characterization of the new histamine H4 receptor agonist VUF 8430. *Br. J. Pharmacol.* 157, 34–43. doi: 10.1111/j.1476-5381.2009.00200.x

Lodovici, M., Casalini, C., Cariaggi, R., Michelucci, L., and Dolara, P. (2000). Levels of 8-hydroxydeoxyguanosine as a marker of DNA damage in human leukocytes. *Free Radic. Biol. Med.* 28, 13–17. doi: 10.1016/S0891-5849(99)00194-X

Lucarini, L., Durante, M., Lanzi, C., Pini, A., Boccalini, G., Calosi, L., et al. (2017). HYDAMTIQ, a selective PARP-1 inhibitor, improves bleomycin-

induced lung fibrosis by dampening the TGF-β/SMAD signalling pathway. *J. Cell. Mol. Med.* 21, 324–335. doi: 10.1111/jcmm.12967

Lucarini, L., Pini, A., Gerace, E., Pellicciari, R., Masini, E., and Moroni, F. (2014). Poly(ADP-ribose) polymerase inhibition with HYDAMTIQ reduces allergen-induced asthma-like reaction, bronchial hyper-reactivity and airway remodelling. *J. Cell. Mol. Med.* 18, 468–479. doi: 10.1111/jcmm.12197

Lucarini, L., Pini, A., Rosa, A. C., Lanzi, C., Durante, M., Chazot, P. L., et al. (2016). Role of histamine H4 receptor ligands in bleomycin-induced pulmonary fibrosis. *Pharmacol. Res.* 111, 740–748. doi: 10.1016/j.phrs.2016.07.037

Manni, M. L., Mandalapu, S., McHugh, K. J., Elloso, M. M., Dudas, P. L., and Alcorn, J. F. (2016). Molecular mechanisms of airway hyperresponsiveness in a murine model of steroid-resistant airway inflammation. *J. Immunol.* 196, 963–977. doi: 10.4049/jimmunol.1501531

Marcos-Garcés, V., Harvat, M., Molina Aguilar, P., Ferrandez Izquierdo, A., and Ruiz-Saurì, A. (2017). Comparative measurement of collagen bundle orientation by Fourier analysis and semiquantitative evaluation: reliability and agreement in Masson's trichrome, Picrosirius red and confocal microscopy techniques. *J. Microsc.* 267, 130–142. doi: 10.1111/jmi.12553

Martin, M. M., Buckenberger, J. A., Jiang, J., Malana, G. E., Knoell, D. L., Feldman, D. S., et al. (2007). TGF-beta1 stimulates human AT1 receptor expression in lung fibroblasts by cross talk between the Smad, p 38 MAPK, JNK, and PI3K signaling pathways. *Am. J. Physiol. Lung Cell. Mol. Physiol.* 293, L790–L799. doi: 10.1152/ajplung.00099.2007

Masini, E., Bani, D., Vannacci, A., Pierpaoli, S., Mannaioni, P. F., Comhair, S. A. A., et al. (2005). Reduction of antigen-induced respiratory abnormalities and airway inflammation in sensitized guinea pigs by a superoxide dismutase mimetic. *Free Radic. Biol. Med.* 39, 520–531. doi: 10.1016/j.freeradbiomed.2005.04.006

Masini, E., Lucarini, L., Sydbom, A., Dahlén, B., and Dahlén, S.-E. (2013). "Histamine in asthmatic and fibrotic lung disorders" in *Histamine H4 Receptor: A Novel Drug Target in Immunoregulation and Inflammation*. ed. H. Stark (London, Great Britain: Versita), 145–171.

McGrath, J. C., Drummond, G. B., McLachlan, E. M. E., Kilkenny, C., and Wainwright, C. L. (2010). Guidelines for reporting experiments involving animals: the ARRIVE guidelines. *Br. J. Pharmacol.* 160, 1573–1576. doi: 10.1111/j.1476-5381.2010.00873.x

Moore, B. B., and Hogaboam, C. M. (2008). Murine models of pulmonary fibrosis. *Am. J. Physiol. Lung Cell. Mol. Physiol.* 294, 152–160. doi: 10.1152/ajplung.00313.2007

Mukhopadhyay, P., Rajesh, M., Cao, Z., Horvth, B., Park, O., Wang, H., et al. (2014). Poly (ADP-ribose) polymerase-1 is a key mediator of liver inflammation and fibrosis. *Hepatology* 59, 1998–2009. doi: 10.1002/hep.26763

Mullane, K. M., Kraemer, R., and Smith, B. (1985). Myeloperoxidase activity as a quantitative assessment of neutrophil infiltration into ischemic myocardium. *J. Pharmacol. Methods* 14, 157–167. doi: 10.1016/0160-5402(85)90029-4

Nanthakumar, C. B., Hatley, R. J. D., Lemma, S., Gauldie, J., Marshall, R. P., and Macdonald, S. J. F. (2015). Dissecting fibrosis: therapeutic insights from the small-molecule toolbox. *Nat. Rev. Drug Discov.* 14, 693–720. doi: 10.1038/nrd4592

Pacher, P., Liaudet, L., Bai, P., Virag, L., Mabley, J. G., Haskó, G., et al. (2002). Activation of poly(ADP-ribose) polymerase contributes to development of doxorubicin-induced heart failure. *J. Pharmacol. Exp. Ther.* 300, 862–867. doi: 10.1124/jpet.300.3.862

Paz, Z., and Shoenfeld, Y. (2010). Antifibrosis: to reverse the irreversible. *Clin. Rev. Allergy Immunol.* 38, 276–286. doi: 10.1007/s12016-009-8157-7

Pini, A., Shemesh, R., Samuel, C. S., Bathgate, R. A. D., Zauberman, A., Hermesh, C., et al. (2010). Prevention of bleomycin-induced pulmonary fibrosis by a novel antifibrotic peptide with relaxin-like activity. *J. Pharmacol. Exp. Ther.* 335, 589–599. doi: 10.1124/jpet.110.170977

Pini, A., Viappiani, S., Bolla, M., Masini, E., and Bani, D. (2012). Prevention of bleomycin-induced lung fibrosis in mice by a novel approach of parallel inhibition of cyclooxygenase and nitric-oxide donation using NCX 466, a prototype cyclooxygenase inhibitor and nitric-oxide donor. *J. Pharmacol. Exp. Ther.* 341, 493–499. doi: 10.1124/jpet.111.190660

Plantier, L., Cazes, A., Dinh-Xuan, A.-T., Bancal, C., Marchand-Adam, S., and Crestani, B. (2018). Physiology of the lung in idiopathic pulmonary fibrosis. *Eur. Respir. Rev.* 27:170062. doi: 10.1183/16000617.0062-2017

Rosa, A. C., Pini, A., Lucarini, L., Lanzi, C., Veglia, E., Thurmond, R. L., et al. (2014). Prevention of bleomycin-induced lung inflammation and fibrosis in mice by naproxen and JNJ7777120 treatment. *J. Pharmacol. Exp. Ther.* 351, 308–316. doi: 10.1124/jpet.114.215152

Sime, P. J., Xing, Z., Graham, F. L., Csaky, K. G., and Gauldie, J. (1997). Adenovector-mediated gene transfer of active transforming growth factor-beta1 induces prolonged severe fibrosis in rat lung. *J. Clin. Invest.* 100, 768–776. doi: 10.1172/JCI119590

Smolle, J., Fiebiger, M., Hofmann-Wellenhof, R., and Kerl, H. (1996). Quantitative morphology of collagen fibers in cutaneous malignant melanoma and melanocytic nevus. *Am. J. Dermatopathol.* 18, 358–363. doi: 10.1097/00000372-199608000-00005

Swigris, J. J., Kuschner, W. G., Jacobs, S. S., Wilson, S. R., and Gould, M. K. (2005). Health-related quality of life in patients with idiopathic pulmonary fibrosis: a systematic review. *Thorax* 60, 588–594. doi: 10.1136/thx.2004.035220

Tatler, A. L., and Jenkins, G. (2012). TGF-β activation and lung fibrosis. *Proc. Am. Thorac. Soc.* 9, 130–136. doi: 10.1513/pats.201201-003AW

Thannickal, V. J., and Horowitz, J. C. (2006). Evolving concepts of apoptosis in idiopathic pulmonary fibrosis. *Proc. Am. Thorac. Soc.* 3, 350–356. doi: 10.1513/pats.200601-001TK

Wang, Z. Q., Auer, B., Stingl, L., Berghammer, H., Haidacher, D., Schweiger, M., et al. (1995). Mice lacking ADPRT and poly(ADP-ribosyl)ation develop normally but are susceptible to skin disease. *Genes Dev.* 9, 509–520. doi: 10.1101/gad.9.5.509

Wilson, M. S., and Wynn, T. A. (2009). Pulmonary fibrosis: pathogenesis, etiology and regulation. *Mucosal Immunol.* 2, 103–121. doi: 10.1038/mi.2008.85

Wynn, T. A. (2007). Common and unique mechanisms regulate fibrosis in various fibroproliferative diseases. *J. Clin. Invest.* 117, 524–529. doi: 10.1172/JCI31487

Wynn, T. (2008). Cellular and molecular mechanisms of fibrosis. *J. Pathol.* 214, 199–210. doi: 10.1002/path.2277

Wynn, T. A., and Ramalingam, T. R. (2012). Mechanisms of fibrosis: therapeutic translation for fibrotic disease. *Nat. Med.* 18, 1028–1040. doi: 10.1038/nm.2807

Zampeli, E., and Tiligada, E. (2009). The role of histamine H4 receptor in immune and inflammatory disorders. *Br. J. Pharmacol.* 157, 24–33. doi: 10.1111/j.1476-5381.2009.00151.x

Conflict of Interest Statement: The authors declare that the research was conducted in the absence of any commercial or financial relationships that could be construed as a potential conflict of interest.

frontiers in Pharmacology

REVIEW
published: 01 July 2019
doi: 10.3389/fphar.2019.00724

Gene Therapy Tools for Brain Diseases

Selene Ingusci[1], Gianluca Verlengia[1,2], Marie Soukupova[1], Silvia Zucchini[1,3] and Michele Simonato[1,2]*

[1] Department of Medical Sciences and National Institute of Neuroscience, University of Ferrara, Ferrara, Italy, [2] Division of Neuroscience, University Vita-Salute San Raffaele, Milan, Italy, [3] Technopole of Ferrara, LTTA Laboratory for Advanced Therapies, Ferrara, Italy

Neurological disorders affecting the central nervous system (CNS) are still incompletely understood. Many of these disorders lack a cure and are seeking more specific and effective treatments. In fact, in spite of advancements in knowledge of the CNS function, the treatment of neurological disorders with modern medical and surgical approaches remains difficult for many reasons, such as the complexity of the CNS, the limited regenerative capacity of the tissue, and the difficulty in conveying conventional drugs to the organ due to the blood–brain barrier. Gene therapy, allowing the delivery of genetic materials that encodes potential therapeutic molecules, represents an attractive option. Gene therapy can result in a stable or inducible expression of transgene(s), and can allow a nearly specific expression in target cells. In this review, we will discuss the most commonly used tools for the delivery of genetic material in the CNS, including viral and non-viral vectors; their main applications; their advantages and disadvantages. We will discuss mechanisms of genetic regulation through cell-specific and inducible promoters, which allow to express gene products only in specific cells and to control their transcriptional activation. In addition, we will describe the applications to CNS diseases of post-transcriptional regulation systems (RNA interference); of systems allowing spatial or temporal control of expression [optogenetics and Designer Receptors Exclusively Activated by Designer Drugs (DREADDs)]; and of gene editing technologies (CRISPR/Cas9, Zinc finger proteins). Particular attention will be reserved to viral vectors derived from herpes simplex type 1, a potential tool for the delivery and expression of multiple transgene cassettes simultaneously.

Keywords: gene therapy, central nervous system, viral vector, gene regulation, brain disease

OPEN ACCESS

Edited by:
Ioanna Andreadou, National and Kapodistrian University of Athens, Greece

Reviewed by:
Michelino Di Rosa, University of Catania, Italy
Kyle David Fink, University of California, Davis, United States

****Correspondence:***
Selene Ingusci
selene.ingusci@unife.it

Specialty section:
This article was submitted to Experimental Pharmacology and Drug Discovery, a section of the journal Frontiers in Pharmacology

Received: *28 December 2018*
Accepted: *05 June 2019*
Published: *01 July 2019*

Citation:
Ingusci S, Verlengia G, Soukupova M, Zucchini S and Simonato M (2019) Gene Therapy Tools for Brain Diseases. Front. Pharmacol. 10:724. doi: 10.3389/fphar.2019.00724

INTRODUCTION

Even if scientific research has made great progress over the last decade in identifying pathogenic mechanisms and treatment strategies, neurological disorders affecting the central nervous system (CNS) are still incompletely understood. The majority of these disorders lack a cure or, at least, reasonably effective treatments. Reasons are certainly multifold and include the complexity of the CNS, the limited regenerative capacity of the tissue, and the difficulty in conveying conventional drugs to the organ across the blood–brain barrier (BBB). Neurons, the principal cells of the nervous tissue, are not only morphologically and physiologically heterogeneous, but also strictly organized to form complex circuits. Neural stem cells ensure only a limited replacement of only specific neuronal types. The BBB expresses a selective permeability for molecules that possess a limited range of molecular

weight and lipophilicity, preventing the entry of large-molecule drugs and of the majority of small-molecule drugs.

In this context, gene therapy is emerging as an attractive therapeutic option, because it can result in a stable or inducible expression of therapeutic gene(s), and can allow a nearly specific expression in target cells. Although much remains to be done before it becomes routine practice, the potential of gene therapy for the treatment of CNS diseases is amply demonstrated by numerous preclinical and clinical studies (Simonato et al., 2013).

A large part of the work needed to finally reach the stage of clinical application consists in the refinement of the tools needed for a safe, targeted, and regulated gene delivery. In this review, we will discuss the most commonly used gene therapy tools for delivery in the CNS and the strategies that can be employed for regulating therapeutic gene expression.

GENE THERAPY

The idea behind gene therapy derives from an assumption of great simplicity: by introducing into the cells the "correct" copy of a defective gene whose malfunction causes a disease, its product, a functional protein, will be able to revert the pathological phenotype. This assumption may be correct for monogenic diseases caused by alterations in the coding sequence or in regulatory regions of a single gene, and if these alterations lead to loss of function without production of a pathogenic protein. However, many diseases have a pattern of multiple altered genes. Moreover, the regulation of gene expression is often complex and difficult to reconstruct. According to a new, broader definition, all drugs that contain an active substance that includes or consists of a recombinant nucleic acid (DNA or RNA), administered to a human being for the purpose to adjust, repair, replace, add, or remove a gene sequence, can be defined gene therapy (Klug et al., 2012).

The introduction of a functional gene, called transgene, within the cell nucleus is a complex operation that starts with the choice of a delivery system (gene therapy vector). A good vector should fulfill many requirements (Kay et al., 1997; Gardlik et al., 2005; Shillitoe, 2009):

- Manipulation: the vector should be easily manipulated for recombination and propagation in suitable hosts.
- High cloning capacity: the vector should allow the introduction of one or more genes and regulatory sequences that guarantee the desired spatial and temporal restriction of transgene expression.
- Minimal invasiveness: the vector should not cause uncontrolled or undesired alterations of the host genome. The integration of a vector into the cellular genome can induce insertional mutagenesis.
- Selectivity for the cellular target: the transgene should be expressed exclusively in the target cells.
- Absence of immunogenicity: the vector should not contain genes that induce immune responses or other factors that may be harmful to the body.
- Stability over time: the vector should be transferred unaltered in the cell progeny and/or must allow a correct and prolonged expression of the transgene(s).

Available gene therapy vectors belong to two broad categories: viral and nonviral vectors.

Nonviral Vectors

Nonviral vectors offer some advantages, like reduced pathogenicity, low cost, and simple production techniques (Zhang et al., 2004; Ramamoorth and Narvekar, 2015). However, DNA delivered by nonviral vectors must overcome a number of extracellular and intracellular barriers, limiting the efficiency of transfection (Howell et al., 2003; Matsumoto et al., 2009). In fact, the transfection efficiency is limited by the premature release of the genetic material into the bloodstream and its subsequent degradation by serum nucleases when administered intravenously, while the endocytosed DNA is in large part degraded along the endosome/lysosome pathway before it reaches the nucleus (Ogris et al., 1999; Perez-Martinez et al., 2011).

In addition to direct injection and microinjection of DNA into the nucleus, physical methods and chemical carriers have been developed to improve delivery of naked DNA to cells and tissues (Li and Huang, 2006; Ramamoorth and Narvekar, 2015). Commonly used nonviral delivery tools are cationic polymers and cationic lipids, whose efficiency is dependent on cationic charge, saturation, and linker stability (Jayant et al., 2016). Several strategies have been explored to increase the stability of DNA in the circulation. Polyethylene glycol (PEG) is one example (Dufes et al., 2005; Huang et al., 2007). Another approach is the use of bio-responsive polymers that exploit the chemical–physical properties of the biological microenvironment (pH, presence of reducing agents, etc.) to promote the release of the genetic material exclusively intracellularly. Other tested strategies are acetyl bonds, which degrade at the pH of the endosomal environment (Knorr et al., 2007; Wolff and Rozema, 2008), or disulfide bridges, which are reduced in the cytosol (Piest et al., 2008).

Viral Vectors

Independent of their origin, order, and family, viruses have evolved very fine strategies to reach and penetrate specific cellular targets. Their use in gene therapy lies in their innate ability to deliver and express genetic information into host cells. Replication-defective viral vectors (Bouard et al., 2009) commonly derive from wild-type viruses in which the therapeutic gene(s) are inserted into the viral genome by replacing the "wild" genes essential for the lytic cycle, thereby preventing the virus to replicate and exert cytotoxic effects in target cells. These genes, however, can be replaced by trans-acting factors through the development of specific cell lines or the use of helper viruses during the manufacturing process (Zhou et al., 1996; Von Seggern et al., 1998; Morris et al., 2010). Among all viral vectors, the most characterized and used for targeting the CNS have been derived from retroviruses, adenoviruses, adeno-associated viruses, and herpes simplex viruses (Teschemacher et al., 2005; Bourdenx et al., 2014; Artusi

et al., 2018). These vectors differ in payload capacity, cell tropism (**Table 1**), and ability to integrate into the host genome, which may affect the duration of transgene expression. Advantages and disadvantages, potential CNS application, and side effects for each of the above-mentioned vectors will be briefly discussed below.

Retroviral/Lentiviral Vectors

The *Retroviridae* family consists in a broad range of small RNA viruses whose common feature is to replicate through a DNA intermediate. γ-Retrovirus and lentivirus belong to this family (Cooray et al., 2012). The former is more suitable for *ex vivo* gene therapy applications, because it does not efficiently infect nondividing cells and because it is difficult to reach high viral titers (Gardlik et al., 2005). The latter infects both proliferating and quiescent cells, ensuring long-term gene expression in the absence of inflammatory responses (Case et al., 1999; Sutton et al., 1999; Sakuma et al., 2012).

While the lentiviral integrative nature ensures stable and persistent expression of the transgene, it also entails the risk of insertional mutagenesis. However, gene editing allowed to develop safe lentiviral vectors with specific integration sites (Lombardo et al., 2007). To increase the safety of lentiviral vectors, the viral genome can be split in multiple plasmids, thereby making recombinant virus generation very unlikely (Milone and O'Doherty, 2018). In addition, envelope glycoproteins (gp) can be pseudotyped to redirect viral particles to specific targets (Yee et al., 1994; Aiken, 1997; Sinclair et al., 1997; Maurice et al., 2002; Verhoeyen et al., 2003).

Since lentiviral vectors transduce neurons effectively, they have been tested for the treatment of Alzheimer's disease (AD) and Parkinson's disease (PD) (Azzouz et al., 2002; Jarraya et al., 2009; Palfi et al., 2014; Katsouri et al., 2016; Palfi et al., 2018).

TABLE 1 | Main features of the most commonly employed viral vectors for CNS gene therapy.

Viral vector	Payload	Tropism
Retrovirus vectors	up to 9 kb	Proliferating and quiescent cells
Lentiviruses		
Adenovirus vectors	7–10 kb	Dividing and non-dividing cells
1st generation (subtype C)	~ 35 kb	Respiratory epithelium (blood cells)
Helper-dependent (gutless)		Highly efficient in targeting hepatocytes, less in lung, cardiac muscle, vascular neuronal tissue or dendritic cells
Adeno-associated vectors	~4.8 kb	Different serotypes with different tropism; typical is tropism for hepatocytes, myocytes, and neuronal cells
Herpes Simplex 1 vectors	~40 kb	Actively dividing tumor cells like
Replication-competent (oncolytic)	30–50 kb	glioblastoma, hepatocellular carcinoma or melanoma cells
Replication-defective	up to 150 kb	Nondividing neuronal cells
Amplicon vectors		Neurons, glial cells, epithelial cells

Adenoviral Vectors

Adenoviruses are linear double-stranded DNA viruses with a genome size of 35–40 kb encoding approximately 30–40 genes. There are 100 serotypes of adenovirus, 57 of which have the potential to infect humans. These are divided into seven subgroups, A to G, that differ in cellular tropism (Khare et al., 2011; Lee et al., 2017). The most frequently utilized for gene therapy are types 2 and 5 (Campos and Barry, 2007), both belonging to subtype C (Chang et al., 2008).

Adenoviral vectors transduce efficiently dividing and nondividing cells, with no risk of integration in the host cell genome (Lee et al., 2017). Their main limitations are high immunogenicity; transient transgene expression (from 2 weeks to a few months); and high risk of cytopathic effects (Christ et al., 1997; Ritter et al., 2002; Lowenstein and Castro, 2003; Lowenstein and Castro, 2004; Cucchiarini, 2016). New generations of adenoviral vectors partially overcome these limitations (Lowenstein and Castro, 2002; Gardlik et al., 2005; Campos and Barry, 2007).

Adenoviral vectors have been widely studied for the treatment of tumors (Dobbelstein, 2004; Rein et al., 2006; Sharma et al., 2009; Lenman et al., 2018). In addition, preclinical studies have been conducted in rodent models of PD and Huntington disease (HD) (Choi-Lundberg et al., 1998; Bemelmans et al., 1999).

Adeno-Associated Vectors

Adeno-associated viruses (AAVs) are small, non-enveloped, single-stranded DNA viruses belonging to the *Parvoviridae* family. Despite the size limitation, they are considered the most promising vehicle for gene therapy targeting the CNS because they are clinically safe and effective in transducing dividing and quiescent cells, while capable of establishing a long-term transgene expression. More than 150 clinical trials with a good safety profile and significant clinical benefit in many genetic diseases used AAV vectors (Penaud-Budloo et al., 2018). The AAV genome contains only three genes, replication (*rep*), assembly (*aap*), and capsid (*cap*) (Naso et al., 2017), necessary for viral replication, integration, and packaging (Berns and Giraud, 1996; Nakai et al., 1999; Musatov et al., 2002). AAVs can persist in the host cell in an episomal state, only a small fraction integrating into the host cell genome (Bouard et al., 2009).

More than 12 different AAV serotypes have been isolated (Duan, 2016). Each of these has specific features, including: differences in cellular tropisms (Nakai et al., 2005; Mandel et al., 2006), depending on different capsid surface proteins (Kaludov et al., 2001; Wu et al., 2006; Bell et al., 2011; Shen et al., 2011); differences in transduction efficiency; and differences in ability to evade the host immune response and to cross the BBB (Zhang et al., 2011; Yang et al., 2014). Many serotypes transduce efficiently neurons and glial cells (Davidson et al., 2000; Wang et al., 2003a; Burger et al., 2004; Aschauer et al., 2013). Refinement of AAV vector features and increased brain uptake have been obtained by pseudotyping approaches, like mixing of capsids and genome from different viral serotypes (Grimm et al., 2008; Mao et al., 2016; Hammond et al., 2017); insertion of peptide motifs from phage libraries (Chen et al., 2009); or enrichment of the capsid

through random incorporation of peptide motifs (Choudhury et al., 2016; Deverman et al., 2016; Korbelin et al., 2016; Chan et al., 2017).

Owing to the small sized genome, AAV vectors are capable of accommodating less than 5 kb of exogenous DNA (Wang et al., 2014; Chira et al., 2015). However, strategies are under development for delivering larger genes. One approach could be using truncated forms of genes and/or promoters that maintain the properties of their full-length counterpart (Wang et al., 2000; Kodippili et al., 2018; Zhang et al., 2018). An alternative strategy has been developed by taking advantage of the AAV innate ability to undergo a genomic intermolecular recombination that can give rise to head-to-tail DNA concatamerization (Yan et al., 2005). In this context, the DNA sequence of an oversized expression cassette can be split and packaged in two (Duan et al., 1998; Yan et al., 2000; Duan et al., 2001; Ghosh et al., 2008; Trapani et al., 2014) or even three (Maddalena et al., 2018) independent AAV vectors. Upon concomitant infection of the host, these multiple vectors may give rise to DNA concatamers, which can reconstitute the whole cassette (Maddalena et al., 2018). The efficiency of this multiple-vector strategy is obviously significantly lower than the single-vector strategy (Duan et al., 2001), and attempts are ongoing to improve the situation (Ghosh et al., 2008).

The therapeutic potential of AAV-based gene therapy has been tested in many different neurological disorders (Kaplitt et al., 2007; Eberling et al., 2008; Worgall et al., 2008; Christine et al., 2009; Souweidane et al., 2010; Mittermeyer et al., 2012; Rafii et al., 2014; Tardieu et al., 2014; Mendell et al., 2017).

Herpes Simplex Vectors

The first Herpesvirus vector has been derived from Herpes Simplex Virus type 1 (HSV-1) (Palella et al., 1988), an enveloped ubiquitous virus with a double-stranded linear DNA genome. Hallmarks of HSV-1 are the short replication cycle and the ability to travel *via* retrograde axonal transport from the primary infection site to the sensory neurons of the CNS, where it establishes a life-long latency in an episomal form (Studahl et al., 2017). Since then, three types of HSV-1 based vectors have been developed: replication-competent, replication-defective, and amplicon vectors (Artusi et al., 2018). Replication-competent vectors are used in oncology for their ability to complete a lytic cycle in the presence of permissive cellular environments (Ikeda et al., 2000; Todo, 2008). Replication-defective and amplicon vectors are tested as gene transfer tools for the CNS (Goverdhana et al., 2005; Berges et al., 2007).

The large genome (152 kb) of HSV-1 encodes about 80 genes, half of which can be removed to make room for up to 50 kb of foreign DNA in the case of replication-defective vectors and up to 150 kb for amplicon vectors (Simonato et al., 2000). HSV-1 vectors maintain high infectivity, ability of both retrograde and anterograde transport, and potential to establish a latent infection in the episomal form (Lachmann, 2004). Traditional limitations in their application are residual toxicity towards the infected cells (Goverdhana et al., 2005) and the short-term expression of the transgene due to rapid silencing mechanisms (Lachmann et al., 1996).

New HSV-Based Vectors for Delivering Multiple Expression Cassettes

Disorders of the CNS are often not a result of single gene mutation or of a single molecular mechanism but have instead a multifactorial origin. As a result, the therapeutic gene(s) and/or the regulation sequence to be delivered very often exceed the payload capacity of viral vectors (Thomas et al., 2003). HSV-1 vectors represent an attractive solution for this issue, because of their large genomic size and capacity to host large amounts of foreign DNA. As noted above, however, the first generations of replication-defective HSV-1 vectors were hindered by highly significant limitations, including toxicity and short-term expression of the transgenes (Marconi et al., 1999). Many recent studies have been aimed to solve these problems.

The HSV productive cycle is characterized by a temporally regulated cascade of gene expression, during which three distinct classes of transcripts are expressed in a sequential manner. The immediate early genes (IE or α) are first expressed, followed by the early (E or β) and late (L or γ) genes. IE genes are required not only for establishment of a lytic reproductive cycle, but also to overcome innate immune responses, to block cell division, and to prevent host cell apoptosis and epigenetic repression of viral genes. The engineering of mutant HSV-1 vectors devoid of α genes shuts off viral replication and remarkably reduce cytotoxicity (Krisky et al., 1998). Deletion of two IE genes, ICP4 and ICP27, gave rise to the first (ΔICP4) and second (ΔICP4/27) generation of HSV-1 vectors (Shepard and DeLuca, 1991; Wu et al., 1996). These early generations were able to establish a long-term expression without the ability to reactivate, but the residual presence of ICP0 was responsible of cytotoxic effects in transduced cells. The consequent deletion of ICP0 gave rise to a third generation of vectors that were devoid of toxicity but displayed short-term expression of the transgene (Samaniego et al., 1997). To overcome this hurdle, a novel generation of HSV-1 vectors (**Figure 1**) was engineered by inserting the transgene expression cassette into the viral latency-associated transcript locus, a genome region that is protected from silencing during latency by the presence of insulator sequences (CTRL) that act as boundary elements to shield the locus against epigenetic modifications (Bloom et al., 2010). This new generation of highly defective vectors offers a large payload capacity while displaying no sign of toxicity upon *in vitro* infection of diverse cell types (Miyagawa et al., 2015). The *in vivo* injection of this new class of HSV-based vectors into different brain regions of naive rats yielded a robust and persistent (up to 6 months) neuron-specific expression of transgenes inserted in the ICP4 locus, without evidence of toxicity or inflammatory cell infiltration, suggesting that the ICP4 locus may be an option to achieve a sustained and prolonged transgene expression in neurons (Verlengia et al., 2017). A further modification of the viral backbone (the deletion of the UL41 gene that may contribute residual toxicity) further improved the levels of transgene expression. UL41-deleted vectors displayed an improved, long-lasting and neuron-specific transgene expression without any evidence of toxicity (Miyagawa et al., 2017). Recently, in order to overcome the rapid transcriptional repression of transgenes cloned outside the ICP4

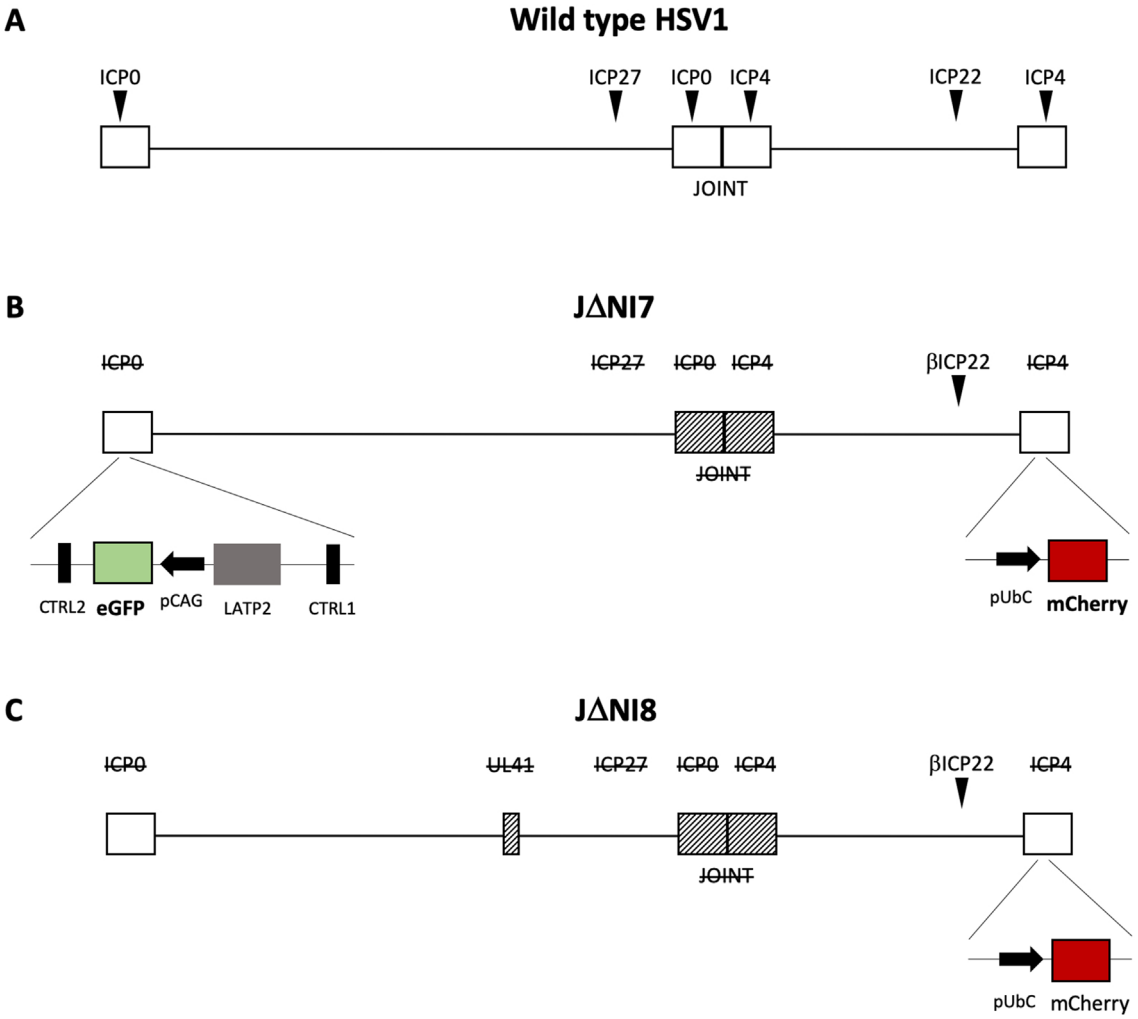

FIGURE 1 | Schematic drawing of the genomes of new HSV-1 vectors. Compared to the wild-type genome **(A)**, the derivative vectors JDNI7 **(B)** and JDNI8 **(C)** are deleted for the joint region and the ICP0, ICP4, and ICP27 immediate-early genes, while the ICP22 immediate-early gene is converted to early-expression kinetics by promoter modification. Moreover, both viral backbones are engineered for the insertion of a ubiquitin C promoter (UbCp)-mCherry cassette within the ICP4 locus. The JDNI7 **(B)** backbone is further modified by the insertion of a CAG promoter-eGFP expression cassette into the LAT (Latency Associated Transcript) intron region, flanked by the LATP2 enhancer region, and CTCF-binding motifs (CTRL2). The last generation of HSV-based vectors, JDNI8 **(C)**, is also deleted for UL41, the gene encoding the virion host shutoff (vhs) protein.

locus, the backbone was further engineered with specific cellular anti-silencing elements, inserted to prevent the formation of heterochromatin at the transgene promoter level. Different types of anti-silencing elements were evaluated, but the most effective in increasing neuronal transgene expression in both *in vitro* and *in vivo* assays was A2UCOE (Han et al., 2018). In conclusion, these new replication-defective backbones seem to hold the features and the flexibility of options needed for gene therapy applications in the CNS.

Amplicon vectors (**Figure 2**) are the other promising class of HSV-1-based vectors. Amplicons maintain all structural, immunological, and host range properties of the wild-type virus, but only two elements, the viral origin of replication (*ori*) and the capsid packaging sequence (*pac*), are retained from their original genome, the other part consisting of a concatemer repetition of the foreign DNA (Epstein, 2009b). The major advantage of this gene transfer tool is that the total deletion of viral genes allows the insertion of up to 150 kb of exogenous DNA. The number of concatameric repeats depends on the size of the expression cassette, i.e., short sequences allow the insertion of more copies of the gene of interest. Furthermore, the complete absence of all viral genes strongly reduces the risk of reactivation, complementation, or recombination with latent HSV-1 genomes (Epstein, 2009a). The downside is that amplicon propagation is rather difficult, because cell lines able to complement all viral proteins in trans are not available. Therefore, first generation of amplicon vectors was propagated by transfection of amplicon plasmids into cells, which were then superinfected with an HSV-1 helper virus. Unfortunately, this approach leads to a significant (about 1%) contamination with helper virus (Pechan

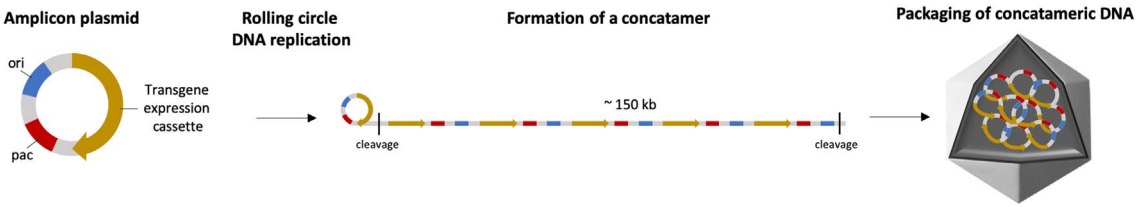

FIGURE 2 | Schematic representation of an amplicon vector. The amplicon plasmid contains the sequences for viral DNA replication (ori, blue) and the packaging signal (pac, red), flanking the transgene expression cassette. In the presence of an HSV-1 helper virus in permissive cells, the amplicon DNA plasmid is replicated as head-to-tail concatemers, cleaved into 150 kb linear DNA and packaged in HSV capsids.

et al., 1996). A promising alternative is the use of the LaL helper virus, in which the packaging sequence can be deleted by Cre-lox specific-site recombination, reducing the helper contamination to 0.05–0.5% (Zaupa et al., 2003). Despite the fact that amplicon vectors have been widely used for exploring the mechanisms of CNS function, only few studies have focused on their use for gene therapy (Cuchet et al., 2007). Recently, ultrapure amplicons produced using a highly defective helper virus have been employed to silence brain-derived neurotrophic factor (BDNF) expression in an animal model of epilepsy (Falcicchia et al., 2016). Apart from the production difficulties, amplicon vectors suffer from a relatively short-time expression of the transgenes in the living organism. Most likely, the presence of bacterial sequences in the amplicon genome causes transgene silencing by forming inactive chromatin (Suzuki et al., 2006). Therefore, the current research in this field focuses on the development of new, helper virus independent production techniques and on means to obtain long-term expression of the transgene.

CARGO

Genes Encoding Therapeutic Proteins

The question that comes together with the development of suitable vectors for gene transfer in the CNS is which genes to transfer. The first, most obvious option is genes encoding a therapeutic protein. This may be the correct copy of a defective gene whose malfunction causes the disease, but also a gene encoding a therapeutic protein that could not be peripherally administered, not being able to cross the BBB. In this last instance, the protein could be diffusible (i.e., produced and secreted by the infected cell) to produce a by-stander effect in adjacent cells (Simonato, 2014).

Apart from genes encoding therapeutic proteins, however, there are other cargo options for CNS gene therapy vectors, like gene editing, chemogenetic, and optogenetic tools.

Gene Editing Tools

A step forward was made in gene therapy with the development of gene editing tools that can correct genetic defects directly in the host DNA. These tools generate a double strand break (DSB) at a precisely desired location, and the break allows to take advantage of the fine strategies that cells have evolved to detect and repair DNA damage. The DSB can lead to gene disruption by non-homologous end joint (Lieber, 2010), or gene addition or repair by homologous recombination using an exogenously supplied repair template (Li and Heyer, 2008). The most promising gene editing system is the Clustered Regularly Interspaced Short Palindromic Repeats/Cas (CRISPR/Cas) system (Gaj et al., 2016; Ahmad et al., 2018). The delivery platforms described in this review are obviously essential for this new and powerful therapeutic tool.

Chemogenetic and Optogenetic Tools

The complexity of the mammalian brain has no comparison: dozens of billions of interconnected neurons, with complex morphology and circuit interaction, capable of exchanging electrical signals with a precise temporal scan in the order of milliseconds. A great challenge is to develop the ability to control only one type of cell in the brain without affecting others. Electrical, physical, pharmacological, and genetic methods are traditionally used to manipulate cells and synapses (Carter and Shieh, 2015). However, all these methods lack temporal and spatial resolution and can cause stimulation, inhibition, or inactivation of off-target cells and processes. To overcome these limitations, new genetic tools referred to as "chemogenetic" and "optogenetics" have been developed.

Designer Receptors Exclusively Activated by Designer Drug

Chemogenetics is the processes in which proteins are engineered to interact specifically with a small molecule (Sternson and Roth, 2014). Different proteins involved in CNS disorders have been engineered to this aim, including enzymes (Bishop et al., 1998; Cohen et al., 2005; Dar et al., 2012), and G protein-coupled receptors (GPCRs; Zemelman et al., 2003; Magnus et al., 2011). The latter include allele-specific GPCRs (Strader et al., 1991), Receptors Activated Solely by a Synthetic Ligand (RASSLs; Coward et al., 1998), and Designer Receptors Exclusively Activated by Designer Drugs (DREADDs; Armbruster et al., 2007). The first chemogenetically engineered GPCR was the β-adrenergic receptor (Strader et al., 1991). Following mutations at the β-adrenergic receptor binding site, the responsiveness to the natural ligand disappeared and a new specificity was obtained to ketonic and catechol esterase agonists. Several years later, RASSLs receptors were developed, based on human κ-opioids, that lost their affinity for the endogenous peptide ligand (dynorphin) and gained specificity for small and safe drugs such as spiradoline (Coward et al., 1998).

Together with optogenetics, the DREADDs technology is currently the most used tool for *in vivo* manipulation of the activity of genetically defined neuronal populations. An example of DREADDs technology is the use of modified muscarinic receptors, hM3Dq for stimulation and hM4Di for inhibition, which have lost their affinity for endogenous acetylcholine, but can be activated by a synthetic ligand (clozapine-N-oxide, CNO) that crosses the BBB (Armbruster et al., 2007; Alexander et al., 2009). Compared to previous techniques, chemogenetics based on DREADDs confers the ability to regulate and manipulate in a non-invasive manner the activity of specific neuronal circuits. Combined with the set of gene therapy tools described above, DREADDs can be delivered and almost selectively expressed in the neuronal subpopulation of interest, for example serotoninergic (Teissier et al., 2015; Urban et al., 2016) or glutamatergic neurons (Krashes et al., 2014; Zhu et al., 2014; Zhu et al., 2016).

DREADDs are useful tools for basic scientific research but may also refine gene therapy approaches for neurodegenerative disorders in which changes in neuronal activity play an important role. Neuronal hyperactivity and hyperexcitability of the cerebral cortex and hippocampus are common features of epilepsy and AD (Badawy et al., 2009; de Haan et al., 2017). On demand attenuation of seizures was achieved after delivery of AAV vectors carrying the hM4Di receptor under the control of the *CamkIIα* promoter (Katzel et al., 2014). Moreover, transient cholinergic-specific stimulation led to a striking improvement in motor scores in a rodent model of PD including gait and postural abnormalities (Pienaar et al., 2015).

Optogenetic Approaches

The term optogenetics indicates a methodology that allows to control the activity of specific neurons within intact neuronal circuits (Deisseroth, 2011). The idea of using the light as a tool to control neuronal function was originally put forward by Francis Crick (Crick, 1979). In the 1970s, biologists discovered that some microorganisms generate proteins that, in response to visible light, regulate the flow of charges across the membranes (Oesterhelt and Stoeckenius, 1971). These proteins, termed opsins, are photosensitive trans-membrane proteins that, when illuminated at defined frequencies, induce transmembrane ion fluxes and, thereby, changes in the electrical activity of the cell. There are two major classes of opsins, which differ in sensitivity to light and absorption properties, and cause activation or inhibition of neurons (Deisseroth, 2015):

- Channelrhodopsin (ChR): a blue light activated cation-channel from *Chlamydomonas reinhardtii*, used to excite neurons (Nagel et al., 2003);
- Halorhodopsin (NpHR): a yellow light activated chloride-pump from *Natronomonas pharaonic*, used to inhibit neurons (Chow et al., 2010).

Through viral vectors, the gene coding for an opsin can be integrated into target neurons, leading to expression of the opsin protein on the membrane. A nearby source of light, set on the right wavelength and frequency, can then interact with it, activating or inhibiting neuronal activity. The introduction of mutations to existing opsin variants allowed to overcome certain problems associated with light delivery. For example, the ChR chETA mutant displays faster channel closing and increased temporal control (Gunaydin et al., 2010). The C1V1 mutant can be excited by longer wavelengths, allowing deeper penetration of the tissue (Yizhar et al., 2011). At the same time, light delivery tools have been improved and optimized for *in vivo* studies (Liu et al., 2015).

The use of optogenetics as therapeutic tools for neurological disorders has been investigated in PD, AD, and epilepsy (Kravitz et al., 2010; Zahedi et al., 2013; Seeger-Armbruster et al., 2015). Enhanced excitation of pyramidal neurons is a common feature of many forms of epilepsy, and its control may lead to therapeutic effects. NpHR delivery into these neurons promptly and dramatically reduced seizures upon light stimulation. Enhancing inhibitory activity of interneurons *via* transfection of the excitatory opsin ChR also resulted in reduced seizure frequency and severity upon light stimulation (Krook-Magnuson et al., 2013). Optical inhibition of the subthalamic nucleus in PD models significantly improved akinesia and ameliorated levodopa-induced dyskinesia (Yoon et al., 2014; Yoon et al., 2016).

REGULATION OF GENE EXPRESSION

As previously mentioned, precise regulation of gene expression is essential for any gene therapy approach. A good gene regulation system should be adjustable over a broad dose range; should exert no off-target effect; does not influence endogenous gene expression; should be region or cell specific; and should allow to quickly turn off and on transgene expression (Naidoo and Young, 2012). Regulation of gene expression, in terms of increasing or decreasing levels of a specific gene product or in terms of directing the information to a desired target tissue, can occur at different levels. In this section, we will discuss the gene regulation strategies currently used in gene therapy, e.g., at the transcriptional level, by means of tissue specific and inducible promoters; and at post-transcriptional level, by means of RNA interference techniques.

Transcriptional Level: Tissue Specific and Inducible Promoters

Regulation or RNA transcription depends on the euchromatin and heterochromatin state and on the interaction of transcription factors with regulatory DNA elements, including promoters (**Table 2**), insulators, enhancers, and silencers.

Ubiquitous and Tissue-Specific Promoters

Promoters are the main elements that determine the strength and cellular specificity of gene expression. Ubiquitous and constitutive promoters are strongly active in a wide range of cells and tissues. Therefore, ubiquitous expression promoters are used in gene therapy when targeting a specific cell type is not required, i.e., transgene expression is sought in the broadest possible spectrum of cells. Promoters frequently employed to drive exogenous DNA

TABLE 2 | Regulation of gene expression at transcriptional level.

Promoter	Specificity	Size (bp)	Details	References
CAG	Ubiquitous	1,718	Hybrid construct consisting of the cytomegalovirus (CMV) enhancer fused with the chicken beta-actin promoter	(Qin et al., 2010)
EF1α	Ubiquitous	1,179	Human elongation factor 1 alpha promoter	(Qin et al., 2010)
UBC	Ubiquitous	1,177	Human ubiquitin C promoter	(Qin et al., 2010)
SV40	Ubiquitous	627	Simian virus 40 promoter	(Qin et al., 2010)
CMV	Ubiquitous	589	Human cytomegalovirus immediate early enhancer and promoter	(Qin et al., 2010)
PGK	Ubiquitous	511	Mouse phosphoglycerate kinase 1 promoter	(Qin et al., 2010)
Syn1	Neuron	495	Human synapsin 1 promoter	(Kugler et al., 2001; Kugler et al., 2003; McLean et al., 2014)
NSE	Neuron	1,800	Neuron-specific enolase promoter	(Peel et al., 1997)
GFAP	Astrocytes	681–2,200		(Smith-Arica et al., 2000; Lee et al., 2008)
MAG	Oligodendrocytes	1,500–2,200	Human myelin associated glycoprotein	(von Jonquieres et al., 2013)
MBP	Oligodendrocytes	1,900	Myelin basic promoter	(von Jonquieres et al., 2016)
F4/80	Microglia	667		(Rosario et al., 2016)
CD68	Microglia	460		(Rosario et al., 2016)
PAG	Glutamatergic neurons	2,400	Phosphate-activated glutaminase promoter	(Rasmussen et al., 2007)
vGLUT	Glutamatergic neurons	7,000	Vesicular glutamate transporter promoter	(Rasmussen et al., 2007)
GAD	GABAergic neurons	10,000	Glutamic acid decarboxylase promoter	(Rasmussen et al., 2007)
Tetracycline ON/ OFF system	Inducible promoter		Advantages: rapid *in vivo* induction or inhibition kinetics, low toxicity. Limitations: high basal transgene expression.	(Gossen et al., 1995; Xiong et al., 2006)
Rapamycin regulation system	Inducible promoter		Advantages: low basal expression, trigger by low doses, crosses BBB. Limitations: immunosuppressive properties of rapamycin.	(Rivera et al., 1996)

expression in a non-cell specific manner include cytomegalovirus (CMV) immediate-early; enhancer/chicken-β actin (CAG); human ubiquitin C (UBC); simian virus 40 early (SV40); human elongation factor 1α (EF1α); and mouse phosphoglycerate kinase 1 (PGK). Previous works have described the relative strengths of commonly used transcriptional regulatory elements both *in vitro* and *in vivo* (Pasleau et al., 1985; Martin-Gallardo et al., 1988; Oellig and Seliger, 1990; Yew et al., 1997; Manthorpe et al., 1993; Hartikka et al., 1996). CAG, EF1α, and CMV are the strongest among those analyzed. However, the CMV promoter exerts variable results, being very strong in some cell types and rather weak in others (Qin et al., 2010).

The use of cell-type specific promoters may be useful for confining the transgene expression to a specific cell type. Limitations for their use in gene therapy include their low level of expression and their large genomic size. In principle, however, specifically labeling a population of neurons or glial cells might allow to achieve the therapeutic goal without incurring in off-target effects. The synapsin-1 (Syn1) and the neuron-specific enolase (NSE) promoter are used for their ability to selectively drive transgene expression in neurons (Peel et al., 1997; Kugler et al., 2001; Kugler et al., 2003; McLean et al., 2014), while the glial fibrillary acidic protein (GFAP) promoter results in astrocyte-specific expression (Smith-Arica et al., 2000; Lee et al., 2008). Transgene expression can be specifically targeted to oligodendrocytes by the myelin basic protein (MBP) (von Jonquieres et al., 2013) or the human myelin associated glycoprotein (MAG) promoter, the latter in both a full-length and a truncated version (von Jonquieres et al., 2016). High level of microglial cells specificity can be obtained with the F4/80 promoter (Rosario et al., 2016).

The balance between excitatory and inhibitory signals, basically the equilibrium between glutamatergic and GABAergic neurotransmission, can be often disrupted in diseases like epilepsy. Therefore, targeting specifically GABAergic or glutamatergic neurons may be needed for many applications. The phosphate-activated glutaminase (PAG) or the vesicular glutamate transporter (vGLUT) promoter ensures ~90% glutamatergic neuron-specific expression, whereas the glutamic acid decarboxylase (GAD) promoter ensures ~90% GABAergic neuron-specific expression (Rasmussen et al., 2007).

Promoters are not the only elements necessary for transcriptional regulation. Combining regulation elements of different kinds such as promoters, enhancers, introns, and polyadenylation signals by creating hybrid sequences allows modulation of the expression levels. The levels of transgene expression may be strongly influenced by a rapid epigenetic silencing of the exogenous promoters. To protect the promoter and the whole expression cassette from heterochromatization, insulator elements have been tested for their ability to maintain transcriptionally competent whole portions of DNA, regardless of the tissue type and the integration site (Chung et al., 1993; Bell et al., 1999). As reviewed extensively elsewhere, these protective elements are divided into enhancer-blocking insulators, whose function is mediated by the CTCF-binding factor (Gaszner and Felsenfeld, 2006; Phillips and Corces, 2009) and barrier insulators, whose mechanism of action is less known (West et al., 2002; Gaszner and Felsenfeld, 2006; Raab and Kamakaka, 2010). The first well-characterized vertebrate

insulator derived from the chicken β-globin locus associated with a constitutive DNAse I, the hypersensitive site-4 called cHS4 (Chung et al., 1993). cHS4 exhibits both enhancer-blocking activity and barrier activity (Yao et al., 2003). Many studies concerning the delivery of retroviral vectors showed that the inclusion of the cHS4 element allows to increase transgene expression (Rivella et al., 2000; Emery, 2011). Others, such as the ubiquitous chromatin opening element (UCOE) derived from the human HNRPA2B1-CBX3 locus (A2UCOE), show increased stability of transgene expression due mainly to resistance to DNA methylation-mediated gene silencing (Zhang et al., 2010). Other elements to consider include enhancer elements, whose insertion significantly affects the expression levels of the transgene (Hartikka et al., 1996). Often used in genetic engineering is the CMV enhancer (eCMV), whose presence in cultured cells strongly increases the expression of the transgene when under the control of PDGF-β (platelet-derived growth factor-β) promoter, conferring efficient neurons specific gene expression (Yew et al., 1997; Gruh et al., 2008).

Inducible Promoters

For many applications, it is desirable to modulate the expression of the transgene by switching it on or off. Unregulated long-term overexpression of certain transgenes can cause side effects in the CNS, such as aberrant reorganization of the tissue and activation of compensative pathways and/or inactivation/saturation of activated pathways. A finer regulation can be achieved using inducible promoters. These systems are obtained by incorporating in the vector (or in a separate vector) a cassette driving the constitutive expression of a transcription factor (transactivator) able to activate or block the expression of the transgene depending on the availability of a soluble molecule that can be administered systemically.

The Tet On/Tet Off Regulation System

A commonly used regulation system is based on the mechanism of tetracycline resistance in prokaryotes. Two variants are available (**Figure 3**), both relying on tetracycline to deactivate (Tet-off system) or activate gene expression (Tet-on). In the Tet-off system, the transgene is under the transcriptional control of the tet operator (tetO), a fragment of DNA responsive to the transactivator tTA, composed of the tet-repressor (tetR) fused to the VP16 viral protein transactivation domain. The transgene is expressed only when tTA binds tetO in the absence of doxycycline, an analogue of tetracycline. Otherwise stated, the presence of tetracycline or its analog in the culture medium or in the organism reversibly induces the transactivator to detach from the operator, causing the transgene to "switch off." The Tet-on system was developed by inducing random mutations in the tetR. One mutation resulted in a protein with opposite function, which was named reverse tet-repressor (rtetR). This mutant protein, when fused to the VP16 transactivation domain (reverse transactivator, rtTA), drives transgene expression only in the presence of doxycycline (Gossen et al., 1995).

Tetracycline-based regulatory systems hold a great potential for gene therapy applications. They ensure rapid *in vivo* induction or inhibition kinetics (Xiong et al., 2006) and low toxicity—tetracycline and its derivatives have been used for decades for their antimicrobial activity (Pasquale and Tan, 2005). Limitations are mainly due to high basal transgene expression, in particular when the expression is driven by a constitutive promoter. Recently, a second generation of tetracycline-regulated system containing a shortened CMV minimal promoter was found to increase regulation efficiency and display low basal expression (Agha-Mohammadi et al., 2004). Modifications in the tetO sequence (TRE-tight1) driven by an NSE were found to improve gene expression efficiency and to reduce the leaky basal transcription (Tian et al., 2009).

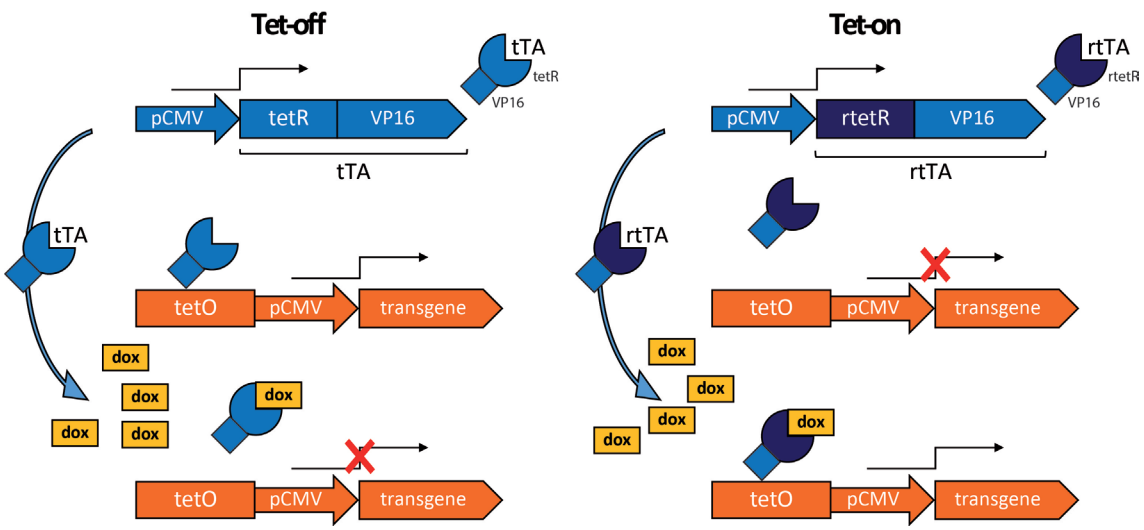

FIGURE 3 | Tetracycline regulation system. In this example, the constitutively active human cytomegalovirus promoter (pCMV) drives the expression of the tetracycline transactivator (tTA) or of the tetracycline reverse transactivator (rtTA), consisting respectively of the tet-repressor (tetR) or reverse tet-repressor (rtetR) fused to the VP16 transactivation domain. Tet-off: tTA binds the tet operator (tetO) to drive transgene expression in the absence, but not in the presence of doxycycline (dox). Tet-on: rtTA binds to tetO and drives transgene expression in the presence, but not in the absence of dox.

For CNS applications, it is necessary to obtain adequate concentrations of doxycycline in the brain, which is difficult due to the limited ability of this drug to cross the BBB (Nau et al., 2010). However, new rtTA variants containing mutations in the doxycycline contact domain enhance sensitivity to doxycycline, resulting in a reduction of the concentrations required for transgene regulation (Das et al., 2004; Zhou et al., 2006). The majority of CNS applications involving the tetracycline-regulated system used viral vectors for the construct delivery, e.g., lentiviruses (Georgievska et al., 2004; Pluta et al., 2005), adenoviruses or AAVs (Ebert et al., 2005; Lee et al., 2005; Le Guiner et al., 2014), and resulted in a tightly regulated gene expression. For example, the lentiviral vector-mediated delivery of GDNF regulated by a Tet-on system in a PD rat model resulted in a precise regulation of transgene expression and in neuroprotection of nigral DA neurons (Chen et al., 2014).

The Rapamycin Regulation System

The rapamycin regulation system is based on the interaction between two inactive transcription factors, a DNA binding domain and a DNA transcriptional activation domain. Each transcription factor is fused to heterologous binding domains for rapamycin. The DNA binding domain is fused to three copies of the FK-binding protein (FKBP), while the DNA activation domain is fused to a lipid kinase, FKBP12 rapamycin-associated protein (FRAP) (Rivera et al., 1996; Kang et al., 2008). Rapamycin allows their interaction, thus forming an active, heterodimeric transcription factor that drives the expression of the transgene (**Figure 4**).

This system holds many of the features required for clinical use. First, rapamycin is a clinically approved drug, used as an antifungal and antitumor molecule that can be administered orally and can cross the BBB (Dutta et al., 2014). Second, the system ensures low basal expression of the transgene in the absence of rapamycin, but can be triggering by low doses of the drug (Naidoo and Young, 2012). The limitations are mainly related to the immunosuppressive properties of rapamycin, dependent on blockade of the mTOR signaling pathways. The rapamycin analogues "rapalog" (e.g., AP21967) were engineered by adding substituents that prevent the binding to mTOR (Bayle et al., 2006).

A limited number of studies tested this system in the CNS by delivering it through lentiviral (Vogel et al., 2008), AAV

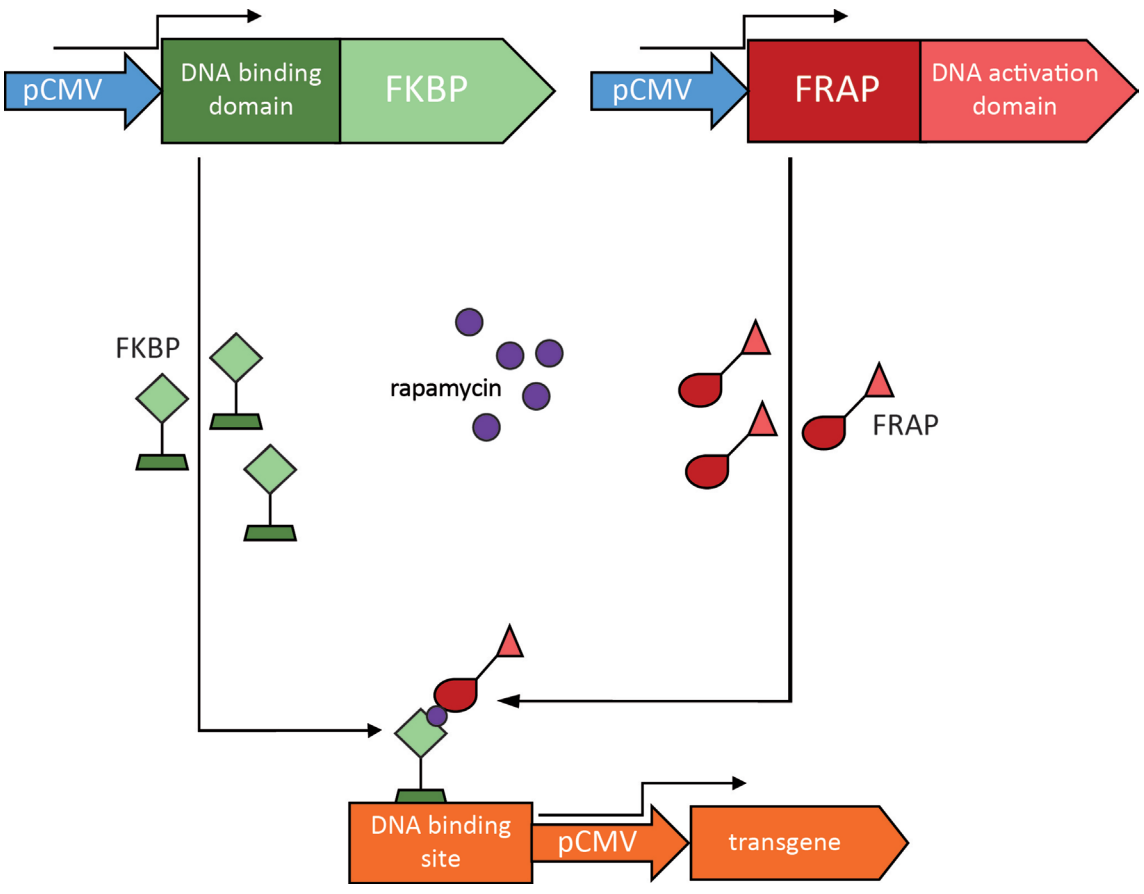

FIGURE 4 | Rapamycin regulation system. In this example, the constitutively active human cytomegalovirus promoter (pCMV) drives the expression of two transcription factors, one consisting of the FK-binding protein (FKBP) fused to a DNA binding domain (in green), the other consisting of an FKBP12 rapamycin-associated protein (FRAP) fused to a DNA activation domain (in red). Rapamycin enables dimerization of the transcription factors and the resulting heterodimer is able to drive expression of the transgene of interest.

(Sanftner et al., 2006), and HSV-1-based vectors (Wang et al., 2003b). A dose-dependent response to rapamycin was observed after delivering into the rat striatum a rapamycin regulated AAV2-GDNF vector, by evaluating GDNF biogenesis and accumulation under various rapamycin dosing regimens. In addition, chronic administration with clinically compatible regimens of rapamycin provided GDNF protein levels similar to those reported to be neuroprotective in PD animal models (Hadaczek et al., 2011).

Post-Transcriptional Gene Regulation

The term "post-transcriptional gene regulation" refers to approaches designed to enhance degradation or block translation of a target mRNA. The prototypical example is RNA interference (RNAi, **Figure 5**), a physiological and evolutionarily conserved gene silencing mechanism normally present in eukaryotic cells, which is mediated by a group of noncoding small RNAs (Mattick and Makunin, 2006). Although many types of small RNAs have been identified, the main classes seem to be short interfering RNAs (siRNAs), microRNAs (miRNAs), and piwi-interacting RNAs (piRNAs) (Gomes et al., 2013). Guided by the interaction with Argonaute proteins, these small RNAs can mediate the degradation or the inhibition of translation of a specific mRNA, making it possible to fine-tune gene expression (Hock and Meister, 2008). In 2018, the US Food and Drug Administration approved Patisiran, the first ever RNAi therapy licensed for clinical use. Patisiran is a formulation of lipid nanoparticles that can be intravenously administered to deliver siRNAs designed to suppress the production of transthyretin, which aggregates into amyloid fibrils that cause nerve damage in patients with hereditary transthyretin amyloidosis (Coelho et al., 2013; Adams et al., 2018).

Neurodegenerative diseases resulting from a single gene mutation that causes gain-of-function or accumulation of a mutant protein are potential candidates for RNAi. Unfortunately, RNA molecules do not cross the BBB, thus requiring the use of viral or nonviral vectors for CNS delivery. This may result in widespread changes in expression levels in unrelated genes due to nonspecific degradation of nontarget mRNAs (Jackson et al., 2003; Persengiev et al., 2004; Scacheri et al., 2004) and saturation of endogenous silencing pathways (Grimm et al., 2006).

For example, RNAi has been investigated in HD, an autosomal-dominant neurodegenerative disorder caused by a CAG trinucleotide repeat expansion in the huntingtin (HTT) gene (Kremer et al., 1994). A potential therapeutic strategy for HD is to reduce mutant HTT expression by using shRNA or miRNA molecules against HTT mRNA. Using RNAi against HTT mRNA does not imply the down-regulation of only the mutated protein, but also of the wild-type protein that plays an important role in neuronal survival (Reiner et al., 2003). To reduce off-target effects, a series of bioinformatic programs have been developed to predict the hypothetical target mRNAs for

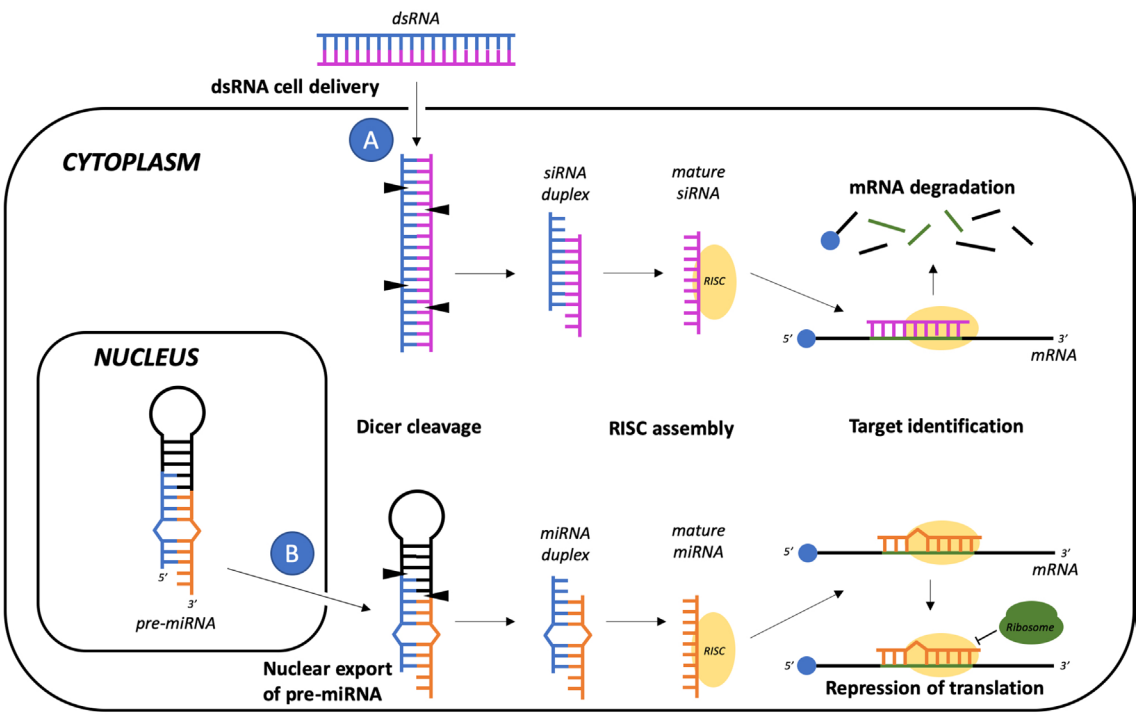

FIGURE 5 | RNA interference-gene silencing pathways mediated by siRNA or miRNA. Even though siRNAs precursors are commonly delivered into the target cells as exogenous double-stranded RNAs **(A)** while the pre-miRNA hairpin structure is exported from the nucleus after nuclear transcription and processing **(B)**, in the cytoplasm these small RNA sequences both share common pathways of maturation and target mRNA recognition, which respectively involve DICER cleavage and association of one strand of the duplex with the RNA-induced silencing complex (RISC). Both the siRNA-RISC and the miRNA-RISC complexes may then sequence-specifically hybridize the target mRNA, leading to mRNA degradation or to translation repression.

each specific miRNA. These programs take into account target complementarity, evolutionary conservation among species, and the thermodynamic stability of the heteroduplex formed by the interaction between miRNAs and mRNAs (Reynolds et al., 2004). Several studies have shown a significant reduction in HTT mRNA together with improved motor function in mouse models of HD upon brain delivery of AAV vectors encoding for shRNA designed to target HTT mRNA (Harper et al., 2005; Rodriguez-Lebron et al., 2005). However, evidence of side effects prompted new studies using artificial miRNAs for gene silencing. This approach improved the therapeutic effect in the absence of any detectable detrimental effect up to 9 months after treatment (Boudreau et al., 2009; Drouet et al., 2009), and has been employed in many subsequent preclinical studies not only on HD (Miniarikova et al., 2016; Pfister et al., 2017; Pfister et al., 2018) but also on superoxide dismutase 1-linked amyotrophic lateral sclerosis (Foust et al., 2013; Borel et al., 2018).

New promising tools acting at a post-transcriptional level are short antisense oligonucleotides (ASO, **Figure 6**) with RNA/DNA-based structures that can sequence-specifically hybridize RNA, turning it into a target for RNase H-mediated degradation (Wu et al., 2004). The main advantages of ASOs are a higher affinity to target compared with small RNAs, which results in decreased or null off-target toxicity, and the ability to cross the cell membrane to bind RNAs in the cytoplasm or even in the nucleus (Geary et al., 2015). ASOs have been intensively tested in human neurodegenerative disorders. For example, ASOs that selectively decrease human tau mRNA have been shown to reduce tau protein deposition and neuronal loss in a mouse model of AD (DeVos et al., 2017). Moreover, ASOs developed for targeting the mutated form of HTT (mHTT) are currently in clinical development for HD. Initial results with a non-allele specific ASO indicate absence of toxicity and reduced levels of mHTT (Tabrizi et al., 2019). Clinical trials with allele-specific ASOs for mHTT are also ongoing (Potkin and Potkin, 2018).

CONCLUSIONS

The rapid progress of viral and nonviral vector systems has increased the probability of success of CNS gene therapy as an alternative to existing pharmacological treatments. However, all the delivery systems developed thus far have advantages and disadvantages and, therefore, the search for an ideal one continues. A lesson

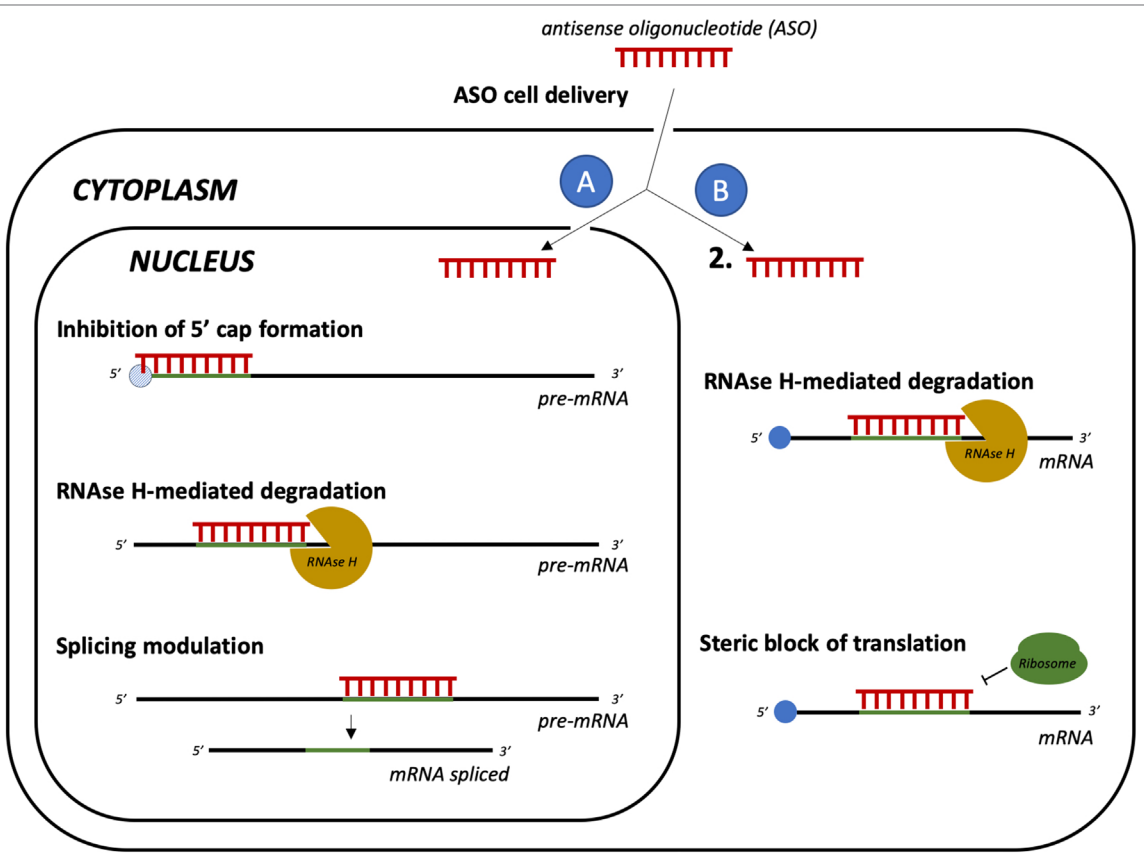

FIGURE 6 | Gene silencing by delivery of antisense oligonucleotides (ASO). Cell-delivered ASOs can act as translation repressors with different mechanisms. If ASOs reach the nucleus **(A)**, they can form heteroduplexes with the pre-mRNA, which can result in inhibition of 5' cap formation, recruitment of RNAse H, and mRNA degradation. They may also even act as splicing modulators. In the cytoplasm **(B)**, ASOs can hybridize with the target mRNA, leading to RNAse H-mediated degradation or to steric block of ribosome binging, resulting in impaired translation.

learned from the research performed to date is that delivery tools do not necessarily adapt to all applications, but should be chosen according to the specific situation and need. Understanding the rules of transcriptional and post-transcriptional gene regulation will allow to improve our techniques. In addition, optogenetic and chemogenetic approaches can provide a precise temporal and spatial regulation of gene expression, and the recent introduction of genome-editing technologies allows the direct manipulation of the genome. Therefore, even if more work will be needed to overcome the remaining hurdles, gene therapy now holds a strong promise to become a safe and effective option for CNS diseases in the not too distant future.

AUTHOR CONTRIBUTIONS

SI, GV, and MSi wrote the largest part of the article. MSo wrote the chapter on amplicons, and SZ wrote the chapter on viral vectors.

FUNDING

This work was supported by grants from the European Community (FP7-PEOPLE-2011-IAPP project 285827 [EPIXCHANGE] and FP7-HEALTH project 602102 [EPITARGET]).

REFERENCES

Adams, D., Gonzalez-Duarte, A., O'Riordan, W. D., Yang, C. C., Ueda, M., Kristen, A. V., et al. (2018). Patisiran, an RNAi therapeutic, for hereditary transthyretin amyloidosis. *N. Engl. J. Med.* 379 (1), 11–21. doi: 10.1056/NEJMoa1716153

Agha-Mohammadi, S., O'Malley, M., Etemad, A., Wang, Z., Xiao, X., and Lotze, M. T. (2004). Second-generation tetracycline-regulatable promoter: repositioned tet operator elements optimize transactivator synergy while shorter minimal promoter offers tight basal leakiness. *J. Gene. Med.* 6 (7), 817–828. doi: 10.1002/jgm.566

Ahmad, H. I., Ahmad, M. J., Asif, A. R., Adnan, M., Iqbal, M. K., Mehmood, K., et al. (2018). A review of CRISPR-based genome editing: survival, evolution and challenges. *Curr. Issues Mol. Biol.* 28, 47–68. doi: 10.21775/cimb.028.047

Aiken, C. (1997). Pseudotyping human immunodeficiency virus type 1 (HIV-1) by the glycoprotein of vesicular stomatitis virus targets HIV-1 entry to an endocytic pathway and suppresses both the requirement for Nef and the sensitivity to cyclosporin A. *J. Virol.* 71 (8), 5871–5877.

Alexander, G. M., Rogan, S. C., Abbas, A. I., Armbruster, B. N., Pei, Y., Allen, J. A., et al. (2009). Remote control of neuronal activity in transgenic mice expressing evolved G protein-coupled receptors. *Neuron* 63 (1), 27–39. doi: 10.1016/j.neuron.2009.06.014

Armbruster, B. N., Li, X., Pausch, M. H., Herlitze, S., and Roth, B. L. (2007). Evolving the lock to fit the key to create a family of G protein-coupled receptors potently activated by an inert ligand. *Proc. Natl. Acad. Sci. U. S. A.* 104 (12), 5163–5168. doi: 10.1073/pnas.0700293104

Artusi, S., Miyagawa, Y., Goins, W. F., Cohen, J. B., and Glorioso, J. C. (2018). Herpes simplex virus vectors for gene transfer to the central nervous system. *Diseases* 6 (3), E74. doi: 10.3390/diseases6030074

Aschauer, D. F., Kreuz, S., and Rumpel, S. (2013). Analysis of transduction efficiency, tropism and axonal transport of AAV serotypes 1, 2, 5, 6, 8 and 9 in the mouse brain. *PLoS One* 8 (9), e76310. doi: 10.1371/journal.pone.0076310

Azzouz, M., Martin-Rendon, E., Barber, R. D., Mitrophanous, K. A., Carter, E. E., Rohll, J. B., et al. (2002). Multicistronic lentiviral vector-mediated striatal gene transfer of aromatic L-amino acid decarboxylase, tyrosine hydroxylase, and GTP cyclohydrolase I induces sustained transgene expression, dopamine production, and functional improvement in a rat model of Parkinson's disease. *J. Neurosci.* 22 (23), 10302–10312. doi: 10.1523/JNEUROSCI.22-23-10302.2002

Badawy, R. A. B., Harvey, A. S., and MacDonell, R. A. L. (2009). Cortical hyperexcitability and epileptogenesis: understanding the mechanisms of epilepsy—Part 2. *J. Clin. Neurosci.* 16 (4), 485–500. doi: 10.1016/j.jocn.2008.10.001

Bayle, J. H., Grimley, J. S., Stankunas, K., Gestwicki, J. E., Wandless, T. J., and Crabtree, G. R. (2006). Rapamycin analogs with differential binding specificity permit orthogonal control of protein activity. *Chem. Biol.* 13 (1), 99–107. doi: 10.1016/j.chembiol.2005.10.017

Bell, A. C., West, A. G., and Felsenfeld, G. (1999). The protein CTCF is required for the enhancer blocking activity of vertebrate insulators. *Cell* 98 (3), 387–396. doi: 10.1016/S0092-8674(00)81967-4

Bell, C. L., Vandenberghe, L. H., Bell, P., Limberis, M. P., Gao, G. P., Van Vliet, K., et al. (2011). The AAV9 receptor and its modification to improve in vivo lung gene transfer in mice. *J. Clin Invest.* 121 (6), 2427–2435. doi: 10.1172/JCI57367

Bemelmans, A. P., Horellou, P., Pradier, L., Brunet, I., Colin, P., and Mallet, J. (1999). Brain-derived neurotrophic factor-mediated protection of striatal neurons in an excitotoxic rat model of Huntington's disease, as demonstrated by adenoviral gene transfer. *Hum. Gene Ther.* 10 (18), 2987–2997. doi: 10.1089/10430349950016393

Berges, B. K., Wolfe, J. H., and Fraser, N. W. (2007). Transduction of brain by herpes simplex virus vectors. *Mol. Ther.* 15 (1), 20–29. doi: 10.1038/sj.mt.6300018

Berns, K. I., and Giraud, C. (1996). Biology of adeno-associated virus. *Curr. Top Microbiol. Immunol.* 218, 1–23. doi: 10.1007/978-3-642-80207-2_1

Bishop, A. C., Shah, K., Liu, Y., Witucki, L., Kung, C. Y., and Shokat, K. M. (1998). Design of allele-specific inhibitors to probe protein kinase signaling. *Curr. Biol.* 8 (5), 257–266. doi: 10.1016/S0960-9822(98)70198-8

Bloom, D. C., Giordani, N. V., and Kwiatkowski, D. L. (2010). Epigenetic regulation of latent HSV-1 gene expression. *Biochim. Biophys. Acta* 1799 (3-4), 246–256. doi: 10.1016/j.bbagrm.2009.12.001

Borel, F., Gernoux, G., Sun, H., Stock, R., Blackwood, M., Brown, R. H., Jr., et al. (2018). Safe and effective superoxide dismutase 1 silencing using artificial microRNA in macaques. *Sci. Transl. Med.* 10 (465), eaau6414. doi: 10.1126/scitranslmed.aau6414

Bouard, D., Alazard-Dany, D., and Cosset, F. L. (2009). Viral vectors: from virology to transgene expression. *Br. J. Pharmacol.* 157 (2), 153–165. doi: 10.1038/bjp.2008.349

Boudreau, R. L., McBride, J. L., Martins, I., Shen, S., Xing, Y., Carter, B. J., et al. (2009). Nonallele-specific silencing of mutant and wild-type huntingtin demonstrates therapeutic efficacy in Huntington's disease mice. *Mol. Ther.* 17 (6), 1053–1063. doi: 10.1038/mt.2009.17

Bourdenx, M., Dutheil, N., Bezard, E., and Dehay, B. (2014). Systemic gene delivery to the central nervous system using Adeno-associated virus. *Front. Mol. Neurosci.* 7, 50. doi: 10.3389/fnmol.2014.00050

Burger, C., Gorbatyuk, O. S., Velardo, M. J., Peden, C. S., Williams, P., Zolotukhin, S., et al. (2004). Recombinant AAV viral vectors pseudotyped with viral capsids from serotypes 1, 2, and 5 display differential efficiency and cell tropism after delivery to different regions of the central nervous system. *Mol. Ther.* 10 (2), 302–317. doi: 10.1016/j.ymthe.2004.05.024

Campos, S. K., and Barry, M. A. (2007). Current advances and future challenges in Adenoviral vector biology and targeting. *Curr. Gene. Ther.* 7 (3), 189–204. doi: 10.2174/156652307780859062

Carter, M., and Shieh, J. (2015). *Guide to research techniques in neuroscience*. 2nd. edition. Cambridge, MA: Academic Press.

Case, S. S., Price, M. A., Jordan, C. T., Yu, X. J., Wang, L., Bauer, G., et al. (1999). Stable transduction of quiescent CD34(+)CD38(-) human hematopoietic cells by HIV-1-based lentiviral vectors. *Proc. Natl. Acad. Sci. U. S. A.* 96 (6), 2988–2993. doi: 10.1073/pnas.96.6.2988

Chan, K. Y., Jang, M. J., Yoo, B. B., Greenbaum, A., Ravi, N., Wu, W. L., et al. (2017). Engineered AAVs for efficient noninvasive gene delivery to the central and peripheral nervous systems. *Nat. Neurosci.* 20 (8), 1172–1179. doi: 10.1038/nn.4593

Chang, S. Y., Lee, C. N., Lin, P. H., Huang, H. H., Chang, L. Y., Ko, W., et al. (2008). A community-derived outbreak of adenovirus type 3 in children in Taiwan between 2004 and 2005. *J. Med. Virol.* 80 (1), 102–112. doi: 10.1002/jmv.21045

Chen, S. S., Yang, C., Hao, F., Li, C., Lu, T., Zhao, L. R., et al. (2014). Intrastriatal GDNF gene transfer by inducible lentivirus vectors protects dopaminergic neurons in a rat model of parkinsonism. *Exp. Neurol.* 261, 87–96. doi: 10.1016/j.expneurol.2014.06.022

Chen, Y. H., Chang, M., and Davidson, B. L. (2009). Molecular signatures of disease brain endothelia provide new sites for CNS-directed enzyme therapy. *Nat. Med.* 15 (10), 1215–1218. doi: 10.1038/nm.2025

Chira, S., Jackson, C. S., Oprea, I., Ozturk, F., Pepper, M. S., Diaconu, I., et al. (2015). Progresses towards safe and efficient gene therapy vectors. *Oncotarget* 6 (31), 30675–30703. doi: 10.18632/oncotarget.5169

Choi-Lundberg, D. L., Lin, Q., Schallert, T., Crippens, D., Davidson, B. L., Chang, Y. N., et al. (1998). Behavioral and cellular protection of rat dopaminergic neurons by an adenoviral vector encoding glial cell line-derived neurotrophic factor. *Exp. Neurol.* 154 (2), 261–275. doi: 10.1006/exnr.1998.6887

Choudhury, S. R., Harris, A. F., Cabral, D. J., Keeler, A. M., Sapp, E., Ferreira, J. S., et al. (2016). Widespread central nervous system gene transfer and silencing after systemic delivery of novel AAV-AS vector. *Mol. Ther.* 24 (4), 726–735. doi: 10.1038/mt.2015.231

Chow, B. Y., Han, X., Dobry, A. S., Qian, X., Chuong, A. S., Li, M., et al. (2010). High-performance genetically targetable optical neural silencing by light-driven proton pumps. *Nature* 463 (7277), 98–102. doi: 10.1038/nature08652

Christ, M., Lusky, M., Stoeckel, F., Dreyer, D., Dieterle, A., Michou, A. I., et al. (1997). Gene therapy with recombinant adenovirus vectors: evaluation of the host immune response. *Immunol. Lett.* 57 (1–3), 19–25. doi: 10.1016/S0165-2478(97)00049-7

Christine, C. W., Starr, P. A., Larson, P. S., Eberling, J. L., Jagust, W. J., Hawkins, R. A., et al. (2009). Safety and tolerability of putaminal AADC gene therapy for Parkinson disease. *Neurology* 73 (20), 1662–1669. doi: 10.1212/WNL.0b013e3181c29356

Chung, J. H., Whiteley, M., and Felsenfeld, G. (1993). A 5' element of the chicken beta-globin domain serves as an insulator in human erythroid cells and protects against position effect in Drosophila. *Cell* 74 (3), 505–514. doi: 10.1016/0092-8674(93)80052-G

Coelho, T., Adams, D., Silva, A., Lozeron, P., Hawkins, P. N., Mant, T., et al. (2013). Safety and efficacy of RNAi therapy for transthyretin amyloidosis. *N. Engl. J. Med.* 369 (9), 819–829. doi: 10.1056/NEJMoa1208760

Cohen, M. S., Zhang, C., Shokat, K. M., and Taunton, J. (2005). Structural bioinformatics-based design of selective, irreversible kinase inhibitors. *Science* 308 (5726), 1318–1321. doi: 10.1126/science1108367

Cooray, S., Howe, S. J., and Thrasher, A. J. (2012). Retrovirus and lentivirus vector design and methods of cell conditioning. *Methods Enzymol* 507, 29–57. doi: 10.1016/B978-0-12-386509-0.00003-X

Coward, P., Wada, H. G., Falk, M. S., Chan, S. D. H., Meng, F., Akil, H., et al. (1998). Controlling signaling with a specifically designed G(i)-coupled receptor. *Proc. Natl. Acad. Sci. U. S. A.* 95 (1), 352–357. doi: 10.1073/pnas.95.1.352

Crick, F. H. (1979). Thinking about the brain. *Sci. Am.* 241 (3), 219–232. doi: 10.1038/scientificamerican0979-219

Cucchiarini, M. (2016). Human gene therapy: novel approaches to improve the current gene delivery systems. *Discov. Med.* 21 (118), 495–506.

Cuchet, D., Potel, C., Thomas, J., and Epstein, A. L. (2007). HSV-1 amplicon vectors: a promising and versatile tool for gene delivery. *Expert Opin. Biol. Ther.* 7 (7), 975–995. doi: 10.1517/14712598.7.7.975

Dar, A. C., Das, T. K., Shokat, K. M., and Cagan, R. L. (2012). Chemical genetic discovery of targets and anti-targets for cancer polypharmacology. *Nature* 486 (7401), 80–U101. doi: 10.1038/nature11127

Das, A. T., Zhou, X., Vink, M., Klaver, B., Verhoef, K., Marzio, G., et al. (2004). Viral evolution as a tool to improve the tetracycline-regulated gene expression system. *J. Biol. Chem.* 279 (18), 18776–18782. doi: 10.1074/jbc.M313895200

Davidson, B. L., Stein, C. S., Heth, J. A., Martins, I., Kotin, R. M., Derksen, T. A., et al. (2000). Recombinant adeno-associated virus type 2, 4, and 5 vectors: transduction of variant cell types and regions in the mammalian central nervous system. *Proc. Natl. Acad. Sci. U. S. A.* 97 (7), 3428–3432. doi: 10.1073/pnas.050581197

de Haan, W., van Straaten, E. C. W., Gouw, A. A., and Stam, C. J. (2017). Altering neuronal excitability to preserve network connectivity in a computational model of Alzheimer's disease. *PLoS Comput. Biol.* 13 (9), e1005707. doi: 10.1371/journal.pcbi.1005707

Deisseroth, K. (2011). Optogenetics. *Nat. Methods* 8 (1), 26–29. doi: 10.1038/nmeth.f.324

Deisseroth, K. (2015). Optogenetics: 10 years of microbial opsins in neuroscience. *Nat. Neurosci.* 18 (9), 1213–1225. doi: 10.1038/nn.4091

Deverman, B. E., Pravdo, P. L., Simpson, B. P., Kumar, S. R., Chan, K. Y., Banerjee, A., et al. (2016). Cre-dependent selection yields AAV variants for widespread gene transfer to the adult brain. *Nat. Biotechnol.* 34 (2), 204–209. doi: 10.1038/nbt.3440

DeVos, S. L., Miller, R. L., Schoch, K. M., Holmes, B. B., Kebodeaux, C. S., Wegener, A. J., et al. (2017). Tau reduction prevents neuronal loss and reverses pathological tau deposition and seeding in mice with tauopathy. *Sci. Transl. Med.* 9 (374), eaa90481. doi: 10.1126/scitranslmed.aag0481

Dobbelstein, M. (2004). Replicating adenoviruses in cancer therapy. *Curr. Top Microbiol. Immunol.* 273, 291–334. doi: 10.1007/978-3-662-05599-1_9

Drouet, V., Perrin, V., Hassig, R., Dufour, N., Auregan, G., Alves, S., et al. (2009). Sustained effects of nonallele-specific Huntingtin silencing. *Ann. Neurol.* 65 (3), 276–285. doi: 10.1002/ana.21569

Duan, D. (2016). Systemic delivery of adeno-associated viral vectors. *Curr. Opin. Virol.* 21, 16–25. doi: 10.1016/j.coviro.2016.07.006

Duan, D., Sharma, P., Yang, J., Yue, Y., Dudus, L., Zhang, Y., et al. (1998). Circular intermediates of recombinant adeno-associated virus have defined structural characteristics responsible for long-term episomal persistence in muscle tissue. *J. Virol.* 72 (11), 8568–8577.

Duan, D., Yue, Y., and Engelhardt, J. F. (2001). Expanding AAV packaging capacity with trans-splicing or overlapping vectors: a quantitative comparison. *Mol. Ther.* 4 (4), 383–391. doi: 10.1006/mthe.2001.0456

Dufes, C., Uchegbu, I. F., and Schatzlein, A. G. (2005). Dendrimers in gene delivery. *Adv. Drug Deliv. Rev.* 57 (15), 2177–2202. doi: 10.1016/j.addr.2005.09.017

Dutta, S., Basak, B., Bhunia, B., Chakraborty, S., and Dey, A. (2014). Kinetics of rapamycin production by Streptomyces hygroscopicus MTCC 4003. *3 Biotech* 4 (5), 523–531. doi: 10.1007/s13205-013-0189-2

Eberling, J. L., Jagust, W. J., Christine, C. W., Starr, P., Larson, P., Bankiewicz, K. S., et al. (2008). Results from a phase I safety trial of hAADC gene therapy for Parkinson disease. *Neurology* 70 (21), 1980–1983. doi: 10.1212/01.wnl.0000312381.29287.ff

Ebert, A. D., Chen, F., He, X., Cryns, V. L., and Bohn, M. C. (2005). A tetracycline-regulated adenovirus encoding dominant-negative caspase-9 is regulated in rat brain and protects against neurotoxin-induced cell death in vitro, but not in vivo. *Exp. Neurol.* 191 Suppl 1, S80–94. doi: 10.1016/j.expneurol.2004.08.024

Emery, D. W. (2011). The use of chromatin insulators to improve the expression and safety of integrating gene transfer vectors. *Hum. Gene Ther.* 22 (6), 761–774. doi: 10.1089/hum.2010.233

Epstein, A. L. (2009a). HSV-1-derived amplicon vectors: recent technological improvements and remaining difficulties - A review. *Mem. Inst. Oswaldo Cruz* 104 (3), 399–410. doi: 10.1590/S0074-02762009000300002

Epstein, A. L. (2009b). Progress and prospects: biological properties and technological advances of herpes simplex virus type 1-based amplicon vectors. *Gene Ther.* 16 (6), 709–715. doi: 10.1038/gt.2009.42

Falcicchia, C., Trempat, P., Binaschi, A., Perrier-Biollay, C., Roncon, P., Soukupova, M., et al. (2016). Silencing status epilepticus-induced BDNF expression with herpes simplex virus type-1 based amplicon vectors. *PLoS One* 11 (3), e0150995. doi: 10.1371/journal.pone.0150995

Foust, K. D., Salazar, D. L., Likhite, S., Ferraiuolo, L., Ditsworth, D., Ilieva, H., et al. (2013). Therapeutic AAV9-mediated suppression of mutant SOD1 slows disease progression and extends survival in models of inherited ALS. *Mol. Ther.* 21 (12), 2148–2159. doi: 10.1038/mt.2013.211

Gaj, T., Sirk, S. J., Shui, S. L., and Liu, J. (2016). Genome-editing technologies: principles and applications. *Cold Spring Harb. Perspect. Biol.* 8 (12), 9023754. doi: 10.1101/cshperspect.a023754

Gardlik, R., Palffy, R., Hodosy, J., Lukacs, J., Turna, J., and Celec, P. (2005). Vectors and delivery systems in gene therapy. *Med. Sci. Monit.* 11 (4), RA110–121.

Gaszner, M., and Felsenfeld, G. (2006). Insulators: exploiting transcriptional and epigenetic mechanisms. *Nat. Rev. Genet.* 7 (9), 703–713. doi: 10.1038/nrg1925

Geary, R. S., Norris, D., Yu, R., and Bennett, C. F. (2015). Pharmacokinetics, biodistribution and cell uptake of antisense oligonucleotides. *Adv. Drug Deliv. Rev.* 87, 46–51. doi: 10.1016/j.addr.2015.01.008

Georgievska, B., Jakobsson, J., Persson, E., Ericson, C., Kirik, D., and Lundberg, C. (2004). Regulated delivery of glial cell line-derived neurotrophic factor into rat striatum, using a tetracycline-dependent lentiviral vector. *Hum. Gene Ther.* 15 (10), 934–944. doi: 10.1089/hum.2004.15.934

Ghosh, A., Yue, Y., Lai, Y., and Duan, D. (2008). A hybrid vector system expands adeno-associated viral vector packaging capacity in a transgene-independent manner. *Mol. Ther.* 16 (1), 124–130. doi: 10.1038/sj.mt.6300322

Gomes, A. Q., Nolasco, S., and Soares, H. (2013). Non-coding RNAs: multi-tasking molecules in the cell. *Int. J. Mol. Sci.* 14 (8), 16010–16039. doi: 10.3390/ijms140816010

Gossen, M., Freundlieb, S., Bender, G., Muller, G., Hillen, W., and Bujard, H. (1995). Transcriptional activation by tetracyclines in mammalian cells. *Science* 268 (5218), 1766–1769. doi: 10.1126/science.7792603

Goverdhana, S., Puntel, M., Xiong, W., Zirger, J. M., Barcia, C., Curtin, J. F., et al. (2005). Regulatable gene expression systems for gene therapy applications: progress and future challenges. *Mol. Ther.* 12 (2), 189–211. doi: 10.1016/j.ymthe.2005.03.022

Grimm, D., Lee, J. S., Wang, L., Desai, T., Akache, B., Storm, T. A., et al. (2008). In vitro and in vivo gene therapy vector evolution via multispecies interbreeding and retargeting of adeno-associated viruses. *J. Virol.* 82 (12), 5887–5911. doi: 10.1128/JVI.00254-08

Grimm, D., Streetz, K. L., Jopling, C. L., Storm, T. A., Pandey, K., Davis, C. R., et al. (2006). Fatality in mice due to oversaturation of cellular microRNA/short hairpin RNA pathways. *Nature* 441 (7092), 537–541. doi: 10.1038/nature04791

Gruh, I., Wunderlich, S., Winkler, M., Schwanke, K., Heinke, J., Blomer, U., et al. (2008). Human CMV immediate-early enhancer: a useful tool to enhance cell-type-specific expression from lentiviral vectors. *J. Gene. Med.* 10 (1), 21–32. doi: 10.1002/jgm.1122

Gunaydin, L. A., Yizhar, O., Berndt, A., Sohal, V. S., Deisseroth, K., and Hegemann, P. (2010). Ultrafast optogenetic control. *Nat. Neurosci.* 13 (3), 387–392. doi: 10.1038/nn.2495

Hadaczek, P., Beyer, J., Kells, A., Narrow, W., Bowers, W., Federoff, H. J., et al. (2011). Evaluation of an AAV2-based rapamycin-regulated glial cell line-derived neurotrophic factor (GDNF) expression vector system. *PLoS One* 6 (11), e27728. doi: 10.1371/journal.pone.0027728

Hammond, S. L., Leek, A. N., Richman, E. H., and Tjalkens, R. B. (2017). Cellular selectivity of AAV serotypes for gene delivery in neurons and astrocytes by neonatal intracerebroventricular injection. *PLoS One* 12 (12), e0188830. doi: 10.1371/journal.pone.0188830

Han, F., Miyagawa, Y., Verlengia, G., Ingusci, S., Soukupova, M., Simonato, M., et al. (2018). Cellular antisilencing elements support transgene expression from herpes simplex virus vectors in the absence of immediate early gene expression. *J. Virol.* 92 (17), e00536–18. doi: 10.1128/JVI.00536-18

Harper, S. Q., Staber, P. D., He, X., Eliason, S. L., Martins, I. H., Mao, Q., et al. (2005). RNA interference improves motor and neuropathological abnormalities in a Huntington's disease mouse model. *Proc. Natl. Acad. Sci. U. S. A.* 102 (16), 5820–5825. doi: 10.1073/pnas.0501507102

Hartikka, J., Sawdey, M., Cornefert-Jensen, F., Margalith, M., Barnhart, K., Nolasco, M., et al. (1996). An improved plasmid DNA expression vector for direct injection into skeletal muscle. *Hum. Gene Ther.* 7 (10), 1205–1217. doi: 10.1089/hum.1996.7.10-1205

Hock, J., and Meister, G. (2008). The Argonaute protein family. *Genome Biol.* 9 (2), 210. doi: 10.1186/gb-2008-9-2-210

Howell, D. P., Krieser, R. J., Eastman, A., and Barry, M. A. (2003). Deoxyribonuclease II is a lysosomal barrier to transfection. *Mol. Ther.* 8 (6), 957–963. doi: 10.1016/j.ymthe.2003.09.011

Huang, R. Q., Qu, Y. H., Ke, W. L., Zhu, J. H., Pei, Y. Y., and Jiang, C. (2007). Efficient gene delivery targeted to the brain using a transferrin-conjugated polyethyleneglycol-modified polyamidoamine dendrimer. *FASEB J.* 21 (4), 1117–1125. doi: 10.1096/fj.06-7380com

Ikeda, K., Wakimoto, H., Ichikawa, T., Jhung, S., Hochberg, F. H., Louis, D. N., et al. (2000). Complement depletion facilitates the infection of multiple brain tumors by an intravascular, replication-conditional herpes simplex virus mutant. *J. Virol.* 74 (10), 4765–4775. doi: 10.1128/JVI.74.10.4765-4775.2000

Jackson, A. L., Bartz, S. R., Schelter, J., Kobayashi, S. V., Burchard, J., Mao, M., et al. (2003). Expression profiling reveals off-target gene regulation by RNAi. *Nat. Biotechnol.* 21 (6), 635–637. doi: 10.1038/nbt831

Jarraya, B., Boulet, S., Ralph, G. S., Jan, C., Bonvento, G., Azzouz, M., et al. (2009). Dopamine gene therapy for Parkinson's disease in a nonhuman primate without associated dyskinesia. *Sci. Transl. Med.* 1 (2), 2ra4. doi: 10.1126/scitranslmed.3000130

Jayant, R. D., Sosa, D., Kaushik, A., Atluri, V., Vashist, A., Tomitaka, A., et al. (2016). Current status of non-viral gene therapy for CNS disorders. *Expert Opin. Drug Deliv.* 13 (10), 1433–1445. doi: 10.1080/17425247.2016.1188802

Kaludov, N., Brown, K. E., Walters, R. W., Zabner, J., and Chiorini, J. A. (2001). Adeno-associated virus serotype 4 (AAV4) and AAV5 both require sialic acid binding for hemagglutination and efficient transduction but differ in sialic acid linkage specificity. *J. Virol.* 75 (15), 6884–6893. doi: 10.1128/JVI.75.15.6884-6893.2001

Kang, C. B., Hong, Y., Dhe-Paganon, S., and Yoon, H. S. (2008). FKBP family proteins: immunophilins with versatile biological functions. *Neurosignals* 16 (4), 318–325. doi: 10.1159/000123041

Kaplitt, M. G., Feigin, A., Tang, C., Fitzsimons, H. L., Mattis, P., Lawlor, P. A., et al. (2007). Safety and tolerability of gene therapy with an adeno-associated virus (AAV) borne GAD gene for Parkinson's disease: an open label, phase I trial. *Lancet* 369 (9579), 2097–2105. doi: 10.1016/S0140-6736(07)60982-9

Katsouri, L., Lim, Y. M., Blondrath, K., Eleftheriadou, I., Lombardero, L., Birch, A. M., et al. (2016). PPARgamma-coactivator-1alpha gene transfer reduces neuronal loss and amyloid-beta generation by reducing beta-secretase in an Alzheimer's disease model. *Proc. Natl. Acad. Sci. U. S. A.* 113 (43), 12292–12297. doi: 10.1073/pnas.1606171113

Katzel, D., Nicholson, E., Schorge, S., Walker, M. C., and Kullmann, D. M. (2014). Chemical-genetic attenuation of focal neocortical seizures. *Nat. Commun.* 5, 3847. doi: 10.1038/ncomms4847

Kay, M. A., Liu, D., and Hoogerbrugge, P. M. (1997). Gene therapy. *Proc. Natl. Acad. Sci. U. S. A.* 94 (24), 12744–12746. doi: 10.1073/pnas.94.24.12744

Khare, R., Chen, C. Y., Weaver, E. A., and Barry, M. A. (2011). Advances and future challenges in adenoviral vector pharmacology and targeting. *Curr. Gene. Ther.* 11 (4), 241–258. doi: 10.2174/156652311796150363

Klug, B., Celis, P., Carr, M., and Reinhardt, J. (2012). Regulatory structures for gene therapy medicinal products in the European Union. *Methods Enzymol* 507, 337–354. doi: 10.1016/B978-0-12-386509-0.00017-X

Knorr, V., Allmendinger, L., Walker, G. F., Paintner, F. F., and Wagner, E. (2007). An acetal-based PEGylation reagent for pH-Sensitive shielding of DNA polyplexes. *Bioconjug. Chem.* 18 (4), 1218–1225. doi: 10.1021/bc060327a

Kodippili, K., Hakim, C. H., Pan, X., Yang, H. T., Yue, Y., Zhang, Y., et al. (2018). Dual AAV gene therapy for duchenne muscular dystrophy with a 7-kb mini-dystrophin gene in the canine model. *Hum. Gene Ther.* 29 (3), 299–311. doi: 10.1089/hum.2017.095

Korbelin, J., Dogbevia, G., Michelfelder, S., Ridder, D. A., Hunger, A., Wenzel, J., et al. (2016). A brain microvasculature endothelial cell-specific viral vector with the potential to treat neurovascular and neurological diseases. *EMBO Mol. Med.* 8 (6), 609–625. doi: 10.15252/emmm.201506078

Krashes, M. J., Shah, B. P., Madara, J. C., Olson, D. P., Strochlic, D. E., Garfield, A. S., et al. (2014). An excitatory paraventricular nucleus to AgRP neuron circuit that drives hunger. *Nature* 507 (7491), 238–+. doi: 10.1038/nature12956

Kravitz, A. V., Freeze, B. S., Parker, P. R. L., Kay, K., Thwin, M. T., Deisseroth, K., et al. (2010). Regulation of parkinsonian motor behaviours by optogenetic control of basal ganglia circuitry. *Nature* 466 (7306), U622–U627. doi: 10.1038/nature09159

Kremer, B., Goldberg, P., Andrew, S. E., Theilmann, J., Telenius, H., Zeisler, J., et al. (1994). A worldwide study of the Huntington's disease mutation. The sensitivity and specificity of measuring CAG repeats. *N. Engl. J. Med.* 330 (20), 1401–1406. doi: 10.1056/NEJM199405193302001

Krisky, D. M., Wolfe, D., Goins, W. F., Marconi, P. C., Ramakrishnan, R., Mata, M., et al. (1998). Deletion of multiple immediate-early genes from herpes simplex virus reduces cytotoxicity and permits long-term gene expression in neurons. *Gene Ther.* 5 (12), 1593–1603. doi: 10.1038/sj.gt.3300766

Krook-Magnuson, E., Armstrong, C., Oijala, M., and Soltesz, I. (2013). On-demand optogenetic control of spontaneous seizures in temporal lobe epilepsy. *Nat. Commun.* 4, 1376. doi: 10.1038/ncomms2376

Kugler, S., Kilic, E., and Bahr, M. (2003). Human synapsin 1 gene promoter confers highly neuron-specific long-term transgene expression from an adenoviral vector in the adult rat brain depending on the transduced area. *Gene Ther.* 10 (4), 337–347. doi: 10.1038/sj.gt.3301905

Kugler, S., Meyn, L., Holzmuller, H., Gerhardt, E., Isenmann, S., Schulz, J. B., et al. (2001). Neuron-specific expression of therapeutic proteins: evaluation of different cellular promoters in recombinant adenoviral vectors. *Mol. Cell Neurosci.* 17 (1), 78–96. doi: 10.1006/mcne.2000.0929

Lachmann, R. (2004). Herpes simplex virus-based vectors. *Int. J. Exp. Pathol.* 85 (4), 177–190. doi: 10.1111/j.0959-9673.2004.00383.x

Lachmann, R. H., Brown, C., and Efstathiou, S. (1996). A murine RNA polymerase I promoter inserted into the herpes simplex virus type 1 genome is functional during lytic, but not latent, infection. *J. Gen. Virol.* 77 (Pt 10), 2575–2582. doi: 10.1099/0022-1317-77-10-2575

Le Guiner, C., Stieger, K., Toromanoff, A., Guilbaud, M., Mendes-Madeira, A., Devaux, M., et al. (2014). Transgene regulation using the tetracycline-inducible TetR-KRAB system after AAV-mediated gene transfer in rodents and nonhuman primates. *PLoS One* 9 (9), e102538. doi: 10.1371/journal.pone.0102538

Lee, C. S., Bishop, E. S., Zhang, R., Yu, X., Farina, E. M., Yan, S., et al. (2017). Adenovirus-mediated gene delivery: potential applications for gene and cell-based therapies in the new era of personalized medicine. *Genes Dis.* 4 (2), 43–63. doi: 10.1016/j.gendis.2017.04.001

Lee, Y., Messing, A., Su, M., and Brenner, M. (2008). GFAP promoter elements required for region-specific and astrocyte-specific expression. *Glia* 56 (5), 481–493. doi: 10.1002/glia.20622

Lee, Y. B., Cosgrave, A. S., Glover, C. P., Bienemann, A., Heywood, D., Hobson, R. J., et al. (2005). Increased utility in the CNS of a powerful neuron-specific tetracycline-regulatable adenoviral system developed using a post-transcriptional enhancer. *J. Gene Med.* 7 (5), 576–583. doi: 10.1002/jgm.694

Lenman, A., Liaci, A. M., Liu, Y., Frangsmyr, L., Frank, M., Blaum, B. S., et al. (2018). Polysialic acid is a cellular receptor for human adenovirus 52. *Proc. Natl. Acad. Sci. U. S. A.* 115 (18), E4264–E4273. doi: 10.1073/pnas.1716900115

Li, S. D., and Huang, L. (2006). Gene therapy progress and prospects: non-viral gene therapy by systemic delivery. *Gene Ther.* 13 (18), 1313–1319. doi: 10.1038/sj.gt.3302838

Li, X., and Heyer, W. D. (2008). Homologous recombination in DNA repair and DNA damage tolerance. *Cell Res.* 18 (1), 99–113. doi: 10.1038/cr.2008.1

Lieber, M. R. (2010). The mechanism of double-strand DNA break repair by the nonhomologous DNA end-joining pathway. *Annu. Rev. Biochem.* 79, 181–211. doi: 10.1146/annurev.biochem.052308.093131

Liu, Y., Jacques, S. L., Azimipour, M., Rogers, J. D., Pashaie, R., and Eliceiri, K. W. (2015). OptogenSIM: a 3D Monte Carlo simulation platform for light delivery design in optogenetics. *Biomed. Opt. Express* 6 (12), 4859–4870. doi: 10.1364/BOE.6.004859

Lombardo, A., Genovese, P., Beausejour, C. M., Colleoni, S., Lee, Y. L., Kim, K. A., et al. (2007). Gene editing in human stem cells using zinc finger nucleases and integrase-defective lentiviral vector delivery. *Nat. Biotechnol.* 25 (11), 1298–1306. doi: 10.1038/nbt1353

Lowenstein, P. R., and Castro, M. G. (2002). Progress and challenges in viral vector-mediated gene transfer to the brain. *Curr. Opin. Mol. Ther.* 4 (4), 359–371.

Lowenstein, P. R., and Castro, M. G. (2003). Inflammation and adaptive immune responses to adenoviral vectors injected into the brain: peculiarities, mechanisms, and consequences. *Gene Ther.* 10 (11), 946–954. doi: 10.1038/sj.gt.3302048

Lowenstein, P. R., and Castro, M. G. (2004). Recent advances in the pharmacology of neurological gene therapy. *Curr. Opin. Pharmacol.* 4 (1), 91–97. doi: 10.1016/j.coph.2003.10.005

Maddalena, A., Tornabene, P., Tiberi, P., Minopoli, R., Manfredi, A., Mutarelli, M., et al. (2018). Triple vectors expand AAV transfer capacity in the retina. *Mol. Ther.* 26 (2), 524–541. doi: 10.1016/j.ymthe.2017.11.019

Magnus, C. J., Lee, P. H., Atasoy, D., Su, H. H., Looger, L. L., and Sternson, S. M. (2011). Chemical and genetic engineering of selective ion channel–ligand interactions. *Science* 333 (6047), 1292–1296. doi: 10.1126/science.1206606

Mandel, R. J., Manfredsson, F. P., Foust, K. D., Rising, A., Reimsnider, S., Nash, K., et al. (2006). Recombinant adeno-associated viral vectors as therapeutic agents to treat neurological disorders. *Mol. Ther.* 13 (3), 463–483. doi: 10.1016/j.ymthe.2005.11.009

Manthorpe, M., Cornefert-Jensen, F., Hartikka, J., Felgner, J., Rundell, A., Margalith, M., et al. (1993). Gene therapy by intramuscular injection of plasmid DNA: studies on firefly luciferase gene expression in mice. *Hum. Gene Ther.* 4 (4), 419–431. doi: 10.1089/hum.1993.4.4-419

Mao, Y., Wang, X., Yan, R., Hu, W., Li, A., Wang, S., et al. (2016). Single point mutation in adeno-associated viral vectors -DJ capsid leads to improvement for gene delivery in vivo. *BMC Biotechnol.* 16, 1. doi: 10.1186/s12896-015-0230-0

Marconi, P., Simonato, M., Zucchini, S., Bregola, G., Argnani, R., Krisky, D., et al. (1999). Replication-defective herpes simplex virus vectors for neurotrophic factor gene transfer in vitro and in vivo. *Gene Ther.* 6 (5), 904–912. doi: 10.1038/sj.gt.3300882

Martin-Gallardo, A., Montoya-Zavala, M., Kelder, B., Taylor, J., Chen, H., Leung, F. C., et al. (1988). A comparison of bovine growth-hormone gene expression in mouse L cells directed by the Moloney murine-leukemia virus long terminal repeat, simian virus-40 early promoter or cytomegalovirus immediate-early promoter. *Gene* 70 (1), 51–56. doi: 10.1016/0378-1119(88)90103-5

Matsumoto, Y., Itaka, K., Yamasoba, T., and Kataoka, K. (2009). Intranuclear fluorescence resonance energy transfer analysis of plasmid DNA decondensation from nonviral gene carriers. *J. Gene. Med.* 11 (7), 615–623. doi: 10.1002/jgm.1338

Mattick, J. S., and Makunin, I. V. (2006). Non-coding RNA. *Hum. Mol. Genet.* 15 Spec No 1, R17–29. doi: 10.1093/hmg/ddl046

Maurice, M., Verhoeyen, E., Salmon, P., Trono, D., Russell, S. J., and Cosset, F. L. (2002). Efficient gene transfer into human primary blood lymphocytes by surface-engineered lentiviral vectors that display a T cell-activating polypeptide. *Blood* 99 (7), 2342–2350. doi: 10.1182/blood.V99.7.2342

McLean, J. R., Smith, G. A., Rocha, E. M., Hayes, M. A., Beagan, J. A., Hallett, P. J., et al. (2014). Widespread neuron-specific transgene expression in brain and spinal cord following synapsin promoter-driven AAV9 neonatal intracerebroventricular injection. *Neurosci. Lett.* 576, 73–78. doi: 10.1016/j.neulet.2014.05.044

Mendell, J. R., Al-Zaidy, S., Shell, R., Arnold, W. D., Rodino-Klapac, L. R., Prior, T. W., et al. (2017). Single-dose gene-replacement therapy for spinal muscular atrophy. *N. Engl. J. Med.* 377 (18), 1713–1722. doi: 10.1056/NEJMoa1706198

Milone, M. C., and O'Doherty, U. (2018). Clinical use of lentiviral vectors. *Leukemia* 32 (7), 1529–1541. doi: 10.1038/s41375-018-0106-0

Miniarikova, J., Zanella, I., Huseinovic, A., van der Zon, T., Hanemaaijer, E., Martier, R., et al. (2016). Design, characterization, and lead selection of therapeutic miRNAs targeting Huntingtin for development of gene therapy for Huntington's disease. *Mol. Ther. Nucleic Acids* 5, e297. doi: 10.1038/mtna.2016.7

Mittermeyer, G., Christine, C. W., Rosenbluth, K. H., Baker, S. L., Starr, P., Larson, P., et al. (2012). Long-term evaluation of a phase 1 study of AADC gene therapy for Parkinson's disease. *Hum. Gene Ther.* 23 (4), 377–381. doi: 10.1089/hum.2011.220

Miyagawa, Y., Marino, P., Verlengia, G., Uchida, H., Goins, W. F., Yokota, S., et al. (2015). Herpes simplex viral-vector design for efficient transduction of nonneuronal cells without cytotoxicity. *Proc. Natl. Acad. Sci. U. S. A.* 112 (13), E1632–1641. doi: 10.1073/pnas.1423556112

Miyagawa, Y., Verlengia, G., Reinhart, B., Han, F., Uchida, H., Zucchini, S., et al. (2017). Deletion of the virion host shut-off gene enhances neuronal-selective transgene expression from an HSV vector lacking functional IE genes. *Mol. Ther. Methods Clin. Dev.* 6, 79–90. doi: 10.1016/j.omtm.2017.06.001

Morris, S. J., Farley, D. C., and Leppard, K. N. (2010). Generation of cell lines to complement adenovirus vectors using recombination-mediated cassette exchange. *BMC Biotechnol.* 10, 92. doi: 10.1186/1472-6750-10-92

Musatov, S., Roberts, J., Pfaff, D., and Kaplitt, M. (2002). A cis-acting element that directs circular adeno-associated virus replication and packaging. *J. Virol.* 76 (24), 12792–12802. doi: 10.1128/JVI.76.24.12792-12802.2002

Nagel, G., Szellas, T., Huhn, W., Kateriya, S., Adeishvili, N., Berthold, P., et al. (2003). Channelrhodopsin-2, a directly light-gated cation-selective membrane channel. *Proc. Natl. Acad. Sci. U. S. A.* 100 (24), 13940–13945. doi: 10.1073/pnas.1936192100

Naidoo, J., and Young, D. (2012). Gene regulation systems for gene therapy applications in the central nervous system. *Neurol. Res. Int.* 2012, 595410. doi: 10.1155/2012/595410

Nakai, H., Fuess, S., Storm, T. A., Muramatsu, S., Nara, Y., and Kay, M. A. (2005). Unrestricted hepatocyte transduction with adeno-associated virus serotype 8 vectors in mice. *J. Virol.* 79 (1), 214–224. doi: 10.1128/JVI.79.1.214-224.2005

Nakai, H., Iwaki, Y., Kay, M. A., and Couto, L. B. (1999). Isolation of recombinant adeno-associated virus vector-cellular DNA junctions from mouse liver. *J. Virol.* 73 (7), 5438–5447.

Naso, M. F., Tomkowicz, B., Perry, W. L., 3rd, and Strohl, W. R. (2017). Adeno-associated virus (AAV) as a vector for gene therapy. *BioDrugs* 31 (4), 317–334. doi: 10.1007/s40259-017-0234-5

Nau, R., Sorgel, F., and Eiffert, H. (2010). Penetration of drugs through the blood-cerebrospinal fluid/blood-brain barrier for treatment of central nervous system infections. *Clin. Microbiol. Rev.* 23 (4), 858–883. doi: 10.1128/CMR.00007-10

Oellig, C., and Seliger, B. (1990). Gene transfer into brain tumor cell lines: reporter gene expression using various cellular and viral promoters. *J. Neurosci. Res.* 26 (3), 390–396. doi: 10.1002/jnr.490260317

Oesterhelt, D., and Stoeckenius, W. (1971). Rhodopsin-like protein from the purple membrane of Halobacterium halobium. *Nat. New Biol.* 233 (39), 149–152. doi: 10.1038/newbio233149a0

Ogris, M., Brunner, S., Schuller, S., Kircheis, R., and Wagner, E. (1999). PEGylated DNA/transferrin-PEI complexes: reduced interaction with blood components, extended circulation in blood and potential for systemic gene delivery. *Gene Ther.* 6 (4), 595–605. doi: 10.1038/sj.gt.3300900

Palella, T. D., Silverman, L. J., Schroll, C. T., Homa, F. L., Levine, M., and Kelley, W. N. (1988). Herpes simplex virus-mediated human hypoxanthine-guanine phosphoribosyltransferase gene transfer into neuronal cells. *Mol. Cell Biol.* 8 (1), 457–460. doi: 10.1128/MCB.8.1.457

Palfi, S., Gurruchaga, J. M., Lepetit, H., Howard, K., Ralph, G. S., Mason, S., et al. (2018). Long-term follow-up of a phase I/II study of ProSavin, a lentiviral vector gene therapy for Parkinson's disease. *Hum. Gene Ther. Clin. Dev.* 29 (3), 148–155. doi: 10.1089/humc.2018.081

Palfi, S., Gurruchaga, J. M., Ralph, G. S., Lepetit, H., Lavisse, S., Buttery, P. C., et al. (2014). Long-term safety and tolerability of ProSavin, a lentiviral vector-based gene therapy for Parkinson's disease: a dose escalation, open-label, phase 1/2 trial. *Lancet* 383 (9923), 1138–1146. doi: 10.1016/S0140-6736(13)61939-X

Pasleau, F., Tocci, M. J., Leung, F., and Kopchick, J. J. (1985). Growth hormone gene expression in eukaryotic cells directed by the Rous sarcoma virus long terminal repeat or cytomegalovirus immediate-early promoter. *Gene* 38 (1–3), 227–232. doi: 10.1016/0378-1119(85)90221-5

Pasquale, T. R., and Tan, J. S. (2005). Nonantimicrobial effects of antibacterial agents. *Clin. Infect. Dis.* 40 (1), 127–135. doi: 10.1086/426545

Pechan, P. A., Fotaki, M., Thompson, R. L., Dunn, R., Chase, M., Chiocca, E. A., et al. (1996). A novel 'piggyback' packaging system for herpes simplex virus amplicon vectors. *Hum. Gene Ther.* 7 (16), 2003–2013. doi: 10.1089/hum.1996.7.16-2003

Peel, A. L., Zolotukhin, S., Schrimsher, G. W., Muzyczka, N., and Reier, P. J. (1997). Efficient transduction of green fluorescent protein in spinal cord neurons using adeno-associated virus vectors containing cell type-specific promoters. *Gene Ther.* 4 (1), 16–24. doi: 10.1038/sj.gt.3300358

Penaud-Budloo, M., Francois, A., Clement, N., and Ayuso, E. (2018). Pharmacology of recombinant adeno-associated virus production. *Mol. Ther. Methods Clin. Dev.* 8, 166–180. doi: 10.1016/j.omtm.2018.01.002

Perez-Martinez, F. C., Guerra, J., Posadas, I., and Cena, V. (2011). Barriers to non-viral vector-mediated gene delivery in the nervous system. *Pharm. Res.* 28 (8), 1843–1858. doi: 10.1007/s11095-010-0364-7

Persengiev, S. P., Zhu, X., and Green, M. R. (2004). Nonspecific, concentration-dependent stimulation and repression of mammalian gene expression by small interfering RNAs (siRNAs). *RNA* 10 (1), 12–18. doi: 10.1261/rna5160904

Pfister, E. L., Chase, K. O., Sun, H., Kennington, L. A., Conroy, F., Johnson, E., et al. (2017). Safe and efficient silencing with a Pol II, but not a Pol lII, promoter expressing an artificial miRNA targeting human Huntingtin. *Mol. Ther. Nucleic Acids* 7, 324–334. doi: 10.1016/j.omtn.2017.04.011

Pfister, E. L., DiNardo, N., Mondo, E., Borel, F., Conroy, F., Fraser, C., et al. (2018). Artificial miRNAs reduce human mutant Huntingtin throughout the striatum in a transgenic sheep model of Huntington's disease. *Hum. Gene Ther.* 29 (6), 663–673. doi: 10.1089/hum.2017.199

Phillips, J. E., and Corces, V. G. (2009). CTCF: master weaver of the genome. *Cell* 137 (7), 1194–1211. doi: 10.1016/j.cell.2009.06.001

Pienaar, I. S., Gartside, S. E., Sharma, P., De Paola, V., Gretenkord, S., Withers, D., et al. (2015). Pharmacogenetic stimulation of cholinergic pedunculopontine neurons reverses motor deficits in a rat model of Parkinson's disease. *Mol. Neurodegener.* 10, 47. doi: 10.1186/s13024-015-0044-5

Piest, M., Lin, C., Mateos-Timoneda, M. A., Lok, M. C., Hennink, W. E., Feijen, J., et al. (2008). Novel poly(amido amine)s with bioreducible disulfide linkages in their diamino-units: structure effects and in vitro gene transfer properties. *J. Control. Release* 132 (3), E12–E13. doi: 10.1016/j.jconrel.2008.09.047

Pluta, K., Luce, M. J., Bao, L., Agha-Mohammadi, S., and Reiser, J. (2005). Tight control of transgene expression by lentivirus vectors containing second-generation tetracycline-responsive promoters. *J. Gene Med.* 7 (6), 803–817. doi: 10.1002/jgm.712

Potkin, K. T., and Potkin, S. G. (2018). New directions in therapeutics for Huntington disease. *Future Neurol.* 13 (2), 101–121. doi: 10.2217/fnl-2017-0035

Qin, J. Y., Zhang, L., Clift, K. L., Hulur, I., Xiang, A. P., Ren, B. Z., et al. (2010). Systematic comparison of constitutive promoters and the doxycycline-inducible promoter. *PLoS One* 5 (5), e10611. doi: 10.1371/journal.pone.0010611

Raab, J. R., and Kamakaka, R. T. (2010). Insulators and promoters: closer than we think. *Nat. Rev. Genet.* 11 (6), 439–446. doi: 10.1038/nrg2765

Rafii, M. S., Baumann, T. L., Bakay, R. A., Ostrove, J. M., Siffert, J., Fleisher, A. S., et al. (2014). A phase1 study of stereotactic gene delivery of AAV2-NGF for Alzheimer's disease. *Alzheimers Dement.* 10 (5), 571–581. doi: 10.1016/j.jalz.2013.09.004

Ramamoorth, M., and Narvekar, A. (2015). Non viral vectors in gene therapy- an overview. *J. Clin. Diagn. Res.* 9 (1), GE01–06. doi: 10.7860/JCDR/2015/10443.5394

Rasmussen, M., Kong, L., Zhang, G. R., Liu, M., Wang, X., Szabo, G., et al. (2007). Glutamatergic or GABAergic neuron-specific, long-term expression in neocortical neurons from helper virus-free HSV-1 vectors containing the phosphate-activated glutaminase, vesicular glutamate transporter-1, or glutamic acid decarboxylase promoter. *Brain Res.* 1144, 19–32. doi: 10.1016/j.brainres.2007.01.125

Rein, D. T., Breidenbach, M., and Curiel, D. T. (2006). Current developments in adenovirus-based cancer gene therapy. *Future Oncol.* 2 (1), 137–143. doi: 10.2217/14796694.2.1.137

Reiner, A., Dragatsis, I., Zeitlin, S., and Goldowitz, D. (2003). Wild-type huntingtin plays a role in brain development and neuronal survival. *Mol. Neurobiol.* 28 (3), 259–276. doi: 10.1385/MN:28:3:259

Reynolds, A., Leake, D., Boese, Q., Scaringe, S., Marshall, W. S., and Khvorova, A. (2004). Rational siRNA design for RNA interference. *Nat. Biotechnol.* 22 (3), 326–330. doi: 10.1038/nbt936

Ritter, T., Lehmann, M., and Volk, H. D. (2002). Improvements in gene therapy: averting the immune response to adenoviral vectors. *BioDrugs* 16 (1), 3–10. doi: 10.2165/00063030-200216010-00001

Rivella, S., Callegari, J. A., May, C., Tan, C. W., and Sadelain, M. (2000). The cHS4 insulator increases the probability of retroviral expression at random chromosomal integration sites. *J. Virol.* 74 (10), 4679–4687. doi: 10.1128/JVI.74.10.4679-4687.2000

Rivera, V. M., Clackson, T., Natesan, S., Pollock, R., Amara, J. F., Keenan, T., et al. (1996). A humanized system for pharmacologic control of gene expression. *Nat. Med.* 2 (9), 1028–1032. doi: 10.1038/nm0996-1028

Rodriguez-Lebron, E., Denovan-Wright, E. M., Nash, K., Lewin, A. S., and Mandel, R. J. (2005). Intrastriatal rAAV-mediated delivery of anti-huntingtin shRNAs induces partial reversal of disease progression in R6/1 Huntington's disease transgenic mice. *Mol. Ther.* 12 (4), 618–633. doi: 10.1016/j.ymthe.2005.05.006

Rosario, A. M., Cruz, P. E., Ceballos-Diaz, C., Strickland, M. R., Siemienski, Z., Pardo, M., et al. (2016). Microglia-specific targeting by novel capsid-modified AAV6 vectors. *Mol. Ther. Methods Clin. Dev.* 3, 16026. doi: 10.1038/mtm.2016.26

Sakuma, T., Barry, M. A., and Ikeda, Y. (2012). Lentiviral vectors: basic to translational. *Biochem. J.* 443 (3), 603–618. doi: 10.1042/BJ20120146

Samaniego, L. A., Wu, N., and DeLuca, N. A. (1997). The herpes simplex virus immediate-early protein ICP0 affects transcription from the viral genome and infected-cell survival in the absence of ICP4 and ICP27. *J. Virol.* 71 (6), 4614–4625.

Sanftner, L. M., Rivera, V. M., Suzuki, B. M., Feng, L., Berk, L., Zhou, S., et al. (2006). Dimerizer regulation of AADC expression and behavioral response in AAV-transduced 6-OHDA lesioned rats. *Mol. Ther.* 13 (1), 167–174. doi: 10.1016/j.ymthe.2005.06.480

Scacheri, P. C., Rozenblatt-Rosen, O., Caplen, N. J., Wolfsberg, T. G., Umayam, L., Lee, J. C., et al. (2004). Short interfering RNAs can induce unexpected and divergent changes in the levels of untargeted proteins in mammalian cells. *Proc. Natl. Acad. Sci. U. S. A.* 101 (7), 1892–1897. doi: 10.1073/pnas.0308698100

Seeger-Armbruster, S., Bosch-Bouju, C., Little, S. T., Smither, R. A., Hughes, S. M., Hyland, B. I., et al. (2015). Patterned, but not tonic, optogenetic stimulation in motor thalamus improves reaching in acute drug-induced Parkinsonian rats. *J. Neurosci.* 35 (3), 1211–1216. doi: 10.1523/JNEUROSCI.3277-14.2015

Sharma, A., Tandon, M., Bangari, D. S., and Mittal, S. K. (2009). Adenoviral vector-based strategies for cancer therapy. *Curr. Drug Ther.* 4 (2), 117–138. doi: 10.2174/157488509788185123

Shen, S., Bryant, K. D., Brown, S. M., Randell, S. H., and Asokan, A. (2011). Terminal N-linked galactose is the primary receptor for adeno-associated virus 9. *J. Biol. Chem.* 286 (15), 13532–13540. doi: 10.1074/jbc.M110.210922

Shepard, A. A., and DeLuca, N. A. (1991). A second-site revertant of a defective herpes simplex virus ICP4 protein with restored regulatory activities and impaired DNA-binding properties. *J. Virol.* 65 (2), 787–795.

Shillitoe, E. J. (2009). Gene therapy: the end of the rainbow? *Head Neck Oncol.* 1, 7. doi: 10.1186/1758-3284-1-7

Simonato, M. (2014). Gene therapy for epilepsy. *Epilepsy Behav.* 38, 125–130. doi: 10.1016/j.yebeh.2013.09.013

Simonato, M., Bennett, J., Boulis, N. M., Castro, M. G., Fink, D. J., Goins, W. F., et al. (2013). Progress in gene therapy for neurological disorders. *Nat. Rev. Neurol.* 9 (5), 277–291. doi: 10.1038/nrneurol.2013.56

Simonato, M., Manservigi, R., Marconi, P., and Glorioso, J. (2000). Gene transfer into neurones for the molecular analysis of behaviour: focus on herpes simplex vectors. *Trends Neurosci.* 23 (5), 183–190. doi: 10.1016/S0166-2236(99)01539-8

Sinclair, A. M., Agrawal, Y. P., Elbar, E., Agrawal, R., Ho, A. D., and Levine, F. (1997). Interaction of vesicular stomatitis virus-G pseudotyped retrovirus with CD34+ and CD34+ CD38- hematopoietic progenitor cells. *Gene Ther.* 4 (9), 918–927. doi: 10.1038/sj.gt.3300479

Smith-Arica, J. R., Morelli, A. E., Larregina, A. T., Smith, J., Lowenstein, P. R., and Castro, M. G. (2000). Cell-type-specific and regulatable transgenesis in the adult brain: adenovirus-encoded combined transcriptional targeting and inducible transgene expression. *Mol. Ther.* 2 (6), 579–587. doi: 10.1006/mthe.2000.0215

Souweidane, M. M., Fraser, J. F., Arkin, L. M., Sondhi, D., Hackett, N. R., Kaminsky, S. M., et al. (2010). Gene therapy for late infantile neuronal ceroid lipofuscinosis: neurosurgical considerations. *J. Neurosurg. Pediatr.* 6 (2), 115–122. doi: 10.3171/2010.4.PEDS09507

Sternson, S. M., and Roth, B. L. (2014). Chemogenetic tools to interrogate brain functions. *Annu. Rev. Neurosci.* 37, 387–407. doi: 10.1146/annurev-neuro-071013-014048

Strader, C. D., Gaffney, T., Sugg, E. E., Candelore, M. R., Keys, R., Patchett, A. A., et al. (1991). Allele-specific activation of genetically engineered receptors. *J. Biol. Chem.* 266 (1), 5–8.

Studahl, M., Cinque, P., and Bergström, T., (2017). *Herpes simplex viruses*. 1st Edition. Boca Raton, FL: CRC Press. p. 440. doi: 10.1201/9780203711828

Sutton, R. E., Reitsma, M. J., Uchida, N., and Brown, P. O. (1999). Transduction of human progenitor hematopoietic stem cells by human immunodeficiency virus type 1-based vectors is cell cycle dependent. *J. Virol.* 73 (5), 3649–3660.

Suzuki, M., Kasai, K., and Saeki, Y. (2006). Plasmid DNA sequences present in conventional herpes simplex virus amplicon vectors cause rapid transgene silencing by forming inactive chromatin. *J. Virol.* 80 (7), 3293–3300. doi: 10.1128/JVI.80.7.3293-3300.2006

Tabrizi, S. J., Leavitt, B. R., Landwehrmeyer, G. B., Wild, E. J., Saft, C., Barker, R. A., et al. (2019). Targeting Huntingtin expression in patients with Huntington's disease. *N. Engl. J. Med.* 380 (24), 2307–2316. doi: 10.1056/NEJMoa1900907

Tardieu, M., Zerah, M., Husson, B., de Bournonville, S., Deiva, K., Adamsbaum, C., et al. (2014). Intracerebral administration of adeno-associated viral vector serotype rh.10 carrying human SGSH and SUMF1 cDNAs in children with mucopolysaccharidosis type IIIA disease: results of a phase I/II trial. *Hum. Gene Ther.* 25 (6), 506–516. doi: 10.1089/hum.2013.238

Teissier, A., Chemiakine, A., Inbar, B., Bagchi, S., Ray, R. S., Palmiter, R. D., et al. (2015). Activity of raphe serotonergic neurons controls emotional behaviors. *Cell Rep.* 13 (9), 1965–1976. doi: 10.1016/j.celrep.2015.10.061

Teschemacher, A. G., Wang, S., Lonergan, T., Duale, H., Waki, H., Paton, J. F., et al. (2005). Targeting specific neuronal populations using adeno- and lentiviral vectors: applications for imaging and studies of cell function. *Exp. Physiol.* 90 (1), 61–69. doi: 10.1113/expphysiol.2004.028191

Thomas, C. E., Ehrhardt, A., and Kay, M. A. (2003). Progress and problems with the use of viral vectors for gene therapy. *Nat. Rev. Genet.* 4 (5), 346–358. doi: 10.1038/nrg1066

Tian, X., Wang, G., Xu, Y., Wang, P., Chen, S., Yang, H., et al. (2009). An improved tet-on system for gene expression in neurons delivered by a single lentiviral vector. *Hum. Gene Ther.* 20 (2), 113–123. doi: 10.1089/hum.2008.018

Todo, T. (2008). "Armed" oncolytic herpes simplex viruses for brain tumor therapy. *Cell Adh. Migr.* 2 (3), 208–213. doi: 10.4161/cam.2.3.6353

Trapani, I., Colella, P., Sommella, A., Iodice, C., Cesi, G., de Simone, S., et al. (2014). Effective delivery of large genes to the retina by dual AAV vectors. *EMBO Mol. Med.* 6 (2), 194–211. doi: 10.1002/emmm.201302948

Urban, D. J., Zhu, H., Marcinkiewcz, C. A., Michaelides, M., Oshibuchi, H., Rhea, D., et al. (2016). Elucidation of The behavioral program and neuronal network encoded by dorsal raphe serotonergic neurons. *Neuropsychopharmacology* 41 (5), 1404–1415. doi: 10.1038/npp.2015.293

Verhoeyen, E., Dardalhon, V., Ducrey-Rundquist, O., Trono, D., Taylor, N., and Cosset, F. L. (2003). IL-7 surface-engineered lentiviral vectors promote survival and efficient gene transfer in resting primary T lymphocytes. *Blood* 101 (6), 2167–2174. doi: 10.1182/blood-2002-07-2224

Verlengia, G., Miyagawa, Y., Ingusci, S., Cohen, J. B., Simonato, M., and Glorioso, J. C. (2017). Engineered HSV vector achieves safe long-term transgene expression in the central nervous system. *Sci. Rep.* 7 (1), 1507. doi: 10.1038/s41598-017-01635-1

Vogel, R., Mammeri, H., and Mallet, J. (2008). Lentiviral vectors mediate nonimmunosuppressive rapamycin analog-induced production of secreted therapeutic factors in the brain: regulation at the level of transcription and exocytosis. *Hum. Gene Ther.* 19 (2), 167–178. doi: 10.1089/hum.2007.125

von Jonquieres, G., Frohlich, D., Klugmann, C. B., Wen, X., Harasta, A. E., Ramkumar, R., et al. (2016). Recombinant human myelin-associated glycoprotein promoter drives selective AAV-mediated transgene expression in oligodendrocytes. *Front. Mol. Neurosci.* 9, 13. doi: 10.3389/fnmol.2016.00013

von Jonquieres, G., Mersmann, N., Klugmann, C. B., Harasta, A. E., Lutz, B., Teahan, O., et al. (2013). Glial promoter selectivity following AAV-delivery to the immature brain. *PLoS One* 8 (6), e65646. doi: 10.1371/journal.pone.0065646

Von Seggern, D. J., Kehler, J., Endo, R. I., and Nemerow, G. R. (1998). Complementation of a fibre mutant adenovirus by packaging cell lines stably expressing the adenovirus type 5 fibre protein. *J. Gen. Virol.* 79 (Pt 6), 1461–1468. doi: 10.1099/0022-1317-79-6-1461

Wang, B., Li, J., and Xiao, X. (2000). Adeno-associated virus vector carrying human minidystrophin genes effectively ameliorates muscular dystrophy in mdx mouse model. *Proc. Natl. Acad. Sci. U. S. A.* 97 (25), 13714–13719. doi: 10.1073/pnas.240335297

Wang, C., Wang, C. M., Clark, K. R., and Sferra, T. J. (2003a). Recombinant AAV serotype 1 transduction efficiency and tropism in the murine brain. *Gene Ther.* 10 (17), 1528–1534. doi: 10.1038/sj.gt.3302011

Wang, D., Zhong, L., Nahid, M. A., and Gao, G. (2014). The potential of adeno-associated viral vectors for gene delivery to muscle tissue. *Expert Opin. Drug Deliv.* 11 (3), 345–364. doi: 10.1517/17425247.2014.871258

Wang, S., Petravicz, J., and Breakefield, X. O. (2003b). Single HSV-amplicon vector mediates drug-induced gene expression via dimerizer system. *Mol. Ther.* 7 (6), 790–800. doi: 10.1016/S1525-0016(03)00094-7

West, A. G., Gaszner, M., and Felsenfeld, G. (2002). Insulators: many functions, many mechanisms. *Genes Dev.* 16 (3), 271–288. doi: 10.1101/gad.954702

Wolff, J. A., and Rozema, D. B. (2008). Breaking the bonds: Non-viral vectors become chemically dynamic. *Mol. Ther.* 16 (1), 8–15. doi: 10.1038/sj.mt.6300326

Worgall, S., Sondhi, D., Hackett, N. R., Kosofsky, B., Kekatpure, M. V., Neyzi, N., et al. (2008). Treatment of late infantile neuronal ceroid lipofuscinosis by CNS administration of a serotype 2 adeno-associated virus expressing CLN2 cDNA. *Hum. Gene Ther.* 19 (5), 463–474. doi: 10.1089/hum.2008.022

Wu, H., Lima, W. F., Zhang, H., Fan, A., Sun, H., and Crooke, S. T. (2004). Determination of the role of the human RNase H1 in the pharmacology of DNA-like antisense drugs. *J. Biol. Chem.* 279 (17), 17181–17189. doi: 10.1074/jbc.M311683200

Wu, N., Watkins, S. C., Schaffer, P. A., and DeLuca, N. A. (1996). Prolonged gene expression and cell survival after infection by a herpes simplex virus mutant defective in the immediate-early genes encoding ICP4, ICP27, and ICP22. *J. Virol.* 70 (9), 6358–6369.

Wu, Z., Miller, E., Agbandje-McKenna, M., and Samulski, R. J. (2006). Alpha2,3 and alpha2,6 N-linked sialic acids facilitate efficient binding and transduction by adeno-associated virus types 1 and 6. *J. Virol.* 80 (18), 9093–9103. doi: 10.1128/JVI.00895-06

Xiong, W., Goverdhana, S., Sciascia, S. A., Candolfi, M., Zirger, J. M., Barcia, C., et al. (2006). Regulatable gutless adenovirus vectors sustain inducible transgene expression in the brain in the presence of an immune response against adenoviruses. *J. Virol.* 80 (1), 27–37. doi: 10.1128/JVI.80.1.27-37.2006

Yan, Z., Zak, R., Zhang, Y., and Engelhardt, J. F. (2005). Inverted terminal repeat sequences are important for intermolecular recombination and circularization of adeno-associated virus genomes. *J. Virol.* 79 (1), 364–379. doi: 10.1128/JVI.79.1.364-379.2005

Yan, Z., Zhang, Y., Duan, D., and Engelhardt, J. F. (2000). Trans-splicing vectors expand the utility of adeno-associated virus for gene therapy. *Proc. Natl. Acad. Sci. U. S. A.* 97 (12), 6716–6721. doi: 10.1073/pnas.97.12.6716

Yang, B., Li, S., Wang, H., Guo, Y., Gessler, D. J., Cao, C., et al. (2014). Global CNS transduction of adult mice by intravenously delivered rAAVrh.8 and rAAVrh.10 and nonhuman primates by rAAVrh.10. *Mol. Ther.* 22 (7), 1299–1309. doi: 10.1038/mt.2014.68

Yao, S., Osborne, C. S., Bharadwaj, R. R., Pasceri, P., Sukonnik, T., Pannell, D., et al. (2003). Retrovirus silencer blocking by the cHS4 insulator is CTCF independent. *Nucleic Acids Res.* 31 (18), 5317–5323. doi: 10.1093/nar/gkg742

Yee, J. K., Miyanohara, A., LaPorte, P., Bouic, K., Burns, J. C., and Friedmann, T. (1994). A general method for the generation of high-titer, pantropic retroviral vectors: highly efficient infection of primary hepatocytes. *Proc. Natl. Acad. Sci. U. S. A.* 91 (20), 9564–9568. doi: 10.1073/pnas.91.20.9564

Yew, N. S., Wysokenski, D. M., Wang, K. X., Ziegler, R. J., Marshall, J., McNeilly, D., et al. (1997). Optimization of plasmid vectors for high-level expression in lung epithelial cells. *Hum. Gene Ther.* 8 (5), 575–584. doi: 10.1089/hum.1997.8.5-575

Yizhar, O., Fenno, L. E., Davidson, T. J., Mogri, M., and Deisseroth, K. (2011). Optogenetics in neural systems. *Neuron* 71 (1), 9–34. doi: 10.1016/j.neuron.2011.06.004

Yoon, H. H., Min, J., Hwang, E., Lee, C. J., Suh, J. K., Hwang, O., et al. (2016). Optogenetic inhibition of the subthalamic nucleus reduces levodopa-induced dyskinesias in a rat model of Parkinson's disease. *Stereotact. Funct. Neurosurg.* 94 (1), 41–53. doi: 10.1159/000442891

Yoon, H. H., Park, J. H., Kim, Y. H., Min, J., Hwang, E., Lee, C. J., et al. (2014). Optogenetic inactivation of the subthalamic nucleus improves forelimb akinesia in a rat model of Parkinson disease. *Neurosurgery* 74 (5), 533–540. doi: 10.1227/NEU.0000000000000297

Zahedi, A., Defea, K., and Ethell, I. (2013). Optogenetics to target actin-mediated synaptic loss in Alzheimer's. *Optogenetics: Optical Methods for Cellular Control* 8586, 6. doi: 10.1117/12.2000480

Zaupa, C., Revol-Guyot, V., and Epstein, A. L. (2003). Improved packaging system for generation of high-level noncytotoxic HSV-1 amplicon vectors using Cre-loxP site-specific recombination to delete the packaging signals of defective helper genomes. *Hum. Gene Ther.* 14 (11), 1049–1063. doi: 10.1089/104303403322124774

Zemelman, B. V., Nesnas, N., Lee, G. A., and Miesenbock, G. (2003). Photochemical gating of heterologous ion channels: Remote control over genetically designated populations of neurons. *Proc. Natl. Acad. Sci. U. S. A.* 100 (3), 1352–1357. doi: 10.1073/pnas.242738899

Zhang, F., Frost, A. R., Blundell, M. P., Bales, O., Antoniou, M. N., and Thrasher, A. J. (2010). A ubiquitous chromatin opening element (UCOE) confers resistance to DNA methylation-mediated silencing of lentiviral vectors. *Mol. Ther.* 18 (9), 1640–1649. doi: 10.1038/mt.2010.132

Zhang, H., Yang, B., Mu, X., Ahmed, S. S., Su, Q., He, R., et al. (2011). Several rAAV vectors efficiently cross the blood-brain barrier and transduce neurons and astrocytes in the neonatal mouse central nervous system. *Mol. Ther.* 19 (8), 1440–1448. doi: 10.1038/mt.2011.98

Zhang, S., Xu, Y., Wang, B., Qiao, W., Liu, D., and Li, Z. (2004). Cationic compounds used in lipoplexes and polyplexes for gene delivery. *J. Control. Release* 100 (2), 165–180. doi: 10.1016/j.jconrel.2004.08.019

Zhang, W., Li, L., Su, Q., Gao, G., and Khanna, H. (2018). Gene therapy using a miniCEP290 fragment delays photoreceptor degeneration in a mouse model of Leber congenital amaurosis. *Hum. Gene Ther.* 29 (1), 42–50. doi: 10.1089/hum.2017.049

Zhou, H., O'Neal, W., Morral, N., and Beaudet, A. L. (1996). Development of a complementing cell line and a system for construction of adenovirus vectors with E1 and E2a deleted. *J. Virol.* 70 (10), 7030–7038.

Zhou, X., Vink, M., Klaver, B., Berkhout, B., and Das, A. T. (2006). Optimization of the Tet-On system for regulated gene expression through viral evolution. *Gene Ther.* 13 (19), 1382–1390. doi: 10.1038/sj.gt.3302780

Zhu, H., Pleil, K. E., Urban, D. J., Moy, S. S., Kash, T. L., and Roth, B. L. (2014). Chemogenetic inactivation of ventral hippocampal glutamatergic neurons disrupts consolidation of contextual fear memory. *Neuropsychopharmacology* 39 (8), 1880–1892. doi: 10.1038/npp.2014.35

Zhu, Y. J., Wienecke, C. F. R., Nachtrab, G., and Chen, X. K. (2016). A thalamic input to the nucleus accumbens mediates opiate dependence. *Nature* 530 (7589), 219–+. doi: 10.1038/nature16954

Conflict of Interest Statement: The authors declare that the research was conducted in the absence of any commercial or financial relationships that could be construed as a potential conflict of interest.

frontiers in Pharmacology

ORIGINAL RESEARCH
published: 12 July 2019
doi: 10.3389/fphar.2019.00776

Paclitaxel-Loaded Nanosponges Inhibit Growth and Angiogenesis in Melanoma Cell Models

Nausicaa Clemente[1], Monica Argenziano[2], Casimiro Luca Gigliotti[1], Benedetta Ferrara[2], Elena Boggio[1], Annalisa Chiocchetti[1], Fabrizio Caldera[3], Francesco Trotta[3], Elisa Benetti[2], Laura Annaratone[4], Simone Ribero[4], Stefania Pizzimenti[5], Giuseppina Barrera[5], Umberto Dianzani[1], Roberta Cavalli[2] and Chiara Dianzani[2]*

[1] Department of Health Sciences and Interdisciplinary Research Center of Autoimmune Diseases (IRCAD), UPO, Novara, Italy, [2] Dipartimento di Scienza e Tecnologia del Farmaco, University of Torino, Torino, Italy, [3] Department of Chemistry, University of Torino, Torino, Italy, [4] Department of Medical Sciences, University of Torino, Torino, Italy, [5] Department of Clinical and Biological Sciences, University of Torino, Torino, Italy

OPEN ACCESS

Edited by:
Ioanna Andreadou,
National and Kapodistrian University of Athens, Greece

Reviewed by:
Yoichi Matsuo,
Nagoya City University, Japan
Young-IL Jeong,
Pusan National University Yangsan Hospital, South Korea

***Correspondence:**
Roberta Cavalli
roberta.cavalli@unito.it

Specialty section:
This article was submitted to Experimental Pharmacology and Drug Discovery, a section of the journal Frontiers in Pharmacology

Received: 08 February 2019
Accepted: 17 June 2019
Published: 12 July 2019

Citation:
Clemente N, Argenziano M, Gigliotti CL, Ferrara B, Boggio E,Chiocchetti A, Caldera F, Trotta F, Benetti E, Annaratone L, Ribero S, Pizzimenti S, Barrera G, Dianzani U, Cavalli R and Dianzani C (2019) Paclitaxel-Loaded Nanosponges Inhibit Growth and Angiogenesis in Melanoma Cell Models. Front. Pharmacol. 10:776. doi: 10.3389/fphar.2019.00776

This study investigated the effects of free paclitaxel (PTX) and PTX-loaded in pyromellitic nanosponges (PTX-PNS) in reducing *in vitro* and *in vivo* melanoma cell growth and invasivity, and in inhibiting angiogenesis. To test the response of cells to the two PTX formulations, the cell viability was evaluated by MTT assay in seven continuous cell lines, in primary melanoma cells, both in 2D and 3D cultures, and in human umbilical vein endothelial cells (HUVECs) after exposure to different concentrations of PTX or PTX-PNS. Cell motility was assessed by a scratch assay or Boyden chamber assay, evaluating cell migration in presence or absence of diverse concentrations of PTX or PTX-PNS. The effect of PTX and PTX-PNS on angiogenesis was evaluated as endothelial tube formation assay, a test able to estimate the formation of three-dimensional vessels *in vitro*. To assess the anticancer effect of PTX and PTX-PNS in *in vivo* experiments, the two drug formulations were tested in a melanoma mouse model obtained by B16-BL6 cell implantation in C57/BL6 mice. Results obtained were as follows: 1) MTT analysis revealed that cell proliferation was more affected by PTX-PNS than by PTX in all tested cell lines, in both 2D and 3D cultures; 2) the analysis of the cell migration showed that PTX-PNS acted at very lower concentrations than PTX; 3) tube formation assay showed that PTX-PNS were more effective in inhibiting tube formation than free PTX; and 4) *in vivo* experiments demonstrated that tumor weights, volumes, and growth were significantly reduced by PTX-PNS treatment with respect to PTX; the angiogenesis and the cell proliferation, detected in the tumor samples with CD31 and Ki-67 antibodies, respectively, indicated that, in the PTX-PNS-treated tumors, the tube formation was inhibited, and a low amount of proliferating cells was present. Taken together, our data demonstrated that our new PTX nanoformulation can respond to some important issues related to PTX treatment, lowering the anti-tumor effective doses and increasing the effectiveness in inhibiting melanoma growth *in vivo*.

Keywords: paclitaxel, melanoma, angiogenesis, tumor growth, mouse model, nanosponges

INTRODUCTION

Melanomas are a heterogeneous group of aggressive and highly metastatic tumors (Radovic et al., 2012), representing the deadliest form of skin cancer. Nearly half of patients with metastatic melanomas harbor a valine–glutamine substitution in codon 600 of the serine/threonine kinase BRAF (BRAFV600 mutation) (Davies et al., 2002). BRAF inhibitors (BRAFi) target selectively the BRAF V600E/K genetic alteration and are widely used to treat melanoma patients harboring BRAFV600 mutation. Treatment with BRAFi results in high response rates. However, responses are short-lived, with a median time to progression of 5.1–8.8 months (Flaherty et al., 2010; Robert et al., 2015). The addition of a MEK inhibitor to a BRAFi extends the median duration of response from 5.6 to 9.5 months (Long et al., 2017).

Similar results have been observed in patients treated with anti–PD-1 (tumor programmed death ligand 1) monotherapy or a combination of anti–PD-1 and anti–CTLA-4 agents. A recent overall survival (OS) analysis of the phase 3 KEYNOTE-006 trial showed a 33-month OS rate of 50% in patients receiving pembrolizumab monotherapy, an anti-PD-1 monoclonal antibody (Robert et al., 2017). Despite the efficacy of BRAF-targeted and PD-1-related immune therapies in treating metastatic melanoma, a significant number of patients exhibit resistance. Although chemotherapeutic drugs, including dacarbazine, cisplatin, and paclitaxel (PTX), have been used, alone or in combination, without significant survival rate improvement (Bhatia et al., 2009), some patients with metastatic melanoma present remarkable responses to chemotherapeutic agents, even in the absence of a response to modern targeted therapies and immunotherapies (Simon et al., 2017).

PTX was originally isolated from the bark of the Pacific yew tree, *Taxus brevifolia*, and phase II clinical trials suggested that it had clinical activity in melanoma (Walker et al., 2005). In addition to the microtubule-stabilizer function and the induction of cytotoxicity, PTX has been found to induce immunogenic cell death, which results in augmented CD8+ T cell priming and cytotoxic activity (Song et al., 2017), regulating the immunosuppressive microenvironment in tumor (Pfannenstiel et al., 2010). However, free PTX showed non-selective distribution and poor water solubility (less than 0.3 μg/ml) (Konno et al., 2003). The common PTX formulation approved consists of Cremophor EL® and ethanol solution, but these solvents present severe side effects. To overcome these limitations, PTX has been embedded in drug nanotherapeutics, including albumin and polymeric micelle nanoparticles to treat several types of tumors (Sofias et al., 2017). These nanoformulations can reduce serious adverse effects of PTX, like allergic reactions, nephrotoxicity, and neurotoxicity, but some of them showed insufficient solubilizing capacity and poor stability (Mittal et al., 2018). For instance, Abraxane®, human serum albumin-bound PTX nanoparticle, approved by FDA in 2005, reduced off-targeted side effects and improved antitumor efficacy, but after i.v. administration, Abraxane® rapidly dissociates into the individual constituents. Moreover, the pharmacokinetics and the biodistribution of PTX are not improved (Chen et al., 2018). Thus, identification of non-toxic formulations capable to deliver PTX to the target site and release it in a sustained manner is needed to avoid the nonspecific biodistribution and to prevent the toxicity due to excessive dose of the drug. The novel pyromellitic nanosponges (PNS) showed the capability to act as PTX nanocarrier able to store and release it slowly and in a prolonged manner.

In this paper, we compare the effectiveness of free PTX and PTX-loaded PNS (PTX-PNS) in inhibiting *in vitro* and *in vivo* melanoma cell growth and invasiveness and in inhibiting angiogenesis.

MATERIALS AND METHODS

Preparation of PTX-Loaded Pyromellitic Nanosponges

PNS were synthetized by reacting β-cyclodextrin with pyromellitic anhydride as crosslinking agent at 1:4 molar ratio (CD/cross-linker). To transform the coarse PNS powder into a nanoformulation suitable for intravenous administration, a top down method was tuned. PNS were suspended in saline solution (NaCl 0.9% w/v) at the concentration of 10 mg/ml and homogenized using a high-shear homogenizer Ultra-Turrax (10 min, 24,000 rpm). Then, a high-pressure homogenization (HPH) step was performed to reduce the PNS size, using a high-pressure homogenizer (EmulsiFlex C5, Avastin, 90 min, 500 bar). The PNS nanosuspension was then purified by dialysis (membrane cutoff 12,000 Da). PTX-PNS were obtained by adding PTX solubilized in 50 μl of isopropanol to the blank PNS nanosuspension. The mixture was stirred at room temperature for 24 h.

Physico-Chemical Characterization of PTX-Loaded Pyromellitic Nanosponges

Size, polydispersity index, and zeta potential values of blank and PTX-PNS were measured by dynamic light scattering using a 90 Plus particle sizer (Brookhaven Instruments Corporation, USA). The measurements were performed using diluted PNS samples at a fixed angle of 90° and at a temperature of 25 °C. For zeta potential determination, the samples were placed in the electrophoretic cell, where an electric field of about 15 V/cm was applied.

The PNS morphology was evaluated by transmission electron microscopy (TEM) analysis, using a Philips CM 10 transmission electron microscope. PNS samples were sprayed on Formvar-coated copper grid and air-dried before observation.

Paclitaxel High Performance Liquid Chromatography (HPLC) Quantitative Determination

PTX quantitative determination was carried out by HPLC analysis using a pump (Perkin Elmer Pump 250B, Waltham, MA) equipped with a spectrophotometer detector (Flexar UV/Vis LC spectrophotometer detector, Perkin Elmer, Waltham, MA). A reverse phase Agilent TC C18 column (150 cm × 4.6 mm, pore size 5 μm; Agilent Technologies, Santa Clara, CA, USA) was used. The column was eluted with acetonitrile/water (60:40) at a flow rate of 1 ml/min. PTX was detected at 227 nm with

a UV/vis detector. The drug concentration was calculated using the external standard method from a standard calibration curve.

In vitro Release Studies

The release kinetics of PTX from PTX-PNS was *in vitro* evaluated. *In vitro* drug release studies were conducted in a multi-compartment rotating cell, comprising a donor chamber separated from the receiving phase by a cellulose membrane (Spectrapore, cut-off = 12,000 Da); 1 ml of PTX-PNS was placed in the donor chamber. The receiving chamber contained 1 ml of phosphate buffer 0.05 M (pH 7.4 or pH 5.5) added with 10% ethanol to assure drug solubility. The receiving phase was withdrawn at regular intervals and completely replaced with the same amount of fresh buffer to maintain sink conditions. The concentration of PTX in the withdrawn samples was detected by HPLC.

Cell Cultures and Treatments

The following human melanoma cell lines were used: A375 from the American Type Culture Collection (ATCC; Manassas VA), M14, JR8, RPMI7932, PCF-2, and LM from Dr. Pistoia (Gaslini Institute, Genoa, Italy). The mouse melanoma B16-BL6 cell line was obtained from RIKEN, Saitama, Japan (RIKEN is Japan's largest comprehensive research institution renowned for high-quality research in a diverse range of scientific disciplines). These cells were cultured in RPMI1640 medium, except A375 that were cultured in DMEM. Both media were supplemented with 10% fetal bovine serum (FBS), 100 units/ml penicillin, and 100 μg/ml streptomycin in a 5% CO_2, 37 °C incubator. Human umbilical vein endothelial cells (HUVECs) were isolated from human umbilical veins by trypsin treatment (1%) and cultured in M199 medium with the addition of 20% FCS, 100 U/ml penicillin, 100 μg/ml streptomycin, 5 UI/ml heparin, 12 μg/ml bovine brain extract, and 200 mM glutamine. HUVEC were grown to confluence in flasks and used at the 2nd–5th passages. Use of HUVEC was approved by the Ethics Committee of the "Presidio Ospedaliero Martini" of Turin and conducted in accordance with the Declaration of Helsinki. Written informed consent was obtained from patients.

PTX was purchased from Bristol-Myers Squibb (Chester, UK).

Isolation and Characterization of Primary Melanoma Cells

The primary melanoma cell line (PMel) was isolated from a 77-year-old Caucasian male patient with a superficial spreading melanoma in vertical growth phase, showing infiltration of the papillary dermis and cutaneous ulceration without metastasis. The study was approved by the Committee for human Biospecimen Utilization (ChBU—Department of Medical Sciences, University of Turin). Written informed consent was obtained from the patient for tissue to be used in research.

The tissue sample, used for the primary cell culture establishment, was collected from the "left-over tissue" (residual tissue not used for diagnostic and therapeutic purposes) at the Department of Medical Sciences, Pathology Unit, University of Torino (Italy), in sterile tubes containing 10 ml of RPMI serum free medium, supplemented with 1% penicillin-streptomycin-fungizone. Primary cell culture isolation was performed as described by Annaratone et al. (2013) with minor modifications. Briefly, the tissue sample was washed three times with the same medium, then finely minced by surgical blades into approximately 1×1 mm fragments which were incubated at 37 °C with collagenase type IV (1 mg/ml; 1 : 1 RPMI, final volume 10 ml), for 3–5 h until complete disaggregation of fragments was obtained. Digested tissue samples were shaken vigorously by hand to disaggregate possible residual large clumps. Collagenase activity was blocked by addition of 10 ml of RPMI with 10% FBS. After centrifugation at 800 rcf for 6 min, the cell pellets were re-suspended in complete culture medium. The final cell suspension was seeded in petri dishes as passage 0 and kept in a humidified incubator with 5% CO_2 at 37 °C in DMEM-F12 medium supplemented with 10% FBS, 10 ng/ml human epidermal growth factor (EGF), 5 mg/ml insulin, 400 ng/ml hydrocortisone, 1% L-glutamine, and 1% penicillin-streptomycin-fungizone (Sigma-Aldrich). Culture medium was changed first at the time of cell attachment and, subsequently, three times a week. After three passages, the cells were characterized for two specific melanoma markers, S100 and HMB45 by immunocytochemistry (ICC). ICC was performed by using an automated slide processing platform (Ventana BenchMark XT Autostainer, Ventana Medical Systems, Tucson, AZ, USA). The anti-S00 and the anti-HMB45 antibodies were purchased from DAKO and used following the manufacturer's instructions (Milan, Italy). Both markers were positive (data not show), confirming the isolation of melanoma-type cells. PMel cells were maintained in standard 2D cell cultures, in DMEM-F12 medium supplemented as described above.

Spheroid Formation of Primary Melanoma (PMel) Cells

PMel cells, cultured in standard 2D condition, were dissociated with trypsin-EDTA into single-cell suspensions. The cells were then seeded on ultra-low attachment (ULA) 96-well flat-bottom plates (Sigma). Optimal seeding densities were established such that melanoma spheroids for both primary cell lines testes fell within a size range of 200 to 500 μm in diameter on day 8, considering appropriate for initiating experimental studies. Representative images of PMel tumor spheroids obtained on day 8, starting from 1×10^4 cells/well, are showed in the **Supplementary data**, **Fig. S1**

MTT Assay

The toxic effect of PTX or PTX-PNS was determined through the 3-(4,5-dimethylthiazol-2-yl)-2,5-diphenyltetrazolium bromide (MTT) assay as previously described (Ciamporcero et al., 2018). This colorimetric assay may be interpreted as a measure of both cell viability and cell proliferation (Sylvester, 2011). Cells were seeded ($0.8 - 1.5 \times 10^3$ cells/well) in 100 μl of serum-supplemented medium and treated with different concentrations of PTX and PTX-PNS. Untreated cells or cells treated with the empty PNS were used as control. After 72 h, the drug was removed and MTT assay was performed. The optical density (OD) of treated and untreated cells was determined at a wavelength of 570 nm

with a microplate reader after 4 h of incubation. Controls were normalized to 100%, and the readings from treated cells were expressed as % of viability inhibition. Eight replicates were used to determine each data point, and five different experiments were performed.

WST-1 Assay

The cytotoxic effect of PTX or PTX-PNS on PMel spheroids was determined by using the 2-(4-iodophenyl)-3-(4-nitrophenyl)-5-(2,4-disulfophenyl)-2H-tetrazolium (WST-1) reagent (Roche, Italy). Cells were seeded (0.8 – 1.5 $\times 10^3$ cells/well) in 100 µl of serum-supplemented medium and treated with different concentrations of PTX, PTX-PNS, or PNS. After 72 h, the drug was removed and the WST-1 assay was performed. The OD of treated and untreated cells was determined at a wavelength of 450 nm with a microplate reader after 4 h of incubation. Controls were normalized to 100%, and the readings from treated cells were expressed as % of viability inhibition. Eight replicates were used to determine each data point, and five different experiments were performed.

Crystal Violet Assay

For the quantitative determination of cells adhering to the plate after the 6 h treatment with different concentrations of PTX, PTX-PNS, or PNS, the violet crystal test was used. The violet crystal is a water-soluble dye with affinity for neutral pH DNA, soluble at acidic pH. The cells were washed after treatment, fixed, and stained with crystal violet-methanol. After careful washing, acetic acid was added and the reading was made with a spectrophotometer at 595 nm. The controls were normalized to 100%, and the readings from treated cells were expressed as % of viability inhibition. Four replicates were used to determine each data point, and five different experiments were performed.

Cell Motility Assays

In the wound-healing assay, after starvation for 24 h in serum-free medium, HUVECs were plated onto six-well plates (10^6 cell/well) and grown to confluence. Cell monolayers were wounded by scratching with a pipette tip along the diameter of the well, and they were washed twice with serum-free medium before their incubation with diverse concentrations of PTX, PTX-PNS, or PNS. Drug concentrations that were not cytotoxic were used for this assay. In order to monitor cell movement into the wounded area, five fields of each wound were photographed immediately after the scratch (T0) and after 24 h (Dianzani et al., 2014). The endpoint of the assay was measured by calculating the reduction in the width of the wound after 24 h and compared to T0, which is set at 100%. The area of wound healing was calculated by using the ImageJ software (Schneider et al., 2012).

In the Boyden chamber (BD Biosciences, San Jose, CA) invasion assay, cells (2×10^3) were plated onto the apical side of 50 µg/ml Matrigel-coated filters (8.2-mm diameter and 0.5-µm pore size; Neuro Probe, Inc.; BIOMAP snc, Milan, Italy) in serum-free medium with or without increasing concentration of PTX, PTX-PNS, or PNS. Nontoxic drug concentrations were used for this assay. Medium containing VEGF-α (10 ng/ml) was placed in the basolateral chamber as a chemo attractant for HUVEC and FCS 20% for melanoma cancer cells (A2058 and B16-BL6). After 6 h, cells on the apical side were wiped off with Q-tips. Cells on the bottom of the filter were stained with crystal violet, and all the fields were counted with an inverted microscope.

Tube Forming Assay

Nontoxic drug concentrations were used for the tube formation assay. HUVECs were seeded onto 48-well plates (5×10^4/well) previously coated with 75 µl of growth factor-reduced Matrigel, with or without increasing concentration of PTX, PTX-PNS, or PNS. The morphology of the capillary-like structures formed by the HUVECs was analyzed by an inverted microscope after 6 h of culture, and photographed with a digital camera. Tubule formation was analyzed with an imaging system (Image-Pro Plus Software for microimaging, Media Cybernetics, version 5.0, Bethesda, MD, USA). Tube formation was evaluated by counting the total number of tubes in three wells, and five different experiments were performed. The results were expressed as % inhibition of untreated control cell.

In vivo Experiments

Eight-week-old female C57BL6/J mice (Charles River Laboratories, Wilmington, MA, USA) were injected subcutaneously (s.c.) with B16-BL6 cells (10^5 cells/mouse). The mice were bred under pathogen-free conditions in the animal facility of the Department of Health Sciences (UPO, Novara, Italy). All experimental procedures were done according to Europeans Guidelines and our Institution's ethics commission. After 7 days from the injections, when average tumor dimension reached 5 mm^3, mice were randomized in a blind fashion into homogenous groups (5 mice per group) and assigned to different treatments. Free PTX or PTX-PNS dissolved in NaCl 0.9% were administrated by tail injection (100 µl/mouse) at the dose of 2.5 mg/kg, every 4 days, for four times. Control mice were injected with empty PNS dissolved in PBS. Treatment-related toxicity was determined by monitoring mouse weight weekly. The tumor size was measured with a caliper, and mice were sacrificed 4 days after the last injection. Euthanasia, collection of tumor samples, tumor weight, and volume determination were performed after 2 weeks from the beginning of treatments.

Histology and Immunofluorescence Anti-CD31 and Anti-Ki-67 on Tumor Sections

Immediately after dissection, tumor samples were embedded in OCT compound (Killik, Bio Optica Milano SpA) and stored at −80 °C until use. Tumor tissues were cut with a cryostat (thickness 4–5 µm) and treated with 4% paraformaldehyde (Sigma-Aldrich) diluted in PBS for 5 min at room temperature to fix the sample on the glass slides. The samples were then blocked with 5% normal goat serum (R&D System) in PBS for 1 h in order to block nonspecific sites to which the primary antibody could bind. To detect CD31 and Ki-67 expression, the primary antibodies used were a polyclonal rabbit anti-CD31

(Abcam, Cambridge, UK) or a monoclonal mouse anti-human Ki-67 antigen (DAKO); both diluted 1:50 and were incubated over night at 4°C in a humid chamber. The secondary antibody used was an anti-rabbit Ig Alexa Fluor 488-conjugated (Thermo-Fisher), or an anti-mouse Ig Alexa Fluor 546-conjugated (Thermo-Fisher); both diluted 1:400, respectively. Then, the sections were stained with 0.5 mg/ml of the fluorescent dye 4,6-diamidino-2-phenylindole-dihydrochloride (DAPI, Sigma-Aldrich) for 5 min to highlight cell nuclei and then mounted using prolong anti-fade mounting medium (SlowFade AntiFADE Kit, Molecular Probes Invitrogen). The sections were then observed by a fluorescence microscope (Leica, Italy) and analyzed by Image Pro Plus Software for micro-imaging 5.0 (Media Cybernetics, version 5.0, Bethesda, MD, USA). Tumor microvessel density (MVD) was measured by evaluating the CD31-positive area; the numbers of positive cells for Ki-67 was calculated in the total tumor area per field upon slide scanning (Panoramic midi II, 3D HISTECH, Budapest, Hungary). Hematoxylin and eosin (Sigma Aldrich, Milan, Italy) staining was performed to assess morphological changes.

Statistical Analysis

Data were expressed as means ± SD. Significance between experimental groups was determined by one-way ANOVA followed by the Bonferroni multiple comparison post-test using GraphPad InStat software (San Diego, CA, USA). Values of $p \leq 0.05$ were considered significant.

TABLE 1 | Physico-chemical characteristics of blank and PTX-loaded PNS formulations.

Formulation	Average diameter ± SD (nm)	Polydispersity index	Zeta potential ± SD (mV)
Blank PNS	307.2 ± 10.6	0.22 ± 0.01	–33.6 ± 4.5
PTX-PNS	316.8 ± 12.1	0.20 ± 0.02	–28.4 ± 3.7

RESULTS

Physico-Chemical Characterization of PTX-PNS

The physico-chemical parameters of PNS before and after loading with PTX are reported in **Table 1**. The PNS nanoformulations showed average diameters of about 300 nm and a negative surface charge. The drug incorporation slightly affected the physico-chemical characteristics. The zeta potential value remained enough high to avoid aggregation phenomena.

TEM analysis showed the spherical morphology of PNS and confirmed their nanoscale sizes, due to the high pressure homogenization step. **Figure 1** (panel A) reports the TEM image of PTX-loaded PNS.

PNS were able to load PTX in a good extent, showing an encapsulation efficiency of about 96.5% and a loading capacity of about 8%.

The release profile of PTX from PTX-PNS was investigated *in vitro* at two pH values (**Figure 1**, panel B). Prolonged *in vitro* release kinetics was demonstrated, and no initial burst effect was observed. The sustained release of PTX from the PTX-PNS confirmed the drug incorporation in the PNS polymer matrix. The percentage of PTX released from the PNS was about 4% at pH 7.4 and 10% at pH 5.5 after 24 h, indicating an enhanced release kinetics at acidic pH.

Effect of PTX and PTX-PNS on Cell Proliferation

To compare the response of cells to free PTX and PTX-PNS, we first analyzed cell viability after 72 h of exposure to different concentrations of PTX (from 10^{-7} to 10^{-9} M) and PTX-PNS or

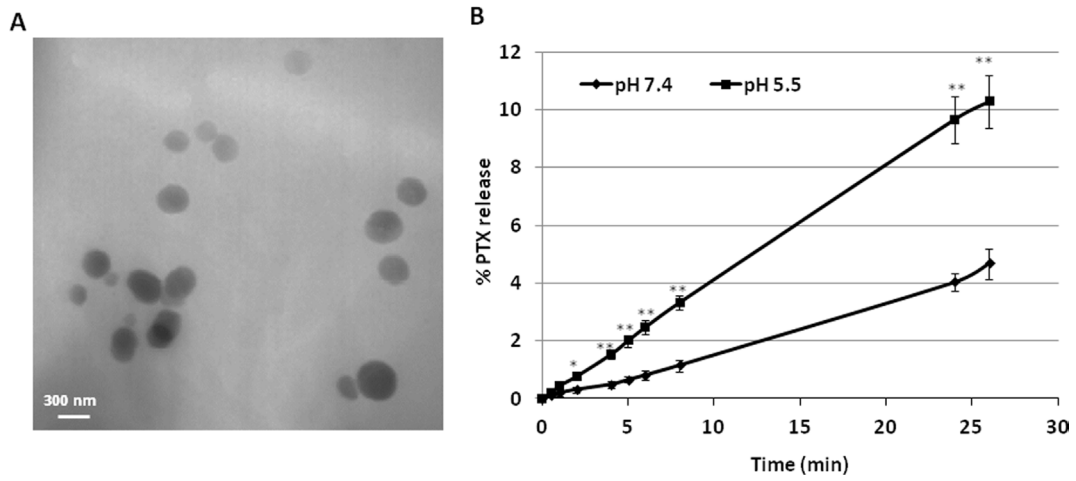

FIGURE 1 | Characterization of PNS formulations. **(A)** TEM image of PTX-loaded PNS; **(B)** *In vitro* release kinetics of PTX from PTX- loaded PNS as a function of pH (pH 7.4 or pH 5.5).

PNS (from 10^{-10} to 10^{-13} M). MTT analysis revealed that cells were more affected by PTX-PNS than by free PTX. The effective concentrations ranged from 10^{-7} to 10^{-8} M for the free PTX in all cell lines; from 3×10^{-9} to 10^{-13} M PTX-PNS in A2058, JR8, PCF2; from 3×10^{-9} to 3×10^{-12} M PTX-PNS in M14; and from 3×10^{-9} to 10^{-12} M PTX-PNS in A375, RPMI7932, and B16-BL6 (**Figure 2**). The empty PNS did not show any toxicity even at highest doses, and the MTT values were similar to those obtained in untreated cells.

Effect PTX and PTX-PNS in Inhibiting Growth of 2D and 3D Cultures of Primary Melanoma Cells

In primary melanoma PMel cells, PTX and PTX-PNS showed an inhibitory activity of growth at different doses. PTX was effective at doses ranging from 10^{-5} to 10^{-9} M, whereas PTX-PNS was effective at doses ranging from 10^{-9} to 10^{-13} M. The empty PNS did not show any toxicity (**Figure 3A**). In 3D spheroids, PTX inhibited the growth at concentrations ranging from 10^{-5} to 10^{-9}M, whereas PTX-PNS inhibited growth at concentrations ranging from 10^{-9} to 10^{-13} M (**Figure 3B**).

Effect of PTX and PTX-PNS in Inhibiting Cell Migration

Tumor growth is favored by tumor angiogenesis, which is continuously activated in cancer resulting in the accumulation of immature and chaotic blood vessels. The acquisition of endothelial cell motility represents the first step of angiogenesis. In order to find the PTX and PTX-PNS nontoxic concentrations in HUVECs, which can be used in the migration test, MTT analysis was performed after 24 h. HUVECs were cultured in the presence and absence of titrated amounts of the different formulations. Results demonstrated that PTX concentration ranging from 10^{-8} to 10^{-10} M and PTX-PNS concentrations ranging from 10^{-12} to 10^{-14} M were nontoxic for HUVEC cells at 24 h (**Supplementary Data**, **Figure S2**). Thus, PTX concentrations in the range of 10^{-8}–10^{-10} M and PTX-PNS concentrations from 10^{-12} to 10^{-14} M were chosen for the wound-healing migration test. Analysis of cells ability to migrate into the scratch showed that only PTX-PNS inhibited HUVEC migration at 10^{-12} M (**Figure 4A** and **B**), while PTX was unaffective.

To confirm these results, cell motility was measured by using a Boyden chamber assay, assessing the capability of directional migration and invasion. In order to find the PTX and PTX-PNS concentrations that were not cytotoxic in HUVECs and melanoma

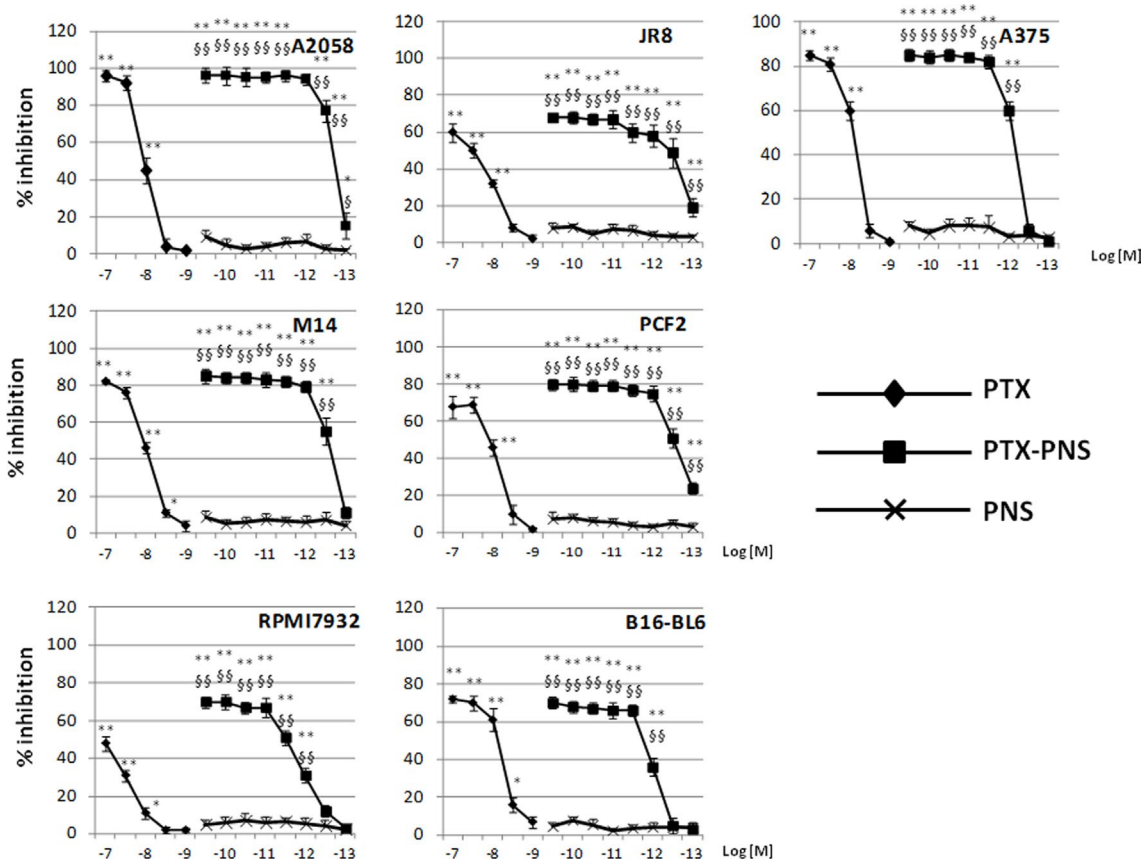

FIGURE 2 | Inhibition of melanoma cell proliferation following PTX and PTX-PNS treatment. Cells were treated with increasing concentrations of PTX (from 10^{-7} to 10^{-9} M) or PTX-PNS (from 10^{-10} to 10^{-13} M) for 72 h. The results are expressed as % inhibition of control and are the mean ± SD of five separated experiments. $^{**}p < 0.01$ *vs* control and PNS, $^{*}p < 0.05$ *vs* control and PNS, $^{§§}p < 0.01$ *vs* PTX, $^{§}p < 0.05$ *vs* PTX.

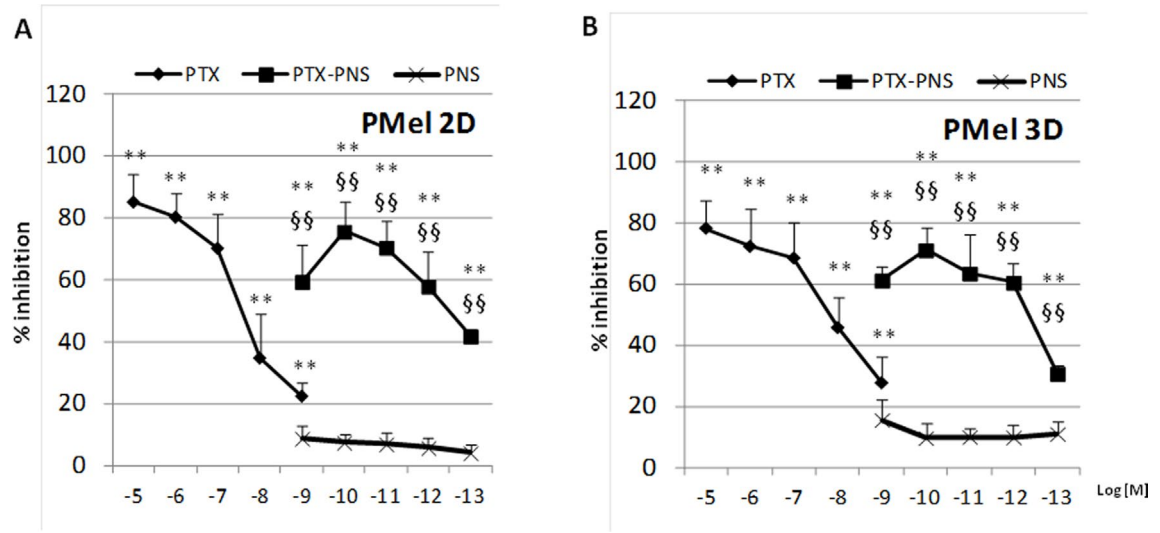

FIGURE 3 | Inhibition of primary melanoma cell growth following PTX and PTX-PNS treatment. Primary melanoma cells **(A)** in 2D or **(B)** in 3D cultures were treated with increasing concentrations of PTX (from 10^{-5} to 10^{-9} M) or PTX-PNS (from 10^{-9} to 10^{-13} M) or PNS (10^{-9} M) for 72 h. The results are expressed as % inhibition of control and are the mean ± SD of five separated experiments. $^{**}p < 0.01$ *vs* control and PNS, $^{§§}p < 0.01$ *vs* PTX.

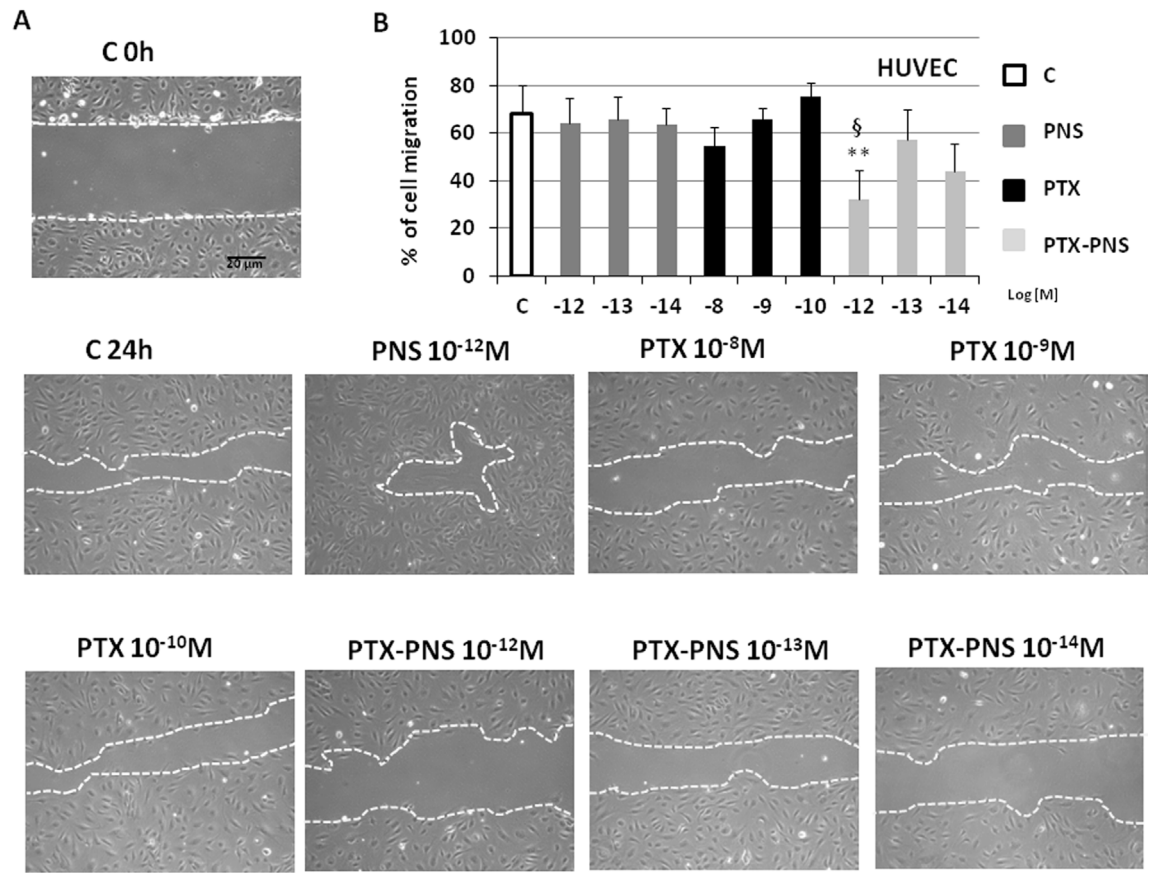

FIGURE 4 | Wound-healing assay of HUVEC treated with different concentrations of PTX and PTX-PNS. A scratch was made through the HUVEC layer, and then, cells were cultured in the absence (C) or in presence of PTX (from 10^{-8} to 10^{-10} M) or PTX-PNS (from 10^{-12} to 10^{-14} M) or PNS (10^{-12} M) for 24 h.
(A) Microphotographs of the wounded area were taken immediately after the scratch (0 h) and after 24 h, in order to monitor cell migration into the wounded area.
(B) The graph shows mean ± SD (n = 5) of assay endpoints measured by calculating the reduction in the width of the wound after 24 h and compared to T0 which is set at 100%. The area of wound healing was calculated by using the ImageJ software. $^{**}p < 0.01$ *vs* C, $^{§}p < 0.05$ *vs* PTX.

cells, crystal violet assay was performed after 6-h treatments with titrated amounts of the diverse formulations. Results demonstrated that cell viability was not affected by any concentration of the drug formulations tested (**Supplementary data, Table S1**). The invasion experiments demonstrated that PTX and PTX-PNS inhibited HUVEC invasion in a concentration dependent-manner; PTX was active at 10^{-8}–10^{-9} M, whereas PTX-PNS affected cell invasion at concentrations ranging from 10^{-12} to 10^{-13} M **(Figure 5A)**. Similar results were obtained for human and mouse melanoma cell lines **(Figure 5B** and **C)**. Representative images of crystal violet staining Matrigel-coated filters of the Boyden chambers were reported in **Supplementary Data**, **Figure S3**.

PTX and PTX-PNS inhibit angiogenesis

The effect of PTX and PTX-PNS on angiogenesis was evaluated in endothelial tube formation assay, which is able to estimate the formation of three-dimensional vessels *in vitro*. HUVECs were seeded onto 24-well plates (5×10^4 cell/well) previously coated with 75 µl of growth factor-reduced Matrigel (BD Biosciences), in the absence or presence of nontoxic concentrations of PTX (10^{-7}–10^{-10}M) or PTX-PNS (10^{-10}–10^{-14}M) (**Supplementary Data**, **Table S1**). The morphology of capillary-like structures formed by HUVEC was analyzed 6 h after culturing. The results showed that PTX and PTX-PNS dose-dependently inhibited endothelial tube formation (**Figure 6A**). Quantification of the

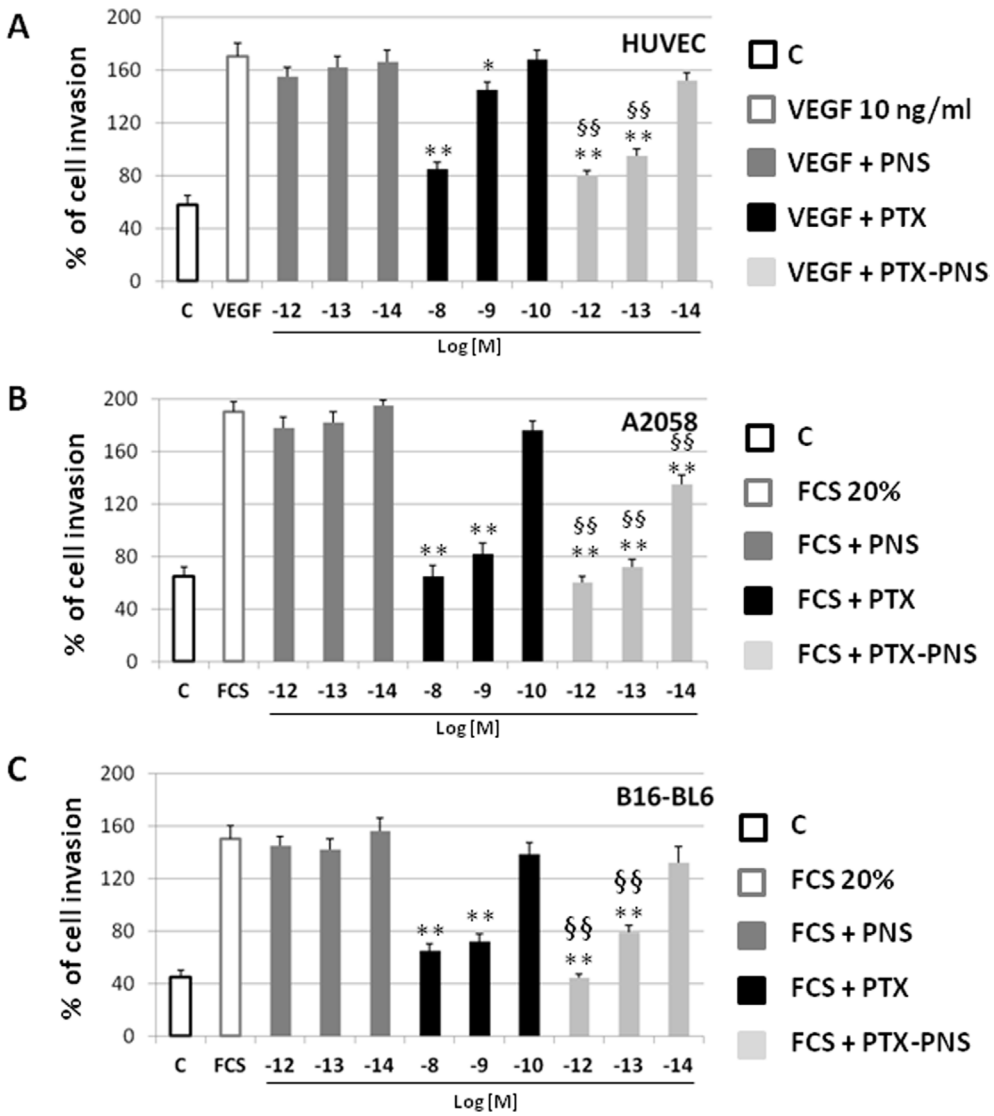

FIGURE 5 | Effect of PTX and PTX-PNS on motility of HUVEC **(A)**, A2058 **(B)**, and B16-BL6 **(C)** assessed by Boyden chamber assay. HUVECs were plated onto the apical side of Matrigel-coated filters in the presence and absence of either PTX (from 10^{-8} to 10^{-10} M) or PTX-PNS (from 10^{-12} to 10^{-14} M). Medium containing VEGF-α (10 ng/ml) or FCS 20% was placed in the basolateral chamber as a chemoattractant for HUVECs or melanoma cell line, respectively. After 6 h, cells on the apical side were wiped off with Q-tips. Cells on the bottom of the filter were stained with crystal violet, and all counted with an inverted microscope. Data are expressed as mean ± SD (n = 5) of number of migrated cells. $^{**}p < 0.01$, *vs* VEGF-α or FCS, $^{§§}p < 0.01$, *vs* PTX.

inhibition is shown in **Figure 6B**. PTX inhibited tube formation at the doses ranging from 10^{-7} to 10^{-9} M, whereas PTX-PNS were more effective inhibiting tube formation at the doses ranging from 10^{-10} to 10^{-13} M.

PTX and PTX-PNS Anticancer Effect in Xenograft Tumor Model

To assess the anticancer effect of PTX and PTX-PNS in *in vivo* experiments, we implanted B16-BL6 cells, in C57/BL6 mice, and we treated animals with the two drug formulations. Results showed that tumor weights (**Figure 7A**), volumes (**Figure 7B**), and growth (**Figure 7C**) were significantly reduced by PTX-PNS treatment compared to those detected in the mice treated with either PBS, empty PNS, or free PTX at the dose of 2.5 mg/kg. By contrast, PTX did not show any significant effect. Analysis of tumor vasculature was assessed by staining CD31 in the tumor sections and showed that vascular density (MVD) was significantly lower in the tumors from mice treated with PTX-PNS than in those treated with either PBS, empty PNS, or free PTX (**Figure 8A** and **B**). The number of positive cells for Ki-67 (**Figure 8C** and **D**) confirmed previous results. All treatments were well tolerated by the animals without significant weight loss in any group.

DISCUSSION

The use of nanodelivery systems offers some advantages that can improve the therapeutic efficacy of anticancer drugs. Indeed, nanoformulations could increase drug concentration at the tumor site, decreasing the total dose administered, and subsequently reducing the side effects (Duchene et al., 2016, Prasad et al., 2018). In particular, cyclodextrin-based nanosponges (NS) have been proposed for cancer nanotherapeutic development (Trotta et al., 2012, Trotta et al., 2014; Swaminathan et al., 2016). The use of NS as nanocarrier for PTX delivery was previously investigated. PTX was encapsulated in NS obtained by reacting CDs with diphenylcarbonate as cross-linker (Ansari et al., 2011).

The *in vivo* behavior of PTX-NS was studied after oral administration to rats, showing an increase of the drug oral bioavailability (Torne et al., 2010). Moreover, PTX showed the capability to be incorporated in a great extent in another type of NS, obtained using carbonyldiimidazole as crosslinking agent (Mognetti et al., 2012). Here, we evaluated the use of PNS as nanovehicle of PTX. Previously, PNS showed non-toxic effect *in vitro* and *in vivo* in acute and repeated dose toxicity studies (Shende et al., 2015). PNS were able to incorporate PTX, increasing its apparent aqueous solubility. Indeed, it has an extremely low aqueous solubility (less

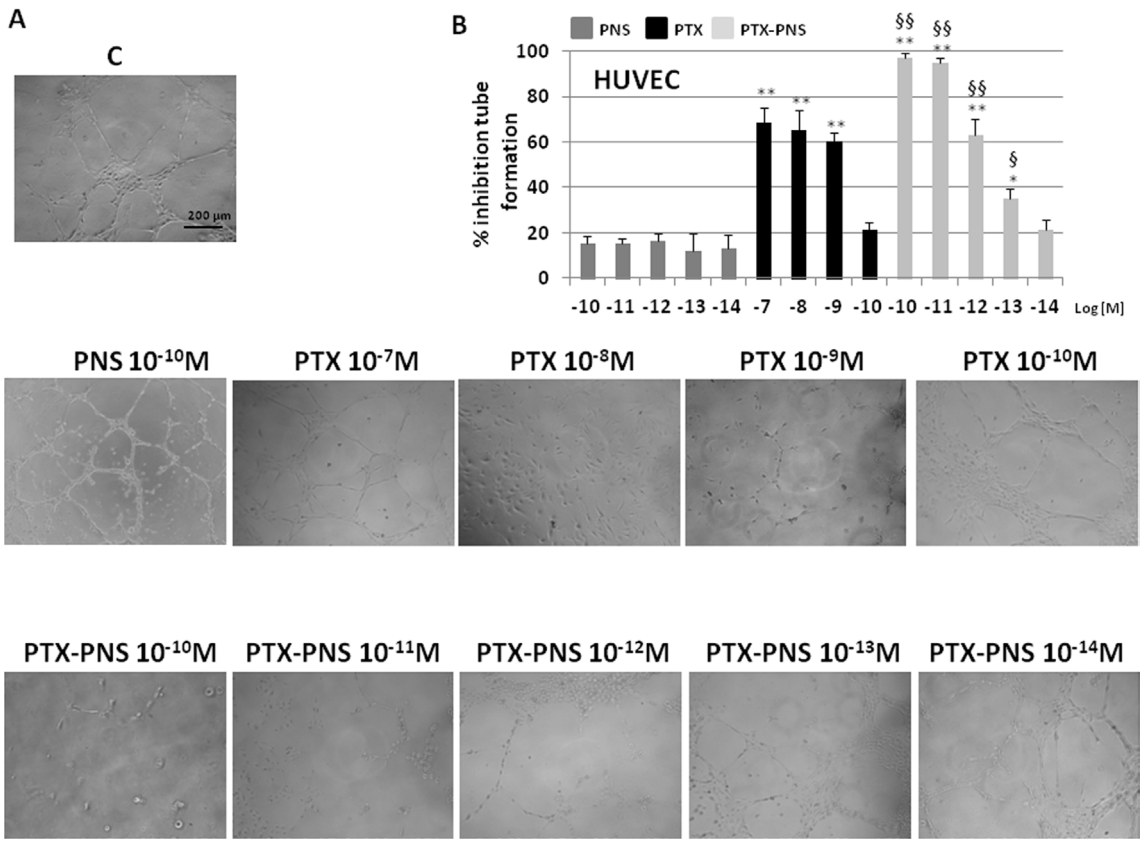

FIGURE 6 | Tube formation assay of HUVEC treated with different concentrations of PTX or PTX-PNS. HUVEC were plated in the presence and absence of PTX (from 10^{-7} to 10^{-10} M) or PTX-PNS (from 10^{-10} to 10^{-14} M). **(A)** The morphology of the capillary-like structures formed by the HUVEC was analyzed by an inverted microscope after 6 h of culture, and photographed with a digital camera. **(B)** The graph shows the tube formation, evaluated by counting the total number of tubes in three wells of five different experiments. The results were expressed as % inhibition of untreated control cells. Data are expressed as mean ± SD. $^{**}p < 0.01$, *vs*.VEGF-α or FCS, $^{*}p < 0.05$, *vs* VEGF-α or FCS, $^{§§}p < 0.01$, *vs*. PTX, $^{§}p < 0.05$, *vs* PTX.

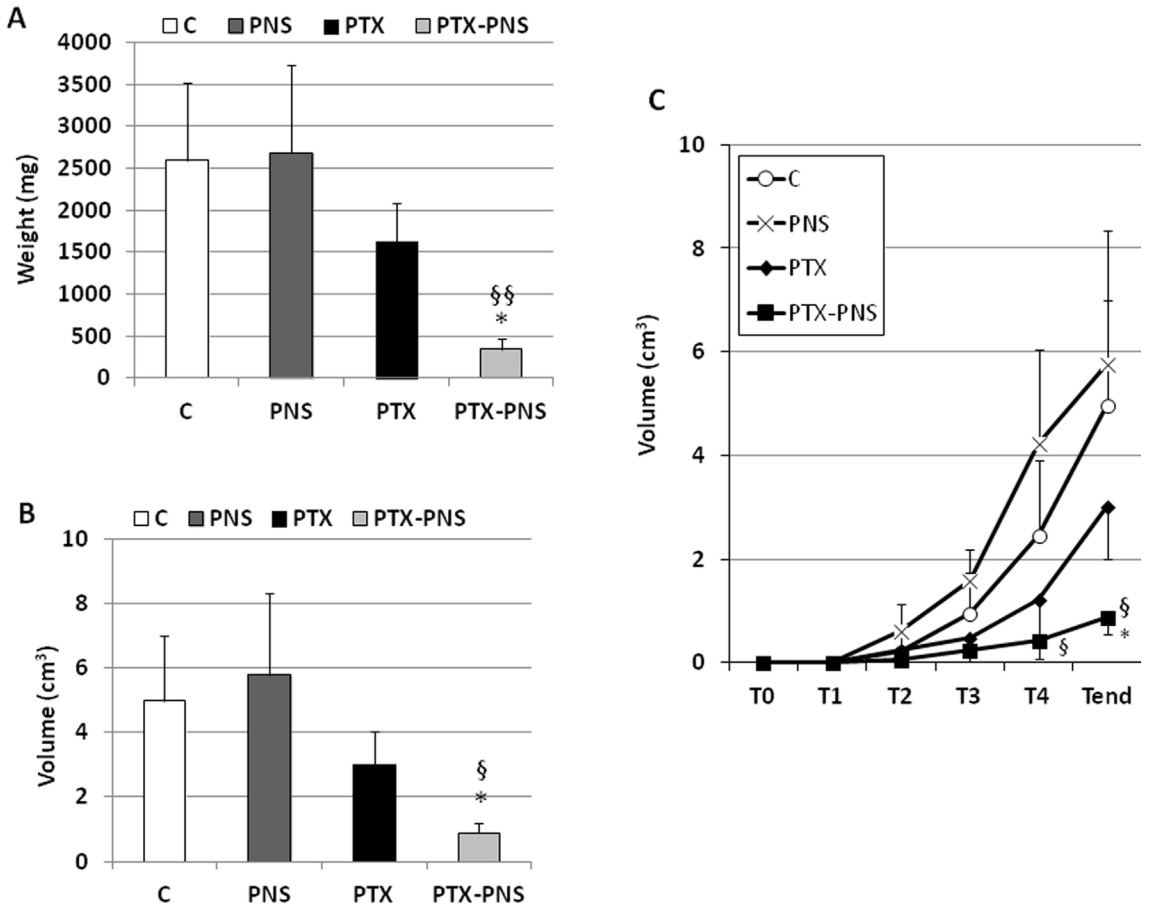

FIGURE 7 | In vivo experiments on mouse melanoma model. C57BL6/J mice were injected subcutaneously with B16-BL6 cells (10^5 cells/mouse). 7 days after the tumor injection, mice were treated every 4 days for 2 weeks by i.v. injection of PTX, PTX-PNS, and PNS (2.5 mg/kg, 100 µl/mouse) or the same volume of NaCl 0.9% as control (five mice/group). Mice were sacrificed at the end of the experiment. Graphs show **(A)** tumor weight (mg, mean ± SD), **(B)** tumor volume curves (cm^3, mean ± SD), and **(C)** tumor growth (cm^3, mean ± SD). Tumors were evaluated every 4 days, after the first treatment performed at T1 (i.e., when they were palpable). Data are expressed as mean ± SD. $^*p < 0.05$, *vs* VEGF-α or FCS, $^{§§}p < 0.01$, *vs*. PTX, $^{§}p < 0.05$, *vs* PTX.

than 0.3 µg/) and it is currently dissolved in a mixture of Cremophor EL® (polyoxyethyleneglycerol triricinoleate 35) and dehydrated ethanol (1:1 v/v) in the commercial intravenous dosage form. The PTX incorporation in the PNS nanostructure was confirmed by the slow and prolonged *in vitro* release kinetics of the drug from PTX-NS. Interestingly, results demonstrated that PTX-PNS inhibited melanoma cell growth more effectively than free PTX. The inhibitory activity on cell proliferation was effective on all of the melanoma cell lines used in this study, including a PMel. Moreover, the cytotoxicity of PTX-PNS was displayed at concentrations which were a thousand times lower than those displayed by free PTX. PTX-PNS significantly inhibited the proliferation of primary tumor cells in both 2D and 3D melanoma cell cultures with the same effectiveness. Results on melanoma spheroid 3D cultures were particularly relevant since 3D-cultured cells acquired morphological and cellular features which are more similar to solid tumors than 2D cultures. In particular, Ma et al. (2012) compared nanoparticle penetration properties of different culture systems and reported that 3D spheroids of HeLa cells displayed similar morphologic features of human solid tumors, including a resistance to chemotherapeutics that could not be observed in 2D cultures. In line with this observation, it has been suggested that 3D spheroids may be a useful simplified model of tumor tissue for *in vitro* testing of anticancer therapeutics (Edmondson et al., 2014; Huang et al., 2015).

The effectiveness of PTX-PNS in 3D cultures demonstrated that this nanoformulation is effective on a tumor-like environment mimicking several features of tumors involved in chemotherapy resistance such as three-dimensional architecture, cell–cell interaction, and hypoxia.

Cancer metastasis is associated with stimulation of cancer cell migration and invasion of the neighboring tissues. In line with previous results, PTX-PNS inhibited cell melanoma invasion at concentrations which were much lower than those displayed by free PTX.

Cancer progression is also associated with stimulation of tumor neoangiogenesis producing newly formed vessels to feed the tumor. This process involves endothelial cell migration and generation of tubule-like structures to form vessels. PTX can reduce endothelial cell migration at concentrations ranging from 10^{-7} to 10^{-9} M, according to previous reports showing taxane effects on cell

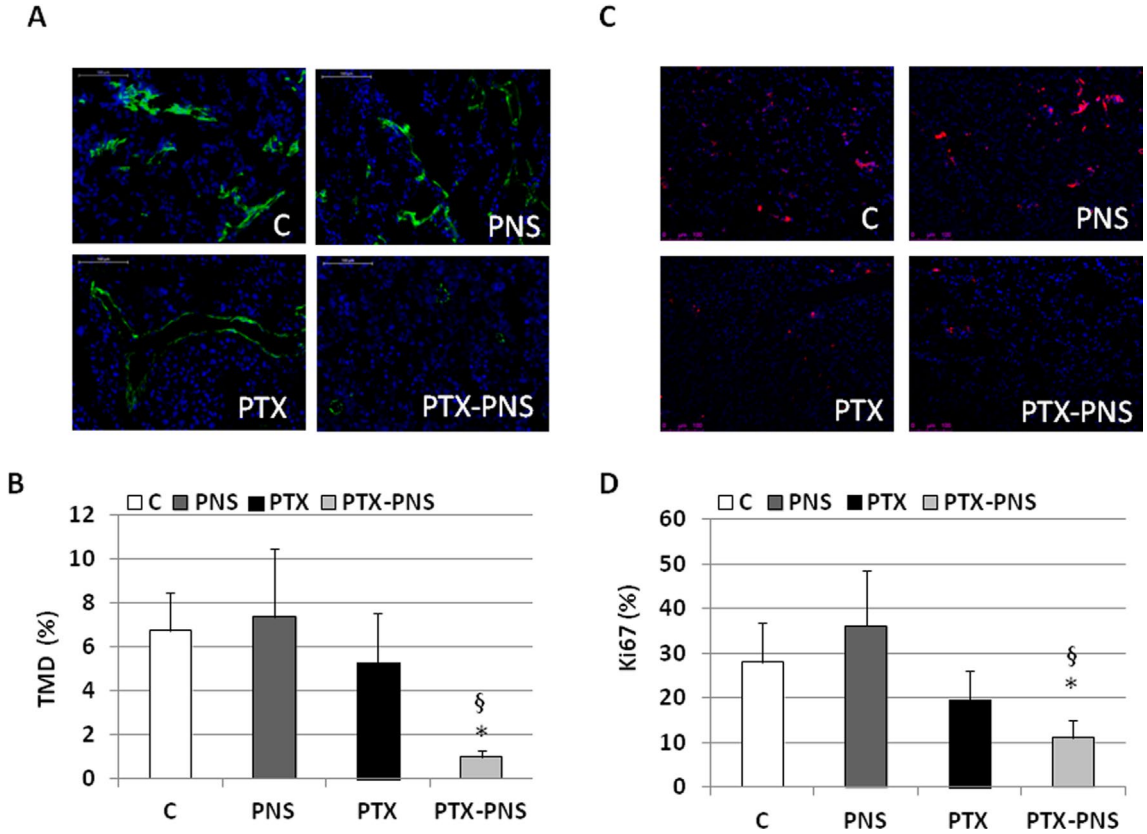

FIGURE 8 | (A) Microphotographs of CD31 staining from a representative experiment (green; magnification 200x). **(B)** Tumor microvessel density (MVD) determined as the percentage of CD31-positive area on the tumor sections. Three randomly selected areas from three tumors from each group were analyzed. **(C)** Microphotographs of Ki-67 staining from a representative experiment (red; magnification 200x). **(D)** % of Ki-67-positive cells among tumor cells. Three randomly selected areas from three tumors from each group were analyzed. *$p < 0.05$ *vs* C and PNS, §$p < 0.05$ *vs* PTX.

migration (Ballestrem et al., 2000). However, also in this case, PTX-PNS was much more effective in inhibiting HUVEC migration and invasion than free PTX. A similar pattern in *in vitro* tubulogenesis of endothelial cells was observed, since the inhibitory effect of PTX was obtained at nanomolar concentrations, in line with previous data from Taraboletti et al. (2002). Intriguingly, PTX-PNS were able to inhibit tubulogenesis at lower concentrations, than free PTX.

Finally, we demonstrated that PTX-PNS was more effective than PTX in inhibiting the *in vivo* growth of melanoma cells in a mouse model also. Indeed, both the weight, the volume, and the growth of melanoma were significantly reduced in mice treated with PTX-PNS whereas no significant inhibition was obtained with the same dose of free PTX. The results on angiogenesis and proliferation rate of tumor cells *in vivo* are in agreement with the *in vitro* experiments since the microvessel density in the tumor and the percentage of Ki-67 positive cells was significantly decreased by treatment with PTX-PNS, whereas no significant effect was obtained upon treatment with free PTX.

Taken together, our data demonstrated that our new PTX nanoformulation can respond to some important issues related to PTX treatment, such as solubility and toxicity. The PTX incorporation in nanosponges might allow to lower the anti-tumor doses and increase its effectiveness in inhibiting melanoma cell model.

ETHICS STATEMENT

All experimental procedures were done according to Europeans Guidelines and our institution's ethics commission.

AUTHOR CONTRIBUTIONS

CD, RC, GB, FT, and UD conceived the project. BF, MA, NC, FC, CLG, EBo, LA, EBe, and SR performed the experiments. SP, AC, and CD analyzed the results. GB, SP, and CD wrote the first draft. All authors revised the manuscript.

ACKNOWLEDGMENTS

This project was funded by the Associazione Italiana Ricerca sul Cancro (IG 20714, AIRC, Milano), Fondazione Amici di Jean (Torino), and Fondazione Cariplo (2017-0535). LA is funded by Fondazione Umberto Veronesi (Post-Doctoral Fellowship 2018). Research was funded by 60% grant of the University of Torino to RC and CD. We are grateful to the Obstetrics and Gynecology Unit, Martini Hospital, Torino, for providing human umbilical cords.

SUPPLEMENTARY MATERIAL

The Supplementary Material for this article can be found online at: https://www.frontiersin.org/articles/10.3389/fphar.2019.00776/full#supplementary-material

FIGURE S1 | Spheroids obtained from primary melanoma cell line PMel.

FIGURE S2 | Effect of PTX and PTX-PNS treatments on HUVEC cell viability assessed by MTT assay at 24h.

FIGURE S3 | HUVECs, A2058 and B16-BL6 cells photographed after the invasion test.

TABLE S1 | Effect of PTX and PTX-PNS treatments on HUVEC, A2058, and B16-BL6 on cell viability assessed by crystal violet staining at 6h.

REFERENCES

Annaratone, L., Marchiò, C., Russo, R., Ciardo, L., Rondon-Lagos, S. M., Goia, M. A., et al. (2013). A collection of primary tissue cultures of tumors from vacuum packed and cooled surgical specimens: a feasibility study. *PLoS One* 8 (9), e75193. doi: 10.1371/journal.pone.0075193

Ansari, K., Torne, J., Vavia, P. R., Trotta, F., and Cavalli, R. (2011). Paclitaxel loaded nanosponges: *in-vitro* characterization and cytotoxicity study on MCF-7 cell line culture. *Curr. Drug Deliv.* 8 (2), 194–202. doi: 10.2174/156720111794479934

Ballestrem, C., Wehrle-Haller, B., Hinz, B., and Imhof, B. A. (2000). Actin-dependent lamellipodia formation and microtubule-dependent tail retraction control-directed cell migration. *Mol. Biol. Cell.* 11, 2999–3012. doi: 10.1091/mbc.11.9.2999

Bhatia, S., Tykodi, S. S., and Thompson, J. A. (2009). Treatment of metastatic melanoma: an overview. *Oncology (Williston Park)* 23, 488–496.

Chen, X., Ling, X., Zhao, L., Xiong, F., Hollett, G., Kang, Y., et al. (2018). Biomimetic shells endow sub-50 nm nanoparticles with ultrahigh paclitaxel payloads for specific and robust chemotherapy. *ACS Appl. Mater. Interfaces* 10 (40), 33976–33985. doi: 10.1021/acsami.8b11571

Ciamporcero, E., Daga, M., Pizzimenti, S., Roetto, A., Dianzani, C., Compagnone, A., et al. (2018). Crosstalk between Nrf2 and YAP contributes to maintaining the antioxidant potential and chemoresistance in bladder cancer. *Free Radic. Biol. Med.* 115, 447–457. doi: 10.1016/j.freeradbiomed.2017.12.005

Davies, H., Bignell, G. R., Cox, C., Stephens, P., Edkins, S., Clegg, S., et al. (2002). Mutations of the BRAF gene in human cancer. *Nature* 417, 949–954. doi: 10.1038/nature00766

Dianzani, C., Minelli, R., Gigliotti, C. L., Occhipinti, S., Giovarelli, M., Conti, L., et al. (2014). B7h triggering inhibits the migration of tumor cell lines. *J. Immunol.* 192, 4921–4931. doi: 10.4049/jimmunol.1300587

Duchene, D., Cavalli, R., and Gref, R. (2016). Cyclodextrin-based polymeric nanoparticles as efficient carriers for anticancer drugs. *Curr. Pharm. Biotechnol.* 17 (3), 248–255. doi: 10.2174/1389201017666151030104944

Edmondson, R., Broglie, J. J., Adcock, A. F., and Yang, L. (2014). Three-dimensional cell culture systems and their applications in drug discovery and cell-based biosensors. *Assay Drug Dev. Technol.* 12, 207–218. doi: 10.1089/adt.2014.573

Flaherty, K. T., Puzanov, I., Kim, K. B., Ribas, A., McArthur, G. A., Sosman, J. A., et al. (2010). Inhibition of mutated, activated BRAF in metastatic melanoma. *N. Engl. J. Med.* 363, 809–819. doi: 10.1056/NEJMoa1002011

Long, G. V., Flaherty, K. T., Stroyakovskiy, D., Gogas, H., Levchenko., E., de Braud, F., et al. (2017). Dabrafenib plus trametinib versus dabrafenib monotherapy in patients with metastatic BRAF V600E/K-mutant melanoma: long-term survival and safety analysis of a phase 3 study. *Ann. Oncol.* 28, 1631–1639. doi: 10.1093/annonc/mdx176

Huang, H., Zhang, P., Chen, H., Ji, L., and Chao, H. (2015). Comparison between polypyridyl and cyclometalated ruthenium(II) complexes: anticancer activities against 2D and 3D cancer models. *Chemistry* 21, 715–725. doi: 10.1002/chem.201404922

Konno, T., Watanabe, J., and Ishihara, K. (2003). Enhanced solubility of paclitaxel using water-soluble and biocompatible 2-methacryloyloxyethyl phosphorylcholine polymers. *J. Biomed. Mater. Res. A.* 65, 209–214. doi: 10.1002/jbm.a.10481

Ma, H. L., Jiang, Q., Han, S., Wu, Y., Cui Tomshine, J., Wang, D., et al. (2012). Multicellular tumor spheroids as an in vivo-like tumor model for three-dimensional imaging of chemotherapeutic and nano material cellular penetration. *Mol. Imaging* 11, 487–498. doi: 10.2310/7290.2012.00012

Mittal, P., Vardhan, H., Ajmal, G., Bonde, G. V., Kapoor, R., Mittal, A., et al. (2018). Formulation, optimization, heamocompatibility and pharmacokinetic evaluation of PLGA nanoparticles containing paclitaxel. *Drug. Dev. Ind. Pharm.* 5, 1–43. doi: 10.1080/03639045.2018.1542706

Mognetti, B., Barberis, A., Marino, S., Berta, G., De Francia, S., Trotta, F., et al. (2012). *In vitro* enhancement of anticancer activity of paclitaxel by a Cremophor free cyclodextrin-based nanosponge formulation. *J. Inc. Phenom. Macrocyclic Chem.* 74 (1-4), 201–210. doi: 10.1007/s10847-011-0101-9

Pfannenstiel, L. W., Lam, S. S., Emens, L. A., Jaffee, E. M., and Armstrong, T. D. (2010). Paclitaxel enhances early dendritic cell maturation and function through TLR4 signaling in mice. *Cell. Immunol.* 263, 79–87. doi: 10.1016/j.cellimm.2010.03.001

Prasad, M., Lambe, U. P., Brar, B., Shah, I., Manimegalai, J., Ranjan, K., et al. (2018). Nanotherapeutics: an insight into healthcare and multi-dimensional applications in medical sector of the modern world. *Biomed. Pharmacoter.* 97, 1521–1537. doi: 10.1016/j.biopha.2017.11.026

Radovic, J., Maksimovic-Ivanic, D., Timotijevic, G., Popadic, S., Ramic, Z., Trajkovic, V., et al. (2012). Cell-type dependent response of melanoma cells to aloe emodin. *Food Chem. Toxicol.* 50, 3181–3189. doi: 10.1016/j.fct.2012.05.047

Robert, C., Karaszewska, B., Schachter, J., Rutkowski, P., Mackiewicz, A., Stroiakovski, D., et al. (2015). Improved overall survival in melanoma with combined dabrafenib and trametinib. *N. Engl. J. Med.* 372, 30–39. doi: 10.1056/NEJMoa1412690

Robert, C., Long, G. V., Schachter, J., Arance, A., Grob, J. J., Mortier, L., Daud, A., et al. (2017). Long-term outcomes in patients (pts) with ipilimumab (ipi)-naive advanced melanoma in the phase 3 KEYNOTE-006 study who completed pembrolizumab (pembro) treatment. *J. Clin. Oncol.* 35 (Suppl. 15). doi: 10.1200/JCO.2017.35.15_suppl.9504

Schneider, C. A., Rasband, W. S., and Eliceiri, K. W. (2012). NIH Image to ImageJ: 25 years of image analysis. *Nat. Methods* 9, 671–675. doi: 10.1038/nmeth.2089

Shende, P., Kulkarni, Y. A., Gaud, R. S., Deshmukh, K., Cavalli, R., Trotta, F., et al. (2015). Acute and repeated dose toxicity studies of different β-cyclodextrin-based nanosponge formulations. *J. Pharm. Sci.* 104 (5), 1856–1863. doi: 10.1002/jps.24416

Simon, A., Kourie, H. R., and Kerger, J. (2017). Is there still a role for cytotoxic chemotherapy after targeted therapy and immunotherapy in metastatic melanoma? A case report and literature review. *Chin. J. Cancer* 36, 10. doi: 10.1186/s40880-017-0179-6

Sofias, A. M., Dunne, M., Storm, G., and Allen, C. (2017). The battle of "nano" paclitaxel. *Adv. Drug Deliv. Rev.* 122, 20–30. doi: 10.1016/j.addr.2017.02.003

Song, Q., Yin, Y., Shang, L., Wu, T., Zhang, D., Kong, M., et al. (2017). Tumor microenvironment responsive nanogel for the combinatorial antitumor effect of chemotherapy and immunotherapy. *Nano Lett.* 17, 6366–6375. doi: 10.1021/acs.nanolett.7b03186

Sylvester, P. W. (2011). Optimization of the tetrazolium dye (MTT) colorimetric assay for cellular growth and viability. *Methods Mol. Biol.* 716, 157–168. doi: 10.1007/978-1-61779-012-6_9

Swaminathan, S., Cavalli, R., and Trotta, F. (2016). Cyclodextrin-based nanosponges: a versatile platform for cancer nanotherapeutics development. *Wiley Interdiscip. Rev. Nanomed. Nanobiotechnol.* 8 (4), 579–601. doi: 10.1002/wnan.1384

Taraboletti, G., Micheletti, G., Rieppi, M., Poli, M., Turatto, M., Rossi, C., et al. (2002). Antiangiogenic and antitumor activity of IDN 5390, a new taxane derivative. *Clin. Cancer Res.* 8, 1182–1188.

Torne, S. J., Ansari, K. A., Vavia, P. R., Trotta, F., and Cavalli, R. (2010). Enhanced oral paclitaxel bioavailability after administration of paclitaxel-loaded nanosponges. *Drug Del.* 17 (6), 419–425. doi: 10.3109/10717541003777233

Trotta, F., Zanetti, M., and Cavalli, R. (2012). Cyclodextrin-based nanosponges as drug carriers. *Beilstein J. Org. Chem.* 8, 2091–2099. doi: 10.3762/bjoc.8.235

Trotta, F., Dianzani, C., Caldera, F., Mognetti, B., and Cavalli, R. (2014). The application of nanosponges to cancer drug delivery. *Exp. Opin. Drug Del.* 11 (6), 931–941. doi: 10.1517/17425247.2014.911729

Walker, L., Schalch, H., King, D. M., Dietrich, L., Eastman, M., Kwak, M., et al. (2005). Phase II trial of weekly paclitaxel in patients with advanced melanoma. *Melanoma Res.* 15, 453–459. doi: 10.1097/00008390-200510000-00015

Conflict of Interest Statement: The authors declare that the research was conducted in the absence of any commercial or financial relationships that could be construed as a potential conflict of interest.

Advantages of publishing in Frontiers

OPEN ACCESS
Articles are free to read for greatest visibility and readership

FAST PUBLICATION
Around 90 days from submission to decision

HIGH QUALITY PEER-REVIEW
Rigorous, collaborative, and constructive peer-review

TRANSPARENT PEER-REVIEW
Editors and reviewers acknowledged by name on published articles

Frontiers
Avenue du Tribunal-Fédéral 34
1005 Lausanne | Switzerland

Visit us: www.frontiersin.org
Contact us: info@frontiersin.org | +41 21 510 17 00

REPRODUCIBILITY OF RESEARCH
Support open data and methods to enhance research reproducibility

DIGITAL PUBLISHING
Articles designed for optimal readership across devices

FOLLOW US
@frontiersin

IMPACT METRICS
Advanced article metrics track visibility across digital media

EXTENSIVE PROMOTION
Marketing and promotion of impactful research

LOOP RESEARCH NETWORK
Our network increases your article's readership